Hungarian Journal
of Industrial Chemistry
Veszprém
Vol. 1. pp. 1-16 (1973)

APPLICATION OF ANALOG COMPUTERS TO THE MEASUREMENT AND EVALUATION OF RESIDENCE TIME DISTRIBUTION

A. LÁSZLÓ and P. ÁRVA

(Department of Chemical Process Engineering,
Veszprém University of Chemical Engineering)

Received: September 6, 1972.

The authors describe a measurement and calculation method which enables direct contact to be made between any optional operational unit and an analog computer. The calculation and evaluation of residence time distribution in the case of absorbers is discussed as an example.

In connection with the above, the expressions which became usual in connection with residence time distribution are modified and transformed in such a way as to obtain quantities everywhere which can be directly fed into an analog computer.

An advantageous property of the method is its high speed, because calculations can be carried out simultaneously with the experiments. In addition, any other variable which is convertible to an electric tension can be directly fed into an analog computer. For example, a chromatograph can be directly connected to an analog machine. Accordingly, concerning its technical utilization the method is also universal.

The residence time distribution of the flowing phases is of paramount importance in the design and operation of chemical industrial operational units.

The above-mentioned fact has been discussed in a paper of basic importance by DANCKWERTS [1]. He defined the most important concepts connected with residence time distribution. It is sufficient to quote his important statement which can be summarized in the following manner: if the residence times of the individual

elements of the flowing phases are different,i.e. they vary according to some sort of distribution, the efficiency of the operational unit (apparatus) is always lower compared to that observed in the case of the identical residence time of the elements. A number of concepts - defined on the basis of DANCKWERTS' paper - are at present widely applied [2 - 7]. These concepts are assumed to be known and they are summarized in Table 1. The only remark to be made in connection with this is that two concepts for time are usually used: t is the time actually measured, whereas θ is dimensionless time referred to the $\bar{t}$ mean or apparent residence time. The connection between these two quantities is expressed by the following equation:

$$\theta = \frac{t}{\bar{t}} = \frac{tv}{V} \qquad (1)$$

Table 1.

Denomination	Experimental curves	Theoretical curves
density function	$C(\theta) = \frac{d\,F}{d\,\theta}$	$\longrightarrow \quad E(\theta) = \frac{d\,I(\theta)}{d\,(\theta)}$
distribution function	$F(\theta) = \int_0^{\infty} C(\theta)\,d\,\theta$	$\longrightarrow \quad 1 - I(\theta) = \int_0^{\theta} E(\theta)\,d\,\theta$
intensity function	-	$\Lambda(\theta) = \frac{E(\theta)}{I(\theta)} = \frac{d}{d\,\theta} \ln I(\theta)$

As to the method of measurement it should be noted that two techniques are used generally: 1. The tracer substance is added to the input stream for only a short period of time in a pulse-like manner, whereupon its addition is disconnected. The c(t) function

of the tracer substance, being the response to the above input pulse, is measured or recorded in the output stream (Fig.1.).

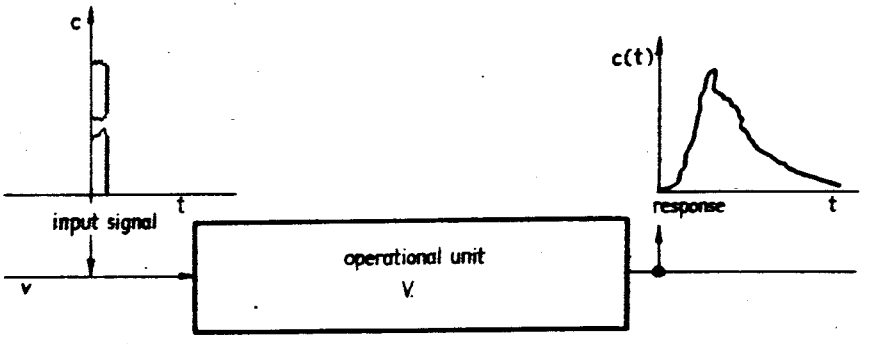

Fig.1. Schematical representation on the study of residence time distribution in the case of pulse-like signal.

2. The tracer substance is added to the input stream at a well-defined (c_o) concentration at a time t = 0 and this (c_o) concentration is maintained in the following (Fig. 2.). This type of signal is

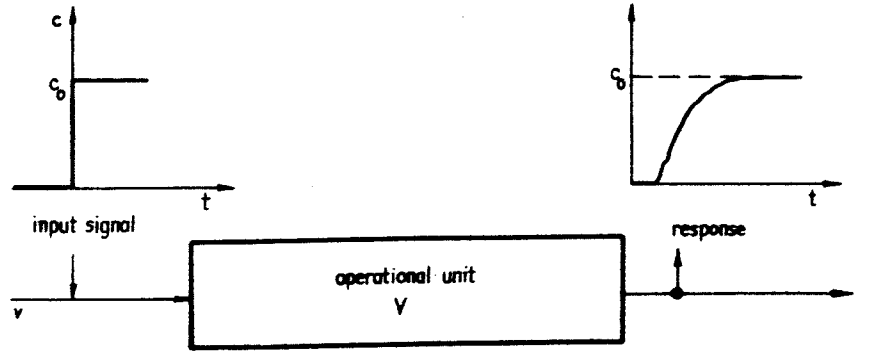

Fig.2. Schematical representation of the study of residence time distribution in the case of jump-like signal.

often called a "jump-like input signal". In such a case, the c(t) concentration of the tracer substance is measured or recorded against time in the exit stream from a time t = 0. In this case the limiting value of the response function c(t) is $c(t) \to (c_o)$ if $t \to \infty$. The ratio of c(t) and (c_o) is the distribution function of the residence time:

$$\frac{c(t)}{c_o} = F(t) \tag{2}$$

In practice, instead of the c(t) function it is advantageous to measure its value multiplied by the volumetric flow rate (v) and divided by the amount of tracer substance brought into the system (Q). This quantity is called function C(t):

$$\frac{c(t)v}{Q} = C(t) \tag{3}$$

The function C(t), as determined experimentally, is identical to the theoretical E(t) residence time distribution density function, if the tracer substance brought into the system truly represents the elements of the streaming phase at the exit side.

According to the well-known laws of mathematical statistics, the connection between the functions described in the foregoing is the following:

$$C(t) \to E(t) = \frac{d\,F}{d\,t}$$

and (4)

$$C(\theta) \to E(\theta) = \frac{d\,F}{d\,\theta}$$

It should be noted that these concepts and measuring methods can not only be applied in connection with continuous operational units of chemical engineering, but also in connection with any other type of engineering activity, where different media flow through any apparatus of a given size and shape, such as, for example, sewage purification and settling tanks.

DESCRIPTION OF THE MEASURING METHOD

The determination of the functions and integrals shown in Table 1. is generally a cumbersome and time-consuming task. Accordingly a measuring technique and a programme was elaborated, the essence is that the experimental data measured in the operational unit are, after suitable and proportional transformation, fed into an analog computer. The latter carries out the calculations simultaneously with the measurement.

The experiments were concerned with adsorption processes occurring in packed columns. However, it should be stressed that the method is of a general nature and can be applied to any operational unit. The calculations were carried out with the momentum method [8, 9, 10].

DESCRIPTION OF THE EXPERIMENTS

The liquid phase applied in the packed column was water and the tracer substance was aqueous NaCl solution. The conductance of the effluent liquid was measured. In the concentration range used in these experiments, the connection between conductance and salt concentration of the liquid is linear. Experiments were carried out with pulse-like and jump-like changes in the amount of the tracer substance.

The connection between the operational unit and the analog computer was established according to Fig. 3. A detector is placed into the liquid leaving the operational unit and the response of the apparatus to the interfering signal is recorded by a potentiometric strip-chart recorder. The sensing device was a conductivity meter equipped with platinum electrodes. A follower potentiometer of 10 kiloohms resistance - this value being matched to the analog computer - was coupled to the shaft actuating the sliding contact of the measuring bridge built into the recorder. A potential

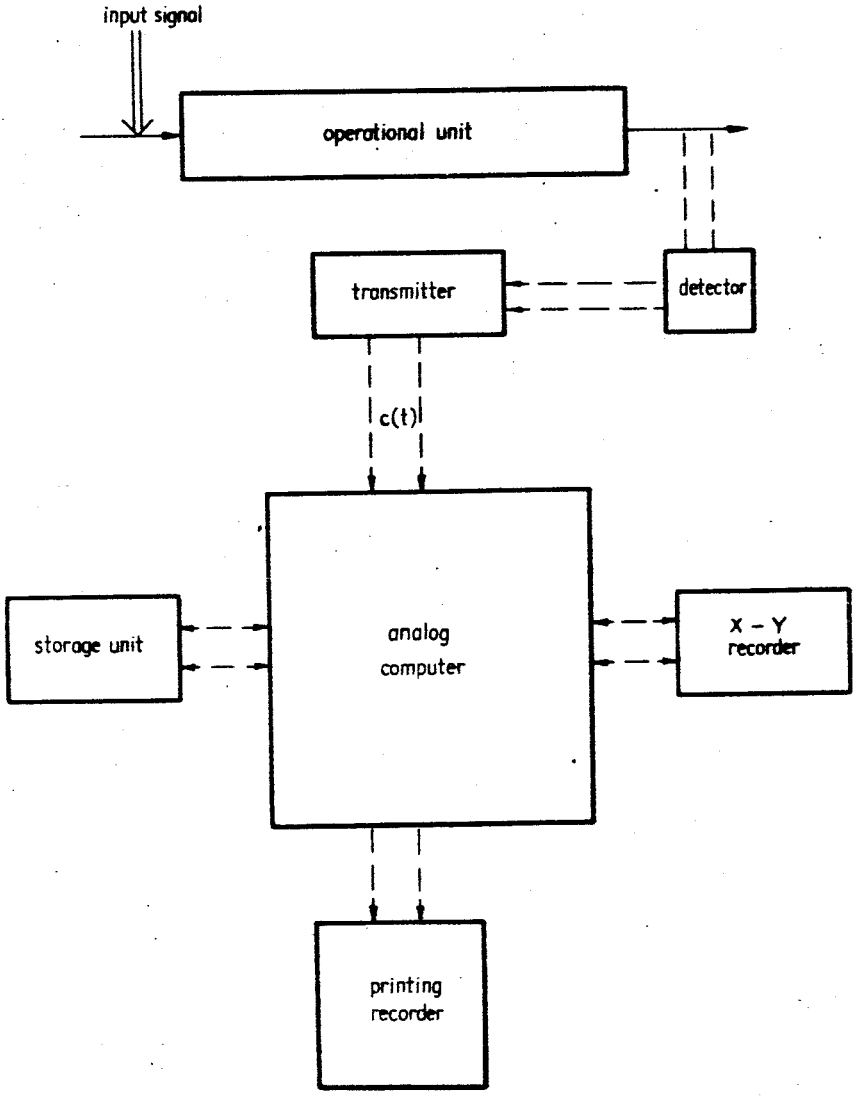

Fig.3. Schematic representation of the connection of the operational unit to the analog computer.

of 10 volts - again matched to the computer - was fed to the end points of the potentiometer. The sliding contact of this potentiometer followed that of the recording potentiometer and, consequently a voltage proportional to that measured by the recorder, i.e. to the conductance of the liquid was obtained between one end and the sliding contact of the follower potentiometer. This voltage can be regarded as equal to the function c(t) and this was fed into the analog computer which carried out the necessary calculations.

It should be noted that the X-Y recorder, which is an accessory of the computer type MEDA 81 T, can also be utilized as a curve reader. Accordingly, the records representing the results can be used in the calculations.

CALCULATIONS

1. Pulse-like Input Signal. The first momentum gives the mean value of the distribution, which in case of a c(t) distribution function is identical to the mean residence time ($\bar{t}$):

$$\bar{t} = \frac{\int_0^\infty t\, c(t)\, dt}{\int_0^\infty c(t)\, dt} = \int_0^\infty t\, C(t)\, dt \qquad (5)$$

The variance σ^2 can be calculated from the experimental data according to the following formula:

$$\sigma^2 = \frac{\int_0^\infty t^2\, c(t)\, dt}{\int_0^\infty c(t)\, dt} \qquad (6)$$

The central variance σ_c^2 is, from the above:

$$\sigma_c^2 = \sigma^2 - \bar{t}^2 \qquad (7)$$

2. Jump-like Input Signal. In this case, the calculation of the momenta is carried out as follows:

The definition of the mean residence time is, according to Eq. (2),

$$\bar{t} = \frac{\int_0^\infty t \, d\, c(t)}{c_0} = \int_0^\infty t \, d\, F(t) \tag{8}$$

The mean residence time cannot be determined with an analog computer. The independent variable is always time and, consequently integration can be carried out only according to time. The expressions referring to a jump-like input signal must be transformed in such a way as to contain integration according to time.

When taking Equation (4) into consideration, Equation (8) can be resolved into two parts:

$$\int_0^\infty t \, d\, F(t) = \int_0^\infty t \, C(t) \, dt = \left[t \, F(t)\right]_0^\infty - \int_0^\infty F(t) \, dt$$

In accordance with practical considerations, the integration is not carried out until infinite time, but a sufficiently large t_m value is chosen at which the value of $F(t_m)$ is practically identical to $F(t_\infty) = 1$. Consequently the value of the integral is t_m and

$$\bar{t} = t_m - \frac{\int_0^{t_m} c(t) \, dt}{c_0} \tag{9}$$

This expression enables the calculation of the mean residence time from experimental data by means of an analog computer.

The definition for the calculation of the variance is the following:

$$\sigma^2 = \int_0^\infty t^2 \, d\, F(t)$$

which, transformed in a way analogous to that described in the forregoing, can be brought to a form allowing the calculations:

$$\sigma^2 = t_m^2 - 2\,\frac{\int_0^{t_m} t\,c(t)\,dt}{c_o} \tag{10}$$

Similarly, for the central variance we have:

$$\sigma_c^2 = t_m^2 - 2\,\frac{\int_0^{t_m} t\,c(t)\,dt}{c_o} - \bar{t}^2 \tag{11}$$

The following experimental data have to be known to calculate the integrals described in Equations (5), (6) and (7), as well as (9), (10) and (11):

Pulse-like input signal:	Jump-like input signal:	
$\int_0^{\infty} c(t)\,dt = I_1'$	$c_o = Y_1'$	(12)
$\int_0^{\infty} t\,c(t)\,dt = I_2'$	$\int_0^{t_m} c(t)\,dt = Y_2'$	(13)
$\int_0^{\infty} t^2\,c(t)\,dt = I_3'$	$\int_0^{t_m} t\,c(t)\,dt = Y_3'$	(14)

Direct calculation of these quantities was also possible if time t was at our disposal in the form of a potential. This method permits a voltage proportional to time to be produced. Indicating the voltage proportional to time by U_t:

$$U_t = K_1 \cdot t \tag{15}$$

and this is the solution of the following differential equation:

$$\frac{d\,U_t}{dt} = K_1 \quad \text{and} \quad U_t(o) = 0 \tag{16}$$

Accordingly, the function $U_t(t)$ can be produced with the programme shown in Fig.4.

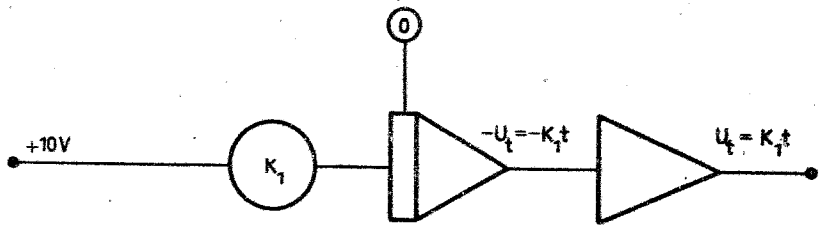

Fig.4. Programme for the production of a voltage proportional to time.

After this, the necessary integrals can be calculated. The computer programme is shown in Fig.5. Constants k_1, k_2, k_3 and k_4 are scale factors. Their values are to be set during the measurement in such a way that the potential produced at the computing units should not be higher than that compatible with the computer. Fig.5. indicates on which units the values of the integrals are read. These do not directly give the values (12), (13) and (14), but rather their products with a constant:

$$I_1' = \frac{I_1}{k_2}$$

$$I_2' = \frac{1}{k_1 k_4} I_2$$

$$I_3' = \frac{1}{k_1^2 k_3} I_3$$

The values of I_1, I_2 and I_3 are read from the computer at the end of the experiment and the momenta can be calculated with the following simple equations:

In the case of a pulse-like input signal:

$$\bar{t} = \frac{k_2}{k_1 k_4} \frac{I_2}{I_1} \qquad (17)$$

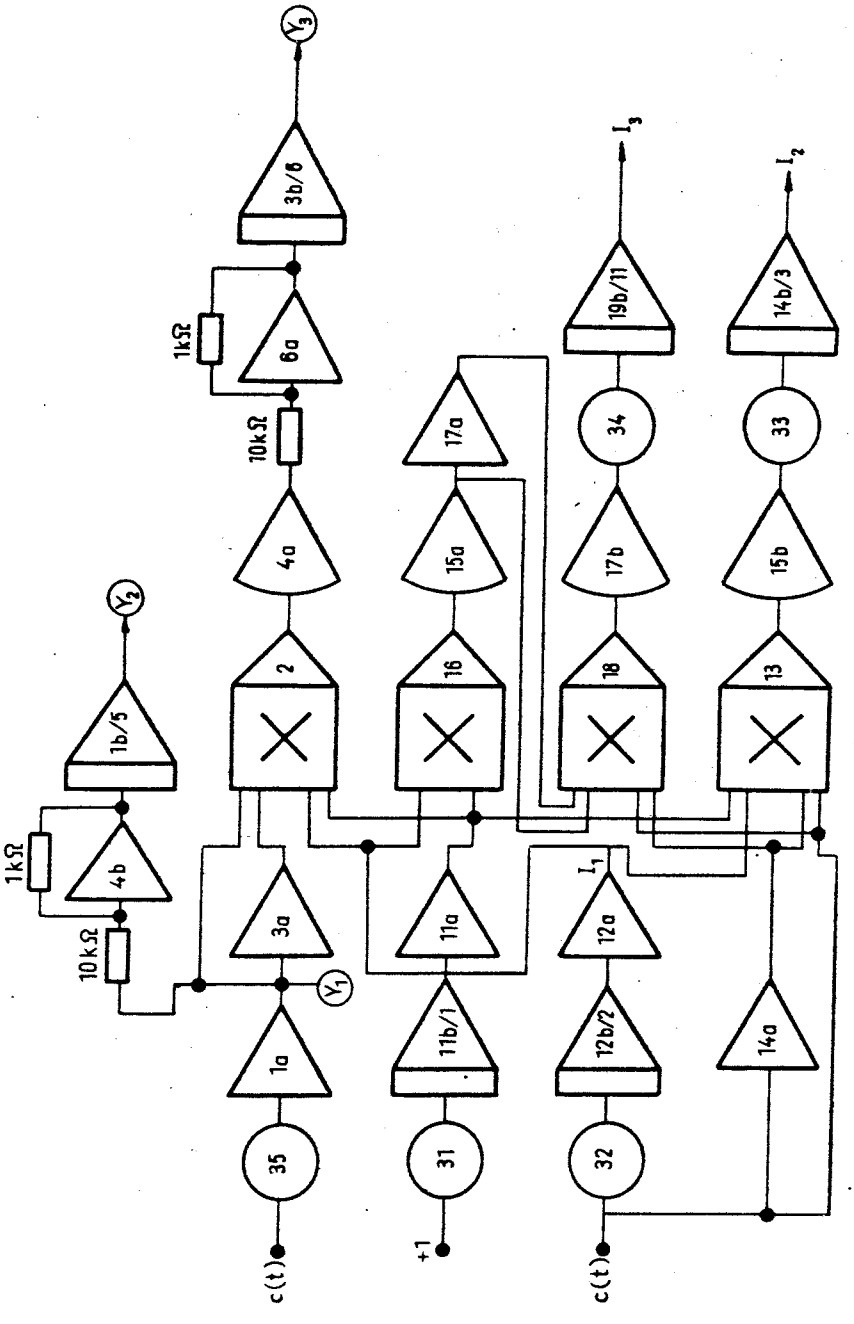

Fig.5. Programme for evaluation of the experiments

$$\sigma^2 = \frac{k_2}{k_1^2 k_3} \frac{I_3}{I_1} \tag{18}$$

In the case of a jump-like input signal:

$$\bar{t} = t_m - \frac{Y_2}{Y_1} \tag{19}$$

$$\sigma^2 = t_m^2 - \frac{Y_3}{k_4 k_1 Y_1} \tag{20}$$

The response curve obtained with a pulse-like input signal together with the calculated values, based on experiments carried out with a packed column, are shown in Fig.6.

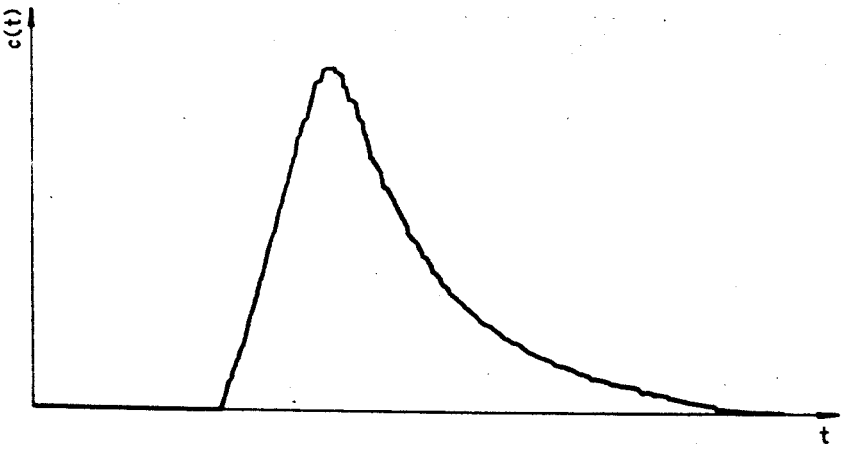

Fig.6. c(t) curve obtained from the analog computer and result of the calculation in the case of pulse-like disturbance

$I_1 = 0.108$ $\bar{t} = 43.9$ sec

$I_2 = 0.237$ $\sigma^2 = 2088$ sec^2

$I_3 = 0.564$ $\sigma_c^2 = 163.4$ sec^2

The response curve obtained with a jump-like input signal, as observed in experiments carried out with a liquid phase streaming in a rotating film-reactor, are shown in Fig.7.

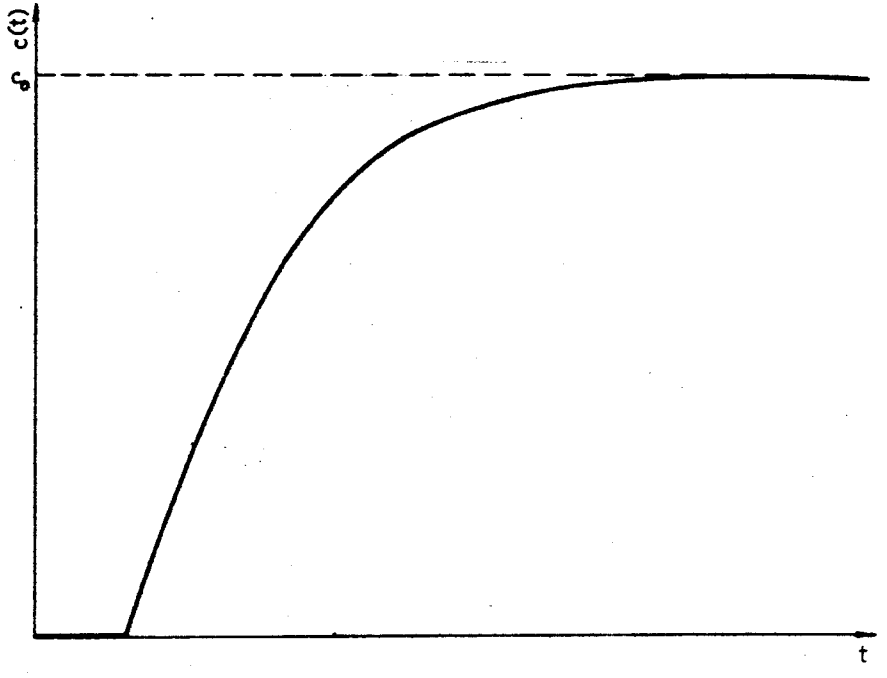

Fig.7. c(t) curve obtained from the computer and result of the calculation in the case of jump-like disturbance

$Y_1 = 0.067$ $\bar{t} = 29$

$Y_2 = 0.489$ $\sigma^2 = 1164$

$Y_3 = 0.296$ $\sigma_c^2 = 435$

Calculations can be carried out by the computer simultaneously with the measurements. The integrals I_1, I_2 and I_3, as functions of time, are present in the computer and their values can be read, printed out or recorded continuously.

According to the discussed method, the analog computer can be applied to construct the functions themselves. For example, in the case of a pulse-like input signal, the value of the integral I_t is proportional to the functions F(t) and I(t) (cf.Table 1.), since the function F(t) can be expressed in the following form:

$$F(t) = \frac{\int_0^t c(t)\,dt}{\int_0^\infty c(t)\,dt} = \frac{I_1(t)}{I_1(\infty)} \qquad (21)$$

Consequently, the function F(t) can be directly obtained from the computer or recorded in the case of a pulse-like input signal.

LIST OF SIGNS

C(t) density function of experimentally determinable residence time distribution (sec^{-1})

c(t) response function furnished by the operational unit upon disturbance ($moles/m^3$)

c_o the value of the jump in the case of jump-like disturbance ($moles/m^3$)

E(t) density function of residence time distribution (sec^{-1})

F(t) distribution function of residence time (dimensionless)

I(t) age distribution function (dimensionless)

I_1 value read on analog computer (cf. Fig.5.)

I_2 value read on analog computer (cf. Fig.5.)

I_3 value read on analog computer (cf. Fig.5.)

I_1' cf. Equation (12)

I_2' cf. Equation (13)

I_3' cf. Equation (14)

k_1, k_2, k_3, k_4 scale factors (cf. Fig.5.)

t time (sec)

$\bar{t}$ mean residence time (sec)

V volume of operational unit (m^3)

v volumetric flow rate of phase (m^3/sec)

Q amount of pilot substance injected (moles)

Y_1 cf. equation (12)

Y_2 cf. equation (13)

Y_3 cf. equation (14)

$A(t)$ intensity function (sec^{-1})

σ^2 second momentum (sec^2) or variance

σ_c^2 second central momentum (sec^2)

REFERENCES

1. DANCKWERTS, P.V., Chem. Eng. Sci. 2, 1 (1953).

2. LEVENSPIEL, O., BISCHOFF, K.B., Adv. Chem. Eng. 4, 95 (1963).

3. KAFAROV, V.V., Metodi kibernetiki v himiya i himitsheskoy technologii, Izd. "Himiya", Moscow (1968).

4. BISCHOFF, K.B., McCRACHEN, A.E., Ind. Eng. Chem. 58, 18 (1966).

5. DANCKWERTS, P.V., Ind. Chemist. 3, 102 (1954).

6. NAOR, P., SINNAR, R., Ind. Eng. Chem. Fund. 2, 278 (1363).

7. HIMMELBLAU, D.M., BISCHOFF, K.B., Process Analysis and Simulation, John Wiley and Sons Inc., New York 1968.

8. van der LAAN, E.Th., Chem. Eng. Sci. 7, 1 (1957).

9. ÁRVA, P., Töltelékes oszlopban történő kétfázisu áramlás matematikai modellezése. Kandidátusi értekezés. (The Mathematical Modelling of Two Phase Flow in Packed Columns. Candidate Thesis.) Moscow, 1970.

10. ARIS, R., Introduction to the Analysis of Chemical Reactors. Prentice-Hall. Englewood Cliffs, N.J. 1965. p. 205.

РЕЗЮМЕ

Автсрами описан метод измерения и вычисления, пригодный для создания непосредвтвенной связи между любым элементом процесса и аналоговой ВМ. В качестве примера показано вычисление и оценка распределения времени пребывания жидкости в случае абсорберов.

В связи с этим изменены выражения, образовавшиеся для распределения времени пребывания, и они превращены таким способом, чтобы везде сфигурировались величины,непосредственно вводимые в ВМ.

Преимуществом метода является его высокая скорость, так как вычисления выполняются одновременно с опытами. Кроме этого, данный метод пригоден к непосредственному введению в АВМ любой другой переменной, превратимой в электрическое напряжение. Так, напр., и хроматограф можно непосредственно подключить к аналоговой АВМ. По этому метод является всеобщим и с точки зрения технологического выполнения.

Hungarian Journal
of Industrial Chemistry
Veszprém
Vol.1. pp. 17-30 (1973)

ALGEBRAIC DESCRIPTION OF TECHNICAL CHEMICAL SYSTEMS I.

THE SIGNIFICANCE OF MODERN ALGEBRAIC METHODS IN CHEMICAL SYSTEMS ENGINEERING

T. BLICKLE

(Research Institute for Technical Chemistry of the Hungarian Academy of Sciences, Veszprém)

Received: June 30, 1972.

The series of papers entitled algebraic description of technical chemical systems has the following chapters:

material systems and transformations,
combination and projection of material systems,
technical chemical operators,
compositions of technical chemical operators,
generalization of the set of technical information.

The possible applications of systems theory, systems engineering and modern algebra in technical chemistry are discussed in the introductory paper, and the position, assignments and expected results of the algebraic treatment are defined. The following tasks are encountered in the study and optimalization of technical chemical systems:

1. Qualitative description and study of technical chemical systems.
2. Study of the functions interpreted on technical chemical systems and of the connections of these functions with one another.
3. Optimalization of static systems.
4. Description, control and optimalization of dynamic systems.

Modern algebraic methods of treatment are adequate for the solution of the first task, a fact that will be confirmed by later papers to be published in this series.

INTRODUCTION

The task of every technical science, and also of technical chemistry is the study of material (or energetical) systems, which - directly or indirectly - serve to satisfy some sort of demand. Accordingly, the task of technical chemistry is the study of systems, which permit the production of a product or final product of the desired properties from the raw material.

Prior to their design, the systems have to be vigorously studied. The claims defining the final product and the transformations producing it must be defined and a theoretical model must be constructed in this manner. The elements of the theoretical model must be scrutinized with regard to the conditions of their realization. When, during the analysis of the theoretical model, the "building bricks" of the system are reached, the physical entities corresponding to these must be found,i.e. the system that is found to be adequate from a theoretical point of view, must be "questioned", bearing in mind the problems of practical realization. The next step is the task of synthetizing, building up the complex physical system and its study while in operation.

In the study of both the theoretical model and the actual operating system as a whole, the treatment based on systems theory is of considerable assistance.

General systems theory was introduced by the justified endeavour towards uniform science. There is no intention here to describe the individual trends, but a few basic concepts taken from the introduction to the selected essays on systems theory,published in 1971 are quoted [1]:

"... Operation research deals with the operation of existing systems, whereas systems engineering is the totality of methods used for designing systems. The two approaches cannot be sharply separated in practice, and from a theoretical point of view they converge to the general systems theory.

- The first step of systems engineering is: specification of what is demanded, and the definition of the claims.

- This is followed by modelling and identification of the given parts of the system. The variables should be chosen and the equations describing their connections should be established.
- The next step after analysis of the equations is the synthesis,i.e. a description of the model of the whole system in accordance with the previously established specification. Systems synthesis mainly consists of the theory of optimalization.
- Finally, the last step of systems engineering is the designing, i.e. the decomposition of the model obtained during synthesis to its physical components".

It is apparent from the foregoing that the formulation of the problems in accordance with systems engineering and the level of demands, which at the present time is a necessity in the study of technical chemistry, have to conform to each other.

The idea of applying the results of systems theory and systems engineering in technical chemistry seemed self-evident, because the results obtained in this way are of general validity and can be utilized in other fields of science.

In order to be able to characterize the technical chemical systems and their characteristics, their mathematical models must be established.

The totality of physically or mentally encompassed elements, in which the elements are in a direct or indirect relation to any of the others, may be defined as a system.

It is an unequivocal fact that technical chemistry deals with materials. These materials in themselves can be regarded as systems. They represent the manifestation of a number of material properties, there are certain relations between these properties and accordingly they can be regarded as elements of the material systems. The totality of these material systems - including also raw materials and final products - comprises the set of material systems.

Chemical technology produces different materials (products) from the given elements of a set of material systems, i.e. it projects the set of material systems upon itself. In mathematics such a system is termed an operator, and accordingly, in the following a system producing a final product from a raw material is termed a chemical technological operator. A system of operators possesses a definite internal structure. In a similar manner to that applied in the case of material systems, a set of technical chemical operator systems can be defined.

During the realization of a concrete technological process, a connection is established between the individual elements of the sets described in the foregoing. The system produced in this manner is termed a technical chemical system, which includes

raw material systems,
operator systems and
final product systems.

The set of these technical chemical systems, together with all the information they contain, represent technical chemistry.

The structure of the systems is demonstrated in the following Figure:

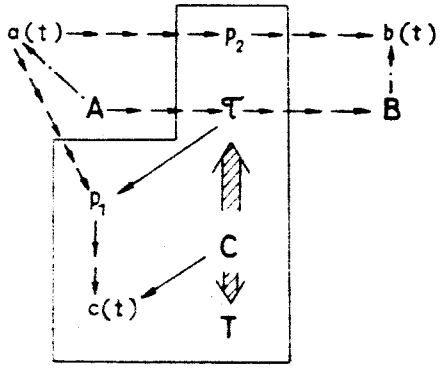

The C technological operator system produces a material system B from material system A. System C comprises (τ) functional and

T existential parts. (τ) is the totality of the elements of the system which are necessary for the operator function, whereas T represents those necessary for the existence of the system. (τ) can be resolved to two operators: p_1 and p_2. The systems are regarded as function systems, so that A corresponds to a(t), B to b(t) and C to c(t). Any changes in a(t) act upon c(t) through operator p_1, and upon b(t) through operator p_2 (where t is time). In general, when studying a system, it was only the function systems and their connections which were studied, and very rarely the structure of the system. However, in our opinion, the latter is the first step. It must be known first, what sort of an operator is adequate to transform system A into system B; knowledge of the concrete function connections comes only after this.

With regard to the foregoing, the main points of view and characteristics of technical chemical systems theory can be summarized in the following.

1. Algebraic description

The process of the satisfaction of the demand can be regarded in the following manner: a system of Γ_o initial state (state of unsatisfied demand), upon the action of the final product A_v - as an operator - becomes state Γ_v (state of satisfied demand):

$$A_v [\Gamma_o] = \Gamma_v \qquad (1)$$

A demand can be e.g. the depression of the temperature of a patient in a feverish state. In this case

Γ_o - is the feverish state,

Γ_v - is the normal state,

operator A_v - is a pharmaceutical product, an antifebrile medicine.

A quantitative and economic description of the satisfaction of the demand can be expressed by the expenses of the satisfaction of the specific demand:

$$N\Gamma = G(A_V) \cdot N\tau(A_V) \qquad (2)$$

where

$N\Gamma$ - is the expense of satisfaction of the specific demand,

$G(A_V)$ - is the amount of product needed for satisfaction of the specific demand,

$N\tau(A_V)$ - is the expense of the final product.

Accordingly, the task is to design an A_V material system which is capable of bringing the passive system from the state Γ_O to state Γ_V with a minimum expense.

The final product A_V, which satisfies the demand, is produced from the raw material A_O by the action of the technical chemical operator T:

$$T\left[A_O\right] = A_V \qquad (3)$$

Consequently, the process in which a demand is satisfied can also be regarded in the following manner: the passive system in state Γ_O is brought to state Γ_V by the joint action of the raw material A_O and the technological operator T. Accordingly, the following is gained by uniting Equations (1) and (3):

$$T\left[A_O\right]\left[\Gamma_O\right] = \Gamma_V \qquad (4)$$

It is apparent that the expenses of the satisfaction of the demand depend on the raw material and on the technological process used. If the A_O raw material is given - and this is the most frequent case - the technological process involving a minimum of expense can be found.

Technological processes are built up of technological stages and accordingly the technological (technical chemical) operator can be resolved into part-operators.

The operator R_1, which carries out the first technological stage, transforms the raw material A_O into an intermediate product A_1:

$$R_1[A_o] = A_1 \tag{5}$$

In the second technological stage, material A_1 is transformed to material A_2 by the action of operator R_2:

$$R_2[A_1] = A_2 \tag{6}$$

and in the n^{th} stage:

$$R_n[A_{n-1}] = A_v \tag{7}$$

Accordingly, the total technological process can be described by:

$$\prod_{i=1}^{n} R_i[A_o] = A_v \tag{8}$$

It follows from the foregoing that the technological process is defined by the following facts: operators that realize the technological stages to be employed and in what order they are employed.

Technical chemical operators - as opposed to mathematical operators - possess a unique structure, which can be characterized by the following formula:

$$R\,[V, A, R]$$

where

V - is the transformation realized by the operator,
A - is the material supply of the operator,
R - is the totality of the operator elements necessary for the operator to exist, i.e. existential structure (e.g. apparatus).

This form of representation differs from the usual methematical representation, but it seems reasonable to immediately write after the operator its structure in brackets, rather than the material system upon which it acts. This form of representation will be used in the following. The transformation of the material system upon the action of the operator will be designated in the

following manner:

$$A_o + T = A_v \tag{9}$$

or

$$A_o + R_1 = A_1 \tag{10}$$

These equations express the same facts as equations (3) and (5), written in the conventional form.

The transformation of the material system may proceed in time:

$$A_{to} + R_1 = A_{tv} \tag{11}$$

where

A_{to} - is the material system introduced at the beginning,
A_{tv} - is the material system taken away after the transformation,

or it may proceed according to place:

$$A_{yo} + R_1 = A_{yv} \tag{12}$$

where

A_{yo} - is the input material flow,
A_{yv} - is the output material flow.

If changes occur with respect to both time and place (unstationary system), the following can be written:

$$A_{to} + A_{yo} + R = A_{tv} + A_{yv} \tag{13}$$

By studying their structure, the operators that realize the technological stages can be resolved to further components.

Operators which bring about one single elementary change - upon whose action only one property of the material system is changed - are termed elementary operators.

Technological stages that include more than one elementary change can be realized by a composition of elementary operators. Operator systems constructed in this manner can be classified into two main groups:

1. The two or more operators which form the operator system - and whose existential structure is identical - act jointly in space and time.

$$R_a \left[V_a, A_a, R_a\right] \wedge R_b \left[V_b, A_b, R_a\right] = R\left[V_a \wedge V_b, A_a \wedge A_b, R_a\right] \qquad (14)$$

This group comprises:

operators of total change,
composite operators.

1.a) Operators of total change are encountered if an elementary operator - due to the permitted single change - would lead to production of a non-existent, fictive material system and consequently the action of further elementary operators is necessary to obtain a real, existent material system. The operator of total change is the combination of the minimum number of elementary operators which permit production of a non-fictive material system as a final product.

For example, the preparation of solid crystalline material from a solution may be regarded as the result of four elementary changes:

separation of material from the solution,
attainment of the crystalline structure,
attainment of form,
attainment of dimensions.

The first operator, which makes the material to be separated from the solution, leads to a fictive system, since there is no solid matter without form and dimensions. Accordingly, in this case the operator of total change comprises four elementary operators.

1.b) If there is no fictive material system among the products of the elementary operators acting together, a composite operator is encountered.

2. The existential structure of the elementary operators is different, the action of the operators is separated in space or time, and any connection between the operators can be realized only through the material system. Depending on the fact, whether the material system ensuring the connection is variable in time or space, we can speak of an

operator block and,
an operator series.

The continually more sophisticated systems, ranging from the elementary operator to the operator series, can be resolved to elementary operators.

Such a resolution of the technological stages and the defining of the possible types of operator structure represents the qualitative description of technical chemical operators.

2. Analytical description and optimalization

The quantitative description is obtained if the $x_1, x_2, \ldots x_n$ functions - their total number being n_F - are interpreted in connection with the elements of the operator structure, and the z function in connection with the change V. The number of the connections between the functions is n_K.

The number of free functions is:

$$n = n_F - n_K \tag{15}$$

The solution of the n_K functions for a system of elementary change is

$$f_i \left[z, x_1, x_2, \ldots x_n, A'', A''', R \right] \tag{16}$$

where

A'' - is the auxiliary material,
A''' - is the packing material.

In the case of any type of systems of composite change the following is gained:

$$RF_i\left[Rf_1,\ R\ f_2,\ \ldots\ z,\ A_r,\ A_t\right] \qquad (17).$$

where

A_r - is the recirculated material,
A_t - is the block auxiliary material.

The expense function will now be considered in connection with the system of elementary change:

$$Nf_i\left[z_o,\ z_v,\ x_1,\ x_2,\ \ldots\ x_n,\ A'',\ A''',\ R\right] \qquad (18)$$

by defining the auxiliary materials $\mathring{A}''$, $\mathring{A}'''$ and the structure $\mathring{R}$, the optimal values of the free functions can be obtained:

$$Nf_i\left[z_o,\ z_v,\ \hat{x}_1,\ \hat{x}_2,\ \ldots\ \hat{x}_n,\ \mathring{A}'',\ \mathring{A}''',\ \mathring{R}\right] \qquad (19)$$

If the most preferable auxiliary materials and structures are chosen, the optimum function of the system of elementary change will be

$$\hat{N}f_i(z_o,\ z_v) \qquad (20)$$

The expense function, considered for a system of composite change, is

$$\hat{N}F_i(\hat{N}\ f_1,\ \hat{N}f_2,\ \ldots\ z_o,\ z_v,\ A_v,\ A_t) \qquad (21)$$

When the preferable values for A_v and A_t are chosen:

$$\hat{N}F_i(z_o,\ z_v) \qquad (22)$$

The permutations of the isomorphous operator systems are the following:

$$N_{e,i} = \hat{N}F_1(z_o, z_1) + \hat{N}F_2(z_1, z_2) + \ldots \hat{N}F_{j+1}(z_j, z_v) \qquad (23)$$

When the most preferable permutation and optimal z_1-z_j values are chosen:

$$\hat{N}_{e,i}(z_o, z_v) \qquad (24)$$

The permutation of the operators of different changes gives the expense of the technological system:

$$\sum_i \hat{N}_{e,i} = N\tau\ (P_M, A_o, A_v) \qquad (25)$$

where P_M represents the permutations, the various permutations being the technological procedures. When the most preferable are chosen from among these:

$$\hat{N}\tau(A_o, A_v) \qquad (26)$$

and an adequate starting material is chosen:

$$\hat{\hat{N}}\tau(A_v) \qquad (27)$$

Returning to equation (2) and taking (27) into consideration, the expense of satisfying the specific demand is obtained:

$$N\Gamma = G(A_v) \cdot \hat{\hat{N}}_\tau\ (A_v) \qquad (28)$$

To find the A_v pertaining to the minimal $N\Gamma$; this is

$$\hat{N}\Gamma$$

which was the original task.

So far it was not mentioned that part of the functions interpreted in connection with qualitative elements does change or fluctuate in time, even in the case of systems of continuous operation (e.g. the temperature of input cooling water).

The task of process control is to change a second input signal, in the case of variations in a first input signal, in such a way as to have an unchanged output signal.

If there are fluctuations in the input signal - to keep these fluctuations between given limits is the controlling task - the optimum defined in the foregoing, together with the expense pertaining to the optimum, will also be changed. The smaller the fluctuation, the lower the original expense of the system; at the same time, the controlling operation, intended to decrease the fluctuations in the input signal, acts as an expense-increasing factor.

Accordingly, the preferable control degree must be found by means of a further optimalization calculation.

The controlling operation applied may be regarded as optimal, if the input signals are controlled so as to attain minimal total expenses.

On the basis of the foregoing, the most important questions, which must be dealt with during the application of systems theory in technical chemistry, can be summarized.

1. Qualitative description and study of technical chemical systems.

2. Study of the functions interpreted in connection with technical chemical systems and of the connections of these functions with one another.

3. Optimalization of static systems.

4. Description, control and optimalization of dynamic systems.

REFERENCES

1. Rendszerelmélet. Válogatott tanulmányok.(Systems Theory. Selected Studies.) Közgazgadási és Jogi Könyvkiadó, Budapest, 1971.

РЕЗЮМЕ

В серии сообщений под заглавием"Алгебраическое описание систем технической химии" предположено автором заниматься следующими разделами:

материальные системы и превращения,
объедимение материальных систем и их проекция,
операторы технической химии,
композиция операторов технической химии,
генерирование множеств информаций технической химии.

В вводной публикации показаны возможности применения теоремы систем, системотехники и современной алгебры в технической химии, и определены место, задачи и ожидаемые результаты алгебраического способа подхода. При изучении и оптимизации систем технической химии предстоят следующие задания:

1. Качественное описание систем технической химии и их испытание.
2. Изучение функций, действующих в данной системе технической химии, а также и их взаимных связей.
3. Оптимизация статических систем.
4. Описание динамических систем, их управление и оптимизация.

Для решения первой из указанных задач исключительно пригодным является алгебраический способ подхода, как это будет представлено в следующих сообщениях серии.

Hungarian Journal
of Industrial Chemistry
Veszprém
Vol.1. pp. 31-52 (1973)

STUDIES ON THE HYDRODYNAMICS OF FLUIDIZED LAYERS I. MEASURING METHODS FOR THE DETERMINATION OF THE EXPANSION OF FLUIDIZED LAYERS

T. BLICKLE and Z. ORMÓS

(Research Institute for Technical Chemistry of the Hungarian Academy of Sciences, Veszprém)

Received: June 30, 1972.

Knowledge of the expansion of fluidized layers is important both with regard to calculations connected with heat and material transfer processes, and for apparatus design. The expansion of the layer can - among others - be characterized by the void fraction of the fluidized bed. The determination methods of the void fraction can be divided into three groups:

a) those applicable in the case of fluidization with a liquid or a gas,

b) those applicable only in the case of liquid fluidization,

c) those applicable only in case of fluidization with a gas.

The authors describe the measuring techniques published in literature according to the above grouping. A report is presented on the research work carried out to investigate the applicability of measuring techniques, the elaboration of new techniques, and to improve those already known. The conditions of the applicability and the possibilities of methods for the determination of the free volume ratio are summarized in a tabular form.

An important characteristic of fluidized layers is the degree of expansion of the layer. The degree of expansion can be characterized by the height of the layer/the minimum height of layer ratio; by the density of the layer and by the void fraction. The

height of the layer/the minimum height of layer ratio - if the weight of the layer, and the characteristics of the particles and of the apparatus are known - and the density of the layer - if the densities of the solid and the fluid are known - can be calculated from the void fraction; accordingly, the knowledge of the free volume ratio is sufficient for characterization of the layer expansion.

The clearing of the conditions of the layer expansion is important both from the point of view of the calculations of heat and material transport processes, and from that of apparatus design. In addition to measuring techniques for the determination of layer expansion (void fraction), in the present series of papers the following problems will also be dealt with: characteristics and calculation methods concerning the expansion of layers fluidized with a gas or liquid, the influence of auxiliary processes (e.g. mechanical stirring, etc.) on layer expansion, and other hydrodynamic problems.

Numerous techniques are known for the determination of fluidized layer expansion. These can be divided into three groups:

a) those applicable in the case of fluidization with a liquid or gas,

b) those applicable only in the case of fluidization with a liquid, and

c) those applicable only in the case of fluidization with a gas.

In the following, the determination methods of void fraction published in literature will be described in accordance with the above grouping. The new techniques that have been elaborated and the improvements carried out on existing techniques will also be dealt with.

a) The Void Fraction Determination Methods in the Case of Fluidization with a Liquid or Gas

Determination of Void Fraction on the Basis of the Layer Height

The simplest and most frequently used method for the determination of the void fraction is that based on the measurement of the height of the layer. This can be used both in case of liquid and gas fluidization.

The calculation directly follows from the definition of void fraction:

$$\bar{\varepsilon}' = \frac{V_r - V}{V_r} \tag{1}$$

If the volumes of the solid material and layer are expressed, after rearrangement the following is gained:

$$\bar{\varepsilon}'_y = \frac{Y - \frac{G}{\gamma \cdot F}}{Y} \tag{2}$$

By means of Eq. (2) the void fraction can be simply calculated from the characteristics of the layer, the solid particles and the apparatus.

During the experiments a large number of measurements were made with various solid materials, liquids and gases. The method based on layer height determination gave very good results in the cases of liquid fluidization, whereas in case of gas fluidization its accuracy was poor, because the boundary of the layer was not sufficiently sharp and consequently the determination of the layer height was difficult. A further drawback of this method is that only the mean void fraction can be determined.

The experiments - including the parallel determinations - led to the conclusion that both in liquid and with a gas fluidization the scattering of the measured void fraction values vary depending on the extent of layer expansion and three distinct ranges can be defined.

In the case of fluidization with a liquid, the first stage of layer expansion - where the range $0.50 < \bar{\varepsilon}'_Y < 0.65$ is valid - the scattering of the void fraction values is relatively high, about ± 2 %. Although the layer height is well defined, the influence of the low reading error on the void fraction can be strongly felt. In the second stage of expansion $0.65 < \bar{\varepsilon}'_Y < 0.75$ the scattering of the measured values is lower, about ± 1 %. In this range, the upper boundary of the layer can be well determined and, the small reading error has no significant influence upon the determined void fraction values. In the third range $0.75 < \bar{\varepsilon}'_Y < 0.9$ the upper boundary of the layer tends to diffuse, because upon the increase of the flow velocity, the smaller particles reach a state of levitation. Considerable errors in the measured layer height are possible, which result in an increased scattering of the void fraction values; the scattering is about ± 2 %.

In the case of fluidization with a gas, the scattering of the void fraction values is generally higher than in the case of fluidization with a liquid. In the first range $0.5 < \bar{\varepsilon}'_Y < 0.6$ the scattering of the values is ± 2 %, this figure being equal to that measured in the case of fluidization with a liquid. The layer is relatively well defined and the layer height can be easily determined. In the second range of layer expansion $0.6 < \bar{\varepsilon}'_Y < 0.8$ the scattering of the values is large, it amounts to ± 3 %, and a thin layer is formed whose height can be measured only with considerable difficulty because the boundary of the layer is diffuse and variable in time. In the third range $0.8 < \bar{\varepsilon}'_Y < 0.9$ the scattering of the results is lower, about ± 2 %, despite the fact that the determination of the layer height is no better than in the previous case, only the same fluctuations in layer height manifest themselves to a lower degree in the void fraction value.

Despite the drawbacks described in the foregoing, the void fraction values determined with other methods or calculated with various equations are generally comparable with those obtained by layer height measurements, because the latter method is the simplest and most reliable of all the methods known for the determination of void fraction, provided that adequately trained personnel carry out a sufficient number of determinations and the application of glass apparatus is possible. The method is based, in accordance with the definition of void fraction, on the measurement of the layer volume.

Determination of Void Fraction Based on the Measurement of a Pressure Drop in the Fluid [1, 2]

A technique was elaborated for the determination of the void fraction in fluidized layers, based on the measurement of the pressure drop in the fluid [1, 2]. As it is known, the pressure drop of the fluid across the fluidized layer is nearly equal to the layer weight with reference to a unit cross section:

$$\Delta p_Y = \frac{G}{F}\,\frac{\gamma - \gamma'}{\gamma} \tag{3}$$

or, in another form:

$$\Delta p_Y = Y(1 - \bar{\varepsilon}')(\gamma - \gamma') \tag{4}$$

Eq. (4) could be applied for the calculation of the void fraction only if the height of the layer was also measured. However, the latter value enables the free volume ratio to be calculated without measuring the pressure drop.

If a suitable pair of static pressure-sensing tubes are placed into the layer in such a way that there is a height difference (y) between their positions, the pressure drop in the fluid along

a given length of the layer can be measured. If this pressure drop is expressed in accordance with Eq. (4), the following is gained:

$$\Delta p_y = y(1 - \bar{\varepsilon}')(\gamma - \gamma') \tag{5}$$

Eq. (5) could be directly applied for the determination of the free volume ratio on the basis of the pressure drop in the fluid. However, the following experimental, empirical finding should be taken into consideration. If the pressure drop values of the fluid across the fluidized layer obtained by actual measurement are compared to those determined on the basis of the layer weight according to Eq. (3), it is seen that the two sets of values are not always in exact agreement. In the evaluation of experimental results, a difference of about ± 5 % was found between the measured and calculated data in the case of liquid fluidization;in the case of gas fluidization this difference may be as high as ± 20 %. This error can be eliminated, if Eq. (5) is divided by Eq. (3), since the equation so obtained takes into consideration the deviation of the pressure drop from the theoretical value:

$$\varepsilon'_{\Delta p} = 1 - \frac{G}{y\,\gamma\,F} \cdot \frac{\Delta p_y}{\Delta p_Y} \tag{6}$$

The void fraction of the fluidized layer can be determined to a satisfactory accuracy by Eq. (6) in a given place of the layer, if the pressure drop is measured across the whole layer and across a length (y) at a given place of the layer [2,3]. The accuracy of the method can further be increased if the pressure drop across a layer of (Y) height is calculated by summation of the pressure drops measured across portions of the length (y):

$$\Delta p_Y = \sum_{i=1}^{i=n} \Delta p_{yi} \tag{7}$$

where $Y = n \cdot y$.

A schematic representation of the apparatus used for the measurements in connection with the above considerations is shown in Fig.1. An interesting feature of the apparatus is that condens-

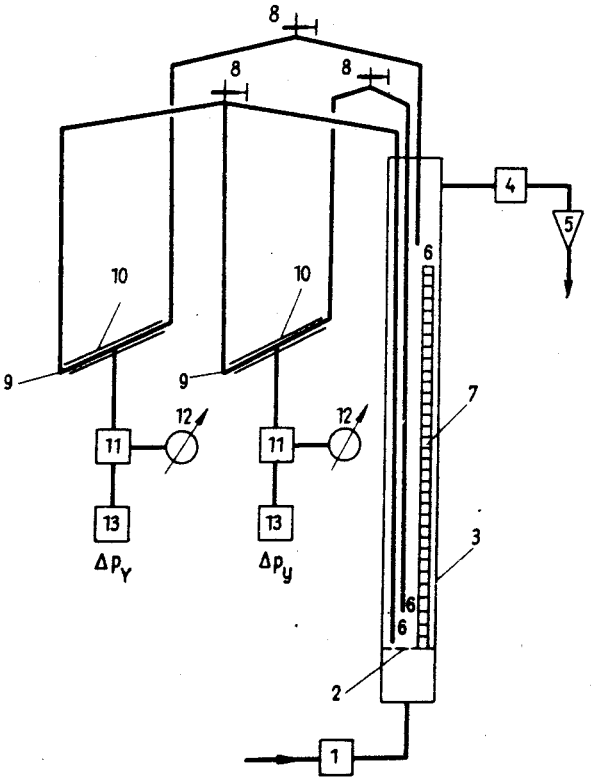

Fig. 1.

1 - quantity meter
2 - support plate
3 - glass apparatus
4 - cyclone
5 - effluent
6 - pressure measuring probes
7 - scale, subdivided in mm.
8 - deaeration stopcock
9 - oblique-tube type pressure gauge
10 - capacitor plates
11 - capacity measuring device
12 - meter
13 - potentiometric recorder

er plates were placed on the oblique-tube type micromanometer tubes and the capacity - proportional to the displacement of the manometer liquid - was measured. The capacity values, which are proportional to the pressure drop, were recorded by a potentiometric strip-chart recorder,whereby not only the pressure drop values, but also any fluctuations in them could be determined. In experiments where fluidization was carried out with a gas, slightly acidified water was used as the pressure gauge fluid, whereas in the case of fluidization with water, carbon tetrachloride was applied. Pressure drop across the total height of the layer, along a 2 cm portion on its bottom,as well as the layer weight and layer thickness were determined.Knowing the specific gravity of the particles and the I.D. of the apparatus, the void fraction of the lower part of the layer was calculated by Eq.(6), whereas the mean void fraction of the whole layer was determined from the layer height value by Eq. (2).

Fig.2. shows the difference between the mean free volume ratio (determined by layer height measurement), and that pertaining to the lower part of the layer (determined by measurement of the pressure drop along a given height) plotted against the mean value determined by layer height measurement for the case of fluidization of sand with water and air, respectively. It is apparent from the Figure that both in the case of fluidization with a gas and with a liquid there is a difference between the values determined with the two methods, but this difference is slight in the case of fluidization with a liquid.This experimental result is in good agreement with that obtained by COEURET and LE GOFF [4], who studied changes in the void fraction along the axis of the layer - among other methods - by conductance measurements. They came to the conclusion that the decrease of voidage along the height axis is not significant, i.e. the void fraction pertaining to the lower part of the layer differs (is lower) only slightly from the mean value, if a narrow fraction of particles is studied.

It is also apparent from Fig.2. that in the case of fluidization with a gas there is a considerable deviation between the compared values.This considerable difference originates from the fact

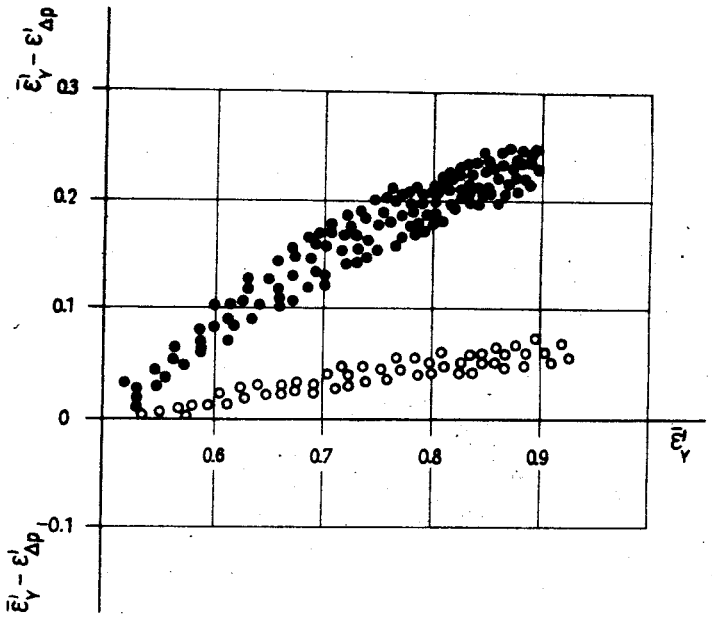

Fig.2. o - sand-water system; • - sand-air system

that in systems fluidized with a gas, the mean void fraction is substantially different from that of both the dense and the thin layers, and it was the dense layer in which the void fraction was determined on the basis of the pressure drop. The difference shown in the Figure is, to a good approximation, equal to the difference of the void fraction of the dense layer and the mean void fraction.

In addition to the apparatus described in the foregoing, another apparatus was constructed in which a pair of probes could be moved along the height and along the radius of the apparatus, whereby the pressure drop produced across a 1 cm portion of the layer

could be determined. The pressure drop was measured by high-sensitivity micromanometers filled with alcohol. In the experiments the pressure drop was measured along the height and at different distances from the axis of a layer fluidized with different air flow rates. The void fraction values were calculated from the measured pressure drops with Eq. (6) in such a way that the Δp_Y values were determined by summation of the measured pressure drop values in accordance with equation (7).

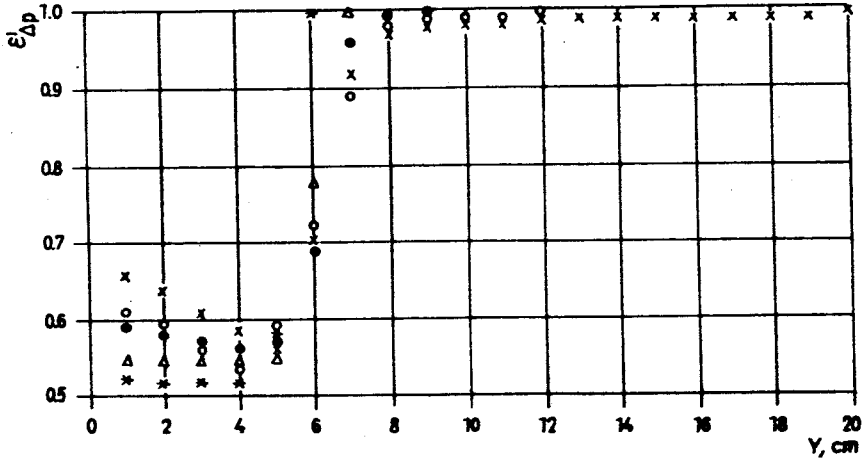

Fig.3. Sand-air system.

d = 0.1 - 0.2 mm
• - u' = 0.132 m/sec
x ÷ u' = 0.04 m/sec
o - u' = 0.265 m/sec
Δ - u' = 0.067 m/sec
x - u' = 0.595 m/sec

Fig.3. snows the mean void fraction values measured at five different air flow rates, determined on the basis of the pressure drop at different distances from the middle of the layer, plotted against the distance measured from the fritted plate, in the case of fluidization of sand of d = 0.1 to 0.2 mm particle size with air. It is apparent from the Figure that there is a jump-like change in the void fraction values at a height of about 6 cm, as measured from the fritted plate (Y_m = 5.4 cm).

The mean values of void fractions determined on the basis of pressure drop measurement at different heights of the layer were compared to the mean void fraction values obtained by calculation on the basis of layer height determinations and it could be concluded that the deviation was smaller than ± 5 % and consequently the accuracy of the method is adequate and therefore it can be applied to the determination of the mean void fraction. The method described in the foregoing, based on pressure drop determination in the fluid, are especially important in connection with experiments where the wall of the apparatus is opaque. Both the mean void fraction of the layer and the dependence of the free volume ratio on place can be determined relatively easily and quickly even in such cases. By means of the apparatus shown in Fig.1. it is possible to record continuously the value of the pressure drop and consequently changes and fluctuations of it and of the void fraction in time can also be recorded. A drawback of the technique is that the mean void fraction is not determined directly, and the probes brought into the layer slightly disturb the motion of the particles.

Determination of the Void Fraction on the Basis of γ-Ray Absorption [5, 6]

A method was elaborated for the determination of the void fraction of layers fluidized with a gas by application of a radiating isotope [5].

The phenomenon of γ-ray absorption makes it possible to determine the thickness and real density of solid and liquid materials as absorbents with reference to the unit area. According to the basic law of the phenomenon, the γ-radiation of I_{γ_o} intensity, having passed a material of ρ_F "surface density", is weakened according to the formula:

$$I_\gamma = I_{\gamma_o} \cdot e^{-\alpha \rho_F} \qquad (8)$$

By expressing the "surface density" the following Equation holds:

$$\rho_F = \frac{2.3}{\alpha} \cdot \log \frac{I_{\gamma_o}}{I_\gamma} \tag{9}$$

The void fraction can be calculated from the "surface density", if the length of the layer (y) in which the γ-rays are absorbed, is known:

$$\varepsilon'_\gamma = 1 - \frac{\rho_F}{\rho \cdot y} \tag{10}$$

The above basic principles were considered in the void fraction determination based on γ-ray absorption.

A chromium-51 isotope was used radiating γ-photons of 0.33 MeV energy as a radiation source in the gas fluidization experiments. The apparatus was made so as to allow exact determination of the position of the practically point-like radiation source in the layer [5].

An improved model of this apparatus was produced [6]. This apparatus also enables experiments of fluidization with liquids to be carried out. In the experiments made with water, a sodium-51 isotope radiating γ-photons of 1.27 MeV energy was used as a radiation source.

Accordingly, the determination of the void fraction of a fluidized layer based on γ-ray absorption can be used with fluidization both with a liquid and a gas, and this technique makes it possible to determine changes in the void fraction along the radius and also along the bed height [6].

It is a drawback of the technique that due to the radiating isotope used it requires a "hot" laboratory, and expensive instruments are needed.

b) Void Fraction Determination Methods in the Case of Fluidization with a Liquid

Determination of the Void Fraction Based on the Measurement of the Layer Density [7]

In the case of fluidization with a liquid, the void fraction of the layer can be determined on the basis of the bed density [7].

The apparent layer density can be obtained from the densities of the fluid and solid material:

$$\rho_r = \varepsilon' \rho' + (1 - \varepsilon')\rho \tag{11}$$

By expressing the void fraction the following is gained:

$$\varepsilon'\rho_r = \frac{\rho - \rho_r}{\rho - \rho'} \tag{12}$$

Accordingly, in order to be able to calculate the void fraction, one has to know densities of the solid and the liquid, and the density of the layer has to be determined. The latter was determined by a hydrometer. This method was compared to that based on layer height determination; the two methods showed good agreement [7]. The layer density method is very simple. However, it can be carried out only rarely. It can be used only with apparatus having transparent walls and it furnishes information only on the mean void fraction. In such cases, the method based on layer height measurement can be applied equally well, the latter method being simpler and more reliable for mean void fraction determination. A further drawback of the density method is the use of a hydrometer which interferes with the free motion of the particles and the diameter of the apparatus has to be considerably larger than that of the hydrometer.

Determination of the Void Fraction Based on the Measurement of the Conductance of the Layer [7]

In the case of fluidization with a liquid, the void fraction of the layer can be determined on the basis of the conductance of the layer [7]. The method is based on the fact that the conductance of the layer depends on the magnitude of the space between the particles, because any changes in the voidage also cause the useful cross section to be changed. Having established a calibration curve, the metnod is applicable both in the case of electrically insulating and of electrically conducting solid particles.

An experimental apparatus was constructed, its schematic drawing is shown in Fig.4. This differs from the apparatus already

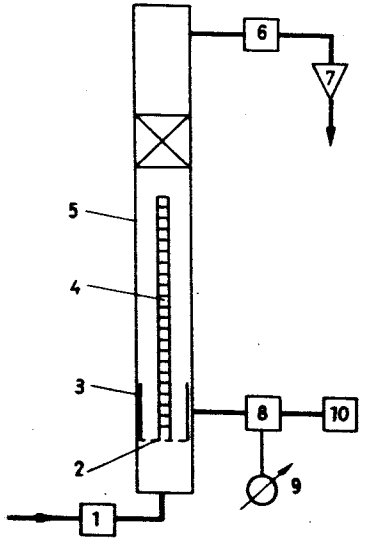

Fig.4.

1 - flow meter
2 - support plate
3 - platinum electrodes
4 - scale, subdivided in mm
5 - Perspex glass apparatus
6 - cyclone
7 - effluent
8 - conductivity meter
9 - meter
10 - potentiometric recorder

described [7] inasmuch as instead of the conductivity meter operating at 2000 c.p.s. frequency, a special conductivity meter of exceptionally wide measuring range, operated at 50 c.p.s. frequency was used. The Perspex glass apparatus was of 5 x 5 cm^2 cross section and there were platinum electrodes placed on the opposite sides in order to measure the conductance of the fluidized layer.

Experiments were carried out with sand and porous burnt clay fluidized in tap-water. The conclusion was reached that the current proportional to the conductance of the fluidized layer (I) divided by the current proportional to the conductance of the liquid (I_o) gives, to a good approximation, the void fraction of the layer:

$$\varepsilon_v' = \frac{I}{I_o} \qquad (13)$$

The differences between the respective void fraction values determined by the layer height measurement on the basis of Equation (2) and by conductivity measurement on the basis of Equation (13) plotted against void fraction values determined from layer height determinations are shown in Fig.5. As it is apparent from the Figure, the values determined with the two methods show a very good agreement and even the highest difference is below ± 10 %.

Accordingly, this method can be applied for void fraction determination in measurements carried out with fluidization with a liquid. An advantageous property of the method is that it can also be used with an opaque-walled apparatus, and the result of the measurement can easily be recorded. Moreover, if more than one pair of independent electrodes is placed into the apparatus at different levels, the distribution of the void fraction can also be determined. The dependence of the void fraction on place (along the height and radius) can also be determined in such a way that an adequately shaped, movable probe is brought into the layer and used for conductivity determination. For example, COEURET and LE GOFF [4] used for such experiments, in an apparatus for fluidization with a liquid, 10 cm in diameter, a conductivity probe movable in the layer and comprising electrodes of

5 mm diameter and 20 mm length, fastened at a distance of 15 mm from each other. In this way, they determined - among others - variations in the void fraction along the axis of the apparatus.

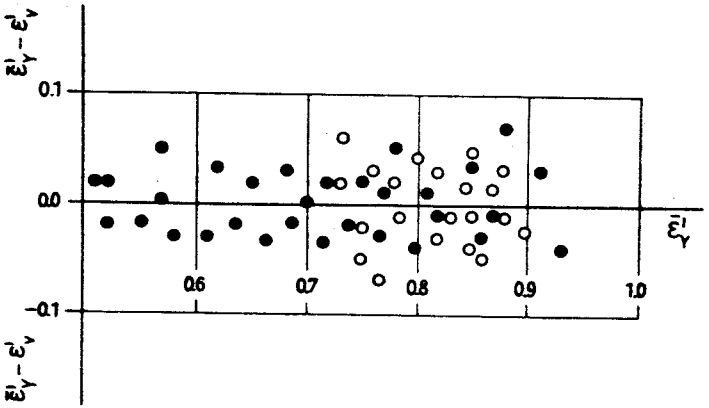

Fig.5. o - burnt clay - water system; • - sand - water system.

Despite its numerous advantages, the method can rarely be applied, because the particles fluidized in a liquid frequently release components which are soluble in the liquid and alter its conductance. Furthermore, every change which tends to alter the conductance of the liquid or the particles - such as adsorption, ion exchange, and change in temperature, etc. - naturally interferes with the method and affects its accuracy to a high degree.

c) Void Fraction Determination Methods in the Case of Fluidization with a Gas

Determination of the Void Fraction on the Basis of X-ray Absorption [8]

GROHSE [8] proposed a method for the determination of the void fraction based on X-ray absorption. The basic principle of the technique is similar to that using the absorption of γ-rays emitted by a radiation source. The X-ray absorption method cannot be easily realized in practice because it necessitates an expensive apparatus. In addition to the above, the place requirement of the method is high, and due to the radiation hazard it requires a separate laboratory to be established. These factors contribute to the difficulties of sprending of the technique.

Void Fraction Determination Based on the Measurement of Layer Capacity

The void fraction at various places of a layer fluidized with a gas can be determined in the following way: small pairs of capacitor plates are placed into the layer and the capacity of these condensers is determined [9]. If the capacitor plates are sufficient small, the distribution of the void fraction along the radius and the height can also be determined.

Void fraction determination technique based on the capacity measurement was improved so as to make it possible to determine the void fraction of the whole layer [10]. The essence of the method is as follows: capacitor plates were placed on two opposite walls of the Perspex glass apparatus of rectangular cross-section and an overflow tube was applied over the capacitor plates. The capacity determinations were carried out according to a definite

Table I. Measuring Methods for the Determination of the Void Fraction of Fluidized Layers

Method	The fluid is		Applicable		The walls are		The method is	
	liquid	gas	$\bar{\varepsilon}$	$\varepsilon' = f(Y,r)$	transparent	opaque	simple	cumbersome
based on layer height determination	+	+	+	-	+	-	+	-
based on the measurement of the pressure drop in the fluid	+	+	+	+	+	+	+	-
based on γ-ray absorption	+	+	+	+	+	+	-	+
based on layer density	+	-	+	-	+	-	+	-
based on the conductance of the layer	+	-	+	+	+	+	-	+
based on X-ray absorption	-	+	+	-	+	+	-	+
based on the capacity of the layer	-	+	+	+	+	+	-	+

system, but the details will not be dealt with here. The results of the capacity measurements enabled the void fraction of the fluidized layer to be calculated, as well as the height and void fraction of the dense and the thin layers, respectively [10, 11]. It was found that the relative error of the experimental void fraction determinations was ± 5 %.

It is easier to carry out the technique based on capacity measurement in the laboratory than either of those based on γ-ray or X-ray absorption. The capacitive method can also be used with apparatus whose walls are opaque. Despite the advantages detailed in the foregoing, this method is rarely applied, partly because it requires instrumentation and partly because the measurement is rather cumbersome and time-consuming.

The conditions and possibilities of the application of the different void fraction determination methods are summarized in Table I.

Used symbols

d particle diameter (m)

F cross section of apparatus (m^2)

G weight of solid particles present in the layer (kp)

I current in the case of a fluidized layer (amperes)

I_o current in the case of pure liquid (amperes)

I_γ intensity of γ-radiation after absorption (counts/sec)

I_{γ_o} intensity of γ-radiation before absorption (counts/sec)

u' linear velocity of fluid as referred to the total cross section of the apparatus (m/sec)

V volume of solid particles present in the layer (m^3)

V_r volume of the layer (m^3)

y given distance along the height of the layer (m)

Y Height of the layer (m)

α mass absorption coefficient ($m^3/kp.sec^2$)

γ density of solid particles (kp/m^3)

γ' density of fluid (kp/m^3)

Δp_y pressure drop of fluid across a length y of the layer (kp/m^2)

Δp_Y pressure drop of fluid across the total height (Y) of the layer (kp/m^2)

ε' value of voidage at a given place of the layer (dimensionless)

$\bar{\varepsilon}'$ calculated mean void fraction of the layer (dimensionless)

ε'_v void fraction calculated on the basis of the conductance of the layer (dimensionless)

$\bar{\varepsilon}'_Y$ mean void fraction determined on the basis of the measurement of the layer height (dimensionless)

ε'_γ void fraction determined on the basis of γ-ray absorption (dimensionless)

$\varepsilon'_{\Delta p}$ void fraction determined on the basis of the pressure drop measurement in the fluid (dimensionless)

$\varepsilon_{\rho r}$ void fraction determined on the basis of the layer density measurement (dimensionless)

ρ density of solid particles ($kp\ sec^2/m^4$)

ρ' density of fluid ($kp\ sec^2/m^4$)

ρ_r density of fluidized layer ($kp\ sec^2/m^4$)

ρ_F "surface density": mass of the solid particless with reference to a unit surface area ($kp\ sec^2/m^3$)

References

1. BLICKLE, T., Theoretical and Experimental Studies on the Realization of Some Material Transfer Processes by Fluidization. Dissertation. Budapest, 1967.

2. ORMÓS, Z., Studies on the Extension of Fluidized Layers. Dissertation. Vegyipari Egyetem, Veszprém, 1968.

3. ORMÓS, Z., Proceedings of the 2nd Conference on Applied Physical Chemistry. Akadémiai Kiadó. Budapest, 1971.Vol.2. p.143.

4. COURET, F., LE GOFF, P., I.Conference on Some Aspects of Physical Chemistry. Budapest, 1966. Publication No.2. Vol. III. p. 323.

5. HODANY, L., ORMÓS, Z., Conference of Intensive Chemical Technological Processes, Kecskemét, 1964. Proc. p. 225.

6. HODANY, L., BLICKLE, T., I. Conference on Some Aspects of Physical Chemistry, Budapest, 1966. Publication No.2. Vol. III. p. 335.

7. BLICKLE, T., BORLAI, O., Vortragstagung des Fach-Verbandes Verfahrenstechnik Halle 1961.

8. GROHSE, E.W., A.I.Ch.E. Journal, 1, 358 (1955)

9. JOTTRAND, R., Chem. Eng. Sci. 1, 81 (1951)

10. BLICKLE, T., Studies on Fluidized Systems. Dissertation, Budapest, 1958.

11. BLICKLE, T., Apparatus, Applications and Calculations in Connection with Fluidization. Akadémiai Kiadó, Budapest, 1963.

РЕЗЮМЕ

Знание распространения псевдоожиженных слоев является важным с точек зрения как расчета процессов передачи тепла и материалов, так и проектировки установок. Распространение слоя — между прочим — можно характеризовать долей свободного объема. Методы, подходящие к измерению доли свободного объема можно подразделить в три группы:

а/ применимые при флюидизации как с жидкостью так и газом,
б/ применимые только при флюидизации с жидкостью,
в/ применимые только при флюидизации с газом.

Находимые в литературе методы измерения описаны авторами в указанной группировке, далее дан ими отчет о результатах исследовательской работы, выполненной по испытанию применимости методов измерения, по разработке новых методов измерения и усовершенствованию известных методов. Условия и возможности применения методов определения доли свободного объема составлены в таблице.

Hungarian Journal
of Industrial Chemistry
Veszprém
Vol.1. pp. 53-62 (1973)

HYDROFORMYLATION OF PROPYLENE WITH HYDROGEN, $Rh_4(CO)_{12}$ AND CARBON MONOXIDE*

G. CSONTOS**, B. HEIL, L. MARKÓ and P. CHINI***

(Department of Organic Chemistry, Veszprém University of Chemical Engineering)

Received: July 7, 1972.

Propylene reacts with H_2 and $Rh_4(CO)_{12}$ at room conditions to yield butyraldehydes and $Rh_6(CO)_{16}$. With higher olefins, isomerization and hydrogenation are observed as side reactions. The rate of butyraldehyde formation is of the first order with respect to $Rh_4(CO)_{12}$ and H_2, and is inhibited by CO, when the latter - if present - is incorporated into the reaction product and partially converts the system into a catalytic one with regard to rhodium. The rate determining step is apparently the reaction of $Rh_4(CO)_{12}$ with H_2 to give mononuclear rhodium carbonyl hydrides and the hydroformylation of propylene is accomplished by these latter species.

The hydroformylation of olefins with rhodium as catalyst [1] is of considerable potential industrial importance because of the high activity and good selectivity of this metal compared to the classical catalyst cobalt. The kinetics and mechanism of hydroformylation in the presence of $Rh_4(CO)_{12}$ has been studied [2], but up

*Paper presented at the Symposium on the Chemistry of Hydroformylation and Related Reactions, 31.5-2.6.1972, Veszprém (Hungary).

**Research Group for Petrochemistry of the Hungarian Academy of Sciences, Veszprém.

***Istituto di Chimica Generale dell'Università, Milano (Italy).

to the present time many details of the reaction sequence have remained obscure. It is therefore of both theoretical and practical interest to obtain further data regarding the reactions occurring in the rhodium containing hydroformylation reaction mixture.

RESULTS and DISCUSSION

$Rh_4(CO)_{12}$ reacts in toluene under ambient conditions with H_2 and propylene to form normal- and iso-butyraldehyde and $Rh_6(CO)_{16}$ [3]. If the concentration of propylene is high, the reaction is complete at 23°C in about 30 minutes and 90-100 per cent yields of aldehyde can be achieved as expected from Equation (1):

$$3\ Rh_4(CO)_{12} + 4\ H_2 + 4\ C_3H_6 \longrightarrow 4\ C_3H_7CHO + 2\ Rh_6(CO)_{16} \qquad (1)$$

Fig.1. shows the aldehyde formation during a typical experiment.

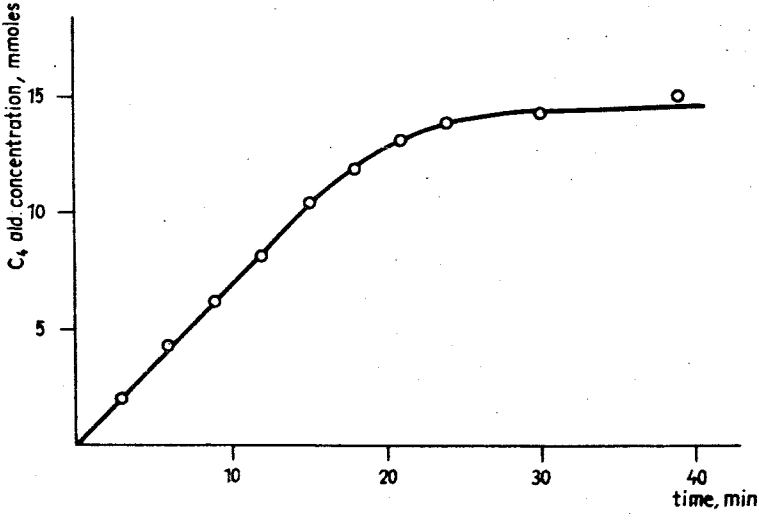

Fig.1. Stoichiometric hydroformylation of propylene in toluene with .0134 moles $Rh_4(CO)_{12}$ at 23°C in the presence of hydrogen; propylene pressure 77.5 mm Hg; hydrogen pressure 388 mm Hg.

This reaction is actually a stoichiometric hydroformylation similar to that described for $Co_2(CO)_8$, H_2 and olefins [4] and thus its study should also provide some information with regard to the catalytic process. Experiments were therefore carried out to determine the kinetics of the aldehyde formation. Only propylene was used as an olefin in these experiments, since preliminary investigations had revealed that higher olefins rapidly isomerize under the conditions used, thus making the evaluation of kinetic data more difficult. In addition, some hydrogenation of the higher olefins was also observed as a side reaction.

The initial rate of butyraldehyde formation was found to be of the first order with respect to p_{H_2} (as shown in Fig.2.), whereas the concentration of $Rh_4(CO)_{12}$ had no effect. The influence

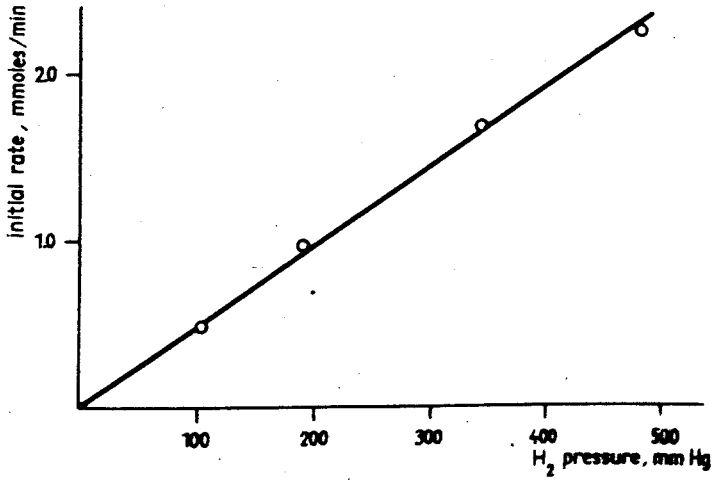

Fig.2. Dependence of initial rate on hydrogen pressure in the absence of carbon monoxide (.0134 moles $Rh_4(CO)_{12}$ in toluene; temp. 23°C; propylene pressure 155 mm Hg).

of propylene concentration is shown by the results compiled in Table 1. At low concentrations of propylene, the yield of butyralde-

hyde was appreciably lower than the theoretical 1.33 moles/mole $Rh_4(CO)_{12}$, whereas at high propylene concentrations the rate of butyraldehyde formation was only slightly influenced by $p_{C_3H_6}$.

Table 1. Effect of propylene pressure on hydroformylation (.0134 moles $Rh_4(CO)_{12}$ in toluene; temp. 23°C; hydrogen pressure 232 mm Hg)

propylene pressure (mm Hg)	initial rate of C_3H_7CHO formation (10^{-3} moles/min)	iso/normal aldehyde ratio	aldehyde formed (moles/mole $Rh_4(CO)_{12}$)
22	0.22	2.0-3.0	0.77
51	0.35	2.0-3.0	0.87
78	0.43	1.7-1.9	1.12
142	1.04	1.6-1.7	1.24
245	1.32	1.6-2.0	-

Carbon monoxide exerts a strong inhibiting effect on the initial rate of C_4 aldehyde formation, as shown by Fig.3.; the dependence is approximately described by $(p_{CO})^{-1}$.

It was found that carbon monoxide admixed to the $H_2 + C_3H_6$ gas mixture participates in the reaction and thereby increases the aldehyde yield above 1.33 moles/mole $Rh_4(CO)_{12}$; until the present time, the highest yields achieved were between 3.5-4 moles of C_3H_7CHO/mole $Rh_4(CO)_{12}$. The incorporation of CO into the product obviously decreases its concentration in the reaction mixture and in the gas phase, which leads under appropriate conditions to a characteristic increase of reaction rate within one experiment as shown in Fig.4. By simultaneously monitoring the reaction by IR spectroscopy (for $Rh_4(CO)_{12}$) and gas chromatography (for C_3H_7CHO) it could be shown that as long as the CO concentration is suffi-

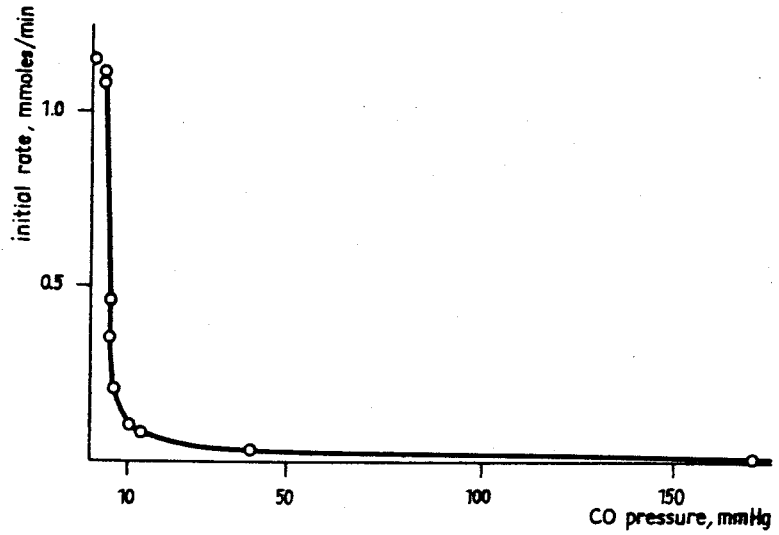

Fig.3. Dependence of initial rate on carbon monoxide pressure (.0134 moles $Rh_4(CO)_{12}$ in toluene; temp. 23°C; hydrogen pressure 232 mm Hg; propylene pressure 155 mm Hg).

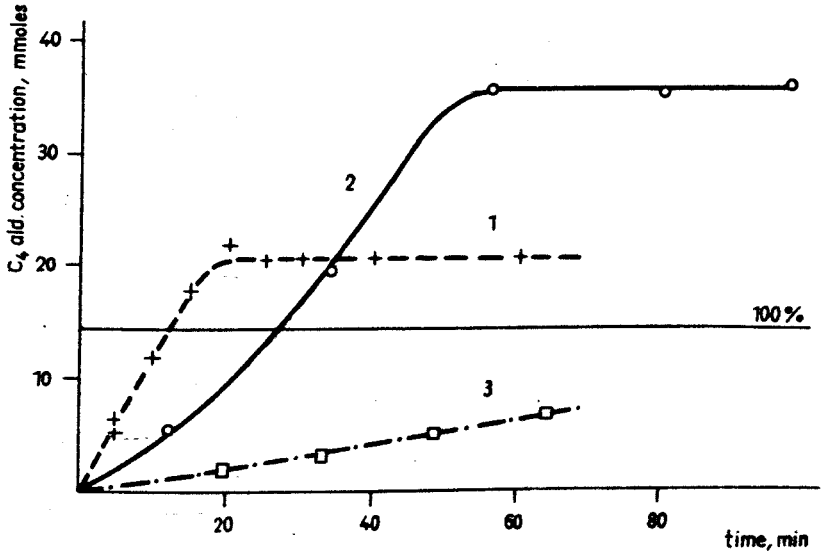

Fig.4. Butyraldehyde concentration vs. time at different carbon monoxide pressure: 1 - CO pressure: 2.5 mm Hg; 2 - CO pressure: 5.1 mm Hg; 3 - CO pressure: 9.8 mm Hg. (.0134 moles $Rh_4(CO)_{12}$ in toluene; temp. 23°C; hydrogen pressure 232 mm Hg; propylene pressure 155 mm Hg).

cient, the decline in the $Rh_4(CO)_{12}$ concentration is moderate (the formation of butyraldehydes is in part due to a "catalytic" effect), while after CO has been consumed, the transformation of $Rh_4(CO)_{12}$ becomes very rapid (Fig.5.).

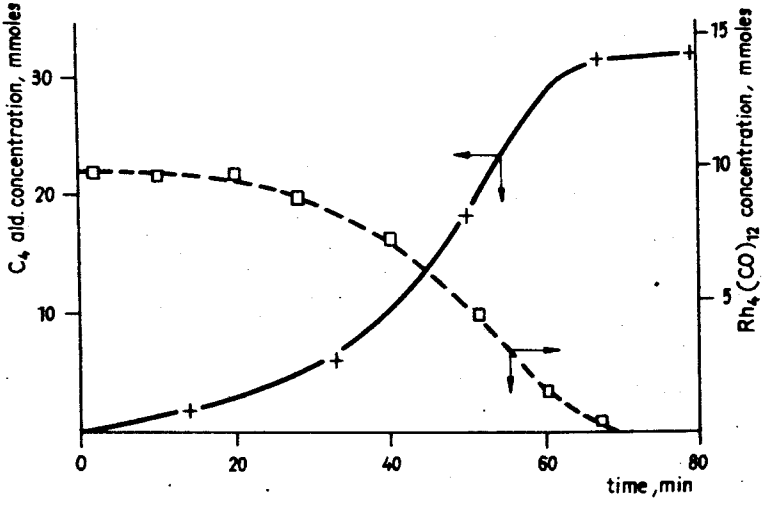

Fig.5. Butyraldehyde and $Rh_4(CO)_{12}$ concentration vs. time (starting $Rh_4(CO)_{12}$ concentration .0098 moles; temp. 23°C; hydrogen pressure 232 mm Hg; propylene pressure 155 mm Hg; carbon monoxide pressure 6 mm Hg).

Under the reaction conditions used, the spontaneous decomposition of $Rh_4(CO)_{12}$ to $Rh_6(CO)_{16}$ and CO cannot be avoided. If no carbon monoxide is added to the gas mixture, the actual p_{CO} is therefore rather ill defined and the kinetic data obtained with the CO-free system can be regarded only as aproximate. For this reason, the kinetics of butyraldehyde formation were also determined at constant low partial pressures of carbon monoxide.

At the actual chosen concentration of carbon monoxide the CO set free by the spontaneous decomposition of $Rh_4(CO)_{12}$ was

negligible compared to the quantity of CO added and, at the same time, the rate of butyraldehyde formation was still sufficiently high for practical measurements.

The most remarkable difference was found in the influence of the $Rh_4(CO)_{12}$ concentration. As shown in Fig.6., the initial rate of butyraldehyde formation under constant p_{CO} was of the first order with regard to $Rh_4(CO)_{12}$. The apparent contradiction between the results obtained with and without carbon monoxide can be explained by the compensating effect of CO liberated from $Rh_4(CO)_{12}$, when no carbon monoxide is added to the reaction mixture.

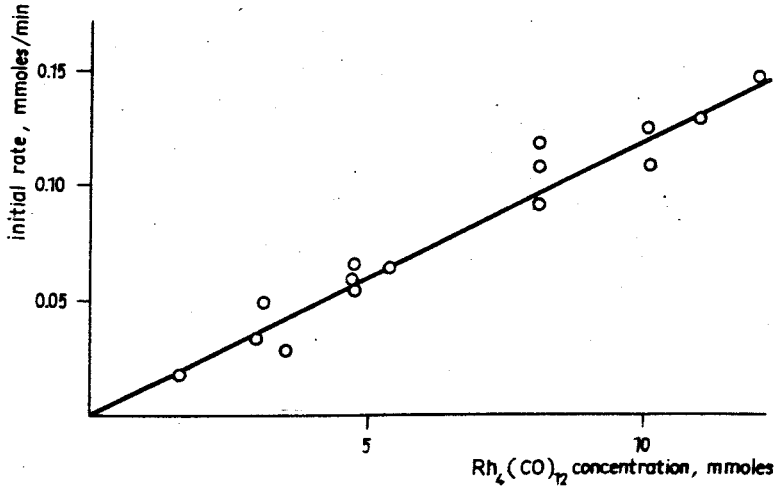

Fig.6. Dependence of initial rate on $Rh_4(CO)_{12}$ concentration (temp. 23°C; hydrogen pressure 232 mm Hg; propylene pressure 155 mm Hg; carbon monoxide pressure 6 mm Hg). The full and open circles refer to two series of experiments.

The results can most appropriately be interpreted by assuming the rupture of the Rh_4 cluster to mononuclear rhodium-carbo-

nyl hydrides as being the rate determining stage. For this process, the following mechanism is suggested:

$$Rh_4(CO)_{12} \rightleftharpoons Rh_4(CO)_{11} + CO \qquad (2)$$

$$Rh_4(CO)_{11} + H_2 \xrightarrow{\text{(rate determining stage)}} \text{mononuclear rhodium-carbonyl hydrides} \qquad (3)$$

The above scheme accords with the observed kinetics

$$\frac{d\,(\text{aldehyde})}{dt} = k\left[Rh_4(CO)_{12}\right]\frac{p_{H_2}}{p_{CO}}$$

This explanation of the experimental results is further supported by those measurements, which show that the rate of $Rh_4(CO)_{12}$ decomposition to $Rh_6(CO)_{16}$ is only very slightly influenced by the absence or presence of propylene (see Table 2.).

Table 2. Effect of propylene on the decomposition of $Rh_4(CO)_{12}$ (starting $Rh_4(CO)_{12}$ concentration .0067 moles in o-xylène; temp. 35°C; hydrogen pressure 310 mm Hg; carbon monoxide pressure 18 mm Hg).

propylene pressure (mm Hg)	percentage of $Rh_4(CO)_{12}$ decomposed in 1 min.
0	0.4
47	0.6
470	1.35

The rate measurements yielded no information on the reaction of the mononuclear rhodium carbonyl hydrides with propylene and the association of the mononuclear fragments to $Rh_6(CO)_{16}$. It is now evident that the actual hydroformylation reaction cycle responsible for aldehyde formation has to be kinetically studied under catalytic conditions (75°C, 100-200 atm.), for this atmos-

pheric system may show how the transformation of $Rh_4(CO)_{12}$ emerges into the catalytically active species ($HRh(CO)_x$). Since this latter process necessarily constitutes the first step in catalytic hydroformylation experiments, the results may be useful for the interpretation of induction periods eventually observed.

EXPERIMENTAL

Materials. All gases were analyzed by GLC. The toluene solvent was purified by distillation, followed by preparative gas-chromatography on a PEG column at 150°C. 0.1 per cent n-Heptane was used as an inner standard.

$Rh_4(CO)_{12}$ was prepared from $Rh_2(CO)_4Cl_2$ at 80°C and 300 atm. CO in the presence of moist $NaHCO_3$ in hexane. The product was separated by chilling the solution to -78°C and purified by recrystallization from hexane.

Apparatus. Experiments were performed in a 50 ml thermostated flask equipped with a magnetic stirrer, silicon rubber tap and a small cup for the $Rh_4(CO)_{12}$, the latter could be overturned from the outside without opening the reaction vessel. Pressure was maintained at 800 mm Hg by a mercury seal.

Reaction of $Rh_4(CO)_{12}$ with Propylene and H_2. $Rh_4(CO)_{12}$ (1 ... 10 mg) was measured into the small cup and the reaction vessel was securated three times with the gas mixture used. 1...2 ml solvent was injected by a syringe through the silicon rubber tap and stirred for 20 minutes to ensure saturation. Reaction was started by turning the cup and dropping the $Rh_4(CO)_{12}$ into the solvent where it completely dissolved within less than 1 minute. 10...20 µl samples were taken at regular intervals from the reaction mixture with a syringe and stored before analysis at -78°C. The aldehyde formed was determined by GLC (50 m PEG column, 150°C), its quantity was estimated with reference to the n-heptane standard (area of n-heptane to C_4 aldehydes= = 1.60). If the reaction rate was low, the $Rh_4(CO)_{12}$ content of

the same samples could be determined by IR spectroscopy, based on the intensity of the 1890 cm^{-1} band.

Acknowledgement

The generous assistance of the Hungarian Oil and Gas Research Institute in the preparation of $Rh_4(CO)_{12}$ is appreciated.

REFERENCES

1. MARKÓ, L., "Hydroformylation of Olefins with Carbonyl Derivatives of Noble Metals as Catalysts" in Aspects of Homogeneous Catalysis, Vol. II (Ed. R. Ugo) Milan, 1971. (in press)

2. HEIL, B., MARKÓ, L. and BOR, G., Chem. Ber. 104, 3418 (1971)

3. CHINI, P., MARTINENGO, S. and GARLASCHELLI, G., Proc. Chem. Hydroformyl. Related. React., Veszprém (Hungary) 31.5-2.6. 1972.

4. PINO, P., ERCOLI, R. and CALDERAZZO, F., Chim. Ind. (Milano) 37, 782 (1955)

РЕЗЮМЕ

При обычных условиях пропилен взаимодействует с водородом и $Rh_4(CO)_{12}$ при образовании бутиральдегида и $Rh_6(CO)_{16}$. В случае более высоких олефинов наблюдались в качестве побочных реакций изомеризация и гидрогенизация. Скорость образования бутиральдегида пропорциональна концентрации $Rh_4(CO)_{12}$ или H_2, а обратно пропорциональна концентрации CO. При наличии последней, она встроится в продукт реакции, и система практически превращается в процесс катализированный родием. Определяющим скорость этапом очевидно является реакция $Rh_4(CO)_{12}$ с водородом, когда образуется гидрид карбонила родия с одним ядром, а гидроформилирование пропилена происходит через этот одноядровый комплекс.

Hungarian Journal
of Industrial Chemistry
Veszprém
Vol.1. pp.63-88 (1973)

CALCULATION OF EXTRACTION COLUMNS FOR LUBRICATING OIL REFINING

Mrs. E. KÁNTOR, M. MAGYAR and Gy. MÓZES

(Hungarian Oil and Gas Research Institute, Veszprém)

Received: August 7, 1972.

Modern chemical engineering work requires all the transport phenomena to be known which accompany the physical or chemical changes that occur in operational units.

A few years ago, studies were started which were aimed at finding a method that would enable the modelling of the operational units, procedures and apparatus used in the mineral oil and the petrochemical industry. This work was based on the known fundamentals of theoretical reactor techniques.

MATHEMATICAL DESCRIPTION OF THE EXTRACTION OF A MULTI-COMPONENT SYSTEM

It is known from literature [1, 2, 3] that the study of transport phenomena is based on the continuity rule, whose general expression is the following:

$$\operatorname{div} J - \frac{\partial \rho A}{\partial t} = 0 \qquad (1)$$

It follows from Equation (1) that the flux density vector is an unequivocal function of the density of the component. It is not possible to apply this formula in the case of systems in which the individual composition cannot be determined. This diffi-

culty can also be overcome in the case of multi-component systems such as those encountered in the mineral oil and petrochemical industry in the following way: Equation (1) is divided by the mean density of the system, and accordingly the concentration will be characterized by the mass fraction in the equation. The general continuity equation expressed with mass fractions was described in literature [1 - 7] and this was applied for modelling the complex systems.

$$-\frac{\partial X_A}{\partial t} = \nabla X_A v - D\nabla^2 X_A + \omega\beta X_A \pm \nu_A r(X_A) \qquad (2)$$

The individual components are not known in complex systems. However, analytically well-defined component groups can always be separated and the mass fraction of these can be accurately determined.

The studied systems cannot be modelled with the application of the Equation (2) since they contain two or more phases. It is readily understood that with regard to phase distribution the definable component groups do not behave as individual compounds. Consequently, a second modification was introduced inasmuch as Equation (2) was not applied to each group of components, instead we selected the group most characteristic of the complex system. This group was termed the "basic component group" and the operational units were modelled only with the variations of this group in time. In this way the system could be described with a single mathematical expression that could be handled in a simple manner. Due to the twofold simplification, the mass flow equation expressed with the original density becomes distorted, since the dimension of Equation (2) is (hr^{-1}), and consequently the diffusion, material transfer, and kinetic constants contained in the equation cannot be compared to the constants determined during the basic research. However, the given complex systems can be very adequately described by these constants which are characteristic of the given system.

With the technique briefly described in the foregoing, we succeeded in modelling the asphalt-blowing reactor cascade of the Zala Mineral Oil Company [5], dimensioning the blowing reactors, their scaling-up and technological optimalization [6]. Commissioned by the International Atomic Energy Commission, it was developed a new technology based on similar theoretical fundamentals for embedding isotope waste in bitumen; this procedure was realized both in a batchlike and in a continuous process and dimensioning and designing problems were also solved [7].

At present, we are engaged in modelling a number of procedures and apparatus for the mineral oil industry using the above method. From these, the modelling of the phenolic mineral oil extraction column of the Duna Mineral Oil Company [8] will be described in this paper.

A number of methods were proposed in literature for the modelling and calculation of extraction processes. It is a unanimuous opinion that in the case of more than four components, these methods - which can be regarded as classical today - do not yield reliable results [9]. Accordingly, Equation (2) was selected as the basis of the modelling.

Extraction is a continuous, stationary operation in which no chemical reaction occurs and diffusion inside the phases is not dominant and, accordingly it is justified to take into consideration only two terms of the Equation (2): the convective and the transfer terms:

$$- B(X_A^{\alpha}{}_o - X_A^{\alpha}) + V_E k_{trans}(X_A^{\alpha} - X_{A^*}^{\alpha}) = 0 \qquad (3)$$

Equation (3) is a relationship which was applied for the basic component group and this allowed to solve the questions connected with lubricating oil extraction.

EXPERIMENTS

Calculations were carried out concerning the industrial-scale extraction column operated at the Duna Mineral Oil Company for a number of various feedstock—phenol systems. From among these, the calculations concerning a residue—phenol system will be dealt with here. The residue was obtained from a mineral oil of Romashkino origin by propane deasphalting. However, it should be stressed that the used method can also be applied to systems built up with other extraction solvents and other extraction columns.

The calculation of the extraction process by Equation (3) can be carried out only if the mass fraction of the basic component group designated by X_A^α in the lubricating oil, containing ten of thousands of components, can be determined in some way. For this purpose, the complex system had to be simplified to two groups of components, these two groups being different with regard to behaviour from the viewpoint of extraction.

Selection and Determination of the Basic Component Group

One of the two above-mentioned component groups - designated in the following by "A" - is immiscible or only partially miscible with the solvent, whereas the other - designated group "C" - is totally soluble in the solvent under the conditions of the extraction. The extracting solvent is component "B".

It is a basic requirement that the component groups follow the requirements of mass balance under the conditions encountered in the extraction process. In addition, the evaluation of the equilibrium states which develop among these component groups must unequivocally be possible.

Component group "A" comprises saturated aliphatic and naphtenic mineral oil hydrocarbons, whereas "C" is a group composed of monocyclic and polycyclic aromatic hydrocarbons.

From among the processes for the separation of saturated and aromatic hydrocarbons that are at present known, the elution liquid chromatographic technique was found to be most suitable. Aromatic and saturated hydrocarbons can be sharply separated from each other, provided that the adsorbent and the eluents are suitably chosen.

Chromatographic separation was carried out on a column of 23 mm I.D.and 1500 mm length,filled with wide-pore silica gel made in the German Democratic Republic. 3 per cent - with reference to the weight of the adsorbent - of the oil to be separated, dissolved in hexane,was placed on the adsorption column. 1,000 ml analytical-grade n-hexane, 1,000 ml analytical-grade benzene and 1,000 ml analytical-grade acetone were used as eluents.The eluates obtained with these solvents were separated from the solvents, their weights and refractive indices were determined. The first eluate, mainly comprising saturated hydrocarbons, is in the following described as component group "A", immiscible or only partially miscible with the solvent. The eluates obtained with benzene and acetone were united and designated as component group "C", mainly containing monocyclic and polycyclic aromatic hydrocarbons and resinuous substances.

The chromatographic analysis of a number of corresponding raffinate-extract pairs and feedstocks was carried out and it was found that the component balance established for the "A" and "C" component groups of the raffinate-extract pairs was in most cases in agreement with the content of the feedstock on the corresponding component to an accuracy of 1 per cent by weight.

The determination of the amounts of component groups "A" and "C" by the chromatographic technique is rather time-consuming. It was consequently studied the possibility of the determination of the composition on the basis of an additive qualitative parameter. There is a considerable difference between the refractive indices of fractions eluated with hexane and benzene, respectively; the determination of the refractive index is a simple, rapid procedure

and it requires only a small amount of sample; furthermore, the connection between the refractive indices on the mixtures made of the pure hexane and benzene fractions, and their composition is a linear one. Accordingly, this qualitative characteristic was chosen as the basis of the concentration determination in the following. The concentrations of the "A" or "C" components in any of the feedstocks or extraction products can be calculated by a simple proportion if the refractive indices of the components and in addition those of the hexane eluate corresponding to the 100 per cent component "A" content and of the benzene eluate corresponding to the 100 per cent component "C" content are known.

In order to check whether the "A" and "C" component concentration values thus calculated conform to the requirements of mass balance, and to what extent they agree with the results of chromatographic analysis, they were compared with the component balances calculated on the basis of refractive indices. It was found that the difference between the component balance of the raffinate--extract pair and the corresponding component content of the feedstock is lower than one per cent.

In order to illustrate the foregoing, the "A" and "C" component content determined respectively by chromatography and refractive index measurement, the component balance of a feedstock, prepared from Romashkino crude oil, and in addition those of raffinate-extract pairs prepared from the same under different operational conditions and with different yields, as calculated with the two different methods, are summarized as an example in Table 1.

A comparison of the component amounts and balances determined by chromatography and those calculated on the basis of the refractive index measurement reveal that most of the data determined by these two techniques agree within 2 per cent. It should be stressed that in the Equation (3), which is the basis of the calculations, the basic component group designated X_A^a is always the mass fraction or amount (in percentage by weight), of the component group "A", calculated in accordance with the foregoing and referred to the refined phase.

Table 1. Component "A" and "C" amounts and balances in feedstock and a few extraction products, determined by chromatographic separation and calculated on the basis of refractive indices

Designation of material	Yield of extraction operation, wt.%	Chromatographic analysis				Refractive index, n_D^{70}	Calculated on the basis of refractive index			
		Composition		component balance			Composition		component balance	
		A, wt.%	C, wt.%	"A" comp.	"C" comp.		A, wt.%	C, wt.%	"A" comp.	"C" comp.
Limit raffinate	-					1.4613	100.0	0.0	100.0	0.0
Limit extract	-					1.5353	0.0	100.0	0.0	100.0
Feedstock										
A	100.0	60.10	39.90	60.10	39.90					
B	100.0	61.50	38.50	61.50	38.50					
mean		60.80	39.20	60.80	39.20	1.4920	60.40	39.60	60.40	39.60
Experiment No.6. Raffinate	47.36	85.25	14.75	40.37	6.98	1.4715	88.10	11.90	41.77	5.59
Experiment No.6. Extract	52.64	37.30	62.70	19.63	33.00	1.5104	35.54	64.46	18.73	33.91
Total				60.00	39.98				60.50	39.50
Experiment No.12. Raffinate	85.50	69.70	30.30	59.59	25.90	1.4857	68.91	31.09	59.41	26.09
Experiment No.12. Extract	14.50	13.10	85.90	1.90	12.45	1.5269	13.24	86.76	0.85	13.65
Total				61.49	38.35				60.26	39.74
Experiment No.21. Raffinate	25.40	83.70	16.30	21.26	1.59	1.4704	89.59	10.41	23.66	1.74
Experiment No.21. Extract	74.60	52.60	47.40	39.24	35.35	1.5002	49.32	50.68	35.16	39.44
Total				60.50	36.94				58.82	41.18

During the industrial-scale experiments it were determined the relationship between raffinate qualities, yield data and technological parameters. As an example, the results obtained in experiments on the Romashkino residue oil-phenol system are described.

Industrial-scale experiments

Calculations were carried out in connection with the phenol refining column of the annual 300,000 to 350,000 tons capacity operated at the Duna Mineral Oil Company.

The extraction column is 33.1 metres high, 4 metres in diameter and equipped with 24 plain grids and 2 bubble cap plates. Its simplified drawing is shown in Fig.1.

In order to increase the sharpness of separation, water feeding and a temperature gradient were applied. Phenol is introduced over the top plate, the feedstock and an azeotropic water--phenol mixture, containing approximately 90 per cent by weight water, is introduced at the 21st plate.

The temperature gradient is controlled by circulation-type reflux. A given portion of the continuous phase is withdrawn and then after cooling in an external heat-exchanger is fed back below the plate. The raffinate and the extract solution are removed after adequate settling, at the column head and at the bottom.

The values of the material stream entering into and leaving the column in cu. metres per hour units, and the temperatures at different points of the column can be read from the instruments. There are nine sampling places on the column. The solvent-refined top-product is taken from the top of the column, and the solvent--extracted bottom product from its lower part. Sampling points designated I - V. are the sampling nozzles located at the upper section of the column, between the 5th and 13th plain grids, and locate the raffinate-extract phase boundary. In addition, two further samples can be taken from the lower third of the column, from

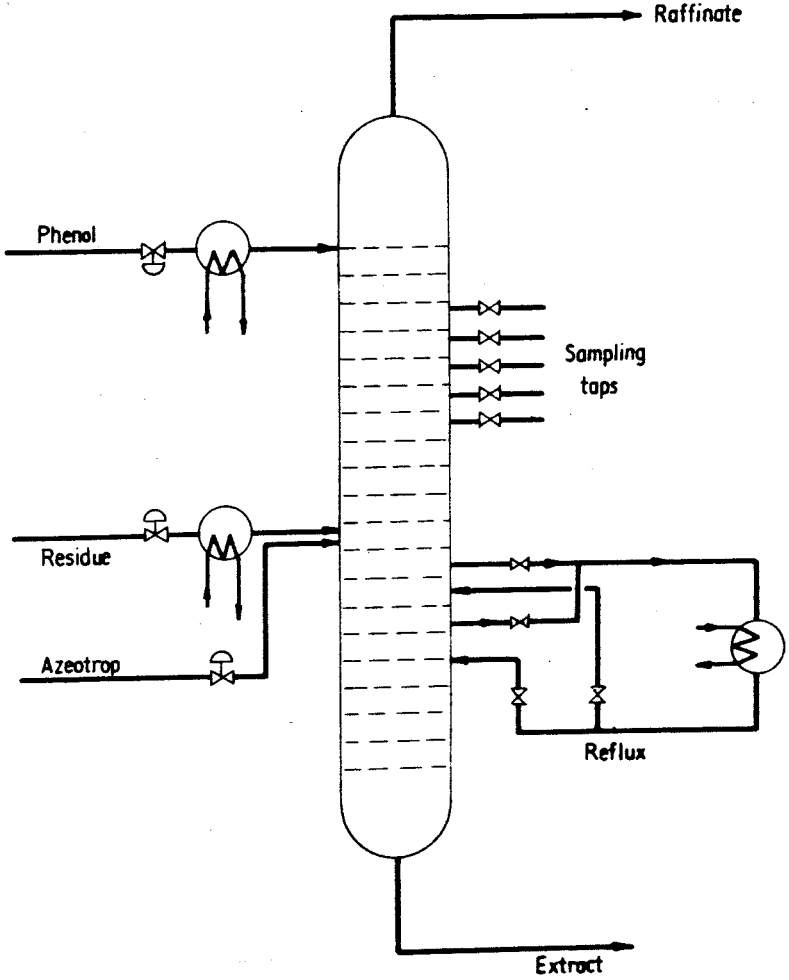

Fig.1. The extraction column.

the point of extract reflux removal, from under the 22nd and 24th plates. Due to technical difficulties, samples were not taken regularly from the extract reflux removal point under the 24th plate. In addition to solvent-containing samples taken from the column, solvent-free raffinate, extract, feedstock and azeotrope samples were also taken in each industrial-scale experiment.

In the laboratory processing of the 9 or 8 samples taken from the extraction column it was endeavoured to separate the phases in such a way as to obtain a composition identical to that actually prevailing at the place of sampling in the industrial extraction column. For this purpose the molten and homogenized samples were allowed to settle at a temperature equal to that measured at the sampling point of the extraction column. Separation to raffinate and extract phases was carried out in this way in a discontinuous-operation laboratory extraction apparatus.

The solvent was separated from the raffinate and extract phases by evaporation and the solvent content of the two phases was calculated. It was also determined the refractive indices of the solvent-free oils and from these were calculated the "A" and "C" component content of the oil with the method described in the previous section. The percentage composition of the three-component phases was calculated afterwards.

The compositions of the phases also were calculated as referred to the collective amounts of raffinate and extract phases; these data, plotted against the length of the extraction column are shown in Fig.2. The Figure shows, as an example, the results obtained in the laboratory processing of samples taken during a given industrial experiment of the phenolic refining of a Romashkino residue. The most important parameters were the following: top temperature 80°C, bottom temperature 60°C, feed 32 m^3/hr. oil, oil to solvent ratio 1/2.1, water content of phenol 3.05 wt.%. The concentration profile developed along the length of the extractor was determined in all industrial experiments. It is apparent from the Figure that the raffinate-extract phase boundary in this experiment was very sharp in the extraction column and was located between the 4th and the 5th plate.

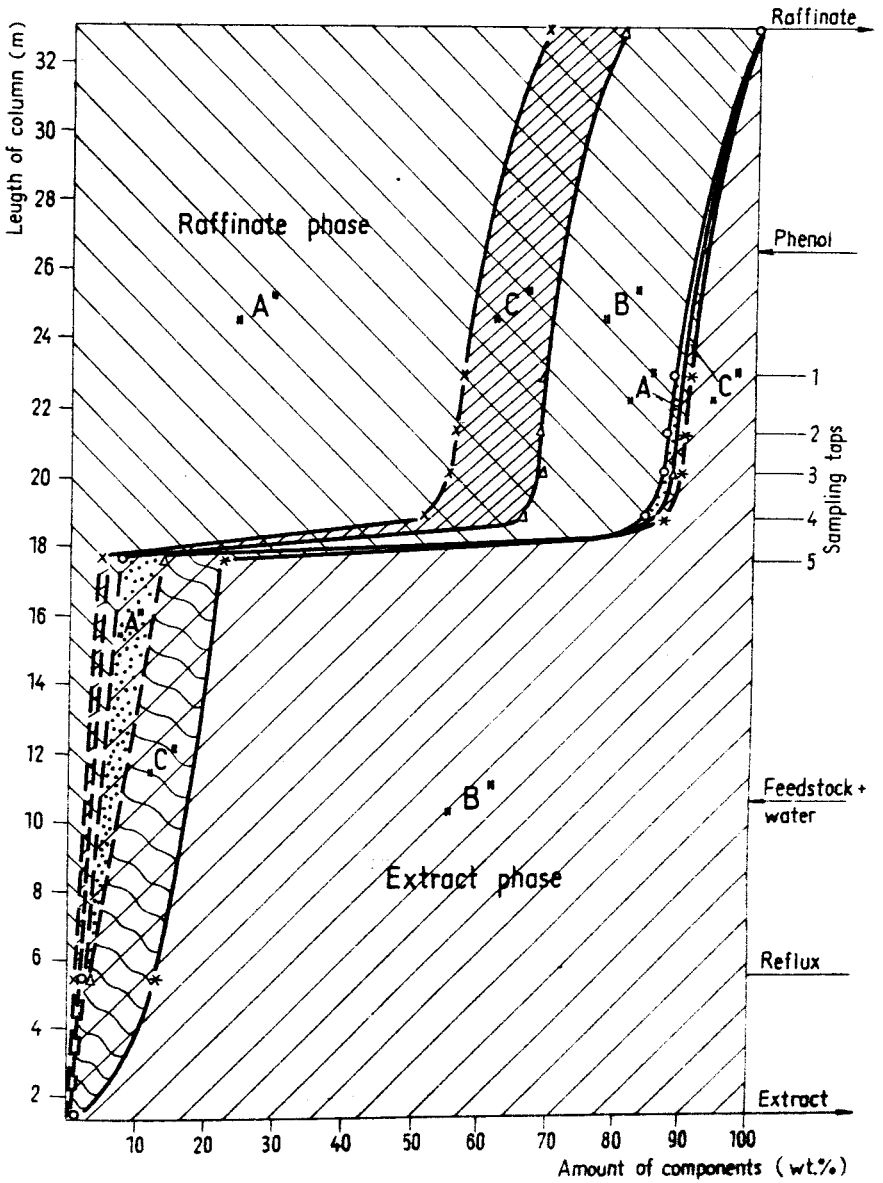

Fig.2. Concentration distribution of components along the length of the column at the experiment of December, 11.

EVALUATION OF THE INDUSTRIAL-SCALE EXPERIMENTS

After the laboratory analysis - according to the foregoing - of the samples taken during the industrial-scale experiments carried out with different parameters, the values of the combined mass transfer coefficient k_{trans} were calculated on the basis of the Equation (3). The "B" total feed expressed in cu. meters per hour represents the amount of feedstock, phenol and azeotropic mixture. V_E is the free volume between the feeding point of the feedstock and the sampling point of the extraction column. The actual concentration of component "A" at the sampling point of the raffinate phase is $X_A^{\alpha}o$, whereas the concentration of component "A" in the feedstock-solvent system is X_A^{α}, expressed in mass fraction.

The value of $X_A^{\alpha}*$ was determined by laboratory equilibrium measurements, at a temperature equal to that of the industrial extraction column and at an identical water content in the phenol and at the oil/solvent ratio prevailing at the point of sampling. In these experiments, a half-hour stirring and a one-hour settling period were applied. This time is sufficient for the equilibrium state to be reached. $X_A^{\alpha}*$ represents the component "A" content of the raffinate phase obtained in the equilibrium measurements.

The calculation of the combined mass transfer coefficient is shown, as an example, in Table 2. The data which were constant during an industrial experiment were especially emphasized. The data necessary for the calculations, which are different at each individual sampling point, were summarized. The first five columns of the Table contain the basic data necessary for the calculation of k_{trans}, whereas the sixth column contains the calculated k_{trans} values.

Theoretically, within one given industrial-scale experiment and at identical technological parameters, identical k_{trans} values should be obtained at any sampling point which is over the oil feeding level on the extractor. This was verified by the

Table 2. Calculation of the k_{trans} coefficient on the basis of the industrial-scale experiment of June, 7.

Constant data:

Feedstock component "A" 0.615
Oil/solvent vol. ratio 1:2.27
Mass fraction of oil at feeding 0.7592
Water content of phenol 2.55 wt.%
$X_A^{\alpha}o = 0.615 \cdot 0.7592 = 0.467$
$B = 132.4\ (m^3/hr.)$

Sample designation	B/V_E	Raff. "A" mass fraction	Raff. phase A + C mass fraction	X_A^{α}	X_{A*}^{α}	k_{trans}
Raffinate	0.540	90.90	80.15	0.729	0.756	5.25
I.	1.029	76.76	76.62	0.588	0.611	5.37
II.	1.176	77.79	75.14	0.585	0.611	5.22
III.	1.321	77.43	75.42	0.584	0.611	5.67
IV.	1.528	76.47	75.85	0.580	0.611	5.52
V.	1.796	75.66	75.93	0.575	0.611	5.25
E. refl. II.	-6.724	59.78	75.92	0.454	0.690	0.14
E. refl. I.	-2.354	61.76	73.68	0.455	0.690	0.04
Extract	-1.236	61.35	65.50	0.402	0.691	0.24
Upper section mean k_{trans}						5.38
Lower section mean k_{trans}						0.14

experiments, since the k_{trans} values calculated for the six sampling points of the upper section showed a good agreement in each industrial-scale experiment. The k_{trans} values calculated for the individual sampling points differ from the mean value by max. ± 0.29 units which corresponds to a scattering of ± 5 per cent.

It is apparent from the Table illustrated as an example, and it was also observed in all the industrial-scale experiments that there is a difference between the k_{trans} coefficients, determined for a section of the extraction column over the oil feeding point and those determined for a section below it, which amounts to an order of magnitude. This is readily understood since enrichment of component "A" in the raffinate phase occurs in the upper section, whereas samples taken from the lower section contain very low amounts of raffinate phase, and even these contain very low concentrations of component "A": it is the enrichment of component "C" which is dominant in the extract phase. The absolute values of the transfer coefficients are very low in the lower section and the mean deviation from the mean value is ± 0.1 unit.

After having come to the conclusion that the X_A^α values can be calculated to a satisfactory accuracy by means of the combined material transport coefficient, i.e. that the elaborated method enables calculation of the X_A^α values - of decisive importance as regards the quality of the desired product - to a satisfactory accuracy, there remained no further task than to determine the values of k_{trans} as a function of the technological parameters by industrial-scale experiments:

$$K_{trans} = f(B, \text{wt.\% water}, T, \text{oil/solvent ratio})$$

These connections are illustrated in Fig.3. It is apparent from the Figure that the value of k_{trans} shows a considerable - though not linear - increase with increasing temperature. Increasing oil feeding rate causes a slight increase, increasing oil/solvent ratio causes a considerable increase in its value; increasing water content causes the k_{trans} value to decrease.

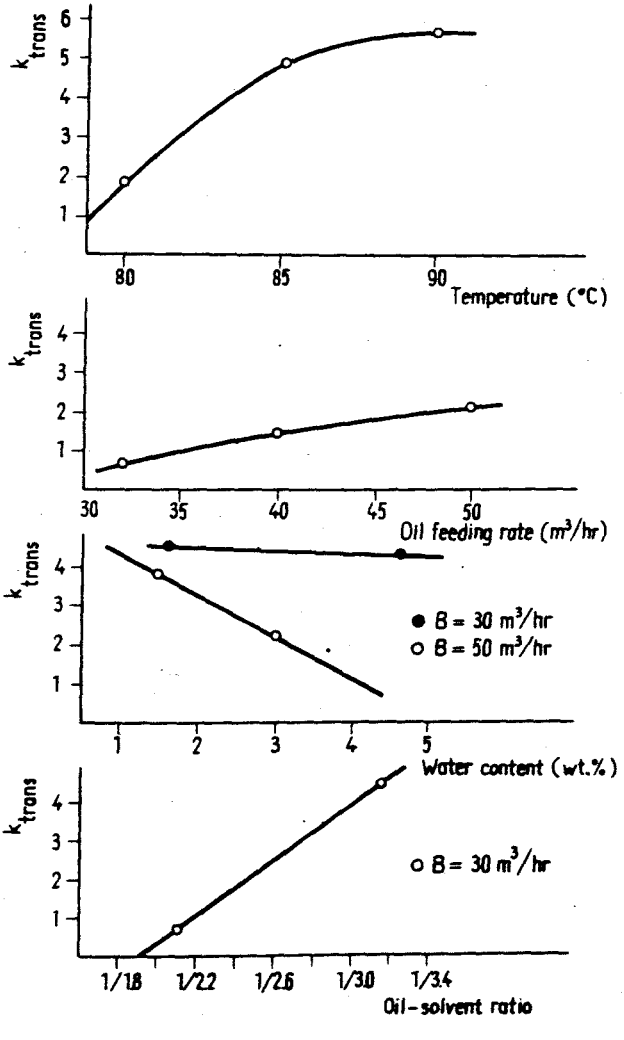

Fig.3. Changes in the transfer coefficient, plotted against various technological parameters.

Knowing the connection between the technological parameters and the combined material transfer coefficient, the k_{trans} values, corresponding to realistic parameter limits, can be established by interpolation to adequately varied values of the individual parameters or by slight extrapolation. Knowing these k_{trans} values, the X_A^{α} values can be calculated. If a sufficient number of experimental data is available, the solvent-free raffinate "A" component concentration values can be calculated by dividing the X_A^{α} values by the experimentally determined mean solvent content expressed in mass fraction. These values are brought into correlation by means of a calibration curve with one of the qualitative parameters of the raffinate which is important from a practical point of view.

Each of the starting materials studied by us - heavy paraffin distillates made of various raw mineral oils and residues mentioned in the foregoing - were processed to motor oil. Consequently, the parameter important from a practical point of view was the viscosity index of the raffinate which had been deparaffinized to a solidification point of -15 to -16°C.

A calibration curve was prepared representing the connection between the refractive index of the paraffin-containing oil and the viscosity index of the deparaffinized oil for the feedstocks and the raffinates made from them. This calibration curve is shown in Fig.4. It is apparent from the Figure that this connection can be determined only with a certain error.

The connection between the refractive index and the concentration of component "A" is also known, since the value of "A" is calculated on the basis of the measured refractive index values, as described in the previous Section. Accordingly, the quality of the product can unequivocally be characterized by the X_A^{α} and "A" component concentration values used for the calculation, and by the data on the refractive index and viscosity index.

During the industrial-scale experiment the raffinate yield data were also determined, partly on the basis of instrument

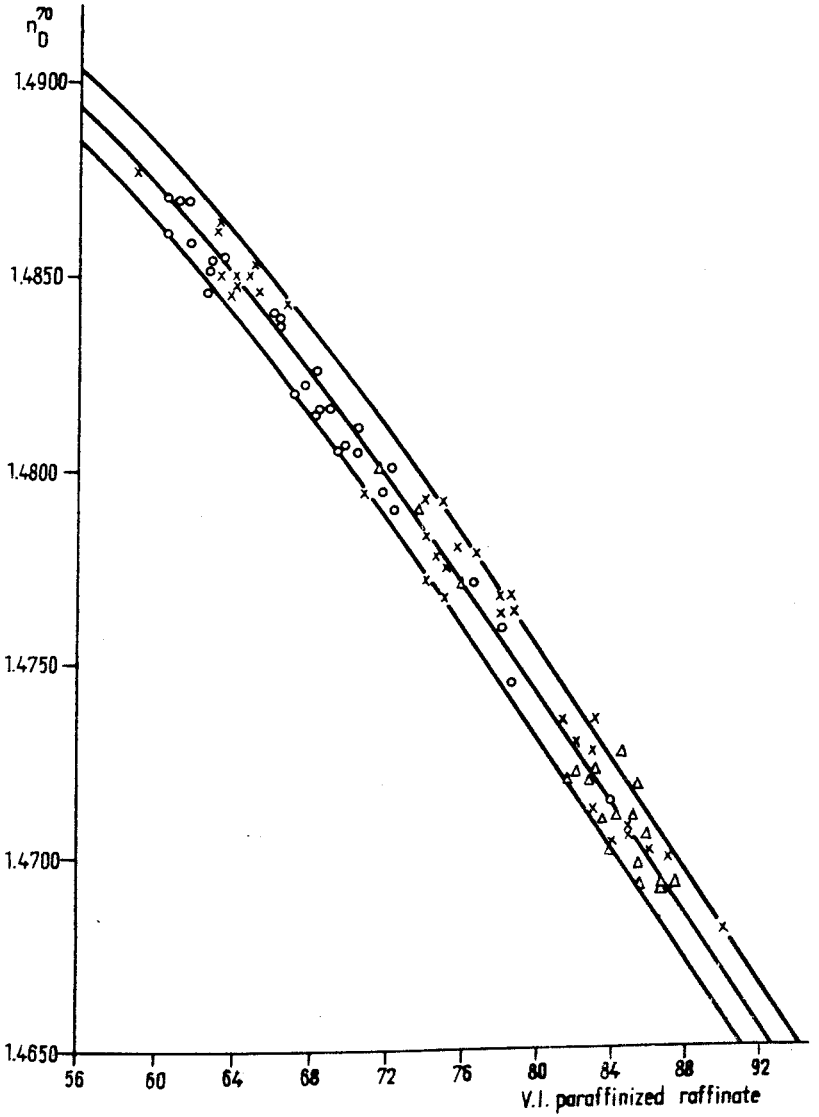

Fig.4. Refractive indices at 70°C of solvent-free raffinates, plotted against the viscosity index of the deparaffinized products. o residue, produced in 1966; x residue, produced in 1968; Δ residue, produced in 1969-1970.

Table 3. Main results of industrial-scale experiments carried out at the phenol refining plant of the Duna Mineral Oil Company with Romashkino residue

Time of experiment	Experimental conditions					k_{trans}	x_A^{α}	Raffinate, n_D^{70}	Deparaffinized raff.V.1.	Raffinate yield (wt.%)
	oil feed (m^3)	water content (wt.%)	oil/solvent ratio	top temperature (°C)	bottom temperature (°C)					
1969.										
VI. 7.	39.8	2.55	1/2.2	92	75	5.84	0.734	1.4712	84	58.7
X. 9.	39.7	3.16	1/2.0	81	61	1.51	0.681	1.4715	84	65.3
XI. 24.	50.0	3.05	1/2.0	79	61	2.20	0.695	1.4720	82	62.3
XII. 11.	32.0	3.05	1/2.1	80	60	0.70	0.643	1.4760	78	70.8
XII. 12.	30.3	1.60	1/3.1	80	61	4.54	0.743	1.4693	89	57.4
XII. 13.	30.0	4.60	1/3.2	79	62	4.31	0.697	1.4692	89	61.0
1970.										
I. 9.	50.4	1.50	1/2.0	80	63	3.87	0.717	1.4708	85	58.0
I. 10.	45.3	2.50	1/2.2	85	67	5.00	0.718	1.4702	86	59.7
I. 21.	45.4	2.60	1/2.2	90	71	5.60	0.687	1.4707	85	64.1
I. 22.	46.0	2.70	1/2.2	89	60	1.37	0.641	1.4722	82	60.3

readings and tank levels, and partly on the additive qualitative characteristics such as e.g. density and refractive index. The range of the parameters studied in the case of the Romashkino residue was as follows:

Volume ratio oil/phenol	1/2 ... 1/3.3
Water content of phenol (wt.%)	1.5 ... 5.0
Oil feeding rate (m^3/hr.)	30 ... 50
Top temperature of extractor (^oC)	80 ... 90
Bottom temperature of extractor (^oC)	60 ... 70

The influence of these parameters upon the raffinate yields and quality was studied in ten industrial-scale experiments. The experimental data and the main results are summarized in Table 3.

In Table 3. the yield data, k_{trans} values were summarized as the function of the technological parameters. The k_{trans} and the yiels values were determined by graphical interpolation for all of the following variations: different temperatures at 5^oC steps, oil feeding rates at 5 (m^3/hr.) steps, phenol water content values at 0.5 wt.% steps and oil-solvent ratios in 1/0.2 and 1/0.4 steps, within the above mentioned ranges of the individual parameters.

The X_A^α values were calculated using the transfer coefficients. With the aid of the above-mentioned connections and calibration curve a connection was established between the component "A" concentration and refractive index, and the viscosity index of the deparaffinized raffinates.

The relations between product quality, yield and technological parameters were calculated on the basis of the ten industrial-scale experiments for 300 different variations of the technological parameters. The results of these calculations were plotted on nomographs similar to that shown, as an example, in Fig.5. Each nomograph shows the raffinate yield and refractive index data pertaining to constant temperature and oil feeding rate as a function of the oil/solvent ratio for the cases of various water contents in the phenol.

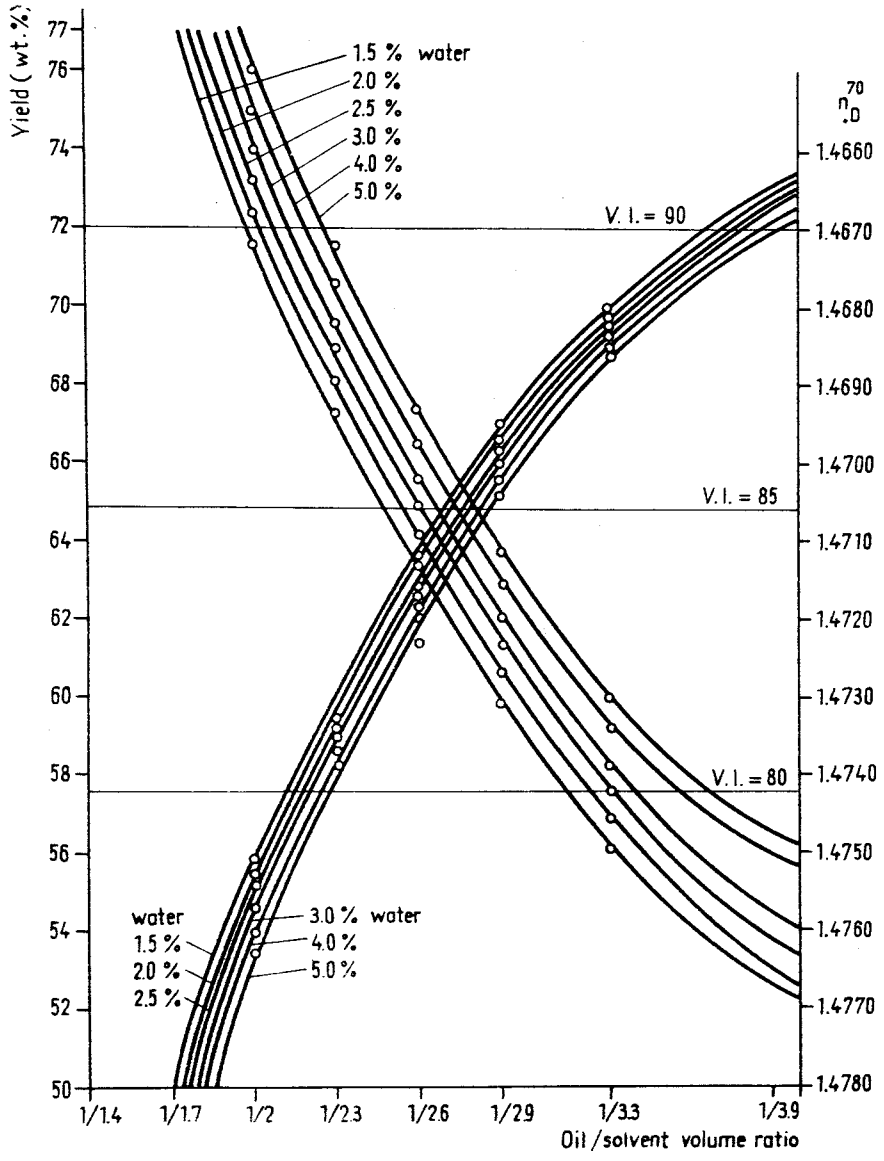

Fig.5. Variations in refractive index and yield of raffinate produced at 30 m^3/hr oil feeding rate and 80°C column top temperature, plotted against oil/solvent ratio.

In conclusion calculations were carried out in order to determine the optimum working conditions. For this purpose, Equation (3) was rearranged to the following form:

$$\frac{B}{k_{trans}} = \frac{V_E}{\frac{X_{A}^{\alpha}o - X_{A}^{\alpha}}{X_{A}^{\alpha} - X_{A}^{\alpha *}}}$$

This form of the Equation corresponds to the functional relation $y = \frac{c}{x}$. The value of V_E i.e. the total volume from the feeding point to the raffinate removal point of the extraction column is constant; in the case of the industrial-scale column it was 245.2 m^3. If it is constructed a system of coordinates on whose ordinate the $\frac{B}{k_{trans}}$ values and on whose abscisse the

$$\left[\frac{X_{A}^{\alpha}o - X_{A}^{\alpha}}{X_{A}^{\alpha} - X_{A}^{\alpha *}}\right]$$

values are plotted, we obtain a hyperbole. The concentration values of the quantity in brackets are interrelated according to the following:

$$X_{A}^{\alpha}o < X_{A}^{\alpha} < X_{A}^{\alpha *}$$

The above expressions were derived from data pertaining to various working conditions and they are illustrated in Fig.6. On the branch of the hyperbole adjacent to the y axis it were found pairs of values corresponding to higher feeding rates and poorer product qualities, whereas on the branch adjacent to the x axis the corresponding values of small amounts and good product qualities were found. Accordingly, the y axis is a coordinate proportional to quantity and the x axis is one proportional to quality. The technological optimum requires the maximum possible yield of

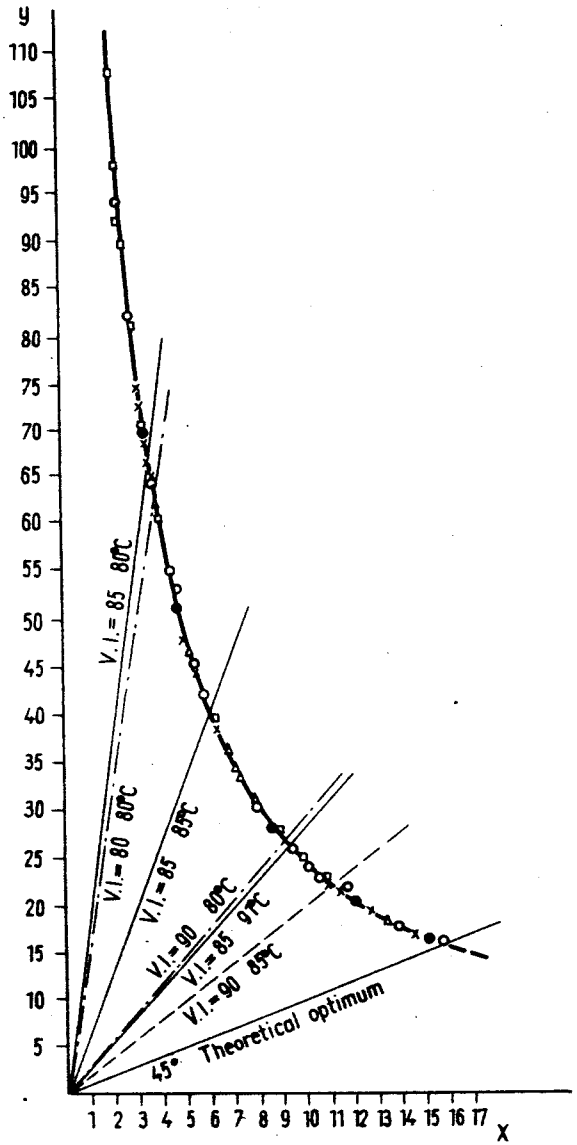

Fig.6. x and y values calculated from basic data defined for various experimental parameters. Oil/solvent ratio: o 1/3.3; Δ 1/2.9; x 1/2.6; • 1/2.3; □ 1/2.0.

product and simultaneously the best possible quality. However, these two characteristics are found on the two branches of the hyperbole in opposite directions, and consequently the optimum is expressed by the point of intersection of the hyperbole with a straight line drawn from the origo at a slope of 45 degrees. It is apparent from Figure 6. that this value is best approximated by the results of raffinations carried out at higher temperature, at 85 to 90°C.

The significance of the method lies in the fact that for one given feedstock-solvent system it is sufficient to determine these connections once and afterwards the production can continue. The technological data, which result in a produced of a required quality at the highest possible yield can be established for any raffinate quality.

However, the principles and methods described in the foregoing can not only be applied to extraction-type raffination processes carried out in industrial-size extraction columns, but also enable other techniques, used in mineral oil technology for processing multi-component mineral oil distillates and derivates - simplified by adequately chosen key fraction to two-component groups - to be studied and controlled.

USED SYMBOLS

B	total feeding rate (m^3/hr)
D	diffusion coefficient (m^2/hr)
J	flux density (amount/m^2hr)
k_{trans}	combined material transport coefficient = $\omega\beta$ (hr^{-1})
r(x)	reaction rate, expressed with mass fraction (hr^{-1})
t	time (hr)

v	linear velocity (m/hr)
V_E	volume of extractor (m^3)
X	mass fraction (dimensionless)
β	mass transfer coefficient (m/hr)
Δ	sign of difference
∇	sign of nabla vector (m^{-1})
ν	stoichiometric coefficient
ρ	density (kg/m^3)
ω	transfer surface area (m^2/m^3)

Indices

lower:

A refers to component "A"

A° is the initial value of component "A"

A^* is the equilibrium value of component "A"

upper:

α sign of one phase

REFERENCES

1. BENEDEK, P., LÁSZLÓ, A., A vegyészmérnöki tudomány alapjai (Fundamentals of Chemical Engineering Science). Budapest, Müszaki Könyvkiadó, 1964.

2. BIRD, R.B., STEWART, W.E., LIGHTFOOT, E.N., Transport Phenomena, New York, John Wiley, 1960.

3. SASVÁRI, Gy., Vegyipari folyamatok matematikai modelljeiről (On the Mathematical Models of Chemical Engineering Processes). Lecture. Hungarian Academy of Sciences, 1969.

4. MAGYAR, M., Lecture held at the Jubilee Scientific Session, Hungarian Academy of Sciences - MŰKKI, Veszprém - Budapest, 1972.

5. MAGYAR, M., MÓZES, Gy. et al., Magyar Kémikusok Lapja 23, 160, 105, 257, 326, 363 (1968)

6. MAGYAR, M., Kémiai Közlemények, 31, 399 (1969);
Ibid. 34, 175 (1970)

7. MAGYAR, M., MÓZES, Gy. et al., MÁFKI Közleményei, 12, 125 (1971); 1972 (in press)

8. KÁNTOR Mrs. M., Dissertation, Veszprém, 1972.

9. PERRY, J.H., Chemical Engineers' Handbook, Vol. II. Budapest, Müszaki Könyvkiadó, 1969.

РЕЗЮМЕ

Современный труд инженера химика сегодня уже потребует, чтобы ему были ясны и транспортные явления, сопровождающие химические или физические изменения, которые протекают в отдельных элементах процессов.

Несколько лет тому назад начались студии, целью которых являлась разработка метода, пригодного для моделирования нефтепромышленных и нефтехимических элементов процессов, производственных процессов и установок, исходя из уже известных теоретических основ по реакторной технике.

Hungarian Journal
of Industrial Chemistry
Veszprém
Vol.1. pp.89-114 (1973)

DESCRIPTION OF THE THERMAL DECOMPOSITION OF NAPHTHAS

V. ILLÉS, K. WELTHER and L. SZEPESY

(Hungarian Oil and Gas Research Institute, Veszprém)

Received: September 16, 1972.

In a laboratory tubular reactor at atmospheric pressure and in a temperature range of 580-830°C the pyrolysis of a straight-run Romashkino naphtha cut with a boiling range of 40-160°C was investigated.

New characteristics were introduced to characterize the degree of the decomposition of the naphthas. Substituting the conversion in kinetic equations developed for flow reactors by the decomposition grade, appropriate correlations were derived for describing the overall decomposition rate of the naphthas.

It was demonstrated that in the temperature and residence time ranges of industrial pyrolysis processes, the expansion and the yield distribution of the main reaction products depend only on the decomposition grade.

For predicting the product distribution in naphtha pyrolysis a simplified kinetic model was elaborated.

INTRODUCTION

Roughly half the annual world production of ethylene of nearly 20 million tons is produced by the pyrolysis of gaseous hydrocarbons, the other half is produced by the pyrolysis of liquid petroleum fractions, mainly of naphthas [1].

Despite the large and rapidly increasing production capacities for the pyrolysis of hydrocarbons, relatively few and often contradictory data were published in literature regarding the description of the pyrolysis process, reaction kinetics and product distribution. Most publications deal with the investigation of gaseous hydrocarbons. Very limited detailed and reliable data are available concerning the description of the pyrolysis of liquid hydrocarbon mixtures and naphthas.

To characterize the degree of decomposition in the pyrolysis of naphthas the "severity function" introduced by LINDEN et al. was generally used in the past [2, 3]. Recently, ZDONIK and his associates introduced the "kinetic severity function" based on the conversion on n-pentane under the given pyrolysis conditions and the $\int kdt$ values calculated by a first-order kinetic equation are used to define the degree of decomposition for naphthas.

On the basis of the previous investigations, the sum of the conversions of the feed components weighed by their mole fractions on the one hand, and the relative expansion on the other hand were introduced for characterizing the decomposition grade for hydrocarbon mixtures, and methods were elaborated for the calculation of the overall decomposition rate and the description of product yield curves, respectively [5, 7].

In this publication the application of the above mentioned methods will be described for the evaluation of the pyrolysis of a straight-run Romashkino naphtha cut carried out in a laboratory tubular reactor at atmospheric pressure and in a temperature range of 580-830°C. The specification of the naphtha investigated was as follows:

Density (g/cm^3)	0.7077
Boiling range (°C)	40-160
Molecular weight (average)	111
n-Paraffins (wt.%)	38.7
iso-Paraffins (wt.%)	37.9
Cycloparaffins (wt.%)	17.3
Aromatics (wt.%)	6.0

DECOMPOSITION GRADE FOR NAPHTHA

Between expansion and decomposition grade the correlation can be given by Equation (1) [5-7]:

$$E = 1 + (E_v - 1)X \quad (1)$$

where E expansion,

$E_v = \sum_j^k \sum_i^{k'} y_j \nu_{ji}$ limiting value of expansion,

ν_{ji} = overall stoichiometric coefficients of the reaction products,

$X = \sum_j^k y_j x_j$ decomposition grade.

As regards its form and physical meaning Equation (1) is the same as the correlation between expansion and conversion for the pyrolysis of individual hydrocarbons [8, 9]. The only difference is that in the case of the pyrolysis of hydrocarbon mixtures, instead of the conversion and the stoichiometric coefficients, the sum of the conversions of the feed components weighed by their mole fractions will be introduced.

In the case where the conversions cannot be determined with sufficient precision because of the large number of components or analytical difficulties (mainly for petroleum fractions), in possession of the expansion (E) and limiting expansion (E_v) values and rearranging Equation (1) the decomposition grade can be estimated by the "relative expansion", given in Equation (2) [5, 6].

$$X = \frac{E - 1}{E_v - 1} \quad (2)$$

The detailed gas chromatographic analysis of the products made it possible to determine the conversions of the components and the decomposition grade of the naphtha investigated was defined by the sum of the conversions of the feed components weighed by their mole fractions.

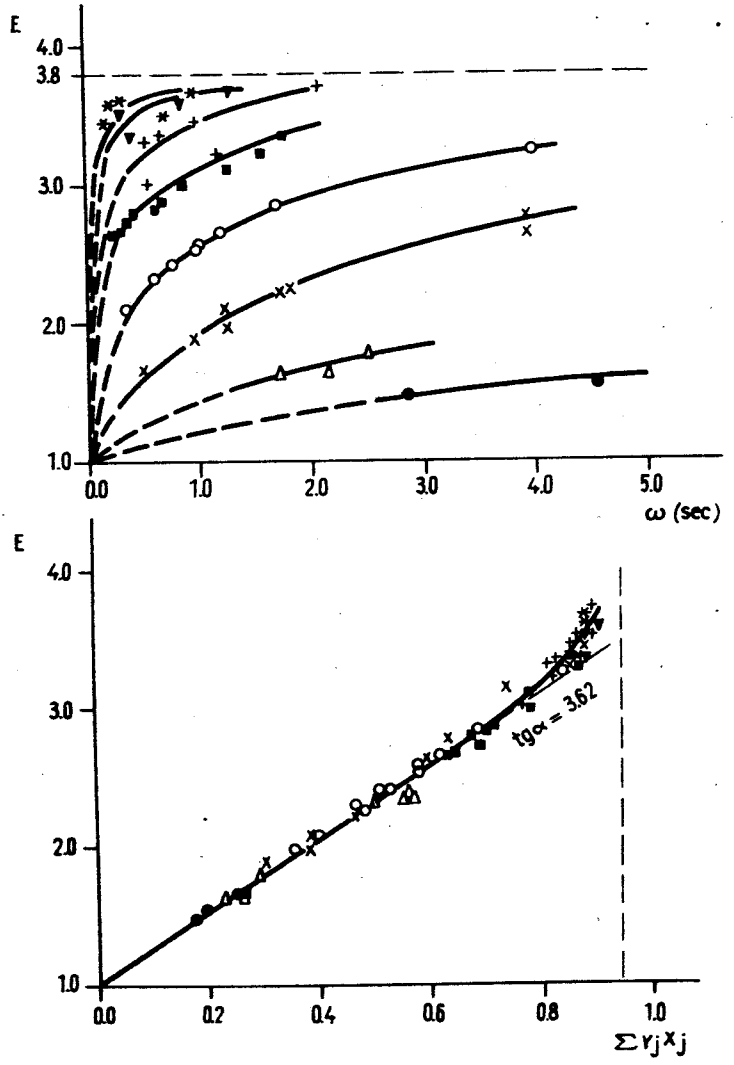

Fig.1. Expansion as a function of the fictive reaction time and the decomposition grade. • 581°C; Δ 624°C; x 660°C; o 699°C; 737°C; + 773°C; ⋇ 834°C.

In Fig. 1 the expansion is plotted as a function of the fictive reaction time and the decomposition grade, respectively. The naphtha feed contained 6 wt.% aromatics that practically do not decompose under the given conditions. For this reason the decomposition grade varies only up to the 0.94 value, which is marked by a dotted line in Fig. 1 and in the forthcoming figures. From the top figure in Fig. 1 the limiting expansion value was estimated to be 3.62. As can be seen from the bottom figure, the variation of expansion as a function of the decomposition grade can be approximated by a single curve independently of the temperature.

DESCRIPTION OF THE OVERALL DECOMPOSITION RATE

A description of the overall decomposition rate for the individual components of the feed naphtha, as well as for the naphtha cut investigated, was carried out by using the kinetic equations for the individual hydrocarbons. Substituting the conversion in these equations by the conversions of the hydrocarbons composing the naphtha (x_j) and by the decomposition grade (X) characteristic for the given naphtha, respectively, the overall decomposition rate for the individual feed components and the naphtha cut, respectively, can be calculated. This method was previously applied for the description of the pyrolysis of binary, ternary and six-component hydrocarbon mixtures [5-7].

As examples in Fig. 2 the conversion of 2,4-dimethylpentane, and in Figs. 3 and 4 the decomposition grades of the naphtha cut are shown as a function of the true and fictive reaction time. The conversion curves for the individual hydrocarbon are similar in shape to the curves for the naphtha cut i.e. by increasing the temperature the rises of the curves - which are proportional to the decomposition rate - steeply increase.

To describe the overall decomposition rate i.e. the conversion curves shown in the figures, an integral as well as a differential method were applied [8, 9].

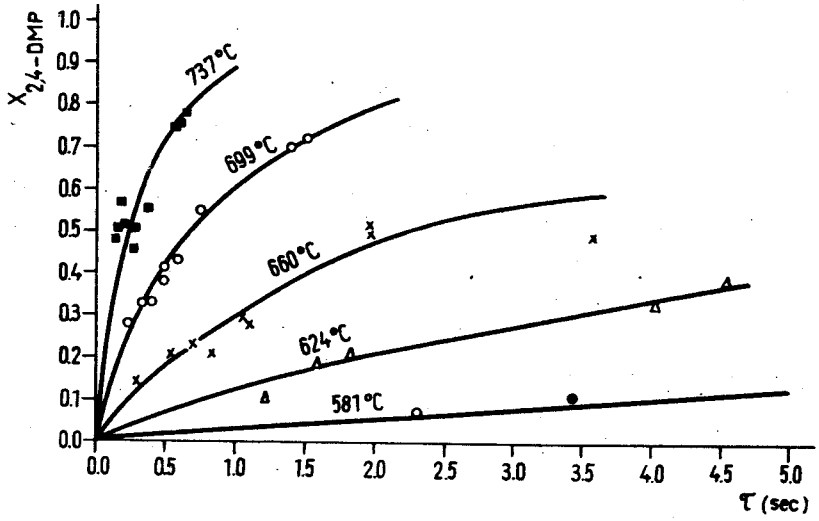

Fig. 2. Conversion of 2,4-dimethylpentane as a function of the true reaction time in naphtha pyrolysis. — Calculated by Eq.(5)

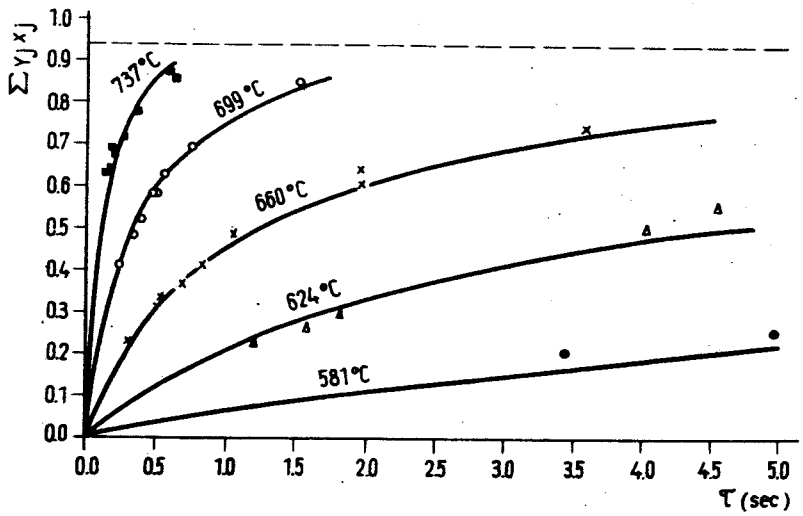

Fig. 3. Decomposition grade vs. true reaction time. — Calculated by Eq. (5).

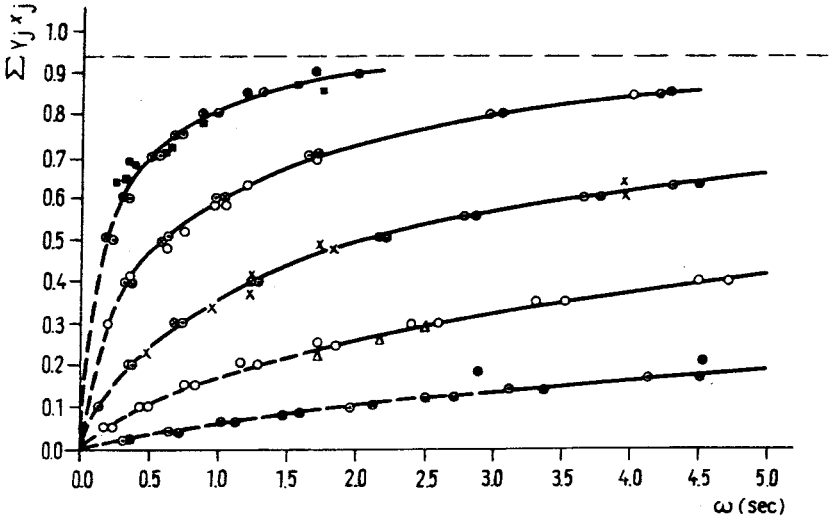

Fig.4. Decomposition grade vs. fictive reaction time.
⊠ Calculated by Eq. (4). ⊙ Calculated by Eq. (7).

Integral Method

In the first step of the evaluation, the decomposition rate constants were calculated for the measured data by using the first-order reaction kinetic equations valid for flow reactors. The calculated k values were plotted against conversion for 2,4--dimethylpentane and against the decomposition grade for the naphtha cut in Figs. 5 and 6, respectively. The figures show that in accordance with the results obtained from the data of the pyrolysis of individual hydrocarbons and model mixtures, the decomposition rate constants calculated by the first-order kinetic equation decrease with increasing conversion and the degree of this decrease depends on the temperature. The values given in Figs. 5 and 6 measured at a given temperature can be approximated by the

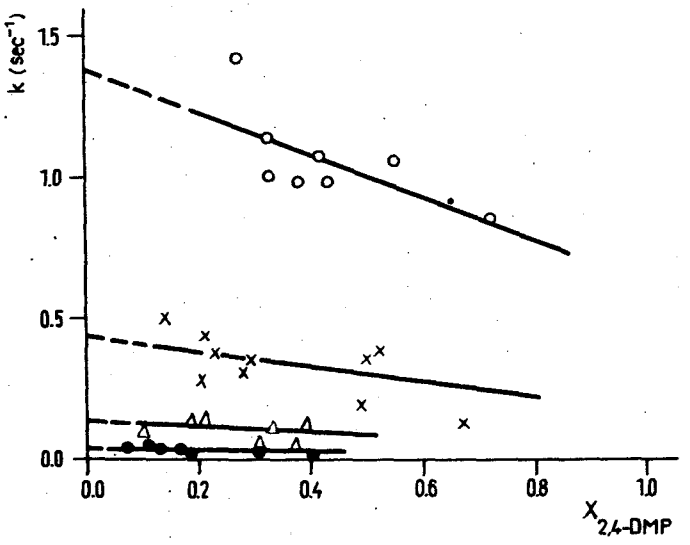

Fig. 5. Decomposition rate "constants" for 2,4-dimethylpentane vs. conversion. • 581°C; Δ 624°C; x 660°C; o 699°C.

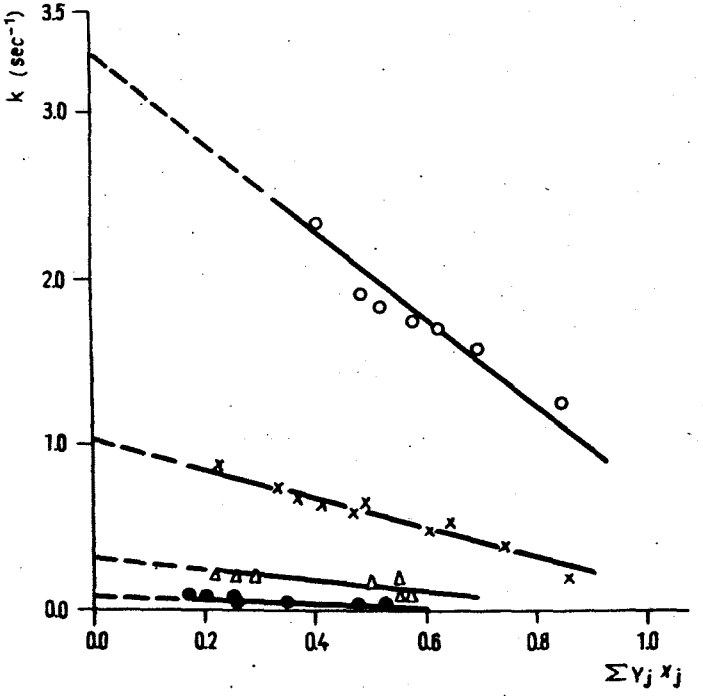

Fig. 6. Decomposition rate "constants" for naphtha vs. decomposition grade. • 581°C; Δ 624°C; x 660°C; o 699°C.

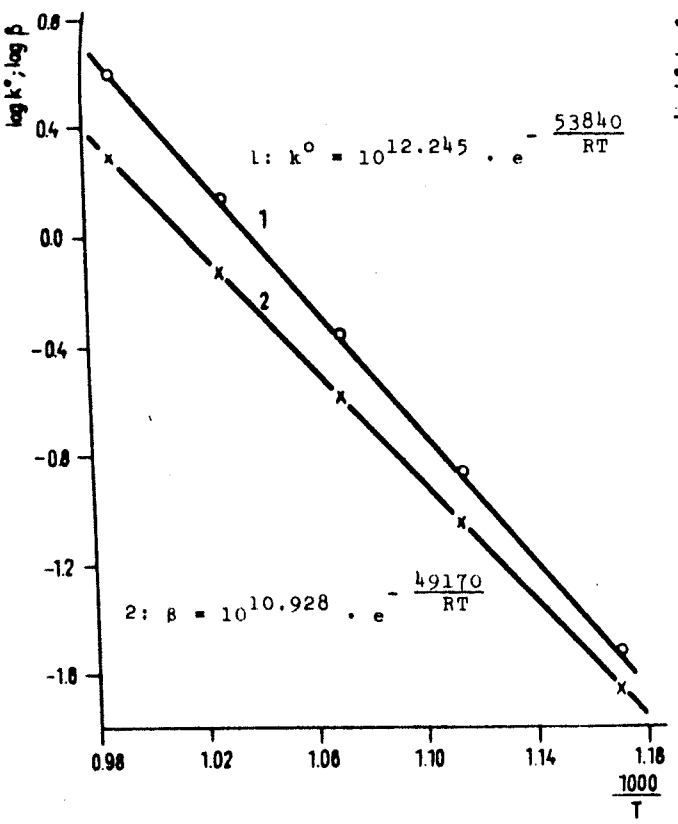

Fig. 7. Arrhenius-plot of the decomposition rate constant (k^o) and the restraining coefficient (β) for 2,4-dimethylpentane.

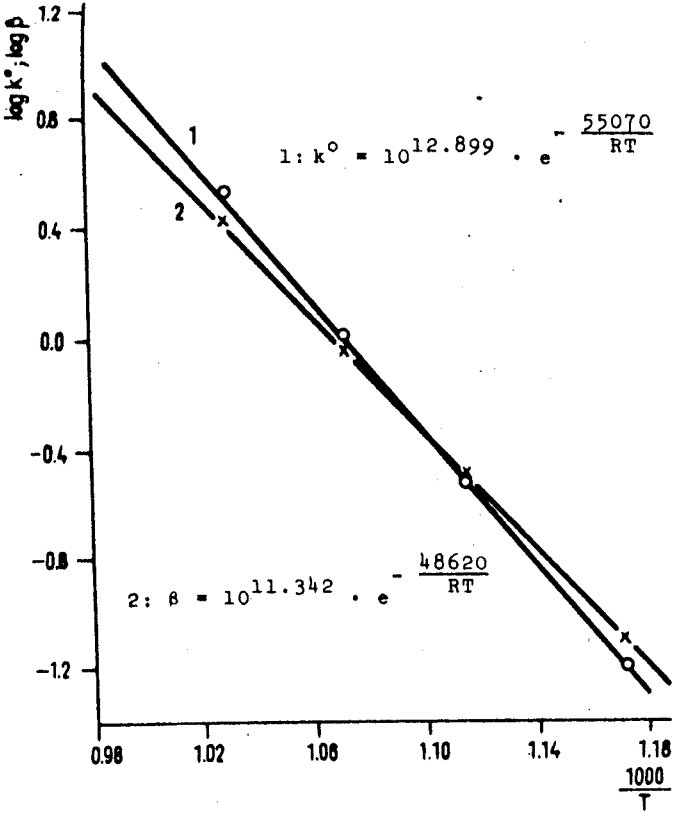

Fig. 8. Arrhenius-plot of the decomposition rate constant (k^o) and the restraining coefficient (β) for naphtha.

following linear relationship:

$$k = k^{o} - \beta X \qquad (3)$$

where k^{o} decomposition rate constant at zero conversion,
β restraining coefficient.

The (k^{o}) and (β) constants can be determined from Figs. 5 and 6.

Figs. 7 and 8 show the decomposition rate constants and restraining coefficients plotted against the temperature for 2,4--dimethylpentane and naphtha. It can be seen that the temperature dependence of both constants can be described by Arrhenius-type equations.

Substituting Equation (3) into the integrated rate equations for first-order reactions the following correlations were obtained between the overall decomposition rate and the fictive and true reaction time [5-9]:

$$w = \frac{1}{k^{o} - \beta X} \left[E_v \, 2.303 \log \frac{1}{1-X} - (E_v - 1) X\right] \qquad (4)$$

$$\tau = \frac{2.303}{k^{o} - \beta X} \log \frac{1}{1 - X} \qquad (5)$$

To check Equations (4) and (5), conversions for 2,4-dimethylpentane as well as decomposition grades for the naphtha were calculated as a function of the fictive and the true reaction times for the measured temperatures. For this calculation, first the k^{o} and β values were calculated for the given temperatures using the Arrhenius-plots in Figs. 7 and 8. Putting these values into Equations (4) and (5), the fictive and true reaction times were calculated for different conversions and decomposition grades, respectively. The full lines in Figs. 2, 3 and 4 represent the calculated curves. The satisfactory agreement between the calculated and measured values confirms that the elaborated method is suitable for the description of the overall decomposition rate of naphthas.

Differential Method

In this method the kinetic equation was used in the linearized form given below [8, 9]:

$$\log (dX/d\omega) = \log (k/C_o) + n \log C \qquad (6)$$

where C_o and C are concentration of the feed components (moles/litre) at the reactor inlet and outlet.

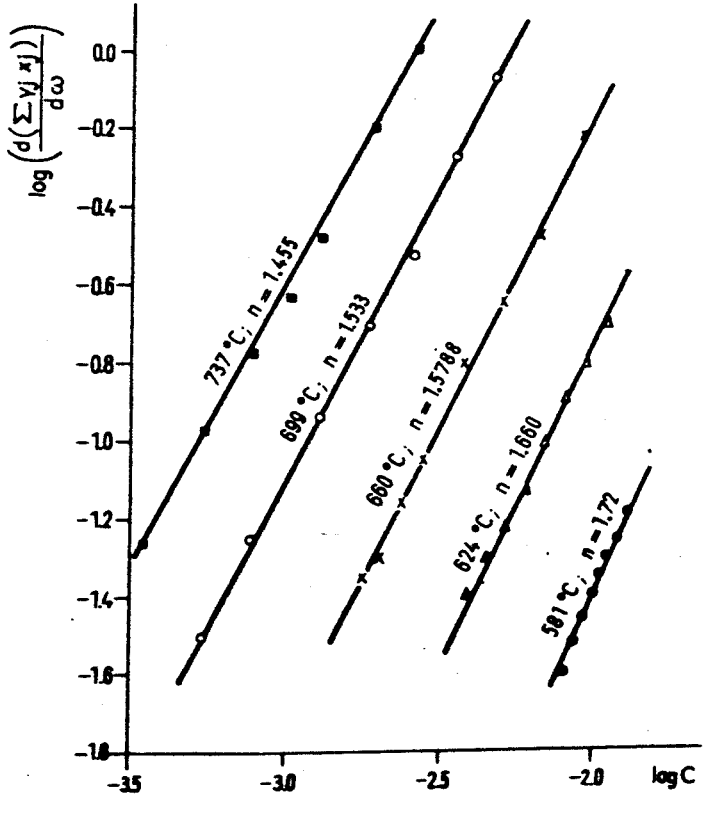

Fig. 9. $\log (\frac{dX}{d\omega}) = \log (\frac{k}{C_o}) + n \log C$ correlation for naphta.

For determining the constants of Equation (6) the curves of the decomposition grade vs. the fictive reaction time (Fig.4) were graphically differentiated and the momentary rates were plotted in logarithmic scale against the actual concentration. This relationship is shown in Fig. 9 for the naphtha investigated.

On the basis of the above figure the k and n values were determined and substituting these values into Equation (7) the decomposition grade values were calculated at different reaction times and temperatures:

$$\omega = \frac{C_o}{k} \int_o^X \left(\frac{1}{C}\right)^n dX \qquad (7)$$

The integration in Equation (7) was performed graphically. The calculated values were plotted in Fig. 4. These data square well with the curves plotted through the measured values which proves the suitability of the method for the description of the overall decomposition rate of naphthas.

DISCUSSION AND INTERPRETATION OF PRODUCT DISTRIBUTION

In Figs. 10-18 the yields of the main reaction products in wt.% are plotted against the decomposition grade of the naphtha cut. It is apparent from the figures that by increasing decomposition there is a considerable change in product distribution. The yields of some products will also be influenced to some extent by the temperature.

The yields of hydrogen and methane continuously increase with the increase of the decomposition grade (Figs.10 and 11). The yield curves run above the tangents constructed to the initial part of the curves, which indicates that the amounts of these products related to the naphtha consumed (the stoichiometric coefficients) increase in the entire decomposition range. These products are stable under pyrolysis conditions. By increasing the temperature at

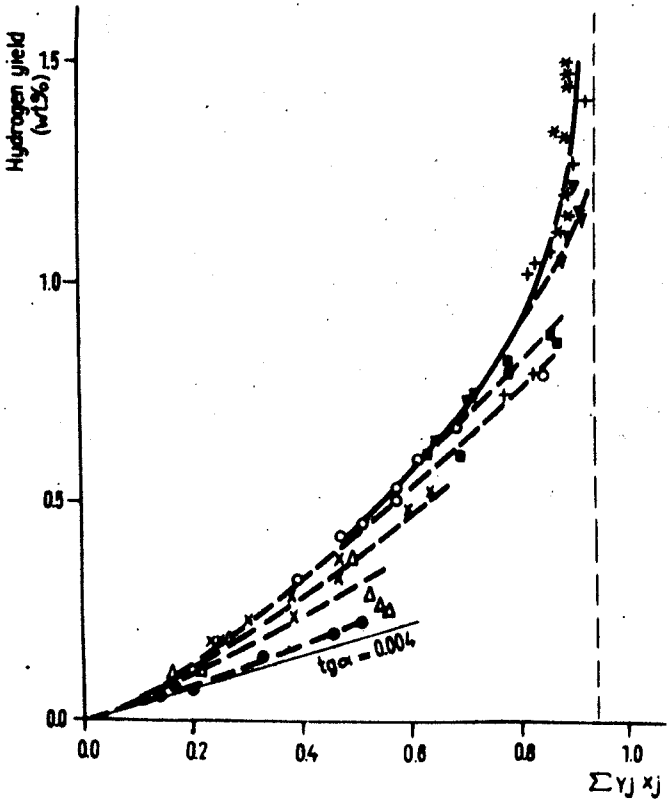

Fig.10. Hydrogen yield vs. decomposition grade
• 581°C; Δ 624°C; x 660°C; o 699°C;
■ 737°C; + 773°C; ▼ 806°C; ✱ 834°C.

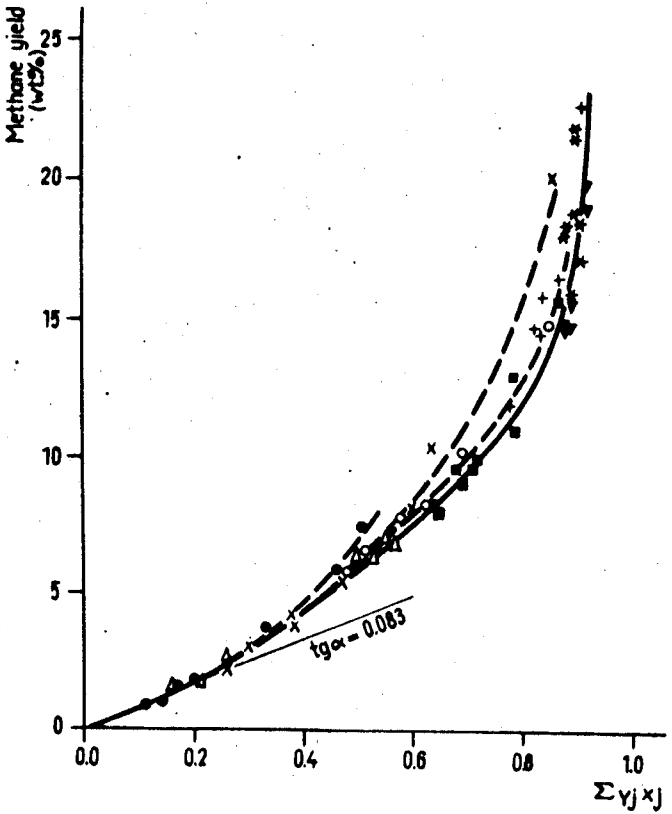

Fig.11. Methane yield vs. decomposition grade
• 581°C; Δ 624°C; x 660°C; o 699°C;
■ 737°C; + 773°C; ▼ 806°C; ✱ 834°C.

a given decomposition, the hydrogen yield increases, and the methane yield slightly decreases.

In Fig. 12 the ethylene yields are plotted against the decomposition grade.

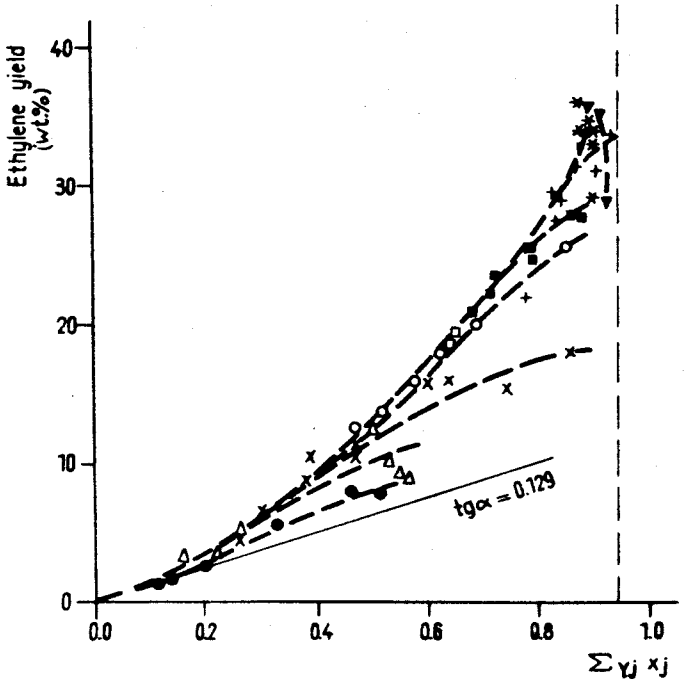

Fig. 12. Ethylene yield vs. decomposition grade. • 581°C; Δ 624°C; × 660°C; o 699°C; ■ 737°C; + 773°C; ▼806°C; * 834°C.

The curves run above the initial tangent i.e. the relative amount of the ethylene considerably increases with increasing decomposition.

Performing the pyrolysis at a higher temperature up to a given decomposition grade, the ethylene yield will increase. It can be observed that the yield curves tend to level out, which indicates that they probably pass through a maximum,at very severe conditions.

The yield curve constructed through the points measured at 806°C shows a definite maximum at about 1 second residence time. Performing the pyrolysis above 800°C with very short (0.1-0.4 second) residence time about 33-34 wt.% ethylene yield related to the naphtha feed can be obtained.

The propylene yield increases with an increased decomposition grade up to a value of about 0.7 (Fig. 13). The yield curve

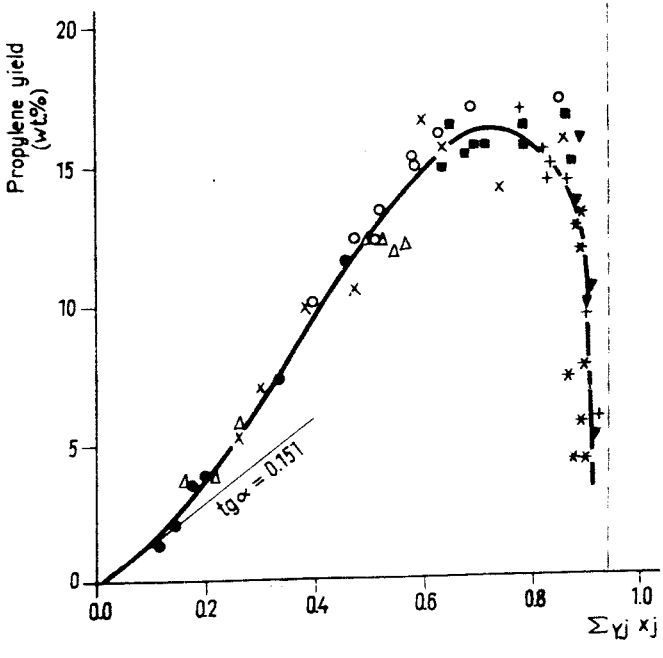

Fig. 13. Propylene yield vs. decomposition grade. • 581°C; Δ 624°C; × 660°C; o 699°C; ■ 737°C; + 773°C; ▼806°C; * 834°C.

runs above the initial tangent, has a maximum at about the 0.7-0.75 decomposition grade and over this the propylene yield sharply decreases. The maximum propylene yield is about 16 wt.%. Under the conditions investigated, the propylene yield curve is independent of the temperature.

Depending on the reaction conditions about 2-10 wt.% ethane is also produced in the pyrolysis process. It can be seen in Fig.14 that the ethane yield increases up to about the 0.85 decomposition

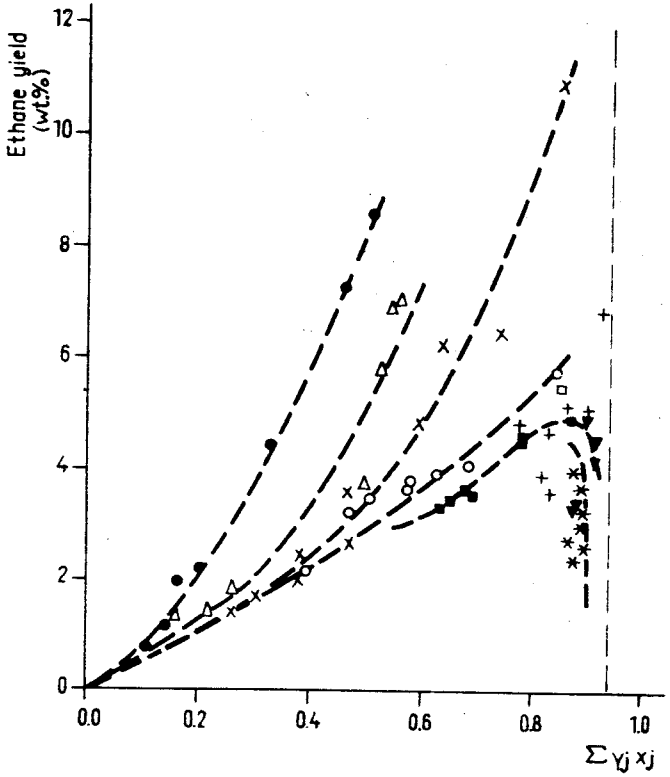

Fig. 14. Ethane yield vs. decomposition grade. ● 581°C; Δ 624°C; x 660°C; ○ 699°C; ■ 737°C; + 773°C; ▼806°C; ✱ 834°C.

grade. At a higher decomposition grade, the yield curves measured above 800°C show a maximum. By increasing the temperature, the ethane yield at a given decomposition grade decreases. The propane yield curves are similar in shape to the ethane curves. The propane yield is one order of magnitude smaller than the ethane yield.

Fig. 15 shows the butylene yields against the decomposition grade. Through the measured values a single curve can be

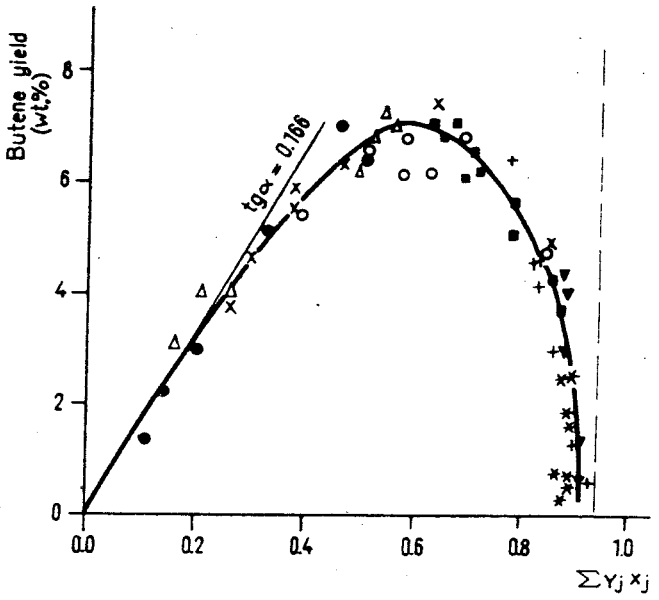

Fig. 15. Butene yield vs. decomposition grade. • 581°C; Δ 624°C; x 660°C; o 699°C; ■ 737°C; + 773°C; ▼ 806°C; * 834°C.

constructed, which means that under the conditions investigated the butylene yield is independent of the temperature. The yield curve shows a maximum at about 0.6 decomposition grade. The maximum butylene yield is about 7 wt.%. The yield curve runs below the tangent constructed to the initial part of the curve, that is the relative amount of the butylene produced decreases with the increasing decomposition grade. The butadiene yield is considerably influenced by the pyrolysis temperature (Fig. 16). At a given decomposition grade, a much higher butadiene yield can be obtained at higher temperatures. The yield curves show a definite maximum at about the 0.6-0.8 decomposition grade. By increasing the temperature, the maximum shifts in the direction of the higher decomposition

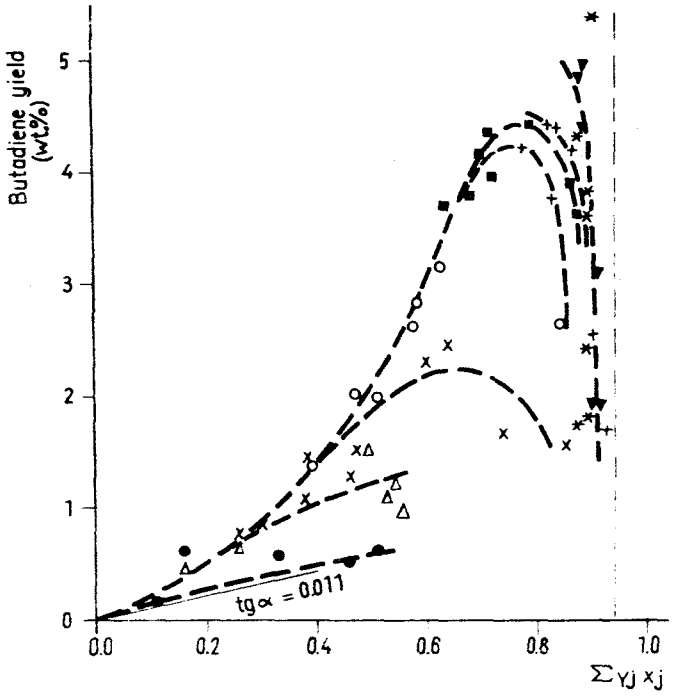

Fig. 16. Butadiene yields vs. decomposition grade. • 581°C; Δ 624°C; x 660°C; o 699°C; ■ 737°C; + 773°C; ▼ 806°C; * 834°C.

grades. The maximum butadiene yield is about 4.5-5.0 wt.%. The shape of the yield curves (the low value of the initial tangent) indicates that the butadiene is mainly formed in secondary reactions.

In naphtha pyrolysis small amounts of pentenes (Fig. 17) and pentadienes are also formed. The yield curve for pentenes shows a maximum at about the 0.6 decomposition grade. The maximum pentenes yield is about 1.6-1.7 wt.%. The yield curves of pentenes as well as of pentadienes are independent of the temperature.

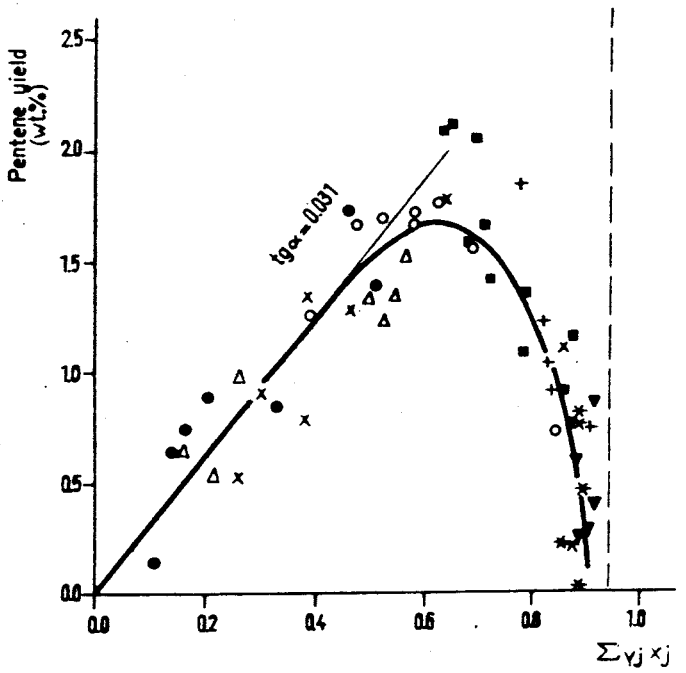

Fig. 17. Yield of pentenes vs. decomposition grade. • 581°C; Δ 624°C; x 660°C; o 699°C; ■ 737°C; + 773°C; ▼ 806°C; ✱ 834°C.

In Fig. 18 the yields of benzene, toluene and styrene are plotted against the decomposition grade. The benzene yield shows a very small increase up to about the 0.5 decomposition grade i.e. practically equal with the benzene content of the naphtha feed. Over the about 0.6 decomposition grade the yield curves rise considerably and over the 0.8 decomposition grade they rise abruptly.

The toluene yield, compared to the toluene content of the naphtha feed, slightly decreases up to about the 0.5 decomposition grade then continuously increases above this value. At a given decomposition grade, the yields of both products decrease by increasing temperature.

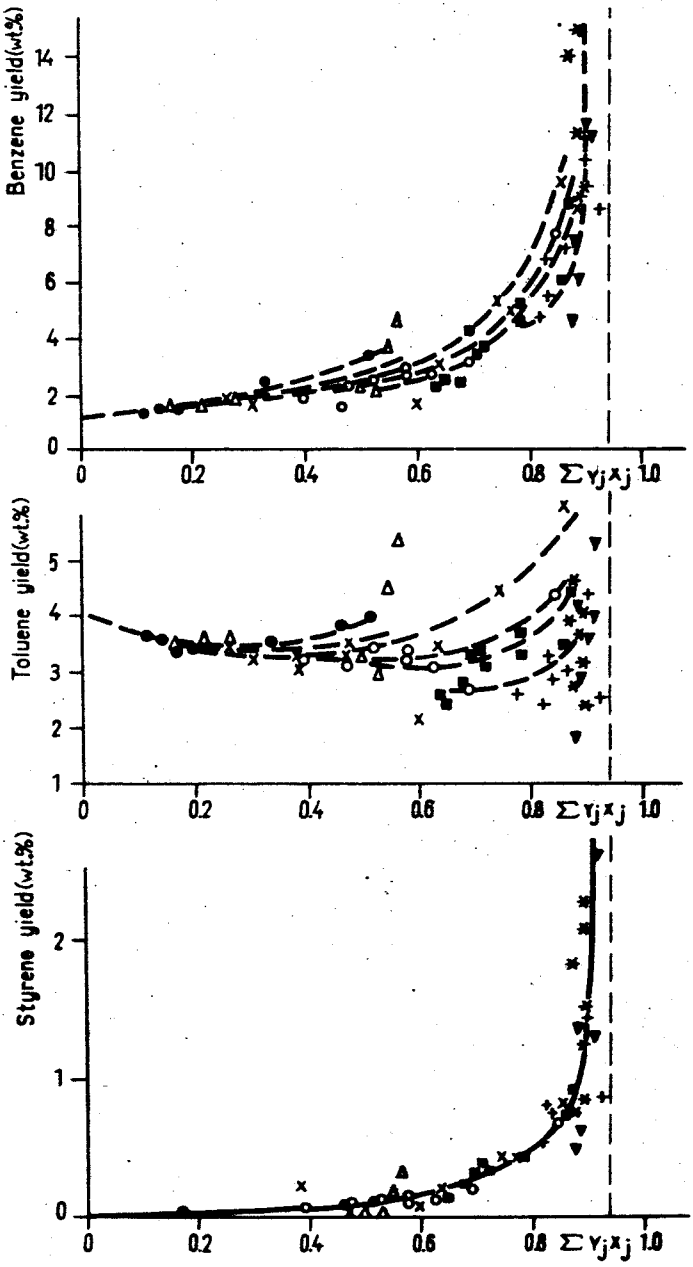

Fig. 18. Yields of benzene, toluene and styrene vs. decomposition grade. • 581°C; Δ 624°C; x 660°C; ■ 737°C; + 773°C; ▼ 806°C; ✱ 834°C.

The yield curve of styrene is independent of the temperature. The styrene curve is similar in shape to the benzene curve, above the about 0.8 decomposition grade it steeply rises. The amount of styrene formed is about one order of magnitude smaller than the amount of benzene.

The above mentioned changes in product distribution are caused by the simultaneous effects of several factors. These changes can to some extent be explained on the basis of the free--radical chain mechanisms.

At a given decomposition grade, the increase in the hydrogen and ethylene yields and the simultaneous decrease in the ethane yield by increasing the temperature are caused by the change of the relative velocities in the hydrogen abstraction and decomposition reactions of the ethyl radicals. By increasing the temperature the velocity of the ethyl radical decomposition will considerably increase compared to the velocity of the hydrogen abstraction, because of the much higher temperature coefficient of the decomposition reaction, which results in an increase of the hydrogen and ethylene yields and an equivalent decrease of the ethane yield.

The decrease in the propane yield by increasing temperature can be explained in a similar way by the different temperature coefficients of the hydrogen abstraction and decomposition reactions of the propyl radicals.

The considerable changes in product distribution by increasing the decomposition grade in naphtha pyrolysis are caused by the secondary reactions among the product olefins and the chain-propagating radicals. From among these reactions the most important are the combination reactions of higher olefins and chain-propagating radicals and the radical decomposition following these reactions.

$$(\text{Olefin})_1 + R_1 \rightleftharpoons \text{Alkyl radical} \rightarrow (\text{Olefin})_2 + R_1' \qquad (8)$$

As a result of the above mentioned decomposition of higher primary olefins (pentenes, butenes) lower olefins (ethylene, propylene) and methane are formed. The rise in the methane as well as in the ethylene and propylene yields and the decrease of the amounts of higher olefins can be explained mainly on the basis of the above reactions.

In the case of higher decomposition grades the hydrogen abstraction reactions among the olefins and chain-propagating radicals also have a considerable effect on product distribution. In these reactions small molecules (H_2, CH_4) as well as vinyl-, allyl- and higher molecular weight unsaturated radicals are formed. The reactions of these radicals among themselves and with the olefins lead to the formation of higher molecular weight dienes and aromatics. As it is apparent in Fig. 18 the amounts of aromatics steeply increase with the decomposition grade above the about 0.6 value.

SIMPLIFIED KINETIC MODEL FOR THE CALCULATION OF PRODUCT YIELDS

In the preceding sections the method for the description of the overall decomposition rate for naphthas was outlined and the constants of the kinetic equations for the naphtha investigated were determined. In these kinetic correlations the decomposition grade introduced instead of the conversion is the dependent variable.

On the basis of the pyrolysis of individual hydrocarbons [8, 9] it was earlier demonstrated that the expansion and yield curves plotted against the conversion were independent of the temperature for most of the hydrocarbons investigated in the temperature and residence time ranges of industrial processes. This means that the expansion and yield curves can be described by mathematical functions containing the conversion as the independent variable.(In most cases this description can be made satisfactory by a poly-

nomial.) In such cases when the temperature independence is not fulfilled, the above curves can be described by functions containing the temperature as a parameter.

It was shown that among the principal reaction products the yield curves of propylene, butenes, pentenes, pentadienes and styrene are independent of the temperature. In the Figures all the measured values were presented. A considerable part of these values were obtained above 1 second residence time. Taking into account only the values measured in the residence time range $0 < \tau < 1$ second of industrial interest, the independence from temperature is also valid approximately for the yield curves of the other products.

To illustrate the above statement, the yield curves of ethylene are shown in Fig. 19 measured in the $0 < \tau < 1$ residence

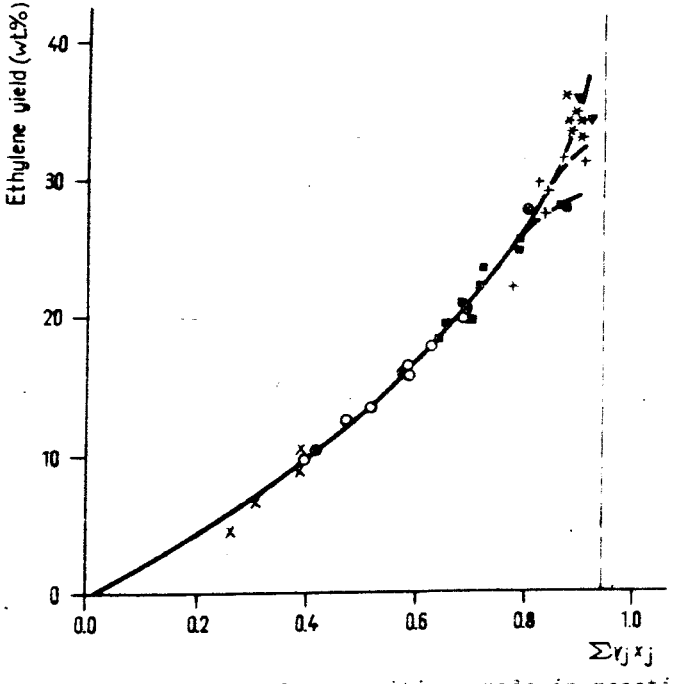

Fig. 19. Ethylene yield vs. decomposition grade in reaction time range of $0 < \tau < 1$ sec. x 660°C; o 699°C; ■ 737°C; + 773°C; ▼ 806°C; ✱ 834°C. ⊗ Calculated values.

time range. The small discrepancies at higher decomposition grades do not cause difficulties in describing the yield curves.

The simplified kinetic model developed for the calculation of the product distribution consists of the kinetic equations suitable for the description of the overall decomposition rate i.e. the changes of the decomposition grade, and of the mathematical equations describing the yield curves as a function of the decomposition grade.

$$X = f(T, \omega, \text{or } \tau)$$
$$H_i = \psi(X) \qquad (9)$$

Fig. 19 also presents some values calculated on the basis of the above model. In this calculations first the decomposition grades were determined for the temperatures investigated using the kinetic constants presented in Fig. 8 and the kinetic Equation (5). The decomposition grade values so obtained were put into the polynomials describing the yield curves and the product yields were determined for the given reaction conditions.

The yields calculated by the above method fit in well with the full line constructed through the measured values which indicates the suitability of the given method for the description of the thermal decomposition of naphthas.

ACKNOWLEDGEMENTS

The authors are indebted to Mrs. J. Simon for the direction of the analytical works and to Mr. Z. Csermely for preparing the computer programme for the description of the yield curves.

USED SYMBOLS

C_o, C total concentration of the naphtha components (undergoing decomposition) at the reactor inlet and outlet, resp. (moles/litre)

E expansion, defined by the ratio of mole numbers of the mixture leaving and entering the reactor (dimensionless)

E_v limiting expansion value (expansion value for the complete decomposition of 1 mole feed mixture)(dimensionless)

H_i yield of the i^{th} reaction product (mole product/mole feed or kg product/kg feed)

k decomposition rate constant (sec^{-1})

k^o decomposition rate constant at zero conversion (sec^{-1})

$\int kdt$ severity function (dimensionless)

n reaction order

R_1, R_i' chain-propagating radicals

ν_{ji} overall stoichiometric coefficient of the i^{th} reaction product in the case of the complete decomposition of the j^{th} component of the feed mixture as individual hydrocarbon (moles product/mole decomposed)

x_j conversion of the j^{th} component in the feed mixture (dimensionless)

X decomposition grade (dimensionless)

y_j mole fraction of component j in the feed mixture (dimensionless)

β restraining coefficient giving the inhibiting effect of the reaction products (sec^{-1})

τ true reaction time (sec)

ω fictive reaction time (sec)

REFERENCES

1. de BLIECK, J.L., CIJFER, H.J., JUNGERHANS, R.J., Erdöl u. Kohle Erdgas Petrochemie 24, 452 (1971)

2. LINDEN, H.R., et al., Ind. Eng. Chem. 47, 2467 (1955)

3. LINDEN, H.R., REID, J.M., Chem. Eng. Progr. 55, 71 (1959)

4. ZDONIK, S.B., GREEN, E.J., HALLE, L.P., The Oil and Gas J. July 10, 192 (1967)

5. ILLÉS, V., Acta Chim. Acad. Sci. Hung. 72, 117 and 133 (1972)

6. ILLÉS, V., Magyar Kémiai Folyóirat 76, 663 (1970)

7. ILLÉS, V., WELTHER, K., SZEPESY, L., The 2nd Conference of Hung. Chem. Soc., Some Applications of Phys. Chem., Veszprém (Hungary), August. 2-5 (1971); Vol. 2, p. 257-265.

8. ILLÉS, V., Acta Chim. Acad. Sci. Hung. 59, 35 (1969); ibid 59, 229 (1969); ibid 67, 41 (1971); ibid 67, 339 (1971)

9. ILLÉS, V., Erdöl u. Kohle Erdgas Petrochemie 25, 464 and 542 (1972)

РЕЗЮМЕ

Бензиновая фракция с пределами точки кипения 40-160°С ромашкинской нефти была подвергнута пиролизу в лабораторном трубчатом реакторе, при давлении 1 атм и в диапазоне температур 580-830°С.

Для характеризовки степени разложения бензиновой фракции введены авторами новые показатели. В кинетических уравнениях разработанных для проточных реакторов была замещена степень разложения, определенная авторами, в место конверсии, и таким образом были получены соотношения подходящие к описанию общей скорости разложения бензиновой фракции.

Авторами показано, что экспансия и выход по основным продуктам реакции — в диапазонах температуры и времени пребывания, принятых при производственном внедрении пиролиза — являются однозначными функциями степени разложения.

На основе найденных соотношений, авторами была разработана упрощенная кинетическая модель для расчета состава смеси реакции пиролиза.

Hungarian Journal
of Industrial Chemistry
Veszprém
Vol.1. pp. 115-140 (1973)

CATALYTIC DEHYDROGENATION OF TETRAHYDROTHIOPHENE TO THIOPHENE

Gy. GÁRDOS, L. HODOSSY* and T. KUN SZABÓ

(Department of Hydrocarbon and Coal Processing, Veszprém
University of Chemical Engineering)

Received: June 9, 1972.

The thermodynamic conditions of the dehydrogenation of tetrahydrothiophene were studied. Experiments were carried out with various types of metal, metal oxide and metal sulphide catalysts in order to increase the rate of the equilibrium reaction,under standardized conditions.

Experiments were carried out using a suitable catalyst to determine the kinetics of the reaction. According to the calculations, the rate-determining partial process is the surface reaction.

Crude oils of high sulphur content contain various organic sulphur compounds in amounts comparable to that of the hydrocarbons. These sulphur compounds may be important raw materials in the production of a number of organic compounds. In the petroleum refining industry, as a result of corrosion hazards, endeavours are made to remove sulphur from the products. However, sulphur removal processes yield sulphur compounds which are inadequate for further processing. Accordingly, any research dealing with the recovery and further processing of organic sulphur compounds found in crude oils is of considerable interest.

---

*Pét Nitrogen Works

The present work deals with the dehydrogenation of a monocyclic sulphide, tetrahydrothiophene, that is also found in crude oils.

The tetrahydrothiophene plant built within the Pét Nitrogen Works primarily serves the demand for gas-scenting agents. However, production on an industrial scale opens up the possibility for the production of other materials based on tetrahydrothiophene. These include two very important products: sulpholane and thiophene. Sulpholane is an important solvent that is used for the recovery of aromatic hydrocarbons present in aromatized petrols. The method is known as the Shell extraction technique.

Thiophene - which can also be produced by the dehydrogenation of tetrahydrothiophene - is another important compound, which is used as a raw material in the pharmaceutical, paint, pesticide and plastics industries [1, 2, 3, 4].

Properties of Thiophene and Tetrahydrothiophene

Physical Properties

The molecular weight of tetrahydrothiophene is 88.174, while that of thiophene is 84.142. There is no major difference between their densities; the density of tetrahydrothiophene at 20°C is almost equal to that of water, its value being 0.9998 g/cm^3, whereas the density of thiophene is 1.0648 g/cm^3. Their boiling points at atmospheric pressure show a rather large difference: tetrahydrothiophene boils at 121.12°C, while thiophene at 84.16°C.

Chemical Properties

Tetrahydrothiophene was first discovered in Persian crude oils. Its odour is poignant. It is miscible with a number of fluids but not with water. It can be oxidized with potassium permanga-

nate; in this reaction sulphone (known commercially as sulpholane) is produced which finds an application as a solvent. It provides crystalline compounds with mercury halides. The latter reaction, on account of the characteristic melting point, is used for identification.

Its stability is higher than that of mercaptans and consequently it can be used for gas scenting. Its sulphides are used to improve the ignition characteristics of Diesel oil. Chlorinated tetrahydrothiophene can be used as a pesticide.

In a similar manner to tetrahydrothiophene, thiophene is a colourless liquid with a slight odour resembling of garlic. Although it is insoluble in water, it is readily soluble in alcohol and ether. It is a reactive compound and its chemical properties are in the main similar to those of benzene: it can be nitrated with nitric acid and sulphonated with sulphuric acid. It forms organic metal compounds with mercury salts, and tends to form complex compounds with various metals.

Its vapours irritate the mucuous membranes. If inhaled for a longer period of time, it causes spasms, and also has an adverse effect on blood cell production. Accordingly it must be handled with care.

Dehydrogenation of Tetrahydrothiophene

YURIEV and BORISOV [5] were the first to produce thiophene from tetrahydrothiophene by dehydrogenation on a platinum-alumina and nickel sulphide-alumina catalyst. After a long interval, YURIEV and TRONOVA [6] reported in another paper on the effect of chromium oxide-alumina catalysts in the transformation of various heterocyclic compounds, including tetrahydrothiophene.

HIRAO and HATTA mentioned in their paper [7] that tetrahydrothiophene can be dehydrogenated to thiophene in the presence of a chromium oxide-alumina catalyst at 500°C.

According to FRIEDMANN [8], tetrahydrothophene is dehydrogenated mostly to thiophene in the presence of elemental sulphur at a pressure of 3 atm and within a period of 10 hours at 160°C with the simultaneous production of a number of other organic sulphur compounds.

OBOLENTSEV and associates [9] studied the dehydrogenation of tetrahydrothiophene in the presence of various industrial catalysts. These authors applied benzene as a diluting component in the dehydrogenation. Their experiments were also supplemented by equilibrium calculations. According to the latter, a temperature of at least 450 to 500°C is necessary for the dehydrogenation to proceed. Decreasing the pressure or dilution with an indifferent component favourably influences the reaction.

MASHKINA and associates [10] studied the dehydrogenating action of the oxides and sulphides of metals of the third to sixth column of the periodic system upon diethyl sulphide and tetrahydrothiophene. Chromium oxide, copper chromite, cobalt molybdate and platinum were found to be the most effective.

Thermodynamics of the Reaction

Dehydrogenation of tetrahydrothiophene to thiophene proceeds according to the following equation:

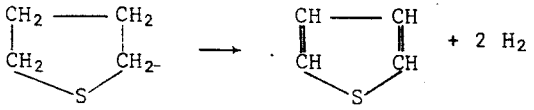

The reaction heats were calculated on the basis of the Franklin-increments [11]. The calculated values are summarized in Table 1. The change in free energy of formation for the reaction was calculated with the FRANKLIN's method [11] as well as with that of van KREVELEN [13]. On the basis of these, the lowest theoretical temperature, at which the reaction is possible, can be determined. The calculated values are shown in Table 2.

Table 1. Heats of Reaction of the Dehydrogenation of Tetrahydrothiophene at Different Temperatures

Temperature °K	ΔH°, Heat of Reaction (kcal/mole)
300	32.910
400	33.252
500	33.540
600	33.752
800	33.844

Table 2. Changes in Free Energy of Formation

Temperature °K	ΔG° (reaction) [11] (kcal/mole)	ΔG° (reaction) [13] (kcal/mole)
300	11.17	11.14
400	4.08	3.87
500	-3.20	-3.44
600	-10.59	-10.70
800	-25.34	-25.56

The values calculated with the two different methods showed good agreement. It can be concluded from the above data that the reaction does not occur at 400°K, whereas it is possible at 500°K. Thiophene can also be hydrogenated an account of the equilibrium reaction. The degree of hydrogenation is negligible at atmospheric or lower pressures.

In the case of a reaction in the gaseous phase, the chemical transformation involves an increase in volume, and accordingly the decrease of pressure or the application of an indifferent diluting component - on account of its partial pressure-decreasing action - promote conversion.

EXPERIMENTS

The aim of the experiments was to study the efficiency of the various catalysts of the metal and metal-oxide-type, in order to find the most preferable to be applied in more detailed studies. The catalysts studied were different industrial products.

A tubular reactor of 11 mm I.D., made of stainless steel, was used for these experiments. The temperature of the reactor was maintained by an electrically heated mercury bath. Reactor temperature could be adjusted by varying the pressure of nitrogen gas conducted over the bath. 20 cm^3 catalyst was placed into the reactor for each experiment.The grain size of the catalyst was brought to 1 to 2 mm by crushing and sieving. The raw material was forwarded into the reactor or into the evaporator connected before the reactor by means of a piston-type pump. The product was recovered in a water-cooled condenser. Uncondensed gases and vapours were collected in a gasometer. Samples were taken from both the condensed product and the gaseous products and the samples were analyzed.

The condensed products were analyzed with a chromatograph, produced by Becker-Delft, type 2040 C-2, equipped with a flame-ionization detector.

The packing material used in the separating column was Celite (C-22) wetted with 25 per cent poly(propylene glycol). The length of the column was 1 m, the rate of the carrier gas stream 3 liters per hour, the temperature was 120°C.

Tetrahydrothiophene produced by the Pét Nitrogen Works was used. The product contained 2.5 per cent tetrahydrofurane as impurity. The diluting material was analytical-grade benzene.

A mixture containing 2 moles of benzene and 1 mole of tetrahydrothiophene was used to compare the catalysts. Experiments were carried out with each catalyst at three temperatures (450, 500 and 550°C) and at three different residence times (0.5, 1.0 and

1.5 sec). The residence time was varied by controlling the pumping rate of the feeding pump and the volumetric rate was varied accordingly. The experiments were carried out at atmospheric pressure.

The effect of the catalysts at a benzene-tetrahydrothiophene molar ratio of 2/1 and a residence time of 1 second is illustrated with the conversion and yield data summarized in Table 3.

Table 3. Effect of Different Types of Catalysts

No.	Catalyst type	THT* conversion %			Thiophene yield %		
		450	500	550	450	500	550
		°C					
1	Cobalt-molybdenum oxide	55.4	60.7	63.0	35.5	40.8	48.3
2	Nickel-tungsten sulphide	15.7	16.9	18.4	9.6	10.0	10.8
3	Platinum-alumina	11.0	27.2	44.0	6.4	16.8	33.1
4	Chromium-alumina	17.6	57.6	81.4	5.6	21.9	40.9
5	Nickel-molybdenum oxide	8.7	10.7	18.7	1.3	3.3	10.1
6	Nickel-alumina	27.6	55.5	84.0	18.7	27.6	54.0
7	Copper chromite	11.1	17.5	41.5	3.6	6.6	25.0

1. Ketjefine 124-1.5
2. Leuna-3076
3. Engelhardt product; 1.6 per cent Pt + Al_2O_3 carrier
4. Leuna-6301
5. Leuna-8199/s
6. Leuna-6524
7. Product of Pét Nitrogen Works; copper(II)-chromium(III)-oxide of the Adkins type

*Generally used abbreviation for tetrahydrothiophene

It is apparent from the data shown in Table 3. that thiophene was formed with all the catalysts used. However, in addition to dehydrogenation to thiophene, other decomposition reactions were also occurring, and this explains the fact that in every case the conversion of THT was higher than the thiophene yield. In addition

to hydrogen, hydrogen sulphide, ethane, propane and butane were detected in the product gases. In addition to the diluent benzene, there was generally mainly tetrahydrothiophene and thiophene in the liquid condensate. Traces of mercaptanes were also found.

On the basis of experiments carried out at 550°C, catalysts of the nickel-alumina, chromium-alumina and cobalt-molybdenum oxide types were found to be most active.

The platinum-alumina catalyst deserves special attention because at a relatively moderate activity it shows a higher selectivity, i.e. the difference between THT conversion and thiophene yield was smaller than in the case of other catalysts. On the other hand, the chromium-alumina catalyst seems to be inadequate for further tests, because - despite the high degree of conversion - its selectivity is poor.

On the basis of the experiments, nickel-alumina, platinum--alumina and cobalt-molybdenum-oxide catalysts were found to be adequate for further detailed studies aimed at finding the parameters of industrial production.

KINETIC ANALYSIS OF THE REACTION

Nickel-alumina was chosen from among the catalysts that were found to be adequate and the kinetics of the reaction were studied in the presence of this catalyst.

The aim of our studies was to obtain data on the relative rates of the elementary processes, on the details of processes occurring on the catalyst and to determine the most preferable parameters in connection with the use of the catalyst.

The experiments were carried out at 550°C and at a molar ratio 10 moles benzene/mole tetrahydrothiophene at different feeding rates. Accordingly, different residence times were obtained for the reactants. The calculations were carried out on the basis of the analytical results obtained for the starting materials and

products. The results of these experiments are given in Table 4. During the calculations, a procedure proposed by NAGY [12] was adopted. This can be summarized as follows: the rate and kinetic equations conforming to the supposed mechanism, pertaining to the stoichiometric equation, were taken from a Table. The partial pressure values were substituted into these equations, and by adopting the sign

$$x = \frac{p_i}{p}$$

the equations were linearized.

The rate values found in the equations can be calculated from the measured data.

Table 4. Dehydrogenation of Tetrahydrothiophene at Various Feeding Rates

Amount of catalyst: 20 g
Temperature: 550 °C
Pressure: 68 mm Hg

Measured data	No. of experiments					
	1.	2.	3.	4.	5.	6.
Feeding rate $B' \cdot 10^2$ (cm^3/sec)	1.815	1.957	2.50	3.15	4.78	6.25
THT concentration in the vapour mixture feed (vol.%)	9.1	9.1	9.1	9.1	9.1	9.1
THT concentration in product vapour (vol.%)	0.66	0.97	1.85	3.44	6.3	8.6
Thiophene concentration in product vapour (vol.%)	8.3	8.0	7.2	5.6	2.8	0.5

If the transformed experimental data, which are in agreement with the equations, are plotted in a diagram, it will be true that from among the rate (kinetic) equations the correct one is that

which yields corresponding pairs of values which lie on a straight line.

The stoichiometric equation of the dehydrogenation of tetrahydrothiophene is the following:

$$C_4H_8S \longrightarrow C_4H_4S + 2\ H_2$$

and the type of the equation is

$$A \longrightarrow B_1 + B_2 \qquad (1)$$

The amount of tetrahydrothiophene brought to evaporation ensures a stream of constant mass rate in the reactor. The amounts of liquid and gaseous products leaving the reactor were measured, together with the composition of the liquid. The diluting component did not take part in the reaction and in order to simplify the calculations it was not taken into account. Compression of the gases after the reactor was given by the difference of the external pressure and the partial pressure of the diluting component, which was 68.0 mm Hg. Taking the stoichiometric Equation (1) into consideration, the rate equation of the reaction is the following:

$$\frac{1}{S} = -\int_{(y_A)_0}^{(y_A)_t} \frac{dy_A}{w} = \int_{(y_{B_1})_0}^{(y_{B_1})_t} \frac{dy_{B_1}}{w} = \frac{1}{2}\int_{(y_{B_2})_0}^{(y_{B_2})_t} \frac{dy_{B_2}}{w} \qquad (2)$$

The factor 1/2 in the third expression of the rate equation originates from the stoichiometric constant.

The density of the raw material fed into the system was 0.889 g/cm^3. From the data given in Table 4., with the mass rate of feed (B), if the mass of the catalyst (m_s) is known, the volumetric rate (S) can be calculated.

$$B = B' \cdot d; \qquad S = \frac{B}{m_s} \qquad (3)$$

Tetrahydrothiophene was fed into the reactor, and thus:

$$(y_A)_0 = \frac{1}{M} ; \quad (y_{B_1})_0 = 0; \quad (y_{B_2})_0 = 0 \tag{4}$$

Taking the equation of the reaction into consideration, for the material balance the following holds:

$$(y_A)_0 - (y_A)_t = (y_{B_1})_t = \frac{1}{2} (y_{B_2})_t \tag{5}$$

The results of the calculations are summarized in Table 5.

Table 5. Values Calculated from the Experimental Data

Calculated values	No. of experiments					
	1.	2.	3.	4.	5.	6.
$B \cdot 10^2$ (g/sec)	1.615	1.740	2.220	2.800	4.250	5.560
$S \cdot 10^3$ (g/g sec)	0.807	0.870	1.110	1.400	2.125	2.780
$(y_A)_0 \cdot 10^2$ (moles/g)	1.135	1.135	1.135	1.135	1.135	1.135
$(y_A)_t \cdot 10^2$ (moles/g)	0.078	0.116	0.222	0.415	0.700	1.060
$1/S \cdot 10^{-3}$ (g sec/g)	1.240	1.150	0.900	0.715	0.470	0.360

It was not possible unequivocally to determine, on the basis of the experimental series, which of the product components influences the reaction rate in addition to the starting material.

Consequently, of the rate equations pertaining to the reaction $A \rightarrow B_1 + B_2$ found in literature all those had to be studied in which the reaction rate is dependent on the partial pressure of the starting material and of a product (Equations 6a to 6e), or on the partial pressure of all the three possible components (Equations 6f and 6g).

1. $W = f(p_A, p_{B_1})$ 2. $W = f(p_A, p_{B_2})$

$$W = \frac{p_A}{a^I + b^I p_A + c^I p_{B_1}}; \qquad W = \frac{p_A}{a^I + b^I p_A + d^I p_{B_2}} \tag{6a}$$

$$W = \frac{p_A}{a^{II} + c^{II}\sqrt{p_{B_1}}}; \qquad W = \frac{p_A}{a^{II} + d^{II}\sqrt{p_{B_2}}} \tag{6b}$$

$$W = \frac{p_A}{(a^{III} + b^{III} p_A + c^{III} p_{B_1})^2}; \quad W = \frac{p_A}{(a^{III} + b^{III} p_A + d^{III} p_{B_2})^2} \tag{6c}$$

$$W = \frac{p_A}{(a^{IV} + b^{IV} p_A + c^{IV}\sqrt{p_{B_1}})^2}; \quad W = \frac{p_A}{(a^{IV} + b^{IV} p_A + d^{IV}\sqrt{p_{B_2}})^2} \tag{6d}$$

$$W = \frac{p_A}{a^V + c^V p_{B_1}}; \qquad W = \frac{p_A}{a^V + d^V p_{B_2}} \tag{6e}$$

3. $W = f(p_A, p_{B_1}, p_{B_2})$

$$W = \frac{p_A}{a^{VI} + c^{VI} p_{B_1} + d^{VI} p_{B_2}} \tag{6f}$$

$$W = \frac{p_A}{(a^{VII} + b^{VII} p_A + c^{VII} p_{B_1} + d^{VII} p_{B_2})^2} \tag{6g}$$

The partial pressures can be substituted by the mole fractions in the gaseous phase:

$$\frac{P_A}{P} = \frac{(y_A)_t}{3(y_A)_o - 2(y_A)_t} \tag{7a}$$

$$\frac{P_{B1}}{P} = \frac{1}{3}\left(1 - \frac{P_A}{P}\right) \tag{7b}$$

$$\frac{P_{B_2}}{P} = \frac{2}{3}\left(1 - \frac{P_A}{P}\right) \tag{7c}$$

By dividing Equations (6) by the total pressure (P), substituting the values given in Equation (7) and ntroducing

$$\frac{P_A}{P} = x$$

we have linearized rate Equation (6):

$$\frac{x}{W} = \left(\frac{a^I}{P} + \frac{2}{3}d^I\right) + \left(b^I - \frac{2}{3}d^I\right)x \quad ; \quad \frac{x}{W} = \alpha^I + \beta^I x \tag{8a}$$

$$\frac{x}{W} = \left(\frac{a^I}{P} + \frac{1}{3}c^I\right) + \left(b^I - \frac{1}{3}c^I\right)x$$

$$\frac{x}{W} = \frac{a^{II}}{P} + \sqrt{\frac{2}{3}}\,\frac{d^{II}}{\sqrt{P}}\sqrt{1-x} \quad ; \quad \frac{x}{W} = \alpha^{II} + \gamma^{II}\sqrt{1-x} \tag{8b}$$

$$\frac{x}{W} = \frac{a^{II}}{P} + \sqrt{\frac{1}{3}}\,\frac{c^{II}}{\sqrt{P}}\sqrt{1-x}$$

$$\sqrt{\frac{x}{W}} = \sqrt{P}\left[\left(\frac{a^{III}}{P} + \frac{2}{3}\,d^{III}\right) + \left(b^{III} - \frac{2}{3}\,d^{III}\right)x\right]$$

$$\sqrt{\frac{x}{W}} = \sqrt{P}\left[\left(\frac{a^{III}}{P} + \frac{1}{3}\,c^{III}\right) + \left(b^{III} - \frac{1}{3}\,c^{III}\right)x\right]$$

$$; \quad \sqrt{\frac{x}{W}} = \alpha^{III} + \beta^{III}x \qquad (8c)$$

$$\sqrt{\frac{x}{W}} = \sqrt{P}\left(\frac{a^{IV}}{P} + b^{IV}x + \sqrt{\frac{2}{3}}\,\frac{d^{IV}}{\sqrt{P}}\,\sqrt{1-x}\right)$$

$$\sqrt{\frac{x}{W}} = \sqrt{P}\left(\frac{a^{IV}}{P} + b^{IV}x + \sqrt{\frac{1}{3}}\,\frac{c^{IV}}{\sqrt{P}}\,\sqrt{1-x}\right)$$

$$; \quad \sqrt{\frac{x}{W}} = \alpha^{IV} + \beta^{IV}x + \gamma^{IV}\sqrt{1-x} \qquad (8d)$$

$$\frac{x}{W} = \frac{a^{V}}{P} + \frac{2}{3}\,d^{V}(1 - x)$$

$$\frac{x}{W} = \frac{a^{V}}{P} + \frac{1}{3}\,c^{V}(1 - x)$$

$$; \quad \frac{x}{W} = \alpha^{V} + \gamma^{V}(1 - x) \qquad (8e)$$

$$\frac{x}{W} = \left(\frac{a^{VI}}{P} + \frac{1}{3}\,c^{VI} + \frac{2}{3}\,d^{VI}\right) - \left(\frac{1}{3}\,c^{VI} + \frac{2}{3}\,d^{VI}\right)x \; ; \; \frac{x}{W} = \alpha^{VI} - \gamma^{VI}x \qquad (8f)$$

$$\sqrt{\frac{x}{W}} = \sqrt{P}\left[\left(\frac{a^{VII}}{P} + \frac{1}{3}\,c^{VII} + \frac{2}{3}\,d^{VII}\right) + \left(b^{VII} - \frac{1}{3}\,c^{VII} - \frac{2}{3}\,d^{VII}\right)x\right] ;$$

$$\sqrt{\frac{x}{W}} = \alpha^{VII} + \beta^{VII}x \qquad (8g)$$

The specific reaction rate (w) can be calculated from the following Equation:

$$w = -\frac{d(y_A)_t}{d(1/S)} \approx -\frac{\Delta(y_A)_t}{\Delta(1/S)} \qquad (9)$$

If $(y_A)_t$ is plotted against 1/S on the basis of Table 5 (Fig.1).

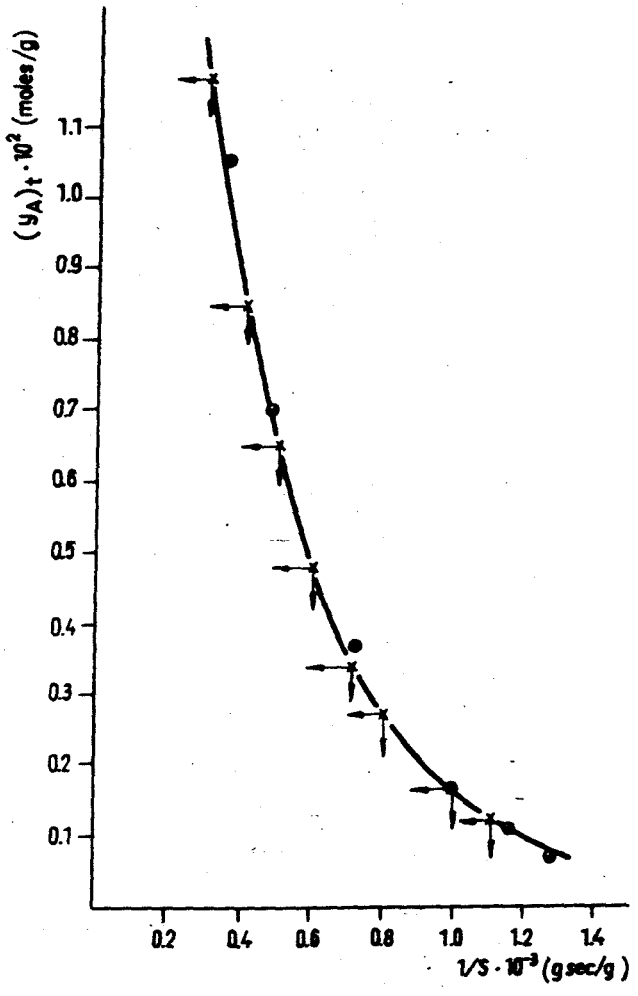

Fig.1. The alteration of THT concentration with the reaction time. ● measured values; x values used in the differentiation.

The difference quotients were calculated by taking the $\Delta(1/S)$ values and the corresponding $\Delta(y_A)_t$ values from Fig. 1. The result of

the calculations is shown in Table 6. Fig.2. was plotted on the basis of Table 6; The Figure shows the difference quotients - which, according to Equation (9), correspond to the specific reaction rates - plotted against $(y_A)_t$.

Table 6. Values of the Difference Quotients as Calculated from Measured Results

Residence time $\frac{1}{S}\cdot 10^{-3}$ (g sec/g)	0.3	0.4	0.5	0.6	0.7	0.8	0.9	1.0	1.1
$(y_A)_t \cdot 10^2$ (moles/g)	1.15	0.86	0.65	0.49	0.38	0.29	0.22	0.17	0.13
$w = \frac{\Delta(y_A)_t}{\Delta(1/S)} \cdot 10^5$ (moles/g sec)	-	2.9	2.1	1.6	1.1	0.9	0.7	0.5	0.4

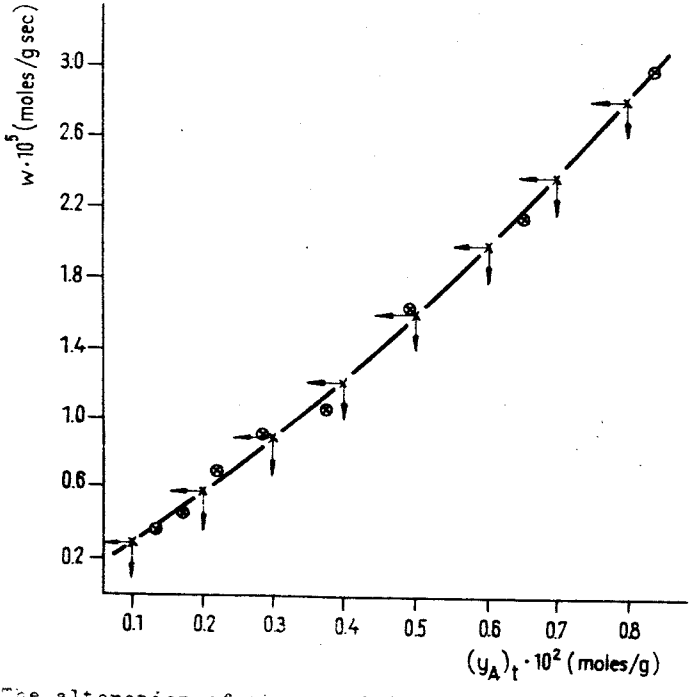

Fig. 2. The alteration of the specific reaction rate with the THT concentration. ⊗ calculated values; x the values of the curve

Knowing the specific reaction rate (w) and the mass of the catalyst, the rate of the dehydrogenation reaction can be written as follows:

$$W = w \cdot m_s \tag{10}$$

The w values, corresponding to increasing $(y_A)_t$ values and necessary for calculation of the linearized rate Equations (8a to 8g), were read from Fig.2. The detailed calculation is shown in Table 7. The linearized rate equations constructed in this manner are shown in Figs. (3a to 3e).

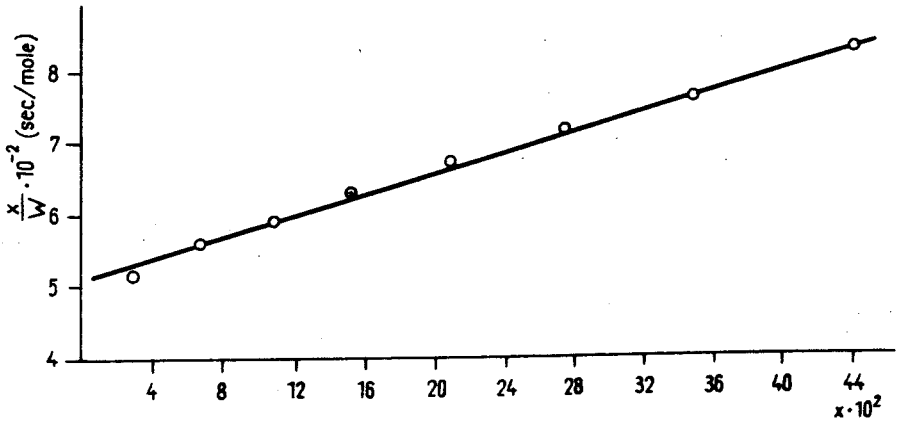

Fig. 3a. The linearized rate equation, based on Equation (8a).

It is apparent from these Figures that the calculated values appear along a straight line only in the case of Figs (3a) and (3e).

From these two the

$$\frac{x}{W} = \alpha^I + \beta^I x$$

equation was accepted which corresponds to Fig. (3a) as the one best fitting the conditions. (The slope of the straight line constructed in Fig. (3e) is negative.)

Table 7. Data of the Linearized Kinetic Equations

$(y_A)_t \cdot 10^2$ (moles/g)	0.1	0.2	0.3	0.4	0.5	0.6	0.7	0.8
$w \cdot 10^5$ (mole/g sec)	0.30	0.60	0.90	1.22	1.58	1.92	2.28	2.66
$W \cdot 10^4$ (mole/sec)	0.60	1.20	1.80	2.44	3.16	3.84	4.56	5.32
$[3(y_A)_0 - 2(y_A)_t] \cdot 10^2$	3.2	3.0	2.8	2.6	2.4	2.2	2.0	1.8
$x = p_A/P = \frac{(y_A)_t}{3(y_A)_0 - 2(y_A)_t} \cdot 10^2$	3.12	6.67	10.70	15.40	20.85	27.30	35.0	44.1
$\frac{x}{W} \cdot 10^{-2}$ (sec/mole)	5.20	5.56	5.94	6.32	6.62	7.12	7.67	8.29
$(1 - x) \cdot 10$	9.69	9.33	8.93	8.46	7.92	7.27	6.50	5.59
$\frac{x}{W}$ ($sec^{1/2}/mole^{1/2}$)	22.8	23.6	24.4	25.15	25.75	26.65	27.65	28.75
$\sqrt{1 - x} \cdot 10$	9.83	9.66	9.45	9.19	8.90	8.52	8.06	7.46
$35.4 - \frac{x}{W}$ ($sec^{1/2}/mole^{1/2}$)	12.6	11.8	11.0	10.25	9.65	8.75	7.75	6.65
$\frac{35.4 - \frac{x}{W}}{\sqrt{1 - x}}$	12.83	12.21	11.63	11.16	10.83	10.27	9.61	8.91

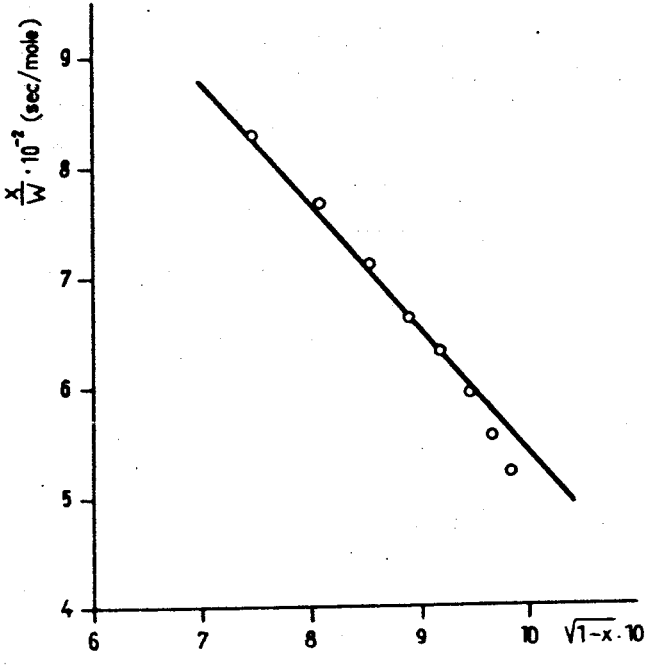

Fig. 3b. The linearized rate equation, based on Equation (8b).

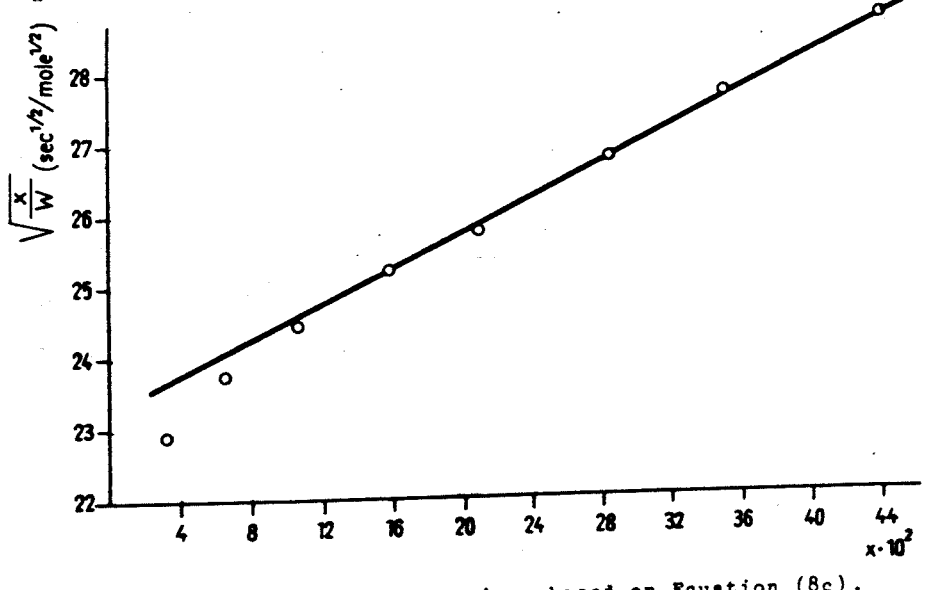

Fig. 3c. The linearized rate equation, based on Equation (8c).

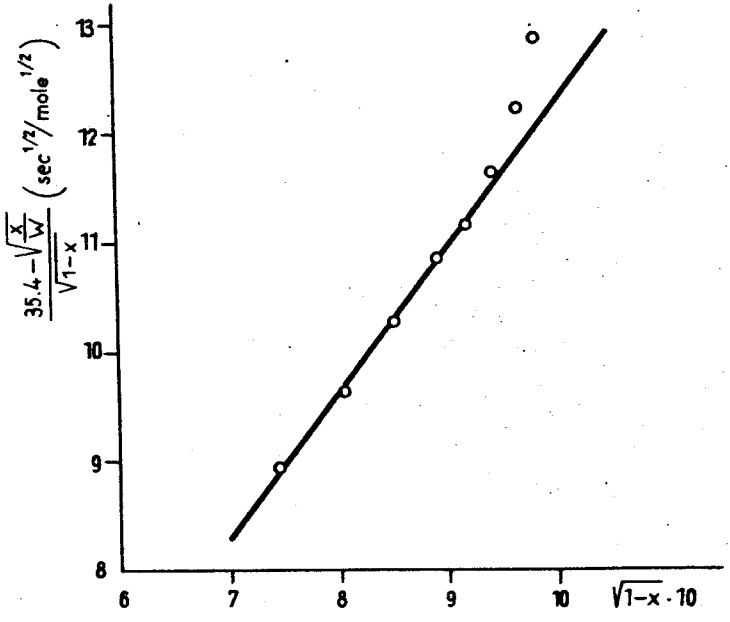

Fig. 3d. The linearized rate equation, based on Equation (8d).

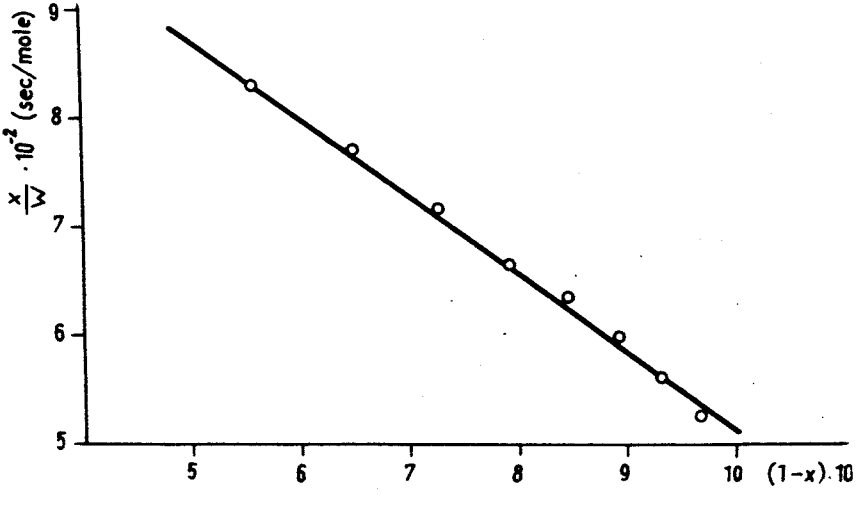

Fig. 3e. The linearized rate equation, based on Equation (8e).

The values of constants α and β can be determined on the basis of Fig. (3a):

$$\alpha^I = 5.05 \cdot 10^2 \text{ (sec/mole)}$$
$$\beta^I = 7.5 \cdot 10^2 \text{ (sec/mole)}$$

A detailed explanation of the meaning of the constants is given in the following:

$$\alpha^I = \frac{a^I}{P} + \frac{2}{3} d^I \qquad \alpha^I = \frac{a^I}{P} + \frac{1}{3} c^I$$

$$\beta^I = b^I - \frac{2}{3} d^I \qquad \beta^I = b^I - \frac{1}{3} c^I$$

$$\frac{a^I}{P} + \frac{2}{3} d^I > 0 \; ; \quad \frac{2}{3} d^I < b^I \neq 0$$

$$\frac{a^I}{P} + \frac{1}{3} c^I > 0 \; ; \quad \frac{1}{3} c^I < b^I \neq 0$$

According to the tables published in literature [11], the surface reaction is the rate-determining partial process in the case of this type of reaction. One of the products formed is adsorbed; consequently both cases of Equation (8a) were studied:

$$W = \frac{p_A}{a + bp_A + cp_{B_1}} = \frac{1}{a} \cdot \frac{p_A}{\left(1 + \frac{b}{a} p_A + \frac{c}{a} p_{B_1}\right)}$$

The corresponding kinetic-equation is:

$$W = k \frac{p_A}{1 + K_A p_A + K_{B_1} p_{B_1}}$$

By comparison of the two equations:

$$k = \frac{1}{a} \; ; \quad K_A = \frac{b}{a} \; ; \quad K_{B_1} = \frac{c}{a} \quad \text{or}$$

$$a = \frac{1}{k} \; ; \quad b = \frac{K_A}{k} \; ; \quad c = \frac{K_{B_1}}{k}$$

When the constants α and β are expressed with rate and equilibrium constants:

$$\alpha = \frac{a}{P} + \frac{1}{3} c = \frac{1}{kP} + \frac{1}{3} \frac{K_{B_1}}{k} = \frac{1}{k} \left(\frac{1}{P} + \frac{1}{3} K_{B_1} \right)$$

$$\beta = b - \frac{1}{3} c = \frac{K_A}{k} - \frac{1}{3} \frac{K_{B_1}}{k} = \frac{1}{k} \left(K_A - \frac{1}{3} K_{B_1} \right)$$

If $K_{B_1} \approx 0$:

$$\alpha = \frac{1}{kP} \rightarrow k = \frac{1}{\alpha P}$$

$$\beta = \frac{K_A}{k} \rightarrow K_A = \beta k = \frac{\beta}{\alpha} \cdot \frac{1}{P}$$

In this case:

$$k = \frac{1}{5.05 \cdot 10^2 \cdot 68} = 2.92 \cdot 10^{-5} \text{ moles/mm Hg sec}$$

$$K_A = 7.5 \cdot 10^2 \cdot 2.92 \cdot 10^{-5} = 2.19 \cdot 10^{-2} \text{ 1/mm Hg}$$

If $K_{B_1} \neq 0$, the values of k, K_A and K_{B_1} cannot be calculated separately.

If component B_2 (hydrogen) is adsorbed, the rate equation is the following:

$$W = \frac{p_A}{a + bp_A + dp_{B_2}}$$

The corresponding kinetic equation is:

$$W = k \frac{p_A}{1 + K_A p_A + K_{B_2} p_{B_2}}$$

In a similar manner to the foregoing:

$$a = \frac{1}{k} \qquad b = \frac{K_A}{k} \qquad d = \frac{K_{B_2}}{k}$$

further

$$\alpha = \frac{a}{P} + \frac{2}{3} d = \frac{1}{k} \left(\frac{1}{P} + \frac{2}{3} K_{B_2}\right)$$

$$\beta = b - \frac{2}{3} d = \frac{1}{k} \left(K_A - \frac{2}{3} K_{B_2}\right)$$

If K_{B_2} 0, the values of k and K_A are identical to those calculated in the foregoing; the values of the physical constants cannot be calculated in the opposite case.

Accordingly, on the basis of the kinetic studies it can be concluded that the dehydrogenation proceeds through the following stages:

1. Adsorption on the catalyst.
2. Chemical reaction on the surface.
3. Desorption.

An analysis of the kinetic equation obtained leads to the following conclusions:

1. The global reaction rate is, through the rate constant, propotional to the surface of the catalyst ($k = F(S_o)\vec{k} K_A$). Accordingly it is preferable to use a dehydrogenating catalyst of as high a specific surface as possible.

2. At low tetrahydrothiophene partial pressures the kinetic equation becomes simpler (the value of $K_A p_A$ may be neglected) and the reaction rate is proportional to the partial pressure of tetrahydrothiophene:

$$W = k \cdot p_A$$

Industrial realization of this condition is uneconomic.

3. Side reactions are negligible at lower temperatures. At the same time, desorption of the products may be accelerated by elevation of the temperature.

The experimental results make it possible to determine the data necessary for reactor design in further experiments carried out on a pilot plant scale.

LIST OF SYMBOLS

A_i	starting components of the reaction
B_i	components of the reaction product
B	mass rate of gas stream (g/sec)
d	density (g/cm^3)
K_{A_i}, K_{B_i}	adsorption equilibrium constants of the components (1/mm Hg)
M	molecular weight
m_s	mass of catalyst (g)
P_{A_i}, P_{B_i}	partial pressures of the components (mm Hg)
P	gas area pressure (mm Hg)
S	volumetric rate of gas stream (g/g sec)
t	time of reaction (sec)
V	catalyst volume (cm^3)
w	specific reaction rate (moles/g sec)

W	reaction rate (moles/sec)
x	conversion (dimensionless)
y_{A_i}, y_{B_i}	concentration of components (moles/g)

REFERENCES

1. FOERST, W., Ullmanns Encyklopädie der technischen Chemie. Vol. XVII. Munich, Urban-Schwarzenberg 1966.
2. SOROKIN, A.N., Khim. Seraorgan. Soedin., Soderzhashch. v Neft. i Nefteprod., Akad. Nauk SSSR, Bashkirsk. Filial 6, 218 (1964)
3. Kratkaya Khimicheskaya Enciklopedia 5, 167. Moscow, Izd. "Sovietskaya Enciklopedia", 1967.
4. TAYTS, S., Khim. Seraorgan. Soedin., Soderzhashch. v Neft. i Nefteprod., Akad. Nauk SSSR, Bashkirsk. Filial 6, 133 (1964)
5. YURIEV, Yu.K., BORISOV, A.E., Zh. Obshch. Khim. 7, 138 (1937)
6. YURIEV, Yu.K., TRONOVA, V.A., Zh. Obshch. Khim. 19, 742 (1949)
7. HIRAO, I., HATTA, H., J. Pharm. Soc. Japan 74, 446 (1954)
8. FRIEDMANN, W., J. Inst. Petroleum 37, 239 (1951)
9. OBOLENTSEV, R.D., GABDULLINA, L.N., GAILYUNAS, G.A., GAISINA,M.G., Khim. Seraorgan. Soedin., Soderzhashch. v Neft. i Nefteprod., Akad. Nauk SSSR, Bashkirsk. Filial 7, 148 (1964)
10. MASHKINA, A.V., SUKHAREVA, T.S., CHERNOV, V.I., Neftekhimiya 7, 301 (1967)
11. LISZI, J., Fizikai-kémiai számitások III. (Physico-Chemical Calculations, III.) Veszprém, Egyetemi Nyomda, 1965.
12. SZABÓ, Z., Kontakt katalizis. Budapest, Akadémiai Kiadó, 1966.

РЕЗЮМЕ

Авторами были изучены термодинамические условия дегидрогенизации тетрагидротиофена. При стандартных условиях реакции были выполнены опыты с применением катализаторов из металла, окиси металла или сульфида металла различного типа, произведенных и в промышленном масштабе, с целью повышения скорости равновесной реакции.

При использовании соответственно выбранного катализатора проводились измерения для определения кинетики реакции. Согласно расчетам авторов, частным процессом определяющим скорость является поверхностная реакция.

Hungarian Journal
of Industrial Chemistry
Veszprém
Vol.1. pp. 141-162 (1973)

BEITRAG ZUR ANWENDUNG DER DÜNNSCHICHTAPPARATE

A. UJHIDY und R. BERKES

(Forschungsinstitut für Technische Chemie der
Ungarischen Akademie der Wissenschaften, Veszprém)

Eingegangen am 18. August 1972.

Bei der Anwendung von Rotationsdünnschichtapparaten können Fälle (z.B. Eindampfung, chemische Reaktionen) vorkommen, wo keine Möglichkeit zur Messung der Filmdicke besteht. In solchen Fällen wird die Filmdicke aus den zweckmässig umgeformten Zusammenhängen von NUSSELT, BRÖTZ und MATOLCSY berechnet. Die Ergebnisse dieser Berechnungen wurden mit aus Versuchsergebnissen bestimmten Filmdicken verglichen. Die Versuche wurden mit Starrflügelrotor und Wischer in Rotationsdünnschichtapparaten von verschiedenen Größen (aktive Oberfläche des Apparates: 0,0396; 0,0578; 0,1140; 0,1260; 0,63; 5,53 m^2) durchgeführt.

Die Kenntnis der Filmdicke ist auch bei der Wasserdampfdestillation erforderlich, weil sie über die Stoff- und Wärmeübertragung und die Leistung des Apparates Aufschluß gibt. Bei den Versuchen wurde die Anwendbarkeit der verschiedenen Verfahren, wie z.B. Rührgefäß, Freifallfilm und Rotationsdünnschichtverfahren, zur Wasserdampfdestillation untersucht. Aus den Untersuchungen konnten einige Hinweise für eine günstigere Durchführung der Wasserdampfdestillation gewonnen werden.

FILMDICKE

Bei mechanisch erzeugten Flüssigkeitsfilmen ist die direkte Messung der Filmdicke sehr umständlich. Die mittlere Filmdicke kann aber aus dem gemessenen Hold-up (H) und aus der aktiven Ober-

fläche des Apparates (F) errechnet werden:

$$\delta = \frac{H}{F} \qquad (1)$$

Anhand dieser Methode hat SCHNEIDER [1] festgestellt, daß mit der Steigerung des Zuflusses und der Zähigkeit die Filmdicke zunimmt, aber von der Umlaufgeschwindigkeit unabhängig ist. Seine Messungen wurden nur mit Wischerrotor durchgeführt.

Eine ähnliche Erscheinung wurde auch von DIETER [2] beobachtet, der die Messungen mit einem Wischerrotor und mit Wasser durchgeführt hat. Die Filmdicke verändert sich vermutlich wegen der praktisch nur zur Filmausbildung notwendigen niedrigen Umlaufgeschwindigkeit (47,2 - 188 m min^{-1}) nicht. Das wird bestätigt dadurch, daß die Filmdicke bei höherer Zähigkeit (8 und 30 cP) und bei höheren Umlaufgeschwindigkeiten als die erwähnten (188-263 m min^{-1}) durch Erhöhung der Umlaufgeschwindigkeit eindeutig zunimmt.

DOMANSZKIJ und Mitarbeiter [3] haben auf Grund der Ergebnisse der mit einem Starrflügelrotor durchgeführten Versuche festgestellt, daß die Filmdicke durch Erhöhung der Umlaufgeschwindigkeit, des Zuflusses und der Zähigkeit eindeutig zunimmt. Die Flügelzahl und die Spaltbreite beeinflussen die Filmdicke, dieser Einfluß ist aber sehr gering.

Nach Messungen von BRESSLER [4] nähert sich die Filmdicke durch Erhöhung der Umlaufgeschwindigkeit des Starrflügelrotors von unten nach oben einem Grenzwert, hingegen erreicht die Filmdicke im Falle des Wischerrotors demselben Grenzwert von oben nach unten. Über diesem Grenzwert wurde kein Unterschied zwischen dem Starrflügel und Wischerrotor festgestellt.

Aus den vorher Mitgeteilten geht hervor, daß die Feststellungen der verschiedenen Verfasser über die Änderung der Filmdicke im Falle der mechanisch erzeugten Flüssigkeitsfilmen einander widersprechen. Deshalb wurden eigene Versuche durchgeführt, um diese Fragen zu klären.

Wir haben auf Grund unserer Versuchsergebnisse festgestellt, daß die Filmdicke im Falle der in den Versuchen angewandten Rotortypen (starrer Flügel und Wischer) durch Erhöhung der Umlaufgeschwindigkeit, des Zuflusses und der Zähigkeit eindeutig zunimmt [5-10]. Bei der Prüfung des Einflusses des Rotortypes stellte es sich heraus, daß die Filmdicke bei dem Starrflügelrotor größer als bei dem Wischerrotor ist. Falls der Flüssigkeitsfilm im Falle des starren Flügels die Spaltbreite ausfüllt, das heißt, die Flügelkanten in den Flüssigkeitsfilm hineintauchen, üben die starren Flügel eine ähnliche Wirkung wie der Wischer aus.

Die aus dem gemessenen Hold-up errechnete Filmdicke nimmt um etwa 8-15 % im Bereich der Umlaufgeschwindigkeit von 80-250 m min^{-1}, während im Bereich der Umlaufgeschwindigkeit von 200-500 m min^{-1} um 10-25 % zu [6, 7, 8]. In praktischer Hinsicht ist dieser letztere Umlaufgeschwindigkeitsbereich, wo die Dünnschichtapparate entweder als Verdampfer, oder als Reaktor, sowohl in laboratoriums-, als auch in Industriegröße zweckmässig betrieben werden können.

Es kann letzten Endes festgestellt werden, daß nur der Zufluß und die Zähigkeit auf die Filmdicke entscheidend wirken, und die Rolle des Flügeltypes, der Flügelzahl und der Spaltbreite viel weniger maßgebend ist [3, 10, 11].

Bei der Anwendung der Rotationsdünnschichtapparate kann ein solcher Fall vorkommen, wo keine Möglichkeit zur Messung des Hold-up besteht, zum Beispiel bei der Eindampfung, wo bei der augenblicklichen Abbrechnung des Zuflusses die ebenso schnelle Abbrechnung der Wärmezufuhr nicht zu verwirklichen ist. Deshalb verhindert die weiterlaufende Verdunstung die Messung des Hold-up.

Eine Möglichkeit für die rechnerische Erfassung der Filmdicke bietet die Verwendung der Zusammenhänge von NUSSELT, BRÖTZ und MATOLCSY [12-15].

Nach einer anderen Methode wird analog zur Strömung im Rohr auch für die Filmströmung aus dem durch die Reibung erzwungenen Druckverlust ein Reibungskoeffizient berechnet, den man zur Errechnung der Filmdicke zu Hilfe nehmen kann [5, 16, 17].

Zur Prüfung der Reproduzierbarkeit der Messungen wurde die Filmdicke nicht nur in einem gegebenen Apparat, sondern auch in den in Tabelle 1. aufgeführten verschiedenen Apparaten untersucht [4, 6. 7, 9, 10].Dadurch wurden auch Wirkungen wie zum Beispiel die Ausknickung und Zentrierung der Welle beseitigt, welche die gleichmäßige Filmausbildung verhindern. Zur Errechnung der Filmdicke können auf diese Weise die von NUSSELT und MATOLCSY angegebenen von uns zweckmäßig umgeformten Zusammenhänge [12-15] mit hinreichender Sicherheit verwendet werden.

Abbildung 1. und 2. zeigen den Einfluß der Flüssigkeitsbelastung auf die Filmdicke im Falle verschiedener Flügelumlaufge-

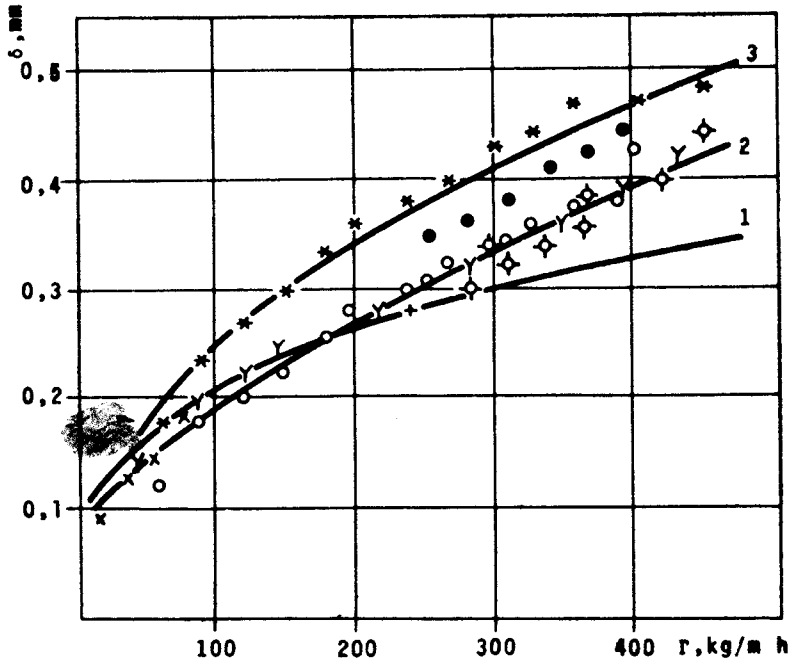

Bild 1. Abhängigkeit der Filmdicke von der Flüssigkeitsbelastung im Falle der verschiedenen Dünnschichtapparate.Rotortyp: starrer Flügel; Zähigkeit: 1,05 cP.Umlaufgeschwindigkeit: 1, 2: 250 m/min; 3: 475 m/min. 1: mit dem Nusseltschen Zusammenhang berechnet; 2, 3: mit dem Matolcsyschen Zusammenhang berechnet.

Tabelle 1. Abmessungen der in den Versuchen angewandten Dünnschichtapparate und die zu diesen gehörenden Bezeichnungen zur Messung der Filmdicke

Bezeichnung des Apparates	Durchmesser (mm)	Aktive Oberfläche (m^2)	Flügeltyp	Spaltbreite (mm)	Wandstärke (mm)	Bezeichnung 250 m/min	Bezeichnung 500 m/min
I	51,9	0,0396	Wischer starr	0,25; 0,70	4,0	x	
II	53,3	0,0578	Wischer starr	0,35	1,5	Y	
III	57,5	0,1140	starr	0,50	4,0	✧	•
IV	80,0	0,1260	Wischer starr	0,40	3,7	o□	* •
V	208,0	0,6300	Wischer	-	4,0	+	
VI	560,0	5,5300	Wischer	-	8,0		Δ

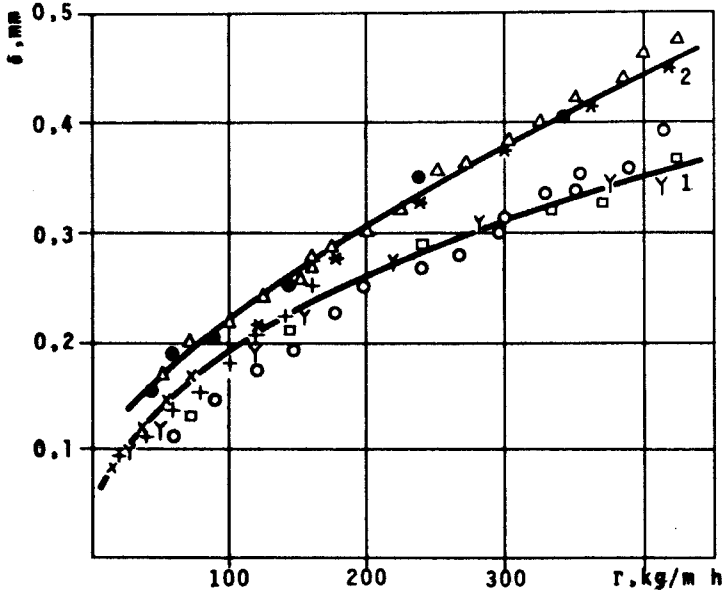

Bild 2. Die Filmdicke in Abhängigkeit von der Flüssigkeitsbelastung bei verschiedenen Dünnschichtapparate-Rotortyp: Wische Zähigkeit: 1,05 cP. Umlaufgeschwindigkeit 1: 250 m/min; 2: 500 m/min. 1, 2: aufgrund des Zusammenhanges von Matolcsy berechnet.

schwindigkeiten und verschiedener Abmessung der Apparate. Die Punkte, bzw. Zeichen sind gemessene Werte, die Kurven wurden berechnet.

Bei Verwendung von Starrflügelrotor kann bis zu einer Flüssigkeitsbelastung von 250 kg/m h und einer Flügelumlaufgeschwindigkeit von 300 m min^{-1}, Im Zähigkeitsbereich von 1-4 cP auch der für Rieselfilme gültige Zusammenhang von Nusselt zur Errechnung der Filmdicke benutzt werden.

$$\delta = \sqrt[3]{\frac{3\,\eta\,G}{\rho^2 g\,\pi\,D}} \qquad (2)$$

wobei

g Erdbeschleunigung ($m\ s^{-2}$)
G Zufluß ($kg\ s^{-1}$)
D Durchmesser (m)
δ Filmdicke (m)
η dynamische Zähigkeit ($kg\ m^{-1}\ s^{-1}$)
ρ Dichte ($kg\ m^{-3}$)

In diesem Bereich hat der Flügel wegen der kleinen Filmdicke in erster Linie für die Ausbildung und Stabilisierung des Filmes zu sorgen.

Im Bereich über der erwähnten Flüssigkeitsbelastung bis zu einer Umlaufgeschwindigkeit von 300 $m\ min^{-1}$ kann der mit einer modifizierten Konstanten korrigierte Zusammenhang von Matolcsy zur Errechnung der Filmdicke benutzt werden (die ursprüngliche Konstante: $5 \cdot 10^{-2}$):

$$\delta = f' \sqrt{\frac{\Gamma \nu}{\rho g}} \qquad (3)$$

wobei

f' modifizierte Konstante (-)
Γ Flüssigkeitsbelastung ($kg\ m^{-1} s^{-1}$)
v Flügelumlaufgeschwindigkeit ($m\ s^{-1}$)

Die modifizierten Konstanten des Matolcsyschen Zusammenhanges zur Errechnung der Filmdicke wurden im Bereich der Zähigkeit von 1-4 cP in Tabelle 2 zusammengefasst.

Tabelle 2

	Starrer Flügel		Wischer	
v ($m\ min^{-1}$)	200-300	300-500	200-300	300-500
f'	$5{,}5 \cdot 10^{-2}$	$5 \cdot 10^{-2}$	$5 \cdot 10^{-2}$	$4{,}35 \cdot 10^{-2}$

Der Matolcsysche Zusammenhang, Gleichung (3), wurde ursprünglich für Wischerrotor entwickelt. Dieser Zusammenhang ist auch im Falle des Starrflügelrotors im Bereich der erwähnten Flüssigkeitsbelastung und Umlaufgeschwindigkeit brauchbar, da der Flüssigkeitsfilm die Spaltbreite schon praktisch voll ausfüllt, so daß starre Flügel wie Wischer wirken.

Diese Feststellung wird dadurch bestätigt, daß derselbe Zusammenhang auch im Falle von starren Flügeln im Bereich der Umlaufgeschwindigkeit von 300-500 m min^{-1} anzuwenden ist genauso wie im Falle des Wischerrotors bis zu einer Umlaufgeschwindigkeit von 300 m min^{-1}.

Beim Wischerrotor ist die Filmdicke im Bereich der Umlaufgeschwindigkeit von 300-500 m min^{-1} ebenfalls mit dem modifizierten Matolcsyschen Zusammenhang zu errechnen.

Der Zusammenhang von Matolcsy ist nur im turbulenten Bereich gültig. Dieser Zusammenhang kann über einer Zähigkeit von 5 cP nicht benutzt werden, da die Strömung bei der in Dünnschichtapparaten gebräuchlichen Flüssigkeitsbelastung und Flügelumlaufgeschwindigkeit schon laminar ist. In solchen Fällen kann der mit einer geeigneten Konstanten korrigierte Zusammenhang von Nusselt, der auch die Zähigkeitveränderung in Betracht zieht, angewandt werden.

Die Korrektionsfaktoren des Nusseltschen Zusammenhanges wurden zur Errechnung der Filmdicke, über Zähigkeiten von 5 cP, in Tabelle 3 zusammengefasst.

Tabelle 3

	Starrer Flügel			Wischer		
η (cP)	4,8	18,6	53,3	4,8	18,6	53,3
f"	1,10	0,855	0,670	0,756	0,585	0,504

Aus den Gesagten ist also zu entnehmen, daß die Flüssigkeitsbelastung und die Zähigkeit die Filmdicke entscheidend beeinflussen. Diese Feststellung bezieht sich auf Flügelumlaufgeschwindigkeiten und Flüssigkeitsbelastungen,die die häufigsten Betriebsparameter von Dünnschichtapparaten (als Verdampfer oder als Reaktor) darstellen.

Bei Durchführung der Eindampfung, Destillation, chemischen Reaktionen und anderer Operationen gibt die Filmdicke Aufschluß über die Strömungsverhältnisse des Flüssigkeitsfilms. Die Leistung des Apparates hängt von der guten Ausnutzung der Oberfläche ab, vorausgesetzt, daß die Benetzung gleichmäßig ist, und der Flüssigkeitsfilm noch nicht so dick ist, daß die filmartige Strömung der Flüssigkeit nicht mehr bestehen würde. Die Erhöhung der Filmdicke führt aber zur Verschlechterung der Stoff- und Wärmeübertragung.

Auch in zwei extremen Fällen der in einem Rotationsdünnschichtapparat durchgeführten Wasserdampfdestillation spielt die Filmdicke eine wichtige Rolle, und zwar, wenn eine kleine Menge der flüchtigen Komponente von großer Menge der nichtflüchtigen Komponente getrennt werden muß, oder wenn die praktisch ganze Menge des zu destillierenden Stoffes flüchtig ist.

WASSERDAMPFDESTILLATION IM DÜNNSCHICHTAPPARAT

Das bekannteste Beispiel für die Trägerdampfdestillation [18, 19] ist die Wasserdampfdestillation von hochsiedenden hitzeempfindlichen Substanzen.Da Wasserdampf als Trägerdampf für viele organische Flüssigkeiten geeignet ist und verwendet wird, spricht man in diesen Fällen von Wasserdampfdestillation. Die Zufuhr des Wasserdampfes hat einmal den Zweck,die destillierbaren Anteile eines Gemisches vom nichtflüchtigen Rückstand abzutrennen und zum anderen zusätzlich den Vorteil, daß eine Siedetemperaturerniedrigung eintritt und damit eine thermisch schonende Behandlung erreicht wird.

Die Wasserdampfdestillation wird besonders zur Reinigung und Trennung von wasserunlöslichen oder nur wenig wasserlöslichen Substanzen unter Normaldruck oder Vakuum in Gleichstrom- oder Gegenstromverfahren angewandt, wie z.B. zur Destillation von Fettsäuren, Fettalkoholen, ätherischen Ölen, Anilin, Tallöl, Benzine, Teerfraktionen usw. Die Steinkohlenteerdestillation verwendet z.B. aus Kohlendioxyd, Stickstoff und Wasserdampf bestehende Abgase als Trägerdampf [19-26].

Das Verfahren der Destillation mit überhitztem Wasserdampf wird in der Technik häufig benutzt, um die Flüchtigkeit hochsiedender Verbindungen zu erhöhen bzw. deren Siedepunkt zu erniedrigen. Diese Methode unterscheidet sich wesentlich von der üblichen Wasserdampfdestillation, bei der ein gesättigter Wasserdampf-Strom in die mit Wasserdampf zu übertreibende Flüssigkeit eingeleitet wird. Die Destillation mit überhitztem, d.h. ungesättigtem Wasserdampf eignet sich infolge der durch den Dampf-Zusatz erzwungenen Temperatur-Erniedrigung innerhalb des Bereiches guter Trennbarkeit besonders zur Trennung hochsiedender Stoffgemische [27, 28]. Zum Unterschied gegenüber der Destillation mit gesättigtem Dampf läßt sich aber nicht nur der Destillationsdruck, bzw. die Destillationtemperatur, sondern auch die Zusammensetzung des Dampfgemisches, d.h. die Wasserdampf-Zufuhr, genau einstellen.

Das theoretische Maßverhältnis der flüchtigen Komponente, G_S zu Wasser G_{DT} im anfallenden Destillat beschreibt Formel (4) [18, 27, 29, 30]:

$$\frac{G_S}{G_{DT}} = \frac{p_S \, M_S}{p_D \, M_W} \qquad (4)$$

wobei p_D, p_S Partialdruck des Wasserdampfes, bzw. des Dampfes des überdestillierten Stoffes, Torr;

M_S, M_W Molekulargewicht des überdestillierten Stoffes und des Wassers.

Bei diskontinuierlicher Wasserdampfdestillation beschreibt Formel (5) die theoretisch notwendige Menge des Wasserdampfes zu einer gewünschten Endkonzentration der flüchtigen Komponente. Bei

dieser Gleichung wird in Betracht gezogen, daß sich der Partialdruck der flüchtigen Komponente mit der Abnahme ihrer Konzentration vermindernt [31-34].

$$G_{DT} = 18 \left(\frac{P}{P_A} - 1\right)(A_1 - A_2) + \frac{P\,N}{P_A} \ln \frac{A_1}{A_2} \qquad (5)$$

wobei

G_{DT} die theoretisch erforderliche Menge des Wasserdampfes, g;

P Gesamtdruck, Torr;

P_A Druck der flüchtigen Komponente, Torr;

A_1 Anfangs-Menge der flüchtigen Komponente, Mol;

A_2 Endmenge der flüchtigen Komponente, Mol;

N Molenzahl der nichtflüchtigen Komponente.

Zur Untersuchung wählten wir als Versuchsgemisch das System Paraffinöl-Nitrobenzol.Die Nitrobenzolkonzentration war etwa 10 %. Die Gleichgewichtskurve des Gemisches wurde nach OTHMER bestimmt.

Es stellte sich heraus, daß eine positive Abweichung von dem Raoultschen Gesetz vorliegt. Deshalb wurden die Werte von P_A aufgrund der Gleichgewichtskurve berechnet.

Im Falle des kontinuierlichen Gegenstromverfahrens wurde die theoretisch notwendige Menge des Wasserdampfes mit Hilfe der Gleichung (6) berechnet.Diese Gleichung kann ausgehend von der Stoffbilanz und Gleichung (4) abgeleitet werden.

$$G_{DT} = 18 \left(\frac{P}{P_S} - 1\right)(A_1 - A_2) \qquad (6)$$

Meistens ist das entstehende Dampfgemisch infolge ungenügender Gleichgewichtseinstellung nicht vollständig mit der flüchtigen Komponente gesättigt. Deshalb muß man mit einer Sättigungszahl (φ) rechnen.

Die Sättigungszahl ist der Quotient der theoretisch benötigten und der praktisch eingeleiteten Menge des Wasserdampfes.

Die Versuche wurden teils in einem diskontinuierlich betriebenen Rührkessel von 2,5 ℓ Inhalt, teils kontinuierlich in einem

Dünnschichtapparat von 0,12 m^2 Heizfläche (Durchmesser: 81 mm) durchgeführt. Der Rührkessel befand sich in einem Thermostat, so konnte man die Kondensation des Wasserdampfes völlig vermeiden. Der Dampfüberhitzer wurde zwischen der Dampfleitung und dem Rührkessel untergebracht und mittels eines Ölbades auf die gewünschte Temperatur gebracht. Die Proben wurden von Zeit zu Zeit genommen,. als sowohl das Gemisch Paraffinöl-Nitrobenzol als auch der überhitzte Dampf die gewünschte und gleiche Temperatur erreichten. Die Nitrobenzol-Gehalte der Proben wurden UV spektrophotometrisch bestimmt.

Der auf die flüchtige Komponente bezogene Wirkungsgrad (η) gibt die übergetriebene Menge in Prozenten an.

Die kontinuierlichen Versuche wurden in einem Dünnschichtapparat vorgenommen. Den Dünnschichtapparat konnte man auch als Freifallfilmapparat einsetzen. Die Versuchsanordnung ist im Bild 3 schematisch dargestellt. Das zu verdampfende vorgewärmte Substanzgemisch wurde aus dem Behälter E mittels einer Dosierpumpe F durch den Stutzen 1 gegen einen umlaufenden Verteilerring gedrückt, der die Flüssigkeit an die Innenseite des Verdampferrohres schleuderte und dadurch für eine gleichmäßige Aufgabe sorgte. Der Zyklon C war zwischen der Dampfleitung und dem Überhitzer D eingebaut, und der überhitzte Wasserdampf wurde durch den Stutzen 3 in den Apparat eingeleitet. Die aufsteigenden Dämpfe traten oben über einen Tropfenabscheider 10 in den Brüdenstutzen 5 und wurden von dort aus zum Kondensator B geleitet. Die nicht verdampften Rückstände sammelten sich unten zusammen und verließen die Apparatur über den Stutzen 4. Die Verdampfungswärme der flüchtigen Komponenten wurde durch den in den Heizmantel eingeleiteten Dampf zugeleitet.

Zur Erzeugung eines turbulenten Filmes standen drei Rührerarten zur Verfügung. Im ersten Fall waren die Flügel als bewegliche, die Wand des Apparates ständig abstreifende Wischer ausgebildet. Das Wischer System Typ Sambay [1, 11] wurde so konstruiert, daß die Flügel in erster Linie die herunterfließende Flüssigkeit und nicht die Wasserdämpfe rührten. Im zweiten Fall waren die Flügel fest an der Welle befestigt [35, 36], und bewegten sich in 0,5 mm Entfernung von der Apparatewand. So wurde in erster Linie der

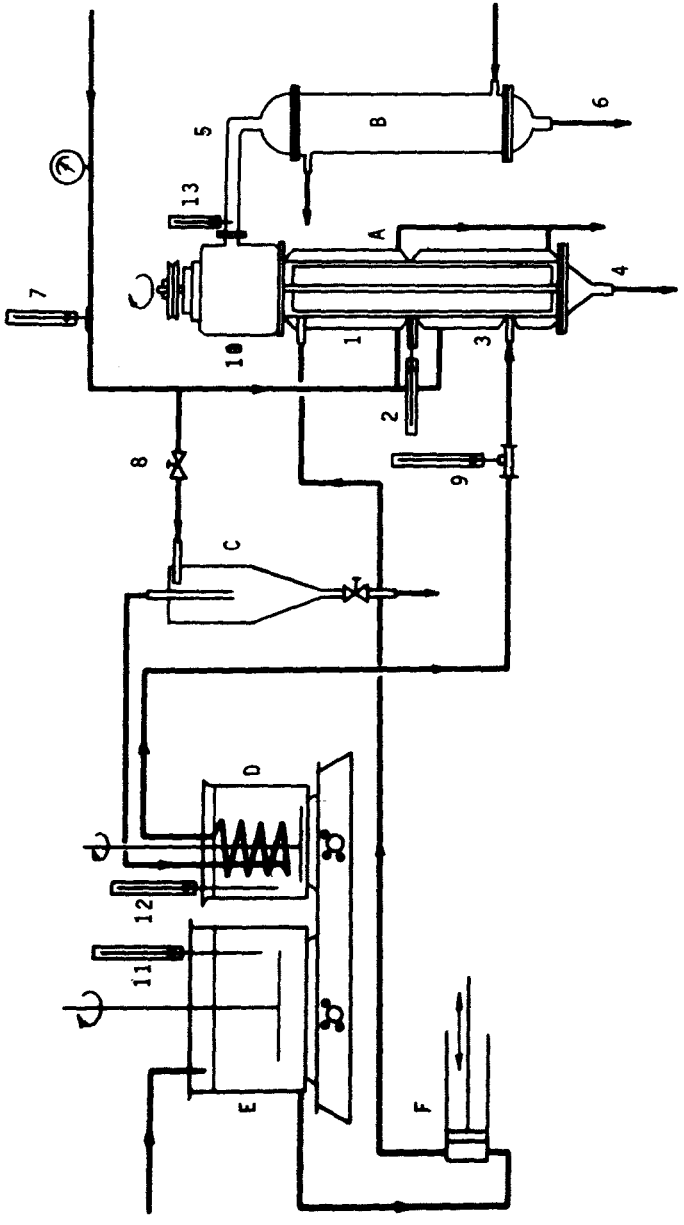

Bild 3. A: Dünnschichtapparat; 1: Zuführstutzen für Modell- 6: Ablaufrohr für Modell-
B: Kondensator; gemisch; gemisch-Wasser;
C: Zyklon; 3: Zuführstutzen für über- 8: Dosierventil für Dampf;
D: Dampfüberhitzer; hitztes Wasserdampf; 10: Tropfenabscheider;
E: Behälter für Modellgemisch; 4: Ablaufrohr für Rückstand; 2, 7, 9, 11, 12, 13:
F: Dosierpumpe; 5: Brüterstutzen; Thermometerstutzen.

Dampf gerührt und die Flüssigkeit mit diesem Dampf in Berührung gebracht. Im dritten Fall waren horizontale Verengungsplatten in den rotierenden Teil der starren Flügel eingebaut [37, 38, 39]. Die Strömungsgeschwindigkeit der Dämpfe steigt in der Nähe der Verengungsplatte wesentlich an, wodurch der Stoffübergang zwischen Dampf und Flüssigkeit verbessert wird.

Die auf den Bildern dargestellten Punkte sind Durchschnittswerte von mehreren parallelen Meßwerten. Im Bild 4 ist der Wir-

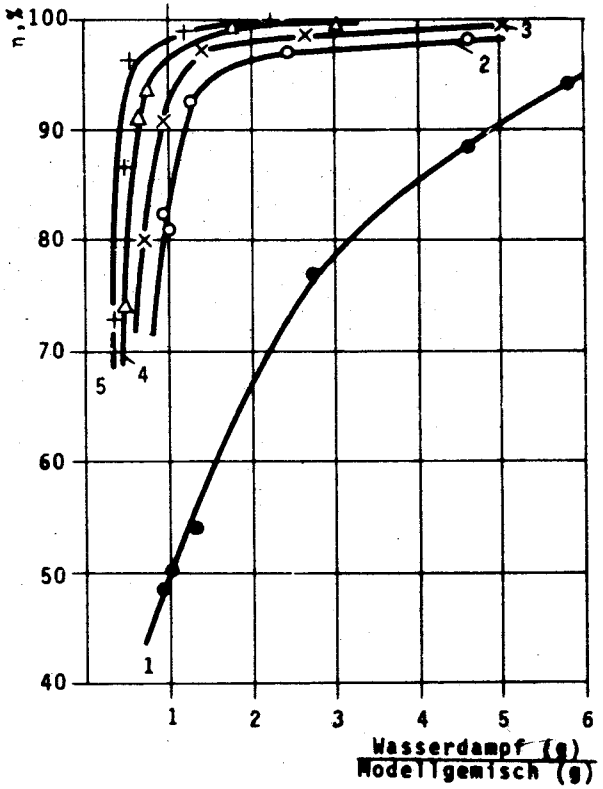

Bild 4. Abhängigkeit des Wirkungsgrads vom $\frac{WD}{M}$ Verhältnis bei verschiedenen Rührwerken. Umlaufgeschwindigkeit: 470 m min^{-1}; t = 126 °C. 1 - Freifallfilm; 2 - Wischer; 3 - starrer Flügel; 4-5 - Rührwerk mit Verengungsplatten

kungsgrad als Funktion des Wasserdampf-Modellgemisch-Verhältnisses bei der Anwendung von Wischern, starren Flügeln, starren Flügeln mit Verengungsplatten und Freifallfilmapparat dargestellt. Die Zufuhr des Wasserdampfes war konstant und zwar 275 g min^{-1}, ausgenommen die Versuche mit Verengungsplatten, wo dieser Wert infolge Flooding 150 g min^{-1} war.

Es ist ersichtlich, daß der Wirkungsgrad beim Freifallfilm viel geringer ist als bei der gerührten Dünnschicht. Es stellte sich heraus, daß der Wirkungsgrad sich beim gerührten Flüssigkeitsfilmen mit dem Typ der Rührwerk etwas verändert. In erster Linie kommt die vorteilhafte Wirkung des mit Verengungsplatten ausgestatteten Flügels zur Geltung. Der Unterschied zwischen den Wischern und starren Flügeln ist nicht sehr ausgeprägt. Die Kurve 5. bezieht sich auf die Versuchsergebnisse bei der Anwendung eines sieben Verengungsplatten tragenden Rührwerkes und die Kurve 4 zeigt die Meßwerte des mit drei Verengungsplatten ausgestatteten Rührwerkes. Der günstige Einfluß des mit Verengungsplatten ausgestatteten Rührwerkes konnte darauf zurückgeführt werden, daß der Kontakt und der Stoffübergang zwischen den Dämpfen und der an der Wand abwärts fließenden Flüssigkeit verbessert wird.

Bild 5 zeigt die Sättigungszahl, bezogen auf das Verhältnis zwischen dem Wasserdampf und dem Modellgemisch unter Anwendung der erwähnten Methoden. Wesentliche Unterschiede konnten nur zwischen Freifall- und gerührtem Film festgestellt werden.

Bild 6 und Bild 7 zeigen die Änderung des Wirkungsgrades und der Sättigungszahl in Abhängigkeit vom Wasserdampf-Modellgemisch-Verhältnis bei verschiedenen Umlaufgeschwindigkeiten des starren Flügelsystems. Der Wirkungsgrad und die Sättigungszahl nehmen bei der Erhöhung der Umlaufgeschwindigkeit zu. Dieser Effekt ist viel geringer beim Wischersystem. Bei Verengungsplatten kann man höchstens von einer ähnlichen Tendenz sprechen.

Die Leistung des Dünnschichtapparates wurde ebenfalls bestimmt. Es wurde festgestellt, daß unter 92-97 prozentigem Wirkungsgrad und 1:1 Dampf-Flüssigkeit-Verhältnis eine Oberflächen-

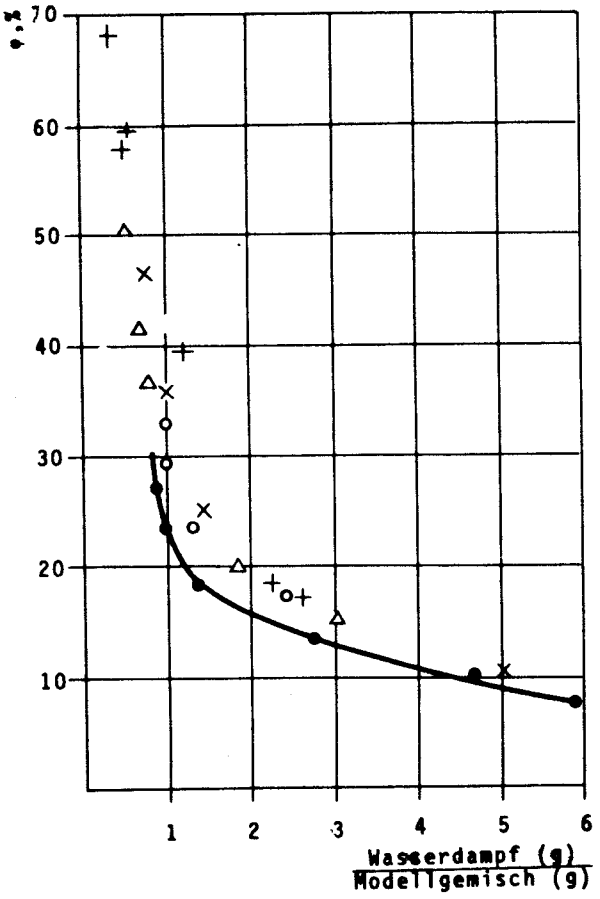

Bild 5. Änderung der Sättigungszahl in Abhängigkeit vom $\frac{WD}{M}$ Verhältnis bei verschiedenen Rührwerken. Umlaufgeschwindigkeit: 470 m min^{-1}; t = 126°C. o - Wischer; x - starrer Flügel; Δ + - Rührwerk mit Verengungsplatten; • - Freifallfilm.

belastung von 200 kg Modellgemisch/h m^2 erreicht werden kann. Es ist noch zu betonen, daß die mittlere Verweilzeit unter den erwähnten Bedingungen etwa 30-50 Sekunden beträgt.

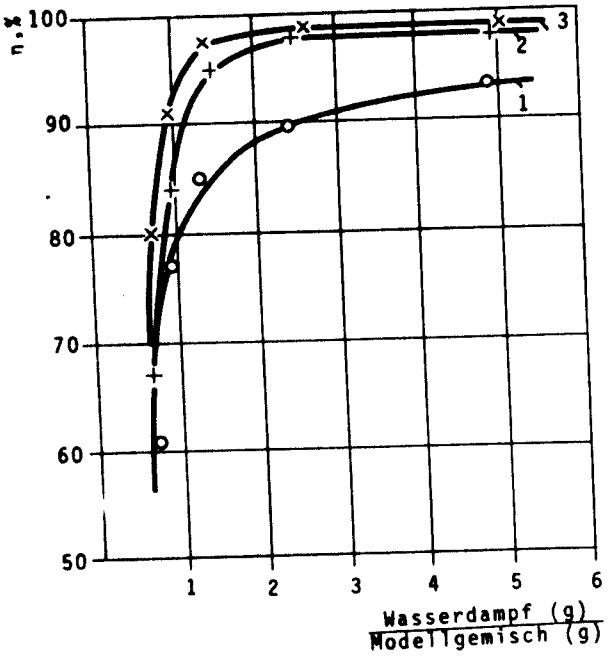

Bild 6. Abhängigkeit des Wirkungsgrads vom $\frac{WD}{M}$ Verhältnis bei verschiedenen Umlaufgeschwindigkeiten des starren Flügels. t = 126 °C. Umlaufgeschwindigkeit: 1: 210 m min^{-1}; 2: 325 m min^{-1}; 3: 470 m min^{-1}

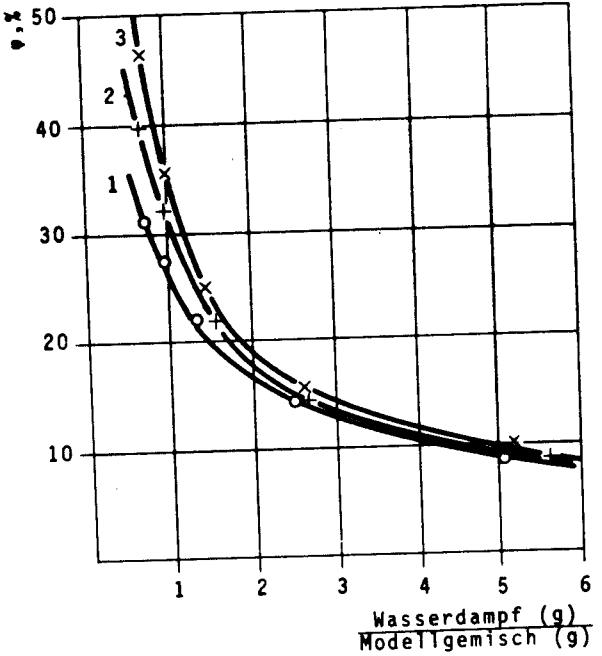

Bild 7. Abhängigkeit der Sättigungszahl von $\frac{WD}{M}$ Verhältnis bei verschiedenen Umlaufgeschwindigkeiten des starren Flügels. t = 126 °C. Umlaufgeschwindigkeit: 1: 210 m min^{-1}; 2: 325 m min^{-1}; 3: 470 m min^{-1}

Vergleicht man die Meßergebnisse der kontinuierlichen Versuche mit denen der diskontinuierlichen, so ist festzustellen, daß die erforderliche Menge des Wasserdampfes unter gleichen Versuchsbedingungen in einem Dünnschichtapparat viel geringer ist. Das ist verständlich, da der Dünnschichtapparat im Gegenstrom arbeitet. Das zeigt Tabelle 4.

Tabelle 4. Vergleich einiger Meßergebnisse von diskontinuierlichen und kontinuierlichen Versuchen

Wirkungsgrad: 75-76 %; t = 126°C.
Wasserdampf-Modellgemisch-Verhältnis: 0,370 g/g.

	Diskontinuierlich	Kontinuierlich	
		starrer Flügel	Verengungsplatten
$\frac{\text{kg Wasserdampf}}{\text{kg Nitrobenzol}}$ theoretisch	16,85	4,16	3,90
$\frac{\text{kg Wasserdampf}}{\text{kg Nitrobenzol}}$ gemessen	17,30	5,00	4,31
Sättigungszahl (%)	97,30	83,40	90,50

Es stellte sich weiterhin heraus, daß die Leistung des Dünnschichtapparates in Vergleich mit dem Rührkessel bezogen auf den Apparaturinhalt etwa 8-10-mal größer ist.

Untersucht man die Sättigungszahl in Abhängigkeit der Ausgangskonzentration der flüchtigen Komponente bei den im Rührkessel durchgeführten Versuchen, so kann man feststellen, daß diese bis zu 1,5 Prozent stark ansteigt (Bild 8).

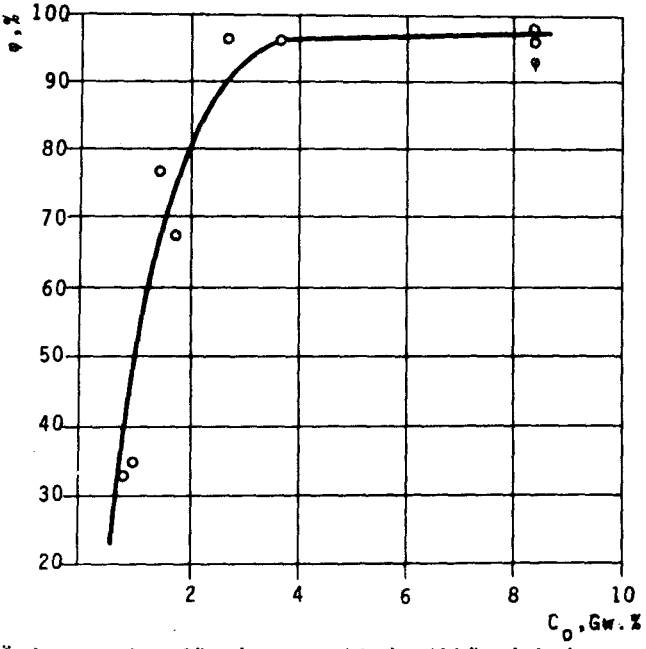

Bild 8. Änderung der Sättigungszahl in Abhängigkeit der Konzentration der flüchtigen Komponente. t = 126°C.

Eine ähnliche Tendenz war auch beim Dünnschichtapparat zu beobachten. Das bedeutet, daß der Stoffübergang besonders bei der Entfernung der unerwünschten flüchtigen Stoffe von geringeren Konzentration eine wichtige Rolle spielt.

LITERATUR

1. SCHNEIDER, R., Chem. Ing. Techn. 27, 259 (1955)

2. DIETER, K., HÜBNER, W., Chemiker-Ztg. 94, 319 (1970)

3. DOMANSZKIJ, I.V., AVBONYKIN, A.F., SOKOLOV, B.N., Zhur. Prikl. Khim. 9, 2009 (1971)

4. BRESSLER, R., Forschungsberichte des Landes Nordheim-Westfalen. Westdeutscher Verlag. Köln. 1960. p. 770.

5. BERKES, R., Müszaki doktori disszertáció. (Dissertation) Veszprém, 1969.

6. BERTY, J., UJHIDY, A., BABOS, B., VIGH, A., Magyar Kémikusok Lapja 12, 101 (1957)

7. UJHIDY, A., BABOS, B., VIGH, A., Magyar Kémikusok Lapja 13, 205 (1958)

8. UNGVÁRY, F., Diplomadolgozat. (Diplomarbeit) Veszprém, 1963.

9. BERKES, R., Diplomadolgozat. (Diplomarbeit) Veszprém, 1967.

10. UJHIDY, A., Kandidátusi disszertáció. (Kandidatendissertation) Veszprém, 1968.

11. UJHIDY, A., BABOS, B., Filmbepárlók, filmreaktorok. (Dünnschichtverdampfer, Dünnschichtreaktoren) Müszaki Könyvkiadó. Budapest, 1967.

12. NUSSELT, W., Z. VDI. 60, 541 (1916)

13. NUSSELT, W., Z. VDI. 67, 206 (1923)

14. BRÖTZ, W., Chem. Ing. Techn. 26, 470 (1954)

15. MATOLCSY, K., Conference on Some Aspects of Physical Chemistry, Budapest. Vol. II. 169 (1966)

16. BRAUER, H., VDI-Forschungsheft 457 22, 6 (1956)

17. BERKES, R., BLICKLE, T., UJHIDY, A., Internation and Calculation of Friction Factor in the Case of Mechanically Agitated Liquid Films. Procedings of the 2nd Conference on Applied Physical Chemistry. Veszprém, August. 2-5. 1971. Vol. 2. p. 179.

18. KIRSCHBAUM, E., Destillier- und Rektifizier Technik, Berlin, 1961. p. 455-456.

19. STAGE, H., Erdöl und Kohle 3, 478 (1950)

20. THORMANN, K., Die Chemische Fabrik. 13, 3 (1940)

21. STAGE, H., Fette-Seifen-Anstrichmittel. 55, 217 (1953)

22. STAGE, H., Ibid. 55, 284 (1953)

23. STAGE, H., Fette-Seifen-Anstrichmittel. 55, 375 (1953)

24. STAGE, H., Ibid. 72, 229 (1970)

25. Schweiz. Pat. 253 949 (1948)

26. US. Pat. 3 151 046 (1964)

27. STAGE, H., Fette-Seifen-Anstrichmittel. 55, 513 (1953)

28. STAGE, H., Ibid. 55, 580 (1953)

29. VOGEL, A.J., A text-book of practical organic chemistry including qualitative organic analysis. Longmans, Green and Co. London, New York, Toronto. 1954. p. 12-16.

30. BELOBORODOV, V.V., Izvesztija Vüszcsih Ucsebnih Zavedenij - Pisevaja Tehnologija. 2, 127 (1967)

31. PERRY, J.H., Chem. Eng. Handbook. McGraw-Hill, New York. 1950. p. 582-584.

32. UJHIDY, A., Müszaki doktori értekezés. (Dissertation) Veszprém, 1960.

33. van WINKLE, M., Distillation. McGraw-Hill, New York. 1967. p. 178-189.

34. CIBOROWSKI, J., A vegyipari müveletek alapjai. (Grundlagen der chemischen Verfahrstechnik) Müszaki Könyvkiadó. Budapest, 1969. p. 391-422.

35. Schweiz. Pat. 305 704 (1952)

36. VERNOIS, G., Seifen-Öle-Fette-Wachse 88, 923 (1962)

37. Magyar szabadalom 152 480 (1962)

38. UJHIDY, A., BABOS, B., FARÁDY, L., Chem. Techn. 18, 652 (1966)

39. UJHIDY, A., BERKES, R., KALAPOS, K., Chem. Techn. 23, 469 (1971)

РЕЗЮМЕ

При применении пленочных роторных аппаратов встречаются случаи (напр. выпаривание, химическая реакция), при которых определение толщины пленки затруднено, или же невозможно. В таких случаях была вычислена толщина пленки из целесообразно преобразованных соотношений НУССЕЛЬТА, БРЕЦ и МАТОЛЬЧИ, которая была сопоставлена с толщиной пленки, определенной из опытных данных. Опыты были выполнены в пленочных роторных аппаратах разных размеров (0,0396; 0,0578; 0,1140; 0,1260; 0,63; 5,53 $м^2$), с применением касающихся и жестких лопастей.

Знание толщины пленки важно и в случае дистилляции с водяным паром, так как получается информация об условиях массо- и теплопередачи, а также и о нагружаемости аппарата. При испытаниях была изучена применимость разных процессов - как например пленочного процесса периодического режима, процесса с пленечным течением и пленочного роторного процесса - для дистилляции с водяным паром. Сведениями опытов была получена информация о том, при каких условиях можно выполнить дистилляцию с водяным паром наиболее преимущественно в случае данного процесса.

Hungarian Journal
of Industrial Chemistry
Veszprém
Vol.1. pp. 163-184 (1973)

ALGEBRAIC DESCRIPTION OF TECHNICAL CHEMICAL SYSTEMS II.*

MATERIAL SYSTEMS AND CHANGES

T. BLICKLE, Mrs. E. BÁTOR and Mrs. Zs. HALÁSZ

(Research Institute for Technical Chemistry of the Hungarian Academy of Sciences, Veszprém)

Received: October 20, 1972.

The material systems of technical chemistry, the changes occurring in these, their interpretation and their mathematical description are presented in this paper.

The qualitative description of the material systems was provided by determining

- the components present in the system,
- the relations between the components and
- the state of the system.

A quantitative description of the systems is presented by a matrix structure.

The technical chemical changes are characterized by the nature and type of the change and so it was possible to define the most important elementary changes.

Technical chemistry deals with material systems and with changes occurring in these [1] and the algebraic description of these will be given in the following.

*The first publication appeared in Hung.J.Ind.Chem. 1, 17 (1973).

DESCRIPTION OF MATERIAL SYSTEMS

Qualitative Description

The starting point for the mathematical formulation of the systems is the following.

The material system is characterized by

- the components present in the system,
- the relations between the components, and
- the state of the system.

According to the above-mentioned characteristics, the material systems can be described by the following mathematical structure:

$$A = A\{\hat{K}, P, T\} \tag{1}$$

where

P - is the pressure,

T - is the temperature,

$\hat{K}$ - is the mathematical structure describing the components and the relations between these components.

The relation between the components may be

- homogenous, such as e.g. in the case of a mixture of liquids or a solution of a solid. The designation of the homogenous relation is the following: $\longrightarrow$
- heterogenous, such as e.g. a liquid dispersed in a gas or a humid solid. The designation of the heterogenous relation is the following: $\longrightarrow$

The components can be characterized by the following structure:

$$K = K\{\alpha_{14}, \alpha_{15}, \alpha_{16}, \beta, \alpha_3, \alpha_4, \alpha_5\} \qquad (2)$$

where the first four elements designate a qualitative, whereas the others a quantitative property:

α_{14} - crystal structure,
α_{15} - chemical structure,
α_{16} - biological structure,
β - the state of the pure components of the material system pertaining to a pressure P and a temperature T. This may be

β_1 - solid
β_2 - liquid
β_3 - gaseous
β_4 - plasma

α_3 - scattering; the distribution of the component in the material system. The distribution may occur according to space co-ordinates or according to time.

The distribution according to space co-ordinates may be characterized by the scattering as used in the probability calculus:

$$\sigma^2 = \frac{\iiint_V (c - \bar{c})^2 \, dv}{\iiint_V dv} \qquad (3)$$

or with the entropy of mixing:

$$s_k = \frac{\iiint_V c \ln c \, dv}{\bar{c} \ln \bar{c} \iiint_V dv} \qquad (4)$$

where

c - is the concentration of the component,
$\bar{c}$ - is the mean concentration of the component,
v - is the volume of the system.

The fluctuation in time of the distribution of the component in a given point is

$$\sigma^2 = \frac{1}{t} \int_0^t (c - \bar{c})^2 \, dt \qquad (5)$$

α^4 - is the characteristic dimension of the state of appearance of the component. Should this not exist, a "zero" is written in the algebraic structure (2) to the corresponding place. The dimension can be described e.g. by the equivalent sphere diameter, mass, volume, surface area, or also by the following expression:

$$\alpha_4^0 = \frac{n}{G} \qquad (6)$$

where

n - is the number of entities in the component,
G - is the mass of the component.

α^5 - form. This can be given by the form factor (φ), by the ratio of characteristic dimensions, etc.

In accordance with Equation (2), a mass of spherical (φ =1) γ-ferric oxide particles, 1 mm in diameter, can be described by the following structure:

$$K_{(\gamma \text{ ferric oxide})} = K\{\gamma, Fe_2O_3 \cdot 0, \beta_1, 0, 1, \varphi = 1\} \qquad (7)$$

It is not always necessary to describe the components by the total mathematical structure. It is sufficient to describe only such elements as are of importance in the given individual case (e.g. which undergo some change in the process where the raw material is transformed to a final product).

If, for example, only the chemical structure of the component is of interest, we may write:

$$K = K\{Fe_2O_3\} \text{ ferric oxide}$$

or if only the state is of importance:

$$K = K\{\beta_1\} \text{ solid component}$$

When writing the expression for the components and the relations between them, the component determining the state of appearance of the system should be written in the first place. If the system is determined not by any one of the components but by their joint entity, the order in which the structure is written is of no consequence. In such a case, the designation of the homogenous relation is $\Longleftrightarrow$ and that of the heterogenous one is $\longleftrightarrow$.

A few examples for the homogenous relation between the components:

liquid mixture: $$\hat{K} = K_1\{\beta_2\} \Longleftrightarrow K_2\{\beta_2\} \quad (8)$$

solution of a solid: $$\hat{K} = K_1\{\beta_2\} \Longrightarrow K_2\{\beta_1\} \quad (9)$$

a solid dissolved in a liquid mixture: $$\hat{K} = [K_1\{\beta_2\} \Longleftrightarrow K_2\{\beta_2\}] \Longrightarrow K_3\{\beta_1\} \quad (10)$$

Examples for a heterogenous relation between the components:

humid solid:

$$\hat{K} = K_2\{\beta_1\} \longrightarrow K_1\{\beta_2\} \quad (11)$$

suspension:

$$\hat{K} = K_1\{\beta_2\} \longrightarrow K_2\{\beta_1\} \quad (12)$$

gas bubbles in a liquid:

$$\hat{K} = K_1\{\beta_2\} \longrightarrow K_2\{\beta_3\} \quad (13)$$

liquid droplets in a gas:

$$\hat{K} = K_2\{\beta_3\} \longrightarrow K_1\{\beta_2\} \quad (14)$$

liquid mixture dispersed in a gas:

$$\hat{K} = [K_1\{\beta_3\} \Longleftrightarrow K_2\{\beta_3\}] \longrightarrow [K_3\{\beta_2\} \Longleftrightarrow K_4\{\beta_2\}] \quad (15)$$

The material systems which can be realized by relations between the components are summarized in Table 1.

Table 1

	Nature of relation	Component 1. Determining / Component 2.	Solid β_1	Liquid β_2	Gaseous β_3
homogenous	⟹	solid β_1		liquid adsorbed at a solid phase	gas dissolved in or adsorbed at a solid phase
	⟺		homogenous solid-solid system; mixed crystal, alloy, glass		
	⟹	liquid β_2	solution of a solid		gas dissolved in a liquid
	⟺			liquid mixture	
	⟹	gas β_3	sublimated matter in a gas	liquid vapour in a gas	
	⟺				gas mixture
heterogenous	→	solid β_1	non-dispersed solid-solid system	liquid moving together with solid	gas moving together with solid
	⟷		mixture of solids	thick slurry	non-dispersed heterogenous solid-gas system
	→	liquid β_2	suspension	emulsion	gas bubbles in a liquid
	⟷		thick slurry	non-dispersed, immiscible liquid-liquid system	non-dispersed liquid-gas system
	→	gas β_3	flue dust in a gas	liquid droplets	
	⟷		non-dispersed heterogenous solid-gas system	non-dispersed liquid-gas system	

Quantitative Description of Material Systems

The material systems can quantitatively be described by a matrix. The line vector (2) giving qualitative description is applied and resolved to two parts: one part describing the component

$$K' (\alpha_{14}, \alpha_{15}, \alpha_{16}, \beta) \tag{16}$$

and the other describing the phase:

$$K'' (\beta', \alpha_3, \alpha_4, \alpha_5) \tag{17}$$

In the case of more than one component and more than one phase, two matrixes are obtained. The component-matrix is the following:

$$\begin{bmatrix} (\alpha_{14})_1 & (\alpha_{14})_2 & \cdots \\ (\alpha_{15})_1 & (\alpha_{15})_2 & \cdots \\ (\alpha_{16})_1 & (\alpha_{16})_2 & \cdots \\ (\beta)_1 & (\beta)_2 & \cdots \end{bmatrix} \tag{18}$$

and the phase-matrix:

$$\begin{bmatrix} (\beta')_1 & (\alpha_3)_1 & (\alpha_4)_1 & (\alpha_5)_1 \\ (\beta')_2 & (\alpha_3)_2 & (\alpha_4)_2 & (\alpha_5)_2 \\ \cdot & \cdot & \cdot & \cdot \\ \cdot & \cdot & \cdot & \cdot \\ \cdot & \cdot & \cdot & \cdot \end{bmatrix} \tag{19}$$

A quantitative matrix containing as many lines as the number of the phases and as many columns as the number of the components in the system is obtained from the above mentioned two matrixes

$$\begin{bmatrix} (\alpha_{14})_1 & \cdots \\ (\alpha_{15})_1 & \cdots \\ (\alpha_{16})_1 & \cdots \\ (\beta)_1 & \cdots \end{bmatrix} \qquad (20).$$

$$\begin{bmatrix} (\beta')_1 & (\alpha_3)_1 & (\alpha_4)_1 & (\alpha_5)_1 \\ \cdot & \cdot & \cdot & \cdot \\ \cdot & \cdot & \cdot & \cdot \\ \cdot & \cdot & \cdot & \cdot \end{bmatrix} \quad \begin{bmatrix} x_{11} & x_{12} & \cdots \\ x_{21} & \cdots & \\ \cdot & \cdot & \\ \cdot & \cdot & \end{bmatrix}$$

where x is the weight fraction.

A further column vector, containing the information valid for the whole material system, is added to the matrix system.

$$\begin{bmatrix} \alpha_1, & t \\ \alpha_2, & y \\ \alpha_3 & \\ \alpha_7, & (T) \\ \alpha_8, & p \\ W & \\ \beta'' & \end{bmatrix} \qquad (21)$$

where

α_1 is time; t_o in the starting state, t_v in the final state, 0 in the case of a stationary system,

α_2 is place; y_o: input, y_v: exit; 0 if there is no change,

α_3 is the scattering of phase distribution,

α_7 is the temperature,

α_8 is the pressure,

W is the mass flux, if $\alpha_1 = 0$, or the mass of the system, if $\alpha_2 = 0$,

β' is the state of the phase,

β'' is the state of the material system.

For example, let us consider a material flux of a rate 15 kilograms per hour, T = 20°C, P = 1 atmosphere, containing uniformly dispersed NaCl particles of 1 millimetre size and of a form factor of 0.7 at a ratio of 0.2, suspended in a solution containing 60 per cent water, 20 per cent ethyl alcohol and 20 per cent NaCl solution. For this case we can write:

$$\begin{bmatrix} 0 \\ y_o \\ 0 \\ 20 \\ 1 \\ 15 \\ \beta_2 \end{bmatrix} \quad \begin{bmatrix} \beta_2 & 0 & 0 & 0 \\ \beta_1 & 0 & 1 & 0{,}7 \end{bmatrix} \quad \begin{bmatrix} 0,16 & 0,48 & 0,16 \\ 0,2 & 0 & 0 \end{bmatrix} \quad \begin{bmatrix} 0 & 0 & 0 \\ NaCl & H_2O & C_2H_5OH \\ 0 & 0 & 0 \\ \beta_1 & \beta_2 & \beta_2 \end{bmatrix}$$

Operations such as addition and subtraction can be carried out with the matrix systems. However, only matrix systems in which the phases and components are same and equal, can be added or subtracted. Should this not be the case, the matrixes should be complemented. Prior to addition or subtraction the x-es are multiplied by W, the elements of the quantitative matrixes thus obtained are reduced and divided by $W_1 + W_2$. The elements of the qualitative matrixes remain unchanged and the reduction of the elements of the column vector is only indicated.

Various functions such as e.g. specific heat, can be interpreted by the matrix structure. In this case, a $C_{i,j}$ value pertains to every $X_{i,j}$ value, and if it is an additive property, the C value put into the column vector can be written in the following form:

$$C = \sum_{ij} \sum x_{ij} \cdot C_{ij} \tag{22}$$

The qualitative mathematical structure can be supplemented by the property designated by C:

$$A\ \{K^+,\ P,\ T,\ C\} \tag{23}$$

where C represents in the above-mentioned example the specific heat of the material system. As already mentioned, only the relevant parameters are given in a number of cases; in the example this may be the specific heat only, and accordingly the short mathematical structure is the following:

$$A\ \{C\} \tag{24}$$

The quantitative description of material systems can also be performed in the following manner.

The component is described by a column vector

$$\begin{bmatrix} \alpha_{14} \\ \alpha_{15} \\ \alpha_{16} \end{bmatrix} \tag{25}$$

and the phase by a line vector

$$[\beta',\ \alpha_5,\ T,\ P,\ y,\ t] \tag{26}$$

(The designations are the same as used in the foregoing.)

In the description of non-streaming material systems the following quantitative parameters are given for all of the components of all of the phases:

g - mass
v - volume
n - numericality
s_k - entropy of mixing

The parameters are indexed according to the components (i) and phases (j), for example:

$$g_{i,j}$$

The following specific quantities are interpreted:

weight fraction:

$$c_{i,j} = \frac{g_{i,j}}{g_j} \tag{27}$$

volume fraction:

$$e_{i,j} = \frac{v_{i,j}}{v_j} \tag{28}$$

phase fraction:

$$\varepsilon_j = \frac{v_j}{\sum_j v_j} \tag{29}$$

density:

$$\rho_{i,j} = \frac{g_{i,j}}{v_{i,j}} \tag{30}$$

mean mass:

$$\bar{g}_j = \frac{g_j}{n_j} \tag{31}$$

specific entropy of mixing:

$$s^o_{i,j} = \frac{s_{i,j}}{g_{i,j}} \tag{32}$$

In the description of streaming material systems the following quantitative parameters may be given:

W - mass flux
p - volume flux
m - numericality
ℓ - flux of entropy of mixing

In a way analogous to the foregoing, the following specific quantities are interpreted:

weight fraction:

$$c_{i,j} = \frac{w_{i,j}}{w_j} \tag{33}$$

volume fraction:

$$e_{i,j} = \frac{p_{i,j}}{p_j} \tag{34}$$

phase ratio:

$$\varepsilon_j = \frac{p_j}{\sum_j p_j} \tag{35}$$

density:

$$\rho_{i,j} = \frac{w_{i,j}}{p_{i,j}} \tag{36}$$

mean mass:

$$\bar{g}_{i,j} = \frac{w_{i,j}}{m_{i,j}} \tag{37}$$

specific entropy of mixing:

$$s^{o}_{i,j} = \frac{\ell_{i,j}}{w_{i,j}} \tag{38}$$

The M_t quantitative matrix of a non-streaming material system:

$$\begin{bmatrix} (\alpha_{14})_1 \ldots\ldots\ldots (\alpha_{14})_i \ldots \\ (\alpha_{15})_1 \ldots\ldots\ldots (\alpha_{15})_i \ldots \\ (\alpha_{16})_1 \ldots\ldots\ldots (\alpha_{16})_i \ldots \\ (\beta)_1 \ldots\ldots\ldots (\beta)_i \ldots \end{bmatrix}$$

$$\begin{bmatrix} (\beta')_1, (\alpha_5)_1, T_1, P_1, t_1 \\ \\ (\beta')_j, (\alpha_5)_j, T_j, P_j, t_j \end{bmatrix} \begin{bmatrix} (g,v,n,s_k)_{1,\ell} \ldots (g,v,n,s_k)_{i,\ell} \ldots \\ \\ (g,v,n,s_k)_{1,j} \ldots (g,v,n,s_k)_{i,j} \ldots \end{bmatrix} \tag{39}$$

The M_g quantitative matrix of a streaming material system:

$$\begin{bmatrix} (\alpha_{14})_1 \ldots\ldots\ldots (\alpha_{14})_i \ldots \\ (\alpha_{15})_1 \ldots\ldots\ldots (\alpha_{15})_i \ldots \\ (\alpha_{16})_1 \ldots\ldots\ldots (\alpha_{16})_i \ldots \\ (\beta)_1 \ldots\ldots\ldots (\beta)_i \ldots \end{bmatrix}$$

$$\begin{bmatrix} (\beta')_1, (\alpha_5)_1, T_1, P_1, y_1 \\ \\ (\beta')_j, (\alpha_5)_j, T_j, P_j, y_j \end{bmatrix} \begin{bmatrix} (w,p,m,\ell)_{1,\ell} \ldots (w,p,m,\ell)_{i,\ell} \ldots \\ \\ (w,p,m,\ell)_{1,j} \ldots (w,p,m,\ell)_{i,j} \ldots \end{bmatrix} \tag{40}$$

The matrixes given in Equations (39) and (40) can, according to the experience, be more easily applied for the quantitative characterization of material systems, than the quantitative matrix described by Equation (20).

TECHNICAL CHEMICAL CHANGES

The changes can be considered as to

the nature of the change and
the type of the change.

The following designations are introduced:

the characteristic is designated by α
the type of the change by ν
the nature of the change by δ
the change by V
the various material fluxes are designated by "o",
the designation of "and" is $\wedge$
and that of "or" is $\vee$.

The nature of the change (δ)

- Linear change: δ_1

in graphic representation: $A_1 \longrightarrow o \longrightarrow A_2$ i.e. material system A_1 is changed to material system A_2. Such changes are e.g. transportation or a change in temperature.

- Combining change: δ_2

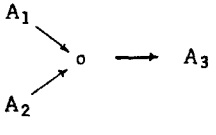

Two material systems are combined to give a third one; e.g. combination of two material streams, dissolution, chemical combination.

- Resolving change: δ_3

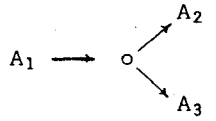

e.g. separation of two material streams, crystallization, chemical dissociation.

- Exchanging change: δ_4

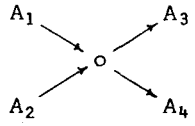

This is the change of the most general nature in which two material streams are changed so as to yield two other material streams. For example, adsorption of a solute, mutual chemical exchange, etc.

From now on "the nature of the change" will be applied in generally sense. In written form an index (1-4) before the V will refer to the nature of the change.

The Types of the Changes

a) Change in the place (α_2): v_1

(The direction of the change is shown by the sign ±.)
The nature of the change may be $\delta_1 \vee \delta_2 \vee \delta_3$.

Linear change:

$$ {}_1v_1^{\pm} = v_1^{\pm} \wedge \delta_1 \tag{41} $$

Such is e.g. transportation.

Combining change:

$$ {}_2v_1 = v_1 \wedge \delta_2 \tag{42} $$

E.g. combination of two totally miscible streams.

Resolving change:

$$ {}_3V_1 = v_1 \wedge \delta_3 \qquad (43) $$

E.g. resolution of a stream into partial streams of identical properties.

b) Change in the scattering (α_3): v_2

A change according to the place or time co-ordinates in the distribution of any of the characteristics is representated by the change in scattering. Increasing scattering is given a positive sign, decreasing scattering a negative sign.

The nature of the change may be: δ_1

$$ {}_1V_2^{\pm} = v_2^{\pm} \wedge \delta_1 \qquad (44) $$

E.g. pressure-equalizer buffer vessel.

c) Change in the dimensions (α_4): v_3

The nature of the change may be: $\delta_1 \vee \delta_2 \vee \delta_3$.

Linear change:

$$ {}_1V_3 = v_3 \wedge \delta_1 \qquad (45) $$

E.g. increasing or decreasing of dimensions.

Combining change:

$$ {}_2V_3 = v_3 \wedge \delta_2 \qquad (46) $$

E.g. supplying a dimensionless body with dimension (freezing).

Resolving change:

$$ {}_3V_3 = v_3 \wedge \delta_3 $$

E.g. abolishment of dimensions (sublimation).

d) Change in the form (α_5): v_4

The nature of the change may be: $\delta_1 \vee \delta_2 \vee \delta_3$.

Linear change may be the change in the form of the material system along a favoured direction (±).

$$ {}_1V_4^{\pm} = v_4^{\pm} \wedge \delta_1 \tag{48} $$

Combining change may be supplying a formless system with form:

$$ {}_2V_4 = v_4 \wedge \delta_2 \tag{49} $$

Resolving change may e.g. be the abolishment of form (melting):

$$ {}_3V_4 = v_4^{*} \wedge \delta_3 \tag{50} $$

e) Change in the temperature (α_6): v_5

The nature of the change may be: $\delta_1 \vee \delta_2 \vee \delta_3$. The change in the temperature may be brought about by processes occurring in the material system (e.g. evaporation, consideration) or by an exchange of energy.

Linear change: change in temperature without external energy exchange:

$$ {}_1V_5^{\pm} = v_5^{\pm} \wedge \delta_1 \tag{51} $$

E.g. heat exchange.

Combining change: the temperature increases by the introduction of external energy:

$$ {}_2V_5 = v_5 \wedge \delta_2 \tag{52} $$

Resolving change: the temperature decreases in consequence of heat extraction:

$$ {}_3V_5 = v_5 \wedge \delta_3 \tag{53} $$

E.g. expansion-type refrigerators.

f) Change in the pressure (α_7): v_6

The nature of the change may be: $\delta_1 \vee \delta_2 \vee \delta_3$.

The change is a linear one, if the change in pressure occurs without the action of external energy:

$$ {}_1V_6^{\pm} = v_6^{\pm} \wedge \delta_1 \qquad (54) $$

such as boiling or condensation.

The change is combining, if the pressure is increased by the action of external energy:

$$ {}_2V_6 = v_6 \wedge \delta_2 \qquad (55) $$

e.g. compression.

The change is resolving, if the pressure is decreased by the action of external energy:

$$ {}_3V_6 = v_6 \wedge \delta_3 \qquad (56) $$

e.g. expansion.

g) Change in the state (α_8): v_7

The nature of the change may be only linear. The direction of the change may be positive:

$$ {}_1V_7^{\pm} = v_7^{+1} \wedge \delta_1 \qquad (57) $$

e.g. a liquid is produced from a solid. Or it may be negative:

$$ {}_1V_7{}^{1} = v_7^{-1} \wedge \delta_1 \qquad (58) $$

e.g. a solid is produced from a liquid. Equations (57) and (58) describe one-step changes in state.

In general form:

$$ A_{yo}[\beta_a] + {}_1V_7^{+1} = A_{yv}[\beta_{a+1}] \qquad (59) $$

$$ a = 1, 2 $$

where A_{yo} = initial,
A_{yv} = final material system

$$A_{yo}[\beta_a] + {}_1V_7^{-1} = A_{yv}[\beta_{a-1}] \qquad (60)$$

$$a = 2,3$$

Two-step changes in state

A gas is produced from a solid:

$$A_{yo}[\beta_1] + {}_1V_7^{+2} = A_{yv}[\beta_3] \qquad (61)$$

A solid is produced from a gas:

$$A_{yo}[\beta_3] + {}_1V_7^{-2} = A_{yv}[\beta_1] \qquad (62)$$

h) Change in the phase ratio (α_9): v_8

The nature of the change: $\delta_2 \vee \delta_3 \vee \delta_4$.

Combining change: a heterogenous system is produced from separate material streams, or - with different wording - material streams are united to a heterogenous system:

$${}_2V_8 = v_8 \wedge \delta_2 \qquad (63)$$

$$A_{yo,1} \circ A_{yo,2} + {}_2V_8 = A_{yv,1} \longrightarrow A_{yv,2} \qquad (64)$$

e.g. preparation of a suspension.

Resolving change is, naturally, the resolution of a heterogenous system

$${}_3V_8 = v_8 \wedge \delta_3 \qquad (65)$$

$$A_{yo,1} \longrightarrow A_{yo,2} + {}_3V_8 = A_{yv,1} \circ A_{yv,2} \qquad (66)$$

e.g. filtration of a suspension.

Exchanging changes place the heterogenous connection to between other phases.

$${}_4V_8 = v_8 \wedge \delta_4 \qquad (67)$$

$$A_{yo,1}[\beta_a \rightarrow \beta_b] \circ A_{yo,2}[\beta_o] + {}_4V_8 =$$

$$= A_{yv,1}[\beta_a] \circ A_{yv,2}[\beta_c \rightarrow \beta_b] \qquad (68)$$

e.g. humid dust separation.

i) Change in the ratio of components within the phase (α_{10}): v_9

The nature of the change is: $\delta_2 \vee \delta_3 \vee \delta_4$.

The change is combining, if heterogenous phases are united to give a homogeneous system:

$${}_2V_9 = v_9 \wedge \delta_2 \qquad (69)$$

$$A_{yo}[\beta_a \rightarrow \beta_b] + {}_2V_9 = A_{yv}[\beta_a \Longrightarrow \beta_b] \qquad (70)$$

The change may be regarded of resolving nature, if a homogenous system is resolved into a heterogenous one:

$${}_3V_9 = v_9 \wedge \delta_3 \qquad (71)$$

$$A_{yo}[\beta_a \Longrightarrow \beta_b] + {}_3V_9 = A_{yv}[\beta_y \rightarrow \beta_b] \qquad (72)$$

e.g. crystallization by cooling.

Exchanging changes occur with transportation of the homogenous relation:

$${}_4V_9 = v_9 \wedge \delta_4 \qquad (73)$$

$$A_{yo}[(\beta_a \Longrightarrow \beta_b) \rightarrow \beta_c] + {}_4V_9 =$$

$$= A_{yv}[(\beta_a \Longrightarrow \beta_c) \rightarrow \beta_b] \qquad (74)$$

e.g. crystallization by salting out.

j) Change in the crystal structure (α_{14}): v_{10}

The nature of the change may be: $\delta_1 \vee \delta_2 \vee \delta_3$.

Linear change is a change in crystal modification; e.g. α-iron is transformed to γ-iron.

$$ {}_1V_{10} = v_{10} \wedge \delta_1 \tag{75} $$

$$ A_{yo}[(\alpha_{14})_1] + {}_1V_{10} = A_{yv}[(\alpha_{14})_2] \tag{76} $$

Combining change is the production of a crystal structure, e.g. in a crystallization process.

$$ {}_2V_{10} = v_{10} \wedge \delta_2 \tag{77} $$

Resolving change is the abolishment of crystal structure, e.g. melting.

$$ {}_3V_{10} = v_{10} \wedge \delta_3 \tag{78} $$

k) Change in chemical structure (α_{15}) and in the distribution of chemical elements among the components (α_{11}): v_{11}

The nature of the change: $\delta_1 \vee \delta_2 \vee \delta_3 \vee \delta_4$

In a linear change no matter is added to the component and none is removed from it, e.g. izomerization.

$$ {}_1V_{11} = v_{11} \wedge \delta_1 \tag{79} $$

$$ A_{yo}[(\alpha_{15})_1] + {}_1V_{11} = A_{yv}[(\alpha_{15})_2] \tag{80} $$

In chemical combination:

$$ {}_2V_{11} = v_{11} \wedge \delta_2 \tag{81} $$

$$ A_{yo,1}[(\alpha_{15})_1] \circ A_{yo,2}[(\alpha_{15})_2] + {}_2V_{11} = $$

$$ = A_{yv}[(\alpha_{15})_3] \tag{82} $$

In chemical decomposition:

$$ {}_3V_{11} = v_{11} \wedge \delta_3 \tag{83} $$

$$ A_{yo}[(\alpha_{15})_1] + {}_3V_{11} = $$

$$ = A_{yv,1}[(\alpha_{15})_2] \circ A_{yv,2}[(\alpha_{15})_3] \tag{84} $$

In chemical exchange:

$$ {}_4V_{11} = v_{11} \wedge \delta_4 \tag{85} $$

$$ A_{yo,1}[(\alpha_{15})_1] \circ A_{yo,2}[(\alpha_{15})_2] + {}_4V_{11} = $$

$$ = A_{yv,1}[(\alpha_{15})_3] \circ A_{yv,2}[(\alpha_{15})_4] \tag{86} $$

1) Change in the biological characteristics: v_2

where the distribution of compounds among the biological systems (α_{12}), the density of the biological individual (α_{13}) and the biological structure (α_{16}) are regarded as characteristic figures.

The nature of the change may be: $\delta_1 \vee \delta_2 \vee \delta_3$.

Linear change is the change of the biological structure.

$$ {}_1V_{12} = v_{12} \wedge \delta_1 \tag{87} $$

$$ A_{yo}[(\alpha_{16})_1] + {}_1V_{12} = A_{yv}[(\alpha_{16})_2] \tag{88} $$

Combining change: growth of the biological individuals.

$$ {}_2V_{12} = v_{12} \wedge \delta_2 \tag{89} $$

$$ A_{yo}[(\alpha_{12})_1] + {}_2V_{12} = A_{yv}[(\alpha_{12})_2] \tag{90} $$

Resolving change: reproduction of the individuals, which brings about an increase in the density of the individuals.

$$ {}_3V_{12} = v_{12}^{+} \wedge \delta_3 \tag{91} $$

$$ A_{yo}[(\alpha_{13})_1] + {}_3V_{12} = A_{yv}[(\alpha_{13})_2] \tag{92} $$

Death of the individual means a decrease in the number of the individuals

$$ {}_3V_{12}^{-1} = v_{12}^{-1} \wedge \delta_3 \tag{93} $$

$$ A_{yo}[(\alpha_{13})_1] + {}_3V_{12}^{-1} = A_{yv}[(\alpha_{13})_2] \tag{94} $$

or:

$$ A_{yo}[(\alpha_{16})_1] + {}_3V_{12}^{-1} = A_{yv}[(0)] \tag{95} $$

Equations (31) to (95) interpret elementary changes. A change is called elementary if only one of the characteristics is changed, even if such a change would lead to a fictive material system (e.g. a material possessing a crystal structure, but, at the same time, without any chemical structure). Consequently, a part of the elementary changes is impossible in itself alone. On the other hand, elementary changes as defined in the foregoing permit all possible real changes to be synthetized.

REFERENCE

1. BLICKLE, T., Hung. J. Ind. Chem. 1, 17 (1973)

РЕЗЮМЕ

Авторы в данном сообщении занимаются материальными системами технической химии, и изменениями происходящими по ним, далее излагают их толкование и математическое описание.

Качественное описание материальных систем было выполнено определением

- компонентов, находящихся в системе,
- взаимных связей между компонентами, и
- состояния системы.

Материальные системы количественно определены матрицным выражением.

Технико-химические изменения были характеризованы видом и типом изменения, таким способом можно было отметить наиболее важные элементарные изменения.

Hungarian Journal
of Industrial Chemistry
Veszprém
Vol.1. pp. 185-206 (1973)

STUDIES ON THE HYDRODINAMICS OF FLUIDIZED LAYERS II. STREAMING OF FLUID, PARTICLE MOTION AND LAYER EXPANSION IN SYSTEMS FLUIDIZED WITH A LIQUID

T. BLICKLE and Z. ORMÓS

(Research Institute for Technical Chemistry of the
Hungarian Academy of Sciences, Veszprém)

Received: August 21, 1972.

Starting from the physical model, basic equations are derived for the flow of the fluid, particle motion and changes in particle density along the radius. These equations enable the fluid-mechanical properties of fluidized systems to be described.

The basic equations derived are applied to systems fluidized with a liquid, and equations are presented for the calculation of the inter-granular liquid flow rate, of the change in grain flow rate along the radius and of the void fraction.

INTRODUCTION

Various theories have been described in literature for the description of the fluid mechanical properties, such as expansion and viscosity of the layer, and the motion of particles, etc., in fluidized layers [1, 2, 3, 4, 5, 6] etc. Based on these theories a number of equations was derived; however, the practical application of these is cumbersome and difficult.

In the following, based on a physical model, the derivation of equations enabling the calculation of the most important fluid

mechanical parameters will be presented. Due to the compositeness of the system and the mathematical difficulties encountered as a consequence of the complicated connections, a large number of approximations and neglections had to be applied and consequently the final conclusions can be regarded only as semi-empirical formulas. However, it was not considered the aim of the present work to elaborated an exact theory - this being, after all, in the opinion of the authors quite impossible due to the complexity and precariousness of the system - but to arrive at connections which enable the fluid mechanical parameters, necessary for design and optimalization, to be calculated to an adequate degree of accuracy.

In order to present a fluid mechanical description of fluidized systems, the physical model illustrated in Fig.1 was taken as a starting point and the following assumptions and restrictions were applied.

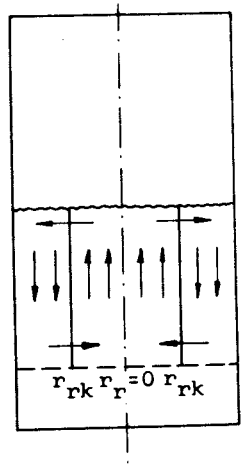

Fig.1

a) The particles in the layer are sphere-shaped; however, they are not necessarily of a uniform size.

b) The streaming of the medium is described by the Navier-Stokes equation. According to this, a rate gradient is built up along the radius.

c) The flow rate of the medium in the direction y is constant, but the velocity of the particles at a point y = 0 is zero and increases with increasing y value. This assumption is not wholly compatible with the uniform flow rate of the medium in the direction y. However, this assumption is justified by the good agreement between data calculated by the obtained formulas and determined experimentally. This will be reported in the next paper of this series.

d) Motion of the particles along the radius is brought about by the dynamic equilibrium of two forces. The rate profile

in the direction of and decreasing with the radius tends to force the particles in the direction of increasing radius. It can be shown that - were there no force of opposite direction - a minimum resistance of the system would be obtained in a extreme state, where all the particles would adhere to the wall of the apparatus and the medium would stream in the space enclosed by the annular cluster of particles. The unoriented motion of the particles, brought about by random fluctuations in the flow rate of the medium, acts against this force of centrifugal nature. If the particles were of uniform size, these fluctuations would cause collisions more rarely and would manifest themselves in a wave-like expansion or contraction. On the other hand, if the size of the particles is not identical, random fluctuations will cause frequent collisions and the particles will be forced - in a manner similar to the process of gas diffusion - in the direction of lower particle density, i.e. in a centripetal direction. In steady state, the radial density distribution of the particles is determined by the equilibrium of these two forces.

In order to present a fluid mechanical description of a fluidized layer, it is necessary to known the values of radial changes in the flow rate of the fluid streaming between the particles, the particle flow rate, and the void fraction.

FLOW OF THE FLUID

In order to describe the flow of the fluid, the Navier-Stokes equations, written for the case of cylindrical co-ordinates, can be used. The equations are the following [7]:

$$\rho' \left(\frac{\partial u'_R}{\partial \tau} + u'_R \frac{\partial u'_R}{\partial r} + \frac{u'_\varphi}{r} \frac{\partial u'_R}{\partial \varphi} + \frac{u'_\varphi}{r} + u'_y \frac{\partial u'_R}{\partial y} \right) =$$

$$= \frac{\partial p}{\partial r} + \mu' \left\{ \frac{\partial}{\partial r} \left[\frac{1}{r} \frac{\partial (r u_R')}{\partial r} \right] + \frac{1}{r^2} \frac{\partial^2 u_R'}{\partial \varphi^2} - \frac{2}{r^2} \frac{\partial u_R'}{\partial \varphi} + \frac{\partial^2 u_R'}{\partial y^2} \right\} + P_R \qquad (1)$$

$$\rho' \left(\frac{\partial u_\varphi'}{\partial \tau} + u_R' \frac{\partial u_\varphi'}{\partial r} + \frac{u_\varphi'}{r} \frac{\partial u_\varphi'}{\partial \varphi} + \frac{u_R' u_\varphi'}{r} + u_y' \frac{\partial u_\varphi'}{\partial y} \right) =$$

$$= - \frac{1}{r} \frac{\partial p}{\partial \varphi} + \mu' \left\{ \frac{\partial}{\partial r} \left[\frac{1}{r} \frac{\partial (r u_\varphi')}{\partial r} \right] + \frac{1}{r^2} \frac{\partial^2 u_\varphi'}{\partial \varphi^2} + \frac{2}{r^2} \frac{\partial u_\varphi'}{\partial \varphi} + \frac{\partial^2 u_\varphi'}{\partial y^2} \right\} + P_\varphi \qquad (2)$$

$$\rho' \left(\frac{\partial u_y'}{\partial \tau} + u_R' \frac{\partial u_y'}{\partial r} + \frac{u_\varphi'}{r} \frac{\partial u_y'}{\partial \varphi} + u_y' \frac{\partial u_y'}{\partial y} \right) =$$

$$= - \frac{\partial p}{\partial y} + \mu' \left[\frac{1}{r} \frac{\partial (r \frac{\partial u_y'}{\partial r})}{\partial r} + \frac{1'}{r^2} \frac{\partial^2 u_y'}{\partial \varphi^2} + \frac{\partial^2 u_y'}{\partial y^2} \right] + P_y \qquad (3)$$

There is no acceleration at a given point of the layer and accordingly we can write:

$$\frac{\partial u_R'}{\partial \tau} \equiv \frac{\partial u_\varphi'}{\partial \tau} \equiv \frac{\partial u_y'}{\partial \tau} \equiv 0 \qquad (4)$$

The pressure does not alter with changing r and φ, and consequently

$$\frac{\partial p}{\partial r} \equiv \frac{\partial p}{\partial \varphi} \equiv 0 \qquad (5)$$

The system is of cylindrical symmetry and so we obtain:

$$\frac{\partial u_R'}{\partial \varphi} \equiv \frac{\partial^2 u_R'}{\partial \varphi^2} \equiv \frac{\partial u_\varphi'}{\partial \varphi} \equiv \frac{\partial^2 u_\varphi'}{\partial \varphi^2} \equiv \frac{\partial u_y'}{\partial \varphi} \equiv \frac{\partial^2 u_\varphi'}{\partial \varphi^2} \equiv 0 \qquad (6)$$

There is no force acting upon the system in the direction r and φ:

$$P_R \equiv P_\varphi \equiv 0 \qquad (7)$$

It is assumed that the system does not flow in the directions r and φ:

$$u'_R \equiv u'_\varphi \equiv \frac{\partial u'_R}{\partial y} \equiv \frac{\partial u'_R}{\partial r} \equiv \frac{\partial^2 u'_R}{\partial y^2} \equiv \frac{\partial u'_\varphi}{\partial y} \equiv \frac{\partial u'_\varphi}{\partial r} \equiv \frac{\partial^2 u'_\varphi}{\partial y^2} \equiv 0 \qquad (8)$$

It follows from assumption (8) that:

$$\frac{\partial u'_y}{\partial y} \equiv \frac{\partial^2 u'_y}{\partial y^2} \equiv 0 \qquad (9)$$

From Equation (1), (2) and (3), considering Equations (4), (5), (6), (7), (8) and (9), we obtain:

$$\frac{dp}{dy} \equiv \mu' \frac{1}{r} \frac{d}{dr} \left(r \frac{du'_y}{dr}\right) + P_y \qquad (10)$$

The pressure in the layer is proportional to the weight of the layer [8]:

$$\Delta p = A_1 [\bar{\varepsilon}(\rho - \rho') + \bar{\varepsilon}'\rho'] gy \qquad (11)$$

from which we obtain:

$$\frac{dp}{dy} = A_1 g [\bar{\varepsilon}(\rho - \rho') + \bar{\varepsilon}'\rho'] \qquad (12)$$

The force acting upon the unit volume is equal to the sum of the force acting upon the particles plus that acting upon the fluid.

The force acting upon one particle is, according to Stokes, proportional to the difference in the velocities of the particle and the fluid [9]:

$$P = a_1(u'_y - u_y) \qquad (13)$$

If the difference is equal to the velocity of the free fall of the particle, it is self-ecident that the force is equal to the Archimedean weight of the particle and we can write:

$$vg(\rho - \rho') = a_1 u_e \qquad (14)$$

The force acting upon the particles present in the unit volume is, as derived from Equations (13) and (14):

$$P = \frac{vg(\rho - \rho')}{u_e} (u'_y - u_y) \tag{15}$$

The force acting upon the fluid present in the unit volume is:

$$P' = \varepsilon'\rho'g \tag{16}$$

The sum of the forces acting upon the particles and the fluid present in the unit volume is, on the basis of Equations (15) and (16), further Equation (5), the following:

$$P_y = \frac{g(\rho - \rho')\varepsilon}{u_e} (u'_y - u_y) + \varepsilon'\rho'g \tag{17}$$

The flow of the fluid can be described, on the basis of Equations (10), (12) and (17), by the following formula:

$$A_1[\bar{\varepsilon}(\rho - \rho') + \bar{\varepsilon}'\rho']g =$$

$$= \mu' \frac{1}{r} \frac{d}{dr} \left(r \frac{du'_y}{dr}\right) + \frac{g\varepsilon(\rho - \rho')}{u_e} (u'_y - u_y) + \varepsilon'\rho'g \tag{18}$$

Motion of the Particles

In the following, the equation describing the motion of the particles will be presented. On the basis of the second Newton's Law, and taking Equation (15) into consideration, we can

$$v\rho \frac{du_y}{d\tau} = \frac{v(\rho - \rho')g}{u_e} (u'_y - u_y) - v(\rho - \rho')g \tag{19}$$

After rearrangement and introduction of relative variables we obtain:

$$\frac{du_{ry}}{d\tau} = \frac{(\rho - \rho')g}{\rho u_e} (u'_{ry} - u_{ry} - 1) \tag{20}$$

The starting condition is:

$$u_{ry}(0) = 0 \tag{21}$$

The solution of Equation (20), taking starting condition - Eq. (21) - into consideration, is:

$$u_{ry} = (u'_{ry} - 1)\left\{1 - \exp\left[-\frac{(\rho - \rho')g\tau}{\rho u_e}\right]\right\} \tag{22}$$

Velocity can be written as the differential quotient of displacement according to time:

$$\frac{dy}{d\tau} = u_e(u'_{ry} - 1)\left\{1 - \exp\left[-\frac{(\rho - \rho')g\tau}{\rho u_e}\right]\right\} \tag{23}$$

The starting condition is:

$$u(0) = 0 \tag{24}$$

The solution of the differential equation, considering starting condition - Equation (24) - is the following:

$$y = (u'_{ry} - 1)u_e\tau - \frac{(u'_{ry} - 1)u_e^2\rho}{(\rho - \rho')g}\left\{1 - \exp\left[-\frac{(\rho - \rho')g\tau}{\rho u_e}\right]\right\} \tag{25}$$

Rearranging Equation (25):

$$y = (u'_{ry} - 1)u_e\tau\left\{\left[1 - \frac{u_e\rho}{(\rho - \rho')g\tau}\right]\left\{1 - \exp\left[-\frac{(\rho - \rho')g\tau}{\rho u_e}\right]\right\}\right\} \tag{26}$$

Let us approximate the exponential expression by the first two members of the series, i.e.:

$$\exp\left[-\frac{(\rho - \rho')g\tau}{\rho u_e}\right] \approx \frac{1}{1 + \frac{(\rho - \rho')g\tau}{\rho u_e}} \tag{27}$$

It was found that a comparative test made with the degree of approximation - Equation (27) - showed the approximation to be

better if a coefficient of 0.85 is used. Accordingly, from Equations (26) and (27) we have:

$$y = 0.85(u'_{ry} - 1)u_e\tau \frac{\frac{(\rho - \rho')g\tau}{\rho u_e}}{1 + \frac{(\rho - \rho')g\tau}{\rho u_e}} \tag{28}$$

By solving the Equation (28) for τ and introducing the dimensionless quantity:

$$A_4 = \frac{g(\rho - \rho')Y_m\varepsilon_m}{\rho u_e^2} \tag{29}$$

we arrive at:

$$2\tau = \frac{y}{0.85\ u_e(u'_{ry} - 1)}\left[1 + \sqrt{1 + \frac{3.4\ \bar{\varepsilon}(u'_{ry} - 1)}{A_4}}\right] \tag{30}$$

The mean velocity of the particles along the height is:

$$\bar{u}_y = \frac{y}{\tau} \tag{31}$$

The mean relative velocity of the particles along the height, as determined from Equations (30) and (31), is

$$\bar{u}_{ry} = \frac{1.7(u'_{ry} - 1)}{1 + \sqrt{1 + \frac{3.4\ \bar{\varepsilon}(u'_{ry} - 1)}{A_4}}} \tag{32}$$

Changes in Particle Density Along the Radius

If a difference in particle density is built up in the fluidized layer along the radius, a streaming of the particles along the radius will start in consequence of this difference.

This equalization process can start only if the particles perform an oscillating motion, since in the case of stationary particles the difference in particle density is not a sufficient cause for the motion. If the particles are floating, their oscillating motion can be observed even by the naked eye. The cause of this phenomenon is - in all probability - the fluctuation of the fluid flow rate in time. The latter has been measured by a number of researchers, e.g. by AEROV [10] among others. The Equation (3) serving the fluid mechanical description of fluidized layers can be derived on the basis of the foregoing.

The volume of the particles moving during unit time from one granular layer into another granular layer in a cylinder jacket of the radius r and the height dy is proportional to the surface area of the particles present at the cylinder jacket ($2\pi r\varepsilon dy$) and to the vibration rate. A fraction of the arriving particles corresponding to the void fraction (ε') enters the neighbouring layer at a distance Y_v, and accordingly the volume of the arriving particles (dv_I) is:

$$dv_I = 2\pi\varepsilon r u_v dy \tag{33}$$

The volume of the particles returning from the neighbouring layer (dv_{II}), if the void fraction was decreased by $\Delta\varepsilon$, while r was increased by Y_v, is the following:

$$dv_{II} = 2\pi\varepsilon u_v dy(r + Y_v)(\varepsilon' - \Delta\varepsilon') \tag{34}$$

The resultant volume of the transient particles (dv_{III}) is, evidently, the difference of the two volumes:

$$dv_{III} = dv_I - dv_{II} \tag{35}$$

and consequently from Equations (33), (34) and (35) we obtain:

$$dv_{III} = 2\pi u_v \varepsilon dy(r\Delta\varepsilon' - Y_v\varepsilon' + Y_v\Delta\varepsilon') \tag{36}$$

The expression $Y_v \Delta\varepsilon'$ is a secondary small value and may be neglected:

$$\Delta\varepsilon' Y_v \approx 0 \tag{37}$$

By approximating the $\varepsilon'(r)$ function by a continuous function:

$$\Delta\varepsilon' \approx Y_v \frac{d\varepsilon'}{dr} \tag{38}$$

From Equations (36), (37) and (38) we obtain:

$$dv_{III} = 2\pi u_v Y_v \varepsilon dy \left(r \frac{d\varepsilon'}{dr} - \varepsilon'\right) \tag{39}$$

The particle volume that passed during unit time can also be expressed by the velocity of the particles along the radius:

$$dv_{III} = 2\pi\varepsilon u_R r dy \tag{40}$$

The particle velocity along the radius is, according to Equations (39) and (40), the following:

$$u_R = - u_v Y_v \left(\frac{\varepsilon'}{r} - \frac{d\varepsilon'}{dr}\right) \tag{41}$$

The distance between the particles may be regarded as equal to the vibrational length of the particles; the product of the latter and the vibration rate may be termed the vibration coefficient:

$$K_v = u_v Y_v \tag{42}$$

The continuity rule is:

$$\frac{\partial u_R}{\partial r} + \frac{u_R}{r} + \frac{\partial u_y}{\partial y} = 0 \tag{43}$$

From Equations (41), (42) and (43) we obtain:

$$K_v \frac{d^2\varepsilon}{dr^2} = -\frac{\partial u_y}{\partial y} \tag{44}$$

Let us take the integral means according to height:

$$\frac{1}{Y} \int_o^Y \frac{\partial u_y}{\partial y} \cdot dy = \frac{1}{Y} [(u_y)_{y=Y} - (u_y)_{y=0}] \tag{45}$$

As a first approximation, arithmetical means may be taken:

$$\bar{u}_y = \frac{(u_y)_{y=Y} + (u_y)_{y=0}}{2} \tag{46}$$

When taking into consideration:

$$(u_y)_{y=0} = 0$$

starting condition, on the basis of Equations (44), (45) and (46) we obtain:

$$K_v \frac{d^2\varepsilon'}{dr^2} = \frac{u'_y}{2Y} \tag{47}$$

By introducting relative variables and the dimensionless expression:

$$A_6 = \frac{R^2 u_e}{2YK_v\bar{\varepsilon}} \tag{48}$$

and considering identity:

$$\varepsilon + \varepsilon' \equiv 1 \tag{49}$$

from Equations (32) and (47) the following formula is obtained:

$$\frac{d^2\varepsilon_r}{dr_r^2} = A_6 \frac{0.85\,(u'_{ry} - 1)}{1 + \sqrt{1 + \frac{3.4\,\bar{\varepsilon}(u'_{ry} - 1)}{A_4}}} \tag{50}$$

Equations (18), (32) and (50) can be regarded the three basic equations which enable the fluid mechanical properties (fluid flow rate between the particles, particle velocity and changes in void fraction) to be described.

The Effect of Layer Viscosity

In the foregoing, the influence of the viscosity of the layer was not taken into consideration. If we were to endeavour to formulate a correct mathematical model, our equations would become complicated to such an extent that their solution would be ab ovo impossible. Accordingly, a very rough approximation, described in the following, was adopted. This approximation is, however, a true model of the systems, as far as the tendencies are concerned. A fluidized layer, a uniform streaming system, will be considered This system streams in the tube as a consequence of the force exerted by the fluid upon the particles. The simplified Navier-Stokes equation (10) can be applied for the description of this process, very much as was done in the description of the streaming of the fluid, the only difference being that in this case it is assumed that the pressure of the layer is zero due to the floating of the particles. The solution of the equation enables the particle velocity in the middle of the layer to be determined in the case of a viscous layer and also if the viscosity is zero. The proposed approximation is that the ratio of the two velocities in the case of a fluidized layer is equal to the velocity ratio thus obtained. Accordingly, the equation - based on Equations (16) and (19), and taking the force acting upon the particles into consideration - will be the following:

$$(\rho - \rho')g\varepsilon(u'_{ry} - u_r) - (\rho - \rho')g\varepsilon = \frac{\mu_{fl} u_e}{R^2}\left(\frac{d^2u_r}{dr_r^2} + \frac{1}{r_r}\frac{du_r}{dr_r}\right) \qquad (51)$$

Considering the state when the particles are no longer accelerated. In this case, taking Equation (22) into consideration, it

is true that:

$$u'_{ry} - \bar{u}_{ry} = 1 \tag{52}$$

Introducing a new symbol:

$$u_r =. \bar{u}_{ry} + \Delta u \tag{53}$$

From Equations (51), (52) and (53) we have:

$$\Delta u(\rho - \rho')g\varepsilon = \frac{\mu_{fl} u_e}{R^2}\left[\frac{1}{r_r}\frac{d(r_r \frac{du_r}{dr_r})}{dr_r}\right] \tag{54}$$

Boundary conditions:

$$\left(\frac{du_r}{dr_r}\right)_{r_r=0} = 0, \quad u_r(1) = 0 \tag{55}$$

By neglecting the changes in particle velocity difference along the radius:

$$\frac{d\Delta u}{dr_r} \approx 0 \tag{56}$$

By the introduction of the dimensionless quantity:

$$A_5 = \frac{\mu_{fl} u_e}{(\rho - \rho')\bar{\varepsilon} g R^2} \tag{57}$$

the solution of Equation (54) is:

$$u_r = \frac{u_{ry}}{1 + A_5} \tag{58}$$

In accordance with the foregoing, u_r is written in place of u_{ry}.

$= u_y/u_e$ in Equation (18), $1.7/(1 + A_5)$ is written in place of 1.7 in Equation (32), and $A_6/(1 + A_5)$ is written in place of A_6 in Equation (50).

Changes in the Liquid Flow Rate between the Particles and in the Particle Velocity along the Radius

In the case of fluidization with a liquid it can be shown by substitution of numerical values that:

$$u_e \ll g\tau \tag{59}$$

By taking this into consideration, from Equation (26) we obtain:

$$y = (u'_{ry} - 1)u_e\tau \tag{60}$$

Accordingly, the mean relative particle velocity - taking the effect of viscosity into consideration - is the following:

$$u_r = \frac{(u'_{ry} - 1)}{1 + A_5} \tag{61}$$

Accordingly, from Equation (50) we obtain:

$$\frac{d^2\varepsilon_r}{dr_r^2} = A_6 \frac{u'_{ry} - 1}{2} \tag{62}$$

In the case of fluidization with a liquid, the value of A_6 is low and consequently it follows from Equation (62):

$$\frac{d^2\varepsilon_r}{dr_r^2} \lesssim 0 \tag{63}$$

On account of the cylindrical symmetry:

$$\left(\frac{d\varepsilon_r}{dr_r}\right)_{r_r=0} = 0 \tag{64}$$

and consequently it follows from Equations (63) and (64), since $(\varepsilon_r)_{r_r} \neq 1$ that:

$$\varepsilon_r \equiv 1 \tag{65}$$

On the basis of Equation (11), if y = Y:

$$A_1 = \frac{\Delta p}{[(\rho - \rho')\bar{\varepsilon} + \rho'\bar{\varepsilon}']gY} \tag{66}$$

From basic Equation (18), considering Equations (61) and (65) we obtain:

$$A_1[\bar{\varepsilon}(\rho-\rho') + \bar{\varepsilon}' - \rho']g = \mu' \frac{1}{r}\frac{d}{dr_r}\left(r_r \frac{du'_{ry}}{dr_r}\right) + g(\rho-\rho')\bar{\varepsilon} + \bar{\varepsilon}'\rho'g \tag{67}$$

By introducing the dimensionless quantity:

$$A_2 = \frac{\mu' u_e}{R^2[(\rho - \rho')\bar{\varepsilon} + \rho'\bar{\varepsilon}']g} \tag{68}$$

and rearranging Equation (67) we obtain:

$$(A_1 - 1) = A_2 \frac{1}{r_r}\frac{d}{dr_r}\left(r_r \frac{du'_{ry}}{dr_r}\right) \tag{69}$$

Boundary conditions:

$$\left(\frac{du'_{ry}}{dr_r}\right)_{r_r=0} = 0; \quad u'_{ry}(1) = 0 \tag{70}$$

The solution of Equation (69) is the following:

$$u'_{ry} = \frac{1 - A_1}{4\ A_2} (1 - r_r^2) \tag{71}$$

With the use of Equation (61), the following formula is obtained from Equation (71):

$$u_r = \frac{1}{1 + A_5} \left[\frac{1 - A_1}{4\ A_2} (1 - r_r^2) - 1 \right] \tag{72}$$

The volume of the particles moving upwards or downwards during unit time is identical; accordingly:

$$\int_0^1 2\pi r_r \bar{\varepsilon} u_r dr_r = 0 \tag{73}$$

From Equations (72) and (73):

$$\frac{1 - A_1}{4\ A_2} = 2 \tag{74}$$

The liquid flow rate between the particles along the radius - on the basis of Equations (71) and (74) - is the following:

$$u'_{ry} = 2\ (1 - r_r^2) \tag{75}$$

The change in particle velocity - on the basis of Equations (72) and (74) - is:

$$u_r = \frac{2\ (1 - r_r^2) - 1}{1 + A_5} \tag{76}$$

The maximum relative particle velocity:

$$u_{rM} = \frac{1}{1 + A_5} \tag{77}$$

CALCULATION OF THE VOID FRACTION IN FLUIDIZATION WITH A LIQUID

On the basis of geometric considerations the following identities are valid:

$$\frac{\pi d^3}{6\, d_I^3} \equiv \varepsilon \tag{78}$$

$$\frac{\pi d^2}{4\, d_I^2} \equiv E \tag{79}$$

It follows from Equations (78) and (79):

$$\frac{8}{6\sqrt{\pi}}\, E^{3/2} \equiv \varepsilon \tag{80}$$

By applying the continuity rule to the streaming of the liquid:

$$\int_0^R 2\pi u_y' E' dr = \pi R^2 U' \tag{81}$$

Considering Equations (65) and (80):

$$E' u_e = U' \tag{82}$$

using the identity:

$$E + E' \equiv 1 \tag{83}$$

we obtain from Equation (82):

$$U' = u_e(1 - E) \tag{84}$$

The particle volume fraction can be obtained from Equation (84) with the application of Identity (80):

$$\varepsilon = \frac{8}{6\sqrt{\pi}}\left(1 - \frac{U'}{u_e}\right)^{3/2} = 0.75\ (1 - U'_r)^{3/2} \tag{85}$$

The formula is valid even at the minimum fluidization velocity:

$$\varepsilon_m = 0.75\ (1 - U'_{rm})^{3/2} \tag{86}$$

The void fraction can be calculated from Equations (85) and (86), considering also Equations (49):

$$1 - \varepsilon' = \frac{1 - \varepsilon'_m}{(1 - U'_{rm})^{3/2}}\ (1 - U'_r)^{3/2} \tag{87}$$

The results of validity tests carried out in connection with Equations (85) and (87), derived for the calculation of the expansion of fluidized layers, will be reported on in the next paper of this series

USED SYMBOLS

a constants

A composite, dimensionless characteristics

d diameter of the particles (m)

E cross section fraction of the particles (m^2/m^2)

E' free cross section fraction (m^2/m^2)

F cross section of the layer (m^2)

g graviational acceleration (m/sec^2)

K_v vibration coefficient (m^2/sec)

p pressure ($kg/m\ sec^2$)

P force acting upon a unit volume ($kg/m^2/sec^2$)

P_y force acting upon a unit volume in the direction y (kg/m^2sec^2)

P_φ force acting upon a unit volume in the direction φ (kg/m^2sec^2)

P_R force acting upon a unit volume in the direction R (kg/m^2sec^2)

r radius co-ordinate (m)

R radius of the layer (m)

u_e fall velocity of the particles (m/sec)

$\bar{u}_y$ mean velocity of the particles along the height, if the viscosity of the layer is zero (m/sec)

$\bar{u}$ mean particle velocity (m/sec)

u_y particle velocity along the height (m/sec)

u_v vibration rate (m/sec)

u_R particle velocity along the radius (m/sec)

u' flow rate of the medium (m/sec)

$\bar{u}'_y$ mean flow rate of the fluid along the height (m/sec)

u'_R flow rate of the fluid along the radius (m/sec)

u'_φ flow rate of the fluid along an angle (m/sec)

u'_y flow rate of the fluid along the height (m/sec)

U' feed rate of the fluid (m^3/m^2sec)

U'_m minimum feed rate of fluid (m^3/m^2sec)

v volume of the particles (m^3)

y height co-ordinate (m)

Y layer height (m)

Y_m minimum layer height (m)

Y_v vibrational lenght (m)

Δp pressure difference ($kg/msec^2$)

ε particle volume fraction (m^3/m^3)

$\bar{\varepsilon}$ mean particle volume fraction (m^3/m^3)

ε_m minimum particle volume fraction (m^3/m^3)

ε_r relative particle volume fraction (dimensionless)

ε' void fraction (m^3/m^3)

$\bar{\varepsilon}'$ mean void fraction (m^3/m^3)

ε'_m minimum void fraction (m^3/m^3)

ε'_r relative void fraction (dimensionless)

μ' viscosity of the fluid (kg/sec m)

μ_{fl} viscosity of the fluidized layer (kg/sec m)

ρ density of the solid phase (kg/m^3)

ρ' density of the fluid (kg/m^3)

τ time (sec)

φ angular co-ordinate (degree)

Markings

A straight line drawn over the symbol: $\bar{}$: mean value.

A letter "r" on the lower right-hand side of the symbol: relative quantity.

No marking on the upper right-hand side of the symbol: solid phase.

A comma on the upper right-hand side of the symbol: ': fluid: liquid or gas.

Relative variables

$$u_r = \frac{u}{u_e} \qquad u_{ry} = \frac{u_y}{u_e}$$

$$u'_r = \frac{u'}{u_e} \qquad u'_{ry} = \frac{u'_y}{u_e}$$

$$U'_r = \frac{U'}{u_e} \qquad U'_{rm} = \frac{U'_m}{u_e}$$

$$r_r = \frac{r}{R} \qquad \bar{u}_{ry} = \frac{\bar{u}_y}{u_e}$$

$$\varepsilon_r = \frac{\varepsilon}{\bar{\varepsilon}} \qquad u_{rM} = \frac{u_M}{u_e}$$

REFERENCES

1. FURUKAWA, J., OHAMAE, T., Ind. Eng. Chem. 50, 82 (1958)
2. SCHÜGERL, K., MERTZ, M., FETTING, F., Chem. Eng. Sci. 15, 1 (1961)
3. PIGFORD, R.L., BARON, T., Ind. Eng. Chem. Fundamentals 4, 81 (1965)
4. ANDERSON, T.B., JACKSON, R., Ind. Eng. Chem. Fundamentals 6, 527 (1967)
5. HETZLER, R., WILLIAMS, M.C., Ind. Eng. Chem. Fundamentals 8, 668 (1969)
6. SAXTON, J.A., FITTON, J.B., VERMENLEN, T., AIChE Journal 16, 120 (1970)
7. R.BEPON BIRD, Transport Phenomena, J. Wiling and Sons. New York, 1960. 81 pp.
8. BRÖTZ, W., Chem. Ing. Techn. 24, 57 (1952)
9. GRUBER, J., Folyadékok mechanikája. Fluid mechanics. Tankönyvkiadó, Budapest, 1963. 181 pp.
10. AEROV, M.E., Zhurnal Prikl. Him. 23, 1009 (1950)

РЕЗЮМЕ

Исходя из физической модели, авторы излагают вывод основных уравнений для движения зерен и измерения плотности зерен вдоль радиуса, пригодных для описания гидродинамических условий псевдоожиженных систем.

Выведенные уравнения применены авторами для систем псевдоожиженных с помощью жидкости, представлены ими соотношения для вычисления скорости жидкости между зернами, скорости зерен вдоль радиуса, а также и доли свободного объема.

Hungarian Journal
of Industrial Chemistry
Veszprém
Vol.1. pp. 207-228 (1973)

STUDIES ON GRANULATION IN FLUIDIZED BED I.

METHODS FOR TESTING THE PHYSICAL PROPERTIES OF GRANULATES

Z. ORMÓS

(Research Institute for Technical Chemistry of the
Hungarian Academy of Sciences, Veszprém)

Received: August 21, 1972.

The knowledge of the properties of granulates is of considerable importance,both as regards application and scientific research work. Methods for the determination of the most important physical characteristics of granulates (such as grain-size distribution,density characteristics, pore space fraction, rolling tendency characteristics, and mechanical strength) published in literature, are described. The results of the research work aimed at checking the applicability of the testing methods and the development of new techniques are reported. The concepts of "loosened bulk density" and "rolling tendency coefficient" are introduced and measuring techniques enabling the determination of these quantities are described. A simple measuring technique is proposed for the determination of the pore space fraction. The technique is based on the identical space filling characteristics of particles of an identical shape. A new measuring method for the determination of the abrasion strength (abrasion resistance) of the granulates is described, which is based on the measurement of the mechanical stress acting in the fluidized layer.

In chemical and related industries (e.g. the food industry) the granulates prepared are used partly as starting materials of further products and partly as final products. Various fields of

application raise various requirements concerning the quality of the granulates. However, the basic principles of qualitative characterization are nearly identical and mainly refer to the physical properties of the granulates.

The main physical characteristics of granulates are the following:

a) grain size distribution and form of the grains,
b) density characteristics,
c) porosity,
d) rolling tendency characteristics,
e) mechanical strength.

Naturally, in addition to the above-mentioned physical parameters, there are other characteristics which may be of importance in some fields of application, e.g. tendency to crumbling, and pressing ability, etc. However, the knowledge of these - although in some cases of considerable importance - is in general not as essential as the physical parameters listed earlier. Several other authors are of the same opinion [1, 2, 3, 4, 5,etc.].The granulates are in some cases, mainly in the pharmaceutical industry, very often qualified in addition to their physical properties on the basis of indirect parameters, such as the physical characteristics of the tablets made of them (e.g. variations in the weight of the tablets, time of falling apart, and abrasion resistance) [6, 7].

In the following, testing methods found in literature for the determination of the most important physical characteristics of granulates will be described, together with a report on the elaboration of new techniques and the improvement of known ones.

GRAIN-SIZE DISTRIBUTION AND FORM OF THE GRAINS

In the study of the granulation process, generally the distribution of heaps of grains of different properties according to

size is to be determined. The grain-size distribution of the starting material to be granulated can rarely be determined by sieve analysis; sliming [8, 9, 10], sedimentation [8, 9, 10] or microscopic examination [3, 9, 11] can be applied instead. The latter method also enables the form of the grains to be observed.

The most widely used method for the determination of the grain-size distribution of granulates is sieve analysis. This test is most frequently carried out by a standard set of sieves [18, 9, 10]. The granulates - especially those obtained by building-up type granulation - are of nearly spherical form, or at least the largest and smallest dimensions of the granulate are not significantly different from each other and consequently the accuracy of the method is satisfactory.

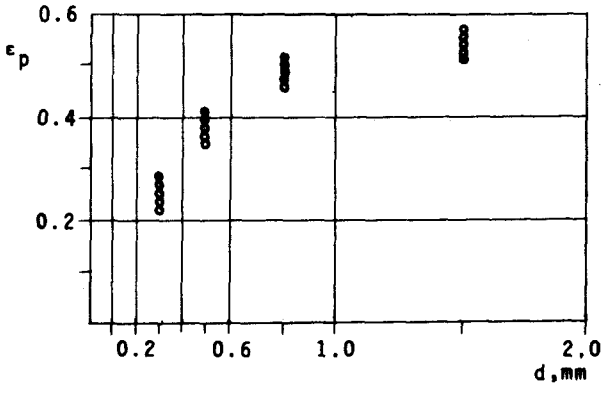

Fig. 1

In the case of granulates prepared by the fluidization granulation technique it was found that the porosity of the granulates increases, i.e. the grain density decreases with increasing dimensions.

Fig. 1 shows the change in pore space fraction plotted against increasing volume in the case of 5 different granulates, prepared from a sand fraction of 0.1 to 0.2 millimetre grain size in a laboratory-scale fluidization granulation apparatus. It can be concluded from the Figure that the grain density of granulate particles exceeding the 0.6 millimetre size is decreased to about one half as compared to that of the ungranulated 0.1 to 0.2 millimetre fraction.

In the opinion of the author, in those cases where - the porosity of the granulates and, together with it -, the grain den-

sity is dependent on grain size, the ratio of the grain spaces is far more characteristic of the granulates than the weight ratio of the individual fractions. The former can be calculated from the weight ratio, if the porosity is known. In this case it is not the weight ratio of the grains, but their volume ratio that is to be considered in the calculation of the average grain size and other average values (e.g. average grain density, etc.) of the granulate.

DENSITY CHARACTERISTICS

In the case of a heap composed of porous grains, real density, grain density and bulk density can be considered.

The Real Density is often difficult to determine, because the simple pyknometer density determination technique [8, 9, 10, 11] does not yield reliable results unless the sample is compact, readily wettable and of small grain size. The Biltz vacuum pyknometer [9] can be used to determine the density of fine powders, if it is possible to find an adequate indifferent measuring liquid. The liquid-medium pyknometer technique can be used for the determination of the real density of masses composed of porous grains only with reservation.

The liquid used for the measurement penetrates the grains to an extent depending on the structure of the grains and the characteristics of the liquid; consequently an intermediate value is obtained which is between the real density and the grain density. In such cases, the Hofsass air-pyknometer can be used; the accuracy of the latter can be increased by using helium instead of air [9].

Grain Density: the mass of grains of unit volume, can be expressed in the following way:

$$\rho_g = \rho(1 - \varepsilon_p) \tag{1}$$

where

ρ_g is the grain density (gram/cu.centimetre),

ρ is the real density (gram/cu.centimetre),

ε_p is the pore space fraction.

The techniques applicable for the determination of the pore space fraction are described in the next chapter.

Bulk Density: the mass of a heap of unit volume of grains. The value of this quantity depends on a number of parameters, such as average grain density, grain-size distribution, and grain form, etc. However, the most influental parameter is - for a given heap of grains - the closeness of packing. Accordingly, three bulk density values can be defined: close-packed bulk density,filled-in bulk density and loosened bulk density.

Close-Packed Bulk Density: the mass of a unit-volume heap of grains pressed together intensively. This value is to some degree dependent on the method of compression [12, 13]. In general, it can be stated that the highest degree of compression and, together with it, the highest close-packed bulk density is attained by vibration brought about in some way, e.g. pneumatically. However, even this value differs only slightly from grain heap densities obtained by some other compression technique, e.g. mechanic or manual compression. Different authors have proposed various techniques for the determination of the close-packed bulk density. For example, NEWITT and CONWAY-JONES [2] used high-frequency vibration, MARKS and SCIARRA [7] repeated manual knocking in a graduated cylinder; according to KONCZ [8], the best method is the application of a Becker-Rosenmüller shaker, etc. Consequently, it is very difficult to compare the measured results. Nevertheless it is a general opinion that - provided proper care is exercised - any of the methods is adequate for the determination of the close-packed bulk density.

Filled-in Bulk Density. The mass of a grain heap, when filled into a vessel of unit volume. In addition to grain size distribution, grain density and grain form, the filled-in bulk density also depends on the size and shape of the volumetric vessel and on the method used to fill in the grains. The values obtained with different techniques differ and this necessitated standardization of the filled-in grain density determination methods [3]. The ap-

paratus consisting of two parts, shown in Fig. 2, serves this purpose [15]. The essence of the measurement is that a 120 millilitre portion of the granulate heap to be tested is poured into the funnel and permitted to freely flow into the graduated cylinder of 100 millilitres capacity. The excess is removed from top of the cylinder and the mass of the latter is weighed. Other authors [9] have proposed the application of a filling apparatus according to Gary and Böhme.

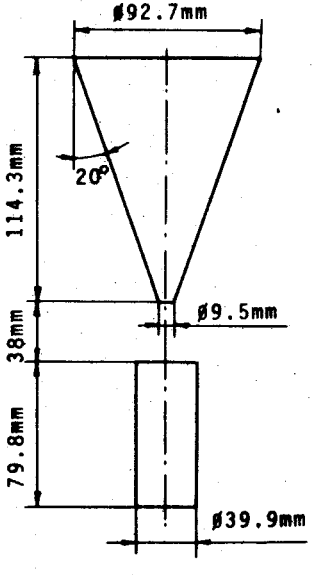

Fig. 2

Loosed Bulk Density: the mass of a unit-volume heap of loosened grains. The loosened heap is produced in the following manner: a granulate heap of known mass is placed into a simple laboratory-scale fluidization apparatus (4-5 centimetres in diameter) and fluidized with air until an expansion of one and a half times or twice the volume of the original, and then the amount of air is decreased until a stationary layer is obtained. The height of the layer is measured and it enables the loosened bulk density to be calculated in a simple manner:

$$\rho_l = \frac{4\,G}{D^2 \pi Y_m} \qquad (2)$$

where

ρ_l is the loosened bulk density (gram/cu.centimetre),

G is the mass of the heap of granulate (gram),

D is the diameter of the apparatus (centimetre),

Y_m is the minimum fluidization layer height (centimetre).

The schematic drawing of the apparatus is shown in Fig. 3. While carrying out the measurement, care should be exercised to ensure that, on the one hand, Y/Y_m should not be higher than 1.5

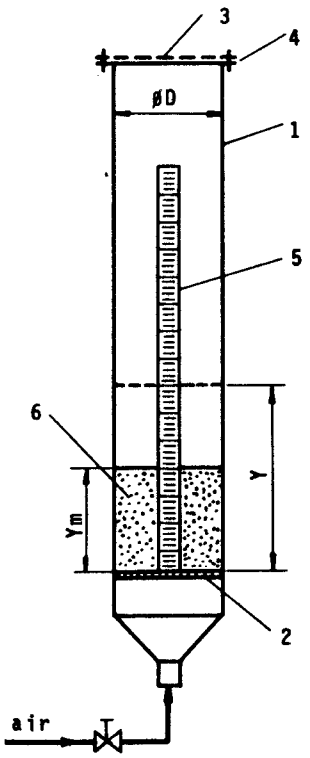

Fig. 3

1. Fluidization apparatus
2. Fritted glass retaining disk
3. Sieve, 15-20 μm
4. Dismountable flange
5. Millimetre scale
6. Loosened grain heap

to 2, in order to avoid the production of flow dust, and, on the other, Y_m/D should be 0.5 to 1.5. The loosened bulk density values determined by the proposed technique are well defined and reproducible, and the apparatus and the procedure are simple. To know the value of the loosened bulk density is important both from the points of view of plant operation and design.

POROSITY

The pore space fraction - which is the ratio volume of the pores present in the grains by total volume of grains - can be determined by a number of techniques. One of these is based on the principle that a non-wetting liquid (mercury) is forced at different pressures into the pores of the grains, the amount of the liquid is measured and thereby it is possible to draw conclusions not only on the pore space fraction, but also on the size of the pores [10, 11]. This measurement, with the use of mercury, can be carried out in an even more simple manner, if it is not necessary to know the distribution of the pore space fraction and the latter can be determined by a suitable pyknometer technique [3, 8, 12].

In the study of the granulation operation it is necessary to determine the pore space fraction on a large number of granulate heaps, moreover, the determinations should be carried out quickly. For this purpose, a simple but adequate pore space fraction determination method was developed in the author's laboratory. The new

method is based on the fact that the void fraction of a relatively narrow grain fraction of practically spherical, compact grains scatters between narrow limits [16]. Any significant deviation from this value is in the case of grains larger than 0.2 millimetre - and, accordingly, generally also in that of the granulates - the consequence of the porosity of the grains and hence it can be used for pore space determination.

The definition of the void fraction is the following:

$$\varepsilon' = \frac{V_r - V}{V_r} = \frac{F \cdot Y - \frac{G}{\rho}}{F \cdot Y} \tag{3}$$

where

ε' is the void fraction,

V_r is the volume of the layer (cu.centimetre),

V is the volume of the solid material present in the layer (cu.centimetre),

G is the mass of the solid material (gram),

ρ is the real density of the solid material (gram/cu.centimetre),

Y is the height of the layer (centimetre),

F is the cross section of the apparatus (sq.centimetre).

On the basis of geometric considerations it is evident that the void fraction, in the case of porous grains, can be written in the following manner:

$$\varepsilon_2' = \varepsilon_1' + (1 - \varepsilon_1') \cdot \varepsilon_p \tag{4}$$

where

ε_2' is the void fraction in the case of porous grains,

ε_1' is the void fraction without pores (taking only the free space between the grains in consideration),

ε_p is the pore space fraction of the grains.

Equation (4) can be written for the point of minimum fluidization:

$$\varepsilon_{m2}' = \varepsilon_{m1}' + (1 - \varepsilon_{m1}') \varepsilon_p \tag{5}$$

and hence the pore space fraction of the grains (ε_p) can be expressed:

$$\varepsilon_p = \frac{\varepsilon'_{m2} - \varepsilon'_{m1}}{1 - \varepsilon'_{m1}} \tag{6}$$

where

ε'_{m1} is the minimum void fraction of a compact granular material of a form similar to that of the porous grains,

ε'_{m2} is the minimum void fraction of the porous granular material.

The minimum void fraction of the porous granular material (ε'_{m2}) is, on the basis of Equation (3), the following:

$$\varepsilon'_{m2} = \frac{Y_m - \frac{G}{F\,\rho}}{Y_m} \tag{7}$$

where

Y_m is the minimum fluidization layer height of the grain fraction (centimetre),

G is the mass of the weighed-in grain fraction (gram),

ρ is the mean real density of the materials building up the grains (gram/cu.centimetre),

F is the cross section of the apparatus (sq.centimetre).

The minimum fluidization layer height of the individual granulate fractions can be determined, as described in the previous section, by means of the simple laboratory fluidization apparatus shown in Fig. 3. The narrower the fraction tested (i.e. the higher the number of fractions into which the heap of granulate was divided), the higher the accuracy of the pore space fraction determination.

During the research work carried out in connection with the layer expansion of fluidized systems, among others the minimum void fraction of relatively narrow grain fractions of quite a number of compact granular materials were determined. Microphotographs of the grains were prepared and compared with those of porous grains and granulates made of various starting materials by different procedures. The minimum void fraction of grain fractions consisting of compact grains of approximately identical form shows a good agreement, and consequently - in the case of grain fractions of a size exceeding 0.2 millimetre - the following values can be substituted into Equation (6):

a) regular, approximately sphere-shaped, porous grains: $\varepsilon_{ml} = 0.45$;

b) less regular, sphere-shaped porous grains, granulates prepared by a rotary (e.g. rotating disk) apparatus: $\varepsilon_{ml} = 0.50$;

c) even less regular, porous grains, granulates prepared by fluidization: $\varepsilon_{ml} = 0.55$;

d) broken, porous grains prepared by crushing or rough disintegration, granulates prepared in a fluidized layer from needle-crystal shaped starting material: $\varepsilon_{ml} = 0.60$.

The determination method can naturally be refined in such a manner that a series of photographs is made of compact grains of various forms, the photograph of the porous grains to be tested is compared with these, and the actual minimum void fraction value is determined by this comparison. However, it is very rarely necessary to carry out this procedure in studies connected with fluidization granulation since the shape of the granulates obtained - except for some needle-crystal shaped starting materials - is approximately identical, and the value of $\varepsilon_{ml} = 0.55$ can be substituted into Equation (6).

Two comparative tests were carried out as regards the applicability of the measuring technique described earlier. The essence

of the first was that the pore space fraction of a number of granulate fractions was determined with the proposed technique, and afterwards three lots of one thousand grains were counted, their mass weighed and the pore space fraction (ε_p^*) calculated by Equation (1). The deviation between the values determined by the two methods plotted against the pore space fraction, as determined on the basis of the minimum void fraction, is shown in Fig. 4. It can be concluded on the basis of the Figure that except for a few cases, the relative deviation is smaller than ± 10 per cent and the agreement is better at medium values, i.e. in the case of granulates of medium size. In the second test, the minimum void fraction of burnt clay grain fractions of known porosity was determined and afterwards the pore space fractions were calculated by Equation (6) in such a way that - based on microscopic comparison - a value of $\varepsilon'_{m1} = 0.50$ was substituted. A comparison of the pore space fractions showed that the relative deviation in this case is also generally below ± 10 per cent.

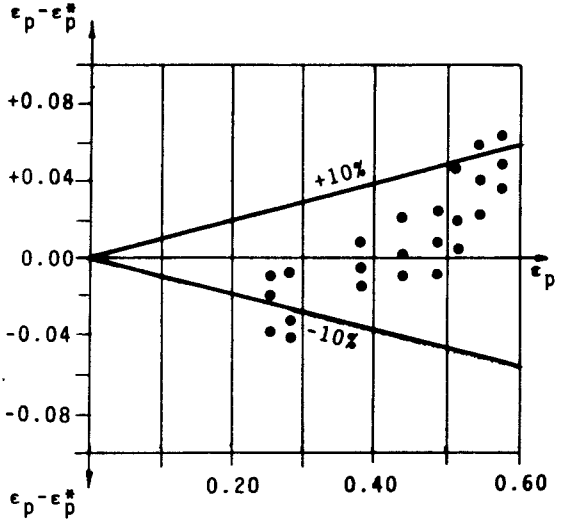

Fig. 4

It is the advantage of the proposed measuring technique that it is simple, rapid, and no expensive equipment is needed.

On the other hand, it is burdened by the drawback that when applying it, the granulate heap to be tested has to be separated to at least 5 to 6 grain fractions. However, this is carried out anyway during the sieve analysis and so the two tests can be connected. The average pore space fraction, characteristic of the

whole heap, can be calculated, knowing the grain size distribution, by weighted averaging.

ROLLING TENDENCY CHARACTERISTICS

Rolling tendency is an important physical property of granular heaps of materials and it is characterized by the internal friction of the heap. The rolling tendency characteristics are generally described by the slump angle of a heap produced in some manner, or by the rate of flow from a funnel of defined dimensions.

In connection with material heaps, a number of angles can be defined,such as slump angle, falling angle, sliding angle, spatula angle, internal friction angle, and inclination angle [17]. Most frequently it is the slump angle from among these, referred to a heap of grains produced by a standardized procedure, which is determined. The essence of one such procedure is that the standardized funnel [15] shown in Fig. 2 is fixed in such a position that its lower end is 4 centimetres above the base and the material to be tested is poured into the funnel until the apex of the material heap produced just reaches the lower end of the funnel. The height of the heap and the diameter of the base circle are measured and the slump angle calculated from these data [3]. Slump angle determination can also be carried out by the Langhaus-apparatus [9].

When a heap of grains flows from a funnel of standardized dimensions, the result can be expressed by the discharge time of the material of the unit mass or unit volume, and by the mass or volume of material discharged during the unit time, etc. For example, GOLD and his co-workers [18] evaluated the results on the basis of the discharge time of a given mass, KANENIWA and IKEKAWA [19] on the basis of the mass discharged during unit time, and LISKE and MÖBUS [20] on the basis of the volume discharged during unit time.

A number of authors dealt with the circumstances of the discharge of granular matter from a funnel, including KANENIWA and IKEKAWA. These authors concluded [19] that, in addition to the properties of the grain heap, the rate of discharge depends, to a large extent, on the diameter of the discharge opening, its length and the cone angle of the funnel, but it is independent of the height of the heap above the opening. The latter statement, with a few exceptions, was also confirmed by other authors [21, 22]. It follows from the aforesaid that it is primarily necessary to standardize the funnel in order to obtain comparable results. For example, the standard funnel shown in Fig. 2 [15] enables the rolling tendency characteristics to be determined. A hundredfold (in grammes) of the density (gram/cubic centimetre) of the solid is poured into the funnel and the time necessary for discharge is measured [3]. Experience shows that the researchers use funnels of different dimensions for this measurement [4, 5, 7, 19, 20].

In the author's opinion, the discharge data are more characteristic of the rolling tendency than the slump angle. This is supported by the fact that the discharge rate shows - in the case of different grain heaps - considerably greater variations, and consequently the method is more sensitive. For example, according to data published by LISKE and MÖBUS [20], the discharge rate from a given funnel corresponding to a slump angle of 46° was 288 millilitres/minute, whereas that corresponding to 44.2° was 370 millilitres/minute. On the other hand, the discharge rate, in the case of certain types of granulate heaps, may fluctuate in time even if the average value is the same [18]. The determination of this fluctuation provides a possibility for further refinements.

Different methods based on the measurement of the discharge rate from a funnel are used in general practice for the determination of the rolling tendency characteristics and consequently it seems desirable to introduce a few improvements in the measuring techniques in order to obtain results that are readily comparable. The grain volume discharged in unit time seems to be more adequate for the comparison of the rolling tendency characteristics of gra-

nulate heaps than the mass of grains discharged in unit time. This is especially true if heaps of different grain density are to be compared. Of course, the average grain density or porosity should be known in this case; a simple and rapid technique for its determination was described in the previous chapter.

The other problem arises as a consequence of the difference of the testing methods. It is the author's opinion that this difficulty could be overcome if the results obtained with different methods were compared with the discharge rate of a generally accepted standard material. The rolling tendency coefficient defined in this manner is

$$\varphi = \frac{v_g}{v_s} \tag{8}$$

where

φ is the rolling tendency coefficient,

v_s is the discharge rate of the standard material (cu.centimetre/second),

v_g is the discharge rate of the granulate under test (cu.centimetre/second).

Narrov fractions of different sizes of a number of different materials were examined and from among the materials available, that consisting of regular glass spheres of approximately 0.15 mm (100 mesh) dimension was found to possess the most advantageous rolling tendency characteristics. This material is a commercial product (GLASS BEADS FOR GAS CHROMATOGRAPHY, approximately 100 MESH, BRITISH DRUG HOUSES LTD., B.D.H. LABORATORY CHEMICALS DIVISION, POOLE, ENGLAND) and consequently it seems to be adequate to be used as a standard in the determination of rolling tendency characteristics.

If in the measurement of discharge rate, amounts corresponding to the same grain space are weighed in from the standard material and from the granulates, and the discharge times of the to-

tal quantities are measured, Equation (8) takes the following form:

$$\varphi = \frac{\tau_s}{\tau_g} \tag{9}$$

where

φ is the rolling tendency coefficient,

τ_s is the discharge time of the standard material (sec),

τ_g is the discharge time of the granulate heap under test (sec).

The time of discharge of a grain space of 100 cubic centimetres (G_s = 296 grammes) of the standard material proposed in the foregoing from the standard funnel shown in Fig. 2 [15] is τ_s = 8 seconds, i.e. v_s = 12.5 cubic centimetres/second. The rolling tendency coefficient of a few grain heaps are given in the following:

glass beads	d = 0.25 millimetre	φ = 0.93
	d = 0.42 millimetre	φ = 0.82
sand	d = 0.10-0.20 millimetre	φ = 0.62
	d = 0.20-0.32 millimetre	φ = 0.68
	d = 0.32-0.40 millimetre	φ = 0.66
	d = 0.40-0.50 millimetre	φ = 0.63
	d = 0.50-0.63 millimetre	φ = 0.62
	d = 0.63-0.80 millimetre	φ = 0.60
	d = 0.80-1.00 millimetre	φ = 0.54

According to the author's experience, the rolling tendency coefficient of granulates prepared by the fluidization process is in the 0.3 to 0.6 range. Probably there exists some material whose discharge rate is greater than that of the standard material proposed, but the rolling tendency coefficient of the overwhelming majority of the materials is between 0 and 1.

MECHANICAL STRENGTH

Mechanical strength means the totality of those properties which express the resistance of the granulates against mechanical stresses [1]. The mechanical stress may be pressure, impingement, and abrasion, etc. Often these actions simultaneously manifest themselves during the operations carried out with the granulates, such as shipment, storage, feeding, and packing. The methods used for the measurement of the mechanical strength of granulates can be classified into two groups. The methods belonging to one group enable the compressive strength to be determined, and the other the abrasive strength.

The underlying principle of the methods used for the determination of the compressive strength of granulates is the following. A compressive stress is put on an individual granulate grain and the force is increased until the grain is crushed. The compression strength is most frequently expressed as the ratio maximum compressive force before crushing per cross sectional area of the grain [1, 2, 4, 23]. The drawback of this method is that it does not adequately model the mechanical stresses acting upon the granulates in their use.

Abrasion resistance of the granulates means their resistance against abrasion effects encountered during their application [5, 7, 24]. Abrasion resistance is most frequently determined by a sieve analysis carried out after the abrasive action and the result is presented as the ratio fraction remaining on a sieve of a given mesh size to the total quantity of sample weighed in. The methods used to produce abrasive mechanical stress are multifarious. MARKS and SCIARRA [7] applied the Roche pulverization tendency testing apparatus [25]. FUNNER and his co-workers [26] shook the granulates in a closed container for a given period of time and afterwards sieved them. DAVIES and his co-workers [5] modified the standard testing procedure developed for the testing of coal [27] and abraded the granulates in a rotary shaking-mixing apparatus. A standard [24] recommends that as long as there is no ade-

quate standard for an abrasion testing apparatus, it is preferable that the interested parties should come to an agreement as to the conditions of the test.

In connection with studies on fluidization granulation, the question arose as to the method to be applied for the determination of the abrasion resistance of granulates. Either the application of some sort of shaking apparatus could be taken into consideration, or abrasion in a fluidized layer could be used. In order to settle this question, a series of experiments were carried out with a granulate heap prepared in a fluidized layer of a sand fraction of 0.1-0.2 millimetre size with gelatine as the binding agent. The experiments were carried out in such a manner that a given quantity of the granulate heap to be tested was exposed to different abrasive stresses for a given period of time. Thereupon the grain size distribution was determined by sieve analysis. The abrasive mechanical stress was brought about in the following manners:

a) A 100 gram portion of the granulate was placed into the receiver of a set of sieves, covered with the lid, and was shaken with a horizontal motion at a frequency of 200/minute on top of a "Labor MIM" shaking apparatus for 10 minutes (R 1),

b) The experiment was repeated with the above-described parameters in such a manner that 25 steel balls of 8 millimetre diameter were placed into the vessel together with the granulate sample (R 2),

c) A 100 gram portion of the granulate was weighed into a 300-millilitre Erlenmeyer flask, the latter was fixed into one of the clamps on the side of a "Labor MIM" shaking apparatus and shaken at a 200/minute frequency for 10 minutes (R 3),

d) A 100 gram portion of the granulate was kept in a fluidized state in a laboratory fluidization apparatus of 5 centimetre diameter (cf. Fig. 3) at a threefold layer expansion (Y/Y_m = = 3) with an air stream for 10 minutes (F 1).

The results of the experiments are summarized in Table 1. X is the ratio average grain diameter of the grain heap after abrasion by average grain diameter of the grain heap to be tested (percentage).

Table 1

	Granulate to be tested	Granulate after abrasion			
		R 1	R 2	R 3	F 1
Average grain diameter (millimetre)	0.55	0.52	0.27	0.38	0.41
X, per cent	100	94	49	69	74

It is apparent from the Table that the horizontal shaking of the granulate is not sufficiently effective (R 1). If there are also steel balls in the vessel when carrying out horizontal shaking, the abrasive stress is too strong (R 2). Shaking in the Erlenmeyer flask (R 3) and abrasion by fluidization (F 1) represent stresses that are nearly equal to each other. It is an advantageous property of the latter technique that it is simpler and it is not dependent on a commercial product such as the shaking apparatus.

Abrasion tests were also carried out with the fractions of the granulate heap. The fractions were kept in a fluidized state by an air stream at a threefold layer expansion for 10 minutes, sieved on a sieve corresponding to the lower dimension limit, and the residual material was measured. The value of the abrasive strength was defined in the following manner:

$$K_s = \frac{G_m}{G} \cdot 100 \qquad (12)$$

where

K_s is the abrasion strength (abrasion resistance) (per cent),

G is the mass of the weighed-in granulate fraction (gram),

G_m is the mass of grains remaining on the sieve corresponding to the lower dimension limit of the granulate fraction (gram).

The following values were obtained for the abrasion strength of the granulate fractions:

d = 0.25 - 0.40 millimetre K_s = 75 per cent
d = 0.40 - 0.63 millimetre K_s = 64 per cent
d = 0.63 - 1.00 millimetre K_s = 62 per cent
d = 1.00 - 2.00 millimetres K_s = 61 per cent

It can be concluded from these data that the abrasion strength of granulates larger than medium is approximately the same, and slightly decreases with increasing size; furthermore, the change in the amount of residual material on the sieve is greater even in the case of medium size than the decrease in average diameter when the whole granulate is subjected to abrasion. The strength of a large number of granulate-fractions was tested and this same tendency was observed in every case. Accordingly, it was concluded that for the evaluation it is sufficient to determine the abrasion strength of the granulate fraction of medium size, i.e. 0.4-0.63 millimetre.

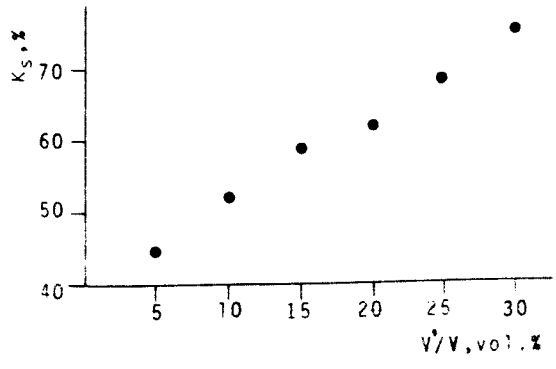

Fig.5

The abrasion strengths of the 0.4-0.63 mm fractions if six granulate heaps are shown, as an example, in Fig.5. The granulates were prepared by fluidization under identical circum-

stances and with the use of different relative amounts of liquid containing the same amount of binding agent. It is apparent from the Figure that the measuring method can be applied for studying the dependence of the abrasion strength on various parameters. The laboratory-type fluidization apparatus (cf. Fig. 3) needed and the procedure of measurement are simple and the results obtained are comparable, because the degree of mechanical stress is independent of the make of the apparatus, as is the case with various types of shaking apparatuses.

REFERENCES

1. RUMPF, H., Chem. Ing. Techn. 30, 144 (1958)
2. NEWITT, D.M., CONWAY-JONES, J.M., Trans. Instn. Chem. Engr. 36, 422 (1958)
3. PANDULA, E., TAKÁCS, G., Ipari Gyógyszerészet (Industrial Pharmacy) Medicina Könyvkiadó, Budapest, 1964.
4. HARWOOD, C.F., PILPEL, N., J. Pharm. Sci. 57, 478 (1968)
5. DAVIES, W.L., GLOOR, Jr.W.T., J. Pharm. Sci. 60, 1869 (1971)
6. MÖBUS, W., Ceskoslov. farm. 18, 109 (1969)
7. MARKS, A.M., SCIARRA, J.J., J. Pharm. Sci. 57, 497 (1968)
8. BERECZKY, É., HENSZELMANN, F., TAMÁS, F., Szilikátipari vizsgálatok II. (Testing Methods in the Silicate Industry II.) Nehézipari Könyvkiadó, Budapest, 1954.
9. KONCZ, J., Portalanitás és porleválasztás (Powder Removal and Powder Separation). Müszaki Könyvkiadó, Budapest, 1970.
10. TAMÁS, F., etc., Szilikátipari laboratóriumi vizsgálatok. (Laboratory Tests in the Silicate Industry). Müszaki Könyvkiadó, Budapest, 1970.

11. ASTM E 20-68 (1968)

12. ERDEY-GRUZ, T., PROSZT, J., Fizikai-kémiai praktikum (Physico Chemical Laboratory Measurements). Tankönyvkiadó, Budapest, 1955.

13. LEADBEATER, C.J., NORTHCOTT, L., HARGREEVES, F., Iron and Steel Spec. Rept. 20, 38 (1947)

14. BUTLER, A.G., RAMSEY, Drug Standards 20, 217 (1955)

15. ASTM D 392-38 (1952)

16. ORMÓS, Z., A fluidizált rétegek kiterjedésének tanulmányozása (Studies on the Expansion of Fluidized Layers. Dissertation for a Doctor's Degree. Veszprém University of Chemical Engineering, 1968.)

17. CARR, L.L., Brit. Chem. Eng. 15, 1541 (1970)

18. GOLD, G., DUVALL, R.N., PALERMO, B.T., SLATER, J.G., J. Pharm. Sci. 57, 2153 (1968)

19. KANENIWA, N., IKEKAWA, N., Chem. Pharm. Bull. (Tokyo) 16, 1433 (1968)

20. LISKE, T., MÖBUS, W., Pharm. Ind. 30, 557 (1968)

21. KAWASHIMA, C., MURATA, N., J. Ceramic. Assoc. (Japan) 63, 88 (1955)

22. TANAKA, T., KAWAI, S., Kagaku Kogaku 20, 144 (1956)

23. LOZHKON, A.F., PASHCHENKO, V.N., Khim. Prom. 44, 451 (1968)

24. CSN Chechoslovak Standard 65 4812

25. SHAFER, E.G., WOLLISH, E.G., ENGER, F.E., J. Am. Pharm. Assoc. Sci. Ed. 45, 114 (1956)

26. FONNER, D.E., BANKER, G.S., SWARBRICK, J., J. Pharm. Sci. 55, 181 (1966)

27. ASTM D-441 (1958)

РЕЗЮМЕ

Знание физических свойств гранулированных зерен важно с точки зрения как использования, так и научной исследовательской работы. Автором изложены методы измерения встречающиеся в литературе, пригодные к определению важнейших физических показателей гранулированных зерен (распределение размеров зерен, показатели плотности, доля объема пор, свойства истечения, прочность), а также дан отчет о результатах исследовательской работы, выполненной в связи с испытанием применимости методов измерения, и разработкой новых методов измерения. Автором введены понятия "плотность разрыхленных множеств зерен" и "коэффициент истечения", и указаны методы измерения применимые для их определения. Дан отчет о разработке простого метода измерения доли объема пор, основанного на одинаковые свойства заполнения пространства зерен подобной формы. Для определения прочности против износа (износостойкости) гранулированных зерен описан автором новый метод измерения, основанный на измерение действия механической нагрузки в псевдоожиженном слое.

Hungarian Journal
of Industrial Chemistry
Veszprém
Vol.1. pp. 229-246 (1973)

DETERMINATION OF OPTIMUM PARAMETERS IN CONNECTION WITH TRANSPORTATION WITH A GAS STREAM

T. BLICKLE and Mrs. E. BÁTOR

(Research Institute for Technical Chemistry of the Hungarian Academy of Sciences, Veszprém)

Received: September 22, 1972.

The specific energy consumption, and - by way of this - the expenditure of the transportation of solid, granular material with a gas stream is highly dependent on the dimensions of the transport conduit and on the working parameters. If the output of the transport system is given, the diameter of the conduit and the amount of transporting gas has to be chosen so as to obtain minimum transportation costs.This problem was solved by the introduction of intermediate variables. A method of calculation is proposed for the determination of the optimum values of the process parameters, such as gas flow rate and volume ratio of solid. The application of the method is illustrated with the example of vertical transportation of sodium bicarbonate.

The way in which problems of transportation - encountered during industrial production - are solved, often contribute in quite a decisive manner to the costs of production. Accordingly, determination of the optimum parameters of the transportation processes applied is closely related to the economic efficiency test of production processes.

Transportation of solid, granular material through pipelines by a gas stream has become more and more popular in almost every branch of industry. The widespread application of this process is

explained by its numerous advantages.The dosts of the installation of the device are low,it can be easily automatized, whereby manual labour can be dispensed with and labour expenses are accordingly reduced. A minimum amount of maintenance is necessary, since there are no moving mechanical parts subject to abrasion and the functioning of the apparatus is highly reliable. The space requirement of the transport conduits is moderate, the pattern of the arrangement of the pipeline is practically unlimited and consequently it can easily be installed even in plants that are already in operation. The conduit lines are hygienic and thus they can also be used in food manufacture. In the chemical industry, the main advantage of the method is that it can be combined with other processes, such as heat exchange, drying, and regeneration of a catalyst, etc. A production process can be made more economical by a combination of such operations.

There is in effect only one drawback to transportation with a gas stream and this is its high energy requirement. The latter may be, at an identical output, as high as five times, or even twenty times as high as that of mechanical devices. The scattering of the energy consumption within extremely wide limits provides a clear indication of the major importance of the actual values of the main dimensions and operating parameters.

THE OBJECTIVE FUNCTION AND CHARACTERISTICS TO BE OPTIMALIZED

The economical aim of optimalization is maximum profit or minimum expenses. However, due to the complicated nature of economic and commercial parameters - which may influence profit in a direct way, i.e. independently of the procedure - it seems more simple to search for a minimum expenditure. The latter is influenced by a number of parameters. However, changes in the parameters of a given process influence only the amortization and energy expenses, and accordingly only these two will be considered as a functional aim [1, 2]:

$$N = N_a + N_e \tag{1}$$

When designing a transport device, the sort of material to be transported, the output, and the starting- and end-points of transportation are usually defined by the problem itself. On the other hand, in the case of transportation with a gas stream it is - within certain limits - up to the designer to decide the quantity of the carrier gas and the diameter of the conduit. During optimalization, the particular values of these two independent variables are sought, at which the sum of the amortization and energy expenses - as related to the unit amount of transported material and the unit path lenght of transportation - are minimal.

In the calculation of the amortization cost, the weight of the transport conduit is taken as the basis:

$$N_a = C_a \frac{\gamma_a \pi}{4 \tau_a G_s} (D_k^2 - D^2) \tag{2}$$

or, expressed with the wall thickness of the conduit:

$$N_a = C_a \frac{\gamma_a \pi}{\tau_a G_s} \delta_a^2 + C_a \frac{\gamma_a \pi \delta_a}{\tau_a G_s} D \tag{3}$$

The cost of energy can be calculated from the pressure drop in the transporting gas:

$$N_e = C_e \frac{\Delta p}{L} \frac{G_g}{\gamma_g G_s} \tag{4}$$

Accordingly, the complete objective function is:

$$N = C_a \frac{\gamma_a \pi}{\tau_a G_s} \delta_a^2 + C_a \frac{\gamma_a \pi \delta_a}{\tau_a G_s} D + C_e \frac{\Delta p}{L} \frac{G_g}{\gamma_g G_s} \tag{5}$$

OPTIMUM VALUES OF THE OPERATIONAL PARAMETERS

The flow characteristics (such as pressure drop, and rate values, etc.) are generally described by the gas flow rate and the volume ratio of the solid. These operational parameters do not appear in the expense function, but they influence the values of the expense terms and at the same time they also depend on the value of the independent variable in the objective function. Accordingly, these parameters will be regarded as intermediate variables.

The relation between the independent and the intermediate variables is the following:

$$G_s = \frac{D^2\pi}{4} \varepsilon_s \gamma_s u_s \tag{6}$$

$$G_g = \frac{D^2\pi}{4} \gamma_g u \tag{7}$$

Considering Equations (6) and (7), Equation (5) can be brought to the following form:

$$N = A_1 + \frac{A_2}{\sqrt{\varepsilon_s u_s}} + A_3 \frac{\Delta p u}{\varepsilon_s u_s} \tag{8}$$

where

$$A_1 = C_a \frac{\gamma_a \pi}{\tau_a G_s} \delta_a^2 \tag{9}$$

$$A_2 = 2\, C_a \frac{\gamma_a \delta_a}{\tau_a} \sqrt{\frac{\pi}{\gamma_s G_s}} \tag{10}$$

$$A_3 = \frac{C_e}{\gamma_s L} \tag{11}$$

The particle flow rate (u_s) and the pressure drop (Δp) are functions of the gas flow rate and the concentration of the solid:

$$u_s = F_1 (u, \varepsilon_s) \tag{12}$$

$$\Delta p/L = F_2 (u, \varepsilon_s) \tag{13}$$

In order to find the optimum of the operational parameters, the extreme value of the objective function (8) according to intermediate variables ε_s and u is found to be:

$$\frac{\partial N}{\partial \varepsilon_s} = -\frac{A_2}{2} \frac{\varepsilon_s \frac{\partial u_s}{\partial \varepsilon_s} + u_s}{(\varepsilon_s u_s)^{3/2}} + A_3 u \frac{\varepsilon_s u_s \frac{\partial \Delta p}{\partial \varepsilon_s} - \Delta p(\varepsilon_s \frac{\partial u_s}{\partial \varepsilon_s} + u_s)}{(\varepsilon_s u_s)^2} = 0 \tag{14}$$

After rearrangement and reduction:

$$\frac{A_2}{2 A_3} = \frac{u}{\sqrt{\varepsilon_s u_s}} \left[\frac{\varepsilon_s u_s \frac{\partial \Delta p}{\partial \varepsilon_s}}{\varepsilon_s \frac{\partial u_s}{\partial \varepsilon_s} + u_s} - \Delta p \right] \tag{15}$$

or

$$\frac{A_2}{2 A_3} = \frac{\Delta p u}{\sqrt{\varepsilon_s u_s}} \left[\frac{\frac{\partial \ln \Delta p}{\partial \ln \varepsilon_s}}{\frac{\partial \ln u_s}{\partial \ln \varepsilon_s} + 1} - 1 \right] \tag{16}$$

By application of simpler designations:

$$\frac{\Delta p\, u}{\sqrt{\varepsilon_s u_s}} = \varphi \tag{17}$$

whence we have

$$\frac{A_2}{2 A_3} = \varphi \left[\frac{1}{\frac{\partial \ln \varepsilon_s}{\partial \ln \varphi} \quad \frac{\partial \ln u_s}{\partial \ln \varphi}} - \frac{1}{2} \right] \tag{18}$$

The partial derivative of the objective function according to (u) is:

$$\frac{\partial N}{\partial u} = -\frac{A_2}{2}\frac{\varepsilon_s \frac{\partial u_s}{\partial u}}{(\varepsilon_s u_s)^{3/2}} + A_3 \frac{(u\frac{\partial \Delta p}{\partial u} + \Delta p)\varepsilon_s u_s - \Delta p\, u \varepsilon_s \frac{\partial u_s}{\partial u}}{(\varepsilon_s u_s)^2} = 0 \qquad (19)$$

After rearrangement we have:

$$\frac{A_2}{2\,A_3} = \frac{\Delta p u}{\sqrt{\varepsilon_s u_s}}\left[\frac{\partial \ln \Delta p}{\partial \ln u_s} + \frac{\partial \ln u}{\partial \ln u_s} - 1\right] \qquad (20)$$

Taking Equation (17) into consideration:

$$\frac{A_2}{2\,A_3} = \varphi\left[\frac{\partial \ln \varphi}{\partial \ln u_s} - \frac{1}{2}\right] \qquad (21)$$

The optimum value of the two operational parameters can be determined from Equations (16) and (20) or (18) and (21). These Equations also provide information on the internal relation between the optimum values of the concentration and gas flow rate:

$$\frac{\partial \ln \Delta p}{\partial \ln u} + 1 = -\frac{\partial \ln u_s}{\partial \ln \varepsilon_s} \qquad (22)$$

Minimum expenditure can be determined for a given transportation assignment if the concrete form of functions (12) and (13) is known, or there are experimental data on the particle flow rate and gas pressure drop as a function of the gas flow rate and solid concentration at the designer's disposal.

Pressure-drop and Rate Relations in Gas-Solid Two-Phase Flow

Due to the flow resistance, the solid granular material brought into the gas stream is accelerated and carried away by the gas stream in the conduit, if the gas flow rate is higher than the terminal free falling velocity of the particles. A gas stream of the flow rate (u_g) carries the solid particles with a free falling velocity of (u_s) this being lower than the former. The relative rate $v = u_g - u_s$ supplies the driving force necessary for transportation. The relative retardation of the material stream alters the composition of the gas-solid mixture in the conduit as compared to the composition of the material fed into the system. As a consequence of collisions and friction occurring during transportation, the solid is slowed down and has to be accelerated again by the gas stream.This continuous rate energy withdrawal manifests itself in a loss in pressure.

The value of the pressure drop is calculated - according to the modern view point - from the equilibrium of forces acting upon one unit volume of the two-phase stream [3-12]. The following simplifications were introduced for the stream of a gas-solid mixture travelling along a straight conduit:

- the flow is stationary and unidimensional,
- the flow rate of the gas and solid along the cross section of the conduit is constant,
- the solid particles are sphere-shaped and of the same size,
- the distribution of the solid material along the cross section of the conduit is uniform,
- the changes in the state of the gas are isothermal.

The equilibrium of the forces acting upon one unit volume of the two-phase stream can be expressed by

$$A\,dp = T_g + T_s + S_g + K \qquad (23)$$

where the individual terms are:

the inertia force of the gas:

$$T_g = \frac{D^2\pi}{4} \varepsilon \frac{\gamma_g}{g} u_g du_g \tag{24}$$

the inertia forces of the solid

$$T_s = \frac{D^2\pi}{4} \varepsilon_s \frac{\gamma_s}{g} u_s du_s \tag{25}$$

the friction forces of the gas:

$$S_g = \frac{D^2\pi}{4} \varepsilon\lambda \frac{dL}{D} \frac{\gamma_g}{2g} u_g^2 \tag{26}$$

the force impeding motion of the solid:

$$K = \frac{D^2\pi}{4} \gamma_s \varepsilon_s (au_s^2 + b)\, dL \tag{27}$$

The latter term accounts for effects arising from the collision, friction and lifting of the solid particles.

Accordingly, considering Equations (24), (25), (26) and (27), the equilibrium equation (23) will take the form

$$dp = \varepsilon \frac{\gamma_g}{g} u_g du_g + \varepsilon_s \frac{\gamma_s}{g} u_s du_s + \varepsilon \frac{\lambda}{D} \frac{\gamma_g}{2g} u_g^2\, dL + \varepsilon_s \gamma_s (au_s^2 + b)\, dL \tag{28}$$

The first term in Equation (28) can be disregarded, if the expansion of the gas stream may be neglected. In the section where the transport is of constant rate, $du_s/dL = 0$ and consequently the second term of Equation (28) may also be neglected. Accordingly, the value of pressure drop in a straight conduit of optional position is

$$\Delta p = \varepsilon \frac{\lambda}{D} \frac{\gamma_g}{2g} u_g^2 L + \varepsilon_s \gamma_s (a u_s^2 + b) L \qquad (29)$$

It must be pointed out that the explanation given for factors a and b in the Equations by various authors differs. According to BARTH and his followers [3-9]

$$a = \frac{\lambda_j}{2 Dg} \qquad (30)$$

$$b = \sin \alpha + \beta_o \cos \alpha \qquad (31)$$

The value of the additional pipe friction coefficient λ_j, as determined by measurement, is generally given as a function of the Froude-number, with the parameters of the transport characteristics. The factor β_o accounts for the work necessary to lift the particles in the case of horizontal transportation.

The motion-retarding force K, in Hungarian literature, based on works by PATTANTYUS [10], PÁPAI [11] and SZŐNYI [12], is considered to be - in addition to the lifting force required in vertical transportation - the result partly of collisions and partly of friction. Assuming the mean of the retaining force originating from collisions in time to be a force that is acting continuously, the following expression is obtained for factor a:

$$a = \frac{k_{1v}}{2g} (1 + C_1 \sin \alpha) \qquad (32)$$

whereas factor b accounts for the vertical lifting of the weight and the friction of the solid material:

$$b = \sin \alpha + k_2 \xi_s \qquad (33)$$

ξ_s is a constant characteristic of the quality of the solid and of the conduit wall.

In addition to the quality of the transported material and the conduit, the values of factors a and b also depend on the concentration of the solid. According to SZŐNYI [12], the k_{lv} collision coefficient included in factor a has - in the case of low solid concentrations ($\varepsilon_s < 0.03$) - a high and practically constant value. The latter decreases with increasing concentration in an exponential manner. The value of the proportionality factor k_2 increases with increasing solid concentration. In a horizontal conduit, the particles whole weight participates in creating a friction force and the value of k_2 tends to 1. A smaller friction force arises, according to experience, in vertical transportation and consequently the value of k_2 can be only a fraction of that encountered in the previous case. In the case of transportation in a dilute stream - especially if the solid particles are elastic - k_2 tends to zero.

The motion equation of the solid material - with the use of the simplifications discussed earlier - can be derived from the equilibrium of the forces acting upon the particles dispersed in one unit volume of the conduit. The resistance of medium - brought about by the relative velocity between the particles and the gas stream - acts as a driving force and this must be in equilibrium with the inertia force of the particles, and the retaining forces originating from friction or/and collision and lifting work:

$$C_h A_h \frac{\gamma_g}{2g} (u_g - u_s)^2 = \frac{D^2\pi}{4} \varepsilon_s \gamma_s dL \left[\frac{u_s}{g} \frac{du_s}{dL} + a u_s^2 + b \right] \qquad (34)$$

Assuming the specific gravity of the gas to be negligible, as compared to that of the solid: $\gamma_s - \gamma_g \approx \gamma_s$, the weight of the solid present in a unit volume can be expressed with the aid of the terminal free falling velocity:

$$\frac{D^2\pi}{4} \varepsilon_s \gamma_s \, dL = C_h A_h \frac{\gamma_g}{2g} v_s^2 \qquad (35)$$

Accordingly, the equation of motion of the solid phase of a two-phase gas-solid system is:

$$\frac{du_s}{dL} = \frac{g}{u_s}\left[\frac{(u_g - u_s)^2}{v_s^2} - au_s^2 - b\right] \tag{36}$$

In the case of the transportation of a stationary rate $du_s/dL = 0$ and by introduction of the gas flow rate as calculated for the empty conduit cross section:

$$u_s = \frac{1}{1 - av_s^2}\left[\frac{u}{\varepsilon} - v_s\sqrt{(1 - av_s^2)b + a\frac{u^2}{\varepsilon^2}}\right] \tag{37}$$

VARIATIONS IN THE EXPENDITURE OF TRANSPORTATION IN THE FUNCTION OF OPERATIONAL PARAMETERS

The formation of expenditure and optimum determination is illustred with the example of the vertical transportation of sodium bicarbonate. The characteristics of the material to be transported are as follows:

$d_o = 9 \cdot 10^{-5}$ metres
$\gamma_s = 2200$ kilograms (weight)/cu.metre
$v_o = 0.45$ metres/second

The transporting gas is air.

For the values of factors a and b of Equations (29) and (37) the experimental values

$a = 8 \cdot 10^{-3}$
$b = 1$

were found in tests carried out in a conduit of the diameter D = 36 millimetres in dilute-stream ($\varepsilon_s < 0.005$) transportation.

The value of the friction coefficient, as referred to the empty tube, is $\lambda = 0.03$. By using data published by WEBER [9], the connection between the concentration of the solid and factor a can be described by the following empirical formula:

$$a = 8 \cdot 10^{-3}\, e^{-0.0585\,\varepsilon_s} \tag{38}$$

The particle flow rate values, as calculated by Equation (37), are illustrated as a function of gas rate in Fig.1. Measured data pertaining to transportation in a dilute stream ($\varepsilon_s < 0.005$) are also included in the Figure. The pressure-drop relations, in accordance with Equation (29) for the case of transportation of sodium bicarbonate are shown in Fig.2.

By substituting the pressure drop and particle flow rate values, as expressed by Equations (29) and (37), into the objective function (8), the specific expenditure of transportation as the function of gas flow rate and solid concentration can be determined. The results of these calculations are illus-

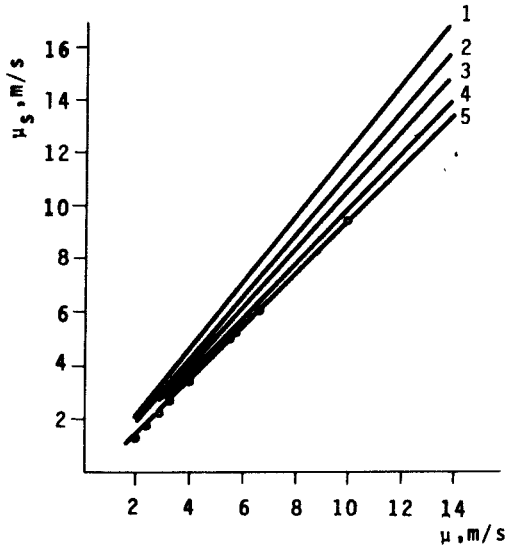

Fig.1. 1 - ε_s = 0.20; 2 - ε_s = 0.15; 3 - ε_s = 0.10; 4 - ε_s = 0.05; 5 - ε_s = 0.01

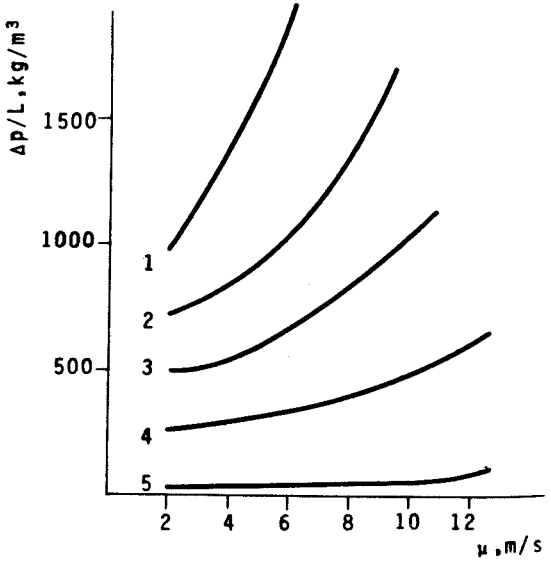

Fig.2. 1 - ε_s = 0.46; 2 - ε_s = 0.31; 3 - ε_s = 0.21; 4 - ε_s = 0.11; 5 - ε_s = 0.01

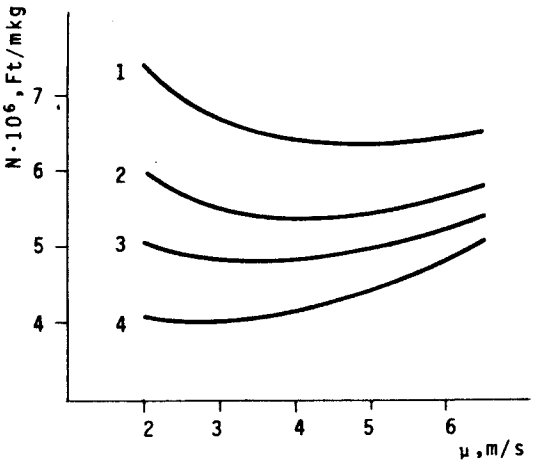

Fig.3. 1 - ε_s = 0.11; 2 - ε_s = 0.21; 3 - ε_s = 0.31; 4 - ε_s = 0.46

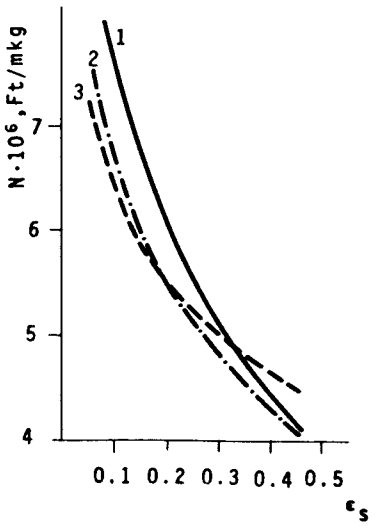

Fig.4. 1 - μ = 2.0 m/sec; 2 - μ = 3.5 m/sec; 3 - μ = 5.0 m/sec

trated in Fig.3 and 4 for an output of 1000 kilograms(weight)/hour if the values of the constants contained in the aim function are the following:

C_a = 30 Forints/kilogram (weight)

γ_a = 7,900 kilograms (weight)/cu.metre

δ_a = 0.01 metre

τ_a = 72,000 hours

C_e = $3 \cdot 10^{-6}$ Forint/metre kilogram (weight)

It is clearly apparent from the Figures that the specific expenditure of transportation shows a monotonous decrease with increasing solid concentration. From an economical point of view it is preferable to choose the parameters of transportation so as to have as high a solid concentration in the transporting conduit as possible.

The transportation expenditure, when examined as a function of the gas flow rate, exceeds a minimum. The flow rate value corresponding to this minimum decreases with increasing solid concentration. The optimum value can be determined by means of Equation (21). The value of the right-hand side of the Equation (NU in the following) as a function of gas flow rate and at various concentrations is shown in Fig.5. The value of the ratio at the left-hand side of Equation (21) is

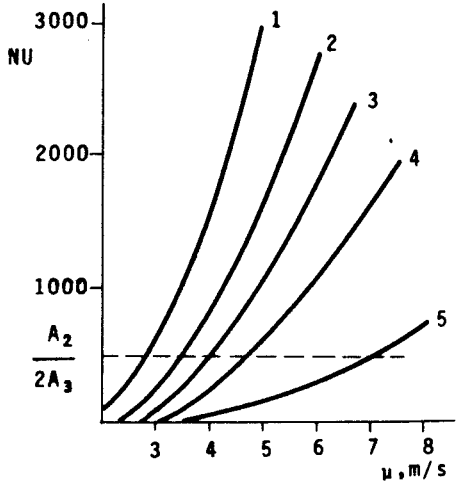

Fig.5. 1 - ε_s = 0.46; 2 - ε_s = 0.31; 3 - ε_s = P.21; 4 - ε_s = 0.11; 5 - ε_s = 0.01

$$\frac{A_2}{2\ A_3} = 484$$

at the values of the economical coefficients given in the foregoing and at an output of 1000 kilograms (weight)/hour. The intersection point of this straight line with the curves of various ε_s parameter values directly gives the optimum gas flow rate pertaining to the actual solid concentration. The relation between the optimum rate and concentration is illustred in Fig.6.If the highest material

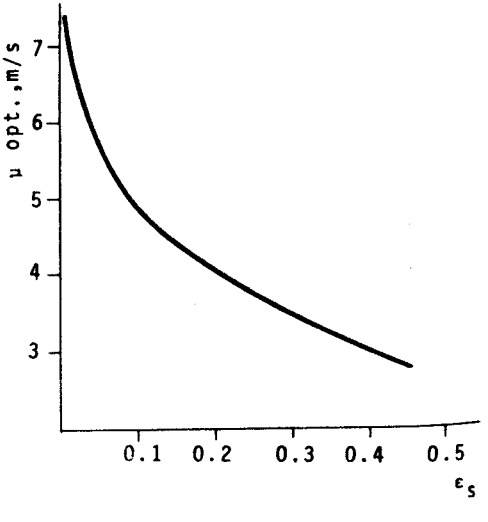

Fig.6.

concentration is substituted into the value of φ, the gas flow rate determined on the basis of Equation (21) gives the lowest possible expense of transportation.

If the optimum values of the operational parameters are known, it is also possible to determine the optimum values of the variables of the original objective function (5). The solid flow rate pertaining to the $U_{optimum}$ and the chosen ε_s values can be calculated from Equation (37), and the diameter of the transport conduit from Equation (6). The amount of gas necessary for the transportation may be determined by Equation (7).

The calculations carried out so far covered the whole range of theoretically possible solid concentrations, from $\varepsilon_s = 0$ to $\varepsilon_s = 1 - \varepsilon_m$. Decisions concerning the practical upper limit of increasing the solid concentration - either by modification of the transport conduit [7] or by application of an auxiliary procedure, without modifying the aim function - require further investigation.

SYMBOLS USED

A - cross section of conduit (sq. metre)

A_h - area of the projection of the particle accumulation in a direction perpendicular to the direction of flow (sq. metre)

C_1 - constant

C_a - cost of the material of the conduit [Forints/kilogram (weight)]

C_e - cost of energy [Forints/metre kilogram (weight)]

C_h - resistance coefficient of the particle accumulation

D - internal diameter of the conduit (metre)

D_k - external diameter of the conduit (metre)

d_o - diameter of the particle (metre)

G_g - weight flow rate of the transporting gas [kilogram (weight)/second]

G_s - weight flow rate of the solid (kilogram (weight)/second)

k_{1v} - collision coefficient measured in a horizontal conduit (metre)$^{-1}$

k_2 - proportionality factor

K - motion-inhibiting force [kilogram (weight)]

L - length of conduit (metre)

N - specific cost of transportation [Forints/metre kilogram (weight)]

N_a - amortization expense ratio [Forints/metre kilogram (weight)]

N_e - energy expense ratio [Forints/metre kilogram (weight)]

p - pressure [kilogram (weight)/sq.metre]

Δp - pressure drop [kilogram (weight)/sq.metre]

S_g - friction forces in the gas [kilogram (weight)]

T_g - inertia force of the gas [kilogram (weight)]

T_s - inertia force of the solid [kilogram (weight)]

u - gas flow rate referred to the total conduit cross section (metres/second)

u_g - actual flow rate of the gas (metres/second)

u_s - flow rate of the solid particles (metres/second)

v - relative rate between gas and solid (metres/second)

v_o - terminal free-falling velocity of single particle (metres/second)

v_s - terminal free-falling velocity of particle in a suspension of porosity ε, (metres/second)

α - slope of the conduit, as compared to the horizontal

γ_a - specific gravity of the conduit material [kilogram (weight)/cu.metre]

γ_g - specific gravity of the gas [kilogram (weight)/cu.metre]

γ_s - specific gravity of the solid [kilogram (weight)/cu.metre]

δ_a - wall thickness of the conduit (metre)

ε - volume ratio of gas

ε_s - volume ratio of solid

ε_m - minimum gas volume ratio

λ - conduit friction coefficient

λ_j - additional conduit friction coefficient

ξ_s - friction coefficient

τ_a - amortization time (sec)

REFERENCES

1. BLICKLE, T., Magyar Kémikusok Lapja 24, 425 (1971)

2. ORMÓS, Z., BLICKLE, T., Magyar Kémikusok Lapja 24, 432 (1971)

3. BARTH, W., Chem. Ing. Techn. 30, 171 (1958)

4. BARTH, W., Chem. Ing. Techn. 32, 164 (1960)

5. MUSCHELKNAUTZ, E., VDI.-Forschungsheft No 476 B25 (1959)

6. MUSCHELKNAUTZ, E., KRAMBROCK, W., Chem. Ing. Techn. 41, 1164 (1969)

7. LIPPERT, A., Chem. Ing. Techn. 38, 350 (1966)

8. BOHNET, M., VDI.-Forschungsheft 507 (1965)

9. WEBER, M., Deutsche Hebe- und Fördertechnik 14, 344 (1968)

10. PATTANTYUS, G.Á., Anyagszállitás légáramban. MTI (Material Transport in an Air Stream. Hung. Acad. of Sciences) Budapest, 1953.

11. PAPAI, L., Darutervezés III. Anyagszállitás légáramban és folyadékárambạn. MTI. (Design of Cranes III. Material Transport in Gas and Liquid Streams. Hung. Acad. of Sciences) Budapest, 1965.

12. SZŐNYI, J., Fluidizációs anyagszállitási vizsgálatok. Kandidátusi értekezés. (Studies on Material Transport by Fluidization. Dissertation for a Candidate's Degree.) Veszprém, 1969.

РЕЗЮМЕ

Удельная затрата энергии транспортировки твердых зернистых материалов при помощи газового потока, и таким путем денежные расходы транспорта в значительной мере зависят от расчета транспортного провода и показателей эксплуатации. При проектировке транспортной системы - в случае определенной мощности транспорта - диаметр провода и количество транспортирующего газа необходимо выбрать с таким расчетом, чтобы расходы транспортировки были минимальными. Задача решена авторами введением вспомогательных переменных. Для определения оптимальных величин показателей процесса - скорость газа, объемная доля твердого вещества - описан метод вычисления. Применение метода представлено на примере вертикального транспорта кислого карбоната натрия.

Hungarian Journal
of Industrial Chemistry
Veszprém
Vol.1. pp. 247-270 (1973)

MATHEMATICAL MODELS FOR RECTIFICATION PROCESSES

M. PARTI and B. PALÁNCZ

(Budapest Technical University, Institute for Chemical Industrial Machines and Agricultural Industries, Budapest)

Received: September 29, 1972.

A large number of mathematical models for the dimensioning of rectifying column and the description of the process of rectification can be found in literature. However, all these models use the concept of plate or column efficiency. In the present paper, a mathematical model is proposed for the case of continuous and non-continuous rectification which, by application of the diffusion model, dispenses with the necessity of the knowledge of the efficiency. Numerical examples were elaborated for the illustration of the models. The calculations were carried out by an electronic computer.

INTRODUCTION

Rectification is an operation which enables a vapour to be obtained that is substantially richer than the liquid left in the still. This operation is very frequently applied in the chemical industry. In the fractionating columns used to carry out the operation, heat and material transfer processes occur simultaneously. In order to determine the main dimensions of such columns, the McCabe-Thiele method is most frequently applied, and the Ponchon-Savarit method [1] in the case of non-constant overflow is used. A number of papers were published in recent years [2] dealing with

this subject and proposing models which enable more accurate theoretical description of the processes. Efforts were made to try to describe the simultaneous heat and material transfer by analytical methods. The most important drawback of the above-mentioned graphical methods is the fact that the determination of the plate or column efficiency is difficult [3].

In the present paper a mathematical model is proposed for the numerical dimensioning of two-component fractionating columns. The treatment is basically valid for plate-type columns, but - with slight modifications - it can also be used for packed columns.

A diffusion model is applied in connection with the plate. The relations are presented for continuous and batch operation, the application is illustrated by a numerical example.

CONTINUOUS OPERATION

As mentioned in the foregoing, graphical methods, and - in the case of certain operational conditions - analytical procedures [e.g. Fenske-Underwood equation (1)] can be used for the determination of the theoretically necessary number of plates in continuous rectifying columns. The real number of plates can be determined if the column or plate efficiency is known.

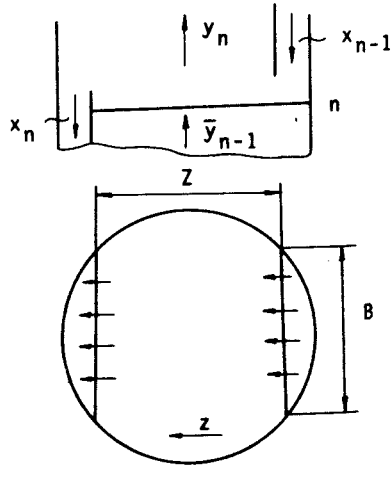

Fig. 1

Mathematical Model

Let be considered the n^{th} plate of the column (Fig. 1). The concentration of the liquid entering the plate (z=0) is x_{n-1}. The liquid,

during its progress along the plate, meets the vapour arising from plate n+1. This vapour is well mixed and consequently its concentration along the co-ordinate z is constant and it leaves the plate enriched in the more volatile component. This concentration is, naturally, a function of the co-ordinate z. The liquid, having passed a plate of the length Z, leaves it at a concentration x_n.

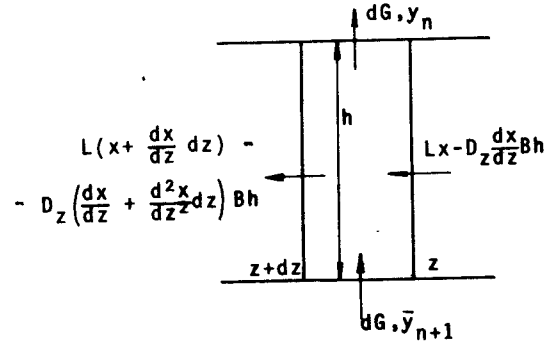

Fig. 2

As a first step, the material balance of the more volatile component is written for an elementary liquid layer of the height h (Fig. 2):

$$L\left(x+\frac{dx}{dz}dz\right)-D_z\left(\frac{dx}{dz}+\frac{d^2x}{dz^2}dz\right)Bh+dGy_n=$$

$$=Lx-D_z\frac{dx}{dz}Bh+dG\bar{y}_{n+1}$$

and

$$L\frac{dx}{dz}dz-D_z\frac{d^2x}{dx^2}dzBh=dG(\bar{y}_{n+1}-y_n) \qquad (1)$$

The material transport between the liquid and the vapour phases can be described by the material transfer coefficient on the side of the vapour:

$$dG(\bar{y}_{n+1}-y_n)=\beta_g(y_n-y^*)dfe \qquad (2)$$

(It is to be mentioned that the vapour concentration varies between the values $\bar{y}_{n+1}$ and y_n and consequently Equation (2) is, at the same time, the equation defining the vapour side transfer coefficient.)

The specific contact area referred to unit volume is introduced:

$$\varepsilon = \frac{dfe}{dV} = \frac{1}{Bh}\frac{dfe}{dz} \tag{3}$$

Considering Equations (2) and (3), Equation (1) becomes

$$L\frac{dx}{dz} - D_z\frac{d^2x}{dz^2}Bh + \beta_g(y^* - y_n)\,Bh\varepsilon = 0$$

With the introduction of the dimensionless variables

$$\xi = \frac{z}{Z}, \quad Pe = \frac{LZ}{BhD_z}, \quad No = \frac{\beta_g \varepsilon Bh}{L}Z$$

the Equation (4) attains the following final form:

$$\frac{dx}{d\xi} - \frac{1}{Pe}\frac{d^2x}{d\xi^2} + No\,(y^* - y_n) = 0 \tag{4}$$

where

$$0 \le \xi \le 1 \quad \text{and} \quad x_{n-1} \le x \le x_n;$$

The calculation of the concentration of the vapour rising from the plate should now be examined. Considering Equation (3), Equation (2) can be written in the form

$$\frac{dG}{dz} = \frac{\beta_g \varepsilon Bh(y_n - y^*)}{y_{n+1} - y_n}$$

but, the molar mass fluxes are constant and accordingly

$$\frac{dG}{dz} = \text{constant} = \frac{G}{z}$$

and consequently

$$\bar{y}_{n+1} - y_n = \frac{L}{G} No(y_n - y^*) \tag{5}$$

For the case of the rectifying section, the ratio L/G can be expressed by the reflux ratio:

$$\frac{L}{G} = \frac{R}{R + 1}$$

and accordingly

$$y_n = \frac{No\,R}{R + 1} (y^* - y_n) + \bar{y}_{n+1}$$

Rearranging:

$$y_n = \frac{\bar{y}_{n+1} + No \frac{R}{R + 1} y^*}{1 + No \frac{R}{R + 1}} \tag{6}$$

The average concentration of the vapour rising from the plate is

$$\bar{y}_n = \frac{1}{Z} \int_0^Z y_n \, dz = \int_0^1 y_n \, d\xi \tag{7}$$

The value of y^* can be determined on the basis of the equilibrium curve

$$y^* = \varphi(x) \tag{8}$$

An equation essentially similar to Equation (5) can be written for the stripping section, with the difference that is this case $\bar{L}$ and $\bar{G}$ values are used which correspond to the change in material flux caused by the feed:

$$y_n = \frac{\bar{y}_{n+1} + \bar{N}o\bar{L}/\bar{G}y^*}{1 + \bar{N}o\bar{L}/\bar{G}}$$

The f^{th} plate, i.e. the plate where the feed enters will now be examined in order to determine the relation between the concentrations in the rectifying and the stripping sections, resp. (cf. Fig. 3).

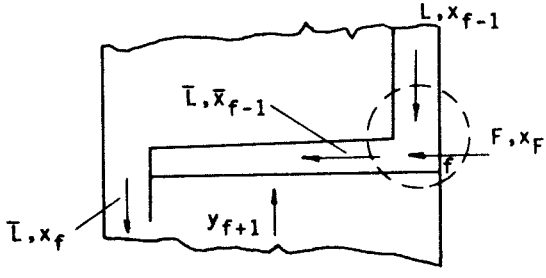

Fig. 3

Supposing that a thorough mixing has occurred between the feed and the liquid leaving plate (f - 1) in the downcomer tube prior to entering the plate, the material balance for the volatile component is:

$$Lx_{f-1} + Fx_F = \bar{L}\bar{x}_{f-1}$$

or

$$x_{f-1} = \frac{\bar{L}}{L}\bar{x}_{f-1} - \frac{F}{L}x_F \qquad (9)$$

It is apparent that only the relation between the material fluxes need to be given. This can be done on the basis of the overall material and heat balances of the feed plate (Fig. 4).

The overall material balance is:

$$L + F + \bar{G} = G + \bar{L}$$

The heat balance is:

$$Li_L + Fi_F + \bar{G}i_{\bar{g}} = Gi_G + \bar{L}i_L$$

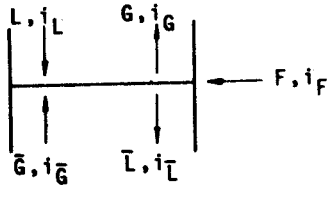

Fig. 4

Assuming that

$$i_L \approx i_{\bar{L}} \quad \text{and} \quad i_G \approx i_{\bar{G}}$$

the ratio of the change in molar flux of the liquid to the feed flux is q:

$$q = \frac{\bar{L} - L}{F} \tag{10}$$

It follows from this and the previous two balance equations that

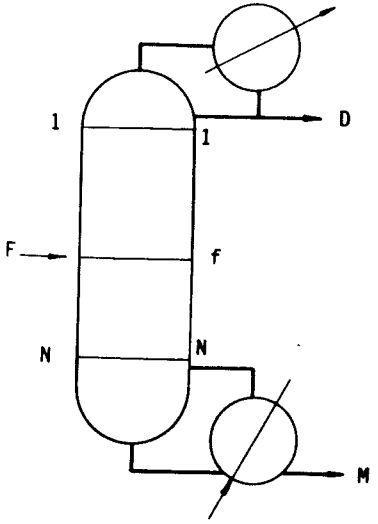

Fig. 5

$$\frac{\bar{G} - G}{F} = q - 1 \tag{11}$$

and

$$q = \frac{i_G - i_F}{i_G - i_L} \tag{12}$$

Summarizing the equations obtained, and taking Fig. 5 into consideration, we obtain

$$\frac{dx}{d\xi} - \frac{1}{Pe}\frac{d^2x}{d\xi^2} + No(y^* - y_n) = 0 \tag{4}$$

where

$$Pe = \begin{cases} LZ/BhD_z & \text{if } 1 \le n \le f-1 \\ \bar{L}Z/BhD_z & \text{if } f \le n \le N \end{cases}$$

$$y_n = \frac{\bar{y}_{n+1} + No\ (L/G)y^*}{1 + No\ (L/G)} \tag{6}$$

where

$$No\ L/G = \begin{cases} \dfrac{\beta_g \varepsilon Bh\ Z}{G} & \text{if } 1 \le n \le f-1 \\ \dfrac{\beta_g \varepsilon Bh\ Z}{\bar{G}} & \text{if } f \le n \le N \end{cases}$$

$$\bar{y}_n = \int_0^1 y_n \, d\xi \tag{7}$$

$$y^* = \varphi(x) \tag{8}$$

$$x_{f-1} = \frac{\bar{L}}{L} \bar{x}_{f-1} - \frac{F}{L} x_F \tag{9}$$

$$\bar{L} - L = Fq \tag{10}$$

$$\bar{G} - G = F(q-1) \tag{11}$$

$$q = \frac{i_G - i_F}{i_G - i_L} \tag{12}$$

In order to make the model complete, the boundary conditions are to be defined.

Boundary Conditions

In the case of Equation (4) (13)

$$x(1) = x_n \qquad 1 \leq n \leq N \tag{13}$$

and

$$\frac{dx}{d\xi}(1) < 0 \tag{14}$$

i.e. the derivative of the concentration function of the liquid leaving the plate is a constant, which is characteristic of the plate (and of the degree of the material transfer) whose value is different at every plate. As a first approximation, it was supposed that the value of this constant was zero. In order to establish the validity of the material balance, the value of the constant was varied by iteration until the material balance was true to the prescribed degree of accuracy. It should be noted here that

the value of Equation (14) cannot be zero, as it is generally assumed in literature [e.g. (5)]; this would be true only in the case of a plate of infinite width.

The concentration of the distillate should be known, i.e.:

$$x_1 < x(\xi) = x_D \qquad 0 \leq \xi \leq 1 \tag{15}$$

Equation (15) should be formulated like this, since it cannot be prescribed that

$$x_1 < x\ (0) = x_D$$

if the value of Z is fixed.

Generally the concentration of the bottom product is also prescribed; however, this is not adequate to be chosen as a boundary condition. Considering Fig. 6 the material balance for the more volatile can be constructed:

$$\bar{L}x_N = \bar{G}\bar{y}_{N+1} + Mx_M$$

and from this

$$x_N = \frac{\bar{G}}{\bar{L}}\bar{y}_{N+1} + \frac{M}{\bar{L}}x_M$$

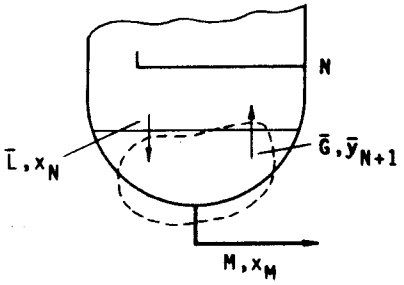

Fig. 6

Assuming equilibrium in the boiler:

$$\bar{y}_{N+1} = \varphi(x_M)$$

and consequently

$$x_N = \frac{\bar{G}}{\bar{L}}\varphi(x_M) + \frac{M}{\bar{L}}x_M \tag{16}$$

The material fluxes can be determined on the basis of the top and bottom product concentrations, as well as the condition - Eq.

(12) -, amount and concentration of the feed, for a given reflux ratio, since

$$R = \frac{L}{D}$$

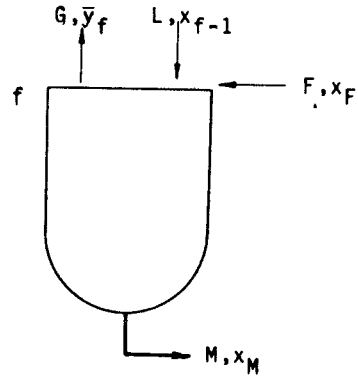

Fig. 7

and on the basis of Fig. 7

$$Fx_F = Dx_D + Mx_M$$

and

$$F = D + M$$

The value of D and M can be determined from this equation, and on the basis of

$$L = RD$$

and

$$G = L + D$$

the material fluxes in the rectifying section are L and G. By the application of the values of q and F and on the basis of Equations (10) and (11), the $\bar{L}$ and $\bar{G}$ values will be known.

Moreover, the location of the feed, i.e. the value of f should be known. Considerations concerning this problem will be described in the following.

Numerical Solution

In the determination of the boundary conditions, cases were considered where the degree of separation was predetermined and the necessary number of plates was sought. The algorithm enabling the calculation of this problem will be described here.

The calculation will be started at the bottom of the column, at the N^{th} plate, considering the conditions

$$x(1) = x_N$$

and

$$\frac{dx}{d\xi}(1) = \text{constant} \quad (N)$$

The equilibrium curve can be written, with the application of the relative volatility, in the following form

$$y^* = \frac{\alpha x}{1 + (\alpha - 1)\, x} \tag{17}$$

where generally $\alpha = \alpha(x)$, i.e. the y^* pertaining to a given x value can be determined. The value of y_n for the lower section is obtained on the basis of Equation (6):

$$y_n = \frac{\bar{y}_{n+1} + y^* \bar{N}o\, \bar{L}/\bar{G}}{1 + \bar{N}o\, \bar{L}/\bar{G}}$$

Accordingly, $x(\xi)$ can be calculated with the application of Equation (4). By proceeding along the plate to the value $\xi = 1$, the function $y_n(\xi)$ is obtained, by whose integration the average concentration of the vapour arising from the plate is obtained [cf. Equation (7)]. If the place of feed has been reached, the change in concentration due to the feed can be calculated by Equation (9), where

$$\bar{x}_{f-1} = x(0)$$

for the f^{th} plate.

Using Equations (10), (11), and (12), the material fluxes, as well as the No and Pe values of the rectifying section can be determined. The calculation is then carried on until the condition

$$x(\xi) \geq x_D$$

comes true. The plate on which this occurs will be the first plate.

Hereupon the calculation is repeated with various feed places taken until the particular feed place giving the minimum number of plates is found.

In order to illustrate the aforesaid, a numerical example will be presented. The calculations were carried out using digital computer type ODRA 1204.

Numerical Example

Data used in the calculation of the example:

D	= 88.8 kilomoles/hour	F	= 216.8 kilomoles/hour
M	= 128 kilomoles/hour	q	= 0.916
x_M	= 0.00565	x_F	= 0.36
$\bar{L}$	= 303.4 kilomoles/hour	x_D	= 0.87
$\bar{G}$	= 174.45 kilomoles/hour	$\bar{p}$	= 0.0782 hour/kilomole
α	= 5	$\bar{e}$	= 303.4 hours/kilomole

where Pe = $\bar{p}L$ and $\bar{e}$ = L No.

The material transfer surface area and the material transfer coefficient were determined on the basis of HOBLER [4], whereas the diffusion coefficient can be calculated on the basis of GERSTER [3].

The results obtained are illustrated in Figs. 8, 9 and 10. Figs. 8 and 9 show the changes in liquid and vapour concentrations along the plate, resp. Fig. 10 shows the concentration of the liquid entering the plate and the average composition of the vapour leaving the plate along the height of the column.

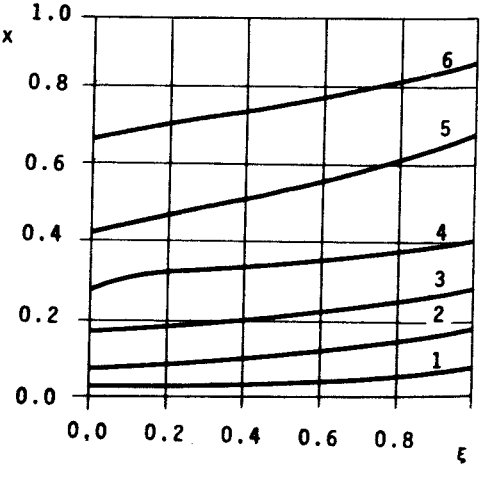

Fig. 8

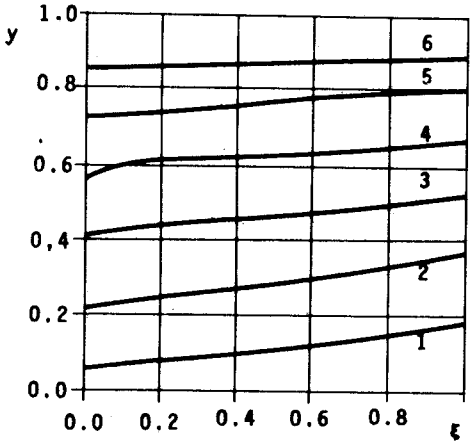

Fig. 9

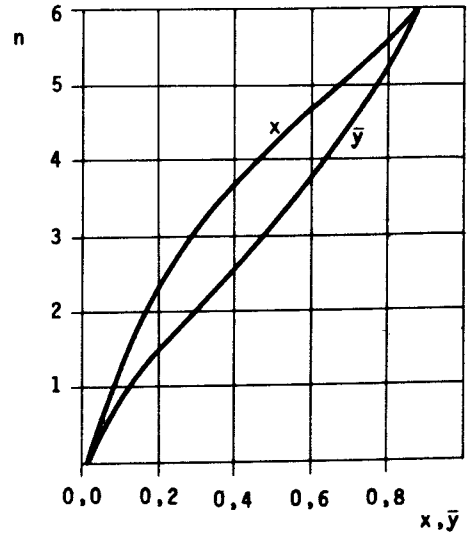

Fig. 10

BATCH OPERATION

In the case of batch fractionating columns, two modes of operation can be distinguished, according to the aim of the process:

- operation with a distillate of constant composition,
- operation at a constant reflux ratio.

From the two modes of operation mentioned above, the first is applied more frequently. This necessitates a continuous variation of the reflux ratio.

A batch fractionating column will now be considered and its mathematical model constructed, together with necessary initial and boundary conditions. Heat and material balances will be employed.

Mathematical Model

The fractionating column is shown in Fig. 11. The material balance of the column will now be constructed for time instants τ and $\tau + d\tau$. The overall material balance is

$$F = (F + \frac{dF}{d\tau} d\tau) + D\, d\tau$$

from where

$$D = -\frac{dF}{d\tau} \qquad (18)$$

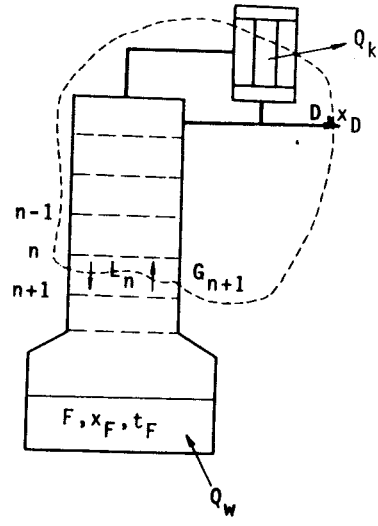

Fig. 11

The material balance for the more volatile component is

$$Fx_F = (F + \frac{dF}{d\tau} d\tau)(x_F + \frac{dx_F}{d\tau} d\tau) + Dx_D\, d\tau$$

and rearranging

$$\frac{dx_F}{d\tau} = -\frac{D}{F}(x_D - x_F) \qquad (19)$$

The following two equations are deduced from the material balances applied to the column.

The overall material balance, for the part enclosed by the control surface is

$$D + L_n = G_{n+1} \qquad (20)$$

The material balance for the more volatile component, for the part enclosed by the control surface is

$$Dx_D + L_n x_n = G_{n+1}\, y_{n+1}$$

from which

$$x_n = \frac{G_{n+1}}{L_n} y_{n+1} - \frac{D}{L_n} x_D \tag{21}$$

Further relations can be derived by constructing the heat balance:

$$Fi_F + qAd\tau = (F + \frac{dF}{d\tau} d\tau)(i_F + \frac{di_F}{d\tau} d\tau) + Di_D d\tau + (D + L_n) M_D r_D d\tau$$

It is supposed that a perfect condensation occurs in the condenser, where the amount of heat to be removed is

$$Q_k = (D + L_n) M_D r_D$$

the same, expressed with the reflux ratio, is

$$Q_k = D(R + 1) M_D r_D$$

The relation can be simplified by supposing the additivity of the enthalpy:

$$i = [xc_1 + (1 - x)c_2]t \tag{22}$$

and

$$\frac{di}{d\tau} = \frac{\partial i}{\partial t}\frac{dt}{d\tau} + \frac{\partial i}{\partial x}\frac{dx}{d\tau}$$

where

$$\frac{di}{dt} = xc_1 + (1 - x)c_2 \tag{23}$$

$$\frac{di}{dx} = (c_1 - c_2)t$$

The above equation can be simplified - the group of Equations (23) is, for the sake of conciseness, not gi[illegible] -

$$qA = F \frac{\partial i_F}{\partial t_F} \frac{dt_F}{d\tau} + F \frac{\partial i_F}{\partial x_F} \frac{dx_F}{d\tau} + D\,(i_D - i_F) + (D + L_n)\, M_D r_D \qquad (24)$$

The following should be added to the connections obtained in the above:

$$t_F = \varphi(x_F) \qquad (25)$$

and

$$\frac{dt_F}{d\tau} = \frac{dt_F}{dx_F} \frac{dx_F}{d\tau} = a(x_F) \frac{dx_F}{d\tau} \qquad (26)$$

from where Equation (24), considering also Equation (19), will become

$$qA = D[i_D - i_F - (x_D - x_F)(\frac{\partial i_F}{\partial t_F} a(x_F) + \frac{\partial i_F}{\partial x_F}) + (1 + R)\, M_D r_D]$$

or

$$qA = D[i_D - i_F - (x_D - x_F)[(x_F c_1 + (1 - x_F)c_2)a(x_F) +$$

$$+ (c_1 - c_2)t_F] + (1 + R)\, M_D r_D] \qquad (27)$$

where the enthalpies i_D and i_F can be calculated from Equation (22), taking the corresponding concentrations x_D and x_F as well as the temperatures t_D and t_F into consideration.

The relations defined in the foregoing have to be supplemented with the equation of the equilibrium curve, as well as with the elementary material balances as written for a plate (cf. section 1.) and the definition of the reflux ratio.

In accordance with the foregoing, the equations can be summarized in the following:

$$\frac{dF}{d\tau} = -D \qquad (18)$$

$$\frac{dx_F}{d\tau} = -\frac{D}{F}(x_D - x_F) \tag{19}$$

$$D + L_n = G_{n+1} \tag{20}$$

$$x_n = \frac{G_{n+1}}{L_n} y_{n+1} - \frac{D}{L_n} x_D \tag{21}$$

$$qA = D\{i_D - i_F - (x_D - x_F)[(x_F c_1 + (1 - x_F)c_2)a(x_F)t_F] +$$

$$+ (1 + R) M_D r_D\} \tag{27}$$

$$y^* = \varphi(x) \tag{8}$$

$$\frac{dx}{d\xi} - \frac{1}{Pe}\frac{d^2x}{d\xi^2} + No(y^* - y_n) = 0 \tag{4}$$

$$y_n = \frac{\bar{y}_{n+1} + No\ L_n/G_{n+1}\ y^*}{1 + No\ L_n{}^*G_{n+1}} \tag{6}$$

$$R = R(\tau) = \frac{L_n(\tau)}{D(\tau)} = \frac{L_n(\tau)}{G(\tau) - L_n(\tau)} \tag{28}$$

$$q = k(t_f - t_F) \tag{29}$$

where t_f is the constant temperature of the heating medium and k is the heat transfer coefficient.

It is supposed in the course of the solution of the set of equations that the molar material fluxes are unchanged along the column in a given time instant (i.e. the dynamic hold-up is constant along the column, but it may be dependent on time).

Conditions

In order to solve the set of equations, the initial and boundary conditions, which, for Equation (4), are the following

$$x(1) = x_n \qquad 1 \leq n \leq N \tag{13}$$

and

$$\frac{dx}{d\xi}(1) = \text{constant}(n) \tag{14}$$

The constant described here is characteristic of the plate mentioned in the foregoing.

The initial conditions are the following:

$$\begin{aligned} F(0) &= F_o \\ x_F(0) &= x_{F_o} \\ t_F(0) &= t_{F_o} \end{aligned} \tag{30}$$

The further conditions are dependent on the mode of operation and accordingly in the first mode

$$x_1 < x(\xi) = x_D = \text{constant} \qquad 0 \leq \xi \leq 1 \tag{15a}$$

and

$$R(0) = R_o \tag{31a}$$

whereas in the second mode of operation

$$x_D(0) = x_{D_o} \tag{15b}$$

and

$$R(\tau) = R_o = \text{constant} \tag{31b}$$

Numerical Solution

While defining the limiting conditions it was supposed that the number of the plates being present in the column is at first not defined, it will be decided on the basis of the initial condition with application of the model. The calculation is carried out according to the following:

the molar material flux of the destillate is determined from the given conditions by Equation (27) and hereafter the material fluxes are determined with the application of the initial value of the reflux ratio and with Equation (20). As the material fluxes are known, the composition of the liquid leaving the last plate ($n \equiv N$) can be determined on the basis of Equation (21) and since the values

$$\begin{aligned} \bar{y}_{N+1} &= \varphi(x_F) \\ y_N^* &= \varphi(x_N) \end{aligned} \tag{8}$$

can be calculated, the change in concentration along the plate can also be determined. The calculation is now carried out in accordance with the procedure described in Chapter 1, from plate to plate, as long as the condition given in Equation (15) is fulfilled. The number of plates determined in this manner will be constant in the following, and accordingly the calculation is carried on with a column of known number of plates.

The rates of changes can be determined on the basis of Equation (18) and (19) and the new values can be calculated if the time scale has been fixed. Accordingly:

$$F(\tau + \Delta\tau) = F(\tau) + \frac{dF}{d\tau}(\tau)\Delta\tau$$

$$x_F(\tau + \Delta\tau) = x_F(\tau) + \frac{dx_F}{d\tau}(\tau)\Delta\tau$$

$$t_F(\tau + \Delta\tau) = t_F(\tau) + \frac{dt_F}{d\tau}(\tau)\Delta\tau$$

The course of further calculations is the following:

1. In the first mode of operation

the above described calculation is first repeated with unchanged reflux ratio and should the condition

$$|x_D - x_{DU}| \leq \varepsilon_k$$

be fulfilled, the reflux ratio need not be modified. In the opposite case, the reflux ratio is to be modified (increased) until the condition is fulfilled (the prescribed margin of error is ε_k).

2. In the second mode of operation

the calculation can be carried on without alteration, with the only remark that

$$x_{DU} = \bar{y}_1$$

i.e. the composition of the vapour leaving the uppermost plate gives the new composition of the distillate.

The calculation is carried on until the prescribed final composition is reached.

In order to illustrate the model a numerical example has been elaborated for the case of a constant reflux ratio. The calculations were carried out with digital computer type ODRA 1204.

Numerical example

Data used (ethyl alcohol-water system):

F_o = 200 kilomoles

x_{Fo} = 0.3

x_{Do} = 0.7

R = 0.52

P = 1 atmosphere

$A = 10$ sq.metres

$k = 200$ kilocalories/sq.metres·hour·$^{\circ}$C

$t_f = 150\ ^{\circ}$C

$p = 0.125$ hour/kilomole

and

$e = 86$ hours/kilomole

$\alpha = 46\ x^2 - 38.2\ x + 10.36$, if $0 \leq x \leq 0.4$

$\alpha = 4{\cdot}16\ x^2 - 8.2\ x + 5.02$, if $0.4 \leq x \leq 0.7$

furthermore

$t_{bp} = 144\ x^2 - 100\ x + 100$, if $0 \leq x \leq 0.4$

$t_{bp} = -8.5\ x + 86.5$ if $0.4 \leq x \leq 1$

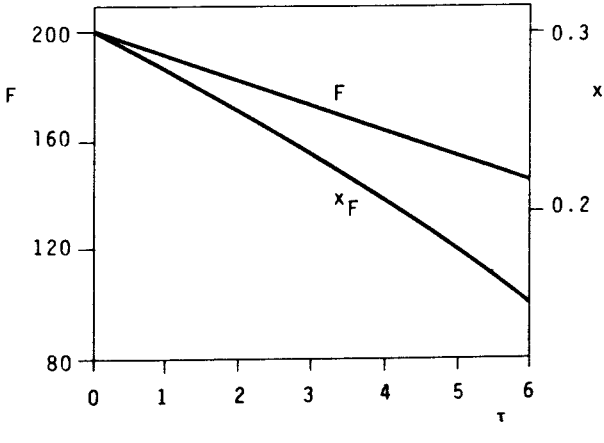

Fig. 12

The constants in the relations referring to the relative volatility or bubble point were determined by parabolic or linear approximation. If a higher degree of accuracy is required, the constants can be determined by regression analysis.

Fig. 12 shows the changes of the quantities F and x_F plotted against time.

The numerical example can be calculated for changing the reflux ratio in the same manner.

CONCLUSIONS

Table 1 clearly illustrates that the value of the initial derivate $dx/d\xi(1)$ considerably differs from zero in the case of a number of plates and this accounts for the consideration of the final plate dimension.

Table 1

Number of plate	$\left.\frac{dx}{d\xi}\right\|_{\xi=1}$
1.	-0.025
2.	-0.032
3.	-0.084
4.	-1,300
5.	-0.350
6.	-0.180

It should be mentioned that the model enables the determination of the composition of the top and bottom products in continuous operation at a given plate number, i.e. in the case of a given column, if the feed plate and the conditions of feed are known. This could make possible the determination of the optimum feed place and calculation of the corresponding top and bottom products in the case of switching over to another product.

Further development of the models may also enable the consideration of a variable takeoff; however, in this case they become very complicated and the calculations are very difficult to carry out.

SYMBOLS USED

a functional relation
c specific heat (kilocalories/kilomole·°C)
fe material transfer surface area (sq.metres)
h height of liquid on the reay (metre)
i molar enthalpy (kilocalories/kilomole)
n number of trays
q heat flux density (kilocalories/sq.metre, hour), dimensionless variable (-)

r latent heat (kilocalories/kilogram)
t temperature (°C)
x concentration of liquid
y concentration of vapour
$\bar{y}$ average concentration of vapour leaving the tray
y* vapour concentration in equilibrium with x
A heat transfer surface area (sq.metre)
B width of plate (metre)
D material flux of destillate (kilomoles/hour), diffusivity (kilomoles/metre hour)
F material flux of feed (kilomole/hour), bottom product (kilomole)
G material flux of gas phase (kilomoles/hour)
M material flux of residue (kilomoles/hour), molecular weight (kilograms/kilomole)
N total number of plates
Q heat removed by the condenser (kilocalories/hour)
R reflux ratio
Pe Peclet-number
No dimensionless quantity

Greek letters

α relative volatility
β heat transfer coefficient (kilomoles/sq.metre·hour)
ε heat transfer surface area (sq.metres/cu.metre)
φ sign of functional relation
ξ dimensionless variable

Indexes

f refers to the feed plate
k refers to the condenser
n serial number of plate
y refers to the vapour side

z direction of the co-ordinate z
D refers to the destillate
F refers to the feed or bottom product
G,$\bar{G}$ refers to the vapour phase
L,$\bar{L}$ refers to the liquid phase
M refers to the residue
N refers to the last plate

REFERENCES

1. TREYBAL, R.E., Mass Transfer Operations. McGraw-Hill Book Co., New York, 1968.

2. WEHNER, J.F., WILCHELM, R.H., Chem. Eng. Sci. 6, 89 (1956)

3. GERSTER, J.A. et al., Tray Efficiencies in Distillation Columns. Final Report from the University of Delaware, New York, 1958.

4. HOBLER, T., Mass Transfer and Absorbers. Pergamon Press, Oxford, 1966.

5. Bubble Tray Design Manual, A.J.Ch.E., New York, 1958.

РЕЗЮМЕ

В литературе известен ряд математических моделей для рассчитивания ректификационных оборудований и для описания процесса ректификации. А все эти модели употребляют коэффициент полезного действия тарелок или колонны. В настоящей работе описан математический модель, упразняющий с пользованием диффузионной модели необходимость знания коэффициента полезного действия. Для иллюстрации моделей выработаны числовые примеры. Расчеты произведены на электронно-вычислительных машин.

Hungarian Journal
of Industrial Chemistry
Veszprém
Vol.1. pp. 271-292 (1973)

MATHEMATICAL MODELLING OF ABSORPTION COLUMNS I.

THE INVESTIGATION OF THE MODELS OF ABSORPTION COLUMNS

P. ÁRVA and F. SZEIFERT

(Department of Chemical Process Engineering, Veszprém
University of Chemical Engineering)

Received: December 7, 1972.

The aim of the authors was the extensive investigation of the problems emerging in the mathematical modelling of packed absorption columns.

A method will be described which can be used for the determination of the concentration distribution in a packed column. The measured data were processed to these calculations, two models, the Piston Flow model (PF), and the Axial-Dispersed Plug-Flow model (ADPF) were used. The comparison made between the measured and calculated data revealed the fact that the ADPF model fulfils the process with satisfactory accuracy between the examined limits.

If the liquid load of the column is increased, the use of the PF model is also favourable.Both models were used in the determination of the component transfer coefficient. The numerical value of the transfer coefficient ($\beta\omega$) obtained by the calculations based on the ADPF model was twenty or fifty per cent higher than the same one of the PF model.

The mathematical modelling of chemical processes is based on the DAMKÖHLER equations [1], which express the conservation laws. Depending on the real application of these equations, different types of models exist [1, 2].

From other viewpoint, the general equations have to be transformed for the description of a given process, using the in-

formation previously obtained in the experiments.The derived equations are in general more or less simpler. It is well known that a simpler model in most cases poorly describes reality, but is easy to handle.

The basic aim was to select a model which works well, where the computation of the results can be carried out quickly and without effort.

In this work, a packed absorption column was investigated. Based on the mentioned mathematical models, the calculated and experimentally determined data were compared and an answer was given for the questions raised previously.

SULPHUR DIOXIDE ABSORPTION IN PACKED COLUMN

Sulphur dioxide is moderately soluble in water, its concentration can be determined - either in liquid or in gas phases - easily and exactly. In view of these favourable properties, this gas was selected from among the others. The equilibrium concentrations of sulphur dioxide existing in the liquid and the gas phase being in contact with each other can be described fairly well by the following equation, which is valid at 15°C and at atmospheric pressure [3, 13]:

$$c_L^* = H\, c_G + c_o^* \qquad (1)$$

where $H = 62.3$ and $c_o^* = 0.0084$ (moles per litre).

The Arrangement of the Absorption Column

The experiments were carried out in the absorption column shown in Fig. 1. The column, built up from seven glass tubes, was filled with Raschig rings. The I.D. of the column was 0.1 metre and the packed height was $Z = 2.13$ metres. The dimensions of the Raschig rings were 10 mm o.d. x 10 mm deep x 1 mm thick.

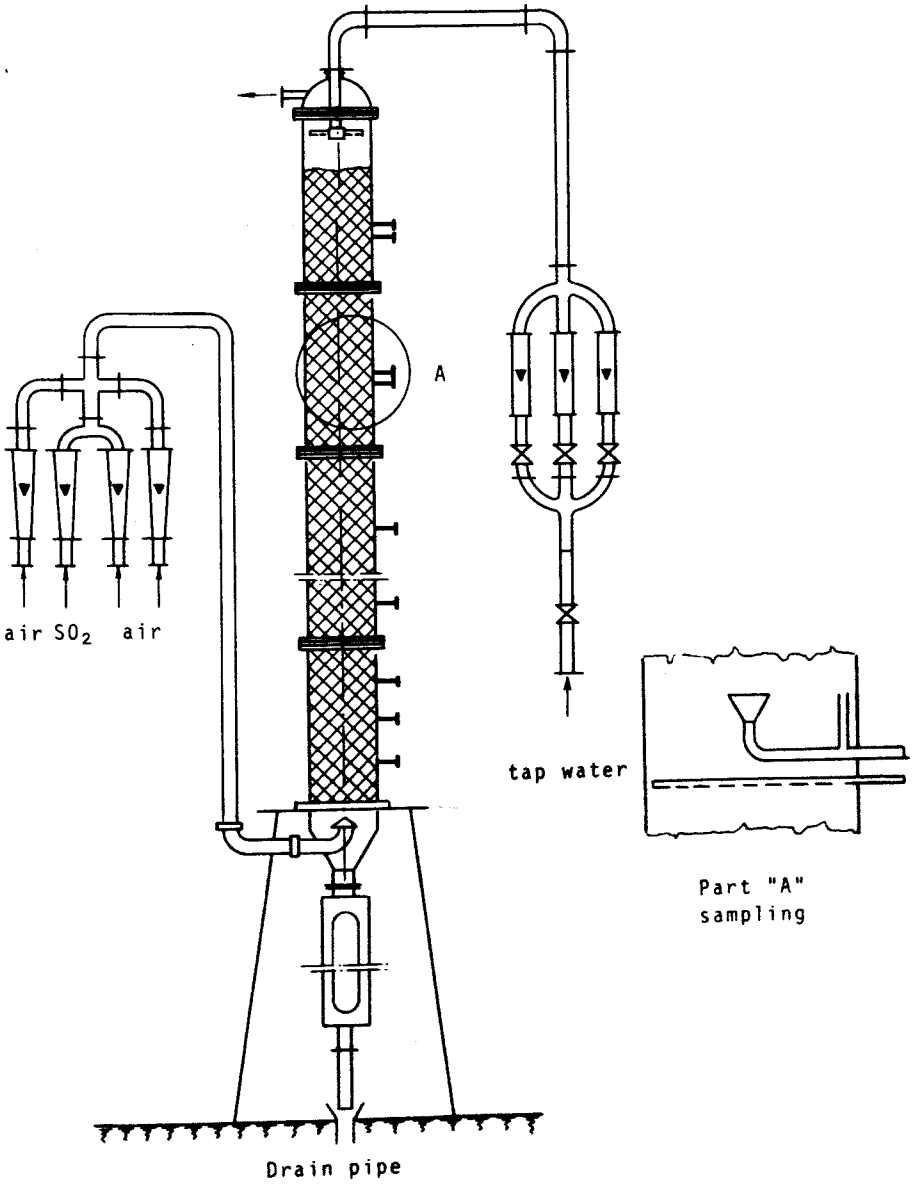

Fig. 1. Packed absorber

The solute free liquor - tapwater - was regulated by a valve, it was led through a rotameter and six liquid feed jets built into the top of the column. Through these the water was evenly sprayed over the rings. The amount of the solution, collected at the bottom of the column was held constant by a level controller and the exit solution was led into the drain-pipe.

A gently heated steel bomb was used as the source of sulphur dioxide and the air which was mixed with it was provided by a blower. The flow rate of air was regulated by a valve and measured by a rotameter. The sulphur dioxide containing air was blown into the bottom of the column, it passed upwards through the packings and came into contact with the liquid and finally left the column through the top. In order to obtain detailed information about the running absorption column, it is generally insufficient to determine the compositions of the gas and liquid phases at the top and bottom of the column, but it is necessary to locate several sampling taps along the packed height.

In addition to the construction of the column, the sampling method is important with regard to the accuracy of the measurement.

The Sampling Methods and Analytics

For the determination of the concentration profiles the liquid and gas phases along the packed column, twenty three sampling taps were mounted, among these eleven were used for taking gas, and the remainder for liquid samples. Near to the bottom of the column, the taps were located near to each other, this arrangement made it easier to determine the higher concentration changes that occurred in the phases.

The sampling is accurate if the composition of the sample is the same as the composition of the bulk phase at the level of the sampling tap. This idea was taken into account in the design of the sampling taps which can be seen in Fig.1. In the design of the shape and dimensions of the taps, special care was taken to ensure that they only slinghtly disturb the flow of the phases.

The gas sampling was carried out by a five millimetres I.D. tube, sealed at one end and perforated along its mantle in the direction of the gas flow. This tube was placed at a right angle to the axis of the column.A small baffle plate was soldered on to the tube to prevent the penetration of the liquid into the holes. The gas samples were free of liquid and their composition well represented the streaming gas phase at the given cross section. The volume of the sample is negligible, so the flow conditions were undisturbed.

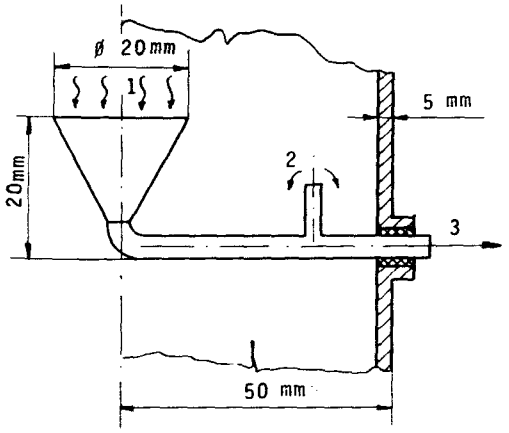

Fig.2. Method of sampling the liquid phase

The sampling of the liquid involved some difficulties, because due to the random arrengement of the rings,the flow of the liquid was uneven along the cross section. Therefore, the sampling tube was fitted with a funnel and a pipe stub as shown in Fig.2.

As it can be seen in Fig. 2., the liquid dripping into the funnel (1) flows through the pipe stub (2) mounted upwards and finally it flows back to the packing. Using this arrangement, the liquid sample, taken at certain intervals, well represents the composition of the bulk liquid.

The sulphur dioxide content of both phases was analyzed iodometrically. The gas samples were sucked into an evacuated flask. Care must be taken by the sampling to fulfil the following relation:

$$t \gg 3600\ V/G$$

where t = duration of sampling (sec)
V = volume of the sampling flask (litres)
G = volume flow rate of gas (litres per hour)

If the sampling does not comply with the above requirements, the results are generally incorrect.

Experiments

Experiments were carried out with liquid loads (L) ranging between 6,370 and 31,850 kilograms per sq.metre per hour, and gas loads (G) ranging between 330 and 2,320 kilograms per sq.metre per hour. The liquid/gas ratio varied between 4 and 48.

By starting the experiments, the liquid and gas feed rates and the sulphur dioxide concentration of the entering gas was adjusted (approx. 4 and 5 vol.% sulphur dioxide). It was found that after five or ten minutes, the column reached the steady state. At the sampling, careful attention was paid to the running of the column. The analysis of the inlet gas gave uncertain results, therefore these concentration data were computed on the basis of the over-all mass balance of the column.

Among the others, two runs were selected, the concentration data of the phases measured during these runs are collated in Table 1. The data represent the sulphur dioxide concentration of the liquid phase, c_L (moles per litre) and that of the gas phase c_G, (volume per cent) along the packed height of the column and at a given liquid and gas load. Table 1. presents the concentration data of the phases in dimensionless form (x_L and y_G). The dimensionless concentration (y_G) was obtained by dividing the actual gas concentration with the same one of the inlet gas. In the case of the liquid, the dimensionless concentration was computed by the equilibrium equation, using the appropriate gas concentration data. The dimensionless concentration data have values between zero and one.

Comments are to be made with regard to the values of c_G and y_G at z=0. The dimensionless concentration of the feed gas at the bottom of the column is equal to one. The data y_G (z=0) in Table 1. represent the concentration data of the gas being in the packed zone at z=0. These concentration data cannot be determined experi-

Table 1. Experimental data

	Run N° 2.				Run N° 55.			
	L = 12,740 ; G = 990				L = 25,480 ; G = 1990			
z (-)	c_L (moles/litre)	c_G (vol.%)	x_L (-)	y_G (-)	c_L (moles/litre)	c_G (vol.%)	x_L (-)	y_G (-)
0.0	0.113	4.63	0.794	0.994	0.083	3.88	0.733	0.976
0.1	0.101	4.33	0.739	0.943	0.073	3.48	0.644	0.875
0.2	0.090	4.00	0.683	0.891	0.064	3.04	0.565	0.764
0.3	0.080	3.65	0.628	0.831	0.055	2.61	0.485	0.656
0.4	0.068	3.26	0.573	0.765	0.046	2.14	0.406	0.538
0.5	0.058	2.88	0.504	0.686	0.036	1.67	0.318	0.420
0.6	0.046	2.48	0.428	0.587	0.027	1.22	0.238	0.307
0.7	0.035	2.06	0.338	0.483	0.020	0.84	0.176	0.211
0.8	0.024	1.60	0.241	0.373	0.012	0.53	0.106	0.133
0.9	0.013	1.05	0.131	0.255	0.005	0.24	0.044	0.060
1.0	0.000	0.46	0.013	0.123	0.001	0.05	0.008	0.012

mentally, they were extrapolated using the concentration data measured at $z > 0$ heights. The results were $y_G(0) = 0.944$ and $y_G(0) = 0.976$, respectively. To increase the accuracy of the extrapolation, the sampling taps were located near to each other at the lower part of the column.

MATHEMATICAL MODELS FOR THE DESCRIPTION OF A PACKED ABSORPTION COLUMN

The dimensions of the Raschig rings are relatively small related to the dimensions of the column. The liquid, streaming downwards through the packings is dispersed into small droplets and films, and the number of these is high. Due to this, both the continuous and dispersed phases are described by a continuous mathematical model. In the examined case, this means that the properties of the phases are regarded as a continuous function along the height of the column. Among the others, two models are frequently used for the description of process units, these are the ideal Piston Flow (PF) model and the Axial-Dispersed Plug-Flow (ADPF) model.

It is presumed by the application of the PF model that the flow rate of the phase is independent along the path and the conductivity factor is zero.

According to these, the PF model can be formulated as follows:

$$\frac{\partial \Gamma}{\partial t} = - v \frac{\partial \Gamma}{\partial z} + \varepsilon \omega \Delta \Gamma \qquad (2)$$

Compared to the general equation used for the description of process units, Eq. (2) is simplified in two points. On the one hand the conductivity term is neglected, on the other it is assumed that the convective flux exist only in the direction of the z co-ordinate.

The most simple ADPF model assumes a conductivity flux along the z co-ordinate and the conductivity factor is independent along

the path:

$$\frac{\partial \Gamma}{\partial t} = - v \frac{\partial \Gamma}{\partial z} + D \frac{\partial^2 \Gamma}{\partial z^2} + \varepsilon \omega \Delta \Gamma \qquad (3)$$

These two models will be used for the description of the packed column.

For the description of the two phase countercurrent absorption column, the following differential equation can be given based on the ideal PF model:

$$\frac{dx_i}{dz} + St_L[A(y_i - 1) + (1 - x_i)] = 0 \qquad (4)$$

$$\frac{dy_i}{dz} + St_G[A(y_i - 1) + (1 - x)] = 0 \qquad (5)$$

where

$$St_L = \frac{(\beta\omega)_i Z}{v_L} \; ; \; St_G = \frac{(\beta\omega)_i Z H}{v_G A} \; ; \; A = \frac{H c_{G,in}}{H c_{G,in} + c_o^*}$$

The differential equations of the ADPF model are:

$$\frac{1}{Pe_L} \frac{d^2 x_D}{dz^2} + \frac{d x_D}{dz} + St_L[A(y_D - 1) + (1 - x_D)] = 0 \qquad (6)$$

$$\frac{1}{Pe_G} \frac{d^2 y_D}{dz^2} - \frac{d y_D}{dz} - St_G[A(y_D - 1) + (1 - x_D)] = 0 \qquad (7)$$

where

$$Pe_L = \frac{v_L Z}{D_L H_L} \; ; \quad Pe_G = \frac{v_G Z}{D_G H_G}$$

Eq. (4) and (5), as well as (6) and (7), describe the process unit only with the help of boundary conditions. These equations express the conservation law. For the evaluation of the boundary conditions, the mass balances to be constructed are valid

at the contact points (z=0 and z=1). Several authors dealt with the problems of the boundary conditions [5, 6, 7], their work was used here, therefore a description of the details has been omitted Taking the PF model, the concentration of the gas in the packing at z=0 is to that of the inlet gas. Similarly, this is the case with the liquid at the opposite end of the packing (z=1), its concentration equals the inlet liquid. These are indicated in the following expression:

$$y_i(z=0) = 1 \tag{8}$$

$$x_i(z=1) = x_{in} \tag{9}$$

For an evaluation of the boundary conditions valid for the ADPF model, the absorption column as a whole has to be examined. The packed part of the column was regarded as a closed system and it was assumed that the properties of both the liquid and gas phases in contact with each other in the packed space are similar to the ideal plug flow. With these assumptions the boundary conditions are:

$$\left.\frac{dx_D}{dz}\right|_{z=0} = 0 \tag{10}$$

$$\left.\frac{dy_D}{dz}\right|_{z=0} + Pe_G[1 - y_D(z=0)] = 0 \tag{11}$$

$$\left.\frac{dy_D}{dz}\right|_{z=1} = 0 \tag{12}$$

$$\left.\frac{dx_D}{dz}\right|_{z=1} + Pe_L[x(z=1) - x_{in}] = 0 \tag{13}$$

The boundary conditions of the ADPF model give the concentration of the phases in the column that can be described with a continuous function, but a discontinuous function described the concentration values at the inlet points.

The differential equations of the models using the boundary conditions were solved [5, 8, 9]. E.g. the solution of Eq. (4) and (5), using the boundary conditions given in Eq. (8) and (9), is as follows:

when $\frac{A\ St_G}{St_L} \neq 1$

$$x_i = \frac{1 - x_{in}}{\frac{A\ St_G}{St_L} - \exp(St_L - A\ St_G)} \{\exp[(St_L - A\ St_G)z] - \frac{A\ St_G}{St_L}\} + 1 \quad (14)$$

$$y_i = \frac{St_G}{St_L} \frac{1 - x_{in}}{\frac{A\ St_G}{St_L} - \exp(St_L - A\ St_G)} \{\exp[(St_L - A\ St_G)z] - 1\} + 1 \quad (15)$$

MIYAUCHI and VERMEULEN [8] solved the equations of the ADPF model for several conditions, these can be found in their paper. The mentioned solutions were applied in the further calculations which were carried out by an electronic computer, Typ. ODRA 1204.

THE EVALUATION OF DATA ON THE BASIS OF THE APPLIED MODELS

First of all the parameters of the equations have to be determined. Knowing the numerical values of the parameters, the solution of the differential equation system presents the x(z) and y(z) functions. Comparing the measured and calculated concentration profile data, the applicability of the models used can be checked. At first the PF model was investigated.

The Determination of the Mass Transfer Coefficient of the PF Model

Being in the possession of the experimental data, the boundary conditions of the PF model enable a computation to be carried

out for all the investigated sections of the column. The feature of the column is constant along its longitudinal axis, the used model involves this statement, therefore the concentration data $x_L(z)$ and $y_G(z)$ determined at the point z can be used for the calculation of the transfer coefficient $(\beta\omega)_i$ being valid for the examined volume unit of the column. The calculations can be carried out with the following expressions:

if $z > 0$ and $\Lambda \neq 1$

$$\beta\omega(z)_i = \frac{v_L}{zZ} \frac{1}{1-\Lambda} \ln \frac{\Lambda\{[1 - x_L(z)] + A[y_G(z) - 1]\}}{\Lambda[1 - x_L(z)] + A[y_G(z) - 1]} \tag{16}$$

if $z = 0$ and $\Lambda \neq 1$

$$\beta\omega(z)_i = \frac{v_L}{Z} \frac{1}{1-\Lambda} \ln \frac{1 - x_{in} + \Lambda[x_{in} - x_L(0)]}{1 - x_L(0)} \tag{17}$$

where $$\Lambda = \frac{A\ St_G}{St_L}$$

Using the measured concentration data of the previously mentioned two runs, the $(\beta\omega)_i$ value were computed and these are presented in Tables 2. and 3.

The values in the Tables 2. and 3. indicate that $(\beta\omega)_i$ is the function of the co-ordinate z, its mean value can be given by Eq. (18):

$$(\overline{\beta\omega})_i = \int_0^1 \beta\omega(z)_i dz \tag{18}$$

The mean values are also presented in Tables 2. and 3.

The deviation of the $(\beta\omega)_i$ values from the average can be given by Eq. (19):

$$h = \frac{1}{(\overline{\beta\omega})_i} \int_0^1 |\beta\omega(z)_i - (\overline{\beta\omega})_i|\, dz \cdot 100, \quad \% \tag{19}$$

Table 2. Calculated from the Data of Run 2.

PF model				ADPF model	
$(\overline{\beta\omega})_i = 7.08\times10^{-3}$; h = 14.5 %; $\Delta c_i = 0.055$				$D_L=1.92\times10^{-3}\,m^2sec^{-1}$; $D_G=3.32\times10^{-3}\,m^2sec^{-1}$ $(\overline{\beta\omega})_D=8.48\times10^{-3}\,sec^{-1}$; $St_L=5.10$; $St_G=5.30$; $\Delta c_D=2.68\times10^{-2}$	
z	x_1	y_i	$(\beta\omega)_i\cdot10^3$	x_D	y_D
0.0	0.797	1.000	8.16	0.800	0.995
0.1	0.711	0.905	9.95	0.736	0.897
0.2	0.627	0.811	7.45	0.652	0.804
0.3	0.544	0.719	6.65	0.569	0.712
0.4	0.462	0.629	6.34	0.487	0.622
0.5	0.382	0.540	6.06	0.406	0.533
0.6	0.303	0.452	5.82	0.327	0.446
0.7	0.225	0.366	5.86	0.249	0.360
0.8	0.149	0.282	6.11	0.172	0.275
0.9	0.073	0.199	7.12	0.096	0.192
1.0	0.000	0.117	8.38	0.022	0.113

Table 3. Calculated from the Data of Run 52.

PF model				ADPF model	
$(\beta\omega)_i = 5.63\times10^{-3}\,sec^{-1}$; h=21.9 %; $\Delta c_i = 0.074$				$D_L=1.92\times10^{-3}\,m^2sec^{-1}$; $D_G=4.68\times10^{-3}\,m^2sec^{-1}$; $(\beta\omega) = 12.2\times10^{-3}\,sec^{-1}$; $St_L=7.35$; $St_G=5.7$; $\Delta c_D = 0.046$	
z	x_i	y_i	$(\beta\omega)_i \cdot 10^3$	x_D	y_D
0.0	0.835	1.000	6.05	0.925	0.998
0.1	0.776	0.952	7.06	0.890	0.957
0.2	0.714	0.899	4.55	0.838	0.911
0.3	0.646	0.843	3.97	0.778	0.860
0.4	0.573	0.983	3.79	0.710	0.801
0.5	0.494	0.718	4.00	0.633	0.734
0.6	0.410	0.648	5.05	0.544	0.657
0.7	0.319	0.573	6.52	0.443	0.570
0.8	0.220	0.491	7.77	0.328	0.471
0.9	0.114	0.404	6.74	0.197	0.357
1.0	0.000	0.309	6.46	0.047	0.234

The equation of the model was solved using the mean $(\overline{\beta\omega})_i$ value and the sulphur dioxide concentrations of the liquid and gas phases were calculated. The computed $x(z)_i$ and $y(z)_i$ values are summarized in Tables 2. and 3. Comparing the x_L and y_G data in Table 1. with the adequate data in Tables 2. and 3., the discrepancies are significant to the model. The deviations between the data can be characterized by the following equation:

$$\Delta c_i = \frac{1}{2} \int_0^1 [|x_L - x_i| + |y_G - y_i|] \, dz \qquad (20)$$

The Determination of the Transfer Coefficient of the ADPF Model

Using this model, not only is the transfer coefficient, or the St number unknown, but also the values of the other parameters, the mixing coefficients of the phases (D_L and D_G) are concealed. The mixing coefficients are included in Peclet numbers Pe_L and Pe_G. For the determination of the numerical values empirical formulas were published in literature [10, 11]:

$$\frac{v_G d_p}{D_G} = 2.4(Re_G)^{-0.2} \cdot 10^{-0.013-0.088 \frac{d_p}{d_k} Re_L} \qquad (21)$$

$$\frac{D_L \rho_L}{\mu_L} = 0.527 \, (Re_L)^{1/2} (Ga_L)^{1/2} \qquad (22)$$

$$Re_L = \frac{v_L d_p \rho_L}{\mu_L} \; ; \; Re_G = \frac{v_G d_p \rho_G}{\mu_G} \; ; \; Ga_L = \frac{d_p^3 g \rho_L^2}{\mu_L}$$

where d_k = diameter of the column (metre)
d_p = nominal diameter of the packing (metre)
ρ_L, ρ_G = liquid or gas density (kilograms per cu.metre)
μ_L, μ_G = dynamic viscosity of the liquid or gas (kilograms per metre per second)
g = gravitational constant (metres per sq.second)

The hold-up of the column was calculated by Eq. (23) [12]:

$$H_L = 3.48 \times 10^{-3} \left(\frac{v_L \rho_L}{d_p}\right)^{0.6} \qquad (23)$$

The numerical values of constants in Eq. (23) were taken from literature [13].

The calculated mixing coefficients are presented in Tables 2. and 3.

For the determination of the $(\beta\omega)_D$ values, the experimentally determined data were used. The previously discussed boundary conditions of the ADPF model are valid only for the closed system and as such, the absorption column has to be regarded as a whole. Therefore it is impossible to calculate the $(\beta\omega)_D$ values for each section, there is only one $(\beta\omega)_D$ value for the whole column. Using the solutions of Eq. (6) and (7), the $(\beta\omega)_D$ value was determined in such a way that Eq. (24) is at minimum:

$$\Delta c_D = \frac{1}{2} \int_0^1 [|x_L - x_D| + |y_G - y_D|]dz \qquad (24)$$

The calculated $(\beta\omega)_D$ values, and the $x(z)_D$ and $y(z)_D$ data are collected in Tables 2. and 3.

Δc_D is characteristic for the deviations between the calculated and measured values, this is also shown in the mentioned Tables.

THE VALUATION OF THE INVESTIGATED MODELS

The P.F. Model

The computed $(\beta\omega)_i$ values depend on z; it is caused either by the deficiency of the model or by the scattering of the measured data. For the determination of the scattering, several parallel runs were made. It was found that the scattering was $c_{measurement}$=

= 0.03. In contrast to this, in the experiments the following data were measured which are summarized in Table 4.

Table 4

$L < 12\,740$	$h \approx 31$ %	$\Delta c_i \approx 0.10$
$L \geq 12\,740$, $G < 990$	$h \approx 19$ %	$\Delta c_i \approx 0.05$
$L \geq 12\,740$, $G \geq 990$	$h \approx 14$ %	$\Delta c_i \approx 0.04$

The data show that the deviation Δc_i is many times higher than the experimental error. The two values approach each other if the liquid load of the column is high. It is assumed that the differences between the measured and calculated concentration values can be deduced both on the inadequacy of the model and experimental errors. The deviation is regarded as the sum of both:

$$\Delta c_i = \Delta c_{measurement} + \Delta c_{model}$$

From the data collected in Table 4., the conclusion can be drawn that if the liquid load is low, the model describes the investigated system imperfectly, here the value of Δc_{model} is approx. 0.07, which means a ten or fifteen per cent deviation between the measured and calculated concentration data. If the liquid load is increased, this deviation lessens in the examined range and finaly reaches the 0.01 value.

On the basis of this, it can be stated that by high liquid loads the PF model can be applied for the design of an absorption column. This statement is also supported by the values of h, which represent the deviations between the $\beta\omega(z)_i$ and the average. If the liquid load is low, the deviation of the $(\beta\omega)_i$ calculated from the experimental results, is 31 per cent, in the higher liquid load range this decreases until 14 per cent. The data suggest that

Table 5

B_L ($\frac{\text{litres}}{\text{hour}}$)	B_G ($\frac{\text{litres}}{\text{hour}}$)	$(\beta\omega)_D$ (10^3/sec)	Δc_D (-)	$\frac{(\beta\omega)_D-(\overline{\beta\omega})_i}{(\beta\omega)_D}$ (%)	$\Delta c_i-\Delta c_D$ (-)	$\Delta c_{mod,D}$
50	2000	2.99	0.048	-37.4	0.045	0.018
	4000	6.58	0.048	48.8	0.035	0.018
	6000	5.82	0.033	37.8	0.032	0.003
	8000	5.85	0.033	61.7	0.082	0.003
	10000	5.60	0.043	64.2	0.076	0.013
100	2000	6.04	0.027	39.8	0.027	0.000
	4000	10.30	0.024	28.8	-0.003	0.000
	6000	9.19	0.023	26.5	0.032	0.000
	8000	11.38	0.033	41.5	0.022	0.003
	10000	11.06	0.029	47.8	0.046	0.000
150	4000	13.00	0.046	53.5	0.034	0.016
	6000	13.18	0.027	24.2	0.001	0.000
	8000	11.32	0.019	1.2	0.008	0.000
	10000	14.56	0.032	23.6	0.007	0.002
	12000	16.27	0.023	46.2	0.042	0.000
	14000	15.17	0.036	45.9	0.024	0.006
200	4000	16.23	0.039	58.6	0.031	0.009
	6000	25.50	0.040	58.8	0.016	0.010
	8000	17.92	0.026	29.4	0.014	0.000
	10000	16.84	0.024	11.2	0.001	0.000
	12000	17.44	0.044	22.3	-0.001	0.014
	13000	17.95	0.046	24.3	0.010	0.016
	14000	19.79	0.027	49.8	-0.009	0.000
250	4000	18.81	0.045	64.9	0.028	0.015
	8000	18.40	0.031	31.9	0.014	0.001
	10000	20.80	0.024	21.9	-0.001	0.000
	11000	16.10	0.042	25.5	-0.012	0.012

with low liquid and gas loads, the PF model is inapplicable either in the project work or in the qualification of a running absorption column.

The ADPF Model

The Δc_D values, characteristic for the deviations between the measured and calculated concentration data, are collected in Tables 2. and 3. Table 5. includes all the measured data, these show that the deviation caused by the application of the ADPF model was not higher than 0.01 in all the cases if $\Delta c_{measured} = 0.03$ is assumed. The mean of the $\Delta c_{measured}$ values is approx. 0.007. Therefore it can be stated that the ADPF model is suitable, between the investigated limits, for the description of the absorption column.

The appropriate ($\beta\omega$) values calculated either on the basis of the PF, or ADPF models do not agree numerically with each other. The ($\beta\omega$) values presented by the ADPF model are higher (Table 5.), this can be attributed to the mixing phenomena which decrease the efficiency of the column. The data show that the transfer coefficients related to the unit volume of the packing were ten or sixty per cent higher of the ADPF model was selected as the basis of the calculations instead of the PF model.

The deviations between the above discussed data reveals the fact that care must be taken by the application of the data published in literature. It is always recommended to check the mathematical model in which the calculations are based.

USED SYMBOLS

c_L^* equilibrium concentration in the liquid phase (moles per litre)

H	equilibrium constant (dimensionless)
c_o^*	intercept of equilibrium straight line (moles per litre)
c_G	concentration in the gas phase (moles per litre)
c_L	concentration in the liquid phase (moles per litre)
L	liquid load (kilograms per sq.metre per hour)
G	gas load (kilograms per sq.metre per hour)
B	feed (litres per hour)
x	dimensionless concentration of the liquid phase
y	dimensionless concentration of the gas phase
Γ	density (mass per cu.metre)
t	time (sec)
z	co-ordinate
ϵ	general transfer factor (metres per second)
ω	specific surface (sq.metres per cu.metre)
D	mixing factor (sq.metres per second)
St	Stanton number (dimensionless)
β	mass transfer coefficient (metres per second)
Z	length of the packed column (metres)
v	velocity (metres per second)
H_L	hold up (dimensionless)
h	deviation from average (per cent)
Δc	mean deviation of the measured and calculated concentrations

Indexes

L	liquid phase
G	gas phase
in	**inlet**

i piston flow model

D axial-dispersed plug-flow model

REFERENCES

1. BENEDEK, P., LÁSZLÓ, A., The Foundation of Chemical Engineering (in Hungarian) Budapest, M.K. 1964.

2. KAFAROV, V.V., Cybernetic Methods in Chemistry and Chemical Technology (in Russian) Moscow, KHIMIJA, 1968.

3. DZSABAGIN, T.K., SZEMJONOV, P.A., ROJ, D.K., Khim. Prom. 11, 870-875 (1963)

4. RAMM, V.M., Absorbcija gazov (The Absorption of Gases), Moscow, KHIMIJA, 1966.

5. WILBURN, N.P., Ind. Eng. Chem. Fundamentals. 3, N° 3, 189 (1964)

6. WEHNER, J.F., WILHELM, R.H., Chem. Eng. Sci. 6, 89 (1956)

7. VAN CAUWENBERGHE, A.R., Chem. Eng. Sci. 21, 203 (1966)

8. MIYAUCHI, T., VERMEULEN, T., Ind. Eng. Chem. Fundamentals. 2, N° 4, 303 (1963)

9. HARTLAND, S., MECKLENBURGH, J.C., Chem. Eng. Sci. 21, 1209 (1966)

10. DE MARIE, F., WHITE, R.R., AIChJ. 473 (1960)

11. OTAKE, T., KUNUGITA, E., Chem. Eng. (Japan) 22, 144 (1958)

12. HOBLER, T., Massoperedacha i absorbcija (Mass Transfer and Absorption) Moscow, I.L. (1963)

13. PERRY, J.H., Chemical Engineers' Handbook (in Hungarian) Bp. M.K. (1968)

РЕЗЮМЕ

Целью авторов являлось многостороннее изучение вопросов, возникших при математическом моделировании насадочных абсорбционных установок.

В работе описан экспериментальный метод, применимый к измерению распределения концентрации складывающегося в насадочной колонне. Полученные измерения были обработаны на основе модели так называемого идеального вытеснения и диффузионной модели, содержащей также и осевое перемешивание. Сопоставление измерных распределений концентрации с вычисленными датами показало, что действительные условия при обстоятельствах опита во всей области описаны диффузионной моделью достаточной точностью. Модель идеального вытеснения является подходящей при более интенсивном режиме работы. Коэффициент передачи компонента был определен на основе обеих моделей. При этом с помощью диффузионной модели были получены значения (β_w) примерно на 20 - 60 % выше, чем при помощи модели идеального вытеснения.

Hungarian Journal
of Industrial Chemistry
Veszprém
Vol.1. pp. 293-306 (1973)

ENERGETIC INTERPRETATION OF DISTILLATION BASED ON NON-EQUILIBRIUM THERMODYNAMICS

A. FONYÓ

(Polytechnical University, Department of Chemical Engineering, Budapest)

Received: January 30, 1973.

Distillation is dealt with as a steady state system of the first degree. The energetic aim in distillation is that the entropy produced by the heat transport is utilized as completely as possible by the entropy consumption of the component separation. Expressions are given for the entropy production of the heat transport emerging at distillation in both the reversible and the real cases. In conclusion, the thermodynamic interpretation of the driving force, efficiency and dynamic behaviour of distillation is indicated.

INTRODUCTION

The first comprehensive thermodynamic analysis of distillation is due to MARKOWSKY and co-workers [1, 2, 3, 4, 5, 6]. Their papers deal with the energy improvement of distillation. The possibilities of the thermodynamic expression for the driving force and its practical characteristics (efficiency) of distillation were investigated by KATAEV and VIGDOROV [7, 8, 9]. In addition, the general work of SZARGUT on the energetics of separation processes predominates, explaining the theory of steady systems of the first degree and enabling the energetic interpretation

of the coupled processes by treating the entropy consuming and entropy producing processes separately [10, 11, 12].

The aim of the present paper is the uniform energetic interpretation of distillation based on non-equilibrium thermodynamics, that may in the future be of assistance in the energetic improvement of this operation, i.e. in the practical implementation of the principles that could be initiated from thermodynamic considerations. During the development of the principles given in this paper the works of HASELDEN [13], TIMMERS [15], PRATT [16], FRATSCHER [14], KING [17] and STUPIN [18] published in this field were used, in addition to those mentioned earlier.

DISTILLATION COLUMN AS A FIRST DEGREE STEADY SYSTEM

Although the linearity of the integral expressions for the transfer processes is questionable in the irreversible thermodynamics, the linearity of the phenomenological equations will be assumed in the mathematical treatment. This proved to be appropriate, and it was possible to interpret the empirical data by the relationships that were derived. In general the entropy source density in this theory is:

$$\phi = \bar{\bar{L}}'_{jk} \bar{\bar{X}}_k : \bar{\bar{X}}_j \tag{1}$$

Disregarding the relaxation processes, the function of entropy source density of a steady system with two variables, which is of the first degree with regard to flux 1 is

$$\frac{\partial \phi}{\partial X_2} = (L'_{12} + L'_{21})X_1 + 2\, L'_{22} X_2 = 0 \tag{2}$$

at the local minimum

$$\phi = L'_{11}X_1^2\left[1 - \frac{(L'_{12} + L'_{21})}{4\ L_{11}L_{22}}\right] = L'_{11}X_1^2(1 - p^2) \qquad (3)$$

where p is the coupling factor, i.e. the degree of the coupling of the entropy processes.

In the case of distillation, the heat flow is flux 1, maintained by an X_1 driving force of constant value due to an external force, and flux 2 is the resulting transfer component flow, which is extinguished because of the ONSAGER relations [19]. In the present case, the entropy produced by the heat transport of the column is decreased by the entropy consuming process of the component separation. The range of the coupling factor is

$$0 \leq p \leq 1 \qquad (4)$$

It is clear that at p = 0 the system is completely irreversible, since $\phi = L_{11}X_1^2$ i.e. only the entropy producing process takes place. If p = 1, ϕ = 0 i.e. the system is reversible, the entropy produced by the heat flow is completely consumed by the entropy consuming process of the component separation.

With respect to energetics in the case of distillation, it should be ensured that the entropy produced by the heat transport be utilized as completely as possible by the entropy consumption of the component separation.

ENTROPY PRODUCTION OF HEAT TRANSPORT

Reversible Rectification

The realization of reversible distillation is well known [1, 2, 20, 21, 22, 23, 24], and will not be dealt with here.

The driving force of the heat flow is the change in the reciprocal of the temperature. From RAOULT's law and the CLAUSIUS-CLAPEYRON Equation can be derived:

$$P = \sum_i \bar{p}_i x_i$$

$$\frac{dP}{dT} = \sum_i \bar{p}_i \frac{dx_i}{dT} + \sum_i x_i \frac{d\bar{p}_i}{dT} = 0 \quad (p = \text{const.}) \tag{5}$$

$$\frac{dp_i}{dT} = \frac{x_i \bar{p}_i}{RT^2} \quad (V_x = 0;\ V_y = \frac{RT}{\bar{p}_i}) \quad (i = 1, 2, \ldots n) \tag{6}$$

Assuming identical latent heats, Equations (5) and (6) and the $\sum_i dx_i = 0$ relation give the driving force of the heat flow:

$$d(\frac{1}{T}) = \frac{R}{\lambda} \sum_i (K_i - 1)\, dx_i \tag{7}$$

Assuming equilibrium at each level of the column, the component and mass balances give the vapour stream in the rectification zone as

$$V = \frac{1}{K_i - 1} (\frac{x_{iD}}{x_i} - 1)\, D \quad (i = 1, 2, \ldots n) \tag{8}$$

Similarly the vapour stream in the stripping zone is

$$V' = \frac{1}{K_i - 1} (1 - \frac{x_{iB}}{x_i})\, B \quad (i = 1, 2, \ldots n) \tag{9}$$

(The values of V and V' can be given for any component and since $K_i = K_i(T,p,x)$, its value changes along the height of the column.) The entropy production of the heat transport for the full height of the column (flux x driving force) is

$$\Phi_Q = \int_{x_{iB}}^{x_{iD}} I_Q\, d(\frac{1}{T}) = \int_{x_{iF}}^{x_{iD}} V\lambda d(\frac{1}{T}) + \int_{x_{iB}}^{x_{iF}} V'\lambda d(\frac{1}{T}) \tag{10}$$

or by substituting Equations (7), (8), (9)

$$Q = RD \sum_i \int_{x_{iF}}^{x_{iD}} \left(\frac{x_{iD}}{x_i} - 1\right) dx_i + RB \sum_i \int_{x_{iB}}^{x_{iF}} \left(1 - \frac{x_{iB}}{x_i}\right) dx_i$$

$$\phi_Q = R\left(D \sum_{i=1}^{n} x_{iD} \ln x_{iD} + B \sum_{i=1}^{n} x_{iB} \ln x_{iB} - F \sum_{i=1}^{n} x_{iF} \ln x_{iF}\right) \quad (11)$$

Since the entropy production of the heat transport given by Equation 11 is equal to the entropy consumption in an isotherm--isobar separation of a mixture, known from thermodynamics (entropy of mixing) [19], but with an opposite sign, so the overall entropy source density is zero:

$$\phi = \phi_Q + \phi_c = 0 \quad (12)$$

and the coupling factor p = 1.

Adiabatic Rectification

Supposing a constant molar overflow, the entropy production of the heat transport under adiabatic circumstances is

$$\phi_Q = \frac{(R + 1)\, D\lambda T_B - [(R + 1)\, D + (q - 1)\, F]\lambda T_D}{T_D\, T_B} \quad (13)$$

It can be shown that under adiabatic circumstances, the entropy production is greater than in the reversible case even at the R_{min} value, i.e. in a column of infinite dimensions (11), since the vapour stream along the entire height of the column is equal to the minimum value of the vapour stream of the "greatest value". The over-all entropy source density is:

$$\phi = \phi_Q + \phi_c > 0 \quad (14)$$

and the coupling factor:

$$0 < |p| < 1$$

Squared Off Cascade, Thermally Coupled Distillation System

In the case of reversible rectification with the complete elimination of the heavy key component in the enriching section, the internal reflux ratio at level h (m^{th} plate) of the column is:

$$\left(\frac{L}{V}\right)_m = R_h = \frac{V_m - D}{V_m} = 1 - \frac{D}{V_m} \tag{15}$$

Since the value of the equilibrium ratio generally diminishes upward in the column, $\frac{dR_h}{dm}$ is positive if the plates are numbered from the top down to the bottom:

$$\frac{d\left(\frac{L}{V}\right)}{dm} = \frac{D}{V_m^2}\frac{dV}{dm} = \frac{dR_h}{dm} > 0 \tag{16}$$

D and V are positive, so (dV/dm) must also be positive, thus the vapour stream must grow downward in the column, that means a gradual heat withdrawal along the enriching section. By a similar treatment it can be shown that for the realization of a reversible rectification, a gradual addition of heat is necessary in the stripping section.

The gradual addition and withdrawal of heat are carried out in practice by using squared off cascades [16, 25,27] or thermally coupled distillation systems [1, 3, 26, 27]. In these systems the entropy production of the heat transport in rectification is less than in the usual adiabatic case,its value, however, cannot attain the value calculated by Equation (11), since the establishment of a reversible rectification requires other conditions too [24] (for instance infinite column sizes, first degree rectification, and a zero pressure drop, etc.). The value of the coupling factor is here:

$$0 < |p| < 1$$

(If p = 0, i.e. only heat transport takes place and there is no component separation and there is no rectification.)

GENERAL THERMODYNAMIC EXPRESSION FOR THE DRIVING FORCE

In thermodynamics the number of transfer units can be defined in general as follows:

$$N_{term} = \int_0^{L_N} \frac{dL_h}{-L_h^*} = \int_0^{S_{ch}} \frac{dS_{ch}}{-S_{ch}^*} \tag{17}$$

(Only the entropy consuming processes are dealt with.)

$$dS_{ch} = \sum_i y_{iD}\, d\left(\frac{G_{ih}}{T}\right) = R \sum_i y_{iD}\, d \ln y_{ih}^g$$

$$S_{ch}^* = \sum_i y_{iD} \left(\frac{G_{ih}^f}{T_h^f} - \frac{G_{ih}^g}{T_h^g}\right) = R \sum_i y_{iD} \ln \frac{y_{ih}^f}{y_{ih}^g} \tag{18}$$

(The above inequalities are strictly valid only under small or moderate pressures, in general fugacities should be written instead of mole fractions in the above relations.)

Substituting, the number of thermodynamic transfer units in the enriching section is:

$$N_{term} = \int_{y_{io}}^{y_{ih}} \frac{\sum_i y_{iD}\, d \ln y_{ih}}{\sum_i y_{iD} \ln \frac{y_{ih}^*}{y_{ih}}} \tag{19}$$

where y_{ih}^* is the equilibrium concentration calculated from the other phase. For the upper part of the column when the pure most volatile component is the overhead product:

$$\lim_{\substack{y_{BD} \to 0 \\ y_{CD} \to 0}} (N_{term}) = \int_{y_{Ao}}^{y_{Ah}} \frac{y_{AD}\, d \ln y_{Ah}}{y_{Ad} \ln \frac{y_{Ah}^*}{y_{Ah}}} = \int_{y_{Ao}}^{y_{Ah}} \frac{d \ln y_{Ah}}{\ln \frac{y_{Ah}^*}{y_{Ah}}} \tag{20}$$

But in this case $y^*_{Ah} - y_{Ah} = \Delta^*$ approaches zero, so Eq. (20) turns into the number of diffusional transfer units as expressed by CHILTON and COLBURN:

$$\lim_{\substack{y_{BD}\to 0,\Delta^*\to 0\\ y_{CD}\to 0,\\ \vdots}} (N_{term}) = \int_{y_{Ao}}^{y_{Ah}} \frac{dy_{Ah}}{y_{Ah} \ln\left(1 + \frac{\Delta^*}{y_{Ah}}\right)} = \int_{y_{Ao}}^{y_{Ah}} \frac{dy_{Ah}}{y^*_{Ah} - y_{Ah}} = NTU \tag{21}$$

using the relationship:

$$\lim_{\Delta^*\to 0} \left[\ln\left(1 + \frac{\Delta^*}{y_{Ah}}\right)\right] = \frac{\Delta^*}{y_{Ah}}$$

THERMODYNAMIC PLATE EFFICIENCY

If a rectification column is analyzed using the concept of the equilibrium stage, the thermodynamic plate efficiency, similarly to the above derivation, is

$$\eta_{term} = \frac{L_N}{L^*_N} = \frac{\sum_i y_{iD} \ln \frac{y_{iN}}{y_{i(N+1)}}}{\sum_i y_{iD} \ln \frac{y^*_{iN}}{y_{i(N+1)}}} \tag{22}$$

the η_{term} turns into the MURPHREE plate efficiency if pure component A is obtained in the enriching section, and $\Delta^* \to 0$, $\Delta \to 0$:

$$\lim_{\substack{\Delta^*\to 0\ y_{BD}\to 0\\ \Delta\to 0\ y_{CD}\to 0\\ \vdots}} (\eta_{term}) = \frac{y_{AD} \ln \frac{y_{AN}}{y_{A(N+1)}}}{y_{AD} \ln \frac{y^*_{AN}}{y_{A(N+1)}}} = \frac{y_{AN} - y_{A(N+1)}}{y^*_{AN} - y_{A(N+1)}} = \eta_M \tag{23}$$

The analysis of the entropy producing process of the heat transport yields the thermal plate efficiency defined by STANDART [30]:

$$\eta^{St}_{term} = \frac{L'_N}{L'^{*}_N} = \frac{V_N H_N - V_{N+1} H_{N+1} + r_N Q_N}{V^{*}_N H^{*}_N - V_{N+1} H_{N+1} + r_N Q_N} \qquad (24)$$

The expressions of the number of transfer units and plate efficiency in the stripping section can be interpreted thermodynamically in a similar way.

ANALYSIS OF THE DYNAMIC BEHAVIOUR

A new method of analysis of dynamic behaviour is the analysis of the entropy production. The GLANSDORF-PRIGOGINE principle [28] can also be verified for discontinuous systems [29] (transfer model). According to this theorem, the production of entropy is at minimum in steady state which is stable with respect to internal changes. Since perturbations are moderated by time, the entropy production decreases approaching the steady state:

$$\frac{d\phi}{dt} \leq 0 \qquad (25)$$

For instance, assuming a disturbance of the steady state in rectification caused by a change in the concentration difference (X'_2) while the temperature difference is kept at a constant value (X_1 = const.):

$$X'_2 \longrightarrow X_2 = X'_2 + \delta X_2 \qquad (26)$$

the I_2 stream is

$$I_2 = L_{21}X_1 + L_{22}X_2 = L_{21}X_1 + L_{22}X'_2 + L_{22}\delta X_2 = I'_2 + L_{22}\delta X_2$$

Since in steady state $I'_2 = 0$

$$I_2 = L_{22}\delta X_2 \qquad (27)$$

and the diagonal elements of the matrix of the transport coefficients are positive ($L_{22} > 0$),

$$I_2 = L_{22}\delta X_2 > 0 \qquad (28)$$

so the δX_2 change in the driving force and the I_2 stream caused by δX_2 are of the same sign.

The entropy production is

$$\phi = L_{11}X_1^2 + 2\,L_{12}X_1(X_2' + \delta X_2) + L_{22}(X_2' + \delta X_2)^2 =$$

$$= \phi'_{min} + 2\,I_2' + L_{22}(\delta X_2)^2 = \phi'_{min} + L_{22}(\delta X_2)^2 \qquad (29)$$

and

$$L_{22}(\delta X_2)^2 = \phi - \phi'_{min}$$

The increase in the entropy production is proportional to the square of the change in the driving force (change of the concentration driving force). From the foregoing it is clear that the pursuit of the minimum entropy production can also be interpreted from dynamic considerations.

USED SYMBOLS

B	molar mass stream of the bottom product
D	molar mass stream of the overhead product
F	molar mass stream of the feed
G	free energy
H	enthalpy of the vapour
I	flow
K	equilibrium ratio
L'	transport coefficient
L	molar liquid stream
L_N	the separation work of the N^{th} plate
N_{term}	number of thermodynamic transfer units
NTU	number of the diffusion transfer units

P total pressure

$\bar{p}$ vapour pressure

p coupling factor

q the liquid fraction of the feed

Q_N the heat loss stream of the N^{th} plate

r_N the heat loss fraction of the vapour stream of the N^{th} plate

R reflux ratio

S entropy

T absolute temperature

t time

V molar vapour stream in the rectification section

V' molar vapour stream in the stripping section

X driving force

δX change in the driving force

x liquid mole fraction

y vapour mole fraction

Δ $y_{AN} - y_{A(N+1)}$

Δ $y^*_{AN} - y_{A(N+1)}$

Φ entropy source density

λ latent heat

Indices

$A,B,C...$ components

j,k transport coefficient endices

i component index

n the number of components

N the number of plate

Q relates to the heat transport

C relates to the component transport

m minimum value

h level of height

f liquid phase index

g vapour phase index

* equilibrium value

Relations are written in a dimensionless form, their homogeneity should be ensured in substitutions.

REFERENCES

1. PLATONOV, V.M., BERGO, B.G., Razdelenie Mnogokomponentnyh Smesey. Khimiya, Moscow. 1965.

2. PETLYUK, F.B., PLATONOV, V.M., GIRSANOV, I.V., Khim. Prom. 40, (10) 723 (1964)

3. PETLYUK, F.B., PLATONOV, V.M., GIRSANOV, I.V., Khim. Prom. 40, (6) 445 (1964)

4. PETLYUK, F.B., PLATONOV, V.M., SLAVINSKII, D.M., Khim. Prom. 41, 206 (1965)

5. PETLYUK, F.B., PLATONOV, V.M., AVETYAN, Khim. Prom. 42, 865 (1966)

6. PLATONOV, V.M., PETLYUK, F.B., ZHVANETSKII, J.B., Khimiya i Tekhn. Topliv i Masel, 16, (3) 32 (1971)

7. VIGDOROV, A.S., KAFAROV, V.V., Zhurn. Prikl. Khim. 38, 1091 (1960)

8. KAFAROV, V.V., VIGDOROV, A.S., Zhurn. Prikl. Khim. 38, 1506 (1960)

9. KAFAROV, V.V., Osnovy Massoperedachy Vysshaya Shkola, Moscow 1966.

10. SZOLCSÁNYI, P., Vegyipari müveleti egységek energetikai analizise. (An Energetic Analysis of Operational Units in the Chemical Industries.) Müszaki Könyvkiadó, Budapest, 1972.

11. SZOLCSÁNYI, P., Folyamatos üzemü diffuziós müveleti egységek matematikai modellezése a nemegyensulyi folyamatok termodinamikája alapján. (Mathematical Simulation of Continuous Diffusional Operational Units Based on the Thermodynamics of Non-equilibrium Process.) Project report. Veszprémi Vegyipari Egyetem, Veszprém, 1970.

12. SZOLCSÁNYI, P., Proceedings of the 2nd Conference on Applied Physical Chemistry. Akadémiai Kiadó. Veszprém. 1971. Vol.2. p. 601.

13. HASELDEN, G.G., De Ingenieur 74, N° 8, Ch 9 - Ch 16, (1962)

14. FRATZSCHER, W., KLÖDITZ, D., W.Z. der T.H. für Chemie "Carl Schorlemmer" Leuna, Merseburg. 10, 134 (1968)

15. TIMMERS, A.C., Proceedings of the Int. Symp. on Distillation Brighton, 1969. I. Ch.E.Publication, p.5:57.

16. PRATT, H.R.C., Countercurrent Separation Processes. Elsevier Publishing Co., Amsterdam, 1967.

17. KING, C.J., Separation Processes, McGraw-Hill. New-York 1971.

18. STUPIN, W.J., The Separation of Multicomponent Mixtures in Thermally-Coupled Distillation Systems. Ph.D. Thesis. University of California. 1970.

19. DODGE, B.F., Chemical Engineering Thermodynamics. McGraw-Hill. New-York, 1944.

20. HAUSEN, H., Z. der Techn. Physik. 13, 271 (1932)

21. BENEDICT, M., A.I.Ch.E. Transactions (CEP) 43, N° 2, 41 (1947)

22. GRUNBERG, J.F., Advances in Cryogenic Eng. Vol.I. Timmerhaus, New-York. 1960.

23. SCOFIELD, H., Advances in Cryogenic Eng. Vol. III. Timmerhaus, New-York. 1960.

24. FONYÓ, Z., Magyar Kémikusok Lapja 28, 123 (1973)

25. FONYÓ, Z., Magyar Kémikusok Lapja 28, N° 6 (1973)

26. FONYÓ, Z., FÖLDES, P., Magyar Kémikusok Lapja 28, N° 7 (1973)

27. DIPAK GUPTA, RAY, S.N., I. and E.C. Process Design and Development. I, N° 4, 255 (1962)

28. GLANSDORF, P., PRIGOGINE, I., Phisica. 20, 773 (1954)

29. DE GROOT, S.R., MAZUR, P., Non-Equilibrium Thermodynamics. Nort-Holland Publ. Co. Amsterdam. 1962.

30. STANDARD, G., Chem. Eng. Sci. 20, 611 (1965)

РЕЗЮМЕ

Дестилляция рассматривается автором, как стационарная система первого порядка. С точки зрения энергетики ставится целью использование наибольшей части энтропии, выделяемой транспортом тепла для сепарации компонентов. Описываются выражения для вычисления производства энтропии теплопередачи для реверсивного и реального процесса. Наконец, сообщается термодинамическое истолкование движущей силы, эффективности динамического поведения ректификации.

Hungarian Journal
of Industrial Chemistry
Veszprém
Vol.1. pp. 307-328 (1973)

STUDIES ON GRANULATION IN A FLUIDIZED BED II. THE EFFECTS OF THE AMOUNT OF THE BINDER ON THE PHYSICAL PROPERTIES OF GRANULES FORMED IN A FLUIDIZED BED

Z. ORMÓS, K. PATAKI and B. CSUKÁS

(Research Institute for Technical Chemistry of the
Hungarian Academy of Sciences, Veszprém)

Received: August 30, 1972.

As the physical properties of granules formed in a fluidized bed with spraying of a binder are considerably affected by the amount of the binder, it is important to know this effect from both theoretical and practical points of view. The most important conclusions on the effects of changes in the amount of the binder, found in literature are summarized. The experimental set up, the methodology and the test methods for the determination of the physical properties of the granules are outlined. The results of the experiments relating to the effects of the amount, concentration and feed rate of the liquid on the physical properties of the granules are shown in the Figures. The experimental results are evaluated and an equation is given for the calculation of the average particle size of the granules.

Granulation is one of the most important processes in many production lines. On the one hand, the granules formed can be used as raw materials for further processes, e.g. for pressing in the pharmaceutical and plastic industries, and for melting in the glass industry, etc., and on the other hand granules can be the final product of a process line, for instance in the cases of fertilizers, plastics, detergents, insecticides, pharmaceuticals in capsules, and products of the food industry, etc.

Granulation is differently defined by various authors [1, 2]. The term "granulation" is used here to mean the grain forming processes in which from a heap of material consisting of small particles, a heap of material that contains greater particles (granules) is formed without a change in the state of most of the solid phase. The particle size distribution of the granules formed by these processes is within relatively narrow limits, but the dimensions of the granules are never so homogeneous as those of tablets, dragees or briquets.

In the last decade, granulation in a fluidized bed became more and more widespread. Granulation in a fluidized bed can be realized in many ways, but that of spraying a binder into the bed is of considerable importance primarily in the pharmaceutical industries, although in recent years it was adopted in other branches of industry (e.g. the granulation of detergents, fertilizers, and foodstuffs etc.). Granulation in a fluidized bed with the spraying of a binder into the bed and the apparatus suitable for its realization were reported in several papers [3, 4, 5, 6, 7, 8, etc.].

The point of granulation in a fluidized bed with spraying is that a liquid material (e.g. solvent) or a solution, melt or suspension of a binder is atomized into the fluidized bed of the particles to be granulated. During this process the mixing, wetting, agglomeration of the particles and the elimination of the solvent content of the granules (drying) or the solidification of the liquid phase in the granules (for instance by setting or by a chemical reaction) take place. The physical properties of granules formed in a fluidized bed with the spraying a binder into the bed are determined by the following independent variables:

a) operational parameters

- the quality, the mean particle size, the particle size distribution and the specific surface area of the substance to be granulated;
- the quality of the binder;
- the physical properties, the concentration and the relative quantity of the granulating liquid;

b) process parameters

- the feed rate of the wetting liquid;
- the expansion of the fluidized bed;
- the ratio of the minimum bed height and the diameter of the bed;
- the extent of the break-up of the granulating liquid;
- the temperature of the fluidizing air at the inlet;

c) the parameters of the apparatus

- the quality of the air distributor plate that supports the bed;
- the shape of the body of the granulator;
- the distance between the atomizer and the distributor plate.

The flow rate of the air ensures the fluidized state is not included since the mean particle size of the granules steadily increases in a batch process, hence to maintain a given bed expansion and an approximately uniform motion of particles it is necessary to continuously increase the flow rate of the air. That means that the gas flow rate is a dependent variable if bed expansion is constrained.

With regard to the operational and process parameters of granulation in a fluidized bed with spraying, here the effects of the amount, feed rate and concentration of the granulating liquid on the physical properties of the granules will be dealt with.

When solving a particular granulation in a fluidized bed with the spraying of a binder, after the selection of the appropriate binder several questions have to be answered. What should be the concentration of the binder in the granulating liquid, what amount of this liquid is needed to attain the required particle size and what feed rate should be applied for the injection into the bed? To determine the optimum values of the parameters just mentioned experiments are needed in almost every case. However, the number of these experiments can be reduced if one knows the effects of the various parameters on the physical characteristics of the granules. These questions were already dealt with by several authors [4, 7, 9, 10, 11] and their relevant conclusions are summarized.

An increase in the amount of the granulating liquid - that means in the case of a constant feed rate an increase in the duration of spraying - at first causes an increase in the mean size of the granules, but later on the growth rate diminishes and an equilibrium emerges [4, 9]. This is caused by the fact that two opposite processes take place simultaneously: a build-up and a break-up and after a certain point agglomeration is offset by attrition effects. MÖBUS [9] studied the change of the particle size distribution of the granules formed as an addition to the mean particle size, and found that by increasing the amount of the granulating liquid the particle size distribution diminishes and later this distribution parameter acquires a constant value in a similar manner to the mean size.

The results on the effect of the feed rate of the granulating liquid on the physical properties of the granules are evaluated in literature by two different methods. RANKELL and co-workers [4] studied the effect of the feed rate of the granulating liquid by increasing the feed rate while keeping the duration of the spraying at a constant value. Hence an increased feed rate also means a greater amount of granulating liquid. They found that the mean particle size of the granules increases linearly with the increase of the feed rate. This conclusion is supported by the investigation of MÖBUS [9] who in addition found that the increase of the feed rate of the granulating liquid also increases the deviation of the particle size distribution. DAVIES and GLOOR [10] studied the effect of the feed rate by varying the feed rate of the granulating liquid while the amount of the latter was kept at a constant value. They found that the increase in the feed rate of the liquid somewhat increased the mean particle size and the wear resistance, bulk density and rollingness of the granules improved. However, it must be stated that these changes are not important except in the case of the mechanical strength.

Several authors referred to the effect of the change of the concentration of the granulating liquid on the physical properties of the granules formed [4, 7, 9, 11].

Emphasis should be placed on the results of DAVIES and GLOOR [11] who studied the effect of the concentration of the granulating liquid on the physical properties of the granules in the cases of four different binders, while keeping the amount of the granulating liquid at a constant value. They found that with the increase of the concentration of the granulating liquid, the mean size and the wear resistance of the granules increase. The trend of the changes is nearly the same, but there are major differences in the numerical values in the cases of the different binders.

THE EXPERIMENTAL APPARATUS AND THE METHOD OF THE EXPERIMENTS

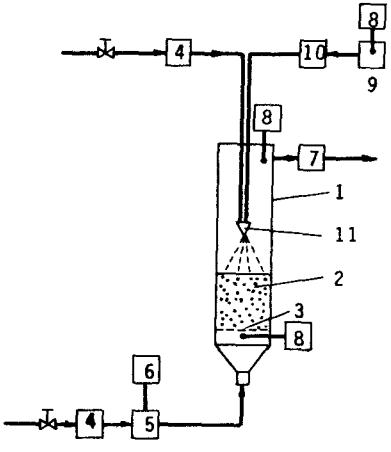

Fig. 1
1 - fluidization apparatus
2 - fluidized bed
3 - underplate
4 - flow meter
5 - preheater
6 - toroidal transformer
7 - cyclone
8 - thermometers
9 - thermostated tank
10 - pump
11 - nozzle

A schematic drawing of the set up used in the experiments on the granulation in a fluidized bed is shown in Fig. 1. The main part of the apparatus is the 0.3 m long granulator of 0.11 metre I.D. The fluidized bed is upheld and air is evenly distributed by the porous glass distributor plate (3). The main air stream enters the conical-cylindrical bottom under the plate via the flow meter (4) and the electric preheater (5). The temperature of the air at the inlet is controlled by the variable transformer (6) and is checked by the thermometer (8). The air leaves the granulator via the cyclone (7) and its temperature is measured by the thermometer (8). The granulating liquid is fed into the nozzle (11) from the thermostated tank (9) by the pump (10).

The amount of the air fed into the nozzle can be measured by the flow meter (4).

In the experiments, the raw material to be granulated was preheated by a hot air stream, and the quantity and temperature of the air were adjusted according to the fluidization properties of the raw material. After the temperature of the air at the outlet attained a given constant value, the atomization of the granulating liquid was started with a given feed rate. Owing to the wetting the particles agglomerate, hence their particle size steadily increases. The minimum fluidization velocity also increases. Therefore, to maintain the same bed expansion and motion of particles, the gas velocity must continuously become greater. Accordingly, the amount of air that ensures the fluid state was increased in accordance with the progress of the agglomeration. Having fed the planned amount of granulating liquid, the product was dried by maintaining the fluid state for a while and after that the physical properties of the product were determined.

As raw material the 0.1 - 0.2 millimetre fraction of quartz sand of a real density of $\rho = 2630$ kilograms per cubic metre, rollingness coefficient [12] of $\varphi = 0.59$ and a minimum fluidization velocity of $u''_m = 0.027$ metre per second were used. The granulating liquids were aqueous gelatine solutions of different concentrations. In the experiments dealt with here not only the dimensions of the apparatus, the raw material and the binder, but the relative expansion of the bed, the mass of the raw material, the temperature of the air at the inlet and the distance of the nozzle from the underplate were constant.

TEST METHODS FOR THE DETERMINATION OF THE PHYSICAL PROPERTIES OF THE GRANULES

In the following the test and calculating methods used for the determination of the physical properties of the granules formed in the experiments are summarized. The test methods were detailed in the first paper of this series [12].

a) The Determination of the Particle Size Distribution and of the Average Particle Size

The particle size distribution was determined by sieve analysis. The granules were separated into the following fractions by a ten-minute sieving with a vibration sieve (VEB Kombinat Medizin und Labortechnik, Typ: Thvr 1, Made in Leipzig GDR):

$(0.1 - 0.2)\times10^{-3}$ m; $(0.2 - 0.4)\times10^{-3}$ m; $(0.4 - 0.6)\times10^{-3}$ m; $(0.6 - 1.0)\times10^{-3}$ m; $(1.0 - 2.0)\times10^{-3}$ m; $(2.0 - 4.0)\times10^{-3}$ m; and above 4.0×10^{-3} metre.

The results of the sieve analysis obtained in weight per cent were also converted into vol. per cent - within the size limits of $(0.1 - 2.0)\times10^{-3}$ metre - by the help of the particle density of each fraction. The mean particle size was calculated on the basis of the vol. per cent composition [12].

b) The Determination of the Porosity

The minimum bed height (Y_m) of known amounts of average samples of the fractions separated by the sieve analysis was determined in the manner described in the first paper of this series [12]. Then the minimum void fraction was calculated as follows:

$$\varepsilon'_{m2} = \frac{Y_m - \frac{G_b}{\rho F}}{Y_m} \qquad (1)$$

The porosity of each fraction can be obtained with these void fractions according to the following equation [12]:

$$\varepsilon_p = 2.2(\varepsilon'_{m2} - 0.55) \qquad (2)$$

For the determination of the volumetric percentage particle distribution, the average granule density of the fractions has to be

known which can be simply calculated with the porosities of the fractions:

$$\rho_{sz} = (1 - \varepsilon_p)\,\rho \tag{3}$$

In this way the porosity and the particle density were determined for each fraction and with the vol. per cent composition of the fractions the average porosity and the average particle density were calculated.

c) The Determination of Wear Resistance

The wear resistance of the granules was determined by abrasion in a fluidized bed under standard circumstances [12]. A given amount of the $(0.4\text{-}0.6)\times10^{-3}$ metre fraction of the bulk to be investigated ($Y_m/D \approx 1$) was charged in a 0.04 metre diameter glass fluidization apparatus having a fritted glass distributor plate, after which the apparatus was closed at the top by a sieve. The particles were kept in fluidized state for ten minutes at a bed expansion of 3 times. After wearing the samples were sieved on a 0.4×10^{-3} metre sieve. The wear resistance was calculated as follows [12]:

$$K_s = \frac{G_m}{G_b} \cdot 100 \tag{4}$$

EXPERIMENTAL RESULTS

The physical properties of granules formed by granulation in a fluidized bed with spraying are affected by many parameters. If a given experiment is repeated even with the utmost care the physical properties of the granules generally are not identical, since it is extremely difficult to maintain the numerous operational and

process parameters at steady values.Therefore, it is indispensable to investigate the repeatability of the experimental results.

a) The Repeatability of the Experimental Results

The repeatability of the experimental results was determined on the basis of ten parallel experiments. Relying upon the preliminary experiments, the mean parameter values were chosen for the experimental circumstances. These and the average values,and the deviation of the most important physical properties of the granules formed are given in Table 1.

Table 1

V'/V = 20 vol. per cent $\quad c' = 60\ kg/m^3$

$w' = 5.9 \times 10^{-5}\ kg/sec \quad c_g = 0.45$ w.%

The characteristics of the granules		Average values	Deviation ± (%)
Particle composition vol. per cent	$d \cdot 10^3$ (m)		
	0.1-0.2	6.6	17.2
	0.2-0.4	26.8	11.3
	0.4-0.6	25.8	7.7
	0.6-1.0	26.3	15.5
	1.0-2.0	14.5	23.4
$\bar{d} \cdot 10^3$ (m)		0.64	6.5
ε_p	(-)	0.38	3.0
ρ_1	(kg/m^3)	811	4.2
ρ_2	(kg/m^3)	840	5.1
ρ_3	(kg/m^3)	1059	3.4
φ	(-)	0.52	5.0

The loosened, apparent and compacted bulk densities and the rollingness coefficients were determined as described in the first paper of this series [7]. The deviation was calculated as

$$\sigma = \pm \sqrt{\frac{\Sigma(\bar{x} - x_i)^2}{n - 1}}$$

where x_i is some property of the granules, n is the number of the determinations and $\bar{x}$ is the arithmetic mean of the results of parallel measurements. Table 1 shows that with respect to the particle composition the deviation of the experiments is significant, therefore in all cases three parallel experiments were carried out and the Figures given show the effects of various parameters, every dot corresponds to the average value of three parallel experiments.

b) The Effect of the Amount and the Feed Rate of the Granulating Liquid on the Physical Properties of the Granules

In a considerable part of our investigations - in about 90 experiments - the effects of the relative quantity and feed rate of the granulating liquid on the physical properties of the granules were investigated. To know the effects of these two variables is important from both the theoretical and practical points of view. The granulating liquid in these experiments was an aqueous gelatine solution of a concentration of $c' = 60$ kilograms per cubic metre. The relative amount of the granulating liquid was varied within the 0 - 30 vol. per cent range at five different feed rates. The relative quantity of the granulating liquid was related to the overall volume of the particles to be granulated (the particle volume of the sand to be granulated was 300×10^{-6} cubic metre). At a constant feed rate the charge of a greater amount of the granulating liquid requires a longer period of time, thus as the relative quantity of the granulating liquid increases the duration of the granulation (t') and the average binder content of the particles ($\bar{c}_g$) also increases.

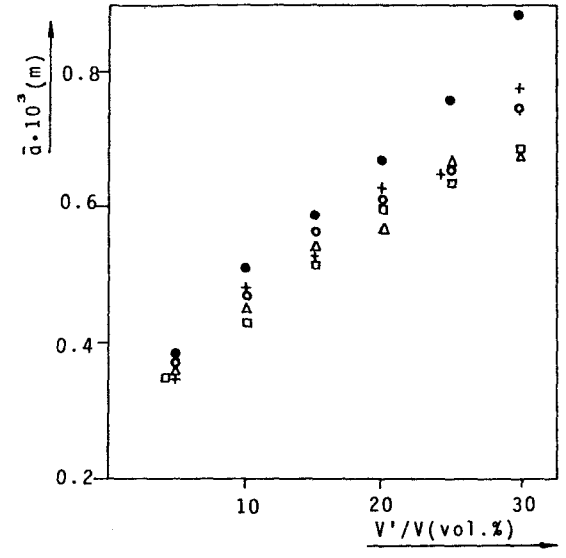

Fig. 2. • - $w' \equiv 2.5 \times 10^{-5}$ kg/sec
o - $w' = 4.2 \times 10^{-5}$ kg/sec; + - $w' = 5.9 \times 10^{-5}$ kg/sec
Δ - $w' = 7.6 \times 10^{-5}$ kg/sec; □ - $w' = 9.2 \times 10^{-5}$ kg/sec

In Fig. 2 the average particle size ($\bar{d}$) is given as a function of the relative quantity of the granulating liquid. When the relative amount of the liquid was increased from 5 vol. per cent, the average particle size increases by about two times. Since a build-up granulation takes place, the increase of the average particle size also causes an increase in the average porosity of the particles ($\bar{\varepsilon}_p$), as shown in Fig. 3.

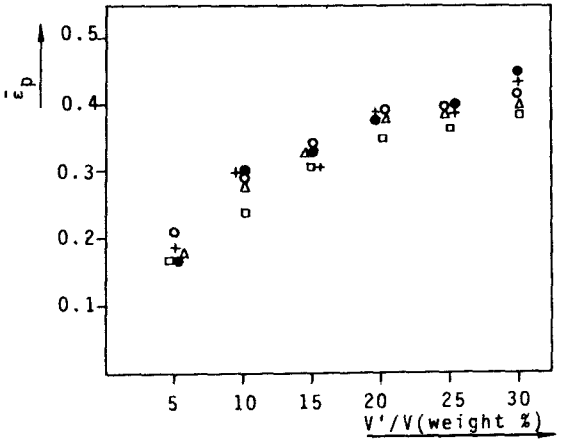

Fig. 3. • - $w' \equiv 2.5 \times 10^{-5}$ kg/sec
o - $w' = 4.2 \times 10^{-5}$ kg/sec; + - $w' = 5.9 \times 10^{-5}$ kg/sec
Δ - $w' = 7.6 \times 10^{-5}$ kg/sec; □ - $w' = 9.2 \times 10^{-5}$ kg/sec

In many respects the amount of the particles that were not granulated is an important indicator. In Fig. 4 the relative amount of the initial particle fraction (in weight per cent) is plotted against the relative amount on the sprayed binder solution.

The effect of the relative quantity of the granulating liquid upon the particle size distribution of the formed granules is shown in Fig.5. The cummulative sieve residue values are plotted in a log-normal diagram. It was found that the particle size distribution of the granules formed in a fluidized bed with spraying can be approximated well by a logarithmic normal distribution function.

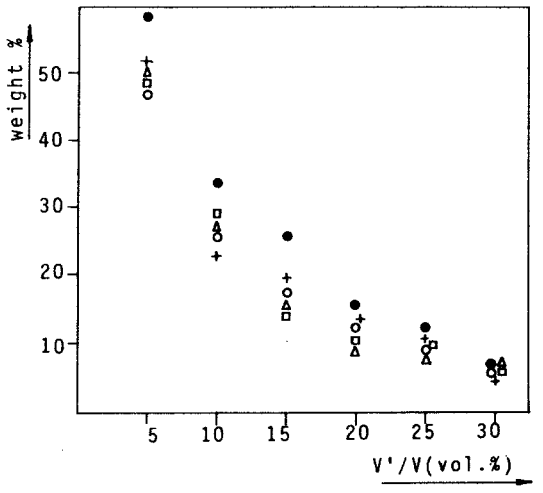

Fig. 4. d = (0.1-0.2)×10^{-3} m
• - w'=2.5×10^{-5} kg/sec; o - w'=4.2×10^{-5} kg/sec
+ - w'=5.9×10^{-5} kg/sec; Δ - w'=7.6×10^{-5} kg/sec
□ - w'=9.2×10^{-5} kg/sec

At three different values of the relative amount of the granulating liquid, the change of the binder concentration was investigated as a function of the size of the granules. In Fig. 6 the binder content of the different fractions is plotted

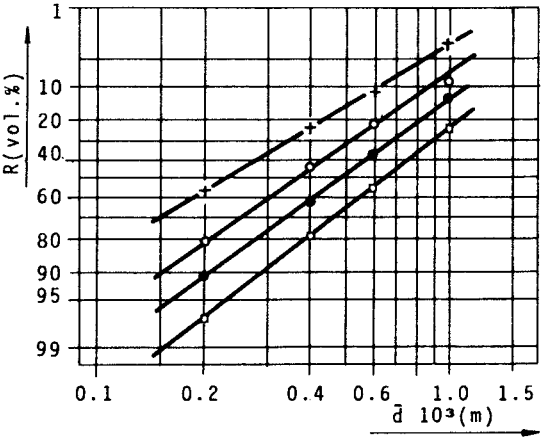

Fig. 5. + - V'/V = 5 v.%; o - V'/V = 10 v.%
• - V'/V = 20 v.%; □ - V'/V = 30 v.%
w' = 5.9×10^{-5} kg/sec

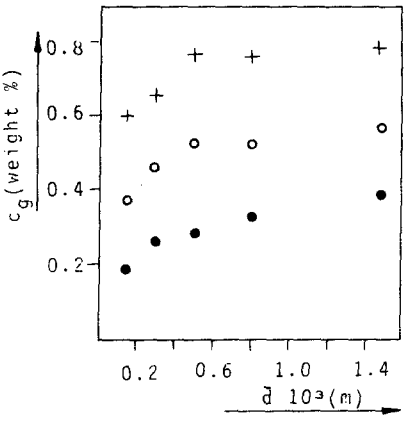

Fig. 6. $\bar{V}'/V$ = 30 vol.%
$\bar{c}_g$ = 0.68 w.%
$\bar{V}'/V$ = 20 vol.%
$\bar{c}_g$ = 0.45 w.%
$\bar{V}'/V$ = 10 vol.%
$\bar{c}_g$ = 0.23 w.%
w' = 5.9×10^{-5} kg/sec

against the overall weight of the dry material. At first the binder content of the granules increases with the growth of the particle size, but above an average particle size of 0.5×10^{-3} metre it aproaches an almost constant level. This agrees well with the statement described in our previous paper [12] that the wear resistance of the granules is approximately the same above the $(0.4\text{-}0.6) \times 10^{-3}$ metre particle size. There is an approximately linear relation between the greater average binder content that prevails with the greater quantity of the liquid and the wear resistance as shown in Fig. 7.

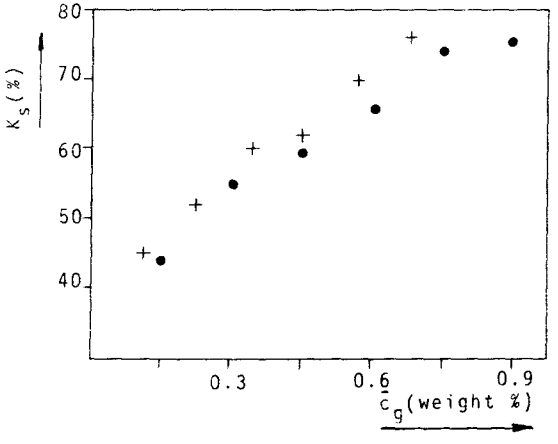

Fig. 7. w' = 5.9×10^{-5} kg/sec
+ - V'/V changes (c' = 60 kg/m^3)
• - c' changes (V'/V = 20 vol.%)

It was found that the increase of the feed rate - within the studied interval - had only a slight effect on the average size, average porosity, and the particle size distribution of the formed granules, provided the overall amount of the liquid sprayed in did not change. However, even in this case, some tendencies can be found, for instance

in Figs. 2 and 3 it is shown that the increase of the feed rate generally somewhat decreases the average particle size and the average porosity, but these tendencies are not so clean-cut and firm as those found in the case of the relative amount of the granulating liquid. This is also supported in Fig. 8 where the particle size distribution of the granules formed with the least, average and greatest feed are plotted in a lognormal diagram. The points fall fairly well along a straight line that indicates that the particle size distribution is nearly identical.

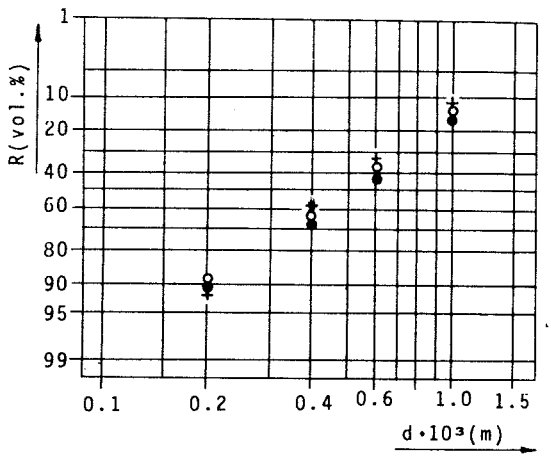

Fig. 8. V'/V≡20 vol.%; •-w'=2.5×10^{-5} kg/sec o-w'=5.9×10^{-5} kg/sec; +-w'=9.2×10^{-5} kg/sec

c) The Effect of the Concentration of the Granulating Liquid and of the Amount of the Binder on the Physical Properties of the Granules

In the next series of experiments the main variable was the concentration of the granulating liquid. The difference between the series of experiments was that in the first one the relative amount of the binder related to the bed weight was kept at a constant value despite the change in the concentration of the granulating liquid, whereas in the second one the amount of the binder also changed with the variation of the concentration. The concentration was varied in the 20 - 120 kilograms per cubic metre range.

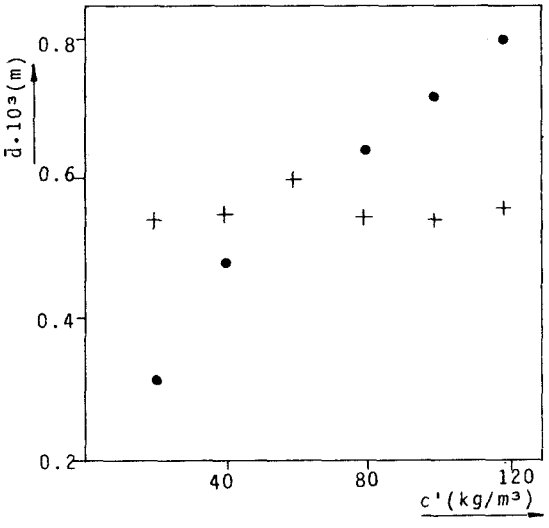

Fig. 9. $w' = 5.9 \times 10^{-5}$ kg/sec
+-$\bar{c}_g$ = 0.45 w.%; •-$\bar{c}_g$ = variable

The change of the concentration of the granulating liquid when the amount of the binder is kept at a constant level does not strongly affect the average size and porosity of the granules formed - at least within the studied concentration range. In Fig. 9 the average size is plotted against the concentration. However, the constant value of the average size does not unequivocally mean that the particle content of the bulk is unchanged. In Fig.10 the amount of the particles that were not granulated is shown as a function of the liquid concentration. It was found that the relative amount of the particles not granulated increases above the concentration of 60 kilograms per cubic metre.

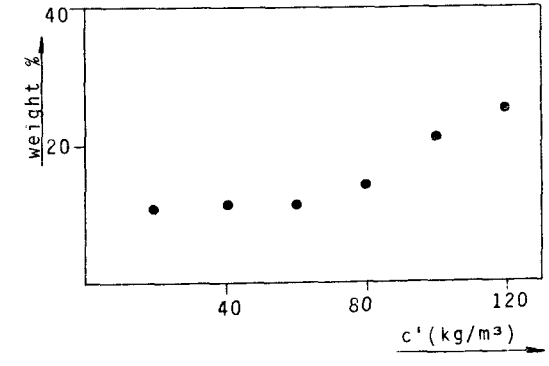

Fig. 10. $d = (0.1\text{-}0.2) \times 10^{-3}$ m
$\bar{c}_g$ = 0.45 w.%; $w' = 5.9 \times 10^{-5}$ kg/sec

When the granulation is carried out with the same amount of granulating liquid of different concentrations, the average particle size and the average porosity increases with an increase in the concentration since in this case the overall quantity of the binder is proportional to the

concentration. The effect of the concentration of the liquid on the average particle size is also shown for this case in Fig. 9.

When the concentration of the granulating liquid - that is the amount of the binder - is increased, the amount of the starting particle fraction approaches a lower limit as shown in Fig. 11. If the amount of the binder is increased by raising the binder concentration - while injecting the same amount of granulating liquid - the wear resistance of the granules increases almost linearly, although at great concentrations it approaches an upper limit (see Fig. 7).

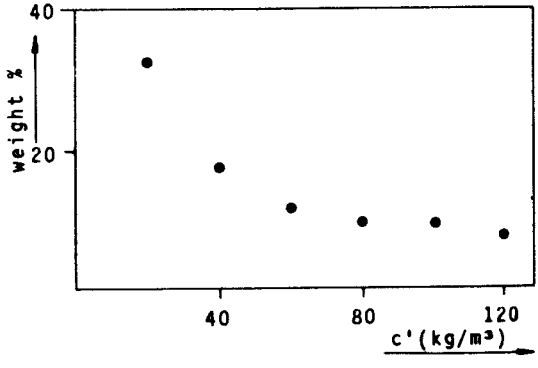

Fig. 11. $d = (0.1\text{-}0.2)\times10^{-3}$ m
$V'/V = 20$ vol.%; $w' = 5.9\times10^{-5}$ kg/sec

DISCUSSION

In the following section conclusions are drawn from the experimental results and wherever it is possible, comparisons are made with the results of other researchers.

The average size of the granules can effectively be enlarged by an increase in the relative quantity of the granulating liquid (Fig. 2). This increase is nearly linear at smaller feed rates, while at the two greatest feed rates it was found that after a certain point the growth of the particles is offset by wear effects and the growth rate diminishes. Several authors reported that after a certain time this latter effect totally compensates for the build-up, and a further addition of the liquid does not have any effect on the average size [9].

The wear resistance of the granules formed determines the value at which this equilibrium state is attained. If quartz sand is granulated with gelatine solutions, granules of high wear resistance are formed, therefore the equilibrium was not reached in the experiments dealt with here.

In build-up granulation the growth of the particle size also causes an increase in the average porosity of the particles. The porosity values show that granules mainly grow by a gradual build-up, since in the case of the linking up of granules the porosities should have been greater than the measured values of about 50 vol. per cent.

In most cases the primary function of granulation is to form a fraction of a given size range in the greatest quantity possible or that the amount of the powder not granulated should be the least possible in the final product. In Fig. 4 it is shown that above the 20 vol. per cent relative liquid quantity the decrease of the amount of the particles not granulated slows down and a further addition of the granulating liquid is unnecessary or it is reasonable only if the wear resistance of the granules is to be increased. From Fig. 7 it is obvious that the wear resistance of the granules - within the studied interval - steadily increases with the relative quantity of the granulating liquid.

If the feed rate of the granulating liquid is increased, the average particle size and the average porosity slightly diminish within the studied range of feed rate. This is inconsistent with the findings of DAVIES and GLOOR [10] that the size of the granules increases with the feed rate of the granulating liquid. The significance of this contradiction is considerably reduced by the fact that the changes found are slight in either case. The feed rate of the granulating liquid mainly affects the strength of the granules and the distribution of the binder in the particle fractions. These changes and the calculating method of the equilibrium and maximum feed rates of the granulating liquid will be dealt with in the next paper of this series in detail.

The experiments carried out to study the effect of the concentration of the granulating liquid showed that the optimum con-

centration of the gelatine solution was between 60-80 kilograms per cubic metre. Above this value the amount of the raw material that was not granulated grew if the amount of the binder was kept at a constant value (Fig. 10). The same optimum concentration is found in Fig. 11, where it is shown that the amount of the particles not granulated decreases up to a concentration of 60-80 kilograms per cubic metre, but later it does not change considerably despite the greater amount of the binder. This can be caused by the fact that together with the concentration, the viscosity of the solution also increases and after a certain limit deteriorates the atomization of the liquid. The average size of the granules is not considerably influenced by the concentration of the granulating liquid, provided the overall quantity of the binder is kept at a constant value (Fig. 9). When the liquid concentration is increased while keeping the relative amount of the granulating liquid at a constant level, the average particle size grows almost linearly, since in this case the greater concentration also means a greater amount of binder (Fig. 9). This conclusion is in agreement with the results of the experiments of DAVIES and GLOOR [11] carried out with gelatine as a binder.

Our conclusions can be summarized on the basis of Fig. 2 and 9 where it is obvious that the mean size of the granules is mainly determined by the overall amount of the binder, independently of the relative amount, feed rate and concentration of the granulating liquid, at least in the studied interval. Relying upon the experimental results the following equation was derived

$$\bar{d} = a_1 \frac{c'w't'}{V\rho\rho'} + a_2 \qquad (5)$$

The values of the constants for the studied model system were determined by a least square fitting method, and it was found that $a_1 = 6.2\times10^{-2}$ metre, $a_2 = 3\times10^{-4}$ metre. The differences between the average particle sizes calculated by Eq. 5 using the above values of the constants and the measured ones are plotted against

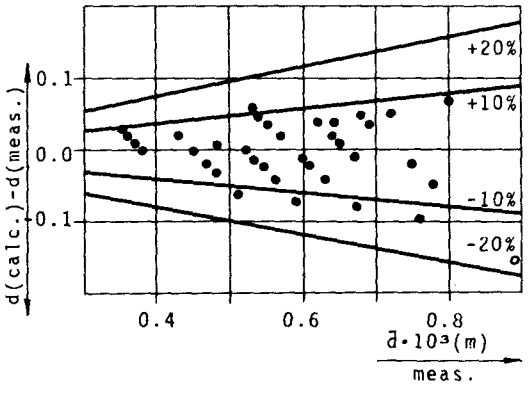

Fig. 12

the measured average particle sizes in Fig. 12. The relative differences between the measured and calculated values were less than ± 10 per cent in most cases.

The dependence of the constants a_1 and a_2 in Eq. 5 on the physical properties of the binder and the granulating liquid was studied in further experiments that will be dealt with in a subsequent paper.

SYMBOLS USED

a_1 constant (metre)

a_2 constant (metre)

c' the concentration of the granulating liquid (kilograms per cubic metre)

c_g the binder content of the granulating liquid (weight per cent)

$\bar{c}_g$ the average binder content of the granules (weight per cent)

D the diameter of the apparatus (metre)

d particle size (metre)

$\bar{d}$ average particle size (metre)

F the cross section of the apparatus (sq. metre)

G_b the mass of the fraction charged in (kilogram)

G_m the mass of the sieve residue (kilogram)

K_s wear resistance (per cent)

R sieve residue (vol. per cent)

T''_b air temperature at the inlet (degree centigrade)

t' the duration of the spraying (second)

u''_m minimum fluidization velocity (metres per second)

V overall volume of the particles to be granulated (cubic metre)

V' the volume of the granulating liquid (cubic metre)

V'/V the relative amount of the granulating liquid (vol. per cent)

w' the feed rate of the granulating liquid (kilograms per second)

Y bed height (metre)

Y_m minimum bed height (metre)

Y/Y_m bed expansion coefficient (dimensionless)

Y_p the distance between the atomizer and the underplate (metre)

ε_{m2} minimum void fraction (dimensionless)

ε_p the porosity of granules (dimensionless)

$\bar{\varepsilon}_p$ average porosity (dimensionless)

ρ real density (kilograms per cubic metre)

ρ_1 loosened bulk density (kilograms per cubic metre)

ρ_2 apparent bulk density (kilograms per cubic metre)

ρ_3 compacted bulk density (kilograms per cubic metre)

ρ_{sz} granule density (kilograms per cubic metre)

$\bar{\rho}_{sz}$ average granule density (kilograms per cubic metre)

ρ' the density of the granulating liquid (kilograms per cubic metre)

σ deviation

φ rollingness coefficient (dimensionless)

REFERENCES

1. RUMPF, H., Chemie Ing. Techn. 30, 144 (1958)
2. NEWITT, D.M., CONWAY-JONES, J.M., Trans Instn. Chem. Engrs. 36, 422 (1958)
3. WURSTER, D.E., J. Pharm. Sci. 49, 82 (1960)
4. RANKELL, A.S., SCOTT, M.W., LIEBERMAN, H.A., CHOW, F.S., BATTISTA, J.V., J. Pharm. Sci. 53, 320 (1964)
5. CONTINI, S., ATASOY, K., Pharm. Ind. 28, 144 (1966)
6. WOLF, G., Pharm. Ind. 30, 552 (1968)
7. LISKE, T., MÖBUS, W., Pharm. Ind. 30, 557 (1968)
8. PILPEL, N., Chem. and Proc. Eng. 50, 67 (1969)
9. MÖBUS, W., Ceskoslov. farm. 18, 109 (1969)
10. DAVIES, W.L., GLOOR, Jr.W.T., J. Pharm. Sci. 60, 1860 (1971)
11. DAVIES, W.L., GLOOR, Jr.W.T., J. Pharm. Sci. 61, 618 (1972)
12. ORMÓS, Z., Hung. Ind. Chem. 1, 207 (1973)

РЕЗЮМЕ

При грануляции в распылительно-псевдоожиженном слое количество связующего вещества имеет значительное влияние на физические свойства образующихся гранул, поэтому знание этого влияния важно с практической и научной точки зрения. Авторы коротко рассматривают важнейшие условия связанные с влиянием изменения количества связующего вещества, найденные в литературе. Описываются экспериментальный аппарат и методы определения физических свойств гранул. Экспериментальные данные, выражающие влияние количества и концентрации, а также скорости подачи гранулирующей жидкости на физические свойства гранул, представляются в таблицах и на рисунках. Экспериментальные данные оцениваются авторами и даются соотношения для вычисления среднего диаметра гранул.

Hungarian Journal
of Industrial Chemistry
Veszprém
Vol.1. pp. 329-342 (1973)

GENERALIZATION OF THE ENTROPY OF MIXING I.

R. TÖRÖS

(Research Institute for Technical Chemistry of the Hungarian Academy of Sciences, Veszprém)

Received: September 26, 1972.

In order to give a theoretical treatment of the mixing process, the formula describing the increase in entropy of the mixing of ideal gases has been generalized and the properties of the quantity thus obtained are dealt with. The entropy of mixing seems to be adequate to serve as a quantitative indication of the degree of permixing.

The second part of this paper reviews the practical application on a simplified fluid mechanical model.

INTRODUCTION

Numerous problems were encountered in the Research Institute for Technical Chemistry of the Hungarian Academy of Sciences in which mixing was an important or even central problem. In the surveyed literature it was found that the papers can be devided into two groups. In one group, mixing is of central interest, but entropy is not mentioned at all. The remainder of the papers include those which deal with entropy, but without mentioning its application in connection with the question of mixing [1]. It also became apparent during these studies that two types of state parameters are necessary for the description of the mixing process:

1. a quantity showing how intensive the mixing process is, and how fast it is, etc. This is a state parameter of intensive type;

2. a quantity showing what changes occur during the mixing operation, i.e. the degree of permixing. This is a state parameter of extensive type.

Undoubtedly a certain degree of arbitrariness cannot be avoided in selecting the quantities of the two types; however, qualitative properties can be stated in connection with both types of state parameters. Such qualitative properties, in the case of the quantity mentioned under 1. are the following:

a) In a domain being mixed, the rate of mixing is certainly different in the various space elements, and consequently, this type of state parameter must be one of the l o c a l type.

b) If the rate of mixing is the same everywhere (homogenous space), the state parameter should be greater if the material is mixed faster and smaller if the mixing is slower.

The qualitative properties of the state parameter described under 2. are the following:

a) The degree of permixing is characteristic of a whole domain and is an extensive measure.

b) The degree of permixing should be higher if the material distribution is more uniform and lower if the material is more inhomogeneous.

For example, a quantity of type 1. may be the current density vector of the material to be homogenized or mixed.

A quantity of type 2. may be some quantity that is a monotonic function of the deviation from the uniform concentration.

In the author's thesis, a quantity has been proposed for the characterization of the degree of permixing. This is a quantity defined by an integral formula obtained by the generalization of the entropy of mixing of ideal gases, if the domain to be mixed is a

set of single connection and measurable. The density of the substance to be mixed is taken as $\rho'(\bar{r},t)$. In this case, if the total mass present in the domain is denoted by M, the quantity: $\frac{\rho'}{M} = \rho(\bar{r},t)$ represents the probability density of an individual particle, selected at random, of the substance. On the basis of the latter function, the quantity can be defined:

$$s = -\int_{(V)} \rho \ln (\rho \Delta V) dV; \quad s_k = \frac{\int \rho \ln \Delta V \rho dV}{\ln \frac{\Delta V}{V}} \tag{1}$$

γ is the density of the substance being permixed, and[1]:

$$\Delta V = \frac{\gamma}{M}$$

ΔV is, according to its meaning, the minimum volume in which the substance to be permixed is present.

As to s, it can be shown that:

1. $$0 < s < s_m$$

where s_m is the value of maximum entropy:

$$s_m = -\ln \frac{\Delta V}{V}$$

2. If the distribution is uniform, then:

$$s = s_m$$

if the distribution is such that the substance to be permixed and the carrier substance are perfectly separated from each other, thus:

$$s = 0$$

These properties offer a reason for using the quantity s for the measurement of the degree of permixing. It would have been

[1] The introduction of ΔV is not only a question of the selection of dimension and zero point, but also that of choice of scale; cf. [2].

preferable to show that s is in a monotonic connection with the uniformity of distribution. However, this was shown only for a special case, numerically, i.e. for the case of a normal distribution. It was found that in such a case there is a monotonic connection between s and the scattering of the distribution:

$$\frac{ds}{d\sigma} > 0$$

1. GENERALIZATION OF THE ENTROPY OF MIXING IN THE CASE OF MORE THAN ONE SUBSTANCE BEING MIXED

Formula (1) can also be generalized if it is not one single substance whose degree of permixing is to be determined. Let us suppose that a number n of substances to be mixed are present in a domain V, each of them in a certain distribution, and let the density of the i^{th} mixed substance be $\rho_i'(r,t)$ $i = 1, 2, \ldots, n$; in this case if M_i is the total mass of the i^{th} substance in the domain, the formula:

$$\frac{\rho_i'}{M_i} = \rho_i(\bar{r},t)$$

is the probability density distribution of an individual particle of the i^{th} substance, selected at random.

The following generalization of Formula (1) will now be considered:

$$S = -\int_{(V)}\int_{(V)}\ldots\int_{(V)}(\rho_1\rho_2\ldots\rho_n)\ln(\Delta V_1\rho_1\Delta V_2\rho_2\ldots\Delta V_n\rho_n)dV_1dV_2\ldots dV_n \quad (2)$$
$$(n)$$

Equation (2) can be transformed by the known functional equation of logarithm:

$$\ln(\Delta V_1\rho_1\ldots\Delta\rho_nV_n) = \sum_{i=1}^{n}\ln\Delta V_i\rho_i \quad (3)$$

By substituting Eq. (3) into Eq. (2) we obtain:

$$S = -\int_{(V)}\int_{(V)}\ldots\int_{(V)} (\rho_1\rho_2\ldots\rho_n)\ \ln\ (\Delta V_1\rho_1\ldots\Delta V_n\rho_n)\ dV_1dV_2\ldots dV_n =$$

$$= -\int_{(V)}\int_{(V)}\ldots\int_{(V)} \sum_{i=1}^{n} (\rho_1\rho_2\ldots\rho_n)\ \ln\ (\Delta V_i\rho_i)dV_1dV_2\ \ldots\ dV_n =$$

$$= -\sum_{i=1}^{n} \int_{(V)}\int_{(V)}\ldots\int_{(V)} (\rho_1\rho_2\ldots\rho_n)\ \ln\ (\Delta V_i\rho_i)dV_1dV_2\ \ldots\ dV_n \qquad (4)$$

The integrals under the sign $\sum$ can now be solved by transformation to multiple integrals, since the factors, which do not contain V_i, can be factored out of the integral according to V_i:

$$S=-\sum_{i=1}^{n} \int_{(V)}\int_{(V)}\ldots\int_{(V)}\left[\int_{(V)}(\rho_1\rho_2\ldots\rho_n)\ln(\Delta V_i\rho_i)dV_i\right]dV_1dV_2..dV_{i-1}dV_{i+1}..dV_n=$$

$$= -\int_{(V)}\int_{(V)}\ldots\int_{(V)}\left[\rho_1\rho_2\ldots\rho_{i-1}\rho_{i+1}\ldots\rho_n \sum_{i=1}^{n}\int_{(V)}\rho_i\ \ln(\Delta V_i\rho_i)dV_i\right]\cdot$$
$$(n-1)$$

$$\cdot\ dV_1dV_2\ \ldots\ dV_{i-1}dV_{i+1}\ \ldots\ dV_n \qquad (5)$$

As a result of these transformations, the quantity s_i is gained in an explicit form:

$$s_i = -\int_{(V)} (\rho_i\ \ln\ (\Delta V_i\rho_i))\ dV_i \qquad (6)$$

s_i is independent on the other variables, and can be factored out from under the integrals. Accordingly, calculation (5) can be continued:

$$S = -\sum_{i=1}^{n} s_i \int_{(V)}\int_{(V)}\ldots\int_{(V)} (\rho_1\rho_2\ldots\rho_{i-1}\rho_{i+1}\ldots\rho_n)\cdot$$
$$(n-1)$$

$$\cdot\ dV_1dV_2\ \ldots\ dV_{i-1}dV_{i+1}\ \ldots\ dV_n$$

The integral can again be resolved to a multiple integral:

$$S = -\sum_{i=1}^{n} s_i \int_{(V)} \rho_1 dV_1 \int_{(V)} \rho_2 dV_2 \ldots \int_{(V)} \rho_{i-1} dV_{i-1} \int_{(V)} \rho_{i+1} dV_{i+1} \ldots \int_{(V)} \rho_n dV_n \tag{7}$$

The values of the individual volume integrals are all unity, since the densities are normalized:

$$\int_{(V)} \rho_i dV_1 = 1 \tag{8}$$

and as a result we obtain:

$$S = \sum_{i=1}^{n} s_i \tag{9}$$

that is to say, if S - as defined by Equation (2) - is regarded as the degree of permixing when a number of substances are simultaneously mixed, the additivity theorem is valid: the degree of permixing, when mixing a number of substances, is the algebraic sum of the various degrees of permixing.

It can be seen by a short calculation that the maximum property shown for s in 1. also holds for S, i.e. S is the functional of the functions $\rho_1, \rho_2, \ldots \rho_n$:

$$S = S[\rho_1, \rho_2, \ldots \rho_n] \tag{10}$$

However, on the basis of formula (9):

$$S[\rho_1 \rho_2 \ldots \rho_n] = \sum_{i=1}^{n} s_i[\rho_i] \tag{11}$$

Consequently, if S is varied according to the variables of ρ_i, and the condition of the extreme value is found, we arrive at:

$$\delta S = 0 \tag{12}$$

If the supplementary condition is included into the method of variation, the following equation is obtained:

$$\sum_{i=1}^{n} \delta s_i[\rho_i] = 0 \tag{13}$$

The ρ_i functions can be varied independently, and consequently:

$$\sum_{i=1}^{n} \delta s_i[\rho_i] = 0 \rightarrow \delta s_i[\rho_i] = 0 \qquad (14)$$

However, the second Equation in (14) involves uniform distribution as a condition. It is apparent that the maximum value of S according to (9) is not unity. If S is divided with maximal values of the sum of s_i-s S will be normalized to unity.

In order to comprehend this, let us consider the quantity:

$$s_i = -\int_{(V)} \rho_i \ln (\Delta V \rho_i)\, dV \qquad (15)$$

Since: $\rho_i \geq 0$

and

$$\rho_i \leq \frac{1}{\Delta V}$$

consequently:

$$\ln (\Delta V \rho_i) \leq 0$$

and thus:

$$s_i \geq 0$$

The maximum value of (15), with the complementary condition:

$$\int_{(V)} \rho_i dV = 1 \qquad (16)$$

can be determined by variation calculus. The task is to determine the extreme value of:

$$\phi = \int [-\rho_i \ln (\Delta V \rho_i) + \alpha \rho_i]\, dV$$

The Euler-equation is:

$$\frac{\partial \varphi}{\partial \rho} = 0$$

where

$$\varphi = -\rho_i \ln (\Delta V \rho_i) + \alpha \rho_i \tag{18}$$

With the substitution of (18), (17) becomes:

$$-\ln \Delta V - (\ln \rho_i + 1) + \alpha = 0$$

$$\rho_i = e^{-(\ln \Delta V - 1 - \alpha)} \tag{19}$$

i.e. we have a uniform distribution which is independent of the space co-ordinates.

The extreme value condition (16) determines α:

$$V e^{-(\ln \Delta V - 1 - \alpha)} = 1$$

$$\alpha = -\ln V$$

$$(\ln \Delta V - 1 - \alpha) = \ln V$$

$$\alpha = \ln \frac{\Delta V}{V} - 1$$

Substituting back into (19):

$$\rho_i = \frac{1}{V}$$

(15) becomes:

$$s_i = -\frac{1}{V} \int \ln \frac{\Delta V}{V} \, dV = -\ln \frac{\Delta V}{V} \tag{20}$$

The property mentioned under (1) has hereby been proven. At the same time, it has also been shown on the basis of (14) that S has its maximum at:

$$\rho_i = \frac{1}{V} \qquad i = 1, 2, \ldots, n$$

whose value is:

$$S_M = -\sum_{i=1}^{n} \ln \frac{\Delta V_i}{V}$$

Accordingly, S is not normalized to 1 and its maximum value is S_M.

$$0 \leq S \leq S_M$$

2. CALCULATION OF THE ENTROPY OF MIXING IN A GENERAL CASE

It is sufficient to show the entropy determination for a single mixed component; if there are more components, the same differential equation is valid on the basis of the same consideration for all of the components as in the case of a single component.

The system of equations, valid for the process of mixing, is the following:

1. The equation of the conservation of mass:

$$\frac{\partial \rho}{\partial t} + \operatorname{div} (\rho \bar{v} - D_1 \operatorname{grad} \rho) = 0 \tag{21}$$

where

$\bar{v}$ is the velocity distribution of substance (metre.second^{-1})

D_1 is the effective diffusion constant (sq.metre·second^{-1})

ρ is the density of the mixed component (kilogram/cu.metre)

In a general case:

$$\rho = \rho(\bar{r},t)$$
$$\bar{v} = \bar{v}(\bar{r},t) \tag{22}$$

where $\bar{r}$ is the position vector.

2. The flow equation pertaining to the rate space, in the usual form of the law of the conservation of impulse:

$$\frac{\partial \rho \bar{v}}{dt} + \operatorname{Div} (P + \rho \bar{v} \circ \bar{v}) = \rho \bar{f} \tag{23}$$

where

Div is tensor-divergence (metre^{-1})

P is the stress-tensor (kilogram·metre^{-1}·second^{-2})

$\bar{f}$ is the vector of mass force (metre·second^{-2})

It is necessary to formulate an assumption in connection with the stress terms and mass forces which give a more exact definition of the nature of the carrier medium. As it is known, such assumptions are the model of the ideal fluid or that of Newtonian fluid, but it may also be any other model [3].

The form of Equation (23) is not identical to that of the Navier-Stokes equation, since the divergence of the first term of (23) and of the diadic tensor of the convective stream cannot be eliminated by Equation (21), only in such cases where the diffusion can be neglected. This assumption is justified in the case of common diffusion; however, if mixing is described by a diffusion-type model, essentially it cannot be neglected. In the following, a flow equation that also takes mixing into consideration will be quoted. The mass forces and the stress-tensor will not be specified, the generalization will still be sustained. The left side of Equation (23) is modified:

$$\frac{\partial \rho \bar{v}}{\partial t} + \mathrm{Div}\,(P + \rho \bar{v} \circ \bar{v}) =$$

$$= \bar{v}\,\frac{\partial \rho}{\partial t} + \rho\,\frac{\partial \bar{v}}{\partial t} + \mathrm{Div}\,P + \mathrm{Div}\,\rho \bar{v} \circ \bar{v} \qquad (24)$$

but:

$$\mathrm{Div}(\rho \bar{v} \circ \bar{v}) = \bar{v}\ \mathrm{div}\ \rho \bar{v} + \rho(\bar{v}, \nabla \circ \bar{v}) \qquad (25)$$

By substituting Equations (24) and (25) back into Equation (23), the multiplicator of $\bar{v}$ van be collected:

$$\bar{v}\,\left(\frac{\partial \rho}{\partial t} + \mathrm{div}\,\rho \bar{v}\right) + \rho\,\frac{d\bar{v}}{ft} + \rho(\bar{v}, \nabla \circ \bar{v}) + \mathrm{Div}\,P = \rho \bar{f} \qquad (26)$$

The first term of Equation (26) is equal to zero, if the term ori-

ginating from the diffusion stream can be neglected in Equation (21):

$$\frac{\partial \rho}{\partial t} + \operatorname{div} \rho \bar{v} = D_1 \Delta \rho \quad 0 \tag{27}$$

Should this not be the case, the simplification of Equation (2) can be carried out only by writing Equation (27):

$$\bar{v} D_1 \Delta \rho + \rho \frac{d\bar{v}}{dt} + \rho(\bar{v}, \nabla \circ \bar{v}) + \operatorname{Div} P = \rho \bar{f} \tag{28}$$

Accordingly, the Navier-Stokes equation will be supplemented with the first term of Equation (28).* It can be added that the Navier-Stokes equation is also different from Equation (28) inasmuch as the medium to be mixed is not incompressible, and consequently:

$$\operatorname{div} \bar{v} \neq 0 \tag{29}$$

since the component being mixed is not present alone in the space of streaming, but together with the carrier. With a view to a more exact formulation, it should also be taken into consideration that the velocity of the molecules of the component to be mixed is not the same as that of those of the carrier medium and accordingly the law of viscosity ought to be taken into account. The system of simultaneous equations thus grows further. Two Navier-Stokes equations are valid for the two velocity spaces, and a conservation law of the type (21) for both substances, one of these (that pertaining to the component to be mixed) also containing a diffusion term. In the two equations of streaming, e.g. the Stokes law of viscosity has to be taken into consideration as a mass force. The friction force has a greater influence upon the mixed component than upon the carrier, and consequently it is sufficient to account for it only in one case:

$$\rho \bar{f} = - 6 \pi \eta r (\bar{v} - \bar{v}') \rho \tag{30}$$

*The attenation of the author was drawn to this fact by Dr.I.Fényes, for which the author expresses his thanks.

where

η is the viscosity of the carrier medium (kilogram·second/sq.metre)

r is the radius of a particle (molecule) of the mixed component (metre)

$\bar{v}, \bar{v}'$ is the rate of the mixed component and of the carrier (metre/second)

Furthermore, if the carrier medium is present at a high density of the incompressibility condition is justified (as against the case of the component being mixed):

$$\operatorname{div} \bar{v}' = 0$$

The equation of streaming becomes simpler. However, it is most reasonable to accept Equations (21) and (28) as basic equations of satisfactory accuracy, which are, at the same time, theoretically accurate.

Summing up, Equations (21) and (28), or (23) are four differential equations for the functions ρ, v_1, v_2, v_3.

The pressure p (stress tensor) is to be regarded as known data of the problem, furthermore the $\bar{f}$ mass force and the initial and boundary conditions. However, if the problem has been solved, by means of these, the value of ρ' and the ρ density function will also be obtained. In this case, Equation (1) gives the degree of permixing by calculation of the integral.

In conclusion it should mentioned that the normal differential equation, describing the changes of the entropy of mixing in time cannot be deduced it has no universal form. This can be explained in the following manner. The entropy of mixing has been regarded as the degree of mixing, whether the task is to mix materials or internal energy. (Equation (1) can be generalized for the simultaneous mixing of both material and internal energy.) Accordingly, the II. law of thermodynamics can be applied, but not the theorems of irreversible thermodynamics describing processes in time. The equations of thermodynamics, describing process in time, always refer to **spontaneous** - although complex - equalization

processes [4]. Mixing is doubtlessly an equalization process, but not a spontaneous one. Therefore a mechanical mixing process cannot be described as a spontaneous equalizing process where the gradient of an intensive quantity is the driving force. E.g. a mixing which produces eddy currents the velocity field has not potential function [1]. If the equalization process was brought about by generalized thermodynamical forces (the gradients of the intensity parameters within the system), the irreversible entropy production brought about in the process (i.e. the entropy of mixing) could be calculated from the equations describing the changes in time, formulated to a continuum [4]. It is outside the scope of this paper, but nevertheless it can be mentioned that mixing could perhaps be described as the tendency of a generally fictive and as yet unknown intensity parameter for equalization. The theoretical foundation seems, on the basis of the foregoing, to be doubtful, but in order to reach only a given aim, not impossible. Only a comparison with practice can tell whether it is successful or not. Consequently, the expansion of the theory in this direction will not be dealt with. (The differential equation of the change in time, which is founded on an empyrical basis and can be checked asymptotically, has been elaborated together with Dr. T. BLICKLE [5].)

REFERENCES

1. TŐRÖS, R., C. Sc. Thesis. Hung. Acad. Sci. Budapest, 1971.

2. VINCE, I., Matematikai Lapok X, (3-4) 255-266 (1959).

3. SKELLAND, A.H.P., Non-Newtonian Flow and Heat Transfer pp. 1-23, John Wiley and S. New York (1967)

4. FÉNYES, I., D. Sc. Thesis. Hung. Acad. Sci. Budapest, 1958.

5. BLICKLE, T. and TŐRÖS, R., A keveredési entrópia heurisztikus differenciálegyenletéről (On the heuristic differential equation of the entropy of mixing; in press.)

РЕЗЮМЕ

Для теоретического описания смешивания автор обобщает выражение приращения энтропии при перемешивании идеальных газов, рассматривает свойства величины, получаемой таким путем. Энтропия смешивания оказывается пригодной для количественного охарактеризования перемешивания.

В следующей части сообщения автор представит практическое применение метода на упрощенной гидродинамической модели.

Hungarian Journal
of Industrial Chemistry
Veszprém
Vol.1. pp. 343-350 (1973)

A METHOD FOR THE CALCULATION OF THE NONPOLAR SOLUBILITY PARAMETER OF UNSATURATED NORMAL HYDROCARBONS

Gy. DEÁK

(Department of Hydrocarbon and Coal Processing,
Veszprém University of Chemical Engineering)

Received: February 2, 1973.

Correlations were derived for the determination of the acentric factor and critical pressure of the homomorphs of unsaturated normal hydrocarbons from the molar liquid volume at a given temperature; with these data the solubility parameter of the homomorph - that is the nonpolar solubility parameter of the unsaturated normal hydrocarbon - can be calculated by the correlation given by LYCKMAN, ECKERT and PRAUSNITZ.

It is often necessary to describe the vapour liquid equilibrium of various systems. In most cases this cannot be done without difficult experiments. Several correlations were derived for the estimation of vapour liquid equilibria. Most of these correlations contain the solubility parameter introduced by HILDEBRAND and SCOTT. In systems that also consist of polar compounds, these correlations apply the solubility parameter split into polar and nonpolar parts. Therefore it is often necessary to calculate the polar and nonpolar solubility parameters of polar compounds.

The regular solution theory of HILDEBRAND and SCOTT has been applied to various problems of chemical engineering [1-4]. This theory contains two temperature dependent parameters for each component, the molar liquid volume (V) and the solubility parameter (δ), which is defined as the square root of the configurational energy per unit volume.

Since appropriate data for their evaluation are frequently unavailable, several generalized relationships were derived to estimate these two parameters at various temperatures. These methods are based on a three-parameter theory of corresponding state [5, 6].

The regular solution theory was applied to correlations for vapour liquid equilibria. The first of the correlations available is the equation of HILDEBRAND for the activity coefficient of component 1 at infinite dilution in solvent component 2:

$$\ln \gamma_1^{\infty} = \frac{V_1(\delta_1 - \delta_2)^2}{RT} \qquad (1)$$

This equation is applicable to regular solutions and has wide applications in systems consisting of hydrocarbons. It is unsuitable for systems involving polar or hydrogen-bonding components.

HILDEBRAND suggested and BLANKS and PRAUSNITZ further developed the idea of splitting the solubility parameter into two parts [7, 8]:

$$\delta^2 = \lambda^2 + \tau^2 \qquad (2)$$

where λ is the solubility parameter ascribed to nonpolar effects and τ is the polar solubility parameter. The value of λ for a polar component is set equal to the solubility parameter of a nonpolar molecule of the same size and shape, and at the same reduced temperature as the polar molecule. The value of τ is obtained by solving Equation (2).The nonpolar molecule used in this context is termed the homomorph of the polar molecule.

The splitting of the solubility parameter of polar compounds has proved to be useful. BLANKS and PRAUSNITZ, WEIMER and PRAUSNITZ,later HELPINSTILL and VAN WINKLE, and finally NULL and PALMER derived various equations for the estimation of the activity coefficient at infinite dilution using τ and λ [8-11]. These relationships are generally capable of predicting the vapour liquid equilibria of different systems consisting of various components.

However, these methods can be used only when the solubility parameter and its two parts can be determined. LYCKMAN, ECKERT and PRAUSNITZ correlated the solubility parameter and the acentric factor and critical pressure for nonpolar or slightly polar compounds. Their correlation is as follows [6]

$$\frac{\delta}{P_c^{1/2}} = \delta_R^{(0)} + \omega\delta_R^{(1)} + \omega^2\delta_R^{(2)} \qquad (3)$$

where P_c is the critical pressure, ω is the acentric factor, $\delta_R^{(0)}$, $\delta_R^{(1)}$ and $\delta_R^{(2)}$ are generalized functions dependent upon the reduced temperature and given by the earlier mentioned authors in tables.

The part of the solubility parameter due to polar effects is more difficult to determine. WEIMER and PRAUSNITZ, and HELPINSTILL and VAN WINKLE provided charts for the calculations of λ from where λ-s are obtained as functions of molar volume and reduced temperatures. NULL and PALMER gave an equation for this purpose which included constants determined by the regression analysis of vapour liquid equilibrium data. The published charts are limited, and so their readings can be rather inaccurate, while NULL's equation can be applied in the cases of such compounds for which the regressional constants were determined.

While predicting the vapour liquid equilibria of various systems consisting of saturated and unsaturated hydrocarbons it was necessary to split the solubility parameter of the unsaturated hydrocarbons according to the polar and nonpolar effects. The earlier mentioned charts were inappropriate for the purpose, partly because of the difficulties in their reading, and partly because their limited range in reduced temperature. The constants in NULL's equation were not available either, so the derivation of a new method was necessary for the estimation of the nonpolar solubility parameter.

As mentioned earlier λ is equal by definition to the solubility parameter of a nonpolar molecule of the same size and shape, and at the same reduced temperature as the polar molecule. The new

method was derived on the basis of this definition. It uses the correlation of LYCKMAN, ECKERT and PRAUSNITZ. First the acentric factor of the hypothetic compound is determined,of which the molar liquid volume at the given reduced temperature is equal to that of the polar hydrocarbon. In possession of this acentric factor, the critical pressure of this hypothetic compound can be determined. Equation (3) can now be used to calculate the solubility parameter of the hypothetic compound, that is the nonpolar solubility parameter of the polar hydrocarbon.

The acentric factor can be calculated by Equation (4) as a function of the temperature and molar liquid volume:

$$\omega = -0.6567970503 + 4.317033425\times10^{-3}\ T - 9.552751262\times10^{-6}\ T^2 +$$

$$+(6.948576691\times10^{-3} - 2.366410236\times10^{-5}\ T + 5.296188633\times10^{-8}\ T^2)\ V +$$

$$+\ (-7.300585551\times10^{-6} + 2.980456572\times10^{-8}\ T - 7.607366498\times10^{-11}T^2)V^2$$

The constants of Equation (4) were determined on the basis of 185 various molar liquid volumes of the C_2-C_{16} normal paraffins embracing the 25 - 105 ^{o}C temperature range by a least square fit method.The values of the molar volumes were calculated according to MEISNER [12]. His equation gives the molar volumes with a relative standard deviation (characterizing the lack of fit) of 0.22 %. Taking into account the internal precision of the molar volume measurements ($\pm$ 0.5 - 1.5 % relative) this fit is quite satisfactory.

The average deviation in the case of the acentric factor was $\pm$ 2.97 %.

In the knowledge of the acentric factor the critical pressure and critical temperature of the hypothetic compound can be calculated by Equations (5) and (6):

$$P_c = 57.96973602 - 113.7754867\ \omega + 74.25657898\ \omega^2 \qquad (5)$$

$$T_c = \exp(6.640208073 - 0.02744984296/\omega + 0.1289717519\ \omega + 0.2985\ \ln\ \omega) \qquad (6)$$

The constants of these equations were determined from the data of the C_2-C_{16} normal paraffins [13, 14] by a least square fit method. A comparison of the critical pressures and temperatures in literature and calculated by Equations (5) and (6) using the acentric factors determined by Equation (4) showed that the average deviation was $\pm$ 2.88 % in the case of the critical pressure and $\pm$ 2.80 % in the case of the critical temperature, taking into account the earlier mentioned 185 data.

Hence the nonpolar solubility parameter of an unsaturated normal hydrocarbon can be calculated by Equations (3)-(6) according to the scheme in the Figure.

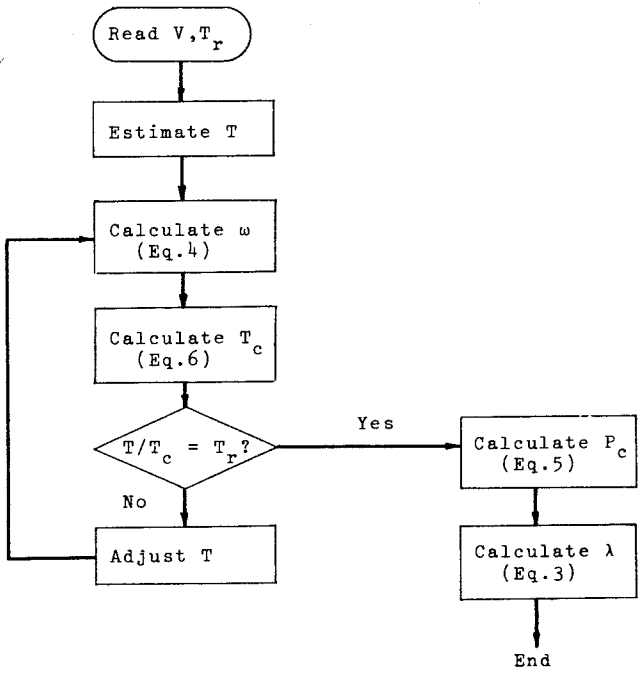

Schematic diagram of the calculation of λ

With the knowledge of the V molar volume and T_r reduced temperature, a T temperature can be estimated, and the acentric factor of that hypothetic normal paraffin can be calculated, that has a V molar volume at the selected temperature (Equation (4)). With Equation (6) the critical temperature of this compound can be calculated. It is now possible to find out what reduced temperature corresponds to the estimated temperature in the case of the hypothetic compound. If this value does not agree with the given reduced temperature, the estimated temperature should be adjusted, and the trials should continue until the deviation is negligible. Accepting the acentric factor that corresponds to this temperature and the given molar volume, the critical pressure of the hypothetic normal paraffin can be determined by Equation (5); the solubility parameter of the hypothetic compound can then be calculated by Equation (3) - which is equal by definition to the nonpolar solubility parameter of the unsaturated normal hydrocarbon.

The method is applicable within the 25 - 105°C temperature range provided that the acentric factor of the hypothetic compound is neither less than 0.105 nor greater than 0.704. This method provides a more precise calculation of the vapour liquid equilibria of systems consisting of C_4 unsaturated hydrocarbons. The results will be published in a subsequent paper.

SYMBOLS USED

P	pressure atm.
R	gas constant
T	temperature (°K)
V	liquid molar volume (cm^3/g mole)
ν	activity coefficient
δ	solubility parameter $(cal/cm^3)^{1/2}$
λ	nonpolar solubility parameter $(cal/cm^3)^{1/2}$
τ	polar solubility parameter $(cal/cm^3)^{1/2}$
ω	acentric factor

REFERENCES

1. HILDEBRAND, J.H., SCOTT, R.L., Regular Solutions, Prentice-Hall Inc. (1962)

2. SHAIR, F.H., PRAUSNITZ, J.M., Am. Inst. Chem. Eng. J. 7, 682 (1961)

3. CHAO, K.C., SEADER, J.D., Am. Inst. Chem. Eng. J. 7, 598 (1961)

4. PRAUSNITZ, J.M., EDMISTER, W.C., CHAO, K.C., Am. Inst. Chem. Eng. J. 6, 212 (1960)

5. LEWIS, G.N., RANDALL, M., Thermodynamics, McGraw-Hill Book Co., New York, Appendix I. (1961)

6. LYCKMAN, E.W., ECKERT, C.A., PRAUSNITZ, J.M., Chem. Eng. Science 20, 703 (1965)

7. HILDEBRAND, J.H., SCOTT, R.L., Solubility of Non-Electrolytes, 3rd edition, Reinhold, New York, (1950)

8. BLANKS, R.F., PRAUSNITZ, J.M., Ind. Eng. Chem. Fundamentals 3, (2) 1 (1964)

9. WEIMER, R.F., PRAUSNITZ, J.M., Hydrocarbon Proc 44, (10) 237 (1965)

10. HELPINSTILL, J.G., VAN WINKLE, M., Ind. Eng. Chem. Proc Des/Dev. 7, 213 (1968)

11. NULL, H.R., PALMER, D.A., Chem. Eng. Progress 65, (10) 47 (1969)

12. MEISNER, J., Ind. Eng. Chem. Fundamentals 11, (1) 83 (1972)

13. Physical Constants of Hydrocarbons C_1 to C_{10}. ASTM Spec. Techn. Pub. No. 109A. (1963)

14. REID, R.C., SHERWOOD, Th.K., The Properties of Gases and Liquids. 2nd edition McGraw-Hill Book Co. New York (1966)

РЕЗЮМЕ

Автор составил соотношения, с помощью которых можно определить фактор ацентричности и критическое давление гомоморфа из жидкофазного молярного объема нормального углеводорода, при определенной температуре. Зная фактор ацентричности и критическое давление - с применением уравнения Лыкмана,Эккерта и Праусница - можно определить параметр растворимости гомоморфа, т.е. часть параметра растворимости ненасыщенного нормального углеводорода, обусловленную полярными влияниями.

Hungarian Journal
of Industrial Chemistry
Veszprém
Vol.1. pp. 351-364 (1973)

INVESTIGATIONS OF THE FLUID MECHANICS IN LIQUID-SPOUTED BED SYSTEMS

Mrs. E. MÉSZÁROS and T. BLICKLE

(Research Institute for Technical Chemistry of the Hungarian Academy of Sciences, Veszprém)

Received: October 31, 1972.

Fluid mechanics in spouted bed processes are dealt with. In an air-water model the pressure drop, the liquid content and the recirculation rate of the system are studied as a function of the gas flow rate and the design characteristics of the apparatus. In addition to the description of the experimental apparatus, test methods, and characteristic results are given. On the basis of the estimated data, the derivation of equations for the pressure drop, recycling rate and liquid fraction in the apparatus are aimed at. The numerous data show that the measured values agree well with the values calculated by the derived equations.

INTRODUCTION

Many kinds of the two-phase gas-liquid flow are known in practice. The flow of gas-liquid systems can be varied depending upon the direction of the flow, and the physical state of the gaseous phase, etc. In the present work, such a liquid-gas flow was investigated that was directed from the bottom to the top of a tube where the liquid is drawn in an inserted tube by a gas flowing with high velocity through a nozzle and where the relati-

vely small residence time of the two-phase flow can be set practically at any value by an internal liquid recirculation. In contrast to the two-phase flow in a tube, where the feed rates and the ratio of the phases are freely selected for both phases, in the studied liquid--spouted bed system the flow of the liquid phase was determined by the system itself, i.e. it depends upon the amount and velocity of the liquid drawn in, the geometrical circumstances and the gas velocity. From this important difference it follows that the relationships derived for the calculation of the flow characteristics of gas-liquid systems cannot be applied without the relationships for the liquid amount and the velocity of the liquid, even if they are also valid for the spouted bed system.

Several equations were derived on the basis of the main variables for the calculations of the characteristics of the two-phase flow [1, 2]. All of these have the inadequacy that they refer only to a certain type of flow, to gases of a given density, some liquid flow rate interval, and a given tube diameter, etc. There is no general relationship such as the coefficient of friction and Reynold's Number diagram which is so useful at the calculation of the single phase flow. Provided the flow processes and all the physical and geometric properties of the system are known, even the best correlations provide a pressure drop with an error of about 25 % and this problem is solved inadequately in the case of volume fractions.

EXPERIMENTAL APPARATUS AND MEASURING TECHNIQUE

The scheme of the apparatus built for the investigation of the fluid mechanics of liquid-spouted bed systems is shown in Fig. 1. The apparatus consists of two concentric cylinders (3, 4). The controlled amount of air (1) is introduced into the inner cylinder (3) through the nozzle (2). The gas flowing with high velocity

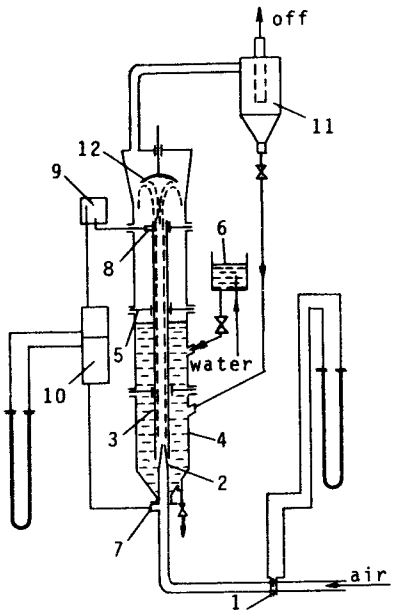

Fig. 1. Liquid-spouted bed. 1 - metering orifice; 2 - nozzle; 3 - inserted tube; 4 - column; 5 - clamping lever; 6 - water tank; 7-8 - pipe end; 9 - liquid separator; 10 - buffer vessel; 11 - cyclone; 12 - baffle plate

draws in the liquid from the space between the two cylinders and carries it away. The gas-liquid mixture proceeds through the inserted tube (3) in a certain type of flow and after bumping into the plate placed at the top of the apparatus (12) the liquid falls back into the space between the two cylinders. In the outer space of the apparatus the liquid moves downwards countercurrently to the flow in the inner cylinder and it once again enters the inner tube at the nozzle. The liquid droplets left in the gas are separated in a cyclone (11) and the gas is carried off into the air.

The pressure drop of the system can be measured as the pressure difference between the (7) and (8) pipe ends. This is the sum

of the pressure drops on the nozzle and on the inner cylinder and it is measured after the liquid separator (9) and damper vessels (10).

The liquid amount in the inserted tube was measured by the frequently applied intermittent method well known in literature. In the lower part of the inserted tube, above the nozzle, a lock was built in which allowed the free flow when open.The measurement consisted of the abrupt closure of the bottom of the system, the liquid collected above the lock was withdrawn and its volume was measured. The standard deviation of the parallel measurements was less than $\pm$ 3 %.

The outer cylinder of the apparatus was assembled from column elements, so the recycling rate of the liquid was measured by separating the column into two parts with a plate built in between two adjacent column elements, which had an opening in the middle, with a diameter corresponding to that of the inserted tube. The liquid collected above the plate was continuously withdrawn, while liquid was added in an amount that corresponded to that of the withdrawn liquid. It was not the volume of the withdrawn liquid that was measured - although some controlling measurements were also carried out in that manner - but the amount of the added water fed under the plate into the bottom of the column via a rotameter, needed to maintain a constant liquid level. Since the identity of the pressure at either side of the plate was ensured, the rotameter directly showed the recirculation rate.

THE EXPERIMENTAL CIRCUMSTANCES AND RESULTS

For the study of the fluid mechanics in liquid-spouted bed systems, the overall pressure drop of the system, the pressure drop of the empty apparatus, the liquid content of the inserted tube, and the liquid recycling rate were measured as a function of the gas velocity, the diameter and length of the inserted tube and

the diameter of the nozzle, in the air-water model system. The pressure drop of the empty apparatus can be measured as the pressure difference between the (7) and (8) pipe ends, provided that only air flows through the apparatus. During the measurements the volume of the water in the apparatus, and the diameter and length of the outer cylinder were constant (1.5 litres, 90 millimetres and 1.5 metres). The gas velocity was varied in such a way that it embraced the 0-90 metres per second interval.

The dimensions of the apparatus were selected for the experiments from the following values:

the length of the inserted tube (millimetres)	400; 600; 800; 1000;
the diameter of the inserted tube (millimetres)	10; 15; 24; 29;
the diameter of the nozzle (millimetres)	2; 4; 6; 8; 10; 12; 14; 16; 18; 20.

The relationships derived between the studied characteristics of flow and the variables will be summarized (the detailed experimental results were published in a Doctor Technicus thesis [3]):

The pressure drop of the empty apparatus increases in a quadratic manner with the increase of the gas velocity and decrease of the nozzle diameter, and is independent of the diameter and length of the inserted tube. The latter seemingly contradicts the accepted relations known in literature, but taking into account the pressure drop of the empty apparatus is the sum of the pressure drops established on the nozzle and on the inserted tube, and the latter is in general smaller by several orders of magnitude, then this contradiction is solved.

Between the overall pressure drop of the system and the independent variables, a relation similar to that of the empty apparatus was found; because of the appearance of the second phase the values of the pressure drop were naturally far greater.

The recirculation rate of the liquid transfer by the gas grows proportionally at the beginning, later it approaches a limit. The growth of the length and diameter of the nozzle decreases,

while the increase of the diameter of the inserted tube increases the recirculation rate.

The liquid content decreases and tends to zero when increasing the gas velocity, while an increase in the length of the inserted tube increases it. The decrease of the nozzle diameter and the increase of the diameter of the inserted tube increase the liquid content.

CALCULATION AND EVALUATION OF THE FLOW CHARACTERISTICS OF LIQUID-SPOUTED BED SYSTEMS

On the basis of the experimental results, efforts were made to attain the derivation of such relationships for the main flow characteristics (pressure drop, recirculation rate, and liquid fraction) that contain only the feed data and the data of the apparatus, and do not contain parameters that are difficult to measure, e.g. the liquid content.

To calculate the liquid fraction the adaptation of a relation previously derived in this Institute was tried. On the basis of the theory of dynamic foams, SASVÁRI [4] derived the following equation for the determination of the liquid fraction:

$$\varepsilon_f = \frac{k}{u_g + k} \tag{1}$$

The reciprocal of Equation (1) is:

$$\frac{1}{\varepsilon_f} = \frac{1}{k}(u_g + k) \tag{2}$$

It is obvious that there is a linear relationship between the reciprocal of the liquid fraction and the gas velocity (u_g). The value of k was determined from the following measured data.

The liquid fractions were calculated from the measured liquid contents by the following equation, derived on the basis of the definition of liquid fraction:

$$\varepsilon_f = \frac{4\,V}{H_B d_B^2 \pi} \tag{3}$$

According to the experimental results since the liquid content (V) not only depended upon the gas velocity, but also on the dimensions of the apparatus, the reciprocals of the liquid fractions were plotted against the gas velocity having these variables as parameters. Straight lines with nearly the same slopes were derived and this confirmed that the value of k is independent of the diameter of the nozzle (d_f) and of the diameter and lenth of the inserted tube (d_B and H_B). From the slope the value of k was found to be 1.7 and so the liquid fraction was calculated by the following equation:

$$\bar{\varepsilon}_f = \frac{1.7}{u_g + 1.7} \tag{4}$$

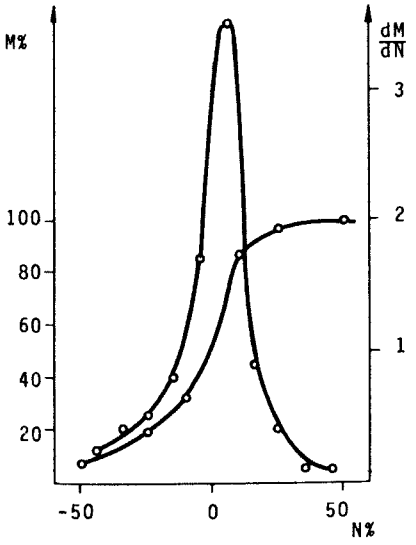

Figure 2. The distribution and frequency of the liquid fraction data

The comparison of the measured and calculated data showed that below a gas velocity of 4 - 5 metres per second the calculated values were invariably smaller than the measured ones. The difference decreased with the decrease of the length of the inserted tube. Above a gas velocity of 5 metres per second the agreement between the two values is good not only in foam, but also in film and mist flow. In Figure 2 the distribution and frequency curves of the differences between the measured liquid fraction values and those calculated by Equation (4) are

shown. It can be seen that the deviations have a nearly normal distribution and their absolute majority is within the ± 10 % deviation range.

At the calculation of the overall pressure drop of the system it was assumed that apart from the outer recirculation space the system can be regarded as a sieve plate column with only one opening on the plate for the distribution of the gas in the liquid. In the sieve plate column the pressure drop consists of the pressure drop on the dry plate, the hydrostatic pressure of the liquid on the plate and the dynamic pressure drop necessary to overcome the surface tension. This latter can be neglected since it is smaller than the others by an order of magnitude.

The overall pressure drop of the system (ΔP_t) was plotted against the sum of the pressure drop of the dry apparatus (Δp) and the hydrostatic pressure (ΔP_h). The hydrostatic pressure was calculated from the measured liquid content by the following equation:

$$\Delta P_h = \frac{4\ V}{d_B^2 \pi} \gamma_f \qquad (5)$$

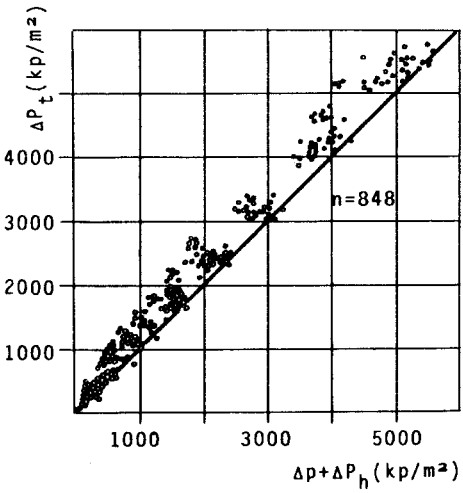

Figure 3

In Figure 3 it is shown that the sum of the pressure drop of the dry column and the hydrostatic pressure is some what less than the overall pressure drop of the system. The measured values are scattered around a straight line of the slope of 1.2.So the overall pressure drop can be calculated by the following Equation:

$$\Delta P_t = (\Delta p + \Delta P_h)\ 1.2 \qquad (6)$$

The pressure drop on the dry column depends upon the gas velocity and on the diameter of the nozzle. So it can be expressed as:

$$\Delta p = a_2 d_f^{a_1} u_{gf}^2 \tag{7}$$

where

d_f is the diameter of the nozzle (metres)

u_{gf} is the gas velocity in the nozzle (metres per second).

The constants were determined from following the measured data.

The pressure drop of the dry column was plotted against the square of the gas velocity in the nozzle, the diameter of the nozzle was the parameter. Straight lines were obtained:

$$\Delta p = a_3 u_{gf}^2 \tag{8}$$

$$a_3 = a_2 d_f^{a_1} \tag{9}$$

Which means that there is a linear relationship between the variables and a_3 can be determined from the slopes. The logarithm of the determined a_3 was plotted against the logarithm of the diameter of the nozzle and according to Equation (9) the intercept of the straight lines was a_1 and their slope gave a_2.

It was found that

$$a_2 = 0.00576$$

$$a_1 = -0.5$$

With these values Equation (7) becomes:

$$\Delta p = 0.00576\, d_f^{-0.5} u_{gf}^2 \tag{10}$$

The comparison of the pressure drops of the dry column calculated by Equation (10) and those measured showed a discrepancy less than ± 10 % in 70 % of the 1200 data.

The hydrostatic pressure drop was calculated on the basis of Equation (5):

$$\Delta P_h = \frac{4\ V}{d_B^2\ \pi} \gamma_f = \varepsilon_f H_B \gamma_f \qquad (11)$$

In Equation (11) the only unknown parameter is the liquid fraction, so it can be calculated. If Equations (4) is substituted into Equation (11) an equation is derived for the hydrostatic pressure drop:

$$\Delta P_h = \varepsilon_f H_B \gamma_f = \frac{k}{u_g + k} H_B \gamma_f = \frac{1.7}{u_g + 1.7} H_B \gamma_f \qquad (12)$$

The comparison of the values calculated by Equation (12) and those measured showed that their discrepancies were less than ±10% in about 50 % of the data. In real foam flows the calculated values were higher, in film-mist transition flows the values were lower than those measured, which means that the best fit was observed in film flows.

The substitution of the relationships for the pressure drop of the dry column and the hydrostatic pressure drop Equation (10) and (12) into Equation (6) gives an equation for the pressure drop of the spouted bed system:

$$\bar{\Delta}P_t = (0.00576\ d_f^{-0.5}\ u_{gf}^2 + \frac{1.7}{u_g + 1.7} H_B \gamma_f)\ 1.2 \qquad (13)$$

In Equation (13) the variables are the length of the inserted tube, and the gas velocity calculated on the diameters of the inserted tube and nozzle. This means that without the knowledge of the liquid feed rate the pressure drop can be calculated in advance. The comparison of the measured and calculated values showed discrepancies that were less than ±25 % in about 80 % of the data.

An equation was derived for the recycling rate (u_f) on the basis of the definition of the volumetric rate:

$$w_f = u_f \varepsilon_f A_t \cdot 3600 \qquad (14)$$

In Equation (14) the liquid fraction is known from Equation (4) so the unknown variable is the actual linear velocity of the

liquid (u_f) which can be calculated using the relation between the recirculation rate and the following measured parameters.

The linear velocity of the liquid can be calculated by Equation (15) from the measured liquid content and recirculation rate:

$$u_f = \frac{w_f}{A_t \varepsilon_f \cdot 3600} = \frac{w_f H_B}{V \cdot 3600} \tag{15}$$

The determined liquid velocity was plotted against the gas velocity having the data of the apparatus as parameters. Straight lines with different slopes and intercepts were obtained.

The equation of the line:

$$u_f = a_4 u_g + a_5 \tag{16}$$

If $u_f = 0$ then:

$$a_5 = - a_4 u_g^* \tag{17}$$

where u_g^* is the gas velocity where the liquid recycling starts.

The substitution into Equation (16) yields:

$$u_f = a_4 u_g - a_4 u_g^* = a_4 (u_g - u_g^*) \tag{18}$$

a_4 and u_g^* in Equation (18) depend upon the following parameters:

$$a_4 = f(H_B, d_B, d_f) \tag{19}$$

and

$$u_g^* = f(H_B, d_B) \tag{20}$$

The Equation (19) and (20) were solved with the following measured data.

u_g^* was plotted against the length of the inserted tube, at constant values of the diameter of the inserted tube. The relationship between the two variables is nearly linear, so the equations for the derived lines are:

If $d_B = 29$ mm; $u_g^* = 5.4(H_B - 0.24) = 5.4\ H_B - 1.3$ (21)

$d_B = 24\text{-}19$ mm; $u_g^* = 4(H_B - 0.25) = 4\ H_B - 1$ (22)

$d_B = 15\text{-}10$ mm; $u_g^* = 2.6(H_B - 0.18) = 2.6\ H_B - 0.5$ (23)

A relationship having both variables simultaneously could not be obtained for u_g^*.

The experimental data showed that a_4 is directly proportional to the length and diameter of the inserted tube and it is inversely proportional to the diameter of the nozzle. So the following equation was derived:

$$a_4 = a_6 \frac{d_B}{d_f} + a_7 \frac{H_B}{d_f} + a_8 \frac{r_h}{d_f} \tag{24}$$

a_6 can be obtained if the $a_4 d_f$ product is plotted against the diameter of the inserted tube with the length of the inserted tube as parameter. The slope of the parallel straight lines obtained gives a_6 and if the intercepts are plotted against the length of the inserted tube, straight lines are obtained once again, where the slope is a_7 and the intercept is a_8.

The following values were obtained for the constants:

$$a_6 = 0.054, \quad a_7 = -10^{-3}, \quad a_8 = 0.57 \times 10^{-3}.$$

With these constants Equation (24) yields:

$$\bar{a}_4 = 0.054 \frac{d_B}{d_f} - 10^{-3} \frac{H_B}{d_f} + 0.57 \times 10^{-3} \frac{r_h}{d_f} \tag{25}$$

Having $\bar{a}_4$ and $\bar{u}_g^*$ Equation (14) is solved on the basis of Equation (18):

$$\bar{u}_f = \bar{a}_4 (u_g - \bar{u}_g^*) \varepsilon_f A_t \cdot 3600 \tag{26}$$

where $\bar{u}_g^*$ can be calculated by Equations (21), (22) or (23) depending upon the diameter of the inserted tube, and $\bar{a}_4$ and ε_f by Equations (25) and (4).

The comparison of the experimental recycling rate and those calculated by Equation (26) showed that their discrepancies were less than ± 10 % in more than 50 % of the 900 data.

To briefly summarize the results, empirical equations (Equations 4, 13, 26) were derived for the calculation of the flow characteristics of the liquid-spouted bed systems (pressure drop, volume fraction and recycling rate) on the basis of nearly 1000-1000 experimental data, which sufficiently describe the system. In these equations, parameters that are easy to determine were employed (gas velocity, and design data), there are no variables that are difficult to measure.

SYMBOLS USED

A_t the cross section area of the inserted tube (m^2)
a_1 a_2 ... a_8 constants
a_2 (kg force.sec^2/m^5) a_3 (kg force.sec^2/m^4) a_5 (m/sec)
d_B the diameter of the inserted tube (m)
d_f the diameter of the nozzle (m)
H_B the length of the inserted tube (m)
k constant
M the distribution of the data in percentage
N the differences between the measured and calculated data in percentage
n the number of measurements
ΔP_h hydrostatic pressure drop (kg force/m^2)
ΔP_t the overall pressure drop of the liquid-spouted bed system (kg force/m^2)
ΔP the pressure drop of the dry column (kg force/m^2)
r_h hydraulic radius (m)
u_f actual liquid velocity (m/sec)
u_g gas velocity calculated on the cross section area of the inserted tube (m/sec)
u_{gf} gas velocity calculated on the cross section area of the nozzle (m/sec)
u_g^* minimum gas velocity needed for the start of the recirculation (m/sec)

V liquid content (m^3)
w_f volumetric liquid feed rate or recirculation rate (m^3/h)
γ_f liquid density (kg force/m^3)
ε liquid fraction
π 3.1415

Variables with a bar are calculated data; those without any bar are measured ones.

REFERENCES

1. SCOTT, W., "Properties of Cocurrent Gas-Liquid Flow" in Advances in Chemical Engineering, Vol. 4, 199-277. Academic Press. New York 1963.

2. HODOSSY, L., Magyar Kémikusok Lapja 1, 29 1968

3. MÉSZÁROS, Mrs. E., Doctor Technicus thesis, Veszprém, 1970.

4. SASVÁRI, Gy., Report on the Research carried out in 1968. MTA MÜKKI Veszprém-Budapest 1969.

РЕЗЮМЕ

Авторами изучаются гидродинамические условия гейзерового способа. Изучают падение давления, содержание жидкости и скорость циркуляции в зависимости от скорости газа и заданных конструктивных параметров. Авторы описывают экспериментальную установку, методы измерения, характерные экспериментальные данные и далее на основе экспериментальных данных пытаются составить уравнения для вычисления падения давления, скорости циркуляции и объемной доли жидкости. Применяя экспериментальные данные большого числа опытов авторы показывают совпадение измеренных данных с данными, вычисленными по составленным соотношениям.

Hungarian Journal
of Industrial Chemistry
Veszprém
Vol.1. pp. 365-378 (1973)

DETERMINATION OF THE VIRTUAL RATE CONSTANT OF A CATALYTIC ISOMERIZATION PROCESS

J. PÓR

(Research Institute for Technical Chemistry of the Hungarian Academy of Sciences, Veszprém)

Received: September 26, 1972.

In connection with catalytic reactions, it is the overall reaction rate that is defined in practice. However, the processes proceed through a number of steps and accordingly it is more preferable to consider each individual partial process. An equation has been derived for the determination of the virtual rate constant of the reaction occurring at the internal surface of the catalyst particles which also contains the figures of mass transfer (external and pore-diffusion). A possibility is hereby given to interact at the most advantageous point, in order to speed up the overall reaction. The overall reaction rate is, at best, equal to that of the surface reaction (if the diffusion hindrance is eliminated) and consequently the latter is preferably determined.

A mathematical estimation has also been derived for the determination of the mass transfer occurring in the boundary layer around the catalyst particles.

INTRODUCTION

Catalytic reactions occurring by the action of a porous catalyst proceed through a number of consecutive partial processes:

1. Diffusion of the reactants onto, and of the products away from the external surface of the catalyst (termed external diffusion).

2. Diffusion of reactants and products within the pores of the catalyst (termed pore diffusion).
3. Adsorption of reactants at the internal surface and desorption of products from the external surface of the catalyst.
4. Reaction at the internal surface of the catalyst.

The above-mentioned partial processes have been given a detailed analysis in the literature [1, 2].

The overall reaction rate is determined by one or more steps.

The reaction rate is defined in the literature - in accordance with industrial practice - by the following equation:

$$r_A = B \frac{dx_A}{dw} \tag{1}$$

It is apparent from Equation (1) that the overall reaction rate refers to the unit mass of the catalyst.

This approach undoubtedly very simple and accordingly it simplified the industrial application; however, it is burdened by a number of drawbacks:

- the effect of the individual partial processes upon the overall reaction rate is not taken into consideration;
- it is valid only for a given catalyst bed, and in the case of a change in any of the parameters of the catalyst bed, the results of the measurement are no longer valid;
- no information is provided on the temperature dependence of the reaction.

It seems more preferable to apply an approach in which the partial processes are, one by one, taken into consideration. By this way, it is possible to speed up the rate-determining step and thereby to modify the overall reaction rate in an advantageous direction. For this purpose it is, however, necessary to know the rate-determining step or steps.

From among the four partial processes described in the foregoing it is only the rate of the surface reaction which is in-

dependent of the geometric parameters of the catalyst bed and accordingly its determination seems to be of paramount importance. It is the rate of the surface reaction that determines the process, if the diffusion hindrance [3] has no role to play in the process. Adsorption cannot be separated from the surface reaction, and consequently an apparent rate constant is used,which also includes the rate constant of the adsorption process.

It can be mentioned as a further advantage of the approach that the empyrical formula of Arrhenius [4] holds for the surface reaction and consequently it is possible to calculate the rate constants of a whole temperature range, if the rate constants for two different temperatures have been determined.

The method is preferably demonstrated on a catalytic isomerization reaction, where a gaseous component is transformed into another similar one, without any change in mole numbers.

DESCRIPTION OF THE MODEL

Let us consider the following process:

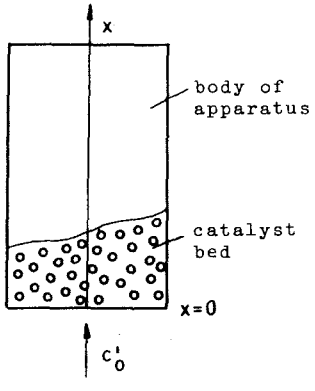

Fig. 1

The reactant c'(o) concentration enters the apparatus at a point x = 0. The molecules of the reactant diffuse into the interior of the catalyst particles, are transformed there and return into the streaming gas mixture of the apparatus, containing the reagent and the product gases.

The gas mixture continuously becomes poorer in the reagent component along the "X" height co-ordinate, and simultaneously the concentration of the product increases in the bulk of the gas.

The sum of the concentration of the product and the reagent is constant, and consequently it is sufficient to follow only the changes in the concentration of the reagent.

THE MATHEMATICAL MODEL

The mathematical model is given by the mass balances, as formulated for the unit volume of the interior of the particle or for the unit volume of the catalyst bed. A detailed description of these will be omitted for the sake of brevity. The following simplifications have been adopted in establishing the mathematical model:

1. The mathematical model holds only for a stationary state, when the concentration in a given cross section of the catalyst bed does not change in time.
2. The concentration of the gas in a given cross section is constant.
3. Radial diffusion in the gas is negligible compared to the convective stream.
4. The catalyst particles are spheres of equal radii and they contact each other only in a point-like manner.
5. The reaction within the pores is of the first order.
6. The process is isothermal.
7. The adsorption process is instantaneous, that is to say, its rate constant may be incorporated into the apparent rate constant of the surface reaction (in this case adsorption and surface reaction have been regarded a single partial process).
8. The particles are homogenous.
9. Any transformation on the outer surface of the particles is negligible. (The internal surface of the particles is larger by several orders of magnitude than the external spherical surface.)

With the above-described simplification in view, the system of differential equations describing the process can be written by means of the differential balance as formulated for the catalyst particle and for the gas.

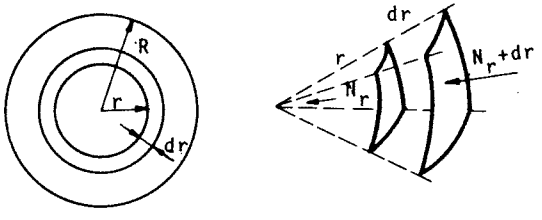

Fig. 2

Fig. 2 shows a section of a spherical catalyst particle, in which diffusion and reaction of the reagent takes place.

The material balance for a unit volume of the particle is the following:

$$4(r + dr)^2\pi\vartheta D \frac{\partial}{\partial r}\left[c(x,r) + \frac{\partial c(x,r)}{\partial r} dr\right] =$$

$$= 4\, r^2\pi\vartheta D \frac{\partial c(x,r)}{\partial r} + 4\, r^2\pi dr a k c(x,r) \qquad (2)$$

Equation (2), after simplifications and carrying out the operations, can be written in the following form:

$$\vartheta D\left[\frac{\partial^2 c(x,r)}{\partial r^2} + \frac{2}{r}\frac{\partial c(x,r)}{\partial r}\right] = a k c(x,r) \qquad (3)$$

After rearrangement:

$$\frac{\partial^2 c(x,r)}{\partial r^2} + \frac{2}{r}\frac{\partial c(x,r)}{\partial r} = \frac{ak}{D^*} c(x,r) \qquad (4)$$

where

$$D^* = \vartheta D \qquad (5)$$

The mass balance of the reacting gas is written for a unit volume of the catalyst bed.

The number of particles present in the unit volume: n [pieces/L^3] depends on the dimensions and order of the particles; this value is constant for the whole bed.

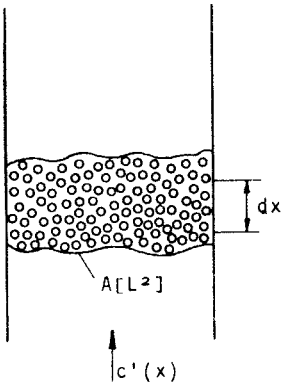

Fig. 3

$$v'A\varepsilon c'(x) = 4\ R^2\pi A dx n\vartheta D[\frac{\partial c(x,r)}{\partial r}]_{r=R} +$$

$$+ A\varepsilon v'[c'(x) + \frac{dc'(x)}{dx}\,dx] \qquad (6)$$

Equation (6) expresses that the decrease in concentration in the bulk of the gas is brought about by diffusion oriented against the surface of the particles.

Having carried out the operations and simplifications, Equation (6) becomes:

$$\frac{dc'}{dx} = -\,b\,[\frac{c(x,r)}{r}]_{r=R} \qquad (7)$$

where

$$b = \frac{4\ R^2\pi nD^*}{\varepsilon v'} \qquad (8)$$

is a factor including the geometrical parameters of the catalyst bed and the linear gas velocity.

Accordingly, the system of differential equations to be solved is the following:

$$\frac{\partial^2 c(x,r)}{\partial r^2} + \frac{2}{r}\frac{\partial c(x,r)}{\partial r} = \frac{ak}{D^*}\,c(x,r) \qquad (9)$$

$$\frac{dc'(x)}{dx} = -\,b\,[\frac{\partial c(x,r)}{\partial r}]_{r=R} \qquad (10)$$

Equations (8) and (9) are in connection through the value of the concentration gradient arising at the external surface of the catalyst particles.

Equation (2) is partial; but having a construction that it can directly be integrated with respect to "r".

The general solution is the following:

$$c(x,r) = \frac{1}{r} [A\ ch(\sqrt{\alpha}\ r) + B\ sh(\sqrt{\alpha}\ r)] \tag{11}$$

where

$$\alpha = \frac{ak}{D^*} \tag{12}$$

A and B are integration constants.

The values of A and B can be calculated by the boundary conditions written for a particle.The boundary conditions are written with reference ot the centre of the particles and to their external surface:

$$[\frac{\partial c(x,r)}{\partial r}]_{r=0} = 0 \tag{13}$$

However, condition (13) cannot be applied, since in the expression $\frac{\partial c}{\partial r}$, "r" is in the denominator and the expression is meaningless if r = 0 is substituted. Instead, the following may be written, as follows from the diffusion process [5]:

$$\lim_{r\to 0} r^2(\frac{\partial c}{\partial r}) = 0 \tag{14}$$

It is apparent that after multiplication by "r^2", the denominator does not contain "r".

The second condition is determined by the circumstances prevailing at the external surface of the particle.

It may be assumed that the concentration of the bulk of the gas is present at the orifice of the pores. (The value of the mass transfer coefficient, k_c, is assumed to be infinite.)

In this case,

$$c'(x) = c(x,R) \tag{15}$$

However, if $k_c \neq \infty$, the Newtonian boundary may be written:

$$D^*[\frac{\partial c(x,r)}{\partial r}]_{r=R} = k_c[c'(x) - c(x,R)] \tag{16}$$

In the case of $k_c = \infty$, Equation (16) becomes Equation (15). The selection of the boundary condition to be applied may be done on the basis of information given by the measurements described in [6]. In some cases, the following calculation may be applied instead of measurements:

k_c may be regarded as infinite, if its value is greater by two orders of magnitude than the value of $D^*[\frac{\partial c(x,r)}{\partial r}]_{r=R}$ that is to say

$$k_c >> D^*[\frac{\partial c(x,r)}{\partial r}]_{r=R} \tag{17}$$

Boundary condition (15) may be applied in this case.

The order of magnitude of the value of k_c can be estimated on the basis of [7] while that of D^* on the basis of [8].

No information whatever is available on the value of $[\frac{\partial c(x,r)}{\partial r}]_{r=R}$ but it can be proved that even the greatest concentration gradient developed along the axis of the catalyst bed is smaller than the concentration gradient of the particle of $c'(o)$ concentration calculated with the assumption $k_c = \infty$ and placed into an infinite environment. Accordingly, the gradient calculated on the basis of this assumption approximates the real value of $[\frac{\partial c(x,r)}{\partial r}]_{r=R}$ from above.

If this value is substituted into Equation (17) and the relation is true, it is also possible to calculate with the boundary condition (15) in the case of the really prevailing concentration gradient.

With application of boundary condition (14),

$$A = C \tag{18}$$

By application of boundary conditions (15) or (16) and Equation (11), the following equation is obtained for the change in concentration along the axis:

$$c'(x) = c'(0)\, e^{-\frac{b}{R}[R\sqrt{\alpha}\ \mathrm{cth}(\sqrt{\alpha}\ R) - 1]x} \tag{19}$$

and

$$c'(x) = c'(0)\, e^{-bk_c \frac{R\sqrt{\alpha}\ \mathrm{cth}(\sqrt{\alpha}\ R) - 1}{D^*[R\sqrt{\alpha}\ \mathrm{cth}(\sqrt{\alpha}\ R) - 1] + k_c R} x} \tag{20}$$

Equations (19) and (20) contain the value of the virtual rate constant, "k", in an implicit manner.

DETERMINATION OF THE APPARENT RATE CONSTANT "k"

Equations (19) and (20) describe the changes in the concentration of the bulk of the gas as a function of the height co-ordinate. The parameters used (geometrical data of the catalyst bed, diffusion coefficient and mass transfer coefficient of the external diffusion) are such that are either at our disposal or can easily be determined [7, 8].

If the concentration of the bulk of the gas, c'(x) is determined along the axis of the catalyst bed in a point of known co-ordinates (it is most preferable to choose the height of the catalyst bed and the concentration of the gas leaving the system), the value of "k" can be calculated with the following transcendent equation:

$$L = \sqrt{\alpha}\ \mathrm{cth}\ (\sqrt{\alpha}\ R) \tag{21}$$

where

$$L = \frac{v'\varepsilon[\ln c'(0) - \ln c'(x)]}{4\ R^2 \pi n\ D^* x} + \frac{1}{R} \tag{22}$$

if boundary condition (15) is applied, and

$$L = \frac{v'\varepsilon k_c [\ln c'(0) - \ln c'(x)]}{k_c \, 4 R^2 \pi n D^* x - D^* \varepsilon v' [\ln c'(0) - \ln c'(x)]} + \frac{1}{R} \qquad (23)$$

if boundary condition (16) is used in the calculations.

Equation (15) is solved for "α" and we have

$$ak = \alpha D^* \qquad (24)$$

Equation (24) gives the product of the virtual rate constant and the specific surface of the catalyst particle.

A similar consideration can also be applied for the case of non-spherical catalyst particles. The only difference is that the differential equations are not written in spherical co-ordinates, and the factor "b" in Equation (7), describing the geometrical paramaters, has to be modified.

Fig. 4 shows particles of cylinder and "flake" shape.

The differential equation for cylindrical particles is the following:

$$\frac{\partial^2 c(x,r)}{\partial r^2} + \frac{1}{r} \frac{\partial (x,r)}{\partial r} =$$

$$= \frac{ak}{D^*} c(x,r) \qquad (25)$$

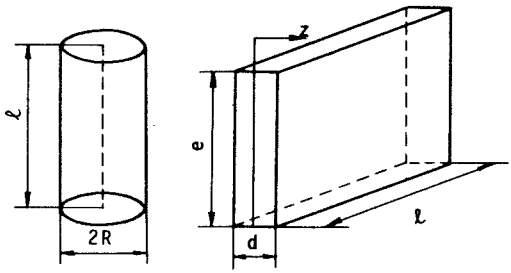

Fig. 4

whereas for "flake"-shaped particles it is:

$$\frac{\partial^2 c(x,z)}{\partial z^2} = \frac{ak}{D^*} c(x,z) \qquad (26)$$

In the case of cylinders, the mass balance of the bulk of the gas is the following:

$$\frac{dc'(x)}{dx} = - b_{cylinder} \left[\frac{\partial (x,r)}{\partial r}\right]_{r=R} \qquad (27)$$

where

$$b_{cylinder} = \frac{2\,R\pi\ell\,nD^*}{\varepsilon v'} \tag{28}$$

and in the case of "flakes"

$$\frac{\partial c'(x)}{\partial x} = -\,b_{flake}\left[\frac{\partial (x,z)}{\partial z}\right]_{z=\frac{d}{2}} \tag{29}$$

$$b_{flake} = \frac{2\,e\ell nD^*}{\varepsilon v'} \tag{30}$$

Mass transport - occurring only at the superficies of the cylinder and at the e.ℓ plate of the "flake" - was taken into consideration when deriving the equations. This omission causes the values of "b" to be taken into account at a value lower than the real one. On the other hand, when describing the model it was assumed that the particles touch in one point only, that is to say, touching of the particles does not decrease the surface area available for diffusion. The errors arising on account of these two omissions influence the value of "b" in an opposite sense, and consequently it is not likely that it causes any considerable deviation in the calculated values.

SUMMARY

The virtual rate constant of catalytic isomerization was determined, with certain suppositions and with the application of the geometric properties of the particles.

In cases where the influence of the external diffusion resistance and that of pore diffusion does not manifest itself, the rate of the surface reaction is equal to the overall reaction rate.

The rates of external diffusion and pore diffusion were also taken into account, and consequently it is possible to select the

rate-determining process. A possibility is given hereby to interact at the most advantageous point in order to attain a more favourable overall reaction rate.

The empyrical formula of Arrhenius holds for the virtual rate constant calculated in accordance with the above, and consequently it is possible to determine the temperature dependence of the reaction from two measurements.

SYMBOLS USED

a	specific surface of catalyst particle, L^{-1}
$c(x,r)$	concentration in the interior of the particle, mole/mole
$c'(x)$	concentration in the bulk of the gas, mole/mole
k	virtual rate constant of the surface reaction, t^{-1}
k_c	mass transfer coefficient of the external diffusion, mole/L^2t
n	number of particles present in the unit volume of the catalyst bed, L^{-3}
r	radial co-ordinate, L
r_A	overall reaction rate, mole/Mt
v'	linear gas velocity, L/t
w	mass of catalyst, M
z	linear co-ordinate in case of "flake"-type particle, L
x	height co-ordinate, L
x_A	conversion, mole/mole
B	feeding rate, mole/t
$D^*=\vartheta D$	effective diffusion coefficient, L^2/t
R	radius of catalyst particles, L

ε free surface fraction of catalyst bed, L^2/L^2

ϑ porosity, L^3/L^3

In the signs, the internationally accepted dimension symbols were used:

L length

M mass

t time

REFERENCES

1. PERRY, J.H., Vegyészmérnökök kézikönyve (Chemical Engineers' Handbook). p. 460., Müszaki Könyvkiadó, 1968.

2. SZABÓ, Z., Kontakt katalizis (Contact Catalysis) p. 391., Akadémiai Könyvkiadó, 1966.

3. SZABÓ, Z., Kontakt katalizis (Contact Catalysis) p. 402., Akadémiai Könyvkiadó, 1966.

4. ERDEY-GRUZ, T., A fizikai kémia alapjai (Fundamentals of Physical Chemistry), Müszaki Könyvkiadó, 1958.

5. TŐRÖS, R., Fülöp, J., A vegyipari müveletek elméletéhez (On the Theory of Chemical Engineering Unit Operations) MTA MÜKKI, 1970.

6. PERRY, J.H., Vegyészmérnökök kézikönyve (Chemical Engineers' Handbook) p. 461., Müszaki Könyvkiadó, 1968.

7. YOSHIDA, F., HOUGEN, O.A., A.I.Ch.E. Journal 8., 5-11 (1962).

8. SZABÓ, Z., Kontakt katalizis (Contact Catalysis) pp. 402-404, Akadémiai Könyvkiadó, 1966.

9. NORMAN, W.S., Absorption, Distillation and Cooling Towers, Longmans, 1961.

10. DENBIGH, K.G., TURNER, J.C.R., Kémiai reaktorok (Chemical Reactors), Müszaki Könyvkiadó, 1971.

РЕЗЮМЕ

При контактных каталитических реакций на практике определяется валовая скорость реакции. Имея в виду то, что процесс происходит в нескольких ступенях, оказывается целесообразным отдельно учитывать частичные процессы. Выведена формула для определения константа виртуальной скорости реакции, происходящей на поверхности гранул катализатора, содержащего характерные данные массопередачи поровой диффузии. Таким образом, дается возможность вмешиваться с целью ускорения валового процесса на самом подходящем месте. Определение скорости поверхностной реакции является целесообразным, ведь скорость валовой реакции и в оптимальном случае (при прекращении диффузионного торможения) может достигать значения последней.

Автором была выведена расценка для определения массопередачи происходящей в граничной пленке вокруг гранул катализатора.

Hungarian Journal
of Industrial Chemistry
Veszprém
Vol.1. pp. 379-400 (1973)

MATHEMATICAL MODELLING OF ABSORPTION COLUMNS II.

PARAMETER SENSITIVITY AND METHODS FOR ITS CALCULATION

P. ÁRVA and F. SZEIFERT

(Department of Chemical Process Engineering,
Veszprém University of Chemical Engineering)

Received: December 7, 1972.

The idea "parameter sensitivity" is defined for various operational units and the models enabling their calculation have been described. The Piston Flow Model (P.F. Model), suitable for the description of two-phase countercurrent operational units has two dimensionless parameters, whereas the Axial Dispersed Plug Flow Model (A.D.P.F. Model) has four. In the case of both models, the number of physical quantities and figures characteristic of the working state included in these dimensionless parameters is very large.

This paper deals with the analytical solution used for the calculation of the sensitivities.

The theoretical connections are supplemented by a number of numerical examples, calculated by both analog and digital computers, presenting an illustration of the practical application of parameter sensitivity.

In the first paper [1] of this series, the mathematical modelling of a packed absorption column was described. An experimental method was presented for the determination of the absorbed component in both of the phases, along the packed column. The experimental results were processed on the basis of the P.F. Model and the A.D.P.F. Model. The mathematical models describe the modelled reality only with a limited accuracy. The inaccuracy of the

models is brought about by two causes. Firstly, they can give only a phenomenological description of reality. The complicated connections and phenomena of a real system are attributed by the model to the collective influence of only two or three factors. For example, in a packed absorption column, the individual elements of the streaming liquid phase may move in any direction of space with a different and variable velocity. In the P.F. Model, this complicated flow pattern is ignored and the process is characterized by mean values. The A.D.P.F. Model characterizes the flow occurring in the real system by two parameters: the mean flow rate and the mixing coefficient. Accordingly, in both cases a schematic pattern is forced upon the reality.

The second reason for the inaccuracy of the parameters is the method of determination. The parameters of the models, such as rate, mixing coefficient, and transfer coefficient, etc., cannot be calculated, but the results of experiments carried out with a real apparatus are processed on the basis of the chosen model. The source of errors is, on the one hand, experimental errors, and, on the other, the errors of the calculation method.

It is our aim in the mathematical description of the operational units to present a description which is,for a given purpose, of adequate accuracy, and as simple as possible. Generally much experimental and calculation work is necessary to produce models which approximate the reality. It is not justified to carry this out if a simpler description also offers satisfactory accuracy. In the solution of such tasks, the knowledge of the parameter sensitivity of the model comes very useful.

The mathematical description of two-phase operational units is often possible by models of the same type, the only difference being the values of the parameters. This paper deals with the generally used P.F. and A.D.P.F. Models.

Studies on the sensitivity of operational units against changes in the parameters proved to be very useful in reactor technique. However, in the field of diffusion operations in chemical engineering there are practically no papers that deal with this problem.

Both for the researcher and the practical worker in the field, the knowledge of how far a change in some property of the apparatus or in the technological parameters may change, the operation of the apparatus is of real practical importance. Such and similar questions may be answered if the parameter sensitivity is known.

The problem of parameter sensitivity is also encountered in the solution of models describing the operational units. This knowledge may also be helpful in choosing the means and methods of calculation.

In the case of all models used in connection with the calculation of operational units, the dependent variables are in all phases the concentration and temperature of the component, and the independent variable is, when a stationary state is examined, the place co-ordinate. In addition to these, a number of parameters, such as e.g. the rate of the phases, transfer coefficients, retention, mixing coefficients, and the concentration of the components along the edges, etc., are applied in the models. This connection is expressed for the variable x_j by the function x_j (z, p_1, p_2, $p_i \cdots p_n$). In the case of a given set of parameter values (p_1, p_2 $\cdots$ p_n) the sensitivity with respect to the parameter p_i can be defined by the following equation:

$$e_{j,i}\ (z,\ p_1,\ p_2\ \cdots\ p_n) = \frac{\partial x_j(z,\ p_1,\ p_2\ \cdots\ p_n)}{\partial p_i} \qquad (1)$$

where x_j is one of the dependent variables and p_i is the parameter with respect to which the sensitivity is examined. Often it is preferable to express this sensitivity in a dimensionless form:

$$E_{j,i} = \frac{p_i}{x_j(z,p_1,p_2,\cdots p_n)}\, e_{j,i} \qquad (2)$$

This paper describes the calculation methods serving the determination of parameter sensitivity on the basis of the most frequently used models.

1. The Sensitivity of the P.F. Model

Two-phase operational units are very frequently described by the following model (cf. Equations (4) and (5) in [1], if A = 1):

$$\frac{dx}{dz} + \frac{\beta\omega Z}{v_L}(y - x) = 0 \tag{3}$$

$$\frac{dy}{dz} + \frac{\beta\omega ZH}{v_G}(y - x) = 0 \tag{4}$$

where

$$x = \frac{c_L}{Hc_{G,in}}; \qquad y = \frac{c_G}{c_{G,in}}$$

The boundary conditions pertaining to the model are the following:

$$y(0) = 1 \tag{5}$$

$$x(1) = x_{in} \tag{6}$$

The model has two dimensionless parameters:

$$St_L = \frac{\beta\omega Z}{v_L} \qquad \text{and} \qquad St_G = \frac{\beta\omega ZH}{v_G}$$

The sensitivity of the model with respect to these two parameters will now be examined.

The following designations for the sensitivity are introduced:

$$e_{11} = \frac{\partial x}{\partial St_L}; \quad e_{21} = \frac{\partial y}{\partial St_L}; \quad e_{12} = \frac{\partial x}{\partial St_G}; \quad e_{22} = \frac{\partial y}{\partial St_G}$$

The functions $x(z)$ and $y(z)$ are obtained at given parameter values, by the solution of Equations (3) and (4) as well as condition Equations (5) and (6).

Let Equations (3), (4), (5) and (6) be differentiated with respect to St_L. In this case, the set of equations expressing the sensitivity with respect to St_L is obtained:

$$\frac{\partial^2 x}{\partial St_L \partial z} + St_L\left(\frac{\partial y}{\partial St_L} - \frac{\partial x}{\partial St_L}\right) + (y - x) = 0 \qquad (7)$$

$$\frac{\partial^2 y}{\partial St_L \partial z} + St_G\left(\frac{\partial y}{\partial St_L} - \frac{\partial x}{\partial St_L}\right) + \frac{\partial St_G}{\partial St_L}(y - x) = 0 \qquad (8)$$

The boundary conditions for this set of differential equations can be derived from Equations (5) and (6). The values y(0) and x(1), i.e. the concentration at which the phases enter the apparatus, are independent of the Stanton figures, and consequently the boundary condition can also be written in the following form:

$$\left.\frac{\partial y}{\partial St_L}\right|_{z=0} = 0 \qquad (9)$$

$$\left.\frac{\partial x}{\partial St_L}\right|_{z=1} = 0 \qquad (10)$$

With application of the signs introduced for the designation of the sensitivity, we may write:

$$\frac{\partial e_{11}}{\partial z} + St_L(e_{21} - e_{11}) + (y - x) = 0 \qquad (11)$$

$$\frac{\partial e_{21}}{\partial z} + St_G(e_{21} - e_{11}) + \frac{\partial St_G}{\partial St_L}(y - x) = 0 \qquad (12)$$

$$e_{21}(0) = 0 \qquad (13)$$

$$e_{11}(1) = 0 \qquad (14)$$

In a similar manner, the following set of differential equations is obtained for the sensitivity with respect to St_G:

$$\frac{\partial e_{12}}{\partial z} + St_L(e_{22} - e_{12}) + \frac{\partial St_L}{\partial St_G}(y - x) = 0 \qquad (15)$$

$$\frac{\partial e_{22}}{\partial z} + St_G(e_{22} - e_{12}) + (y - x) = 0 \qquad (16)$$

$$e_{22}(0) = 0 \qquad (17)$$

$$e_{12}(1) = 0 \qquad (18)$$

The values of the functions $x(z)$, $y(z)$, $e_{11}(z)$, $e_{12}(z)$, $e_{21}(z)$ and $e_{22}(z)$ are obtained from the solution of the set of Differential Equations (3) ... (18), at a given set of parameter values.

Functions $x(z)$ and $y(z)$ can be produced without solving the sensitivity equations. The sensitivities can be obtained without any difficulty if the functions $x(z)$ and $y(z)$ are known in an analytical way by solving the sets of differential equations or by derivating $x(z)$ and $y(z)$. For example, the following equation was obtained for the sensitivity of the concentration y with respect to St_L:

$$e_{21} = [1 - x(1)]\{[1 - \frac{\partial St_G}{\partial St_L} + \frac{1}{St_L} - \frac{1}{St_G}\frac{\partial St_G}{\partial St_L}]\exp(St_L - St_G) \times$$

$$\times[\exp[(St_L - St_G)z] - 1] + \frac{(1 - \frac{\partial St_G}{\partial St_L})\, z \exp[(St_L - St_G)z]}{\frac{St_G}{St_L} - \exp(St_L - St_G)}\} \frac{St_G}{St_L} \qquad (19)$$

It is apparent from the above equation that the sensitivity is a function of the place co-ordinate z and different sensitivity values are obtained at different sets of parameter values.

It has been supposed in the foregoing [cf. Equations (3) and (4)] that the component equilibrium among the phases can be described by a straight line starting from the origo. Equilibrium conditions different from this pattern are often encountered in practice, and consequently the analytical solution of the above sets of differential equations is difficult. Furthermore, the claim for rapid calculations makes it preferable to carry out such a mass of calculations by a computer. In the following, an analog

computer programme is shown for the calculation of the sensitivity. The analog computer enables the calculations to be carried out even in the case of nonlinear sets of equations. The linear case will be discussed here.

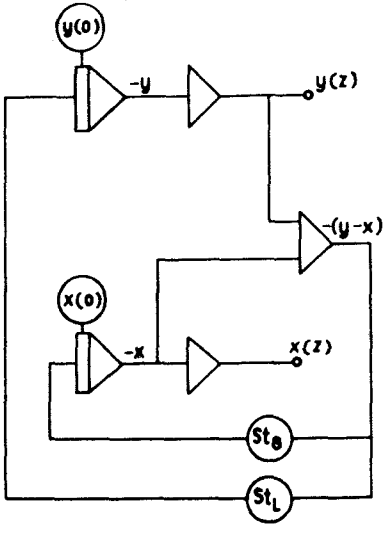

Fig.1. Programme for the solution of Differential Equations (3) and (4)

The analog computer program for the solution of differential Equations (3) and (4) is shown in Fig. 1. The conditional equations are such that only the initial value $y(0) = 1$ is known, but $x(0)$ is unknown, an iterative solution has to be chosen. In the course of this, the initial value fed to the integrator calculating the function is varied until the condition $x(1) = 0$ prescribed for the place $z=1$ is fulfilled. This procedure can, with some practice, be carried out rapidly. It should be noted here that there exists a method for the automation of the iteration.

Having determined the functions x and y, the sensitivity values can - after a similar iteration procedure - be determined with the help of the programme shown in Fig. 2.

Figs. 3 and 4 show the results of the calculations. The values of the functions x, y, e_{11}, e_{21}, e_{12}, and e_{22} are shown in both Figures. As it is apparent from Equations (11), (12), (15) and (16), the differential quotient of the St numbers with respect to each other also appears.

When calculating this differential quotient, different results will be obtained, depending on whether the change in the St number is due to the transfer coefficient ($\beta\omega$) or to the rate of the phase (v_L or v_G).

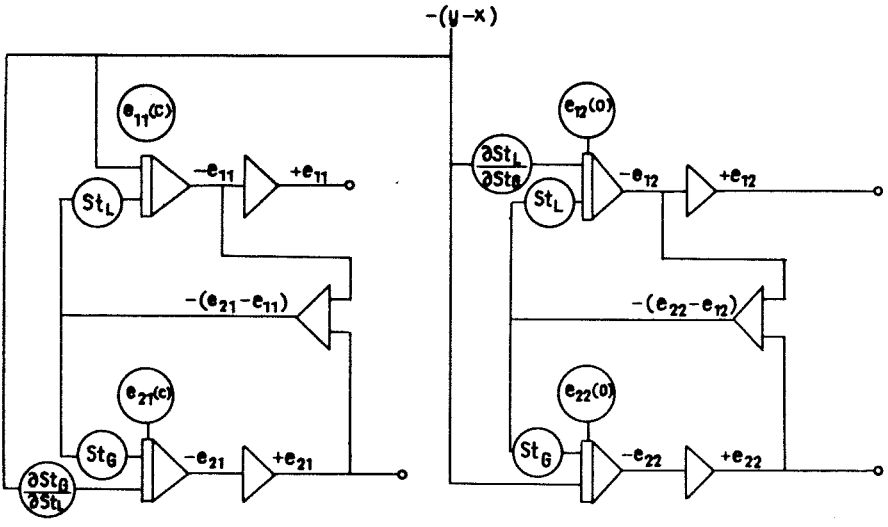

Fig. 2. Programme for the solution of Equations (11), (12), (15) and (16)

Since

$$\frac{\partial St_L}{\partial St_G} = \frac{\partial(\frac{\beta\omega Z}{v_L})}{\partial(\frac{\beta\omega ZH}{v_G})} \tag{20}$$

if $\beta\omega$ changes, but v_L and v_G are constant:

$$\frac{\partial St_L}{\partial St_G} = \frac{v_G}{v_L H} \tag{21}$$

if $\beta\omega$ is constant, we have

$$\frac{\partial St_L}{\partial St_G} = 0 \tag{22}$$

The sensitivity curves for a given system (St_L = 3.48; St_G = = 2.32) and for a case when the parameters St_L and St_G change on

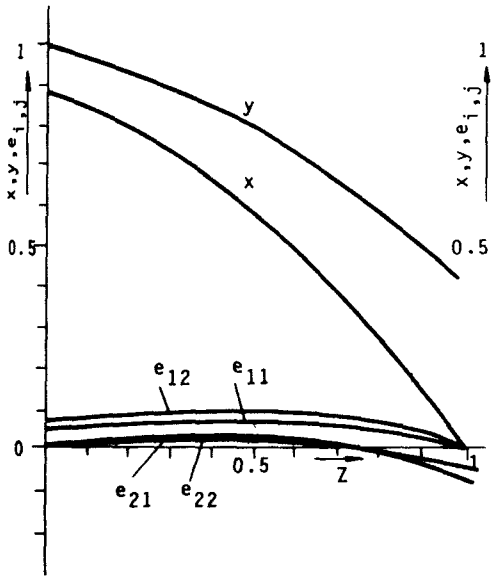

Fig.3. Sensitivity of the variables x and y with respect to St_L and St_G, if the value of $\beta\omega$ is varied (St_L = 3.48, St_G = 2.32)

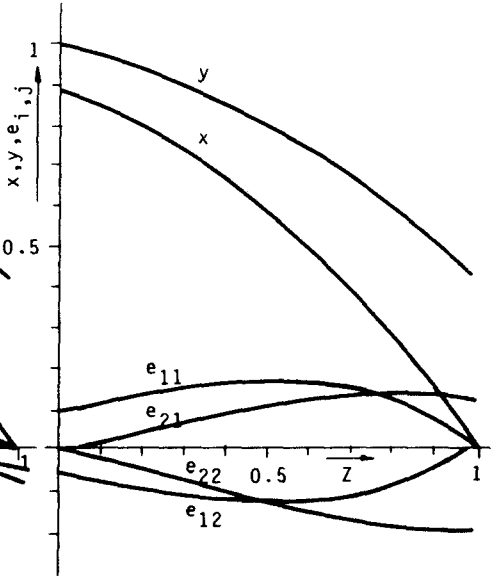

Fig.4. Sensitivity of the variables x and y with respect to St_L and St_G, if v_L or v_G is varied (St_L = 3.48, St_G = 2.32)

account of a change in the transfer coefficient, are shown in Fig. 3. Fig. 4 shows curves that are the result of changes in v_L and v_G. It is apparent from the Figures that the sensitivity curves possess an extreme value. The position of the latter depends on the ratio St_L/St_G. If the ratio $St_L/St_G > 1$, the extreme value at a high z value, whereas it is found at a low z value if $St_L/St_G < 1$.

2. Sensitivity of the A.D.P.F. Model

This model is frequently applied for the description of co-current or counter-current two-phase operational units. The ana-

lytical method of the determination of the parameter sensitivity will be presented here. The model will be described in general for a system in which the equilibrium function is a linear one, but the straight line does not necessarily start from the origo.

The diffusion model may be described in the general form with dimensionless quantities by the following Equation [1]:

$$a_1 \frac{d^2x}{dz^2} + \frac{dx}{dz} + a_2(a_5y + a_6 - x) = 0 \tag{23}$$

$$a_3 \frac{d^2y}{dz^2} - \frac{dy}{dz} - a_4(a_5y + a_6 - x) = 0 \tag{24}$$

Boundary conditions:

$$z = 0, \quad a_3 \frac{dy}{dz} - y + 1 = 0 \tag{25}$$

$$\frac{dx}{dz} = 0 \tag{26}$$

$$z = 1, \quad a_1 \frac{dx}{dz} + x - a_7 = 0 \tag{27}$$

$$\frac{dy}{dz} = 0 \tag{28}$$

Parameters a_1 ... a_7 are present in the differential equation and the boundary conditions. Parameters a_8 and a_9 mean the initial values of the functions x and y and are interesting from the point of view of the calculation.

The set of differential equations pertaining to the sensitivity and the conditional equations may be obtained by the derivation of Equations (24) ... (29). Accordingly, the expression of the sensitivity with respect to parameter a_i (i = 1, 2 ... 9) is the following:

$$a_1 \frac{d^2e_{1,i}}{dz^2} - \frac{de_{1,i}}{dz} + a_2(a_5e_{2,i} - e_{1,i}) + b_1 \frac{d^2x}{dz^2} + b_7y - b_2x + b_8 = 0 \tag{29}$$

$$a_3 \frac{d^2e_{2,i}}{dz^2} - \frac{de_{2,i}}{dz} - a_4(a_5e_{2,i} - e_{1,i}) + b_3 \frac{d^2y}{dz^2} - b_9y + b_4x - b_{10} = 0 \tag{30}$$

The boundary condition of the set of differential equations is the following:

Condition A (i = 1, 2 ... 7):

if z = 0, we have $a_3 \frac{de_{2,i}}{dz} - e_{2,i} + b_3 \frac{dy}{dz} = 0$

and $\frac{de_{1,i}}{dz} = 0$ (31)

if z = 1, we have $a_1 \frac{de_{1,i}}{dz} + e_{1,i} + b_1 \frac{dx}{dz} - f_o = 0$

and $\frac{de_{2,i}}{dz} = 0$ (32)

Condition B (i = 8, 9):

if z = 0, we have $e_{1,i} = f_1$

$e_{2,i} = f_2$

$\frac{de_{1,i}}{dz} = 0$ (33)

and

$\frac{de_{2,i}}{dz} = f_4$

where: $e_{1,i} = \frac{\partial x}{\partial a_i}$; $e_{2,i} = \frac{\partial y}{\partial a_i}$

The meaning of the quantities a_i, b_i and f_i is apparent from Table 1.

Equations (23) ... (33) together represent the A.D.P.F. Model of the parameter sensitivity with the initial and boundary conditions. The part pertaining to x and y can be separated within the model and the solution can be written in the following form:

$$x = \sum_{i=1}^{4} c_i \exp(\lambda_i z) \tag{34}$$

$$y = \frac{1}{a_5} \sum_{i=1}^{4} (1 - \frac{\lambda_i}{a_2} - \frac{a_1}{a_2} \lambda_i^2) c_i \exp(\lambda_i z) - \frac{a_6}{a_5}$$

where λ_i represents the four solutions of the equation

Table 1. Parameter Sensitivity of the A.D.P.F. Model (Symbols)

$a_1 = 1/Pe_L$; $a_2 = St_L$; $a_3 = 1/Pe_G$; $a_4 = St_G$; $a_5 = A$; $St_L = \frac{\beta\omega Z}{v_L}$

$a_6 = x_o^*$; $a_7 = x_{in}$; $St_G = \frac{\beta\omega Z}{v_G}\frac{H}{A}$; $a_8 = x(o)$; $a_9 = y(o)$

Parameters / b_i and f_i	$E_L H_L$	$E_G H_G$	$(\beta\omega)$	v_L	v_G	Z	x_{in}	$x(o)$	$y(o)$
	a_1	a_3	a_2	a_2	a_4	a_2	a_7	a_8	a_9
$b_1 = \frac{\partial a_1}{\partial a_i}$	1	0	0	$\frac{a_1}{a_2}$	0	$-\frac{a_1}{a_2}$	0	0	0
$b_2 = \frac{\partial a_2}{\partial a_i}$	0	0	1	1	0	1	0	0	0
$b_3 = \frac{\partial a_3}{\partial a_i}$	0	1	0	0	$\frac{a_3}{a_4}$	$-\frac{a_3}{a_2}$	0	0	0
$b_4 = \frac{\partial a_4}{\partial a_i}$	0	0	$\frac{a_4}{a_2}$	0	1	$\frac{a_4}{a_2}$	0	0	0
$b_7 = \frac{\partial a_2 a_5}{\partial a_i}$	0	0	a_5	a_5	0	a_5	0	0	0
$b_8 = \frac{\partial a_2 a_6}{\partial a_i}$	0	0	a_6	a_6	0	a_6	0	0	0

$b_9 = \frac{\partial a_4 a_5}{\partial a_i}$	0	0	$\frac{a_4 a_5}{a_2}$	0	a_5	$\frac{a_4 a_5}{a_2}$	0	0	0
$b_{10} = \frac{\partial a_4 a_6}{\partial a_i}$	0	0	$\frac{a_4 a_6}{a_2}$	0	a_6	$\frac{a_4 a_6}{a_2}$	0	0	0
$f_0 = \frac{\partial a_7}{\partial a_i}$	0	0	0	0	0	0	0	0	0
$f_1 = \frac{\partial a_8}{\partial a_i}$	-	-	-	-	-	-	-	1	0
$f_2 = \frac{\partial a_9}{\partial a_i}$	-	-	-	-	-	-	-	1	0
$f_3 = \frac{1}{a_3}(f_2 - b_3 \frac{da_9}{dz})$	-	-	-	-	-	-	-	0	$\frac{1}{a_3}$

$$a_1a_3\lambda^4 + (a_3 - a_1)\lambda^3 - (a_1a_4a_5 + a_2a_3 + 1)\lambda^2 + (a_2 - a_4a_5)\lambda = 0 \tag{35}$$

of the fourth degree, and c_i represents the solutions of the linear set of equations with four unknowns

$$\begin{vmatrix} a_{11} & a_{12} & a_{13} & a_{14} \\ a_{21} & a_{22} & a_{23} & a_{24} \\ a_{31} & a_{32} & a_{33} & a_{34} \\ a_{41} & a_{42} & a_{43} & a_{44} \end{vmatrix} \begin{vmatrix} c_1 \\ c_2 \\ c_3 \\ c_4 \end{vmatrix} = \begin{vmatrix} b_1' \\ b_2' \\ b_3' \\ b_4' \end{vmatrix} \tag{36}$$

The elements of the matrices are the following:

$$\begin{aligned} a_{1i} &= (1 + a_1\lambda_i)\exp\lambda_i \\ a_{2i} &= (1 - a_3\lambda_i)(1 - \frac{1}{a_2}\lambda_i - \frac{a_1}{a_2}\lambda_i^2) \\ a_{3i} &= \lambda_i \\ a_{4i} &= \lambda_i(1 - \frac{1}{a_2}\lambda_i - \frac{a_1}{a_2}\lambda_i^2)\exp\lambda_i \end{aligned} \tag{37}$$

and

$$b_1' = a_7, \quad b_2' = 1, \quad b_3' = 0, \quad b_4' = 0.$$

When $x(z)$ and $y(z)$ are known, the sensitivity model is an inhomogenous differential equation of the fourth degree with constant coefficients. The coefficients of the argumentum of the exponential terms causing the inhomogenous part are identical to the roots of the characteristic equation of the homogenous equation, and consequently the functions $e_{1,i}(z)$ and $e_{2,i}(z)$ take the following form:

$$e_{1,i}(z) = \sum_{i=1}^{4} (K_i + Q_iz)\exp(\lambda_iz) \tag{38}$$

$$e_{2,i}(z) = \frac{1}{a_5}\sum_{i=1}^{4}(1 - \frac{1}{a_2}\lambda_i - \frac{a_1}{a_2}\lambda_i^2)(K_i - L_i + Q_iz)\exp(\lambda_iz) - \frac{b_8 - b_7\frac{a_6}{a_5}}{a_2a_5} \tag{39}$$

Expressions K_i, L_i and Q_i of the equations can be obtained in the following way:

$$L_i = \frac{[b_1\lambda_i^2 + \frac{b_7}{a_5}(1 - \frac{1}{a_2}\lambda_i - \frac{a_1}{a_2}\lambda_i^2) - b_2]c_i + (1 + 2a_1\lambda_i)Q_i}{a_2 - \lambda_i - a_1\lambda_i^2}$$

$$i = 1, 2, 3, 4$$

$$Q_i = c_i\,[\frac{(a_4a_5 - a_3\lambda_i^2 + \lambda_i)[b_1\lambda_i^2 + \frac{b_7}{a_5}(1 - \frac{1}{a_2}\lambda_i - \frac{a_1}{a_2}\lambda_i^2) - b_2]}{3a_1a_3\lambda_i^3 + 2(a_3 - a_1)\lambda_i^2 - (a_2a_3 + a_1a_4a_5 + 1)\lambda_i} +$$

$$+ \frac{a_2a_5[(\frac{b_3}{a_5}\lambda_i^2 - \frac{b_9}{a_5})(1 - \frac{1}{a_2}\lambda_i - \frac{a_1}{a_2}\lambda_i^2) + b_4]}{3a_1a_3\lambda_i^3 + 2(a_3 - a_1)\lambda_i^2 - (a_2a_3 + a_1a_4a_5 + 1)\lambda_i}], \quad i = 1, 2, 3$$

$$Q_4 = \frac{[a_4(b_7 - b_2a_5) + a_2(b_4a_5 - b_9)]c_4 + a_4(a_5b_8 - a_6b_7) + a_2(a_6b_9 + a_5b_{10})}{a_2 - a_4a_5}$$

The values of K_i are given by a set of equations similar to Equation (36), in which the elements of the matrices are the following:

Condition A:

a_{ji} is the same as in Equation (37)

$$b_1' = f_o - \sum_{i=1}^{4}\{[1 + a_1(1 + \lambda_i)]Q_i + b_1\lambda_ic_i\}\exp\lambda_i$$

$$b_2' = \frac{a_5b_8 - a_6b_7}{a_2a_5} + \sum_{i=1}^{4}\{(1 - \frac{1}{a_2}\lambda_i - \frac{a_1}{a_2}\lambda_i^2)[L_i(1 - a_3\lambda_i) + b_3\lambda_ic_i + a_3Q_i]\}$$

$$b_3' = -\sum_{i=1}^{n} Q_i$$

$$b_4' = \sum_{i=1}^{4}(1 - \frac{1}{a_2}\lambda_i - \frac{a_1}{a_2}\lambda_i^2)[\lambda_iL_i - (\lambda_i + 1)Q_i]\exp\lambda_i$$

Condition B:

$$a_{1i} = 1$$

$$a_{2i} = (1 - \frac{1}{a_2}\lambda_i - \frac{a_1}{a_2}\lambda_i^2$$

$$a_{3i} = \lambda_i$$

$$a_{4i} = (1 - \frac{1}{a_2}\lambda_i - \frac{a_1}{a_2}\lambda_i^2)\lambda_i$$

$$b_1' = f_1$$

$$b_2' = a_5 f_2 + \frac{a_5 b_8 - a_6 b_7}{a_2 a_5} + \sum_{i=1}^{4} L_i(1 - \frac{1}{a_2}\lambda_i - \frac{a_1}{a_2}\lambda_i^2)$$

$$b_3' = -\sum_{i=1}^{4} Q_i$$

$$b_4' = a_5 f_4 + \sum_{i=1}^{4}[(1 - \frac{1}{a_2}\lambda_i - \frac{a_1}{a_2}\lambda_i^2)\lambda_i L_i - a_5 Q_i]$$

The solutions of the shape of (34), (38) and (39) can be used only if $a_2 \neq a_4 a_5$ and $a_1 \neq 0$ and $a_3 \neq 0$.

Table 1 contains the values of b_i and f_i for a few given parameters. The meaning of the parameters a_i is given in the Table. The first row contains only such physical quantities with respect to which the sensitivity was studied. The second row shows the a_i parameters which contain these physical quantities. The values of the quantities b_i and f_i vary with respect to which parameter the sensitivity is examined. These values are found in the Table.

In many cases the operational units are such that the coefficients of the differential equations are not constant. For example, the rate of one of the phases varies or the equilibrium connection is a non-linear one. Accordingly, digital computer programmes were prepared in which the set of differential equations was solved with the Runge-Kutta method.

The sort of differential equations pertaining to the sensitivities was solved, for the parameters given in Table 2, with the

Table 2. Parameter sensitivity of the ADPF Model

Pe_L = 10;			Pe_G = 10;		St_L = 4.0;		St_G = 2.0;		x_{in} = 0.0;		A = 1;		x_o^* = 0	
z	x	y	E_{1,D_L}	E_{2,D_L}	E_{1,D_G}	E_{2,D_G}	$E_{1,\beta\omega}$	$E_{2,\beta\omega}$	E_{1,v_L}	E_{2,v_L}	E_{1,v_G}	E_{2,v_G}	$E_{1,x(o)}$	$E_{2,x(o)}$
0.0	0.84	0.97	-0.044	-0.005	-0.038	-0.028	0.183	0.004	-0.297	-0.040	0.196	0.069	1.0	0
0.1	0.83	0.95	-0.035	-0.008	-0.039	-0.032	0.191	0.010	-0.333	-0.083	0.216	0.113	1.1	-0
0.2	0.79	0.92	-0.025	-0.010	-0.042	-0.037	0.211	0.014	-0.399	-0.128	0.255	0.161	1.6	-1
0.3	0.74	0.89	-0.018	-0.011	-0.044	-0.042	0.236	0.016	-0.474	-0.175	0.301	0.212	2.5	-4
0.4	0.69	0.85	-0.010	-0.011	-0.046	-0.047	0.264	0.014	-0.557	-0.225	0.349	0.267	4.9	-15
0.5	0.62	0.81	0.000	-0.008	-0.046	-0.051	0.294	0.009	-0.647	-0.277	0.399	0.328	12.0	-52
0.6	0.55	0.77	0.019	-0.004	-0.045	-0.055	0.328	-0.003	-0.749	-0.331	0.447	0.392	34.0	-177
0.7	0.47	0.72	0.050	0.003	-0.039	-0.054	0.364	-0.024	-0.867	-0.386	0.493	0.461	109.0	-590
0.8	0.38	0.66	0.110	0.014	-0.030	-0.044	0.404	-0.058	-1.016	-0.439	0.532	0.527	355	-1959
0.9	0.27	0.61	0.243	0.028	-0.015	-0.014	0.448	-0.106	-1.235	-0.485	0.559	0.576	1169	-6490
1.0	0.14	0.58	0.702	0.038	-0.004	0.019	0.487	-0.139	-1.754	-0.507	0.569	0.589	3860	-21149

above-mentioned method. The Table contains the sensitivity data with respect to a few more important parameters as a function of z.

3. The Application of Parameter Sensitivity

The knowledge of parameter sensitivity enables a deeper insight to be gained into the properties of the model and the operational unit described by it. From the point of view of unit operations, it provides assistance in the choice among the models describing the operational unit and in judging the merit of a given model. In practical work, it helps to estimate the accuracy of the calculations.

A few numerical examples, illustrating the application of the concept of sensitivity, are presented in the following.

In **design work**, the values of the parameters are taken from the literature. The sensitivity offers a possibility for the estimation of the degree of accuracy that can be claimed of the data taken from the literature.

In the vicinity of a p_s set of values of the parameters we may write

$$x(z,p) = x(z,p_s) + E_{l,i}(z,p_s) \frac{x(z,p_s)}{p_i} \Delta p_i$$

and after rearrangement we obtain

$$\frac{x(z,p) - x(z,p_s)}{x(z,p_s)} = E(p_s,z)_{l,i} \frac{\Delta p_i}{p_i}$$

This equation enables the calculation of the error of the variable x if the relative error of the parameter $(\Delta p_i/p_i)$ is known. A similar procedure may also be applied in the case of the variable y.

Let us estimate the error made with the application of the data given in Table 2, if the expression, taken from the literature, for the calculation of $(\beta\omega)$ is of an accuracy of ± 10 %. The calculation should be carried out for the place $z = 1$. In this place, the sensitivity is (cf. Table 2) $E_{1,\beta\omega} = 0.487$ and $E_{2,\beta\omega} = -0.139$. Accordingly

$$\frac{x(z,p) - x(z,p_s)}{x(z,p_s)} = 0.1 \cdot 0.487 \approx 0.049$$

$$\frac{y(z,p) - y(z,p_s)}{y(z,p_s)} = -0.1 \cdot 0.139 \approx -0.014$$

that is, an error of 10 % in the value of $(\beta\omega)$ results in an error of 4.9 % and 1.4 %, resp. in the calculation of the x and y values in the case of the given system. Similar calculations can also be carried out for the other parameters.

From the point of view of the operator it is interesting to know the effect, for example, of fluctuations in the rate of the phases (v_L and v_G) on the composition of the phases leaving the operational unit. Let us consider a deviation of + 10 % from the predetermined value. In the case of the set of parameters presented in Table 2, this causes the following deviations in the x(o) and y(1) values:

$$\frac{x(o,p) - x(o,p_s)}{x(o,p_s)} = -0.1 \cdot 0.297 \approx -0.030$$

$$\frac{y(1,p) - y(1,p_s)}{y(1,p_s)} = -0.1 \cdot 0.507 \approx -0.050$$

As can be seen, this results in a deviation of 3 % and 5 %, respectively. A change of 10 % in the v_G value results, after a similar calculation, in deviations of 2 % and 6 %, respectively.

In research work the aim is frequently to determine the values of the parameters from the experimental data. If for example

we want to determine the D_L mixing coefficient from measured values of x(t), and the latter can be determined only with an accuracy of 10 %, the error made in the calculation of the parameter is the following:

$$\frac{\Delta D_L}{D_L} = \frac{\frac{\Delta x}{x}}{E_{1,D_L(1)}} = \frac{0.1}{0.7} \approx 0.14$$

Accordingly, it can be calculated with an error of 14 % from the data referring to the place z = 1. The same parameter, when calculated from the measured values of y, could be determined only with an error of 25 %. The sensitivity with respect to E_G is such that its value could be determined with an error even greater than the previous one.

In modelling operational units, a boundary value problem is usually encountered. If we want to use a digital or analog computer in the calculations, the values of the functions taken at the initial points (z = o) have to be given and the solution which satisfies the boundary conditions has to be found by the iteration method. Table 2 also contains the sensitivities with respect to x(o).The absolute value of these is so high that a small deviation from the actual value in the determination of x(o) and y(o) causes a large error in the values of x(z) and y(z). This is the explanation of the fact that two-phase countercurrent operational units cannot be modelled with an analog computer. With the latter, the setting of the x(o) and y(o) values is possible only to a limited accuracy (1-2 %) and even such a small deviation from the actual value causes x(z) and y(z) values to be obtained that are technically unreal. This difficulty is considerably decreased by the use of digital computers, due to the high degree of accuracy that can be realized.

The above examples clearly illustrate the importance and wide range of applicability of the knowledge of the sensitivity.

SYMBOLS USED

a_i parameters (cf. Table 1)

D axial mixing coefficient (m^2/sec)

$e_{j,i}$ sensitivity of the j^{th} dependent variable to alter the value of the i^{th} parameter

$E_{j,i}$ dimensionless sensitivity of the j^{th} dependent variable according to the i^{th} parameter

H Henry-constant (dimensionless)

Pe Peclet-number (dimensionless)

St Stanton-number (dimensionless)

v linear flow rate of the phase (m/sec)

Z length of the column (m)

z space co-ordinate along the length of the column (dimensionless)

x concentration of the absorbed component in the liquid phase (dimensionless)

y concentration of the absorbed component in the gaseous phase (dimensionless)

x_o axis section of equilibrium line (dimensionless)

$\beta\omega$ component transfer coefficient, as referred to unit volume (sec^{-1})

Indices

j refers to the dependent variable (the concentration in the liquid phase is j = 1, that in the gaseous phase is j = 2)

i refers to the parameter

L liquid phase

G gaseous phase

REFERENCE

1. ÁRVA, P., SZEIFERT, F., Hung. J. Ind. Chem. 1, 271 (1973)

РЕЗЮМЕ

Авторами определяется понятие чувствительности параметра для диффузионных элементов процесса, и рассматриваются модели для его вычисления. Модель идеального вытеснения для двухфазных противоточных элементов процесса содержит два, а диффузионная модель, имеющая в виду и осевое смешивание, четыре безразмерных параметра. В обоих моделях используется много физических величин а также величин, характеризующих заводские условия в выражениях безразмерных параметров.

В работе описывается и аналитическое решение для вычисления чувствительностей.

Теоретические выражения дополняются числовыми примерами, решаемыми на аналоговых и цифровых вычислительных машинах, и таким образом, показывается и практическое применение чувствительности параметра.

Hungarian Journal
of Industrial Chemistry
Veszprém
Vol.1. pp. 401-412 (1973)

A DIGITAL CALORIMETER AND ITS APPLICATIONS IN CHEMICAL INDUSTRY

J. FARKAS and F. MOLNÁR

(Research Institute for Heavy Chemical Industries, Veszprém, and CHINOIN Factory of Pharmaceuticals and Chemical Products, Budapest)

Received: March 14, 1973.

In addition to parameters such as temperature, pressure, quantity of streaming material, as well as various other physico-chemical parameters, the quantity of heat is a very important characteristic figure in the chemical, pharmaceutical, and energetical industries, etc., and any other industrial branch where thermal energy is used or produced. Until a few years ago, the simple, accurate and reliable determination was solved by the development of the Digital Calorimeter type DIGITCALOR NORX QM-121. (Hungarian Patent No. 158.601 of the United Chemical Works.)

The above-mentioned continuous-operation, digital calorimeter enables the quantity of heat brought into or carried away from a system by a streaming medium to be determined, both as an instantaneous value and as one integrated for a given period of measurement.

PRINCIPLE OF OPERATION

The quantity of heat absorbed or emitted by a system can be determined on the basis of the following equation:

$$Q = V \gamma c \Delta\theta \qquad \text{kilocalories/hour} \qquad (1)$$

where

V is the amount of heat transfer medium (cu.metre/hour)

γ is the density of the heat transfer medium (kg force/cu.metre)

c is the specific heat of the heat transfer medium (kilocalory/kg force.^{o}C)

$\theta = \theta_{out} - \theta_{in}$ is the temperature difference in the heat transfer medium.

The quantity of heat absorbed or emitted by the system during a period T can be determined by the equation

$$Q = c\,\gamma \int_{o}^{T} V\,\Delta\theta\,dt$$

or, using summarization instead,

$$Q = c\,\gamma \sum_{i=0}^{n} V_i\,\Delta\theta_i\,\Delta t_i \qquad (2)$$

The algorithm of the operation of the digital calorimeter is given by Equation (2).

The amount and temperature difference of the streaming heat transfer medium is measured, the product of the two values is produced, corrected by the constant $c\,\gamma$, and the results obtained are summarized for a given measurement period T by the instrument.

It follows from the algorithm of the operation that the following conditions are to be fulfilled in the measurement:

1. No process involving a latent heat (change in physical state, and chemical reaction, etc.) may occur in the heat transfer medium.

2. The specific heat and specific gravity of the heat transfer medium can be regarded as constant and their temperature dependence can be neglected.

The above conditions are met with in the overwhelming majority of measuring tasks and in such cases the calorimeter operates at the prescribed level of accuracy.

The block diagram of the instrument is shown in Fig.1.

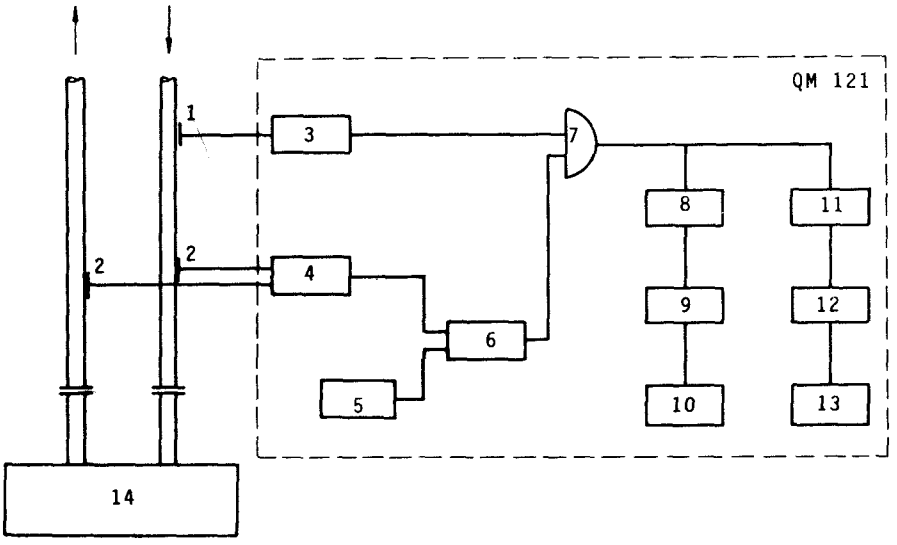

Fig. 1

The volumetric flow rate of the heat transfer medium flowing into system 14 is measured by turbine-type flowmeter 1. Quantity meter 3 transforms the output signal of the turbine-type flowmeter - which is an approximately sine-wave signal of a voltage higher than 10 mV and of a frequency of 0 to 2000 Hz - into a train of pulses corresponding to the level of the TTL logic. This signal is conducted to the first input of AND-gate 7.

The temperature of the medium on entering and leaving is measured by resistance thermometers 2. Temperature difference measuring unit 4 converts the signal of the resistance thermometers into a DC signal: a DC voltage proportional to the temperature difference appears at its output. This voltage is compared to a lineary varied reference voltage by comparator 6. The reference voltage is produced by generator 5. A time-code, proportional to

the temperature difference, appears at the output of comparator 6 in the form of a logic signal of varied switching ratio. The latter signal controls the second input of AND-gate 7 and consequently the AND-gate is open and allows the pulses of the quantity measuring unit to pass for a period proportional to the temperature difference.

The number of pulses appearing at the output of the AND-gate is proportional to the product of the signals conducted to the input of the gate, that is to say, with the heat quantity.

The pulses appearing at the output of AND-gate 7 are counted by counter 8. The content of the counter passes intermediate storage 9 and is shown in a digital form by display 10. Summarization is carried out - via frequency devider 11 and switching amplifier 12 - by electromechanical pulse counter 13.

Fig. 2 illustrates the time diagram of the operation showing: the analog signal of temperature difference meter 4; the linearly varied reference voltage; the controlling signal of comparator 6, the output signal of quantity meter 3, and the train of pulses appearing at the output of the AND-gate.

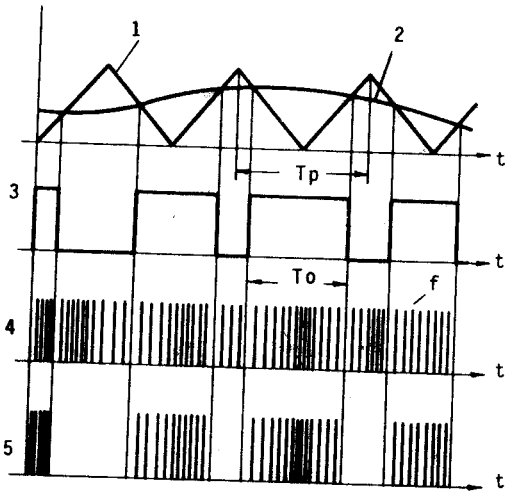

Fig.2. Diagram of operation plotted against time 1: linear reference voltage; 2: voltage proportional to temperature difference; 3: output of comparator (6); 4: output of quantity meter (3); 5: output of AND-gate.

Accordingly, if the pulse train, whose frequency is proportional to the quantity of the streaming medium, is multiplied by the time code proportional to the temperature difference by means of an AND-gate (sampling mul-

tiplication), the number of pulses appearing at the output during one period is

$$N = f\ T_o = k\ V\ \Delta\theta$$

where

- f is a frequency proportional to the quantity (sec^{-1})
- T_o is the time code of the temperature difference, i.e. the "open" time of the AND-gate (sec)
- k is an instrument constant (cf. Fig. 2).

MEASURING UNITS

The simplest calorimetris system comprises the following units:

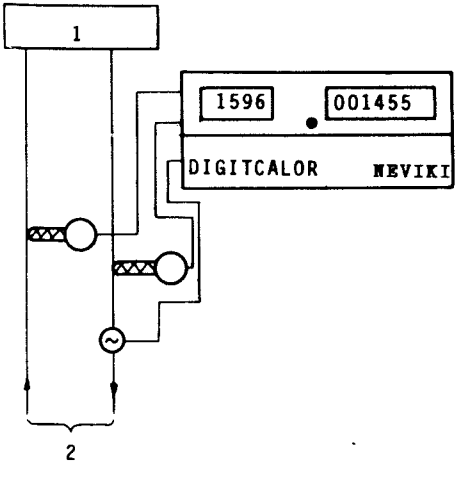

Fig.3. 1 - heat source or heat sink
2 - heat transmitting medium

- TURBOQUANT, turbine-type flow meter
- resistance thermometers in the entering and leaving medium
- electronic section of calorimeter type QM-121 (Fig. 3).

The system composed according to the above enables the instantaneous value of the heat quantity or its integral for a given period of time to be determined.

The instantaneous value is seen on the digital display of the in-

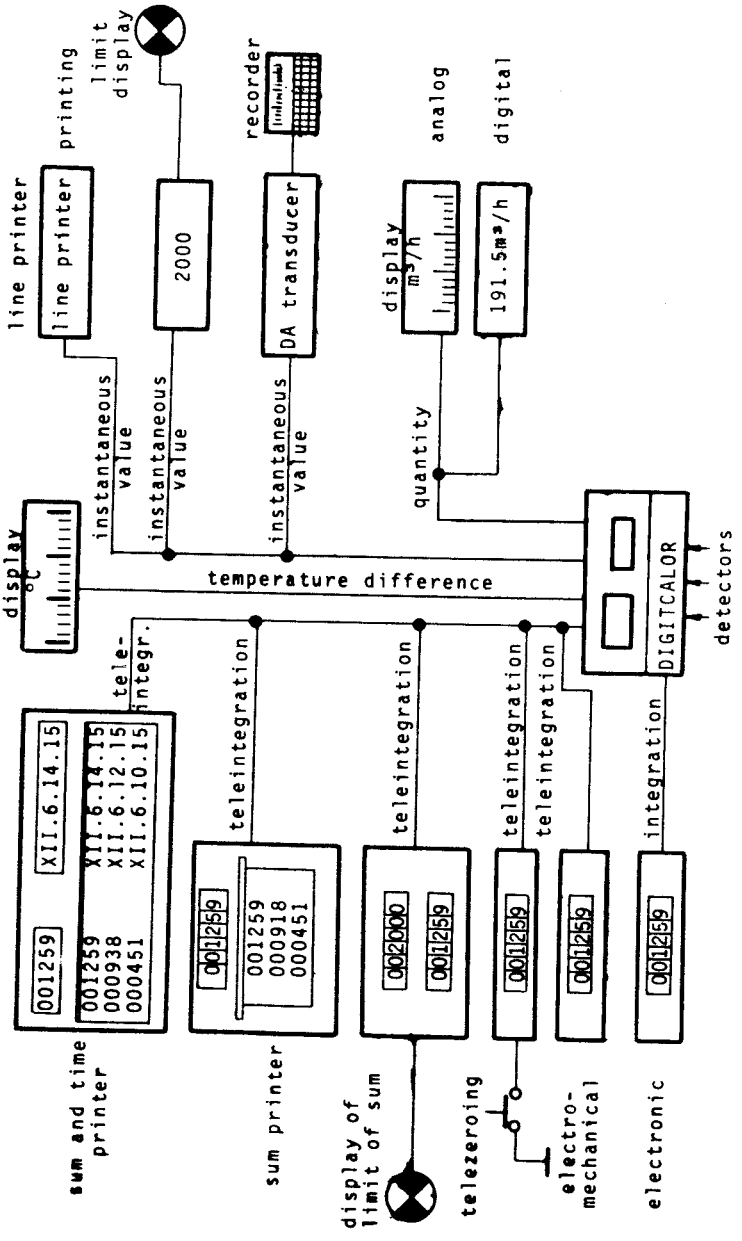
printing
limit display
line printer
line printer
recorder
2000
DA transducer
analog
digital
display m³/h
191.5m³/h
instantaneous value
instantaneous value
instantaneous value
quantity
display °C
temperature difference
DIGITCALOR
detectors
tele-integr.
teleintegration
teleintegration
teleintegration
teleintegration
integration
001259
XII.6.14.15
001259 XII.6.14.15
000938 XII.6.12.15
000451 XII.6.10.15
001259
000918
000451
002000
001259
001259
001259
001259
sum and time printer
sum printer
display of limit of sum
telezeroing
electro-mechanical
electronic

Fig. 4.

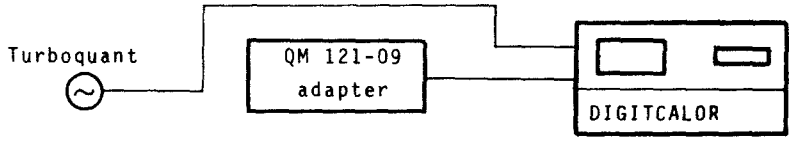

Fig. 5. Measurement of quantity

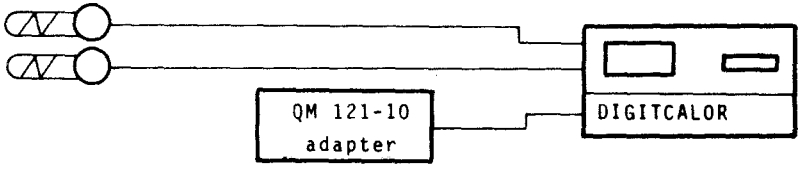

Fig. 6. Measurement of temperature difference

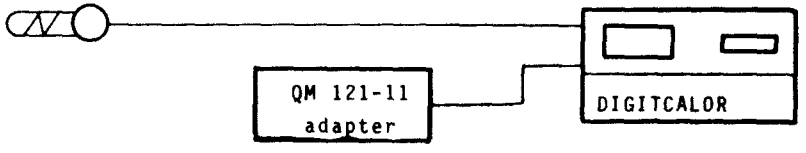

Fig. 7. Measurement of temperature

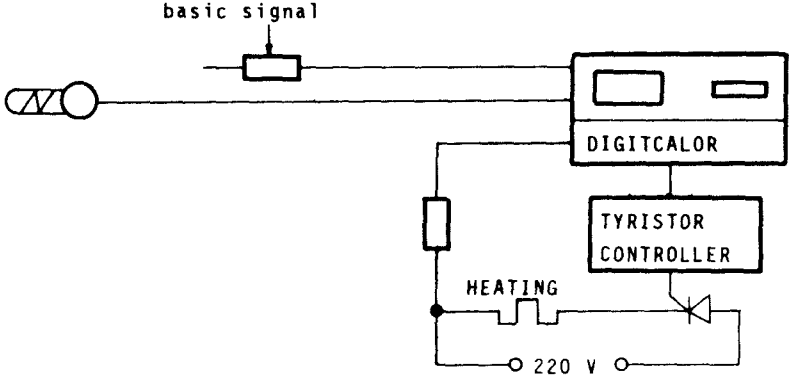

Fig. 8. Temperature regulation

strument, whereas the integral value of the heat quantity can be read from the electromechanical pulse counter built into the front plate of the instrument.

Further data acquisition systems can be connected to the electronic system of the calorimeter; these are illustrated in Fig. 4.

The construction of the calorimeter type QM-121 also enables further parameters to be measured, such as quantity (Fig.5), temperature difference (Fig.6) and temperature (Fig.7).

Fig. 8 shows an interesting measuring setup: by means of thyristors and thyristor controllers, the electronic section of the calorimeter is used as a temperature controller.

INDUSTRIAL APPLICATION

In the description of the fields of application, only those concerned with calorimetric determinations were mentioned. As a consequence of the wide variety of the production and consumption of thermal energy, it is not the aim of the present paper to attempt complete coverage of the field. A few typical possibilities of application are shown and,within these, some technological applications of particular interest from the point of view of chemical industry are described.

Measurement of energy production. In this field, the determination of the heat energy (e.g. hot water) or cold energy (e.g. refrigerated brine) produced by energy producers (e.g. thermal power stations, and refrigerating stations) is the most important task.

The measurement of the heat quantity produced enables continuous production control to be carried out, which is a basic condition of maximum efficiency.

Measurement of energy consumption. The calorimeter enables the energy consumption of a factory, and within this, that of a manufacturing plant or a sub-unit to be measured. The quantity thus determined can also be used for accounting purposes. The energy consumption may represent a considerable fraction of the costs of the production of goods, and consequently, an exact calculation or determination of costs is quite impossible without the measurement of energy.

Technological measurements. The heat effects of chemical reactions are in a quantitative connection with the progress of the reaction and consequently the measurement of heat quantity enables conclusions to be drawn on the progress of a reaction. This may be especially important in cases where no other simple technique of checking is available.

As an example of the application of the Digital Calorimeter for technological purposes, the thermal measurements carried out at the Chinoin Factory for Pharmaceuticals and Chemicals will be described.

In the course of fermentation, biological heat is produced as a consequence of the oxygen uptake of the micro-organisms. The heat produced is dissipated by cooling water.The amount of cooling heat and its input and output temperatures are measured by the Digital Calorimeter. Accordingly, the measured calories give the amount of heat carried away by the cooling water. This is, of course, not identical to the amount of biological heat produced, but the effect of other parameters on the energy balance can be neglected or can be taken into consideration in the evaluation, in view of the fact it is constant.

The results of the measurements are shown in Figs. 9 and 10. Fig.9 shows the thermal pattern of a normal fermentation reaction. It is apparent that there was a period of initial intensive respiration (1), followed by a decrease in the biological heat production due to the decrease in the quantity of carbohydrate present in the fermentor (2), i.e. the necessity of carbihydrate addition,

and the effect of the addition (3). The repeated decrease in carbohydrate concentration was counteracted by renewed addition, and the effect of this is seen in section (5).

Fig. 10 shows the progress of fermentation where infection occurred. After the initial active respiration period (1) a pronounced decrease in biological heat production can be observed (2) which indicates a decrease in respiration and active material production as well.

Results gained in the caloric measurements agree well with those of other instrumental measurements; however, the connections and discrepancies could not be elucidated in all respects.

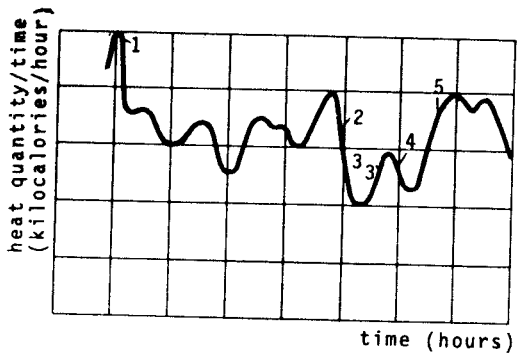

Fig. 9.

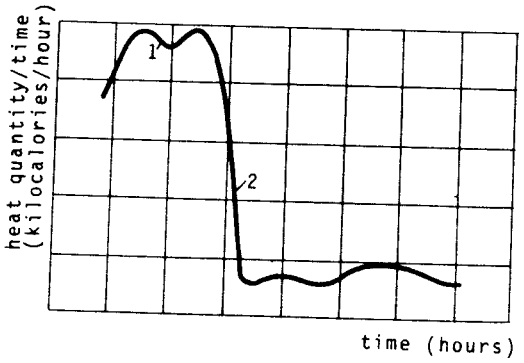

Fig. 10.

The following of chemical reactions with the Digital Calorimeter is of considerable value because it supplies information on the progress of the reaction while the process is occurring and with practically no delay, thereby enabling, if necessary, prompt measures to be taken. The production of the active material in fermentation processes depends on a number of parameters. Consequently, the state of the process can only be defined by the collective examination of these and by knowing the tendency of the

changes. However, these can be decided only afterwards, after carrying out a time-consuming evaluation. On the contrary, the measurement of biological heat is fast and it supplies information characteristic of the essence of the process.

In our opinion, the possibility for the determination of the heat of reaction may become a valuable quantitative parameter in the control of chemical industrial processes.

In conclusions, the technical data of the calorimeter type DIGITCALOR NORX QM-121, described in the foregoing, are set out here:

Range of quantity determination	min. 0.03 to 0.3 cu.metre/hour max. 50 to 500 cu.metre/hour
Range of temperature difference determination	min. 0 to 10°C max. 0 to 100°C
Accuracy	1 %
Sampling frequency	max. 2 seconds
Functions	determination of instantaneous value integration
Display	instantaneous value: 4 decades integral value: 6 decades
Frequency divider of integrator	1:1,000; 1:10,000
Output	for teleintegration by electrochemical pulse counter
voltage	24 Volts
current	300 milliamperes
Mains voltage	220 Volts, 50 Hertz
Ambient temperature	+5 to +50°C
Power consumption	8 voltamperes approx.
Dimensions	230 × 110 × 380 millimetres

Weight	5.5 kg force
Form	laboratory or instrument board pattern

РЕЗЮМЕ

Кроме температуры, давления, интенсивности тока и различных физико-химических параметров в химической, лекарственной, энергетической промышленности, и в других областях промышленности, в которых тепловая энергия потребляется или производится, знание количества тепла имеет большое значение. Простое, точное и достоверное измерение этой величины встречало большие трудности до последнего времени. Для устранения этого недостатка сотрудники института выработали цифровой тепломер типа "Digitcalor NORX QM-121".

Этот цифровой тепломер непрерывного действия пригоден для измерения мгновенного значения и суммы тепла, введенного в систему и отведенного из системы текущей средой.

Hungarian Journal
of Industrial Chemistry
Veszprém
Vol.1. pp. 413-424 (1973)

HYDROFORMYLATION OF SAFROLE: THE MECHANISM OF RING CLOSURE AND FORMATION OF A TETRALIN DERIVATE

J. PALÁGYI, Z. DÉCSY*, G. PÁLYI and L. MARKÓ

(Department of Organic Chemistry, Veszprém University of Chemical Engineering)

Received: March 15, 1973.

5,6,7,8-tetrahydro-2,3-methylenedioxy naphthalene is formed from safrole through γ-(3,4-methylenedioxy phenyl)-butyraldehyde as an intermediate under hydroformylation conditions in the presence of $Co_2(CO)_8$ as catalyst. Ring closure is regarded as an intramolecular electrophilic substitution catalyzed by $HCo(CO)_4$.

The hydroformylation reaction, a typical petrochemical industrial process, has also increased in importance in synthetic organic chemistry. Hydroformylation of natural products can lead to new substances with unusual biological activity.

Eugenol reacts under hydroformylation conditions (120-180°C, 200-400 atm. CO + H , $Co_2(CO)_8$ as catalyst) forming - among other more usual products - 5,6,7,8-tetrahydro-3-methoxy-2-naphthol with 30-40 % yield [1]. The results reported gave no conclusive evidence for the mechanism of ring closure in the formation of the tetralin carbon skeleton.

Experiments performed under similar conditions (150°C, 200-300 atm. CO + H_2, 0.4 mole % $Co_2(CO)_8$ as catalyst) have now shown that the same ring closure also takes place in the case of

*Hungarian Oil and Gas Research Institute, Veszprém

safrole (I) as the starting material. The product of a typical experiment had the following composition:

dihydrosafrole (II)	48 %
5,6,7,8-tetrahydro-2,3-methylenedioxy naphthalene (III)	24 %
C_{11} aldehydes (IVa, Va, VIa)	4 %
C_{11} alcohols (Vb, VIb)	3 %
high boiling products	21 %

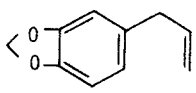

I

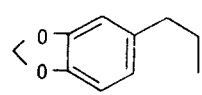

II

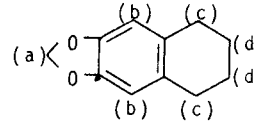

III

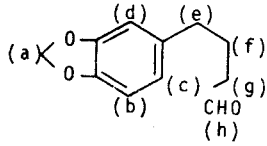

IVa

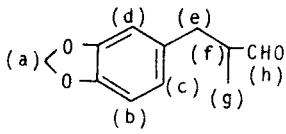

Va

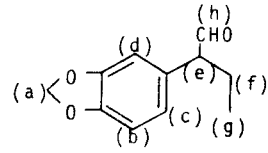

VIa

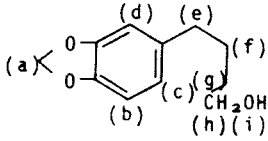

IVb

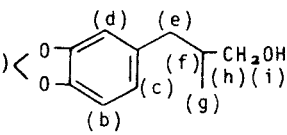

Vb

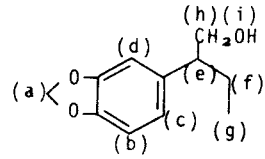

VIb

If the reaction was followed by taking samples from the autoclave at regular intervals, aldehydes IVa, Va and VIa were found to be the intermediates whereas dihydrosafrole (II), the cyclic reaction product III and the alcohols Vb and VIb the end products. This observation suggested the following scheme of reactions:

Table 1. Hydroformylation of safrole with $Rh_4(CO)_{12}$ (0.003 mole %), or $Co_2(CO)_8$ (0.5 mole %) + + PBu_3 (4 mole %) as catalysts

Catalyst	Temperature °C	CO + H_2 pressure atm.	Composition of reaction product, %								
			II	III	IVa	Va	VIa	IVb	Vb	VIb	high boiling
$Rh_4(CO)_{12}$	110	200-300	2	1	24	41	23	-	-	-	9
$Rh_4(CO)_{12}$	180	200-300	3	1	-	-	-	24	39	16	17
$Co_2(CO)_8$ + PBu_3	180	40-60	81	-	-	-	-	-	-	-	19

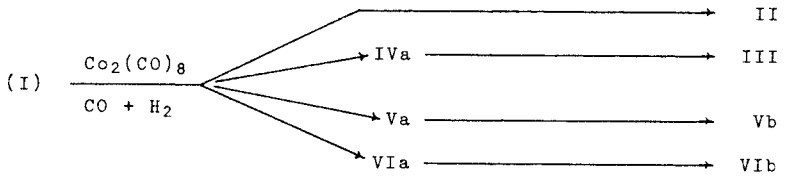

With the exception of IVa ⟶ III, all steps of the above scheme fit into the usual pattern of reactions observed during hydroformylation of olefins and therefore require no comment.

To investigate the mechanism of the ring closure reaction, safrole was also hydroformylated with $Rh_4(CO)_{12}$ as a catalyst. As shown in Table 1, rhodium forms only negligible amounts of compound III. If the $Co_2(CO)_8$ catalyst was modified by adding $P(\underline{n}\text{-}C_4H_9)_3$, dihydrosafrole was the only product of the reaction. Obviously unsubstituted cobalt carbonyls are the favoured catalysts for ring closure.

Regarding the pathway of ring closure, evidently there are two alternatives: both the n-butanol derivate IVb and the n-butyraldehyde derivate IVa may be visualized as intermediates. To clarify this point, two reaction products obtained with $Rh_4(CO)_{12}$ as catalyst at 110 and 180°C were subjected (after distillation to remove dissolved Rh) to further treatment with CO and H_2 in the presence of $Co_2(CO)_8$ as a catalyst. Table 2 shows the results which within the errors of GLC analysis prove aldehyde IVa to be the intermediate compound during the formation of III.

WENDER and co-workers [2] have found that pinacol is transformed under hydroformylation conditions in the presence of $Co_2(CO)_8$ to products which can best be explained by acid catalysis due to $HCo(CO)_4$, a strong acid in polar solvents. Our results can also be interpreted by intramolecular electrophilic substitution of the benzene ring caused by the protonation of aldehyde IVa and the subsequent hydrogenation [3, 4] of the benzyl alcohol derivate VII to the corresponding tetralin derivate, both reactions catalyzed by $HCo(CO)_4$:

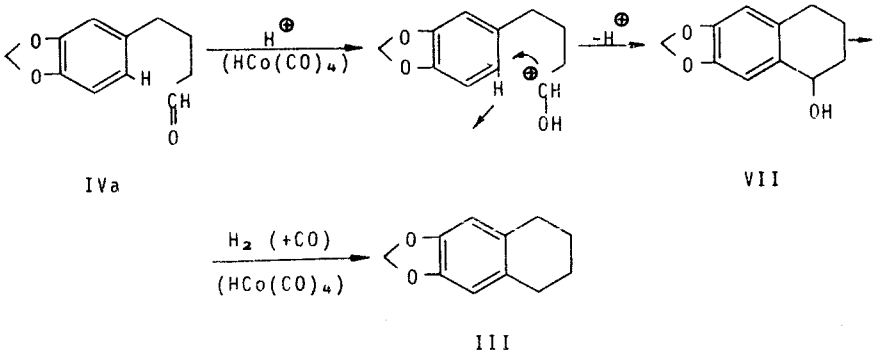

IVa VII III

Table 2. Treatment of the aldehydes IVa-VIa (experiment A) and of the alcohols IVb-VIb (experiment B) with CO + H_2 (150°C, 200-300 atm.) in the presence of 0.4 mole % $Co_2(CO)_8$ as catalyst

Compound	In starting mixture, %		In reaction product, %	
	Exp. A	Exp. B	Exp. A	Exp. B
II	2	3	4	8
III	< 1	< 1	33	2
IVa	27	-	4	-
Va	45	-	3	-
VIa	25	-	2	-
IVb	-	29	-	33
Vb	-	47	13	40
VIb	-	20	9	11
high boiling	-	-	32	6

The proposed S_E mechanism is supported by the observation that the ring closure reaction is strongly dependent on the polarity of the reaction medium. In two parallel experiments performed

in hexane and 1,2-dimethoxy ethane as solvent the yield of III was 7 % and 33 %, respectively. At the same time, the amount of high boiling products was much higher in hexane (25 % and 10 %, respectively) showing that aldehyde IVa - which is transformed mainly into III in a polar medium - is very reactive under hydroformylation conditions and polymerizes if the conditions are unfavourable for ring closure.

Our experiments performed with eugenol as a substrate also revealed a similar mechanism for the ring closure reaction in this case. Typical experimental results which show that the n-butyraldehyde derivative is the precursor of the compound with the tetraline skeleton are summarized in Table 3.

Table 3. Treatment of the aldehydes IVa'-VIa' (experiment A) and alcohols IVb'-VIb' (experiment B) formed from eugenol with CO + H_2 (150°C, 200-300 atm.) in the presence of 0.3 mole % $Co_2(CO)_8$ as catalyst

Compound*	In starting mixture, %		In reaction product, %	
	Exp. A	Exp. B	Exp. A	Exp. B
II'	9	12	5	10
III'	-	22	40	19
IVa'	37	-	-	-
Va'	47	-	14	-
VIa'	7	-	4	-
IVb'	-	14	-	14
Vb'	-	35	-	35
VIb'	-	17	-	14
High boiling	-	-	37	8

*The numbering of eugenol derivatives is based on that of the analogous safrole derivatives, the primes indicating that these compounds contain a methoxy and a hydroxy group instead of the methylenedioxy group in safrole.

The treatment of isosafrole and isoeugenol with synthesis gas in the presence of $Co_2(CO)_8$ at 150° yielded almost exclusively the corresponding dihydro derivatives, whereas with $Rh_4(CO)_{12}$ as catalyst at 100° only the branched chain aldehydes were formed.

EXPERIMENTAL

Hydroformylation of Safrole

162 g safrole and 1.3 g $Co_2(CO)_8$ (0.4 mole %) were charged in a 1000 ml stainless steel rocking autoclave in which a carbon monoxide + hydrogen mixture (1:1) was compressed to 230 atm. The autoclave was heated to 150 ± 5° and maintained at this temperature for 4 hrs. 56 Nl of gas was consumed during this time which amounts to 2.5 mole of gas per mole of safrole. The reaction product (184 g) was discharged and distilled at 140-190°C at 10 Hgmm. The distillate (145 g) was analyzed by GLC (Chromosorb P with 10 % QF-1 at 180°C). The bottom (34 g) was decanted from the metallic cobalt formed by the decomposition of $Co_2(CO)_8$ and was investigated by IR spectroscopy which showed the presence of oligomeric derivatives of safrole or its carbonylated derivatives.

If desired, samples can be taken during the high pressure reaction from the autoclave, and processed and analyzed as indicated above.

Experiments with $Rh_4(CO)_{12}$ or $Co_2(CO)_8$ + PBu_3 as catalyst, as well as the hydroformylation of eugenol were performed similarly.

Identification of the Tetraline Derivative III

The compound was isolated by fractional distillation (bp. 109°C/7 Hgmm). It forms white crystals and melts at 39°C (uncorrected).

The cryoscopic MW determination (in benzene) gave 172 ± 5, the mass spectrometric mole peak (Finnigan Mod. 3000) was at m/e = = 176, these suggested the formula $C_{11}H_{12}O_2$ (calc.: 176).

The structure was assigned on the basis of the ^{1}H-NMR spectra (CCl_4 solution, TMS, 60* and 100** MHz).The signals observed were: δ_1 = 1.66 ppm, br. multiplet at 60 MHz, ill-resolved quintet at 100 MHz with J_1= 0.3 cps, J_2 = 0.4 cps, 4 H, (d)***; δ_2 = 2.53 ppm ill-resolved multiplet, 4 H, (c); δ_3= 5.66 ppm, singlet, 2 H, (a); δ_4 = 6.30 ppm, singlet (even at 100 MHz), 2 H, (b).

Identification of Aldehydes IVa, Va and VIa

The compounds were isolated by fractional distillation and subsequent preparative GLC using a 4 m × 8 mm column packed with 10 % QF-1 on 30/60 mesh Chromosorb W operated at 180°C with 0.9 atm. H_2 carrier inlet pressure. The fractions were collected at room temperature.

The mass spectrometric mole peaks (MS-902, AEI, 70 eV) correspond to the supposed formula $C_{11}H_{12}O_3$ (calc. 192).The M-15 peak is lacking at IVa, M-29 is the base peak at VIa, since M-29 are of very low - and nearly equal - intensity at Va and IVa, thus this process should be attributed to the loss of C_2H_5 and not to that of CHO. The base peak at IVa and Va is the methylenedioxytropylium ion (m/e 135). Other less pronounced features of the spectra are in agreement with this picture.

The ^{1}H-NMR spectra fully agree with the MS assignement. The main characteristics of the NMR spectra (CCl solution, TMS, 60 MHz) are as follows. IVa: δ_1 = 1.85 ppm, quartet, J_1 = 7 cps, J_2 = 8 cps, 2 H, (e); δ_2 = 2.4 ppm, multiplet (6 visible peaks),

*Varian T-60
**JNM PS-100 and XL-100
***for assignment see letters of the formulae

4 H, (f,g); δ_3 = 5.87 ppm, singlet, 2 H, (a); δ_4 = 6.65 ppm, one peak, 3 H, (b,c,d); δ_5 = 9.79 ppm, triplet, J = 1.4 cps, 1 H, (h); Va: δ_1 = 1.03 ppm, doublet, J = 6 cps, 3 H, (g); δ_2 = 2.2-3.2 ppm multiplet, 3 H, (e,f); δ_3 = 5.88 ppm, singlet, 2 H, (a); δ_4 = 6.64 ppm, one peak, 3 H, (b,c,d); δ_5 = 9.75 ppm, doublet, J = 1.0 cps; 1 H, (h); VIa: δ_1 = 0.88 ppm, triplet, J = 7 cps, 3 H, (g); δ_2 = = 1.30-2.15 ppm, multiplet, 2 H, (f); δ_3 = 3.26 ppm, triplet, J = 6 cps, 1 H, (e); δ_4 = 5.94 ppm, singlet, 2 H, (a); δ_5 = 6.67 ppm, one peak, 3 H, (b,c,d); δ_6 = 9.65 ppm, doublet, J = 1.6 cps, 1 H, (h). The most characteristic bands are those of the methyl groups for IVa and Va as well as the bands of the aldehydic protons with special regard to the multiplicity of these bands. These data together with the MS spectra reveal a consistent system of evidence which supports the structural assignment given in formulae IVa-VIa.

IR investigations were in accordance with the above statements; aldehydic ν(C-O) (1630 cm^{-1}) and ν(C-H) (2730 cm^{-1}) bands are present in the spectra of all the three compounds. Bands characteristic for methyl ν(C-H) and ν(C-H) vibrations are absent in the spectra of IVa, while present in those of Va and VIa. The bands characteristic for the $-OCH_2O-$ group (ν(C-H): 2780 cm^{-1}, C-O-C bands: 1248 and 1050 cm^{-1}) are present in all spectra while olefinic absorptions around 1000 cm^{-1} are missing.

Cryoscopic and osmometric (both in benzene) MW measurements (to control the order of magnitude of the MS mole peak measurements) gave 192 ± 6 which agrees well with the supposed formula ($C_{11}H_{12}O_3$) as well as with the mole peak (m/e = 192).

Identification of Alcohols IVb, Vb and VIb

The compounds were separated by means of preparative GLC using a 2 m × 8 mm glass column filled with 22 % QF-1 on 60/72 mesh Celite, at 220°C column temperature and with 140 ml/min Ar carrier. The fractions were collected at -14°C.

Our structural assignment is mainly based on the mass spectra (MS-902, AEI, 70 eV). The mole peaks m/e 194 (48, 29, and 30 respectively) correspond to the supposed formula $C_{11}H_{14}O_3$. The base peak is in all cases the formation of the methylenedioxytropylium ion, m/e = 135 (100). The loss of the hydroxymethylene group (M-31) shows a characteristic trend, the intensity of the corresponding peak decreases sharply with the distance of this group from the aromatic ring: 86 (IVb), 15 (Vb), 9.6 (VIb).

The mass spectral assignation was supported by IR and NMR spectra.

The presence of the ν(O-H) bands (3350 cm^{-1}, s, br.), the characteristic absorptions of the dioxymethylenephenyl group (ν(C-H) (O-CH_2-O) 2780 cm^{-1}, mw; ν(C-O) (C-O-C) 1248 vs and 1050 cm^{-1}, s) is a common feature of the three compounds. The absence of an olefinic double bond stretching band ($\sim$1000 cm^{-1}) as well as aldehydic ν(C-H) and ν(C-O) bands indicates the change of the original safrole and intermediate aldehyde structure. ν(C-H) (methyl) bands are absent in the spectrum of IVb while present at Vb and VIb. The CH_3:CH_2 (C-H str. band) intensity ratio is 1:1 (as supposed) at VIb, while it is far from the theoretical at Vb which can be attributed to the frequency shift of the ν(C-H) absorptions of the methylene group directly attached to the aromatic ring.

The H^1-NMR spectra of the compounds show the following main features (CCl_4 solution, TMS, 60 MHz). IVb: δ_1 = 1.35-1.75 ppm, br. multiplet, 4 H, (f,g); δ_2 = 2.50 ppm, ill-resolved triplet, 2 H, (e); δ_3 = 3.08 ppm, singlet, 1 H, (i); δ_4 = 3.50 ppm, triplet, J = 6 cps, 2 H, (h); δ_5 = 5.86 ppm, singlet, 2 H, (a); δ_6 = 6.62 ppm, one peak, 3 H, (b,c,d). Vb: δ_1 = 0.85 ppm, doublet, J = 7.5 cps, 3 H, (g); δ_2 = 1.35 - 2.05 ppm, multiplet, 1 H, (f); δ_3 = = 2.35 ppm, doublet, J = 7.5 cps, 2 H, (e,i)*; δ_4 = 3.37 ppm, doublet, J = 6 cps, 2 H, (h); δ_5 = 5.89 ppm, singlet, 2 H, (a); δ_6 = 6.63 ppm, one peak, 3 H, (b,c,d). VIb: δ_1 = 0.83 ppm, triplet, J = 6 cps, 3 H, (g); δ_2 = 1.15 - 2.20 ppm, multiplet, 2 H, (f);

*The OH signal is most probably concealed by the (e) doublet.

δ_3 = 1.95 ppm, singlet, 1 H, (i); δ_4 = 2.25 - 2.80 ppm, multiplet, 1 H, (e); δ_5 = 3.58 ppm, doublet, J = 7 cps, 2 H, (h); δ_6 = 5.90 ppm, singlet, 2 H, (a); δ_7 = 6.65 ppm, one peak, 3 H, (b,c,d).

AKNOWLEDGEMENT

Sincere thanks are due to Dr. J. Tamás (Budapest) and Mrs. I. Ötvös (Veszprém) for performing some of the MS and GLC measurements and for valuable discussions of the results. 100 MHz NMR spectra are aknowledged to JEOLCO and Varian as well as one GLC-MS experiment to Finigan A.G.

REFERENCES

1. GASLINI, F., NAHUM, L.Z., J. Org. Chem. 29, 1177 (1964)

2. WENDER, I., METLIN, S., ORCHIN, M., J. Amer. Chem. Soc. 73, 5704 (1951)

3. WENDER, I., GREENFIELD, H., ORCHIN, M., J. Amer. Chem. Soc. 73, 2656 (1951)

4. WENDER, I., GREENFIELD, H., METLIN, M., ORCHIN, M., J. Amer. Chem. Soc. 74, 4079 (1952)

РЕЗЮМЕ

5,6,7,8 - тетрагидро - 2,3 - метилдвуокись нафталина образуется из сафрола через γ - (3,4-метилдвуокись фенил) - бутировый альдегид как переходное соединение в условиях гидроформилирования в присутствии катализатора $Co_2(CO)_8$. Закрытие кольца происходит внутримолекулярным электрофильным замещением, катализированным с $HCo(CO)_4$.

Hungarian Journal
of Industrial Chemistry
Veszprém
Vol.1. pp. 425-442 (1973)

MATHEMATICAL MODELLING OF ABSORPTION COLUMNS III.

THE PRACTICAL USE OF THE PARAMETER SENSITIVITY CONCEPT

P. ÁRVA and F. SZEIFERT

(Department of Chemical Process Engineering,
Veszprém University of Chemical Engineering)

Received: December 7, 1972.

The numerical values of parameter sensitivity based on the data of the previously discussed experiments and the practical use of these values are discussed here.

The sensitivity of concentrations existing either in liquid or in the gas phases were calculated on the base of the Piston Flow (P.F.) model. In these calculations the values of the transfer coefficient of the unit volume and the flow rates of the phases were taken into account. A valuation method is presented which can be used for the calculation of errors in the determination of the parameters. Such errors are due to inaccuracy in the determination of the concentrations. The data of the parameter sensitivity are applied in the valuation of the effects of changes in the operation of absorption columns.

Valuating the Axial Dispersed Plug-Flow (A.D.P.F.) model, the numerical values of the sensitivity as the function of both the mixing and mass transfer coefficients of the phases are presented, and the approximate calculation errors of these data are given. A comparison was drawn between the P.F. and A.D.P.F. models using the sensitivity data calculated by the mixing coefficients determined in a given experiment.

In the first paper of this series [1] an experimental method was discussed which can be used for the determination of the component concentration of phases existing in a packed absorption column.

The mathematical description of counter-current absorption was presented, based on both the P.F. and A.D.P.F. models. The determined and calculated concentration distribution data were compared.

In the second paper, the parameter sensitivity of the models of two phase operation units was discussed and its method of determination was presented.

The parameter sensitivity was defined by the partial change ratio of the concentrations existing in the phases:

$$e_{j,i}(z,p_1, \ldots p_n) = \frac{\partial x_j(z,p_1,p_2 \ldots p_n)}{\partial p_i} \qquad (1)$$

where x_j is one of the dependent variables (e.g. the concentration of the absorbed component in the liquid phase), and p_i is the i-th parameter (e.g. the mass transfer coefficient). Eq. 1. shows that the sensitivity of the j-th variable from the i-th parameter ($e_{j,i}$) depends on the locus co-ordinate (z) and on the values of the other parameters. It is often more expedient to write the sensitivity in dimensionless form:

$$E_{j,i} = \frac{p_i}{x_j(z,p_1,p_2, \ldots p_n)} e_{j,i} \qquad (2)$$

In this paper the practical use of the parameter sensitivity is discussed, the data of the previously published experiments are utilized in the examples.

Based on the P.F. model, the transfer coefficient $(\beta\omega)_i$ was calculated at given liquid and gas feed rates. Knowing these, both for the liquid and gas phases the sensitivity of the soluble component concentration was determined at different parameters [$(\beta\omega)_i$, v_L, v_G].

Using the A.D.P.F. model, similar calculations were carried out, but here in addition to the transfer coefficient $(\beta\omega)_D$ the axial mixing coefficients of both phases (D_L and D_G) were also utilized as parameters.

The calculated values of the x(z), y(z) and $e_{j,i}(z)$ functions of three runs are presented in Figs.1 to 6. If the volumetric feed rate of the absorbent is 100 litres per hour and the flow rate of the gas is 2,000 litres per hour, the value of the mean transfer coefficient calculated by the A.D.P.F. model was $(\overline{\beta\omega})_i = 3.81\times10^{-3}$ one per second ($St_L = 2.3$, $St_G = 7.6$). The calculated concentration distributions x(z) and y(z) are presented in Figs. 1 and 2. If the alteration of St numbers is caused by the variation of the transfer coefficient, the sensitivities at different St_L and St_G dimensionless values as the functions of the column height are presented in Fig. 2, but in this case the St numbers change due to the flux of the given phase.

The construction of Figs. 3, 4, and 5, and 6, are the same, but they are valid for different working characteristics of the column. E.g. Figs. 3 and 4 represent the conditions if the feed rates of the phases are B_L = 100 litres per hour, B_G = 6,000 litres per hour; and Figs. 5 and 6 if B_L = 50 litres per hour and B_G = = 8,000 litres per hour.

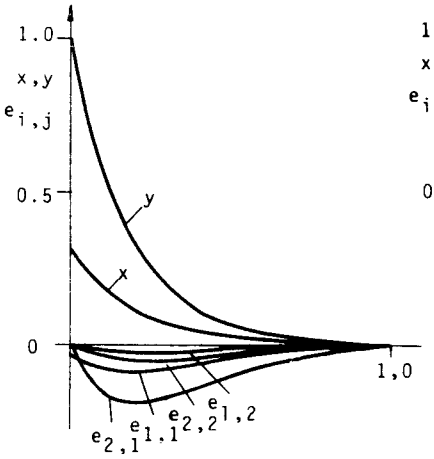

Fig.1. The alteration of liquid and gas phase concentration sensitivity with the transfer coefficient $(\overline{\beta\omega})_i$ St_L = 2.30; St_G = 7.60

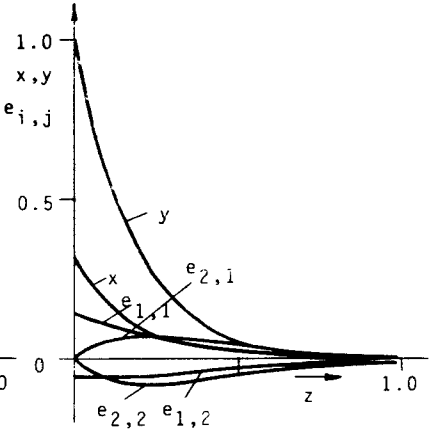

Fig.2. The alteration of liquid and gas phase concentration sensitivity with the flow rates of the phases; St_L = 2.30; St_G = 7.60

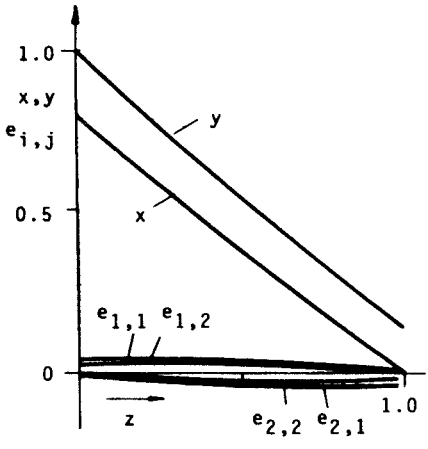

Fig.3. The alteration of liquid and gas phase concentration sensitivity with the mean transfer coefficient $(\overline{\beta\omega})_i$; St_L= 4.08 St_G = 4.51

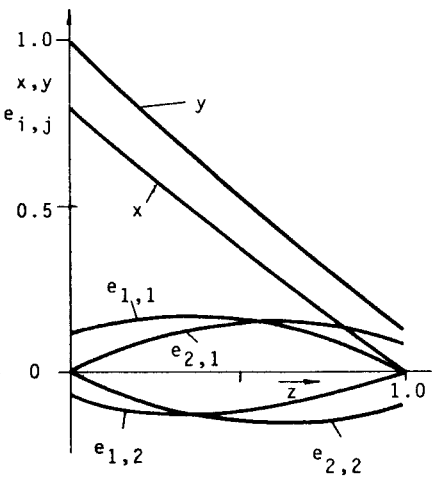

Fig.4. The alteration of liquid and gas phase concentration sensitivity with the flow rates of the phases; St_L = 4.08 St_G = 4.51

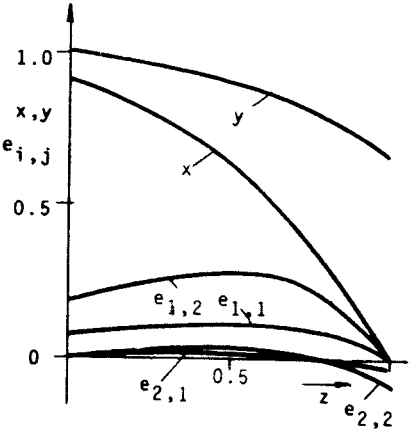

Fig.5. The alteration of liquid and gas phase concentration sensitivity with the mean transfer coefficient $(\overline{\beta\omega})_i$; St_L = 2.70; St_G = 1.12

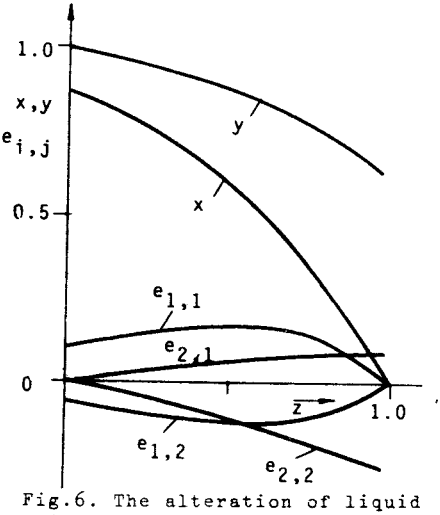

Fig.6. The alteration of liquid and gas phase concentration sensitivity with the flow rates of the phases; St_L = 2.70; St_G = 1.12

The data of the run characterized by the feed rates B_L = 100 litres per hour and B_G = 6,000 litres per hour were also evaluated based on the A.D.P.F.model.In Table 1 and 2 the following data are listed: the calculated dimensionless parameters, the concentration distribution and the data of dimensionless sensitivities calculated at some parameters.

1. The Piston Flow Model

Based on the examination of functions presented in Figs. 1 to 6, the following can be stated:

If the changes of the St number are due to the alteration of the $(\beta\omega)_i$ then for the sensitivities being valid at the top and bottom of the packed height, the following inequalities hold:

$$e_{1,St_L} = e_{1,1}(0) > 0$$
$$e_{2,St_L} = e_{2,1}(1) < 0$$
$$e_{1,St_G} = e_{1,2}(0) > 0$$
$$e_{2,St_G} = e_{2,2}(1) < 0$$

The sensitivity data calculated by the use of St_L or St_G can be transformed to each other:

$$e_{1,1}(0) = e_{1,2}(0) \frac{St_G}{St_L}$$

and

$$e_{2,1}(1) = e_{2,2}(1) \frac{St_G}{St_L}$$

It is also stated that if $St_L > St_G$ then the sensitivity curves reach maximum in the range of $0 < z < 1$, and if $St_L < St_G$ then they reach minimum; in the previous case e_{2,St_L} and e_{2,St_G} and in the latter case e_{1,St_L} and e_{1,St_G} reverse their signs.

For the extreme values the following inequalities hold:

Table 1. B_L = 100 (litres per hour); B_G = 6,000 (litres per hour); Pe_L = 33.3; Pe_G = 234.2; St_L = 5.92; St_G = 6.56; $(\beta\omega)_D$ = 9.19×10^{-3} (one per second)

z	x	y	E_{1,D_L}	E_{2,D_L}	E_{1,D_G}	E_{2,D_G}	$E_{1,\beta\omega}$	$E_{2,\beta\omega}$
0.0	0.819	0.995	-0.013	-0.001	-0.004	-0.005	0.139	-0.001
0.1	0.752	0.894	0.013	0.005	-0.003	-0.004	0.131	-0.023
0.2	0.666	0.798	0.017	0.009	-0.003	-0.004	0.122	-0.048
0.3	0.580	0.705	0.024	0.014	-0.003	-0.003	0.115	-0.077
0.4	0.496	0.613	0.031	0.020	-0.003	-0.003	0.107	-0.112
0.5	0.413	0.522	0.042	0.028	-0.002	-0.003	0.099	-0.156
0.6	0.332	0.433	0.056	0.039	-0.002	-0.003	0.091	-0.214
0.7	0.252	0.346	0.079	0.054	-0.002	-0.002	0.084	-0.296
0.8	0.174	0.261	0.120	0.077	-0.001	-0.002	0.076	-0.424
0.9	0.097	0.171	0.222	0.120	-0.000	-0.002	0.069	-0.664
1.0	0.022	0.098	0.993	0.228	+0.004	+0.036	0.064	-1.254

Table 2. B_L = 50 (litres per hour); B_G = 6,000 (litres per hour); Pe_L = 29.1; Pe_G = 255; St_L = 6.67; St_G = 3.67; $(\beta\omega)_D = 5.82\times10^{-3}$ (one per second)

z	x	y	E_{1,D_L}	E_{2,D_L}	E_{1,D_G}	E_{2,D_G}	$E_{1,\beta\omega}$	$E_{2,\beta\omega}$
0.0	0.964	0.999	-0.013	-0.000	-0.001	-0.001	0.082	0.001
0.1	0.948	0.986	-0.012	-0.003	-0.001	-0.001	0.103	0.016
0.2	0.921	0.970	-0.016	-0.006	-0.002	-0.001	0.141	0.034
0.3	0.886	0.948	-0.021	-0.010	-0.002	-0.001	0.183	0.054
0.4	0.841	0.921	-0.025	-0.014	-0.003	-0.002	0.232	0.075
0.5	0.782	0.885	-0.027	-0.018	-0.004	-0.003	0.288	0.095
0.6	0.705	0.838	-0.028	-0.021	-0.005	-0.004	0.351	0.113
0.7	0.605	0.778	-0.021	-0.023	-0.006	-0.005	0.422	0.122
0.8	0.475	0.699	0.002	-0.021	-0.007	-0.006	0.500	0.112
0.9	0.305	0.596	0.086	-0.011	-0.009	-0.009	0.587	0.060
1.0	0.086	0.469	0.790	0.020	+0.013	+0.011	0.661	-0.104

$$|(e_{2,St})_{max}| < |(e_{1,St})_{max}|$$

or

$$|(e_{2,St})_{min}| > |(e_{1,St})_{min}|$$

Consequently, the sensitivity curves show that the sensitivity of the dependent variables of the examined system changes sharply along the packed height of the column due to the alteration of the parameter. There are also cases in which the concentrations existing inside the section show a marked change - due to the variation of the parameter and the concentrations existing at the top and bottom of the column - remain nearly the same. The quantitative examination of this fact will be discussed later.

The St numbers also alter with the flow rates of the phases. In this case $e_{1,1}(0) > 0$ and $e_{1,2}(0) < 0$, moreover $e_{2,1}(1) > 0$ and $e_{2,2}(1) < 0$. The sensitivities as the function of the z can also have extreme values in the range of $0 < z < 1$, i.e. it is often the case that the concentration existing inside the packed section changes more rapidly - due to the flow rate of the phases - than it changes at the end of the column.

1.1. The Error of the Transfer Coefficient Determination

Generally the experimental data are processed for the calculation of the transfer coefficients being valid in the given unit volume of the absorber $(\beta\omega)_i$. This method was applied in the previous paper [1]. The data published in literature were usually determined as follows: the concentrations of the phases leaving the column were measured, using these data, the driving force, the mean driving force and finally the values of $(\beta\omega)_i$ were calculated. The calculated $(\beta\omega)_i$ is the function of the concentration, i.e. if the concentration determination can be carried out with a definite error so the calculation of the $(\beta\omega)_i$ is also accompanied by another and definite error.

It is assumed that the exact inlet concentration of the phases $y(0)$ and $x(1)$ are known, but the concentration of the produced liquid was analyzed with an error of three per cent. If the sensitivity is known so the evaluation of the error is:

$$h_{1,\beta\omega} = \frac{100}{e_{1,\beta\omega}(0)} \frac{\Delta x(0)}{(\overline{\beta\omega})_i} = h_{1,St_L} = \frac{\Delta x(0)}{St_L e_{1,1}(0)} \cdot 100\ \% \qquad (3)$$

where $h_{1,\beta\omega}$ is the relative error (per cent) of the $(\beta\omega)_i$ determination, and Δx is the absolute error of the concentration determination of the liquid.

E.g. taking the data presented in Fig. 5, where $B_L = 50$ litres per hour and $B_G = 8{,}000$ litres per hour. The calculated $(\overline{\beta\omega})_i$ value was $2.24\ 10^{-3}$ (sec^{-1}).

Corresponding with the given flow rates and transfer coefficient, the $St_L = 2.7$ and $St_G = 1.12$. Using the P.F. model and the mentioned parameters and the boundary conditions of $y(0) = 1$ and $x(1) = 0$, the calculated value of $x(0)$ is 0.885. If the latter is determined with an error of three per cent, $\Delta x = \pm 0.0266$. The value of the sensitivity is $e_{1,1}(0) = 0.0808$, (c.f. Fig. 5). The error in the determination of $(\beta\omega)_i$ can be calculated by Eq. (3):

$$h_{1,\beta\omega} = \frac{1}{0.0808} \frac{\pm 0.0226}{2.70} \cdot 100 = \pm 12.5 \text{ per cent}$$

Using the parameters of the same run, the concentration of the exit gas phase is analysed and worked up in the calculations so that the different error values can be obtained, again assuming three per cent error in the sampling and gas analysis.

Since $e_{2,1}(1) = -0.0335$, the error is

$$h_{2,\beta\omega} = \frac{\pm 0.0192}{-0.0335\ 2.70} \cdot 100 = \pm 21 \text{ per cent}$$

In the examined case, the determination of the concentrations can be carried out with the same accuracy when either the liquid

or the gas phases are analyzed. The error of the transfer coefficient is less if the calculations are based on the concentration data of the liquid phase. This fact is to be taken into account in the experiments.

The error values of all the three runs $h_{1,\beta\omega}$ and $h_{2,\beta\omega}$ are listed in Table 3. The data in Table 3 show that the errors of $(\beta\omega)_i$ values are often higher with an order of magnitude than the errors of the concentration determinations. The selection of the examined phase also plays an important role.

As previously mentioned, the values of the sensitivity depend on z and they can also reach extreme values. This deserves attention if the $(\beta\omega)_i$ values have to be determined. E.g. if the feed rated are B_L = 50 litres per hour and B_G = 8,000 litres per hour, the sensitivity $[e_{1,St}(z)]$ at z = 0.5 reaches maximum. The sensitivity is now $e_{1,St_L}(0.5)$ and this is analyzed with an error of three per cent, the calculation of $(\beta\omega)_i$ results in a value which has an error $h_{1,\beta\omega}$ = 5 per cent compared to the previously mentioned 12.5 per cent error of the same value.

It was mentioned in the previous paper that the concentrations of the phases were simultaneously determined at different heights of the packed absorber. These data were equally used in the calculations.

If the mean value of parameter sensitivity is calculated as follows

$$\overline{e_{1,1}} = \frac{1}{n} \sum_{i=1}^{n} |e_{1,1}(i)|$$

where i is the number of samples and similarly as above, the mean concentration is

$$\bar{x} = \frac{1}{n} \sum_{i=1}^{n} x(i)$$

and the error of the $(\overline{\beta\omega})_i$ calculation can be evaluated. E.g. taking the data of Fig. 5 where $\bar{x}$ = 0.531 and $\bar{y}$ = 0.866 and $\bar{e}_{1,1}$ = = 0.086, as well as $\bar{e}_{2,1}$ = 0.0125. If the calculation of $(\overline{\beta\omega})_i$ is

Table 3

B_L	B_G	$(\overline{\beta\omega})_i$	St_L	St_G	$e_{1,1}(0)$	$e_{2,1}(1)$	$h_{1,\beta\omega}$
(litres per hour)	(litres per hour)	(one per second)	(-)	(-)	(-)	(-)	(per cent)
100	6000	7.08×10^{-3}	4.08	4.51	0.037	-0.041	16
100	2000	3.81×10^{-3}	2.30	7.60	0.0035	-0.0116	120
50	8000	2.24×10^{-3}	2.70	1.12	0.0808	-0.0335	12.5

$h_{2,\beta\omega}$	$\overline{e_{1,1}}$	$\overline{e_{2,2}}$	x(o)	y(1)	$\bar{x}$	$\bar{y}$	$\overline{h_{1,\beta\omega}}$	$\overline{h_{2,\beta\omega}}$
2	0.015	0.023	0.797	0.117	0.388	0.547	19	17.5
5	0.0166	0.07	0.318	0.010	0.07	0.21	5.5	3.9
21	0.086	0.0125	0.885	0.64	0.531	0.866	10	73

based on the liquid concentration data and the analysis was carried out with an error of three per cent, the $(\overline{\beta\omega})_i$ value can be estimated with an error of ten per cent. The error is definitely higher, 73 per cent if the gas concentration data are the basis of the calculation.

The results of similar calculations of the other runs are listed in Table 3.

1.2. The Effect of Flow Rate Changes on the Solute Concentration of the Phases

It is assumed that in a given running condition of the absorption column the liquid feed rate is altered with Δv_L. Now the concentration change of the exit phases have to be estimated. The liquid feed rate change Δv_L causes a ΔSt_L change of the St_L number. The relative alteration of the liquid concentration can be calculated as follows:

$$\frac{\Delta x(o)}{x(o)} = e_{1,1}(o)\,\frac{\Delta St_L}{x(o)} = e_{1,1}(o)\,\frac{St_L}{x(o)}\,\frac{\Delta St_L}{St_L}$$

Using Fig. 6 the deviation of $\Delta x(o)$ can be determined. It is assumed that St_L changes with ten per cent:

$$\frac{\Delta x(o)}{x(o)} = 0.11\,\frac{2.7}{0.885} \cdot 0.1 = 0.0336$$

i.e. the liquid concentration changes with 3.36 per cent. If the flow rate of the liquid phase increases with ten per cent its concentration at the exit point of the column decreases with 3.4 per cent.

The data of an other run were processed, here the flow rates of the phases were B_L = 100 litres per hour and B_G = 6,000 litres per hour, and the error was 6.15 per cent.

The concentration of the gas phase depends on the liquid feed rate. Similar calculations can de used for the determination of the gas phase concentration change effected by the liquid load.

2. The Axial Dispersed Plug-Flow Model

The sensitivity data of liquid and gas phase concentrations are listed in Tables 1 and 2. These data depend on the parameters used in the A.D.P.F. model concept, and refer to the parameter values of the given run.

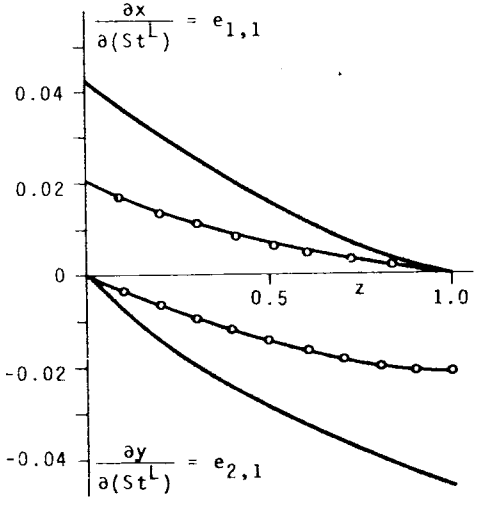

Fig. 7. The comparison between sensitivities calculated by the Piston Flow model and A.D.P.F. model.
B_L = 100 litres per hour;
B_G = 6,000 litres per hour;
—— P.F. model (St_L = 4.08)
-o- A.D.P.F. model (St_L = 5.96)

In Fig. 7 the sensitivity data $e_{1,1}$ and $e_{2,1}$ are presented, both the P.F., and A.D.P.F. models were used in the calculations of these data. (The characteristic phase flow rates of the run were B_L = = 100 litres per hour and B_G = 6,000 litres per hour).

It can be seen from the data that the A.D.P.F. model is less sensible if the St number changes, i.e. the transfer coefficient calculated by the A.D.P.F. model is less accurate.

The sensitivity data listed in the above mentioned Tables are dimensionless. In this case the sensitivity data are related to the real parameters which

are not dimensionless. E.g. the dimensionless sensitivity of the liquid concentration at locus z = 1 is as follows (c.f. Table 2):

$$E_{1,(\beta\omega)_D}(1) = \left.\frac{dx}{d(\beta\omega)_D}\right|_{z=1} \frac{(\beta\omega)_D}{x(1)} = 0.661$$

The $(\beta\omega)_D$ value in the given case is 5.82×10^{-3} (sec^{-1}) and x(1) = = 0.086, the sensitivity is:

$$e_{1,(\beta\omega)_D} = \left.\frac{dx}{d(\beta\omega)_D}\right|_{z=1} = 0.661 \cdot \frac{0.086}{5.82\times10^{-3}} = 9.75 \text{ sec}$$

Similarly to the method discussed concerning the P.F. model, the data of the above mentioned Table can be used for the evaluation of the calculation accuracy.

2.1. The Estimation of the Error Caused in the Determination of Transfer Coefficient

It is assumed that the absorption column is working, and the characteristic parameters are those listed in Table 2. The flow rates and concentrations of the inlet phases are known. The concentration of the outlet liquid is analyzed. This analysis can be carried out with an error of three per cent, i.e. $\Delta x/x(o) = 0.03$. Knowing the sensitivity, the error caused in the calculation of $(\beta\omega)_D$ is:

$$E_{1,(\beta\omega)_D}(0) = 0.082$$

and

$$\frac{\Delta(\beta\omega)_D}{(\beta\omega)_D} = \frac{0.03}{0.082} = 0.366$$

The three per cent error in the determination of the liquid concentration gives an error of 36.6 per cent in the calculation of $(\beta\omega)_D$.

The data listed in the mentioned Table show that $|E_{2,(\beta\omega)_D}| > |E_{1,(\beta\omega)_D}|$ and therefore it is advantageous to base the $(\beta\omega)_D$ calculations on the gas phase concentration data, in the latter case the error is less (29 per cent).

The knowledge of the sensitivity is useful in the different fields of the practical work, e.g. the efficiency of the absorption column can be calculated. It is assumed that the packing of the column is exchanged and another is used which has greater specific surface area, so the $(\beta\omega)_D$ is increased by ten per cent. If the other parameters remain constant, so:

$$\left.\frac{\Delta x}{x}\right|_{z=0} = E_{1,\beta\omega}(0) \cdot 0.1 = 0.082 \cdot 0.1 = 0.08$$

and

$$\left.\frac{\Delta y}{y}\right|_{z=1} = E_{2,\beta\omega}(1) \cdot 0.1 = -0.104 \cdot 0.1 = -0.01$$

consequently, the ten per cent increase in the packing surface area gives only one per cent growth in the column efficiency.

2.2. The Practical Application of the Sensitivity Concept Based on the Mixing Coefficients

The sensitivity data based on the mixing coefficients are also listed in Tables 1 and 2.

It can be seen that the sensitivity data valid at the given parameters change their values with one or two orders of magnitude along the length of the packed column. This refers to the fact that the concentration changes differently along the column due to the mixing. The greatest values of the sensitivity data in the mentioned Tables are those which are valid at locus z=1. In the circumstances given in Table 2, the mixing coefficient of the liquid has a marked influence on the concentration of the exit gas and the effect of the gas mixing coefficient is low. Regarding the data listed in Table 1 the same conclusion can be drawn for the concentration of the exit gas.

Similarly to the above discussed method, the mixing coefficients can be applied for different valuations of the column. These are not discussed here in detail. It is merely mentioned that if the values of the mixing coefficients have to be calculated with the data listed in Table 3 and with the data of the concentration determinations, and the analysis can be carried out with an error of one per cent (at locus z = 0), the results will be ± 0.8 times the liquid mixing coefficient value and ± 2.5 times the gas mixing coefficient value. It is evident that the determination of these data has to be carried out with other methods, e.g. the examination of the residence time distribution can be used.

The data in Tables 1 and 2 show equally that the Pe numbers are high, i.e. the coefficient of the second order differential quotient containing term of the A.D.P.F. model is higher compared to the coefficients of the other terms. If the term of the axial mixing is neglected, the error of the concentration values has to be valuated. (The other parameters are unchanged.) This valuation can be carried out with the data presented in Table 1. The dimensionless sensitivity values related to the converse of Pe numbers were calculated at locus z = 0:

$$E_{1,1/Pe_L}(0) = \frac{\partial x}{\partial(1/Pe_L)}_{z=0} \frac{1/Pe_L}{x(0)} = 0.013;$$

$$E_{1,1/Pe_G}(0) = 0.004; \quad E_{2,1/Pe_L}(1) = 0.228; \quad E_{2,1/Pe_G}(1) = 0.036$$

The alteration of the concentration can be expressed as follows:

$$\Delta x = x\left[\frac{1/Pe_L}{x} \frac{\partial x}{\partial(1/Pe_L)} + \frac{1/Pe_G}{x} \frac{\partial x}{\partial(1/Pe_G)}\right] \qquad (4)$$

and

$$\Delta y = y\left[\frac{1/Pe_L}{y} \frac{\partial y}{\partial(1/Pe_L)} + \frac{1/Pe_G}{y} \frac{\partial y}{\partial(1/Pe_G)}\right] \qquad (5)$$

It is assumed that D_L and D_G are zero, i.e. $Pe_L = Pe_G = \infty$, so the Piston Flow model is valid. In this case:

$$\Delta(1/Pe_L) = 1/Pe_L$$

$$\Delta(1/Pe_G) = 1/Pe_G$$

and using Eq. (4) and (5):

$$\Delta x(0) = 0.819 \cdot (0.013 + 0.004) = 0.014$$

and

$$\Delta y(1) = 0.098 \cdot (0.228 + 0.036) = 0.026$$

and the mean value is:

$$(\Delta c)_i - (\Delta c)_D = \frac{\Delta x(0) + \Delta y(1)}{2} = 0.02$$

The results of the above calculation show that the deviation between the concentrations calculated by the use of the A.D.P.F. and P.F. models is in agreement with the previous experience [1].

SYMBOLS USED

$e_{j,i}$ parameter sensitivity

p parameter

z co-ordinate of locus (dimensionless)

$E_{j,i}$ parameter sensitivity (dimensionless)

v linear flow rate of the phase (metres per second)

$(\beta\omega)_i$ transfer coefficient related to unit volume and based on the Piston Flow model (one per second)

$(\beta\omega)_D$ transfer coefficient related to unit volume and based on the Axial Dispersed Plug Flow model (one per second)

$(\beta\omega)$ transfer coefficient related to unit volume (one per second)

x concentration of the liquid phase (dimensionless)

y concentration of the gas phase (dimensionless)

St Stanton number (dimensionless)

Pe Peclet number (dimensionless)

D	axial mixing coefficient
B	feed rate (litres per hour)
h	relative error (dimensionless)
Δc	deviation of the concentrations (dimensionless)

Indices

D	A.D.P.F. model
L	liquid phase
G	gas phase
i	P.F. model

REFERENCES

1. ÁRVA, P., SZEIFERT, F., J. Hung. Ind. Chem. 1, 271 (1973)

2. ÁRVA, P., SZEIFERT, F., J. Hung. Ind. Chem. 1, 379 (1973)

РЕЗЮМЕ

На основании данных, полученных с использованием ранее опубликованных экспериментальных методов, авторы показывают методы определений численных значений и практическое применение параметрической чуствительности.

На основании модели идеального вытеснения рассчитывалась концентрационная чувствительность для жидкой и газовой фаз по коэффициенту массопередачи, приходящемуся на единицу объема, и по скоростям фазовых потоков. Авторы указывают способ расчета ошибки, которая допускается при определении параметров вследствие ошибки измерения концентрации. Значения параметрической чувствительности используют для оценки влияния тех изменений, которые происходят в режиме работы абсорбционных установок.

Кроме того, авторы приводят численные значения произведенных на основании диффузионной модели расчетов чувствительности по коэффициенту массопередачи и по коэффициенту перемешивания внутри фаз, а также расчетов приближенного значения ошибки, допущенной в вычислениях указанных величин. В условиях проведенного эксперимента данные о чувствительности по коэффициентам перемешивания дали возможность сравнить модель идеального вытеснения с диффузионной моделью.

Hungarian Journal
of Industrial Chemistry
Veszprém
Vol.1. pp. 443-452 (1973)

OLIGOMERIZATION OF SILICATE ANIONS IN PORTLAND CEMENT HYDRATION*

F. TAMÁS

(Research Group for Silicate Chemistry, Veszprém
University of Chemical Engineering)

Received: March 25, 1973.

According to the classic theory of cement hardening, the strength of hardened cement is carried by non-chemical bonds. In this paper the importance of chemical bond formation during cement hardening is emphasized. In this process corner sharing (bridging) common oxygen ions serve as a bond between adjacent SiO_4-tetrahedra. From this point, cement hardening resembles the hardening of plastics: both processes can be described as polymerization reactions with the difference that -C-C-C-C- and Si-O-Si-O-Si- chains (or rings, and sheets etc.) are formed in the latter and former case, respectively. However, as the degree of polymerization in cements is low in contrast to plastics,the term "oligomerization" is suggested. The possible confirmation of the proposed theory and some practical results are outlined.

INTRODUCTION

Building materials can be classified by various principles: e.g. according to their resistance against the attack of water and behaviour to water during hardening (hydraulic and non-hydraulic binders): the system of SYČEV [1] classifies binders according to the process taking place during hardening and consequently divides binders into three classes: hardening by chemical processes (e.g. plastics, and water-glass binders); hardening by physico-chemical

*Presented at the 2nd International Symposium on Science and Research in Silicate Chemistry, Brno, 1972 September.

processes (e.g. portland cement or plaster of Paris);and hardening by physical processes (e.g. the initial period in the hardening of slaked lime).

A further basis of classification might be structural, according to the principal bond type. It is well known that the forces which bond the atoms or molecules of substances can be subdivided into two classes: chemical forces (ionic and covalent bonds) and non-chemical forces (van der Waals bonds, and hydrogen bonds). (The third type of bonding, namely the metallic bond can be disregarded from the point of this study).

Chemical forces are strong, their energy being some hundred kcal/mol.; non-chemical forces are all weak, the van der Waals forces are very weak, while hydrogen bonds somewhat stronger - as a fair approximation, the energy of non-chemical forces can be considered as being 10 kcal/mol.

In the development of the gross strength of a given substance the resultant joint effect of these forces should be taken into consideration: there may be high forces in one direction and the resultant strength is still low if the bonding forces are weak in an another direction: e.g. in the layer structure of orthoboric acid, H_3BO_3 strong chemical bonds exist within the layers, but the separate layers are bonded by van der Waals forces to each another. This is mirrored by the fact that crystals of H_3BO_3 can easily be pulled apart (cleaved) in a direction parallel to the layers.

Among binding materials, water-glass and phosphate base putties and plastics are characterized by the presence of mainly chemical bonds;on the other hand, the strength of plaster of Paris is supplied by the adhesion (i.e. non-chemical bond) developed between the felted gypsum crystals. In the view of POWERS [2] and BRUNAUER [3] non-chemical bonds are responsible for the strength of portland cement, the most important binder also, produced in vast quantities.

However, parallelities exist between the properties and structure of plastics and hardened portland cement, which justify a comparative study between the two groups of materials.

The most important element is C in plastics and Si in portland cement. Although both elements are tetravalent and in the same column of the periodic table, which would indicate similar chemical behaviour, some differences still exist. The most important difference is that no d orbitals exist in the valency shell (n = 2) of the carbon atom, but its ability to form π-bonds is responsible for most of the chemical properties of carbon. Si belongs to the next period (n = 3); silicon possesses d orbitals, but π-bonds do not exist. This is why most of the compounds of corresponding formula differ so characteristically in properties. A striking example: CO_2 and SiO_2. Carbon dioxide is composed of discrete molecules, containing C-atoms of digonal symmetry. However, the strong chemical bonding within the CO_2 molecule is useless, because the intermolecular bonding consists of weak forces. Therefore the thermal energy at $-78^{\circ}C$ supplies the separation of the molecules of solid CO_2, and it occurs as a gas at ordinary temperatures. SiO_2 on the other hand, is a solid of high strength and high refractoriness (m.p. = $1700^{\circ}C$). But SiO_2 contains Si atoms of tetrahedral symmetry, which form an infinite network in all the three dimensions of space; the Si atoms are linked through O-atoms shared always by two Si atoms, so finally the entire quartz crystal is one molecule, its formula being $SiO_{4/2}^{\infty\infty\infty}$. There is no difference between intramolecular and intermolecular bonds in quartz: the entire crystal is held together by strong chemical bonds.

However, the ability to form long chains by polymerization is common with C and Si, though the nature of the chains differ. Carboniferous chains are of -C-C-C-C- formula, but -Si-Si-Si-Si- chains do not exist in silicates: the bonding energy of Si-Si is too low (42 kcal/mol. as contrasted to the 83 kcal/mol. energy of the C-C bond); the Si-O bond on the other hand is strong (124 kcal/mol., the corresponding C-O bond being only 85 kcal/mol.). This suggests the possibility of the formation of stable, strong -Si-O-Si-O-Si-O- chains and its derivatives (double chains, rings, layers, and frameworks, etc.).

Formation of Bridging Oxygen Ions as Strength Carriers

In the formation of Si-O-Si chains, etc., the O-ions of the SiO_4^{4-} tetrahedra receive their energetically advantageous octett shell by utilizing their "internal" reserves: by the formation of bridging oxygen ions, belonging to two Si-ions simultaneously. So a common electron shell of octett symmetry surround the Si-O-Si complex. A stable octett, on the other hand can also be formed by "external help": by metal cations incorporated into the structure, which act as electron donors thus completing the electron-deficient shell. These incorporated ions however interrupt the continuity of the -Si-O-Si- chain, and thus decrease the strength.

A certain amount of energy is needed to break the -Si-O-Si-O- chain. In our view this is done during the burning of clinker (in this study formation of nonsilicate minerals during clinker burning is disregarded): the continuity of -Si-O-Si- chains in natural silicate polymers, e.g. quartz, is interrupted and Ca-ions are incorporated into the structure. The energy needed for this process is transmitted in the kiln. The resulting minerals are no longer polymers: C_2S* and C_3S both contain isolated, i.e. monomeric SiO_4-tetrahedra, as proved by X-ray diffraction. (Formerly O'DANIEL and HELLNER [4], proposed a structure of C_3S which would contain Si_3O_9 trimer rings; but careful later work, mainly by JEFFERY [5] also confirmed the presence of isolated, monomeric SiO_4 tetrahedra in C_3S).

During the reaction of C_2S and C_3S with water the Ca-ions incorporated into the silicate by external energy are expelled from the structure and precipitated as CaO or more correctly $Ca(OH)_2$. This means that the octett-shell, maintained by "external help", i.e. electron donor cations will be replaced by an internal octett shell of bridging O-ions again, and the energy, invested during clinker burning will be regained. This is one of the preconditions for the formation of a stable hardened cement, as only

*Cement chemical notation system is used, together with the conventional system. C = CaO, S = SiO_2.

processes where the free energy is decreased can proceed without external excitation.

The stoichiometry of the hydration reactions, according to BRUNAUER and co-workers [6] in the case of C_3S:

$$2\ Ca_3SiO_5 + 6\ H_2O \rightarrow Ca_3Si_2O_7.3\ H_2O + 3\ Ca(OH)_2$$

and in the case of C_2S

$$2\ Ca_2SiO_4 + 4\ H_2O \rightarrow Ca_{3.3}Si_2O_{7.3}.3.3\ H_2O + 0.7\ Ca(OH)_2$$

The product is very poorly crystalline, whose structure resembles to that of natural tobermorite. Its Ca/Si ratio may vary over a wide range; but this is always lower than in the parent product, being about 1.5 instead of 3.0 in case of C_3S and about 1.65 instead of 2 in case of C_2S.

These phenomena can be well interpreted by the polymerization (or, more correctly, oligomerization, as only products of limited chain lengths are formed) of the monomer C_2S and C_3S. The essence of the reactions in both cases consists of the disproportionation of O-ions:

$$2\ O^- \rightarrow O^0 + O^{2-}$$

where O^- represents O-ions held by Si on one side only (e.g. one of the O-ions in C_2S); O^0 represents an O-ion held by Si on both sides (i.e. a bridging O-ion); and O^{2-} is an O-ion where both valencies are neutralized by a cation.

In our special case, the first equation by Brunauer can be interpreted in such a way that C_2S is dimerized, one of its 8 O^- ions is degraded to O^0; and this counteracted by the formation of one O^{2-}, which latter is bonded to the expelled Ca-ion. Dimerization means that a two-link chain is formed:

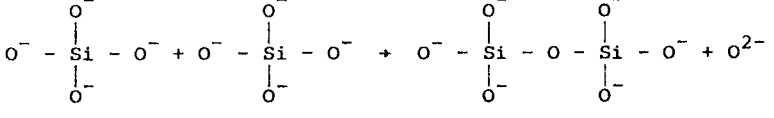

Obviously polymerization may proceed further on, longer chains, and by their linkage, rings, sheets, and space frameworks

may develop. In well-crystallized substances definite complexes are present: e.g. $K_2O.2\ PbO.2\ SiO_2$ is purely dimer, its correct formula being $K_2Pb_2Si_2O_7$ (NÁRAY-SZABÓ and KÁLMÁN [7]). In amorphous or ill.crystallized products, on the other hand (as e.g. in silicate glass, and hydrated portland cement), the concept of equilibria between various complexes of different degrees of polymerization is of utmost importance. The theory of these equilibria is well established for silicate glass (BALTĂ and BALTĂ [8], MASSON [9]), but the concept is similar for hardened portland cement, where C_2S (or C_3S), containing isolated SiO_4 tetrahedra are the monomers, and these become oligomerized during hardening. The process itself resembles the hardening of plastics, e.g. where poly(vinyl chloride):

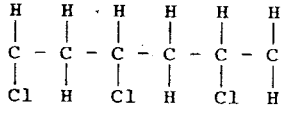

is formed by the polymerization of the monomer vinyl chloride, $CH_2{=}CHCl$.

As stated earlier, complexes of different polymerization degree exist in amorphous or ill-crystallized silicates. The average degree of polymerization can be characterized by:

$$p = \frac{\sum_{x=1}^{\infty} f_x n_x}{2\ n_M}$$

where x is the number of units (in the case of silicates, the number of the SiO_4 groups) in the complex, f_x is the number of linkages (in our case the number of bridging O-ions), n_x is the number of the x-membered complexes, while n_M in the denominator is the number of the monomer mols. Index p may vary between 0 and 1, the first limit being the absence of polymerization, the second complete polymerization into one giant molecule. The summation in the numerator indicates clearly that the formula always gives an average. Thus, from Brunauer's stoichiometry one may think that the hydrate resulting from C_3S is purely dimer, with p = 0.25; but

the same Ca/Si ratio of 1.5 and consequently p = 0.25 may come e.g. also from the equilibrium of 40 % still monomeric and 60 % hexameric complexes.

The following changes occur during the polymerization of C_2S while p changes from 0 to 1:

1. The molecular weight of the complex increases from 172 to ∞.

2. The O/Si ratio changes from 4 to 2.

3. The Ca/Si ratio changes from 2 to 0.

However, the process of polymerization is discontinued after a time, the limit being approx. p = 0.35 or slightly beyond.

The SiOSiOSiO chain, formed during this polymerization is one of the principal conditions to develop the strength of cement. A second important condition is the cross-linkage of these chains, because the linear polymer molecules (linear here obviously means unbranched, not cross-linked complex, with a zig-zag axis, corresponding to the 140° valency angle of the SiOSi bond) could be easily pulled apart by external load along the weak intermolecular bonds, similarly to H_3BO_3, examined earlier.

Possible Proofs of the Theory

1. The direct determination of the mean molecular weight, e.g. by cryoscopic methods, in a suitable solvent. C_2S and most of its hydration products are soluble in acids; but at the same time an instantaneous condensation may take place which, in turn, means that the original anionic structure is not preserved. E.g. the orthosilicic acid may condensate according to the formula below:

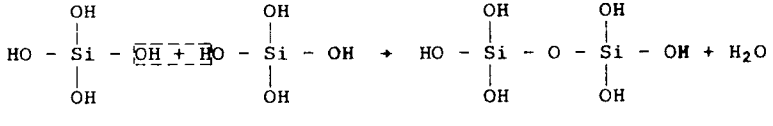

to pyrosilicic acid or even beyond, finally $SiO_2 \cdot n\ H_2O$ will form. The danger of instantaneous condensation can be reduced by using

weak acids and a low temperature dissolution. Obviously a compromise should be sought, because these measures slow down the dissolution process, which brings the same danger again. The use of organic acids of known molar melting point depression is recommended.

2. Instead of molecular weight determination a corresponding property may be examined, e.g. the reactivity of the solution. WIEKER and associates [10] have shown that the reaction rate between silicic acids and molybdate solutions depends on the anionic structure of the silicic acid. The concentration of the product silicomolybdate can easily be measured photometrically. By this method, not only the molecular weight, but also the shape (linear, or ring, etc.) of the molecules can be determined (by calibration with substances of known structures). However, an important limitation: obviously only in cases of a uniform structure. Using a mixture of silicic acids of different molecular size an average value will be obtained.By this method the gradual decrease of the reactivity, i.e. an increase of its molecular weight of the liberated silicic acids as a function of hydration time has been verified [11].

3. The silicic acids, described in the previous paragraph can be separated by paper chromatography [10], thus the individual factors of the average can be studied.

4. The instantaneous condensation mentioned under 1. can be eliminated according to the proposal of LENTZ [12] in such a way that acid dissolution is ensured in the presence of silylating agents, e.g. trimethyl chlorosilane. In this case the original anionic structure remains intact, because the reactive OH or H groups at the end are blocked by the Me_3Si-radical (Me = methyl). E.g. the trimethyl silyl derivative of the orthosilicic acid:

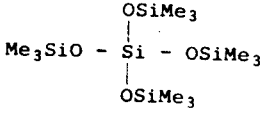

is not capable of instantaneous polymerization, because of the absence of the reactive end groups. The molecular weight or a functional property (e.g. refractive index) of the end-blocked solution can be measured. This method also gives an average only.

5. The end-blocked silicic acid solution can also be separated, e.g. by gas chromatography [12] or by mass spectrometry [13].

6. The proceeding of polymerization can also be determined by indirect methods. For example, by measuring the change in the Ca/Si ratio during hardening (obviously after the selective dissolution of the free lime) Brunauer proved the decrease of this ratio during proceeding hydration. This result accords with the suggested polymerization mechanism of hardening, although Brunauer interprets his results by a different approach.

The formation of cross-links, mentioned earlier, takes place instantaneously during the hardening of silicate cements. The factors influencing the increase of the polymerization degree and cross-linked framework formation are not yet known, although their knowledge would constitute a milestone towards stronger, higher quality binders. An analog example from the history of organic polymers: the technical significance of latex, which contains linear chains of poly(isoprene) is negligible, while cross-linked poly(isoprene) is the polymer, manufactured and utilized in vast quantities: rubber.

By this analogue we endeavoured to affect the hydration of cement so as to produce, in addition to Si - O - Si bonds, cross-linked Si - S - Si bonds too. This can be achieved, e.g. by the addition of compounds containing active sulphur ($SOCl_2$, S_2Cl_2) in such a way that its incorporation into the structure should outpace its decomposition by water. Final strength of cement pastes and concretes produced by this patented method [14] may increase by 40-60 % in contrast to the untreated cement; a further advantage being that the hardening of concrete can be effectively accelerated by steam curing without a loss in final strength.

The endeavour to develop and prove the polymerization mechanism of cement hardening is also significant from a side point: mathematical methods, some practical results, even measurement techniques of the highly advanced theory of organic polymers might be adapted. This will certainly reduce the extent of the fundamental and methodological research needed. Improved knowledge of the

hardening process of cement will constitute a basis for the planned development of new types of cements, having predetermined, controlled properties that are significantly higher than at the present time.

REFERENCES

1. SYČEV, M.M., Silikattechnik 21, 295 (1970)
2. POWERS, T.C., J. Amer. Ceram. Soc. 41, 1 (1958)
3. BRUNAUER, S., Proc. 8th Conf. Silicate Ind. Budapest, p. 205.
4. O'DANIEL, H., HELLNER, E., N. Jahrbuch Miner., (1950) p. 108.
5. JEFFERY, J.W., 3. Symp. Chemistry of Cements, London, 1952.p.30.
6. BRUNAUER, S., COPELAND, L.E., BRAGG, R.H., J. Phys. Chem. 60, 116 (1956)
7. NÁRAY-SZABÓ, I., KÁLMÁN, A., Proc. 6th Conf. Silicate Ind. Budapest, 1963, p. 329.
8. BALTĂ, P., BALTĂ, E., Építőanyag 24, 229 (1972)
9. MASSON, C.R., J. Amer. Ceram. Soc. 51, 134 (1968)
10. WIEKER, W., Építőanyag 24, 188 (1972)
11. TAMÁS, F., FÁBRY, M., Építőanyag 25, 212 (1973)
12. LENTZ, C.W., Inorganic Chemistry 3, 574 (1964)
13. WU, F.F.H., GÖTZ, J., JAMIESON, W.O., MASSON, C.R., J. Chromatography 48, 515 (1970)
14. TAMÁS, F., Method for Increasing the Strength of Cementitious Products. Hung. Patent No. 162 321

РЕЗЮМЕ

Согласно классической теории твердения цемента прочность затвердевшего цемента обусловливают нехимические связи. В этой статье автор обращает внимание на тот факт, что в процессе твердения цемента важную роль играет также и образование химических связей. В данном процессе общие мостовые кислородные ионы обеспечивают связь между тетраэдрами SiO_4, соединяя вершины многогранников. В таком смысле твердение цемента подобно твердению пластмасс с той лишь разницей, что в последнем случае образуются цепи C-C-C-C, а в первом - цепи (и затем, при дальнейшей полимеризации, кольца, слои и т.д.) Si-O-Si-O. Однако, ввиду того, что при твердении цемента имеет место полимеризация значительно меньшей степени, чем в случае пластмасс, автор предлагает использовать здесь понятие "олигомеризации". Данная статья знакомит также с возможностями доказательства предлагаемой теории и представляет практически важные выводы.

Hungarian Journal
of Industrial Chemistry
Veszprém
Vol.1. pp. 453-462 (1973)

STUDIES ON HOMOGENEOUS OLEFIN DISPROPORTIONATION CATALYSTS

L. BENCZE, Á. RÉDEY and L. MARKÓ

(Department of Organic Chemistry, Veszprém University of Chemical Engineering)

Received: August 22, 1973.

Carbon monoxide increases the activity of catalysts composed of tungsten and molybdenum halide complexes and $EtAlCl_2$ for the disproportionation of olefins. Hexacarbonyls as final products and halo carbonyls as intermediates were isolated from the reaction mixtures.

INTRODUCTION

The disproportionation of olefins has undergone a very fast but contradictory development during the last 12 years since the first patent application. The heterogeneous propylene disproportionation is already at present an industrial process, while the disproportionation of longer chain olefins will still remain at the level of laboratory experiments for probably a long time, because of the simultaneous double bond isomerization leading to a low selectivity of the reaction. An increase of catalyst selectivity by the blocking of acidic centres is accompanied with a rapid decrease in activity [1, 2].

The development of the homogeneous catalytic process seems to be somewhat faster; the disproportionation of terminal and internal olefins has been achieved in the last few years [3, 4, 5]. Numerous new catalytic combinations and metals (Ti, Rh, Fe, Co,

etc.) [6, 7] have been reported, in addition to those based on molybdenum and tungsten which were applied from the beginning. However, although a large number of active catalysts are already known, only a few investigations on the catalytic mechanism have so far been reported.

Following the first successful disproportionation experiments a trans alkylidenation mechanism was proposed for propylene disproportionation

$$\begin{matrix} CH_3 - CH = CH_2 \\ CH_3 - CH = CH_2 \end{matrix} \rightleftharpoons \begin{matrix} CH_3 - CH \\ \| \\ CH_3 - CH \end{matrix} + \begin{matrix} CH_2 \\ \| \\ CH_2 \end{matrix} \qquad (1)$$

This general scheme was confirmed by the disproportionation of 2-propene-^{14}C [9]. However, it still remained a problem, that the "quasi cyclobutane intermediate" state proposed for this reaction requires thermaly forbidden electron transitions according to the HOFFMAN–WOODWARD rule [10]. This problem could be solved by the assumption that since the trans alkylidenation has to take place partly or entirely within the co-ordination sphere of the transition metal, the d orbitals of the transition metal also have to be considered in these calculations. The Hoffman–Woodward rule extended in this sense was found to be applicable for the disproportionation of olefins: the process can be described by the combination of the d orbitals of one transition metal and the pi orbitals of two olefins [11].

The homogeneous catalysts used for the disproportionation of olefins are generally composed of a transition metal compound (such as WCl_6) and a cocatalyst such as $EtAlCl_2$ or BuLi [12]. The cocatalyst probably functions partly to produce free co-ordination sites which can be used by the olefin molecules and partly to maintain the necessary electron concentration for the reaction. According to the proposed mechanism, at least two co-ordination sites are required on the transition metal. The experimental observations that disproportionating activity is shown by catalyst combinations with an Al(Li)/W(Mo) ratio of ≥ 2 are in accordance with this theory.

Very little is known about the formation of the catalytically active species. Suggestions for this process were first made by MENAPACE et al. [12] for the two component WCl_6 + BuLi catalyst system:

$$W^{VI}Cl_6 + 2\ R^-Li^+ \longrightarrow W^{IV}R_2Cl_4 + 2\ LiCl \qquad (2)$$

$$\begin{array}{l} W^{IV}R_2Cl_4 \xrightarrow{-2\ R^\cdot} W^{IV}Cl \\ \qquad\qquad\qquad\quad \Big\Updownarrow 2\ \text{olefin} \\ \qquad\quad \Big\downarrow \xrightarrow[-2\ R^\cdot]{2\ \text{olefin}} W^{IV}(\text{olefin})_2Cl_4 \end{array} \qquad (3)$$

$$W^{IV}(\text{olefin})_2Cl_4 \rightleftharpoons W^{IV}Cl_4 + \text{products} \qquad (4)$$

$$\Big\uparrow \text{2 new olefin} \Big\downarrow$$

According to the schema above, the free co-ordination sites are formed by the decomposition of dialkyltungsten tetrachloride. Following this the trans alkylidenation takes place by an intramolecular transformation of the bis olefin complex. Some suggestions were made regarding the oxidation and co-ordination states of the transition metal in Equations (2)-(4), but no experimental proof was presented. The experiments described in this paper were directed towards the isolation of stable derivatives of these intermediates to elucidate some steps of the disproportionation mechanism.

RESULTS AND DISCUSSION

For all experiments cis,trans-2-pentene was chosen as model olefin. Using CALDERON's WCl_6 + EtOH + $EtAlCl_2$ catalyst it was observed that this was very sensitive to air and moisture, whereas Ar, N_2, H_2 or CO and small quantities of PPh_3 or pyridine did not alter its activity appreaciably and CO even increased its selec-

tavity [13]. It was, therefore, concluded that CO, phosphines and pyridine may function as ligands of the transition metal in these catalytic systems.

In order to eliminate the moisture sensitive WCl_6 at first Mo and W compounds were sought that were not sensitive to air and which combined with $AlEtCl_2$ would give active disproportionation catalysts. When 2-pentene was added to the benzene solution of a $AlEtCl_2$ and a ML_2Cl_4 type compound (where L = Py, PPh_3 or 1/2 $C_2H_4(PPh_2)_2$; M = Mo or W) the olefin was consumed by a Friedel--Crafts type reaction for the alkylation of benzene in a few minutes and the disproportionation reaction could not be studied under such conditions [14]. However, using chloro benzene as a solvent (which is more difficult to alkylate than benzene), a homogeneous master solution could be prepared which had the desired disproportionating catalytic activity and was not disturbed by the alkylation of the aromatic ring. The activity of these catalysts significantly increased under CO and approached that of the CALDERON system [15].

Investigating the WPy_2Cl_4 + $EtAlCl_2$ + 2-pentene + chloro benzene reaction mixture by IR spectroscopy, a very strong, sharp absorption band could be observed at 1980 cm^{-1} in addition to some smaller peaks in the ν_{CO} range. This strong band indicated the presence of $W(CO)_6$ which was proved by the subsequent isolation of $W(CO)_6$ from these reaction mixtures. The yield of $W(CO)_6$ reached about 30 per cent and thus surpassed the yield of some of the previously known high pressure syntheses.

By comparing the $W(CO)_6$ content and the catalytic activity of catalyst master solutions (Fig.1) it was shown that an increase of $W(CO)_6$ leads to a decrease of activity. The increase of catalytic activity under carbon monoxide could not, therefore, be attributed to the $W(CO)_6$ formed in the reaction mixture,but to tungsten derivatives having oxidation states between IV and O. It was assumed that the formation of the free sites necessary for co-ordination of olefin (in the catalytic reaction) or carbon monoxide (in metal carbonyl formation) to the metal atom is a result of alkylation (5) and the subsequent decomposition of metal alkyls (6):

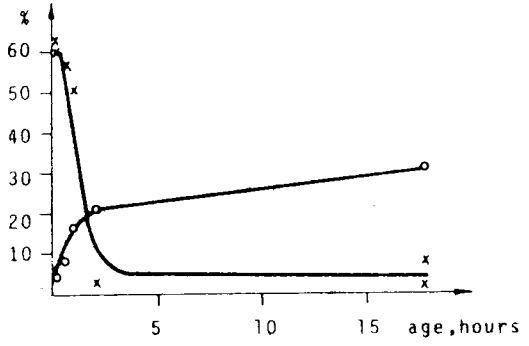

Fig.1. Yield of $W(CO)_6$ and disproportionation activity as functions of the age of the catalyst master solution. o - yield of $W(CO)_6$; x - conversion of 2-pentene in 3 minutes reaction time

$$ML_2Cl_4 + 2\ EtAlCl_2 \rightarrow MEt_2L_2Cl_2 + AlCl_3 \qquad (5)$$

$$MEt_2L_2Cl_2 \xrightarrow{\text{solvent (S)}} ML_2Cl_2S_n + 2\ Et^{\cdot} \qquad (6)$$

These free co-ordination sites can then be occupied either by olefins:

$$ML_2Cl_2S_n + 2\ \text{olefin} \rightleftharpoons ML_2(\text{olefin})_2Cl_2 + n\ S \qquad (7)$$

or by carbon monoxide:

$$ML_2Cl_2S_n + 2\ CO \rightleftharpoons ML_2(CO)_2Cl_2 + n\ S \qquad (8)$$

If olefin and CO is also present at the same time the following equilibrium must be taken into account:

$$ML_2(\text{olefin})_2Cl_2 + 2\ CO \rightleftharpoons ML_2(CO)_2Cl_2 + 2\ \text{olefin} \qquad (9)$$

Such types of VIb metal-halo-carbonyls are already known. Some of these derivatives (like L = PPh_3) are "CO carriers" [16]:

$$M(PPh_3)_2(CO)_2Cl_2 + CO \rightleftharpoons M(PPh_3)_2(CO)_3Cl_2 \qquad (10)$$

To confirm the probability of the above reactions $ML_2(CO)_2Cl_2$ or rather $ML_2(CO)_3Cl_2$ type complexes had to be detected during the disproportionation reaction carried out under carbon monoxide. Although the formation of such compounds was observed in the WPy_2Cl_4 containing systems, their isolation in a pure state failed. Efforts were more successful in the case of the catalyst composed of $Mo(PPh_3)_2Cl_4$ and $AlEtCl_2$:

$$Mo(PPh_3)_2Cl_4 + 2\ EtAlCl_2 \xrightarrow[\text{olefin, solvent}]{CO} Mo(PPh_3)_2(CO)_3Cl_2 \quad (11)$$

The isolation of these complexes supports the assumption that the active catalyst combination contains a low (but not 0) oxidation state transition metal atom having available co-ordination sites. However, the formation of free co-ordination sites does not require the presence of olefins, since the appropriate halo carbonyl complexes can also be prepared from the CO-treated catalyst master solutions in the absence of olefin with good yield.

The halo molybdenum and tungsten carbonyls were prepared previously only by the oxidative transformation of the corresponding carbonyls. Our qualitative observations have been developed to a preparative method which enables the preparation of halo carbonyls by reductive carbonylation with 30-35 per cent yields.

Based on these results, the method described above was also applied in the study of the highly active catalysts derived from $WOCl_4$ or WCl_6 and $AlEtCl_2$ at a molar ratio of W/Al = 1/4. The formation of intermediate unsubstituted halo carbonyls and $W(CO)_6$ was also observed here. $W(CO)_4Cl_2$ was isolated from these reaction mixtures in the form of its stable triphenylphosphine derivative $W(PPh_3)_2(CO)_3Cl_2$. Molybdenum halides reacted similarly [17].

As a matter of fact, all of these results confirm the Menapaces hypothesis and complete it by the reactions occurring under CO atmosphere:

$$W(olefin)_2Cl_4 \xrightarrow[olefin]{CO} W(CO)_2Cl_4 \xrightarrow{PPh_3} W(PPh_3)_2Cl_4 \quad (12)$$

$$W(CO)_2Cl_4 \xrightarrow[olefin]{EtAlCl_2} W(CO)_2(olefin)_2Cl_2 \qquad (13)$$

$$\uparrow\downarrow +CO \quad -olefin$$

$$W(CO)_6 \xleftarrow[CO]{EtAlCl_2} W(CO)_4Cl_2 \xrightarrow[acetone]{PPh_3} W(PPh_3)_2(CO)_3Cl_2 + CO$$

Carbon monoxide is generally known as a catalyst poison and behaves here similarly: it expels the olefins from the catalyst. Despite this the rate of disproportionation is increased in its presence, which suggests the $M(PPh_3)_2(CO)_nCl_2$ (n = 2, 3) type compounds ("the poisoned catalysts") formed in these reaction mixtures are also good catalysts in combination with $EtAlCl_2$ or $AlCl_3$. This assumption was confirmed experimentally: the mixtures of $ML_2(CO)_nCl_2$ (where L = PPh_3 or $AsPh_3$ and M = Mo or W) and $EtAlCl_2$ or $AlCl_3$ (Al/M = 4/1) in chlorobenzene solvent catalyzed the disproportionation of 2-pentene present in a 2-500 fold excess of the equilibrium olefin mixture within 3-5 min [18].

EXPERIMENTAL

General. All manipulations were carried out under Ar or CO at room temperature. Hexane, benzene and cis, trans-2-pentene (Fluka) were distilled from K-Na alloy, chlorobenzene and methylene chloride (Reanal) from phosphorous pentoxide before use. All were stored under Ar.

Molybdenum and tungsten complexes were prepared from purum WCl_6 and $MoCl_5$ (Koch-Light)(Fluka) as described in literature [19, 20]. $EtAlCl_2$ was prepared from Et_3Al and $AlCl_3$ and purified by distillation [21].

The IR spectra were recorded on a double-beam Carl Zeiss UR 20 spectrophotometer.

Catalytic experiments

a) A solution (5 ml) of cis-2-pentene in n-pentane (1/1) and 0.05 ml $EtAlCl_2$ was added to a suspension of 29 mg WPy_2Cl_4 in 5 ml chlorobenzene. After 1 hour, the mixture was hydrolyzed and analyzed by GLC. Based on the quantity of cis-2-pentene introduced, the reaction product contained 14.1 per cent cis, trans-2-butene, 45.7 per cent cis, trans-2-pentene and 27.3 per cent cis, trans-3--nexene. The rest of the olefins were converted to polymers.

b) Several parallel runs were performed with the above catalyst under Ar and CO. After a 15 minute reaction, the conversions of 2-pentene ranged between 7-22 per cent under Ar and 48-51 per cent under CO; since the equilibrium composition was reached under carbon monoxide, the rate of reaction must have been rather high. This was confirmed by utilizing even shorter reaction times: conversion of 2-pentene was 40.6 per cent after 1 minute, 41.8 per cent after 3 minutes and 47.2 per cent after 5 minutes.

c) To study the connection between $W(CO)_6$ content and catalytic activity, a master solution was prepared from 300 mg WPy_2Cl_4, 0.9 ml $EtAlCl_2$ and 50 ml chlorobenzene. This was stirred under CO and samples were taken at certain intervals. 5 ml of the sample was given to 5 ml of a mixture of n-pentane and 2-pentene (1/1) and the conversion of 2-pentene after 3 minutes reaction time was used as a measure of the activity. The concentration of $W(CO)_6$ was determined in another part of the sample by IR spectroscopy and an extinction vs. concentration curve using the extinction measured at 1980 cm^{-1}.

d) $W[C_2H_4(PPh_2)_2]_2Cl_3$, $W[C_2H_4(PPh_2)_2]Cl_4$ and $Mo(PPh_3)_2Cl_4$ behaved similarly to WPy_2Cl_4 under the conditions of a), b) and c).

e) 5 ml of a solution of cis-2-pentene in pentane (1/1) containing 0.05 ml $EtAlCl_2$ was added to a suspension of 0.05 g $W(PPh_3)_2(CO)_3Cl_2$ in 5 ml chlorobenzene under Ar. A homogeneous solution was formed. After 1 hour, the reaction mixture was hydrolyzed and GLC analysis indicated the presence of 13.4 per cent 2-

-butenes, 49.7 per cent 2-pentenes, 26.2 per cent 3-hexenes and traces of higher olefins.

Preparative Experiments

f) The master solutions made according to c) were steam distilled after 2-3 hours reaction time. $M(CO)_6$ (M = Mo or W) precipitated on the wall of the condenser in the form of white crystals, before an appreciable distillation of chlorobenzene has started. Yield 10-30 per cent.

g) A solution of 0.05 ml $EtAlCl_2$ in 3 ml 2-pentene was given to a solution of 190 mg $Mo(PPh_3)_2Cl_4$ in 3 ml chlorobenzene. Rapid disproportionation reaction was observed. Adding pentane (5-10 ml) a precipitate formed due to the diminished solubility of the complexes. This solid portion of the product was separated and dissolved in a small quantity of acetone upon which 20-30 mg $Mo(PPh_3)_2(CO)_3Cl_2$ precipitated.

REFERENCES

1. BANKS, R.L., Belg. Pat. 620 440.
2. BANKS, R.L., Belg. Pat. 633 418.
3. CALDERON, N. and HUNG YU CHEN, Belg. Pat. 698 075.
4. CALDERON, N., HUNG YU CHEN and SCOTT, K.W., Tetrahedron Lett., 1967, 3327.
5. ZUECH, E.A., Chem. Commun. 1968, 1182.
6. German Pat. Appl., 6 806 210.
7. MOULIJN, J.A. and BOELHOUWER, C., J. Chem. Soc. D., 1971, 1170.
8. BRADSHAW, C.P.C., HOWMAN, E.J. and TURNER, L., J. Catalysis 7, 269 (1967)
9. MOL, J.C., MOULIJN, J.A. and BOELHOUWER, C., Chem. Commun. 1968, 633.

10. WOODWARD, R.B. and HOFFMAN, R., J. Amer. Chem. Soc. 87, 2046 (1965)
11. CALDOW, G.L. and MacGREGOR, R.A., J. Chem. Soc. A., 1971, 1654.
12. WANG, J.L. and MENAPACE, H.R., J. Org. Chem. 1968, 33.
13. BENCZE, L. and MARKÓ, L., Magyar Kémikusok Lapja, 1972, 213.
14. BENCZE, L. and MARKÓ, L., unpublished results.
15. BENCZE, L. and MARKÓ, L., J. Organometal. Chem., 1971, 271.
16. COLTON, R., SCOLLARY, G.R. and TOMKINS, I.B., Aust. J. Chem. 21, 15 (1968)
17. BENCZE, L., J. Organometal. Chem. 37, C 37 (1972)
18. BENCZE, L. PÁLYI, G., and MARKÓ, L., 5th Intern. Conf. Organometal. Chem., Moscow, 1971, Vol. 2. p. 194.
19. BLIGHT, D.G. and KEPERT, D.L., J. Chem. Soc. A., 1968, 534.
20. BOORMAN, P.M., GREENWOOD, N.N. and HILDON, M.A., J. Chem. Soc. A., 1968, 2466.
21. GROSSE, A.V. and MAVITY, J.M., J. Org. Chem., 5, 106 (1940)

РЕЗЮМЕ

Окись углерода в реакции диспропорционирования олефинов увеличивает активность используемого катализатора, состоящего из галогенидных комплексов вольфрама и молибдена и из $EtAlCl_2$. Из реакционной смеси были выделены в качестве конечных продуктов гексокарбонилы и в качестве интермедиеров галогенокарбонилы.

Hungarian Journal
of Industrial Chemistry
Veszprém
Vol.1. pp. 463-474 (1973)

STUDIES ON GRANULATION IN A FLUIDIZED BED III.

CALCULATION OF THE FEED RATE OF GRANULATING LIQUID

Z. ORMÓS, K. PATAKI and B. CSUKÁS

(Research Institute for Technical Chemistry of the
Hungarian Academy of Sciences, Veszprém)

Received: March 17, 1973.

In granulation in a fluidized bed, the appropriate selection of the feed rate of the granulating liquid is very important since this parameter, in addition to its effect on the formation of the granulates, considerably influences the capacity of the apparatus. The results of experiments on the effect of the feed rate of granulating liquid on the physical properties of the granulates formed in a fluidized bed (average particle size, the relative amount of the particles not granulated, wear strength, and the inhomogeneities of the binder distribution) are given. On the basis of the heat and liquid balances of the process, correlation is given for the maximum and equilibrium liquid feed rates.

A very important process parameter of the batch granulation in a fluidized bed is the feed rate of the granulating liquid. To attain the optimum average particle size, a well defined quantity of the given binder solution is needed. The liquid can be sprayed in the fluidized bed at different feed rates, i.e. during various lengths of time. Thus the appropriate choice of the feed rate of the granulating liquid, basically determines the duration of the granulation and hence the capacity of the apparatus.

In the first paper of this series [1] - where the relationships between the amount of the binder and the physical properties

of the formed granulates were dealt with - the effect of the feed rate on the physical properties of the granulates was also touched upon to ensure the completeness of the paper. The results of other authors - RANKELL and all. [2], MÖBUS [3] and DAVIES and GLOOR [4] were also given. It was pointed out that the results were evaluated in literature in two different ways. Some authors changed the feed rate while keeping the duration of the spraying at a constant value [2, 3], while others kept the quantity of the granulating liquid constant [4] - hence the results are difficult to compare.

On the basis of the experimental results it was deduced that the average diameter and average porosity and the particle size distribution of the formed granulates were only slightly influenced by the variation within certain limits of the feed rate of the granulating liquid, provided that the overall amount of the binder was kept constant. Therefore, the influence of the feed rate was neglected in addition to those parameters that had greater effects on the above mentioned properties of the granulates.

In the present paper the influence of the feed rate of the granulating liquid on the average particle size, the relative amount of the particles not granulated, the wear strength and the homogeneity of the binder distribution will be dealt with in details. On the basis of the heat and liquid balances of the process, correlations were derived for the upper limit of the liquid feed rate and for the approximately optimum feed rate.

EXPERIMENTAL APPARATUS AND METHODS

The experimental laboratory granulating apparatus and the applied experimental methods will not be described here in detail, since they do not depart from those described in the previous paper of this series [1].The 0.1-0.2 millimetre fraction of quartz sand was used as basic material and an aqueous gelatine solution of a concentration of $c' = 60$ kilograms per cubic metre was used as the granulating liquid. In the experiments dealt with in this

paper, the concentration of the granulating liquid, the mass of the material to be granulated, the relative expansion of the fluidized bed, the temperature of the air at the inlet and the distance between the atomizer and the underplate were kept at constant values, in addition to the characteristics of the apparatus and the basic material and the binder. The air feed rate of the atomizer was increased with the feed rate of the granulating liquid to ensure a nearly identical liquid dispersion throughout the measurements, so that the specific air consumption was always about 2.5 kilograms air per kilogram liquid.

The test and calculation methods for the physical properties of the granulates formed were summarized in the previous paper of this series [1] while the test methods were detailed in the first paper [5].

In some cases the relative humidity of the air at the outlet and the liquid content of the bed were determined several times during the granulation at various liquid feed rates. The liquid content of the bed was determined by drying the samples taken from the bed in a drying oven until constant weight. The relative humidity of the air at the outlet was measured by an ASSMANN psychrometer redesigned to this purpose. These measurements had two objectives: they provided data for the establishment of the heat and liquid balances of the process and helped in deciding whether the change of state of the air flowing through the apparatus is really adiabatic as suggested in literature [2, 6].

At the two extreme values of the feed rate of the granulating liquid, the concentration of the binder was determined as a function of the size of the granulates. The average binder content of the granulates was determined by dissolving NaCl in the granulating liquid. Having concluded the granulation, the dry product was fractioned and from the average samples of identical mass, the labelled binder was extracted by hot distilled water. The conductivity of thermostated solutions of identical volumes of the samples were measured by bell-shaped electrodes. In the knowledge of the relationship between the conductivity and concentration of the NaCl solution, the binder content was determined from the measured conductivity.

EXPERIMENTAL RESULTS

The effects of the feed rate on the physical properties of the granulates were studied by altering the feed rate at four different values of the relative amount of the granulating liquid (V'/V = 5; 10; 20; 30 vol per cent) while keeping the other parameters at constant values. The studied feed rates were as follows: w' = (2.5; 4.2; 5.9; 7.6 and 9.2) $\times 10^{-5}$ kilogram per second. When the feed rate is changed while the relative amount of the granulating liquid is kept constant, the duration of the granulation also changes,with smaller feed rate it is longer, and with greater feed rate is shorter. Because of the repeatability of the experimental results [1] three parallel experiments were carried out in every case so the dots in the following Figures correspond to the average value of three parallel experiments.

The average diameter of the granulates is plotted against the feed rate of the granulating liquid in Fig.1. The average particle size tends to be decreased by the increase of the feed rate, though the dots are rather scattered.(The straight lines in the Figure do not show anything more than the tendencies of the changes!) When the relative amount of the granulating liquid is greater, the decrease of the particle size is greater. While at a relative liquid amount of

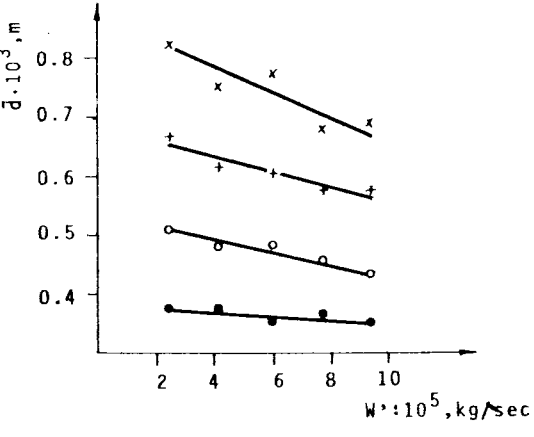

Fig.1. x - V'/V = 30 vol. per cent
+ - V'/V = 20 vol. per cent
o - V'/V = 10 vol. per cent
• - V'/V = 5 vol. per cent

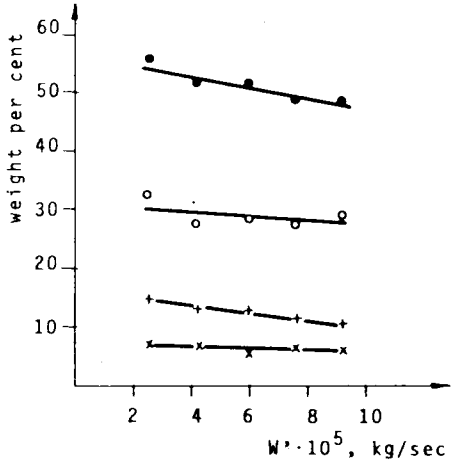

Fig.2. d = (0.1 - 0.2)x10^{-3} m
•-V'/V = 5 vol. per cent
o-V'/V = 10 vol. per cent
+-V'/V = 20 vol. per cent
x-V'/V = 30 vol. per cent

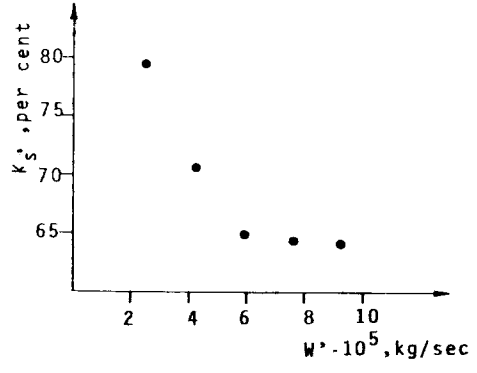

Fig.3. V'/V = 20 vol. per cent

V'/V = 5 vol.per cent, the increase of the feed rate by about four times decreases the average particle size by only about 7 per cent at a relative liquid amount of V'/V = 30 vol. per cent this change is almost 16 per cent.

In Fig. 2 the weight fraction of the particles not granulated is plotted against the feed rate at four different values of the relative amount of the granulating liquid. With the increase of the feed rate there is a slight decrease of this weight fraction. The greatest effect was found at the smallest liquid amount (V'/V = 5 vol. per cent), where the amount of the particles not granulated decreases by about 7 weight per cent when the feed rate is increased from 2.5x10^{-5} kilogram per second to 9.2x10^{-5} kilogram per second, which represents a relative decrease of 12.5 per cent.

In Fig. 3 a more profound change is shown, the wear strength is plotted

against the feed rate of the granulating liquid. After an initial sharp drop, the wear strength approaches a lower limit with the increase of the feed rate, despite the fact that the amount of the binder does not vary.

In Fig. 4 the binder content is plotted against the particle size at two different feed rates. The tendencies are identical in both cases, the binder content at first increases with the particle size, but later it attains a nearly constant value. From the Figure it is clear that if a given amount of the binder solution is sprayed in the bed with high velocity, that is during a short time, there are greater differences between the binder content of the particles of different size than in the case of granulation with small feed rates.

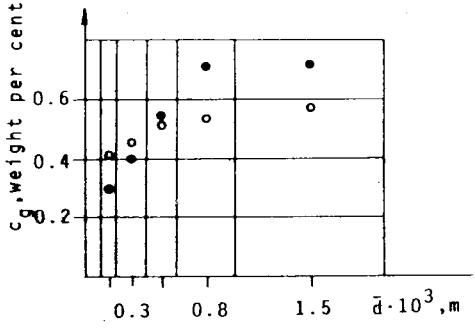

Fig.4. • - w' = 8.4×10^{-5} kilogram per second; o - w' = 3.4×10^{-5} kilogram per second; V'/V = 20 vol. per cent

The temperature and relative humidity of the air was measured at the inlet and at the outlet. In the Mollier diagram of the humid air, the point corresponding to the measured relative humidity of the air at the outlet was determined from the conditions of the air at the inlet, supposing an adiabatic drying process. The dry bulb temperature corresponding to this point is the "adiabatic temperature", (T_a''). The comparison of T_a'' and the measured temperature at the outlet makes it possible to see how the process approaches the ideal adiabatic one. The differences between the measured temperatures and those obtained from the psychrometric diagram are plotted against the measured temperatures in Fig. 5. The discrepancies between the temperature of the air at the outlet

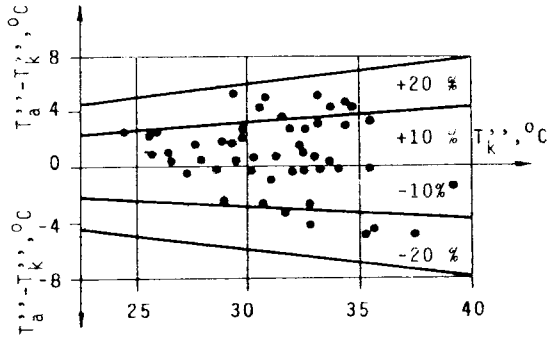

Fig. 5

and the adiabatic temperature were in every case less than ± 20 per cent and in 75 per cent of the cases the differences were not greater than ± 10 per cent.

DISCUSSION

According to Fig. 1, 2, 3 and 4 the changes in the physical properties of the granulates due to the increase of the feed rate of the granulating liquid are not of the type that would make it possible to determine a well defined optimum value of the feed rate. The increase of the feed rate is undesirable on the one hand, because of the worse binder distribution and because of the decrease in the wear strength, while it is desirable on the other hand, because of the greater capacity and because a slight decrease in the amount of the particles not granulated.

The feed rate of the granulating liquid cannot be selected arbitrarily. Both the experimental results and the theoretical considerations show that there is a maximum value of the feed rate above which granulation in a fluidized bed cannot be realized.This

greatest feasible value of the feed rate is determined by the air velocity corresponding to the required bed expansion and by the air temperature at the inlet; after a certain feed rate, the heat content of the air flow is insufficient for the removal of the liquid sprayed in. In such cases, the amount of the granulating liquid retained in the bed continuously increases and at a critical liquid content characteristic of the given system, the fluid movement of the bed cannot be maintained even by a further increase of the air velocity.

The maximum liquid feed rate can easily be determined from the liquid mass balance of the process, in the knownedge of the critical liquid content of the bed.

The liquid mass balance:

$$w't'\left(1 - \frac{c'}{\rho'}\right) - F\rho''(x_k'' - x_b'') \int_0^{t'} u''(t)dt - V_p''t'(x_k'' - x_b'') = x_r G \quad (1)$$

Equation (1) can be reduced by the introduction of the average gas velocity (integral mean); the air flow of the atomizer should be expressed as the product of the liquid feed rate and the specific air requirement of the atomizer:

$$w't'\left(1 - \frac{c'}{\rho'}\right) - F\rho''(x_k'' - x_b'')\,\bar{u}''t' - kw't'(x_k'' - x_b'') = x_r G \quad (2)$$

The results on the changes of the velocity of the air required for the movement of the fluidized bed, with respect to time, and the method for the determination of the average air velocity will be published in a following paper on the fluidization properties of the granulates.

Taking the critical liquid content as the liquid content of the bed ($x_r = x_{rk}$), Equation (2) gives the maximum feed rate:

$$w_M' = \frac{x_{rk} G + F\rho''(x_k'' - x_b'')\,\bar{u}''t'}{t'\left(1 - \frac{c'}{\rho'}\right) - kt'(x_k'' - x_b'')} \quad (3)$$

The liquid content of the bed attains the critical value at which the movement of the bed stops, just by the end of the spraying (during a time interval of t') if the feed rate is that corresponding to Equation (3). The correlation helps in finding the feasible range of feed rates, that extends in theory from a feed rate of zero to w'_M. In practice the lower limit is the lowest feed rate where the precondition of the formation of the liquid bonds does not exist because of the very small wetting. In such cases the atomized granulating liquid becomes partly dry before getting in the bed (drying with atomization), and partly it dries on the surface of the particles without the formation of either liquid or solid bonds.

The heat balance of the batch granulation in a fluidized bed with spraying can be used for the determination of the equilibrium liquid feed rate (w'_e). The latter is the feed rate at which the heat content lost by the flowing gas is equal to the heat required for the evaporation of the solvent sprayed in.

The heat balance:

$$F\rho''c''_p(T''_b - T''_k)\int_o^{t'} u''(t)dt = [w't'(1 - \frac{c'}{\rho'}) - G\int_o^{t'} x_r(t)dt]r' + Q_v \qquad (4)$$

The term on the left hand side of Equation (4) can be reduced by the introduction of the average gas velocity ($\bar{u}''$); moreover, the Q_v heat loss can be neglected in the case of appropriate heat insulation, since the temperature of the bed does not differ significantly from the room-temperature.

$$F\rho''c''_p(T''_b - T''_k)\bar{u}''t' = [w't'(1 - \frac{c'}{\rho'}) - G\int_o^{t'} x_r(t)dt]r' \qquad (5)$$

The liquid feed rate can be equated to that of the equilibrium liquid feed rate defined above. In that case there is no accumulation of the liquid in the bed, so the equation reduces once again:

$$F\rho''c''_p(T''_b - T''_k)\bar{u}''t' = w'_e t'(1 - \frac{c'}{\rho'})\, r' \qquad (6)$$

From Equation (6) the equilibrium feed rate of the granulating liquid is:

$$w'_e = \frac{F\rho''\bar{a}''c''(T''_k - T''_k)}{r'(1 - \frac{\rho''}{\rho'})} \qquad (7)$$

The practical use of this equation is facilitated by the fact that the temperature of the air at the outlet (T''_k) can be aproximated well with the help of the psychrometric diagram, in the knowledge of the characteristics of the air at the inlet, since $T''_k \approx T''_a$ (see under the heading "Experimental Results").

The applicability of Equations (3) and (7) were checked by the solution of several problems. The data needed were substituted into Equations (3) and (7) in the case of the studied model and the following values were obtained: $w'_e = 6\times10^{-5}$ kilogram per second; $w'_M = 10.5\times10^{-5}$ kilogram per second.

The feed rates obtained by the equations are quite feasible and they are compatible with the experimental observations. The calculated maximum feed rate was somewhat higher than the value of 9.2×10^{-5} kilogram per second found to be just employable. But is has to be remembered that at this feed rate an appreciable experiment was carried out so the critical liquid content of the bed was not attained. Hence the higher limit of the feasible feed rates can be well approximated by Equation (3). The equilibrium feed rate calculated by Equation (7) is a good mean value in the feasible interval. Lower rates should be applied for the granulation only if the wear strength of the granulates is to be increased or if small amounts of some additives are to be introduced and distributed in the bed (e.g. in the pharmaceutical industry). The decrease of the feed rate according to Fig. 3. and 4. increases the wear strength of the granulates and helps in the relatively homogeneous distribution of materials fed in small amounts with the granulating liquid, independently of the particle size.

SYMBOLS USED

c' concentration of the granulating liquid (kilogram per cubic metre)

c_g the binder content of the granules (weight per cent)

c''_p heat capacity of the gas (kilocalories per kilogram per Degree Centigrade)

d particle size (metre)

$\bar{d}$ average particle size (metre)

F cross section area of the apparatus (square metre)

G the mass of the bed (kilogram)

k the specific air requirement of the atomizer (kilograms per kilogram)

K_s wear strength (per cent)

r' latent heat of the solvent (kilocalories per kilogram)

Q_v heat loss (kilocalories)

T''_a air temperature at the outlet from the psychrometric diagram (Degree Centigrade)

T''_k air temperature at the outlet (Degree Centigrade)

t time (second)

t' the duration of granulation (second)

u'' gas velocity (metres per second)

$\bar{u}''$ average gas velocity (metres per second)

V the overall volume of the particles to be granulated (cubic metre)

V' the volume of the granulating liquid (cu.metre)

V'/V the relative amount of the granulating liquid (vol. per cent)

V''_p air flow of the atomizer (kilogram per second)

w' feed rate of the granulating liquid (kilogram per second)

w'_e equilibrium feed rate of the granulating liquid (kilograms per second)

w'_M maximum feed rate of the granulating liquid (kilograms per second)

x''_b absolute humidity of the air at the inlet (kilograms per kilogram)

x''_k absolute humidity of the air at the outlet (kilograms per kilogram)

x_r liquid content of the bed (kilograms per kilogram)

x_{rk} critical liquid content of the bed (kilograms per kilogram)

ρ' density of the granulating liquid (kilograms per cu.metre)

ρ'' density of the gas (kilograms per cu.metre)

REFERENCES

1. ORMÓS, Z., PATAKI, K., CSUKÁS, B., Hung. J. Ind. Chem. 1, 307 (1973)
2. RANKELL, A.S., SCOTT, M.W., LIEBERMAN, H.A., CHOW, F.S., BATTISTA, J.V., J. Pharm. Sci. 53, 320 (1964)
3. MÖBUS, W., Ceskoslow. farm. 18, 109 (1969)
4. DAVIES, W.L., GLOOR, Jr. W.T., J. Pharm. Sci. 60, 1869 (1971)
5. ORMÓS, Z., Hung. J. Ind. Chem. 1, 207 (1973)
6. SCOTT, M.W., LIEBERMAN, H.A., RANKELL, A.S., BATTISTA, J.V., J. Pharm. Sci. 53, 314 (1964)

РЕЗЮМЕ

При грануляции, происходящей в псевдоожиженном слое, очень важен выбор соответствующей скорости подачи гранулирующей жидкости, поскольку этот параметр не только влияет на образование гранул, но и в значительной мере определяет производительность установки.

Авторы рассматривают влияние, оказываемое скоростью подачи гранулирующей жидкости на физические свойства (средний диаметр частиц, относительное число негранулировавшихся частиц, износостойкость, негомогенное распределение связующего вещества) образующихся гранул. На основании уравнений материального и теплового баланса была выведена зависимость для определения максимального и равновесного значения скорости подачи жидкости.

Hungarian Journal
of Industrial Chemistry
Veszprém
Vol.1. pp. 475-492 (1973)

STUDIES ON GRANULATION IN FLUIDIZED BED IV.

EFFECTS OF THE CHARACTERISTICS OF THE FLUIDIZED BED THE ATOMIZATION AND THE AIR DISTRIBUTOR UPON THE PHYSICAL PROPERTIES OF THE GRANULATES

Z. ORMÓS, K. PATAKI and B. CSUKÁS

(Research Institute for Technical Chemistry of the
Hungarian Academy of Sciences, Veszprém)

Received: July 18, 1973.

It is important to know the influence of the characteristics of the granulator and the procedure upon the physical properties of the granulates produced, both from the point of view of the granulator design and the determination of the optimum operating parameters. However, few papers dealing with the above-mentioned questions are to be found in literature. The effect of the following factors: ratio minimum bed height to diameter of bed, degree of expansion of the fluidized bed, degree of dispersion of the granulating liquid, distance of the atomizer as measured from the air distributor and the type of the distributor upon the physical properties of the granulates produced was studied in a laboratory-size fluidized bed granulator of batch operation. In the evaluation of the experiments, the results are compared with the conclusions published in literature and the nearly optimum values for the above-mentioned variables are given.

From among the parameters having an influence upon the physical properties of granulates produced in a fluidized bed, the effect brought about by changes in the relative amount of the granulating liquid, the rate of addition of the latter, its concentration, and the total amount of binder fed in were investigated

in the previous papers of this series [1, 2]. Approximative formulae were presented on the basis of those experiments for the calculation of the mean diameter of granules and the feed rate of the granulating liquid. The present paper deals with such characteristic parameters of the procedure and the apparatus that are of importance mainly in connection with the design and operation of fluidized bed granulators. These parameters are the following:

- ratio of the minimum bed height to the diameter of the bed;
- degree of expansion of the fluidized bed;
- degree of dispersion of the granulating liquid;
- distance of the atomizer from air distributor plate;
- performance of the air distributor plate.

As an introduction, conclusions of other authors in connection with the effect of the above-mentioned variables so far published in literature are summarized. The experimental results and conclusions drawn from them are then described.

In the design of fluidized bed granulators when deciding the size of the material container, or in the case of an existing apparatus, when determining the charge weight, the question of the preferable ratio minimum bed height to bed diameter arises. Simple fluid mechanical considerations also lead to the conclusion that this geometric simplex may have an optimum value or optimum value range. It is known from literature on fluidization [3, 4] that an increased danger of channel formation, (slugging) is encountered both with too shallow and with too high beds. These irregularities have an adverse effect on the mixing, heat and mass-transfer processes and also on the granulation. In addition, the ratio bed height to bed diameter may influence the probability of collision between the atomized liquid droplets and the particles, and also the rate of agglomeration [5]. In spite of the probably considerable influence of this variable on the physical properties of the granules produced, and of its economic importance (maximum utilization of the capacity of the apparatus), no paper so far published deals with this question in the manner that it deserves.

The degree of bed expansion is a very important characteristic of fluidization and its effect must be taken into consideration in all processes carried out by fluidization. In the case of fluidized bed granulation, an appropriate choice of the degree of bed expansion is of decisive importance regarding the final size distribution particle of the product [5, 6, 7, 8]. An increase in bed expansion tends to decrease the mean granule size [5, 8] because the more vigorous motion results increased abrasion. Another factor which makes higher bed expansion undesirable is an increase in elutriation. On the other hand, too small bed expansion brings about decreased mixing, heat and mass transfer, leading to the formation of "lumps" beyond the prescribed size limit. Accordingly, the optimum value of bed expansion is always a compromise between processes which are adverse as regards granulation and which tend to act against each other.

It is very difficult to determine accurately the degree of the dispersion of the granulating liquid, i.e. the size, and size distribution of the atomized droplets. Consequently, the effect of this parameter was studied only in an indirect manner. For example, in the case of two-fluid atomizers, which are most frequently applied in the practice of fluidized bed granulators, the effect of the pressure and flow rate of the atomizing air upon the physical properties of the produced granules were studied [8, 9]. The opinion of the different authors on this question is divergent. According to the paper of SCOTT and his co-workers [5], containing mainly theoretical considerations, it is to be expected that the mean drop size of the spray influences the process of granulation. The authors ascribe this to two facts: first, increasing the degree of dispersion also increases the specific surface area of the droplets and together with it the rate of evaporation of the latter. Secondly, the size, size distribution and number of atomized droplets influence the probability of collision between the droplets and solid particles, and thus also the rate of agglomeration. However, no experiments were carried out to study the influence of the degree of atomization. According to the work of MÖBUS [8], changing the pressure of the atomizing air between certain limits

does not appreaciably influence the physical properties of the granules. Unfortunately, experimental results were not published and accordingly it is impossible to determine even the pressure range studied. Detailed experimental data have been published by DAVIES and GLOOR [9]. In contrast to the above-mentioned author, they found that upon increasing the atomizing air pressure from 0,5 to 2.0 kg/cm², the mean granule size was decreased from 438 to 292 μ.

The vertical distance of the spray nozzle from the air distributor is restricted between certain limits [5, 7]. The lower limit that can be taken into consideration is defined by the condition that the atomized liquid must not wet the distributor plate because this would lead to the formation of large lumps, clogging of the distributor and stopping of particle motion. The upper limit of the location of the atomizer is determined by the spray cone angle and the bed height, on the basis of the condition that the atomized granulating liquid should not wet the wall of the granulator. Opinions differ as to whether or not the variation of the height of the nozzle between the above-mentioned limits influences the physical properties of the granules. According to MÖBUS [8], changing the position on the nozzle does not appreciably influence the physical properties of the granules. On the other hand, various authors have observed that increasing the distance between the atomizer and the distributor brings about a decrease in the mean granule diameter [6, 9]. The change can be termed as considerable. For example, experiments carried out by RANKELL and his co-workers showed that the mean granule size was decreased from 500μ to half this value when the atomizer in a granulator, 0.3 m in diameter, was lifted from a height of 0.75 to 1.5 m [6]. The phenomenon was mainly explained by the following consideration: in the case of a highly positioned atomizer, the spray drying that is undesired from the point of view of granulation, become prevalent.

In the case of fluidized bed granulators, mainly perforated plates, sieves and porous plates are applied as distributors. A number of points simultaneously have to be taken into consideration when choosing the distributor. Economic considerations re-

quire a distributor plate that is simple, inexpensive, easy to procure, and causes a low pressure drop. Fluid mechanical considerations would require gas distributor plates made of sintered glass or metal, fireclay, or other similar porous materials, in order to obtain optimum fluidization motion and to avoid irregularities in the fluidization process [3, 4]. This question can be solved satisfactorily only if the influence of the quality of the distributor on the physical properties of the granulates produced is known. As far as the authors know, no other researchers have so far dealt with such studies.

Having reviewed the literature connected with the subject it can be stated that the parameters in question include some whose effect has yet not been studied in any way; in the case of others, mainly theoretical conclusions were drawn and the latter were checked by a few experiments only. In some cases the conclusions of various authors were contradictory to each other. To summarize it can be stated that the data in literature are insufficient to determine the approximately optimum values of the different parameters.

EXPERIMENTAL APPARATUS AND METHODS

A detailed description of the laboratory-size fluidized bed granulator used for the experiments and the experimental techniques will be dispensed with, because they are similar to those described in the second paper of this series [1]. The materials used in the experiments were a quartz sand fraction of $(0.1\text{-}0.2)\times 10^{-3}$ m particle size and a granulating liquid which was an aqueous gelatine solution of $c' = 60$ kg/m³ concentration. The relative amount of the granulating liquid as referred to the total particle volume of the starting material to be granulated ($V'/V = 20$ % by volume), the feed rate of the granulating liquid ($w' = 5.9\times 10^{-5}$ kg/sec) and the input temperature ($T_D'' = 70$ °C) were kept constant.

EXPERIMENTAL RESULTS

The results of the research work carried out in order to study the influence of the technical and apparative parameters listed at the beginning of the present paper will now be described. The influence of changes in the individual parameters upon the mean particle size of the granulated material obtained, the mean porosity of the granules and the relative amount of the "product fraction" are illustrated in the Figures. Considering the conclusions on the reproducibility of the experimental results, published in the second paper of the series [1], three parallel experiments were carried out for each experimental point. The points drawn into the Figures represent the mean value of three such parallel results. It should be noted in connection with the Figures that the only reason to connect the experimental points with straight lines was to illustrate the trends of the changes.

a) Influence of Changes in the Minimum Initial Bed Height and Bed Expansion on the Physical Properties of the Granules

In the case of a given diameter of the granulator, the minimum bed height of the material to be granulated can be altered by changing the amount of the material fed in. In the first experimental series, the initial particle volume was increased from 200×10^{-6} to 600×10^{-6} m^3, in steps of 100×10^{-6} m^3. Simultaneously, the minimum initial bed height showed an approximately threefold increase. Of course, in proportion with increasing the amount of the material, the amount of granulating liquid was also increased, so as to have a constant relative amount of granulating liquid as referred to the particle volume of the material to be granulated.

Fig. 1 shows the changes in mean granule diameter and mean porosity of granulated material plotted against the minimum initi-

al bed height. With increasing minimum initial bed height, the mean granule size shows at first an abrupt decrease and later on it converges to a limiting value. In addition, it is apparent that the change in mean granule size is strikingly large as the minimum starting bed height is increased from 6.4×10^{-2} to 8.7×10^{-2} m. The mean porosity of the granules closely follows any changes in the mean granule diameter. The relative amount of a granule fraction and any changes in this amount depending on the parameter under test are index numbers of considerable importance from the point of view of production. Fig. 2 shows the changes in the relative amount of the granules of the dimension $(0.2 \text{ to } 2.0)\times10^{-3}$ m plotted against the minimum starting bed height. The weight ratio of the granule fraction conforming to the limits $(0.2 \text{ to } 2.0)\times10^{-3}$ m is the highest (0.81 %) at a minimum starting bed height of 6.4×10^{-2} m. Further increasing the initial bed height is very disadvantageous from the point of view of this parameter.

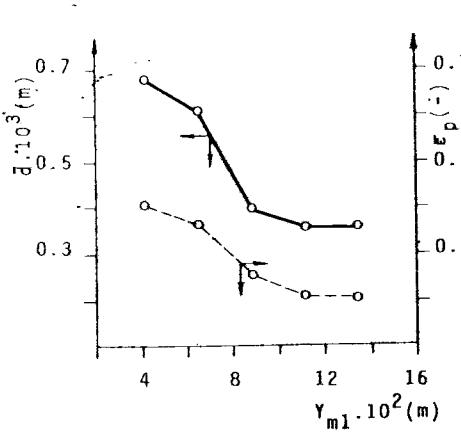

Fig. 1. $c' = 60$ kg/m³
$V'/V = 20$ vol.%
$w' = 5.9\times10^{-5}$ kg/sec

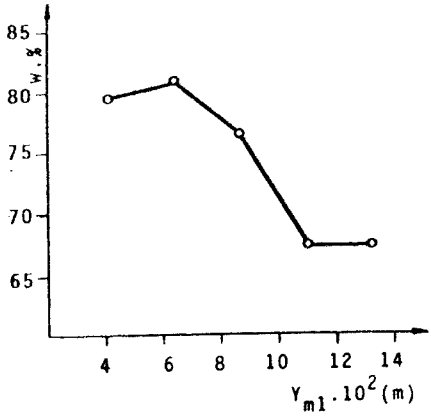

Fig. 2. d = $(0.2\text{-}2.0)\times10^{-3}$ m

The degree of expansion of the fluidized bed can be characterized in the simplest way by the ratio height of the fluidized

bed to the minimum bed height. During the granulation experiments, this ratio was approximately maintained at the predetermined value. With progressive agglomeration, the minimum bed height also changes (it generally increases). Accordingly, from time to time the air supply was stopped for a short period, the minimum bed height was determined, and the air flow rate was adjusted so as to obtain the same relative bed expansion.

In the experiments described so far, the ratio bed height to minimum bed height was the same ($Y/Y_m \approx 1.6$). In the study of the effect of bed expansion, the value Y/Y_m was increased from 1.3 to 2.5, in steps of 0.3, with the other parameters kept constant.

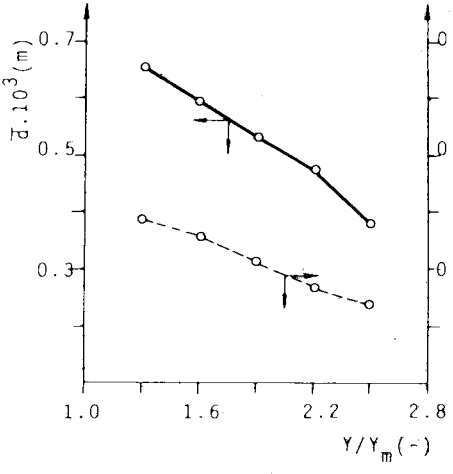

Fig. 3. c' = 60 kg/m³
V'/V = 20 vol.%
w' = 5.9x10⁻⁵ kg/sec

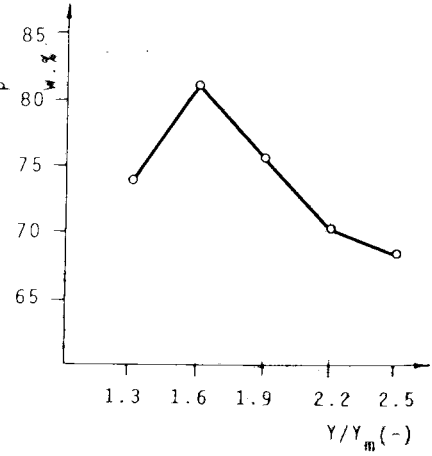

Fig. 4. d = (0.2-2.0)x10⁻³ m

Fig. 3 shows the changes in the mean granule size and the mean porosity plotted against the degree of bed expansion. While increasing the ratio height of the fluidized bed to the minimum bed height from 1.3 to 2.5, the mean granule size showed a - near-

ly linear - decrease. Upon increasing the bed expansion, the mean porosity of the granulates also decrease nearly linearly in the range studied. It is apparent from Fig. 4 that the weight fraction of the granules of the $(0.2 \text{ to } 2.0)_{\times}10^{-3}$ m size range first increases and thereupon it gradually decreases with increasing bed expansion. The maximum value is at - or near to - a bed expansion of 1.6.

b) Influence of Liquid Dispersion and Location of the Atomizer on the Physical Properties of the Granules

In the case of the two-fluid atomizer used in these experiments, the degree of liquid dispersion can be influenced by adjusting the pressure of the atomizing air. With constant feed rate of the liquid to be atomized, the degree of liquid dispersion is increased by increasing the air pressure. In order to determine the connection between the two variables, it would have been necessary to measure the drop size distribution in the atomized stream, and the variations of the latter as a function of the air stream. However, such a detailed study of atomization was beyond the scope of the present experiments and it was considered sufficient, in order to be able to draw conclusions of a qualitative nature, to study the effect of the degree of liquid dispersion in an indirect manner, through the influence of the changes in the atomizing air stream.

In the next series of experiments, the only changed parameter was the air mass flow of the atomizer. The atomizing air flow in these experiments was increased from $(6.7 \text{ to } 30.5)_{\times}10^{-5}$kg/sec in four steps. It is apparent from Fig. 5 that the mean particle size of the granulated material is not influenced to an appreciable degree even if the atomizing air flow is changed considerably. The mean granule diameter changes in the $(0.57 \text{ to } 0.66)_{\times}10^{-3}$ m range: at first it increases and thereupon it slightly decreases. The mean porosity of granules shows an abrupt increase and afterwards

its value remains constant. The relative amount of the granulated fraction corresponding to the size range $(0.2 \text{ to } 2.0)\times10^{-3}$ m changes according to a curve passing a flat maximum when plotted against increasing air atream - as shown in Fig. 6. However, it should be noted that when further increasing the atomizing air flow, at a value of 43.3×10^{-5} kg/sec, the experiment could no longer be evaluated. Accordingly, the changes in the physical properties of the granules brought about by the atomizing air stream are not as slow and gradual as could be judged on the basis of Figs. 5 and 6, but abrupt changes can be observed under a lower and over an upper limiting value. The explanation for this fact is that adequate dispersion of the liquid stops under a certain given air stream, whereas too fast an atomizing air stream virtually "shoots" the liquid into the layer and the material to be granulated clots unto the air distributor plate.

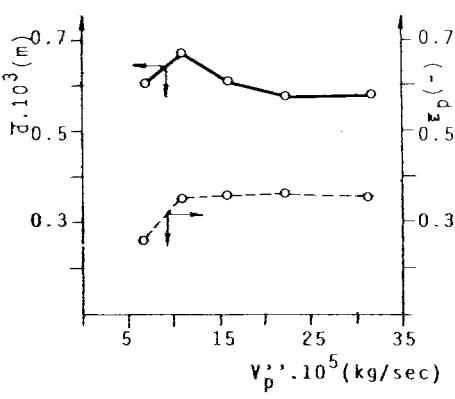

Fig. 5. c' = 60 kg/m³
V'/V = 20 vol.%
w' = 5.9×10^{-5} kg/sec

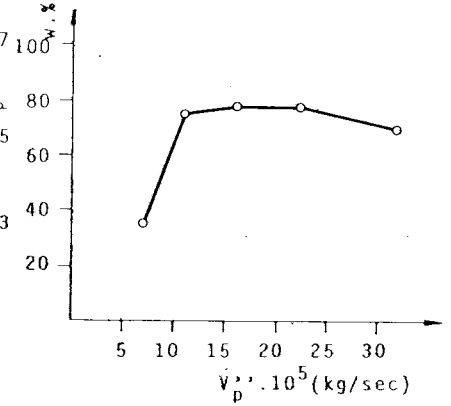

Fig. 6. d = $(0.2\text{-}2.0)\times10^{-3}$ m

The task of the next experimental series was to determine the effect of changes in the height of the atomizer on the physi-

cal properties of the granules produced. In these experiments, the vertical distance of the atomizer, as measured from the air distributor plate, was changed from 9.10^{-2} to 24.10^{-2} m in steps of 3.10^{-2} m.

At the same time, all other variables were maintained at a constant value. The mean particle size and mean porosity of the obtained granules plotted against the distance of the atomizer as measured from the air distributor is shown in Fig. 7, determined

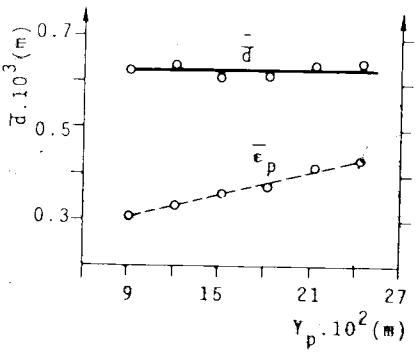

Fig. 7. c' = 60 kg/m³
V'/V = 20 vol.%
w' = 5.9×10^{-5} kg/sec

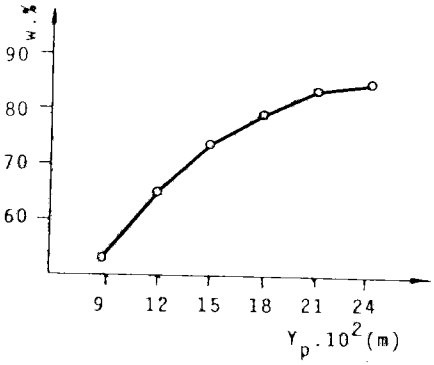

Fig. 8. d = $(0.2-2.0)\times10^{-3}$ m

in these experiments. It is apparent from the Figure that the height of the location of the atomizer does not influence the mean granule diameter to a considerable degree within the studied range. The mean granule size value fluctuates between about 0.60×10^{-3} and 0.65×10^{-3} m. In this case, the mean porosity does not follow the changes in mean diameter, but it gradually increases with the increasing distance between the air distributor plate and the atom-

izer. Location of the atomizer has a most marked influence on the granule size distribution of the product. This is illustrated by Fig. 8 which shows changes in the relative amount of the granule fraction corresponding to the predetermined size range - $(0.2\text{-}2.0)\times 10^{-3}$ m - plotted against the distance between the atomizer and the distributor. By lifting the atomizer from a height of 9.10^{-2} to 24.10^{-2} m, the amount of granules of product fraction was increased, according to the trend apparent from the Figure, from ∿ 53 % to ∿ 86 % by weight.

c) Influence of the Quality of the Air Distributor on the Physical Properties of the Granules

The influence of the quality of the distributor on the physical properties of the granules was studied with the application of four different distributors, under otherwise identical conditions. The distributor plates studied were the following: porous glass plates, sieves of 25×10^{-6} and 90×10^{-6} m openings, and a perforated plate of 12 mm perforations with a free surface ratio of 0.45; in order to prevent the escape of the granules, a sieve of 25×10^{-6} m openings was placed under the latter.

These experiments revealed the result that the mean granule size, mean porosity and particle size distribution of the granulated material obtained are practically independent on the quality of the air distributor.

EVALUATION OF THE EXPERIMENTAL RESULTS

According to the results of the present experiments, increasing the minimum starting bed height of the starting material decreases the mean granule size, and together with it, the mean

porosity of the final product. An explanation for this phenomenon can be given - as has already been pointed out in the introduction - by two reasons. Increasing the starting bed height over a certain limit, this results in decreased uniformity of the fluidization, slugging and strong bubble formation being produced. The latter brings about an increase in the degree of regranulation. The second important effect of increasing the initial bed height in fluidized bed granulation is that - as far as the ratio of the wetted surface area of the bed to the total surface area is unchanged - increasing the bed height decreases the probability of the solid particles meeting a liquid droplet. In granulation tasks, it is generally required that as much of the product as possible should conform to the size limits defined by the purpose of application.

With this in mind, and on the basis of Fig. 2 and other experimental findings, it can be stated that in fluidized bed granulators it is preferable to choose an initial bed height that corresponds to 1/2 to 2/3 of the bed diameter (i.e. the inner diameter of the granulator). In the case of initial bed higher than that, the amount of particles left ungranulated will increase and the amount of the granules of product fraction will decrease.

In the case of a given starting material and a given binder, the degree of regranulation primarily depends on the intensity of the motion of the particles and on the degree of bed expansion. The decisive importance of this parameter regarding final granule composition was confirmed by the present experiments and is also in agreement with the findings of other authors [5, 6, 7, 8]. According to Fig. 3, the mean granule diameter and porosity show an abrupt decrease with increasing bed expansion, due to the increased abrasion of the granules. It can be concluded on the basis of Fig. 4 that the approximately optimum value is a relative bed expansion to about 1.6 times the initial value.

The experimental results illustrated in Figs. 5 and 6 justify the conclusion that the degree of liquid dispersion has, within certain limits, no appreciable influence upon the physical proper-

ties of the granules produced in the process. Increasing the atomizing air flow, primarily influences the particle size distribution however, as it is apparent from Fig. 6, in the middle part of the studied range, over a rather wide interval, even this influence is negligible. The amount of the "product fraction" is practically unchanged when the specific amount of atomizing air is increased to double its value, from 1.8 to 3.6 kg air/kg liquid.

The conclusions of the authors as to the influence of the degree of atomization agree with the opinion of MÖBUS [8] and disagree with the experimental results of DAVIES and GLOOR [9]. In addition to the different experimental conditions and techniques, this discrepancy can be explained by the fact that the drop size distribution of the atomized liquid, or any changes in it, were unknown in both cases and consequently the experimental results cannot be compared.

Some authors [6, 9] observed a decrease in mean granule size if the distance of the atomizer, as measured from the air distributor plate, was increased. In their opinion this is caused by the fact that the drops must travel a longer way to reach the bed if the position of the atomizer is higher. In this case, the smaller droplets may dry and lose their adhesive property. In the opinion of the authors of the present paper, whether the above-mentioned process - undesired with regard to granulation - does or does not occur, is determined not only, and not primarily by the position of the atomizer. Factors such as, e.g. the temperature of air leaving the bed, the concentration of the granulating liquid, and the fineness of the spray, etc., are responsible in this respect. The above process did not occur in the range studied in the present experiments and it can be stated on the basis of Fig. 7 that when changing the distance of the atomizer, as measured from the distributor, within the practically feasible range, the mean granule size remains unchanged. However, an interesting phenomenon can be observed on Fig. 7. This is the following: the higher position of the atomizer leads (even in the case of decreasing mean particle size) to the production of granules of higher porosity. This observation can be explained by the fact that increasing the

distance of the nozzle from the air distributor plate, granule production can also occur in a bed of lower density, where the abrasive and compacting effects are less pronounced than in a fluidized bed of higher density. In the case of an unchanged cone angle of spray, the higher position of the atomizer increases the wetted surface area of the bed, i.e. the wetting is more uniform; and consequently the amount of granules of "product fraction" is increased (cf. Fig. 8). Of course, this can be true only up to a certain limit, since in the case of a too highly positioned nozzle, part of the granulating liquid wets the wall of the granulator instead of the bed as was pointed (out in the introduction), this is disadvantageous from several points of view.

On the basis of the results of these experiments and the experience on granulation acquired over several years, the following formula is proposed for the determination of the approximately optimum distance of the atomizer as measured from the air distributor plate:

$$Y_a = Y_{m1} + 0.8 \frac{D_b}{2 \operatorname{tg} \frac{\alpha}{2}} \qquad (1)$$

Equation (1) expresses that the granulating liquid is to be atomized on top of the dense layer ($Y_d \approx Y_m$) in such a way - in order to prevent "carry up to the wall" - that the diameter of the circular wetted patch on top of the dense layer is 0.8 times the diameter of the apparatus.

The result obtained in connection with the influence of the type of distributor is of major importance. It can be concluded that it is unnecessary to apply distributors made of a porous plate, whose production on an industrial scale is difficult and expensive, and whose resistance against flow is high. The particle size distribution and other physical properties of the granulated material by the granulation process remain unchanged, if instead of a porous plate, a sieve of adequate mesh is used as a support. A perforated plate of large free cross sectional area is placed under the sieve to supply mechanical strength.

The results reported in the present paper were applied in the design of the pilot-plant and the industrial-scale fluidized bed granulator. The correctness of the design principles is confirmed by the fact that the physical properties of the granules produced by the equipment, correspond in every way to the predetermined standard.

SYMBOLS USED

c'	concentration of the granulating liquid (kg/m³)
D_b	diameter of the apparatus (m)
$\bar{d}$	mean granule diameter (m)
d	particle size or sieve pore size (m)
T_b''	temperature of input air (°C)
V	total particle volume of material to be granulated (m³)
V'	volume of granulating liquid (m³)
V_p''	atomizing air stream (kg/sec)
V'/V	relative amount of granulating liquid (vol.%)
w'	feed rate of granulating liquid (kg/sec)
Y	height of the fluidized bed (m)
Y_m	minimum bed height (m)
Y_{m1}	minimum starting bed height (m)
Y/Y_m	degree of bed expansion (dimensionless)
Y_d	height of the dense layer (m)
Y_a	distance of the spray nozzle, as measured from the air distributor (m)
α	angle of spray (degree)
$\bar{\varepsilon}_p$	average porosity of granules (dimensionless)

REFERENCES

1. ORMÓS, Z., PATAKI, K., CSUKÁS, B., Hung J. Ind. Chem. 1, 307 (1973)

2. ORMÓS, Z., PATAKI, K., CSUKÁS, B., Hung. J. Ind. Chem. 1, 207 (1973)

3. LEVA, M., Fluidizáció (Fluidization) Műszaki Könyvkiadó, Budapest (1964)

4. BLICKLE, T., A fluidizációs eljárás készülékei, alkalmazása és számitásai (Apparatuses, Applications and Calculations of the Fluidization Process). Akadémiai Kiadó, Budapest, 1963.

5. SCOTT, M.W., LIEBERMAN, H.A., RANKELL, A.S., BATTISTA, J.V., J. Pharm. Sci. 53, 314 (1964)

6. RANKELL, A.S., SCOTT, M.W., LIEBERMAN, H.A., CHOW, F.S., BATTISTA, J.V., J. Pharm. Sci. 53, 320 (1964)

7. LISKE, T., MÖBUS, W., Pharm. Ind. 30, 557 (1968)

8. MÖBUS, W., Ceskoslov. farm. 18, 109 (1969)

9. DAVIES, W.L., GLOOR, Jr.W.T., J. Pharm. Sci. 60, 1869 (1971)

10. ORMÓS, Z., Hung. J. Ind. Chem. 1, 207 (1973)

РЕЗЮМЕ

В целях проектирования установок, гранулирующих посредством псевдоожиженного слоя, и определения оптимальных условий их работы важно знать каков действие оказывают технологические и аппаратурные характеристики на физические свойства образующихся гранул. В литературе встречается лишь незначительное число работ, подробно занимающихся этим вопросом. Авторы данной статьи на основании экспериментов, проведенных в условиях лабораторного реактора периодического действия с псевдоожиженным слоем, определили отношение минимальной высоты слоя/к диаметру слоя, зависимость размера слоя от скорости газа, а также то, в какой степени влияет на физические свойства гранул вид воздухораспределительной пластины и расстояние распылительной головки от этой пластины. Кроме того, авторы сравнили свои экспериментальные результаты с соответствующими литературными данными, и далее представили оптимальные значения вышеупомянутых переменных.

Hungarian Journal
of Industrial Chemistry
Veszprém
Vol.1. pp. 493-512 (1973)

STUDIES ON THE HYDRODYNAMICS OF FLUIDIZED LAYERS III. CALCULATION OF LAYER EXPANSION IN SYSTEMS FLUIDIZED WITH A LIQUID

Z. ORMÓS and T. BLICKLE

(Research Institute for Technical Chemistry of the Hungarian Academy of Sciences, Veszprém)

Received: April 5, 1973.

The equations for the calculation of the void fraction of layers fluidized with a liquid, most widely known from literature, and those derived from the first paper of the series are briefly described. The equations are transformed to a form which can readily be applied in practice even in the case of porous particles. The mean values of the "constant coefficients" of the equations, and the dependence or independence of the different "constants" on the various parameters was studied. The calculation methods are evaluated by the comparison of void fraction values determined experimentally and calculated by the proposed equations.

The expansion of fluidized layers can - among others - be characterized by the void fraction [1]. A number of calculation methods are known for the determination of the void fraction of layers fluidized with a liquid on the basis of the flow rate of the liquid, the diameter of the particles and other parameters. In the previous paper of the present series, an equation was derived in a theoretical manner which enables the void fraction of layers fluidized with a liquid to be calculated [2].

The present paper briefly summarizes the most important equations for the calculation of void fractions known from litera-

ture. Equations taken both from literature and proposed by the authors are evaluated critically. In the course of the latter, the dependence or independence of the "constant coefficients" of the equations on the parameters of the liquid and of the particles was studied, and the applicability of the equations was put to a trial by the comparison of results obtained, on the one hand, by calculation with the equations, and, on the other, by experimental measurements.

METHODS FOR THE CALCULATION OF THE VOID FRACTION OF LAYERS FLUIDIZED WITH A LIQUID

When deriving equations for the calculation of the void fraction of fluidized systems and studying the laws of such systems, a number of researchers have come to the conclusion that the void fraction is proportional to the flow rate of the fluid and the falling rate of the individual particles.

To a considerable degree, RICHARDSON and ZAKI [3] promoted the theories related to the expansion of fluidized layers known up to now. The equations they proposed describe the dynamic equilibrium of the individual particles as a function of the particulars of the layer and of the apparatus. The following groups were determined by analysis:

$$\frac{U'}{u_e} = f\left(Re, \frac{d}{D}, \bar{\varepsilon}'\right) \tag{1}$$

The data relating to layer expansion were given in the following form:

$$\frac{U'}{u_e} = \bar{\varepsilon}_c'^{\,a_1} \tag{2}$$

According to the above equation, the function flow rate of the liquid vs. void fraction, when drawn in a lg-lg co-ordinate system, gives a straight line whose slope is a_1. The experimental data were examined by this method and the following equations were presented for the calculation of a_1:

$$a_1 = (4.35 + 17.5 \frac{d}{D}) Re^{-0.03}, \quad \text{if } 0.2 < Re < 1 \tag{3}$$

$$a_1 = (4.45 + 18.0 \frac{d}{D}) Re^{-0.1}, \quad \text{if } 1 < Re < 200 \tag{4}$$

$$a_1 = 4.45 \cdot Re^{-0.1}, \quad \text{if } 200 < Re < 500 \tag{5}$$

$$a_1 = 2.39, \quad \text{if } 500 < Re < 500 \tag{6}$$

The Reynolds-number contained in these expressions is the following:

$$Re = \frac{U' \, d \, \rho'}{\mu'} \tag{7}$$

JOTTRAND [4] proposed two equations for the calculation of the void fraction of fluidized layers. One of these is essentially identical to Equation (2) described in the foregoing, whereas the other is the following:

$$\lg \frac{u_e}{U'} = a_2 (1 - \bar{\epsilon}_c') \tag{8}$$

Equation (8) represents, according to the author, a good approximation if the void fraction is within the range of 0.7 to 1 and the value of a_2 is 2.63.

In his book on fluidization, BLICKLE [5] proposed - among others - the following expression for the calculation of the void fraction:

$$\bar{\epsilon}_c' - \epsilon_m' = \frac{U' - U_m'}{u_e} \tag{9}$$

It has already been pointed out in connection with the examination of the above Equation that a better agreement with expe-

rimental data can be obtained by application of the following supplemented formula [6]:

$$\bar{\varepsilon}_c'^2 - \varepsilon_m'^2 = a_3 \frac{U' - U_m'}{u_e} \tag{10}$$

SAXTON and his co-workers [7] proposed an equation for the calculation of the void fraction of layers fluidized with a liquid based upon the cell-model theory of homogeneous fluidization:

$$(1 - \bar{\varepsilon}_c')^{-1/3} - (1 - \varepsilon_m')^{-1/3} = 18.8\ Re\ Ar^{-0.86} \tag{11}$$

where the Reynolds-number is equal to Equation (7) and the Archimedes number is the following:

$$Ar = \frac{(\rho - \rho')\rho' d\ g}{\mu'^2} \tag{12}$$

Connections describing the streaming of the fluid, the motion of the particles and the layer expansion in systems fluidized with a liquid were derived, starting from the physical model; these were described in the first paper of the present series [2]. The following equation was obtained for the expansion of layers fluidized with a liquid [2]:

$$\bar{\varepsilon}_c' = 1 - 0.75\ (1 - \frac{U'}{u_e})^{3/2} \tag{13}$$

In the practical application of the above equation it was found that the value of the constant differs in practice from the theoretically derived value of 0.75 to a considerable degree, and consequently the equation can be written in the following form [6, 8]:

$$\bar{\varepsilon}_c' = 1 - a\ (1 - \frac{U'}{u_e})^{3/2} \tag{14}$$

Considering that Equation (14) is valid even at the minimum fluidization rate, the following equation can be given for the calculation of the void fraction [2]:

$$\bar{\varepsilon}'_c = 1 - \frac{1 - \varepsilon'_m}{(1 - \frac{U'_m}{u_e})^{3/2}} (1 - \frac{U'}{u_e})^{3/2} \qquad (15)$$

In the following, the applicability of Equations (2), (8), (10), (11), (14) and (15) is examined according to the two points of view mentioned in the introduction of the present paper. Naturally, in addition to these equations, a large number of calculation methods have been described in literature [5, 6, 9, 10, 11, 12, 13, etc.]. However, the description and evaluation of these is outside of the scope of the present paper whose intention is only to illustrate the applicability of a few of the more widely known calculation methods and to compare them with the Equations (14) and (15) derived by the authors.

EXPERIMENTAL AND MEASUREMENT TECHNIQUES

The technique based on the determination of layer height was applied for the determination of the mean void fraction in the experimental studies on the expansion of layers fluidized with a liquid. The experiments were carried out in a cylindrical glass apparatus with a diameter D = 0.04 m which contained a fritted glass disk of the porosity of G2 in order to sustain the fluidized layer. The height of the latter was measured, to an accuracy of a few millimetres, by means of a scale secured to the wall of the apparatus and the mean void fraction was calculated with the following formula:

$$\bar{\varepsilon}'_Y = \frac{Y - \frac{G}{\rho F}}{Y} \qquad (16)$$

The quantity of the streaming liquid (water) was measured with a rotameter. The linear flow rate was calculated from the volumetric flow rate and the cross sectional area of the apparatus.

The minimum void fraction values were calculated from the minimum fluidization layer height by means of Equation (16). The minimum layer height was determined by measuring the layer height produced upon slow reduction of the liquid flow rate.

The minimum fluidization rate was obtained from the measured mean void fraction-flow rate values by extrapolation of the flow rate to the minimum void fraction.

The mean falling rate of the tested particle fractions was determined, having plotted the liquid flow rate against the measured mean void fraction values in a lg-lg plot, by graphical extrapolation of the liquid flow rate to the value of $\bar{\varepsilon}' \to 1$.

The mean porosity of the particles was determined by application of a technique, based on the identical space filling properties of particles of similar shape, proposed by the authors of this paper [14].

EXPERIMENTAL RESULTS

The experiments on layer expansion were carried out with a total of 29 particle fractions prepared of 5 different materials. The streaming liquid in the experiments was tap water of 12 - 14 ^{o}C temperature. The extent of layer expansion was determined with each particle fraction at 13 to 15 different flow rates. The dependence of the void fraction of the layer on the flow rate of the liquid is not presented in detail, merely the most important data are summarized in tabular form.

The most important physical properties of the examined granular materials (such as density, and porosity), the mass of the material weighed in for the experiment, the mean size and the size limits of the tested grain fractions, as well as the experimental data pertaining to the minimum void fraction, minimum fluidization rate and the mean falling rate of the particles are summarized in Tables 1. to 5. shown in the following.

Table 1. System glass beads—water

ρ = 2960 kg/m^3, ε_p = 0, G = 0.08 kg

	$\bar{d} \cdot 10^3$ (m)	ε'_{mt}	$U'_m \cdot 10^2$ (m/sec)	$\bar{u}_e \cdot 10^2$ (m/sec)
1	0.15	0.44	0.06	2.0
2	0.18	0.44	0.12	2.5
3	0.25	0.44	0.20	3.2
4	0.42	0.44	0.30	4.2

Table 2. System sand—water

ρ = 2635 kg/m^3, $\bar{\varepsilon}_p$ = 0, G = 0.05 kg

	$d \cdot 10^3$ (m)	ε'_{mt}	$U_m \cdot 10^2$ (m/sec)	$\bar{u}_e \cdot 10^2$ (m/sec)
1	0.10 - 0.20	0.51	0.08	1.2
2	0.20 - 0.32	0.51	0.13	2.5
3	0.32 - 0.40	0.51	0.19	3.9
4	0.40 - 0.50	0.51	0.26	5.0
5	0.50 - 0.63	0.51	0.39	5.9
6	0.63 - 0.80	0.51	0.64	7.0
7	0.80 - 1.00	0.51	1.10	9.0

Table 3. System hematite—water

$\rho = 4150\ kg/m^3$, $\bar{\varepsilon}_p = 0.12$, $G = 0.09\ kg$

	$d \cdot 10^3$ (m)	ε'_{mt}	$U'_m \cdot 10^2$ (m/sec)	$\bar{u}_e \cdot 10^2$ (m/sec)
1	0.10 - 0.20	0.56	0.10	1.5
2	0.20 - 0.32	0.56	0.30	4.0
3	0.32 - 0.40	0.55	0.60	6.0
4	0.40 - 0.50	0.55	0.95	7.5
5	0.50 - 0.63	0.56	1.30	9.5
6	0.63 - 0.80	0.57	1.70	12.0
7	0.80 - 1.00	0.57	2.20	15.0

Table 4. System porous nickel spheres—water

$\rho = 7450\ kg/m^3$, $\bar{\varepsilon}_p = 0.32$, $G = 0.13\ kg$

	$d \cdot 10^3$ (m)	ε'_{mt}	$U'_m \cdot 10^2$ (m/sec)	$\bar{u}_e \cdot 10^2$ (m/sec)
1	0.20 - 0.32	0.60	0.5	7.0
2	0.32 - 0.40	0.59	0.8	12.0
3	0.40 - 0.50	0.59	1.1	18.0
4	0.50 - 0.63	0.59	1.4	25.0
5	0.63 - 0.80	0.58	1.8	33.0

Table 5. System burnt clay—water

ρ = 2420 kg/m^3, $\bar{\varepsilon}_p$ = 0.50, G = 0.03 kg

	$d \cdot 10^3$ (m)	ε'_{mt}	$U'_m \cdot 10^2$ (m/sec)	$\bar{u}_e \cdot 10^2$ (m/sec)
1	0.20 - 0.25	0.75	0.12	1.4
2	0.25 - 0.32	0.75	0.18	1.8
3	0.32 - 0.40	0.76	0.25	2.4
4	0.40 - 0.50	0.76	0.36	3.2
5	0.50 - 0.63	0.76	0.45	3.8
6	0.63 - 0.80	0.76	0.55	4.6

APPLICATION AND EVALUATION OF THE CALCULATION METHODS

The starting point in the examination of the formulas proposed for the calculation of the void fraction is that these enable determination of the free volume or liquid-filled volume fraction. There is no problem in the case of materials consisting of compact granular materials; however in the case of porous particles the void fraction values determined in practice experimentally refer not only to the free space between the particles, but also include the pore space of the particles filled with the liquid. This is brought about by the fact that the density of the particles is determined in most cases with the pycnometer technique with the application of a liquid which has good wetting properties and in which the material of the particles is insoluble. This means that by this technique practically the density of the solid forming the material of the particles is determined and only the closed pores and channels, or those of such small dimensions as to be impermeable for the liquid may cause some deviation. Moreover, it often

occurs that the density values are simply taken from literature or from handbooks; however, such data most frequently refer to the compact material. Whether it is a density value determined by a pycnometer, or one taken from literature that is substituted into Equation (16), the obtained (experimentally determined) void fraction values include the total volume permeable by the liquid. The aforesaid should be taken into consideration in the evaluation of the calculation methods, because in the case of heap of porous particles this is the only reliable method of evaluation.

Starting from the definition of the void fraction and based on geometric considerations, the following connection between the two kinds of void fraction values may be written:

$$\bar{\varepsilon}'_t = \varepsilon_p + (1 - \varepsilon_p)\,\bar{\varepsilon}'_c \tag{17}$$

Accordingly, in order to be able to carry out the calculation, the mean porosity of the heap of particles has to be known. A simple measuring technique, which can be utilized in an easy way, has been developed by the authors [14].

In the application of Equation (2) described by RICHARDSON and ZAKI [3] the first question is the following: which is the equation that is to be used for the calculation of the "constant" a_1. Calculations were carried out in this respect and it was concluded that in the case of the models encountered in practice it is Equation (4) that is most frequently applicable. Accordingly, on the basis of Equations (2), (4) and (7) the following can be written:

$$\bar{\varepsilon}'_t = \varepsilon_p + (1 - \varepsilon_p)\left(\frac{U'}{u_e}\right) \frac{Re^{0.1}}{4.45 + 18\,\frac{d}{D}} \tag{18}$$

The next question which is encountered is whether the Reynolds number is to be calculated for each separate liquid flow rate. The above problem is unequivocally settled by the data presented in Table 6.

Table 6. System sand—water

$d \cdot 10^3$ (m)	a_1 calculated $\bar{\varepsilon}' = 0.6$	a_1 calculated $\bar{\varepsilon}' = 0.8$	a_1 calculated $\bar{\varepsilon}' = 1$	a_1 measured (mean)
0.10 - 0.20	5.1	4.5	4.3	4.1
0.20 - 0.32	4.4	4.0	3.8	3.7
0.32 - 0.40	4.1	3.8	3.6	3.4
0.40 - 0.50	3.9	3.6	3.5	3.2
0.50 - 0.63	3.8	3.5	3.4	3.0
0.63 - 0.80	3.6	3.4	3.3	2.9
0.80 - 1.00	3.5	3.3	3.2	2.8

As it is apparent from Table 6, the agreement between the a_1 values determined experimentally on the one hand, and calculated with Equation (4) on the other, is best if $\bar{\varepsilon}' = 1$, i.e. if the mean falling velocity of the particles is substituted into the equation.

Considering this fact, Equation (18) can be written in the following form:

$$\bar{\varepsilon}_t' = \varepsilon_p + (1 - \varepsilon_p)\left(\frac{U'}{u_e}\right)\frac{(u_e \, d \, \rho')^{0.1}}{\mu'^{0.1}(4.45 + 18 \frac{d}{D})} \qquad (19)$$

Fig. 1 shows the difference between the void fraction values determined experimentally and calculated by Equation (19), plotted against the experimentally determined value. It can be concluded from the Figure that the relative deviation is in all cases lower than ± 10 %, and in the overwhelming majority of the cases it is lower than + 5 %. Computer evaluation led to the conclusion that the mean relative deviation is ± 2 %.

Equation (8), described by JOTTRAND [4], can - considering Equation (17) - be written in the following form:

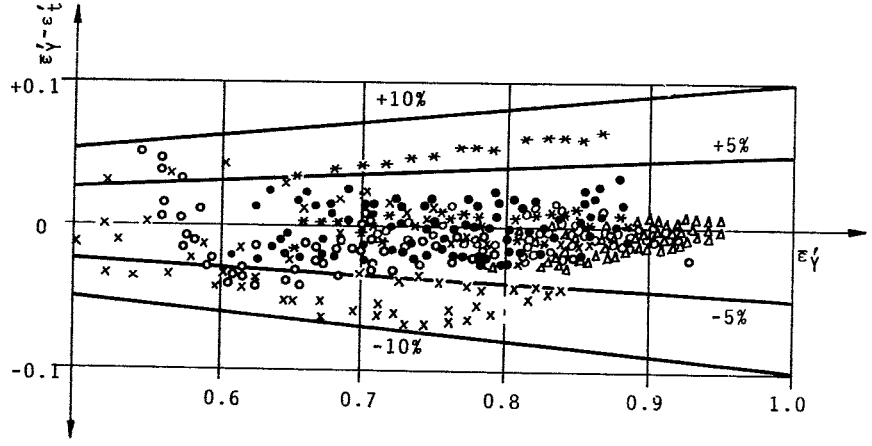

Fig.1. x - glass beads; o - sand; • - hematite; * - porous nickel spheres; Δ - porous burnt clay

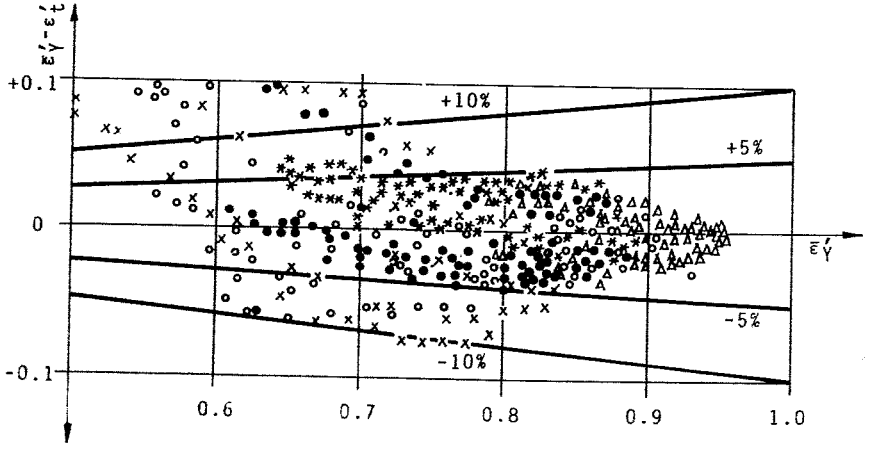

Fig.2. x - glass beads; o - sand; • - hematite; * - porous nickel spheres; Δ - porous burnt clay

$$\bar{\varepsilon}'_t = 1 - \frac{1 - \varepsilon_p}{a_2} \lg \frac{u_e}{U'} \qquad (20)$$

The value of the "constant" a_2 of the equation was determined for the model substances used in the experiments in about 400 cases and $a_2 = 1.75$ was obtained as a mean value. The mean scattering of the "constant" a_2, as a function of flow rate, was found to be $\sigma = \pm 9$ %, whereas the scattering depending on a particle size was $\sigma = \pm 13$ %.

The difference in void fraction values determined experimentally and calculated by Equation (20) ($a_2 = 1.75$), plotted against the experimentally determined value is shown in Fig. 2. It is apparent from the Figure that the relative deviation is, in most cases, lower than ± 10 % and the average relative deviation is +5 and -3 %.

On the basis of Equation (10) [5] and taking Equation (17) into consideration, the following equation can be written:

$$\bar{\varepsilon}'_t = \varepsilon_p + (1 - \varepsilon_p) \left(\frac{\varepsilon'_{mt} - \varepsilon_p}{1 - \varepsilon_p}\right)^2 + a_3 \frac{U' - U'_m}{u_e}^{1/2} \qquad (21)$$

The mean value of the "constant" is $\bar{a}_3 = 1.15$, its mean scattering depending on the flow rate of the liquid is $\sigma = \pm 18$ %, its mean scattering depending on the particle size is $\sigma = \pm 16$ %.

The difference in void fraction values determined experimentally and calculated by Equation (21) ($a_3 = 1.15$), plotted against the experimentally determined value is shown in Fig. 3. It can be concluded from the Figure that except for a few cases the relative deviation is lower than ± 10 %. The mean relative deviation was found to be ± 4 %.

In the examination of Equation (11) derived by SAXTON and his co-workers [7] it was found possible to bring it to a simpler form by substitution of Equations (7) and (12):

$$(1 - \bar{\varepsilon}')^{-1/3} - (1 - \varepsilon'_m)^{-1/3} = \frac{U'}{u_e} \qquad (22)$$

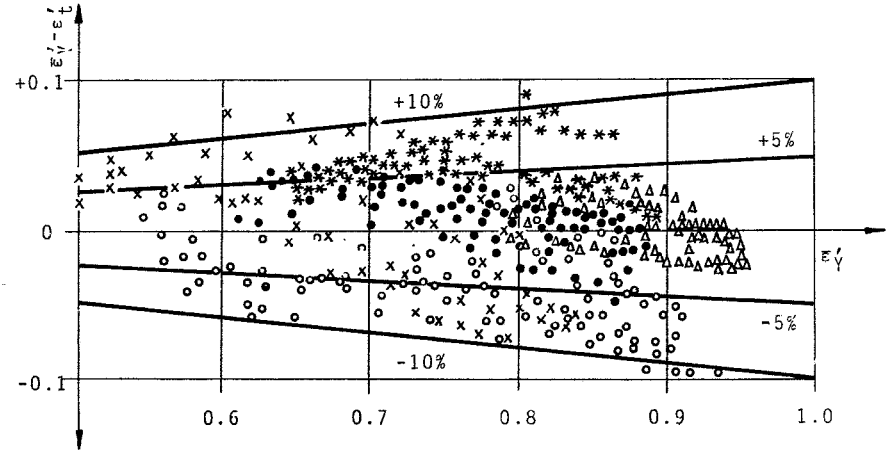

Fig.3. x - glass beads; o - sand; • - hematite; * - porous nickel spheres; Δ - porous burnt clay

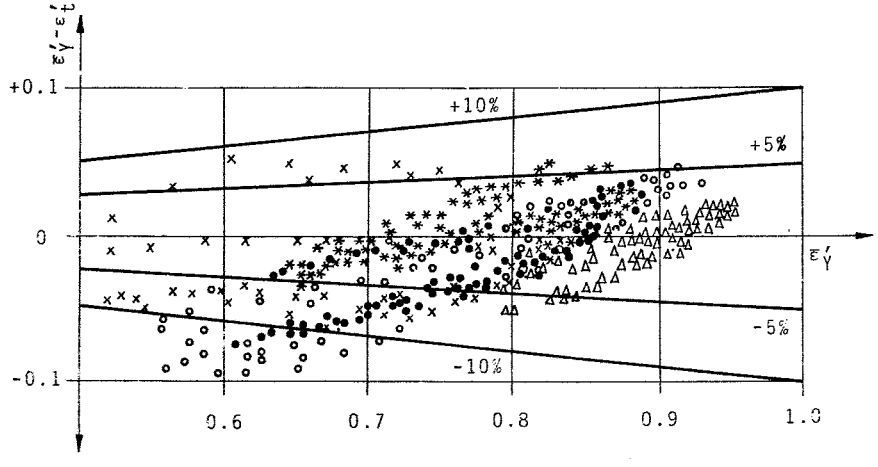

Fig.4. x - glass beads; o - sand; • - hematite; * - porous nickel spheres; Δ - porous burnt clay

On the basis of Equations (22) and (17), the following formula can be written for the calculation of the void fraction:

$$\bar{\varepsilon}'_t = 1 - \frac{(1 - \varepsilon'_{mt})(1 - \varepsilon_p)}{[(1 - \varepsilon_p)^{1/3} + (1 - \varepsilon'_m)^{1/3} \frac{U'}{u_e}]^3} \tag{23}$$

The difference in void fraction values determined experimentally and calculated by Equation (23), plotted against the experimentally determined values, is shown in Fig. 4. It is apparent from the Figure that in the overwhelming majority of the cases the relative deviation is lower than +5 and -10 %. The mean relative deviation is +2 and -5 %.

Taking Equations (14) [2] and (17) into consideration the Equation derived by the authors is the following:

$$\bar{\varepsilon}'_t = 1 - a_4 (1 - \varepsilon_p)(1 - \frac{U'}{u_e})^{3/2} \tag{24}$$

It was found in the experiments that the mean value of the "constant" $\bar{a}_4 = 0.55$, its average scattering depending on the flow rate is $\sigma = \pm 6$ % and its average scattering depending on the particle size is $\sigma = \pm 10$ %. Accordingly, Equation (24) can be written in the following form:

$$\bar{\varepsilon}'_t = 1 - 0.55 (1 - \varepsilon_p)(1 - \frac{U'}{u_e})^{3/2} \tag{25}$$

The difference in mean void fraction values determined experimentally and calculated by Equation (25) plotted against the experimentally determined value is shown in Fig. 5. It is apparent from the Figure that the relative deviation is in all cases lower than ± 10 % and in the overwhelming majority of the cases lower than ± 5 %. The average mean deviation is +3 and -2 %.

Equation (15) [2], as written on the basis of Equation (14) derived by the authors can be brought to a simpler form:

$$\bar{\varepsilon}'_t = 1 - (1 - \varepsilon'_{mt})(\frac{u_e - U'}{u_e - u'_m})^{3/2} \tag{26}$$

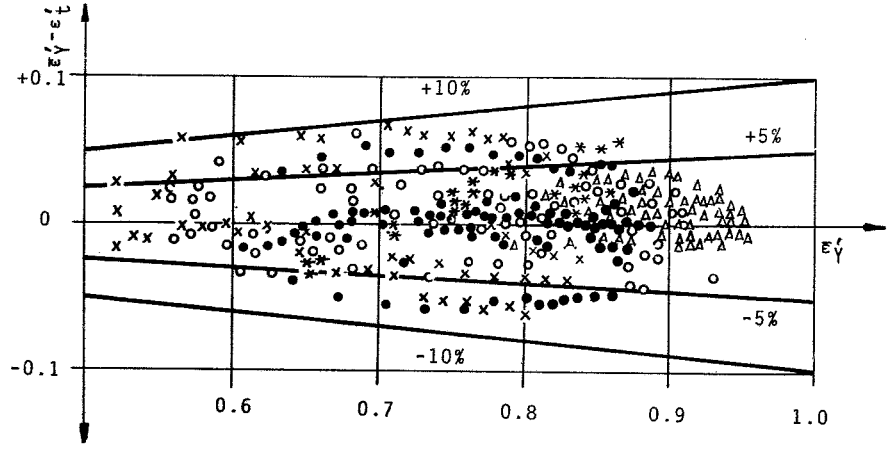

Fig.5. x - glass beads; o - sand; • - hematite; * - porous nickel spheres; Δ - porous burnt clay

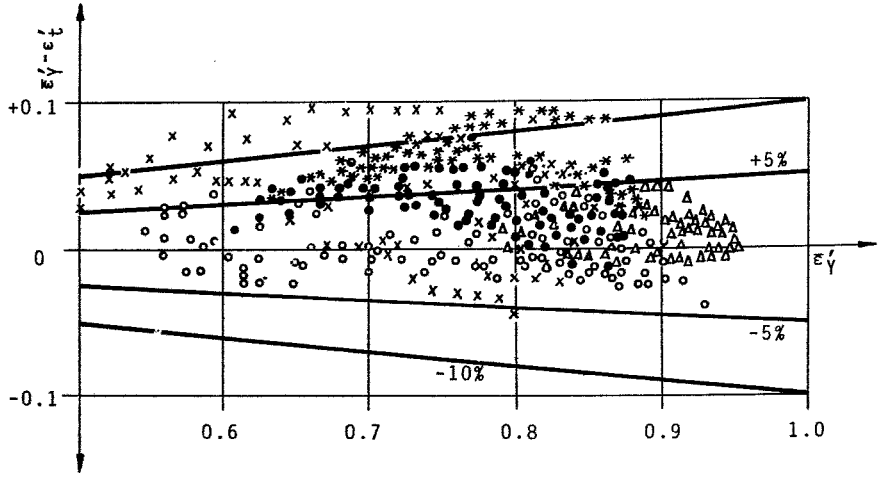

Fig.6. x - glass beads; o - sand; • - hematite; * - porous nickel spheres; Δ - porous burnt clay

The difference in the void fraction values determined experimentally and calculated by Equation (26), plotted against the experimentally determined values, is illustrated in Fig. 6. It can be concluded from the Figure that the relative deviation of the measured and calculated values is in the overwhelming majority of the cases lower than +10 and -5 %. The mean relative deviation is +4 and -2 %.

Summarizing the aforesaid it can be concluded that from among the formulas used for the calculation of the void fraction of layers fluidized with a liquid, Equation (19) derived from the Equation (4) of RICHARDSON and ZAKI [3], and Equation (25) derived from the Equation (14) by the authors of the present paper [2] are those yielding results which best approximate the values determined experimentally.

The agreement was also fairly good in the case of the other examined formulas; however, in case of these the mean relative deviation was on the one hand higher, e.g. Equations (20) and (21), and on the other the higher deviation is asymmetrical, e.g. with Equations (23) and (26). It is to be noted that from among the above Equations (20) and (23) yield values which at higher layer expansions show a good agreement with the experimental data. Equations (19) and (25) describe the layer expansion correctly in the whole range and consequently the application of these is recommended for the calculation of the expansion of fluidized layers.

SYMBOLS USED

a_1, a_2, a_3, a_4 constans

Ar Archimedes-number [cf. Equation (12)]

d diameter of the particles (metre)

$\bar{d}$ mean diameter of the particles (metre)

D diameter of the apparatus (metre)

F cross sectional area of the apparatus (m^2)

g gravitational acceleration (m/sec^2)

G mass of the particles present in the layer (kg)

Re Reynolds-number [cf. Equation (7)]

u_e falling rate of the particles (m/sec)

$\bar{u}_e$ mean falling rate of the particles (m/sec)

U' linear flow rate of the liquid as referred to the total cross sectional area of the apparatus (m/sec)

U'_m minimum fluidization liquid flow rate (m/sec)

Y height of the layer (m)

Y_m minimum layer height (m)

$\bar{\varepsilon}'$ mean void fraction of the layer

$\bar{\varepsilon}'_c$ calculated mean void fraction of the layer

ε'_m minimum void fraction of the layer

ε'_{mt} minimum total void fraction or liquid volume fraction of the layer

ε_p pore volume fraction of the particles

$\bar{\varepsilon}_p$ mean pore volume fraction of the particles

$\bar{\varepsilon}'_t$ calculated mean total void fraction or liquid volume fraction of the layer

$\bar{\varepsilon}'_Y$ mean total void fraction or liquid volume fraction, determined on the basis of layer height measurement

μ' dynamic viscosity of the liquid (kg/sec·m)

ρ density of the particles (kg/m^3)

ρ' density of the liquid (kg/m^3)

REFERENCES

1. BLICKLE, T., ORMÓS, Z., Hung. J. Ind. Chem. 1, 31 (1973)

2. BLICKLE, T., ORMÓS, Z., Hung. J. Ind. Chem. 1, 185 (1973)

3. RICHARDSON, I.J.F., ZAKI, W.N., Trans. Inst. Chem. Engrs. 32, 35 (1954)

4. JOTTRAND, R., Chem. Eng. Sci. 4, 12 (1954)

5. BLICKLE, T., A fluidizációs eljárás készülékei, alkalmazásai és számitásai. (Apparatuses, Applications and Calculations of the Fluidization Technique.) Akadémiai Kiadó, Budapest, 1963.

6. ORMÓS, Z., D. Techn. Thesis.Veszprém University of Chemical Engineering, 1968.

7. SAXTON, J.A., FITTON, J.B., VERMEULEN, T., AIChE Journal 16, 120 (1970)

8. BLICKLE, T., D. Sc. Thesis. Budapest, 1967.

9. SZOLCSÁNYI, P., Magyar Kémiai Folyóirat, 67, 171 (1961)

10. BRÖTZ, W., Chem. Ing. Techn. 24, 57 (1952)

11. BERÁNEK, J., KLUMPAR, J., Chem. Listy. 50, 1673 (1956)

12. LEWA, M., Fluidization, McGraw-Hill Book Company, New York, 1959.

13. HETZLER, R., WILLIAMS, M.C., Ind. Eng. Chem. Fundamentals 8, 668 (1969)

14. ORMÓS, Z., Hung. J. Ind. Chem. 1, 207 (1973)

РЕЗЮМЕ

В данной статье авторы кратко ознакомливают с имеющимися в литературе наиболее распространенными уравнениями, а также с выведенными ими в предыдущей статье данного цикла зависимостями, для вычисления доли свободного объема псевдоожиженных посредством жидкости слоев. Указанные зависимости приводятся к виду, практически непосредственно применимому, распространяющемуся даже на случай пористых частиц. Авторами определены средние значения имеющихся в уравнениях "постоянных сомножителей", кроме того, "постоянные" были проверены на зависимость от различных параметров. Была проведена проверка расчетных методов посредством сравнения полученных экспериментально и рассчитанных по уравнениям значений доли свободного объема.

Hungarian Journal
of Industrial Chemistry
Veszprém
Vol.1. pp. 513-532 (1973)

VERFAHREN ZUR HERSTELLUNG VON FETTSÄUERZUCKERESTERN

A. UJHIDY, J. SZÉPVÖLGYI und Z. SZABÓ*

(Forschungsinstitut für Technische Chemie der Ungarischen
Akademie der Wissenschaften, Veszprém und
*Zentralforschungsinstitut für die Lebensmittelindustrie, Budapest)

Eingegangen am 7. September 1973.

Die Darstellung einer Gruppe der oberflächenaktiven Stoffe, der Fettsäurezuckerester Saccharosepalmitat und Saccharosestearat wurde untersucht, mit besonderer Rücksicht auf die Erhöhung des Monoestergehaltes im Produkt. Die optimalen Parameter der chargenweisen Darstellung des an Monoester reichen Fettsäurezuckeresters im Laboratoriummaßstab werden auf Grund der Versuchsergebnisse angegeben. Versuche zur halbkontinuierlichen Darstellung von Fettsäurezuckerestern im Dünnschichtreaktor wurden ebenfalls durchgeführt.

EINLEITUNG

Die Zuckerester der Fettsäuren werden im allgemeinen durch die Umesterung von C_{15}-C_{20} Fettsäurealkylestern mit einem Zucker in Lösung, in Anwesenheit eines geeigneten Katalysators hergestellt.

Die ersten Versuche zur Darstellung von Zuckerester wurden Mitte des vorigen Jahrhunderts durchgeführt, als BERTHELOT [1] einen Zuckerester durch Erhitzen von Saccharose mit Stearinsäure herzustellen versuchte. LORAND [2] gewann den Zuckerester der Palmitinsäure in der Reaktion von Zucker mit Palmitinsäureanhydrid in Monochloressigsäure als Lösungsmittel, in Anwesenheit eines Magnesiumperchlorat-Katalysators.

Die Umesterung des Methylstearats mit Zucker wurde von OSIPOW und Mitarb. [3] eingehend untersucht in Dimethyl-formamid und Dimethylsulfoxyd als Lösungsmittel.

Die Umesterung ist eine Gleichgewichtsreaktion, und das Gleichgewicht soll durch die rasche Entfernung des in der Reaktion gebildeten Methanols in Richtung der Bildung des Saccharoseesters verschoben werden. Dies kann durch die Erhöhung der Temperatur erreicht werden. Diese Möglichkeit ist aber wegen der Karamelbildung des Zuckers und der Nebenreaktionen begrenzt. Es ist nicht zweckmässig, die Temperatur über 130-135 ^{o}C zu steigern.

Zur Erhöhung der Wirksamkeit der Entfernung des Methanols, und dadurch zur Verschiebung des Gleichgewichtes haben OSIPOW und Mitarb. [4] das Reaktionsgemisch durch einen Dünnschichtverdampfer, worin die Flüssigkeit einen turbulenten Film bildete, umlaufen lassen.

In der Umesterungsreaktion bilden sich der Mono-, und der Diester der Saccharose und unter Umständen höher veresterte Derivate. Vom Gesichtspunkt der praktischen Verwendung aus ist der Saccharosemonoester günstiger als der Diester. Der Monoester löst sich nämlich in Wasser unter Bildung einer kolloidalen Lösung,während der Diester mit Wasser eine schleimige Dispersion gibt. Deswegen ist es zweckmäßig, die Umesterungsreaktion so zu führen, daß der Anteil des Monoesters in dem Produkt maximal sei. OSIPOW [4] erreichte diesen Ziel durch dem Reaktionsgemisch zugesetzte Wasserspuren. Unter dem Einfluß des Wassers reagierten die Polyester mit der freien Saccharose zum Monoester.

Die von OSIPOW [5] im Laboratorium ausgearbeitete Mikroemulsionsmethode bedeutet eine neue Art für die Herstellung von Fettsäurezuckerester. Das Prinzip der Methode liegt darin, daß die ineinander nicht löslichen und daher nur in Anwesenheit eines Lösungsmittels reagierenden Zucker und Methylester in einer sehr feinen Dispersion (Tropfengröße 0,01-0,06 μ) miteinander direkt reagieren können.

Der Gehalt an Monoester in dem Produkt wurde von ZAJIC und BARES [6] dadurch erhöht, daß die Umesterungsreaktion in einem ge-

eigneten Zeitpunkt durch Blockierung des Katalysators, durch Zugabe einer sauren Verbindung eingefroren wurde.

Das Patent [7] verwendete für die Umesterung - von den bisher geschilderten Methoden abweichend - ein Anionenaustauscher--Harz als Katalysator. Das Harz hat den Vorteil, daß es von dem Produkt leicht zu trennen ist. Über die Regenerierung, bzw. wiederholte Verwendung des Harzes wurden aber bisher keine Einzelheiten angegeben.

Die bei der Umesterung verwendeten Lösungsmittel riechen unangenehm und sind toxisch, deswegen soll das Produkt von diesen mit besonderer Sorgfalt befreit werden. Die Lösungsmittelspuren können aber wegen der guten Adsorptionseigenschaften der Fettsäureester nur mühsam entfernt werden. Ein weiteres Problem stellt die Gewinnung des Produktes in relativ reinem Zustand dar.

Die verschiedenen Mitteilungen geben für die Entfernung der letzten Lösungsmittelspuren ferner für die Reinigung des Produktes meistens komplizierte Extraktionsverfahren an [3, 4, 8, 9, 10].

Das Ziel unserer Arbeit war, die Umesterungsreaktion - zur Vermeidung der ziemlich mühsamen Trennung der Mono- und Diester - zweckmäßig so zu führen, daß die Konversion des Zuckers und der Anteil des Monoesters in dem Produkt maximal wird.

Beschreibung der Versuche

Fettsäurezuckerester wurden aus Fettsäuremethylestern durch Umesterung nach drei verschiedenen Methoden hergestellt. Die verwendeten Methoden sind die folgenden:

a) Umesterung nach der Mikroemulsionsmethode,

b) Herstellung von Fettsäurezuckerestern diskontinuierlich,

c) Herstellung von Fettsäurezuckerestern im Dünnschichtreaktor halbkontinuierlich.

Vor der ausführlichen Beschreibung der Versuchsergebnisse werden die zur Analyse des umgeesterten Produktes ausgearbeiteten Verfahren zusammengefasst.

Das in der Umesterungsreaktion erhaltene Produkt wurde von dem Lösungsmittel durch Destillation befreit, die letzten Lösungsmittelspuren wurden danach durch zweistündige Behandlung des Produktes in der Trockenpistole - bei 1-2 Torr und 100 °C - entfernt. Das zur Analyse auf diese Weise vorbereitete Produkt enthielt unreagierten Methylester, Zucker, Seife, Katalysator, ferner Saccharoseester.

Der Methylestergehalt des Produktes wurde nach alkalischer Verseifung durch Messung des entstehenden Methanols bestimmt [11]. Die Methode ist auch zur Bestimmung sehr geringer Mengen von Methanol geeignet, und die Messungen sind gut reproduzierbar.

Der Zucker- und Zuckerestergehalt des Produktes wurde nach Extraktion mit n-Butanol-Wasser Gemisch durch Messung der optischen Drehung der Wasser- bzw. der Butanolphase bestimmt. Bei Kenntnis der Drehung der Butanolphase, des Gewichtes des in der Phase aufgelösten festen Stoffes, ferner der spezifischen Drehung des Saccharosemonostearates bzw. des Distearates kann der Anteil des Mono- und des Diesters in der Probe bestimmt werden. Der Seifengehalt der Probe (K-Stearat, bzw. K-Palmitat) wurde auf folgende Weise bestimmt: zu ein aliquotes Volumen der Butanolphase wurde das gleiche Volumen kohlendioxidfreien destillierten Wassers zugefügt, und mit 0,1 N Salzsäure in Anwesenheit von Methylorange Indikator titriert.

Das durch Destillation von dem Lösungsmittel befreite Rohprodukt enthielt - wegen seiner oberflächenaktiven Eigenschaft - noch etwa 0,2 % Dimethylformamid. Wegen des toxischen Charakters dieser Verbindung soll die Menge des in dem Produkt vorhandenen Dimethylformamids bekannt sein. Der Gehalt an Dimethylformamid des Produktes wurde laut Mitteilung [12] bestimmt. Das Prinzip der Methode ist, daß das Dimethylformamid beim Kochen mit Lauge verseift wird, und sich das entstandene Dimethylamin photometrisch quantitativ bestimmen läßt.

Die Werte der Konversion, der Ausbeute und der Selektivität wurden zur Auswertung der Ergebnisse der Umesterungsversuche aus den Analysenergebnissen auf folgende Weise Bestimmt:

K = [(eingewogenes MSt-unreagiertes MSt)·100]/eingewogenes MSt

A = [SME·100]/eingewogenes MSt

S = [SME·100]/[eingewogenes MSt-unreagiertes MSt]

wobei

K die Konversion (%)
A die Ausbaute (%)
S die Selektivität (%)
MSt Menge des Methylesters (Mol)
SME Menge des Saccharosemonoesters (Mol)

Umesterung nach der Mikroemulsionsmethode

Einerseits um das in Mitteilung [5] beschriebene Mikroemulsions-Laboratoriumsverfahren zu reproduzieren, andererseits zur Ausarbeitung einer eventuellen neuen Darstellungsmethode wurden Versuche zur Synthese von Fettsäurezuckerester nach der Mikroemulsionsmethode in Propylenglykol als Lösungsmittel durchgeführt. Zu einem in Propylenglykol aufgelösten Gemisch von Zucker, Methylstearat und Kaliumkarbonat wurde unter intensivem Rühren Natriumstearat zugefügt. Das Propylenglykol wurde in einem Volumen verwendet, in dem das Gemisch leicht gerührt werden konnte.

Mehrere parallele Versuche wurden mit Reaktionsdauern von 2, 4 und 6 Stunden bei 105 °C durchgeführt. Es wurde festgestellt, daß, obwohl die Konversion mit der Zeit zunahm, die Menge des Saccharoseesters auch nach einer 6-stündigen Reaktionszeit nicht mehr betrug als einige Prozente. Gleichzeitig nahm die Seifenbildung als unerwünschte Nebenreaktion zu.

Weitere Nachteile dieser Methode sind die Folgenden: es ist schwierig, die Emulsion zu erhalten, die Wahrscheinlichkeit der Karamelbildung ist hoch, ferner kann eine Umesterung mit dem als

Lösungsmittel verwendeten Propylenglykol eintreten. Auf Grund dessen ist die Mikroemulsionsmethode laut unserer Erfahrungen zur Erzeugung einer größeren Menge einheitlichen Produktes nicht geeignet.

Diskontinuierliche Umesterung

Unsere Versuche wurden in einem mit Rückflußkühler, Tropftrichter und Thermometer versehenen Dreihalskolben durchgeführt, welcher von außen mit einem Ölbad geheizt wurde. Während der Umesterungsreaktion betrug der Druck im Reaktionsraum 100-150 Torr. Die durch die Siedekapillare eingesaugte Luft rührte das Reaktionsgemisch befriedigend um.

Wurde die Umesterung in Dimethylsulfoxyd bei 90 °C, mit einem 3:1 Molverhältnis von raffiniertem Zucker und Methylester, mit einer Katalysatormenge von 0,049 g K_2CO_3/g Methylester durchgeführt, so betrug die Konversion des Methylesters etwa 80 %, und die Ausbeute 30 %. Mit der Erhöhung der Katalysatormenge nahm die Konversion und die Ausbeute in geringem Maße zu, die Seifenbildung verstärkte sich aber ebenfalls beträchtlich. Unter ähnlichen Reaktionsbedingungen wurde die Umesterung in Dimethylformamid als Lösungsmittel ebenfalls durchgeführt, wo bei einer Konversion von 80-90 % eine Ausbeute von 70-75 % erreicht werden konnte.

Gemäß unseren Versuchen konnte das Dimethylsulfoxyd mit einem Verlust von 20-30 %, und das Dimethylformamid mit einem von 2-5 % regeneriert werden. Im weiteren wurde daher Dimethylformamid als Lösungsmittel verwendet.

Zwei Forderungen müssen bei der Durchführung der Umesterungsreaktion erfüllt werden: neben einer möglichst hohen Konversion soll auch der Monoestergehalt so hoch wie möglich gehalten werden. Durch die richtige Auswahl der Versuchsparameter kann die Konversion bis auf 98-100 % gesteigert werden, wobei es zwecks Erhöhung des Monoestergehaltes wünschenwert ist, laut der Literatur 0,1 % Wasser dem Reaktionsgemisch zuzufügen.

Laut unserer Vorversuchen nimmt aber sowohl die Geschwindigkeit der Umesterungsreaktion, wie auch die Konversion ab, wenn 0,1 % Wasser zu Beginn der Reaktion zum Reaktionsgemisch zugefügt wird.

Als erstes Problem wurde daher untersucht, wie ein Produkt von entsprechender Reinheit mit guter Konversion ohne Zugabe von Wasser erzeugt werden könnte. In jedem Fall wurde Kaliumkarbonat als Katalysator verwendet. Die Versuchsangaben sind in der Tabelle 1. aufgeführt.

Die Versuche No. 1. und 2. zeigten, daß die Zusammensetzung des Produktes mit der Erhöhung der Temperatur günstiger wird, da auch die Geschwindigkeit der Reaktion zwischen dem Diester und Zucker neben der Geschwindigkeit der Entstehung des Diesters bei höherer Temperatur höher wird. Der Grund für die bei 95°C erreichte höhere Konversion liegt darin, daß das Verhältnis Katalysator/ /Methylester in dem Versuch No. 1. größer war.

Diese beiden Versuche waren eigentlich auf die Kontrolle der in der Literatur angegebenen Daten ausgerichtet und zeigten, daß bei diesen Versuchsbedingungen entweder die Konversion, oder die Zusammensetzung des Produktes ungünstig war.

Laut der Literatur kann der Gehalt an Monoester des Produktes auch so gesteigert werden, daß die Aktivität des als Katalysator verwendeten Kaliumkarbonats in einer gewissen Phase der Umesterungsreaktion (wo die Menge des Monoesters erwartungsgemäß die größte ist) blockiert wird, wodurch die unerwünschten Nebenreaktionen beseitigt werden können. Daher wurde der Katalysator in den Versuchen No. 3. und 4. nach einer Reaktionsdauer von 6 Stunden durch Zugabe von beinahe äquivalenten Mengen CH_3COOH bzw. H_3PO_4 blockiert. Diese Methode führt mit der angewandten Reaktionsdauer nicht zum erwünschten Ziel, da am Anfang der Reaktion hauptsächlich Diester entsteht.

Eine andere Möglichkeit zu der Erhöhung des Monoesteranteiles besteht darin, daß die notwendige Menge des Methylesters in Dimethylformamid aufgelöst und in mehreren Portionen dem Gemisch zugeführt wird. Auf diese Weise wurde der Methylester in den Versu-

Tabelle 1. Diskontinuierliche Umesterungsversuche ohne Zugabe von Wasser

No	Reaktions-	Temp.	K_2CO_3/MSt	Zusammensetzung des Produktes (%)					K	A	S	Bemer-
	dauer (St)	(°C)	(g/g)	Zucker	MSt	Seife	SME	SDE	(%)	(%)	(%)	kung
1	12	95	0,107	59,80	0,00	2,75	20,30	14,40	100,0	43,6	43,6	x
2	12	105	0,081	61,50	0,43	1,62	21,60	13,20	82,6	46,2	55,9	x
3	6	120	0,054	59,30	5,64	0,51	16,03	12,80	75,6	34,1	45,0	xx
4	6	120	0,054	57,30	2,58	0,20	15,10	26,70	88,4	32,1	36,3	xx
5	6	120	0,054	64,10	10,77	0,37	9,90	10,00	51,5	21,0	40,7	xxx
6	7	120	0,054	63,30	10,58	0,14	12,40	6,60	52,5	26,5	50,4	xxx
7	7	120	0,054	59,00	5,60	0,50	23,50	10,50	74,8	50,0	66,9	xxxx

Molverhältnis Zucker/Methylester: 2,90
Verhältnis Dimethylformamid/Zucker: 3,3 ml/g

x Zugabe des Katalysators in zwei Portionen, nach Ablauf von 0 und 2 Stunden
xx Blockierung des Katalysators bei dem Versuch No. 86. mit Essigsäure, bei 4. mit Phosphorsäure
xxx MSt in DMF aufgelöst in drei gleichen Portionen nach Ablauf von 0, 1,5 und 3 Stunden zugegeben
xxxx Zugabe von MSt wie bei No. 5. und 6., Zugabe des Katalysators in zwei Portionen nach Ablauf von 0 und 2 Stunden.

chen No. 5., 6. und 7. in drei gleich großen Mengen zu Beginn der Reaktion, nach 1,5 und nach 3 Stunden dem Gemisch zugegeben.

Da das Zucker:Methylester Molverhältnis in dem Reaktionsgemisch in jedem beliebigen Zeitpunkt größer war als 2,9, war es zu erwarten, daß sich hauptsächlich Monoester bildet, und gleichzeitig die Menge des Katalysators und die Reaktionszeit vermindert werden können.

Es wurde aber festgestellt, daß weder die Konversion, noch die Ausbaute die erwünschte Erhöhung aufwiesen, im Gegenteil, die Ergebnisse waren weniger günstig, weil der nach Ablauf von 1,5 Stunden zugefügte Methylester nur 4,5, bzw. 5,5 Stunden lang, während der nach 3 Stunden zugefügte Ester nur 3, bzw. 4 Stunden lang reagieren konnte. Diese Beobachtung unterstützte wiederholt, daß zur Vollendung der Umesterung eine längere Zeit notwendig ist.

Auf Grund der Versuche No. 6. und 7. konnte festgestellt werden, daß es am günstigsten ist, wenn der Katalysator portionsweise dem System zugefügt wird. Sowohl die Konversion, als auch die Zusammensetzung des Produktes ist nähmlich im letzten Fall (No. 7.) günstiger. Der Grund dafür besteht darin, daß auf diese Weise eine beinahe konstante Katalysatorkonzentration in dem System gewährleistet werden kann.

Durch die vorher erwähnte Änderung der Versuchsparameter kann die erwünschte Verbesserung der Zusammensetzung des Produktes laut Angaben der Tabelle 1.nicht erreicht werden. Zur Darstellung eines Produktes mit höherem Monoestergehalt schien es zweckmäßig, Wasser zum Reaktionsgemisch derart zuzuführen, daß die Umesterungsreaktion nicht langsamer bzw. die Konversion des Methylesters nicht niedriger wird.

Den ungünstigen Einfluß des Wassers auf die Reaktion wollten wir so vermeiden, daß das Wasser nicht im Laufe der Umesterungsreaktion zu dem Reaktionsgemisch zugefügt wurde, sondern nach Ablauf der Reaktion. Das wasserhaltige Gemisch wurde nachher 1 Stunde bei einer Temperatur gerührt, welche niedriger war, als die Reaktionstemperatur. Die optimale Zeitdauer dieser Behandlung betrug 1 Stunde, weil sich das Monoester/Diester-Verhältnis nach einer Stunde nicht mehr änderte.

Tabelle 2. Diskontinuierliche Umesterungsversuche und zusätzliches Ausrühren mit Wasser

No	Reaktionsdauer (St)	Temperatur (°C)	Kat/MSt (g/g)	Zusammensetzung des Produktes (%)					K (%)	A (%)	S (%)	Bemerkung
				Zucker	MSt	Seife	SME	SDE				
8	1,5 1	120[x] 95[xx]	0,054	61,30	5,65	1,25	14,20	16,80	74,5	30,1	40,4	
9	3 1	120[x] 95[xx]	0,054	60,10	3,76	0,95	17,30	13,20	83,0	36,7	44,2	
10	4 1	120[x] 95[xx]	0,054	58,10	2,91	0,70	22,30	9,40	87,0	47,3	54,4	
11	6	120[x] 95[x]	0,054	57,60	3,10	0,38	28,30	8,80	86,1	59,8	69,4	
12	1,5 1	120[x] 95[xx]	0,054	39,10	9,15	3,10	37,50	9,33	75,0	48,0	64,1	
13	3 1	120[x] 95[xx]	0,054	37,60	8,66	3,00	41,50	4,06	76,8	53,2	67,1	
14	11 1	95[x] 90[xx]	0,107	56,02	0,14	1,95	31,00	8,50	99,5	66,7	68,0	xxx

15	11 1	105^{x} 95^{xx}	0,081	55,00	0,00	1,50	32,40	8,60	100,0	67,5	67,5	xxx
16	11 1	105^{x} 95^{xx}	0,081	45,80	6,51	1,50	32,90	0,10	77,0	70,0	90,5	xxx
17	11 1	105^{x} 95^{xx}	0,081	33,81	2,98	3,33	32,90	18,20	91,7	42,6	46,4	xxx
18	11 1	105^{x} 95^{xx}	0,081	56,30	0,17	1,26	38,80	0,59	99,4	82,7	83,3	xxx Na_2CO_3
19	11 1	105^{x} 95^{xx}	0,081	43,85	1,40	1,92	26,90	16,90	95,3	42,7	45,0	xxx Na_2CO_3

x während der Reaktion

xx während des Ausrührens mit Wasser

xxx Zugabe des Katalysators in zwei Portionen nach Ablauf von 0 und 4 Stunden

Molverhältnis Zucker/Methylester: 2,88 (No. 8, 9, 10, 11, 14, 15, 18)
2,00 (No. 16, 19)
1,39 (No. 12, 13, 17)

Zum Ausrühren zugegebene Menge von Wassers: 0,10 % (No. 14)
0,13 % (No. 8, 9, 10, 11, 12, 13,
1,20 % (No. 15, 16, 17, 18, 19)

Das Ergebnis der mit Wasserzugabe durchgeführten Versuche ist in der Tabelle 2. ersichtlich.

Die Reaktionstemperatur und die Reaktionsdauer stellen miteinander eng verbundene Parameter dar, deswegen wurde der Einfluß dieser beiden untersucht. Die Erhöhung der Reaktionszeit bei 120°C ergab eindeutig die Zunahme der Konversion und der Ausbeute (Versuche No. 8., 9., 10. und 11). Die Zunahme des Verhältnisses Monoester:Diester mit der Erhöhung der Reaktionsdauer weist ebenfalls darauf hin, daß der Diester in der Anfangsperiode der Reaktion das Hauptprodukt ist.

Aus dem Vergleich des Versuchs No. 11. mit den Versuchen No. 5., oder 3. und 4. (Tabelle 1.) ist es ersichtlich, daß durch ein Ausrühren mit Wasser günstigere Ergebnisse erreicht werden können, als durch Zugabe des Methylesters in drei Portionen, oder durch Blockierung des Katalysators mit Säuren. (Der Katalysator wurde in allen diesen vier Fällen auf einmal, am Anfang der Reaktion dem Reaktiongemisch zugegeben.)

Die Ergebnisse der mit einem Molverhältnis von 1,39 zwischen dem Zucker und Methylester durchgeführten Versuche No. 12. und 13. stimmen mit unseren früheren Feststellungen über den Effekt der Reaktionsdauer überein.

Unsere weiteren Versuche wurden zwecks Vermeidung der Karamelbildung bei niedrigerer Temperatur und mit einer längeren Reaktionszeit durchgeführt. Wegen der längeren Reaktionsdauer wurde der Katalysator zweckmäßigerweise in 2 Portionen zum Gemisch gegeben: 2/3 der gesamten Menge wurde am Anfang der Reaktion, das übrige 1/3 nach Ablauf von 4 Stunden zugefügt.

Weitere Umesterungsversuche wurden bei 95 °C und bei 105 °C, mit der Reaktionsdauer von 11 Stunden, und nachfolgendem einstündigem Ausrühren mit Wasser durchgeführt (Versuche No. 14. und 15.). In beiden Fällen wurde ein Produkt mit höhem Monoestergehalt mit guter Konversion erhalten. Die Seifenbildung wurde in diesen Versuchen durch die herabgesetzte Katalysatormenge geringer, während die Erhöhung der Wassermenge das Verhältnis Monoester/Diester verbesserte.

Auf Grund der durchgeführten Versuche schienen die bei dem Versuch No. 15. angewandten Parameter optimal zu sein. Das Monoester:Diester-Molverhältnis betrug in diesem Fall 5,5:1.

Zwecks Senkung der Selbstkosten des Produktes wurde die Möglichkeit einer Verminderung des Molverhältnisses Zucker:Methylester unter Beibehaltung der optimalen Werte der übrigen Parameter untersucht (Versuche No. 15., 16. und 17.). Es konnte aber festgestellt werden, daß die Verminderung des Molverhältnisses bei der angewandten Temperatur nicht zweckmässig ist.

Neben Kaliumkarbonat wurde auch die katalytische Wirkung des Natriumkarbonats untersucht. Das Natriumkarbonat könnte sich günstiger erweisen, als das Kaliumkarbonat, da es nicht toxisch ist, und dadurch die praktische Verwendung des Produktes nicht stört.

Natriumkarbonat erwies sich sowohl bei einem Molverhältnis von 2,88 zwischen dem Zucker und Methylester, als auch bei dem Molverhältnis von 2,00 (Versuch No. 18. und 19.) als ein günstigerer Umesterungskatalysator und erhöhte in erster Linie die Ausbeute beträchtlich.

So beträgt z.B. das Verhältnis Monoester:Diester bei den in Anwesenheit von Kaliumkarbonat oder Natriumkarbonat durchgeführten Versuchen 5,5 bzw. 93,9 gemäß der Angaben der Versuche No. 15. bzw. 18. Der zweite Wert ist günstiger, als die bisher beschriebenen. Auf Grund dessen sind die optimalen Werte der Parameter hinsichtlich der Konversion und der Bildung des Monoesters die folgenden:

Reaktionstemperatur	105 °C
Reaktionszeit	11 Stunden
Dauer der Behandlung mit Wasser	1 Stunde
Menge des zugefügten Wassers	1,2 % der Gesamtmenge des Reaktionsgemisches
Katalysator	Na_2CO_3
Zugabe des Katalysators	2/3 am Anfang der Reaktion 1/3 nach 4 Stunden
Lösungsmittel	Dimethylformamid
Verhältnis Dimethylformamid/Zucker	3,3 ml/g
Molverhältnis Zucker/Methylester	2,88.

Halbkontinuierliche Umesterung im Dünnschichtreaktor

Wie oben beschrieben, nimmt die Umesterung ziemlich viel Zeit in Anspruch. Um die Reaktionszeit der Umesterung zu vermindern, wurde auf Grund der in der diskontinuierlichen Einrichtung gewonnenen Versuchsergebnisse eine halbkontinuierliche bzw. Rezirkulationseinrichtung im Laboratoriummaßstab entworfen, gebaut und betrieben.

Der Hauptteil der Einrichtung besteht aus einem Rotationsdünnschichtreaktor aus rostfreien Stahl mit einem inneren Durchmesser von 53,3 mm und einer aktiven Oberfläche von 0,057 m^2, mit geteiltem Heizmantel und mit Wischern versehenem Rotor (Typ. Sambay). Die Rohrachse des Rotors wurde in Längsrichtung mehrfach perforiert, um das Absaugen der in der Reaktion entstandenen Methanoldämpfen auch auf diese Weise zu sichern.

Die Einrichtung wurde durch das in dem Heizmantel strömende Glyzerin geheizt, während das Reaktionsgemisch in dem System durch eine Pumpe umgewälzt wurde. Der Druck in Dünnschichtreaktor betrug 100-150 Torr.

Der Vorteil des Dünnschichtreaktors besteht darin, daß das in der Reaktion entstehende Methanol infolge der günstigen Stoffübergangsverhältnisse schon in dem Moment seiner Entstehung entfernt werden kann, so daß die Gleichgewichtsreaktion in Richtung der Bildung der Saccharoseester verschoben werden kann. Der andere Grund, weshalb die Anwendung einer Dünnschichtreaktors zweckmäßig ist, besteht darin, daß voraussichtlich keine Karamelbildung bei der verhältnismäßig hohen Temperatur infolge des kurzen Aufenthaltes der Reaktanten in dem Reaktor eintritt, weil der Temperaturkoeffizient der Reaktion der Karamelbildung kleiner ist, als die der Umesterung.

Da die Umesterung ein langsamer Vorgang ist, wurde das Reaktionsgemisch wegen des kurzen Aufenthaltes im Reaktor zur Erreichung einer guten Konversion in der Abbildung 1. dargestellten Versuchseinrichtung rezirkuliert. Auf diese Weise stand das Reaktions-

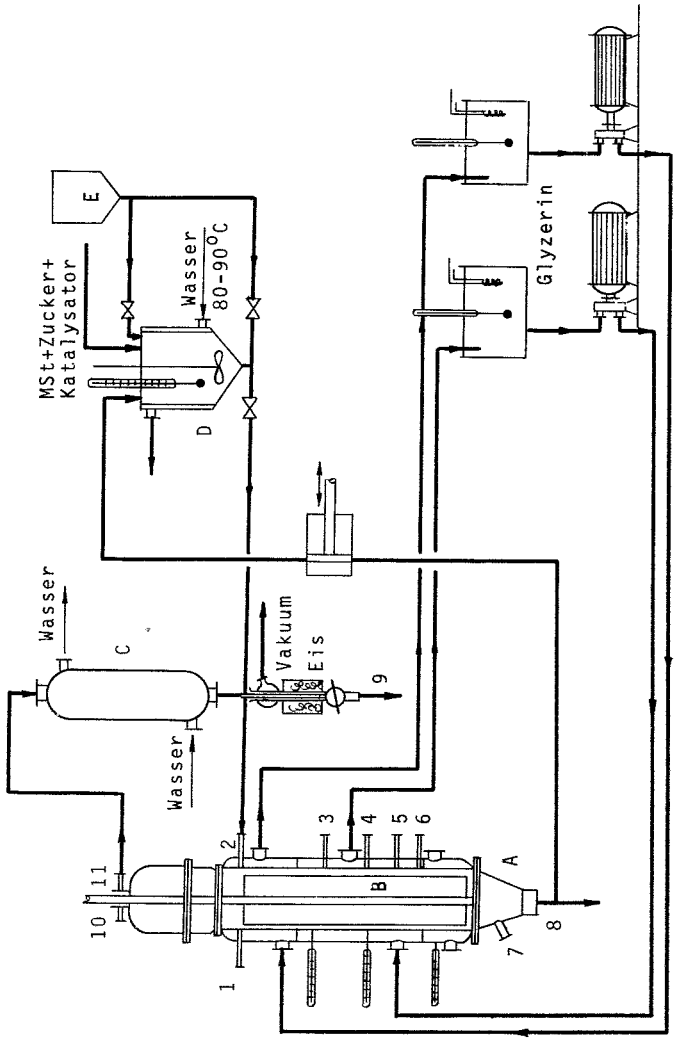

Abb. 1. Die halbkontinuierliche Versuchseinrichtung. 1-6 – Zufuhrstutzen; 7-8 – Produktabnahme; 9 – Methanolabnahme; 10-11 – Methanoldämpfe; A – Dünnschichtreaktor; B – Rotor; C – Kühler; D – Vermischer und Zufuhrbehälter; E – Behälter für Dimethylformamid

gemisch einerseits mit der wärmeren Wand des Filmreaktors in Kontakt, und hielt sich andererseits verhältnismäßig lang in dem Zufuhrbehälter D auf, welcher bei einer Temperatur von 95 °C gehalten wurde.Die durchschnittliche Verweilzeit des Reaktionsgemisches wurde durch Änderung der Geschwindigkeit der Umwälzung reguliert. Diese Geschwindigkeit betrug 22 ml/Min und 100 ml/Min.

Die Erzeugungs- und Betriebskosten der halbkontinuierlichen Versuchseinrichtung liegen höher, als die der diskontinuierlichen Einrichtung. Die Durchführung der Umesterung in einem Dünnschichtreaktor kann also nur in dem Fall als begründet betrachtet werden, wenn die Reaktionszeit der Umesterung bei unveränderter Konversion und Zusammensetzung des Produktes mindestens auf 20 % der in den diskontinuierlichen Versuchen notwendigen Reaktionszeit herabgesetzt werden kann.

Gemäß der durchgeführten Versuche war die optimale Zeitdauer der diskontinuierlichen Umesterung 11 Stunden.

In den halbkontinuierlichen Versuchen wurde das Molverhältnis Zucker:Methylester auf den bei den diskontinuierlichen Versuchen als optimal gefundene Wert 2,9:1 eingestellt.

In unseren Versuchen konnte festgestellt werden, daß das Verhältnis Monoester:Diester durch eine Behandlung des Reaktionsgemisches nach der Beendigung der Reaktion in die Richtung der Bildung des Monoesters verschoben werden kann. Mit diesem Ziel wurden die in der Tabelle 3. zusammengefassten Versuche in der halbkontinuierlichen Einrichtung vorgenommen. Das Reaktionsgemisch wurde 1,5 Stunden lang mit einer Rezirkulationsgeschwindigkeit von 100 ml/Min in der Versuchseinrichtung rezirkuliert, das bei dem gegebenen Volumen einem Rezirkulationsverhältnis von 22,5 entsprach. (Das Rezirkulationsverhältnis gibt an, wievielmal die Pumpe das gesamte Volumen des Reaktionsgemisches innerhalb der gegebenen Reaktionszeit umgewälzt hat.)

Nachher wurde das Reaktionsgemisch nach Zugabe von Wasser (2,1 % auf die Gesamtmenge berechnet) in einem mit Rückflußkühler und Rührer versehenen Rundkolben 1 Stunde bei 95 °C gerührt. Parallel zu diesem Versuch wurde ein analoger Versuch ohne Zugabe von Wasser durchgeführt.

Tabelle 3: Umesterungsversuche im Dünnschichtreaktor und zusätzliches Ausrühren mit Wasser

No	Reaktionsdauer (St)	Temperatur (°C)	Wasser	Zusammensetzung des Produktes (%) Zucker	MSt	Seife	SME	SDE	K (%)	A (%)	S (%)
20	1,5[x]	120	-	57,60	7,70	1,50	19,90	16,10	64,0	28,2	44,1
	1,0[xx]	95	+								
21	1,5[x]	120	-	61,70	6,65	1,30	31,10	0,00	69,0	67,0	97,0
	1,0[xx]	95	+								
22	1,5[x]	130	-	61,20	8,96	0,95	25,50	0,00	58,3	56,0	96,1
	1,0[xx]	95	+								
23	1,5[x]	130	-	63,05	10,10	0,70	23,50	0,00	53,2	51,5	96,7
	1,0[xx]	95	+								

x im Dünnschichtreaktor

xx während des Ausrührens mit Wasser

Molverhältnis Zucker/Methylester: 2,900

Verhältnis K_2CO_3/MSt: 0,087 g/g

Verhältnis Dimethylformamid/Zucker: 3,3 ml/g

Geschwindigkeit der Rezirkulierung 100 ml/Min

Die Durchführung der Umesterung in dem Dünnschichtreaktor bei 120 °C (Versuche No. 20. und 21.) führte zu der Feststellung, daß die Konversion trotz dem hohen Rezirkulationsverhältniss infolge der kurzen durchschnittlichen Verweilzeit gering ist. Eine Behandlung mit Wasser (Versuche No. 21.) verbesserte aber die Zusammensetzung des Produktes wesentlich.

In der bei 130 °C durchgeführten Umesterung nimmt die Konversion mit der Erhöhung der Temperatur nicht zu,sondern ab. Diese Erscheinung kann dadurch erklärt werden, daß die Berührung der Reaktanten infolge des größeren Rezirkulationsverhältnisses intensiver ist, und sich neben der Reaktion des Zuckers mit dem Methylester auch die konkurrierende Reaktion des Zuckers mit dem Diester abspielt. Die Erhöhung der Reaktion zwischen dem Zucker und Diester wird auch durch die Tatsache unterstüzt, daß bei 130 °C, auch ohne Behandlung mit Wasser, ein diesterfreies Produkt erhalten wurde (No. 22.).

In dem mit Wasser behandelten Reaktionsgemisch No. 23. war die Konversion geringer als in dem parallelen mit Wasser nicht behandelten Versuch No. 22. Der Grund dafür ist, daß die Reaktion auch während der einstündigen bei 95 °C durchgeführten Behandlung weiterläuft, die Zugabe von Wasser vermindert aber die Geschwindigkeit der Umesterung.

In der halbkontinuierlichen Einrichtung wurde also nur bei einer Reaktionszeit von 6 Stunden, bei einem Rezirkulationsverhältnis von 15-20 eine genügend hohe Konversion erreicht, wobei die optimale Temperatur des Dünnschichtreaktors 120-125 °C betrug. Zur Erzeugung eines Produktes mit günstiger Zusammensetzung war aber auch bei den optimalen Werten der Parameter ein Ausrühren mit Wasser notwendig.

Wegen des hohen Kostenbedarfs der halbkontinuierlichen Einrichtung, der Verkürzung der Reaktionszeit um nicht mehr als 40-50 %, und wegen der Notwendigkeit des Ausrührens mit Wasser, welche die ganze Technologie in eine diskontinuierliche Technologie umwandelt, ist es deshalb zweckmäßiger, die Umesterungsreaktion diskontinuierlich zu verwirklichen.

Die Verarbeitung des nach dem Ausrühren mit Wasser erhaltenen Reaktionsgemisches

Nach dem Ausrühren mit Wasser wurden die Lösungsmittel in einem Vakuum von 2-5 Torr abdestilliert. Nach dieser Methode destillierte das im Laufe des Ausrührens zugefügte Wasser schon in der Anfangsperiode der Destillation aus.

Da die Destillation bei einer Temperatur von 84-85°C erfolgt, und die Gesamtmenge der Lösungsmittel innerhalb von 2,5-3 Stunden aus dem Gemisch entfernt wird, kann die Konzentration des Mono- und Diesters nach den Gleichgewichtswerten verschoben werden, was eine Zunahme des Gehaltes des Produktes an Diester mit sich bringt. Um das zu vermeiden, wird 0,1-2% Wasser, auf das Anfangsgewicht des destillierten Gemisches berechnet, 30 Minuten nach dem Beginn der Destillation hinzugegeben (ungefähr von dieser Zeit an destilliert das bei dem Ausrühren zugegebene Wasser aus). Das im Laufe der Destillation zugegebene Wasser ändert die Konversion gemäß den Versuchsangaben kaum, die Umesterung kann also am Ende des einstündigen Ausrührens mit Wasser als beendet betrachtet werden, die Zusammensetzung des Produktes ändert sich aber abhängig von der Menge des Wassers wesentlich.

Das günstigste war dasjenige Verfahren, wo Wasser in einer Menge von 0,2-1 % des destillierten Gemisches nach Ablauf einer halben Stunde dem Reaktionsgemisch zugefügt wurde.

Die Verfasser danken dem Ministerium für Schwerindustrie für seine finanzielle Unterstützung.

LITERATUR

1. BERTHELOT, M., Ann. chim. phys. 60, 93 (1860)
2. USP. 1,959,590
3. OSIPOW, L., Ind. Eng. Chem. 48, 1459 (1956)
4. OSIPOW, L., J. Am. Oil Chem. Soc. 34, 185 (1956)
5. OSIPOW, L., J. Am Oil Chem. Soc. 44, 307 (1966)
6. Czech. P. 120.775
7. French P. 1,365,067
8. Brit P. 809,815
9. Brit P. 826,801
10. French P. 1,336,655
11. BLANK, O., Ber. dtsch. chem. Ges. 39, 1326 (1906)
12. KIRK-OTHMER, Encyclopedia of Chemical Technology, 2. Ed. John Wiley and Sons Inc., New-York, 1966. Vol. 10. p. 110.

РЕЗЮМЕ

Авторы изучают метод получения одной из групп поверхностно-активных веществ - сахарных эфиров жирных кислот: пальмитата сахарозы и стеарата сахарозы, причем особое внимание уделяется повышению содержания сложного моноэфира в конечном продукте. На основании экспериментальных данных авторы указывают оптимальные параметры получения сахарных эфиров жирных кислот, при которых в условиях периодически действующей лабораторной установки, они добились высокого содержания сложного моноэфира. Эксперименты проводились в ротационном пленочном реакторе полунепрерывного действия.

Hungarian Journal
of Industrial Chemistry
Veszprém
Vol.1. pp. 533-554 (1973)

ALGEBRAIC DESCRIPTION OF TECHNICAL CHEMICAL SYSTEMS III.

TRANSFORMATIONS OF MATERIAL SYSTEMS

T. BLICKLE and T. BENCZE

(Research Institute for Technical Chemistry of the Hungarian Academy of Sciences, Veszprém and Institute of System Engineering)

Received: February 22, 1973.

Material systems and the changes occurring in them were described with algebraic methods in the previous paper [1]. However, there is a basic connection between the two subjects: the changes occur on the material systems, and produce new ones from them. This may be termed transformation and is described in the following manner;

$$v : \binom{a_o}{a_v} \qquad (1)$$

This expression means that the material system a_o is, as a consequence of the change v_1, transformed to material system a_v. In the following the changes will be discussed and the relations between the mentioned changes and other material systems will be examined.

In technical chemical processes, the changes occur in operational units [2]. The material system of the operational unit is a composition of the starting material system with that of being produced. In the following this will be termed a quasi union of the two material systems and is designated by:

$$\hat{a} = a_o \cup a_v$$

The material system of the operational unit and the change occurring in it is also a description of the technical chemical process. This is termed a change-material composition and is designated by:

$$v_1 \Diamond \hat{a} \tag{3}$$

The content of Equations (1) and (3) being identical:

$$v_1 \left(\begin{matrix} a_e \\ a_v \end{matrix} c\right) \triangleq v_1 \Diamond \hat{a} \tag{4}$$

may be written, provided that:

$$\hat{a} = a_e \cup a_v$$

Expression (4) is called a Z technical chemical transformation, or - briefly - a Z transformation, and its designation is:

$$Z = [v : \left(\begin{matrix} a_e \\ a_v \end{matrix} c\right) \triangleq v_1 \Diamond \hat{a}] \tag{5}$$

An explanation of the concepts so far presented and a few new concepts are given in the following.

Starting and Resultant Material System

Let $A \supset a_i$ be a set of material systems. Four relations are interpreted in connection with this set according to the following:

Elements a_i and a_j are in relation φ_1 if - and only if - they are material streams continuously enterning into an operational unit. Relation φ_1 defines a partial set A_o of the set A:

$$a_i, a_j \in A$$

if

$$a_i \varphi_1 a_j \tag{6}$$

we may write

$$a_i, a_j \in A_o$$

However, instead of designation $A_o = \{a_{o,1}; a_{o,2}; \ldots a_{o,n}\}$ the following can be introduced:

$$A_o = a_{o,1} \circ a_{o,2} \circ \ldots \ldots \circ a_{o,n} \qquad (7)$$

Elements a_i and a_j are in relation φ_2 if - and only if - they are material streams continuously discharging from an operational unit. In a manner totally similar to the previous case we can write:

$$A_v = a_{v,1} \circ a_{v,2} \circ \ldots \ldots \circ a_{v,n} \qquad (8)$$

Elements a_i and a_j are in relation φ_3 if - and only if - they represent the material system of a given operational unit at the beginning of the process:

$$A_o^x = a_{o,1}^x \circ a_{o,2}^x \circ \ldots \ldots \circ a_{o,n}^x \qquad (9)$$

Elements a_i and a_j are in relation φ_4 if - and only if - they represent the material system of a given operational unit at the end of the process:

$$A_v^x = a_{v,1}^x \circ a_{v,2}^x \circ \ldots \ldots \circ a_{v,n}^x \qquad (10)$$

In the following, A_o and A_o^x will be termed starting material systems, A_v and A_v^x resultant material systems.

Change

The definition of ZADEK [3] can be applied to material systems. According to this, the system is the totality of objects which are connected by interactions and mutual connections. The following items of information will be considered as the objects of the material system: crystal structure, chemical structure, biological structure, state, dimensions, distribution, form, temperature, pressure, homogeneous connection and heterogenous con-

nection. The material system is the structure of these, the structure being defined by the mutual connections. It is the objects that alter during a change. The set of objects which form the material system a_i will be denoted by $\eta(a_i)$. In accordance with this, the connection between the change and the material systems will be described by the following equation:

$$v = [\eta(A_o) \cup \eta(A_o^x)] \setminus [\eta(A_v) \cup \eta(A_v^x)] \tag{11}$$

(The symbols that are usual in the theory of sets are used: $A \cap B$ is the common part of sets A and B; $A \cup B$ is the combination of sets A and B; $A \setminus B$ is the difference of sets A and B.)

The change:

$$v = \eta(A_o) \setminus \eta(A_v) \tag{12}$$

will in the following be termed stationary, whereas the change:

$$v^x = \eta(A_o^x) \setminus \eta(A_v^x) \tag{13}$$

will be termed intermitted and the change:

$$v^\circ = [\eta(A_o) \cup \eta(A_o^x)] \setminus [\eta(A_v) \cup \eta(A_v^x)] \tag{14}$$

unstationary.

The changes pertaining to the object difference of the material system were given in the previous paper [1]. The change is termed elementary if the sum of the difference set is one. In this case, the resultant material system produced by the change differs from the starting material system in one object only.

Transformation

On the basis of the aforesaid, the transformation according to Equation (1) can in general be given in the following form: the expression

$$v_1 : \begin{pmatrix} A_o + A_o^x \\ A_v + A_o^x \end{pmatrix} \qquad (15)$$

is termed transformation if the condition:

$$v_1 = [\eta(A_o) \cup \eta(A_o^x)] \setminus [\eta(A_v) \cup \eta(A_v^x)]$$

is fulfilled.

A transformation transforming a set A_o to A_v is termed stationary (v); that transformating A_o^x to A_v^x is termed intermittent (v^x); that transforming $(A_o + A_o^x)$ to $(A_v + A_v^x)$ is termed unstationary (v^o). The transformation can be regarded as the internal transformation of set A, since:

$$A_o, A_o^x, A_v, A_v^x, A_v^x \leq A \qquad (16)$$

If the objects of the starting and resultant material systems are identical, the transformation is, in the algebraic sense of the word, a permutation. For example, the transformation:

$$v_9 \wedge \delta_4 : \begin{pmatrix} K_1 \Rightarrow K_2 \rightarrow K_3 \\ K_1 \Rightarrow K_3 \rightarrow K_2 \end{pmatrix}$$

is a permutation.

The transformation is termed a multiple one, if more than one of the objects of the starting system are changed. A multiple transformation may be homogeneous, when the same change occurs more than once, for example:

$$(v_9 \wedge \delta_2)^2 : \begin{pmatrix} K_1 \rightarrow K_2 \rightarrow K_3 \\ K_1 \Rightarrow K_2 \Rightarrow K_3 \end{pmatrix}$$

As can be seen, the homogeneous transformation is designated by v^m. Here the exponent shows how many times the change occurs. If the starting material system is such that one given change may occur m_t times, but $m < m_t$, the transformation is selective with respect to the material system. For example:

$$v_9 \wedge \delta_2 : \begin{pmatrix} K_1 \rightarrow K_2 \rightarrow K_3 \\ K_1 \Longrightarrow K_2 \rightarrow K_3 \end{pmatrix}$$

It is apparent from the above that the starting and resultant material systems define the change in an unequivocal way, whereas the reverse is not true.

The multiple transformation may be heterogenous, when more than one change occurs. For example:

$$(v_5 \wedge \delta_1) \wedge (v_9 \wedge \delta_2) : \begin{pmatrix} K_1 \rightarrow K_2 \rightarrow K_3, & T_1 \\ K_1 \Longrightarrow K_2 \rightarrow K_3, & T_2 \end{pmatrix}$$

(T_1 and T_2 represent temperatures.)

The transformation is of identical order if the number of the materials of the starting and the resultant material system is the same; if the number of the starting materials is higher, the transformation is of the combining, if lower, it is of the decomposing type:

$$v : \begin{pmatrix} a_{0,1} \circ a_{0,2} \\ a_{v,1} \circ a_{v,2} \end{pmatrix}; \quad v : \begin{pmatrix} a_{0,1} \circ a_{0,2} \\ a_{v,1} \end{pmatrix}; \quad v : \begin{pmatrix} a_{0,1} \\ a_{v,1} \circ a_{v,2} \end{pmatrix} \qquad (16)$$

If it is continuous and not discrete objects that are altered during the change, the degree of change can be given by designating it by s and writing it in the exponent. Two such continuous transformations can be:

$$v_1^{s1} : \begin{pmatrix} a_o \\ a_{v,1} \end{pmatrix} \quad \text{and} \quad v_1^{s2} : \begin{pmatrix} a_o \\ a_{v,2} \end{pmatrix} \qquad (17)$$

and then we set the following postulations:

$$o < s_1 < 1 : \quad o < s_2 < 1$$

if $s_1 = 0$, $a_o = a_{v,1}$

if $s_1 > s_2$, the deviation of $a_{v,1}$ from a_o is greater than that of $a_{v,2}$; i.e. if the changing object is x, we may write

$$|x_{v,1} - x_o| > |x_{v,2} - x_o|$$

The transformation v^s: $(\overset{a_2}{a_1})$ is termed the inverse transformation of v^{-s}: $(\overset{a_1}{a_2})$. In the case of discrete changes, s is an integral number.

The transformation v_1 : $(\overset{A_{0,1}}{A_{v,1}})$ and v_2 : $(\overset{A_{0,2}}{A_{v,2}})$ are termed similar if:

$$v_1 = v_2 \tag{18}$$

The two transformations mentioned in the above are equal if:

$$\begin{aligned} A_{0,1} &= A_{0,2} \\ A_{v,1} &= A_{v,2} \end{aligned} \tag{19}$$

Quasi Union

The quasi union of two material systems is not defined unequivocally; it depends on the properties of the material systems.

The steps of the definition of quasi union are the following:

The Concept of Mean Material Systems

A mean temperature and pressure are supposed for the material systems present in the operational unit; only one state pertains to a given chemical structure and the information as to distribution is disregarded. Accordingly a material system $\bar{a}$ is obtained, whose information content is the following: crystal structure, chemical structure, biological structure, dimensions, form, homogeneous and heterogeneous connection.

The Combination (Union) of Material Systems

The following two rules are valid:

$$a_1 \cup a_1 = a_1 \tag{20}$$

$$a_1 \cup a_2 = \begin{cases} a_1 \Longrightarrow a_2 \\ a_2 \Longrightarrow a_1 \\ a_1 \rightarrow a_2 \\ a_2 \rightarrow a_1 \end{cases} \tag{21}$$

knowing the material systems it is possible to decide which equality is the appropriate one.

Accordingly, the quasi union of the operational unit can be defined, taking the aforesaid into consideration, in the following manner:

$$\hat{a} = A_o \cup A_o^x \cup A_v \cup A_v^x \tag{22}$$

The particular components of the material system $\hat{a}$ present in the operational unit are the auxiliary materials. A filling auxiliary material ($\hat{a}$") is termed that is added to the system at the beginning of the process and can be removed in an unchanged state at the end of the process:

$$\hat{a}" = A_o^x \cap A_v^x \tag{23}$$

A material system introduced continuously into the operational unit and leaving it in an unchanged state is termed recirculating auxiliary material ($\hat{a}$):

$$\hat{a} = A_o \cap A_v \tag{24}$$

The material system changing during the process can be described by:

$$\hat{a}' = A_o \setminus A_v \cup A_v \setminus A_o \cup A_o^x \setminus A_v^x \cup A_v^x \setminus A_o^x \tag{25}$$

On the basis of Equations (22) to (25) we can write:

$$\hat{a} = \hat{a}' \cup \hat{a}" \cup \hat{a}" \tag{26}$$

Permutations

According to the algebraic interpretation, the following transformations can be regarded as permutations:

$(v_5 \Lambda \delta_1) \Lambda (v_5 \Lambda \delta_1)^{-1}$ heat exchange

$(v_7 \Lambda \delta_1) \Lambda (v_7 \Lambda \delta_1)^{-1}$ e.g. rectification

$v_9 \Lambda \delta_4$ e.g. hypersorption

None of the other transformations is a permutation.

Connection Between the Starting Material Systems and the Change

Certain starting material systems postulate the occurrence of a given change.

Such are the following:

A_o postulates v_1. If there are two entering material streams $(A_{0,1} \circ A_{0,2})$ they postulate $v_8 \Lambda \delta_2$ in order to reach the state $A(K_1 \leftrightarrow K_2)$. The reverse of the above is that two leaving material streams postulate $v_8 \Lambda \delta_3$.

If the temperature of the entering material streams is different, the v_5 temperature change will occur, whereas in the case of a difference in pressure the result will be the v_6 change in pressure.

A homogeneous system may be formed, i.e. the change $v_9 \Lambda \delta_2$ may occur if the entering material system or that present in the operational unit is heterogeneous. If both material systems are gases, the change $v_9 \Lambda \delta_2$ always occurs; if they are liquids, the change occurs in most of the cases; if they are solids, the change does not occur.

Connection Between the Material System and the Change

The starting and the resultant material systems and the change are in such a connection as to determine the third one, if the other two are given. However, this system cannot in all cases be totally free, there are some restrictions. These are summarized in the following.

A considerable part of the change may act on any type of material system, there being no restrictions. Such changes are: transportation ($v_1 \Lambda \delta_1$), change in scattering ($v_2 \Lambda \delta_1$), increasing or decreasing the dimensions ($v_3 \Lambda \delta_1$), any type of change in temperature or pressure [$v_5 \Lambda (\delta_1 V \delta_2 V \delta_3)$, $v_6 \Lambda (\delta_1 V \delta_2 V \delta_3)$].

The combination of material streams is possible only in the case of two input material streams, the separation only in the case of two output material streams. The same holds for transformations $v_8 \Lambda \delta_2$ and $v_8 \Lambda \delta_3$; however, there are further restrictions. The heterogeneous system resulting from the change $v_8 \Lambda \delta_2$ may be $\delta_a \rightarrow \delta_b$, $\delta_a \leftrightarrow \delta_b$ or $\delta_b \rightarrow \delta_a$, depending on material properties and the quantitative relations. In the case of solid-liquid systems, the heterogeneous system may be changed on addition or on removal of one of the materials; this holds both for $v_8 \Lambda \delta_2$ and $v_8 \Lambda \delta_3$.

A change in the form is possible only in the case of a solid system, production of form in the case of a "fictive solid material", the demolition of form in the case of a "fictive liquid or gas".

It is self-evident that the change which transforms heterogeneous ones: $v_8 \Lambda \delta_2$ postulates a heterogeneous input system which - except for the case of a solid-solid heterogeneous system - may be changed to a homogeneous one. The case is just the opposite with the change of the $v_8 \Lambda \delta_2$ type, with the difference that this change can separate neither a solid-solid nor a gas-gas homogeneous system.

The change $v_8 \Lambda \delta_2$ transposes a heterogeneous connection, and accordingly the starting material consists of at least two mate-

rial streams, at least one of them being a heterogeneous system. The same holds true of the resultant material system. Consequently, a minimum of three components must be present, from which two or less may be solid, because such a type of change is not possible between exclusively solid materials. Furthermore, not more than one of the components may be a gas, since a heterogeneous gas-gas system cannot exist. The change $v_9 \wedge \delta_4$ transposes a homogeneous connection in the following general system:

$$A_o\{[K_1(\beta_a) \Longrightarrow K_2(\beta_b)] \rightarrow K_3(\beta_c)\} + v_9 \wedge \delta_4 =$$

$$= A_v\{K_1(\beta_a) \rightarrow [K_2(\beta_b) \Longrightarrow K_3(\beta_c)]\} \qquad (27)$$

where a, b and c may be 1, 2 and 3.

The following abbreviations were applied in the description of the combinations, for example:

$$A\{[K_1(\beta_2) \Longrightarrow K_2(\beta_1)] \rightarrow K_3(\beta_3)\} = (2,1,3) \qquad (28)$$

Accordingly, the possible triple combinations are the following:

(1,1,1) (2,2,2) (3,3,3) (28.a)

(1,1,2) (1,1,3) (2,2,1) (2,2,3) (3,3,1) (3,3,2) (28.b)

(1,2,3) (28.c)

The laws decreasing the number of the possible combinations are the following:

a) No change in state occurs, and consequently the starting and the resultant materials are of the same combination;

b) A gas-gas heterogeneous system cannot exist;

c) A solid-solid homogeneous system cannot be decomposed by a solid;

d) In the case of the homogeneous connection of materials od the same state, the direction $\Longrightarrow$ is optional, $\beta_a \Longrightarrow \beta_b = \beta_b \Longrightarrow \beta_a$, whereas in the case of materials of different states, the direction is determined by the form of appearance;

e) A solid material may enter from a solid homogeneous system only into another homogeneous system;

f) A solid material present in a gas may not be exchanged for another solid;

g) A solid-solid system may be formed only from a homogeneous system;

h) Only one change may take place;

i) A change must take place;

j) A solid present in a gas may not be exchanged by a liquid, neither can a liquid be exchanged by a gas.

The combination remains unaltered by the change, only the system goes over from one permutation into another; taking the prohibitive laws into consideration, the remaining changes are the following:

From the line (28.a) there remains only the combination (2,2,2):

$$[\beta_2 \Longrightarrow \beta_2'] \rightarrow \beta_2'' \quad = \quad [\beta_2 \Longrightarrow \beta_2''] \rightarrow \beta_2'$$

The permutations of the second combination of line (28.b) are the following:*

	(1,1,2)	(1,2,1)	(2,1,1)
(1,1,2)	d	e	+
(1,2,1)	e	+	d
(2,1,1)	+	d	+

The permutations of the second combination of line (28.b) are the following:

	(1,1,3)	(1,3,1)	(3,1,1)
(1,1,3)	d	e	+
(1,3,1)	g	+	d
(3,1,1)	+	e	f

*The cases which do occur in reality are designated by + in the Table, whereas those prohibited are indicated by the code letter of the prohibiting law.

The permutations of the third combination of line (28.b) are the following:

	(2,2,1)	(2,1,2)	(1,2,2)
(2,2,1)	d	+	+
(2,1,2)	+	+	d
(1,2,2)	+	d	+

The permutations of the fourth combination of line (28.b) are the following:

	(2,2,3)	(2,3,2)	(3,2,2)
(2,2,3)	d	+	+
(2,3,2)	+	+	d
(3,2,2)	+	d	+

The permutations of the fifth combination of (28.b) are:

	(3,3,1)	(3,1,3)	(1,3,3)
(3,3,1)	d	b	+
(3,1,3)	b	b	b
(1,3,3)	+	b	+

The permutations of the sixth combination of (28.b) are:

	(3,3,2)	(3,2,3)	(2,3,3)
(3,3,2)	d	b	+
(3,2,3)	b	b	b
(2,3,3)	+	b	+

The permutations of the combinations of line (28.c) are:

	(1,2,3)	(1,3,2)	(2,1,3)	(2,3,1)	(3,1,2)	(3,2,1)
(1,2,3)	i	+	d	h	h	+
(1,3,2)	+	i	h	+	d	h
(2,1,3)	d	h	i	+	+	h
(2,3,1)	h	+	+	i	h	d
(3,1,2)	h	d	+	h	i	j
(3,2,1)	+	h	h	d	j	i

Starting material	Change	
A_o	$v_1\wedge\delta_1 \vee v_2\wedge\delta_1 \vee v_3\wedge(\delta_2\vee\delta_3)\vee(v_6\vee v_5)\wedge(\delta_1\vee\delta_2\vee\delta_3)$	1
$A_{0,1} \circ A_{y0,2}$	$v_1\wedge\delta_2$	2
A_{y0}	$v_1\wedge\delta_3$	3
$A\{\beta_a\}\circ A\{\beta_b\}$	$v_8\wedge\delta_2$	4
$A\{\beta_a \leftrightarrow \beta_b\}\circ A\{\beta_b\}$	$v_8\wedge\delta_2$	5
$A\{\beta_a \rightarrow \beta_b\}\circ A\{\beta_b\}$	$v_8\wedge\delta_2$	6
$A\{\beta_a \leftrightarrow \beta_b\}$	$v_8\wedge\delta_3$	7
$A\{\beta_a \leftrightarrow \beta_b\}$	$v_8\wedge\delta_3$	8
$A\{\beta_2 \rightarrow \beta_1\}$	$v_8\wedge\delta_3$	9
$A\{K[\beta_1,(\alpha_5)_1]\}$	$v_4\wedge\delta_1$	10
$A\{K^+[\beta_1,\alpha_4,o]\}$	$v_4\wedge\delta_2$	11
$A\{K^+[\beta_a,o,\alpha_5]\}$	$v_4\wedge\delta_3$	12
$A\{\beta_a\}$	$v_7\wedge\delta_1$	13
$A\{\beta_a\}$	$v_7^{-1}\wedge\delta_1$	14
$A\{\beta_1\}$	$(v_7\wedge\delta_1)^2$	15
$A\{\beta_3\}$	$(v_7\wedge\delta_1)^{-2}$	16
$A\{\beta_a \rightarrow \beta_b\}$	$v_9\wedge\delta_2$	17
$A\{\beta_a \Longrightarrow \beta_b\}$	$v_9\wedge\delta_3$	18
$A\{\beta_a \rightarrow \beta_b\}\circ A\{\beta_c\}$	$v_8\wedge\delta_4$	19
$A\{\beta_a \Longrightarrow \beta_a' \rightarrow \beta_b\}$	$v_9\wedge\delta_4$	20
$A\{\beta_a \Longrightarrow \beta_a' \rightarrow \beta_b\}$	$v_9\wedge\delta_4$	21
$A\{\beta_a \Longrightarrow \beta_b \rightarrow \beta_b'\}$	$v_9\wedge\delta_4$	22
$A\{\beta_a \Longrightarrow \beta_b \rightarrow \beta_c\}$	$v_9\wedge\delta_4$	23
$A\{\beta_a \Longrightarrow \beta_b \rightarrow \beta_c\}$	$v_9\wedge\delta_4$	24
$A\{K[(\alpha_{14})_1,\beta_1]\}$	$v_{10}\wedge\delta_1$	25
$A\{K[(\alpha_{15})_1]\}$	$v_{11}\wedge\delta_1$	26
$A\{K[(\alpha_{15})_1] \rightarrow K[(\alpha_{15})_2]\}$	$v_{11}\wedge\delta_2$	27
$A\{K[(\alpha_{15})_1]\}$	$v_{11}\wedge\delta_3$	28
$A\{K[(\alpha_{15})_1] \rightarrow K[(\alpha_{15})_2]\}$	$v_{11}\wedge\delta_4$	29
$A\{K[(\alpha_{16})_1,\beta_1]\}$	$v_{12}\wedge\delta_1$	30
$A\{K[(\alpha_{16})_1,\alpha_{16},\beta_1]\}$	$v_{12}\wedge\delta_2$	31
$A\{K[(\alpha_{16})_1,\alpha_{16},\beta_1]\}$	$v_{12}\wedge\delta_3$	32
$A\{K[(\alpha_{16})_1,\beta_1]\}$	$v_{12}\wedge\delta_4$	33

	Product	Remark
1	A_v	any material
2	A_v	any material
3	$A_{v,1} \circ A_{v,2}$	any material
4	$A\{\beta_a \rightleftarrows \beta_b\}$	a = 1,2,3 b = 1,2,3
5	$A\{\beta_b \rightarrow \beta_a\}$	a = 1,2 b = 1,2
6	$A\{\beta_a \leftrightarrow \beta_b\}$	a = 1,2 b = 1,2
7	$A\{\beta_a\} \cdot A\{\beta_b\}$	a = 1,2,3 b = 1,2,3
8	$A\{\beta_a \rightarrow \beta_b\} \cdot A\{\beta_b \rightarrow \beta_a\}$	a = 1,2 b = 1,2
9	$A\{\beta_1 \leftrightarrow \beta_2\} \circ A\{\beta_2\}$	
10	$A\{K[\beta_1,(\alpha_5)_2]\}$	
11	$A\{K[\beta_1,\alpha_4,\alpha_5]\}$	
12	$A\{K[\beta_a,o,o]\}$	a = 2,3
13	$A\{\beta_{a+1}\}$	a = 1,2
14	$A\{\beta_{a-1}\}$	a = 2,3
15	$A\{\beta_2\}$	
16	$A\{\beta_1\}$	
17	$A\{\beta_a \Rightarrow \beta_b\}$	a = 1,2,3 b = 1,2,3 a ≠ b ≠ 1
18	$A\{\beta_c \rightarrow \beta_b\}$	a = 1,2,3 b = 1,2,3 a = b ≠ 3
19	$A\{\beta_a\} \cdot A\{\beta_c \rightarrow \beta_e\}$	a,c,e=1,2,3 (one only twice, 3 only once)
20	$A\{\beta_a \Rightarrow \beta_a' = \beta_b \rightarrow (\beta_a' \cdot \beta_b)\}$	a = 2, b = 1,2,3
21	$A\{\beta_b \Rightarrow \beta_a' \rightarrow \beta_a\}$	a, b = 1,2,3 a ≠ b
22	$A\{\beta_a \Rightarrow \beta_b' \rightarrow \beta_{b'}\}$	a=1,3; b=1,2,3: a ≠ b; a = 3; b = 2
23	$A\{\beta_a \Rightarrow \beta_c \rightarrow \beta_b\}$	a = 1,2; b,c = 1,2,3; a ≠ b ≠ c
24	$A\{\beta_c \Rightarrow \beta_c \rightarrow \beta_a\}$	a,b,c = 1,2,3 a ≠ b ≠ c
25	$A\{K[(\alpha_{14})_2,\beta_1]\}$	
26	$A\{K[(\alpha_{15})_2]\}$	
27	$A\{K[(\alpha_{15})_3]\}$	
28	$A\{K[(\alpha_{15})_2] \Rightarrow K[(\alpha_{12})_2]\}$	
29	$A\{K[(\alpha_{15})_2] \Rightarrow K[(\alpha_{13})_2]\}$	
30	$A\{K[(\alpha_{15})_2,\beta_1]\}$	
31	$A\{K[(\alpha_{15})_2,\alpha_{12},\beta_1]\}$	
32	$A\{K[(\alpha_{14})_2,\alpha_{12},\beta_1]\}$	
33	$A\{K[\alpha_{14},\alpha_{15}]\}$	

The chamical change v_{11} postulates a homogeneous material system, $v_{11}\Lambda\delta_2$ acts in the case of at least two input, and $v_{11}\Lambda\delta_3$ at least two output components. $v_{11}\Lambda\delta_4$ acts in the case of two input and two output components.

Micro-biological changes (v_{12}) postulate a solid material.

The connections between the changes and the material systems are summarized in the Table.

Total Changes

Let the sum of elementary changes, consisting of such a minimum number of terms as not to permit the occurrence of a fictive material system among the products, be termed a total change. The following principles may be defined for the production of total changes on the basis of the elementary changes:

a) The starting material and the product of the elementary chemical changes may be homogeneous only, and the chemical change is to be complemented to a total change in accordance with this.

b) If the product of the chemical reaction is a solid, β_1^+ and it is complemented by supplying a crystal structure.

c) If a solid, is produced in the change, β_1^{+++}, i.e. it is complemented by supplying a crystal structure, shape and dimensions; the reverse is true in the case of a disappearance.

d) If the product of the change is a liquid, β_2^+, it is complemented by supplying dimensions.

e) In the line $0 \rightarrow \Longrightarrow$only one step is possible in the course of the elementary change.

For the sake of brevity, only those signs were given which are of some importance in the examination.

The chamical changes are always written as quasi-homogeneous ones and they are complemented with elementary changes, depending on the phases, so as to obtain total changes.

For example:

$$Na_2CO_3 + H_2O + CO_2 = 2\ NaHCO_3$$

The description of a chemical reaction as a quasi-homogeneous change:

$$A\{K[H_2O,\beta_2] \Longrightarrow K[Na_2CO_3,\beta_1] \Longrightarrow K[CO_2,\beta_3]\} + \nu_{11}\Lambda\delta_2 =$$

$$= A\{K[H_2O,\beta_2] \Longrightarrow K[NaHCO_3,\beta_1]\}$$

The supplementary elementary changes are the following:

$$A\{K[H_2O,\beta_2]\} \circ A\{K[\alpha_{14},Na_2CO_3,\beta_1,\alpha_4,\alpha_5]\} + \nu_2\Lambda\delta_2 =$$

$$= A\{K[H_2O,\beta_2] \rightarrow K[\alpha_{14},Na_2CO_3,\beta_1,\alpha_4,\alpha_5]\}$$

$$A\{K[H_2O,\beta_2] \rightarrow K[\alpha_{14},Na_2CO_3,\beta_1,\alpha_4,\alpha_5]\} + \nu_8\Lambda\delta_2 =$$

$$= A\{K[H_2O,\beta_2] \Longrightarrow K^{+++}[\alpha_{14},Na_2CO_3,\beta_1,\alpha_4,\alpha_5]\}$$

$$A\{K[H_2O,\beta_2] \Longrightarrow K^{+++}[\alpha_{14},Na_2CO_3,\beta_1,\alpha_4,\alpha_5]\} + \nu_{11}\Lambda\delta_1 =$$

$$= A\{K[H_2O,\beta_2] \Longrightarrow K^{++}[O,Na_2CO_3,\beta_1,\alpha_4,\alpha_5]\}$$

$$A\{K[H_2O,\beta_2] \Longrightarrow K^{++}[O,Na_2CO_3,\beta_1,\alpha_4,\alpha_5]\} + \nu_4\Lambda\delta_3 =$$

$$= A\{K[H_2O,\beta_2] \Longrightarrow K^{+}[O,Na_2CO_3,\beta_1,\alpha_4,O]\}$$

$$A\{K[H_2O,\beta_2] \Longrightarrow K^{+}[O,Na_2CO_3,\beta_1,\alpha_4,O]\} + \nu_3\Lambda\delta_3 =$$

$$= A\{K[H_2O,\beta_2] \Longrightarrow K[O,Na_2CO_3,\beta_1,O,O]\}$$

$$A\{K[H_2O,\beta_2] \Longrightarrow K[O,Na_2CO_3,\beta_1,O,O]\} \circ A\{K[CO_2,\beta_3]\} + \nu_9\Lambda\delta_2 =$$

$$= A\{K[H_2O,\beta_2] \Longrightarrow K[O,Na_2CO_3,\beta_1,O,O] \rightarrow K[CO_2,\beta_3]\}$$

$$A\{K[H_2O,\delta_2] \Longrightarrow K[O,Na_2CO_3,\delta_1,O,O] \rightarrow K[CO_2,\delta_2]\} + \nu_9\Lambda\delta_2 =$$

$$= A\{K[H_2O,\delta_2] \Longrightarrow K[O,Na_2CO_3,\delta_1,O,O] \Longrightarrow K[CO_2,\delta_3]\}$$

$$A\{K[H_2O,\delta_2] \Longrightarrow K[O,NaHCO_3,\delta_1,O,O]\} + \nu_3\Lambda\delta_3 =$$

$$= A\{K[H_2O,\delta_2] \rightarrow K^{+++}[O,NaHCO_3,\delta_1,O,O]\}$$

$$A\{K[H_2O,\delta_2] \rightarrow K^{+++}[O,NaHCO_3,\delta_1,O,O]\} + \nu_{10}\Lambda\delta_2 =$$

$$= A\{K[H_2O,\delta_2] \rightarrow K^{++}[\alpha_{14},NaHCO_3,\delta_1,O,O]\}$$

$$A\{K[H_2O,\delta_2] \rightarrow K^{++}[\alpha_{14},NaHCO_3,\delta_1,O,O]\} + \nu_4\Lambda\delta_2 =$$

$$= A\{K[H_2O,\delta_2] \rightarrow K^{+}[\alpha_{14},NaHCO_3,\delta_1,O,\alpha_5]\}$$

$$A\{K[H_2O,\delta_2] \rightarrow K^{+}[\alpha_{14},NaHCO_3,\delta_1,O,\alpha_5]\} + \nu_3\Lambda\delta_2 =$$

$$= A\{K[H_2O,\delta_2] \rightarrow K[\alpha_{14},NaHCO_3,\delta_1,\alpha_4,\alpha_5]\}$$

$$A\{K[H_2O,\delta_2] \rightarrow K[\alpha_{14},NaHCO_3,\delta_1,\alpha_4,\alpha_5]\} + \nu_4\Lambda\delta_3 =$$

$$= A\{K[H_2O,\delta_2]\} \rightarrow A\{K[\alpha_{14},NaHCO_3,\delta_1,\alpha_4,\alpha_5]\}$$

$$A\{K[H_2O,\delta_2]\} \rightarrow A\{K[\alpha_{14},Na_2CO_3,\delta_1,\alpha_4,\alpha_5]\} + \nu_{11} =$$

$$= A\{K[\alpha_{14},NaHCO_3,\delta_1,\alpha_4,\alpha_5]\} \rightarrow A\{K[H_2O,\delta_2]\}$$

Partial Transformations

In the overwhelming majority of cases, the total transformations do not go on to completion, but only partially. For example, the symbol of the transformation corresponding to crystallization:

$$\nu_{10} \wedge \delta_3 \quad : \begin{pmatrix} \beta_2 \Longrightarrow \beta_1 \\ \beta_2 \rightarrow \beta_1 \end{pmatrix}$$

expresses that according to the "picture" there is no solid (β_1) dissolved ($\Longrightarrow$) in the liquid (δ_2). If the transformation occurs only partially, crystallization can be expressed by the following symbol:

$$\nu_{10} \wedge \delta_3 \quad : \begin{pmatrix} \beta_2 \Longrightarrow \beta_1 \\ \beta_2 \Longrightarrow \beta_1 \rightarrow \beta_1 \end{pmatrix}$$

If the crystallization is continued on the produced material system $\beta_2 \Longrightarrow \beta_1 \rightarrow \beta_1$, a material system $\beta_2 \Longrightarrow \beta_1 \rightarrow \beta_1$ is obtained again, despite the fact that the two systems differ from each other. This difference is a quantitative one; however, up to now, quantitative discriminations were not made. Neither will the definition of the concrete quantity of the materials be needed in the following algebraic description; it is only necessary that a system of definitions be applied which enables the materials of different quantities to be discriminated. This was already carried out in transformations where the change is continuous by the introduction of the degree of change. Such transformations are the following:

$$(\nu_1 \vee \nu_2 \vee \nu_3 \vee \nu_4 \vee \nu_{10} \vee \nu_{11} \vee \nu_{12}) \wedge \delta_1$$

$$(\nu_5 \vee \nu_6 \vee \nu_{12}) \wedge \delta_2$$

There is no need for a separate discrimination of quantity in the case of these transformations. Similarly, it is not necessary to introduce such a designation in the transformations which do not occur individually.

$$(\nu_7 \vee \nu_8 \vee \nu_{11}) \wedge (\beta_2 \vee \beta_1)$$

The other transformations are dealt with in more detail.

In the formation and dissolution of a heterogeneous connection, the output material system is equal to the unified material

system in such a way that the quantity of one of the phases is changed. The quantitative parameter is designated by p and q and the only reservations are that $0 < p, q < 1$ and that $\beta_a^{p_1}$; $\beta_a^{p_2}$ if $p_1 > p_2$ and $\beta_a^{p_1}$ means in this case a larger quantity of material than $\beta_a^{p_2}$.

Accordingly:

$$v_8\Lambda\delta_i:\begin{pmatrix}\beta_a\rightarrow\beta_b^{p_1}\circ\beta^{q_1} & p_1>p_2 & i=3 \text{ and } p_2=0 & \text{corresponds to a perfect decomposition}\\ \beta\rightarrow\beta^{p_2}\circ\beta^{q_2} & p_1<p_2 & i=2 \text{ and } p_2=1 & \text{corresponds to a perfect combination}\end{pmatrix}$$

The following equationa are valid:

$$p_1 + q_1 = 1$$

$$p_2 + q_2 = 1$$

$$p_1 + p_2 = 1$$

In cases where the above Equations hold, q_1 and q_2 will not be written in the following.

In the case of the formation and dissolution of the homogeneous connection, in a way similar to the above, we may write:

$$v_9\Lambda\delta_i:\begin{pmatrix}\beta_a\rightarrow\beta_b^{p_1}\rightarrow\beta_b & p_1>p_2 & i=3 & p_2=0 & \text{perfect decomposition}\\ \beta_a\rightarrow\beta_b^{p_2}\rightarrow\beta_b & p_1<p_2 & i=2 & p_2=1 & \text{perfect combination}\end{pmatrix}$$

In the case of chemical combination and decomposition:

$$v_{11}\Lambda\delta_i:\begin{pmatrix}[\beta_a\rightarrow\beta_b]^{p_1}\rightarrow\beta_c & p_1>p_2 & i=2 & p_1=1 & \text{total combination}\\ [\beta_a\rightarrow\beta_b]^{p_2}\rightarrow\beta & p_1<p_2 & i=3 & p_1=0 & \text{total decomposition}\end{pmatrix}$$

In changes of state, materials of both the states are present in the starting and resultant material systems:

$$(v_7 \wedge \delta_1)^i: \begin{pmatrix} \beta_1^{p_1} \Longrightarrow \beta_2 & p_1 > p_2 & i=1 & p_2=0 & \text{total change} \\ \beta_1^{p_2} \Longrightarrow \beta_2 & p_1 < p_2 & i=-1 & p_2=1 & \text{total change} \end{pmatrix}$$

In the translocation of a heterogeneous connection:

$$v_8 \wedge \delta_4: \begin{pmatrix} \beta_a \rightarrow \beta_b^{p_1} \circ \beta_c \rightarrow \beta_b \\ \beta_a \rightarrow \beta_b^{p_2} \circ \beta_c \rightarrow \beta_b \end{pmatrix} \quad \text{if} \quad p_2 = \begin{cases} 0 \\ 1 \end{cases} \quad \text{total change}$$

In the translocation of a homogeneous connection:

$$v_9 \wedge \delta_4: \begin{pmatrix} \beta_a \Longrightarrow \beta_b^{p_1} \rightarrow \beta_b \Longrightarrow \beta_c^{q_1} \rightarrow \beta_c & p_2 = 1 & q_2 = 0 \\ \beta_a \Longrightarrow \beta_b^{p_2} \rightarrow \beta_b \Longrightarrow \beta_c^{q_2} \ \beta_c & p_2 = 0 & q_2 = 1 \end{pmatrix} \quad \text{total change}$$

In chamical exchange:

$$v_{11} \wedge \delta_4: \begin{pmatrix} [\beta_a \Longrightarrow \beta_b]^{1-p_1} \Longrightarrow [\beta_c \Longrightarrow \beta_d]^{p_1} \\ [\beta_a \Longrightarrow \beta_b]^{1-p_2} \Longrightarrow [\beta_c \Longrightarrow \beta_d]^{p_2} \end{pmatrix} p_2 = \begin{cases} 0 \\ 1 \end{cases} \quad \text{total change}$$

Finally, in changes of the type $v_1 \wedge (\delta_2 \vee \delta_3)$ the quantitative parameter relates to the ratio of the split material stream, i.e.:

$$v_1 \wedge \delta_i: \begin{pmatrix} a_1^{p_1} \circ a_1^{1-p_1} & p_2 = 1 & i = 2 \\ a_1^{p_2} \circ a_1^{1-p_2} & p_1 = 1 & i = 3 \end{pmatrix}$$

REFERENCES

1. BLICKLE, T., BÁTOR, E. and HALÁSZ, Zs., Hung. J. Ind. Chem. 1, 163 (1973)

2. BENEDEK, P., LÁSZLÓ, A., The Foundations of Chemical Engineering Science. Müszaki Könyvkiadó. Budapest, 1964.

3. BLICKLE, T., Hung. J. Ind. Chem. 1, 17 (1973)

РЕЗЮМЕ

В предыдущей сообщеении этой темы (1) алгебраическими методами описывались материальные системы и происходящие в них изменения. Основная зависимость образуется между происходящими в материальной системе изменениями и получающимися вследствие их новыми системами. Это называют преобразованием и обозначают следующим образом:

$$v_1 : \begin{matrix} a_o \\ a_v \end{matrix} \qquad 1.$$

Вышеуказанное выражение означает, что под действием изменения v_1 материальная система a_0 преобразуется в систему a_v. Далее авторы рассматривают различные изменения и исследуют зависимости, которые имеют место между указанными изменениями и остальными материальными системами.

Hungarian Journal
of Industrial Chemistry
Veszprém
Vol.1. pp. 555-562 (1973)

THERMAL STABILITY OF CHEMICAL REACTORS

A. LÁSZLÓ and Mrs.J. DENCS

(Department of Chemical Process Engineering,
Veszprém University of Chemical Engineering)

Received: October 18, 1973.

The occurrence of thermal instability of large chemical reactors is a well known fact. Experience has shown that during the start and shut down periods, the instability can be considerable and even dangerous. On more than one occasion it was observed that a relatively small change of the feed rate (B), the concentration (c_0) or the temperature of the feed (T_0) caused a rapid drop of the temperature and conversion of a working reactor, characterized by high temperature and high degree of conversion. There are apparent contradictions in the observations of reactors running at low temperature and with a small degree of conversion, that an insignificant alteration of the previously mentioned parameters resulted in a sudden increase of temperature and conversion. In practice, this latter phenomenon was called "ignition", independently from the fact whether burning or an increase of the catalyst temperature only took place. A different type of instability could be observed and also reproduced at certain critical parameter values, when the working condition of a reactor changed suddenly between the mentioned limits, and regarding the thermal phenomena, an oscillation came into existence.

Summing up the experiences, it can be stated that there are narrow unstable domains in the working conditions of a reactor which cannot be described merely by the heat balance of the system.

WAGNER [1] first elucidated the causes of this phenomenon in his theoretically well grounded work. Due to the Second World War his article was not widely available, and van HEERDEN [2] again

elaborated the conditions of the stability in 1953. BILOUS and AMUNDSON's article [3] published in 1955, examined this thermal stability, and for this the linearisation of their mathematical model was used. As a result, numerous researchers have dealt with the problem. VOLTER and SALNIKOV summarized the published statements in their book [4].

In the present work it will be shown that in the thermal sense both the extreme types of reactors, i.e. the adiabatic and isotherm reactors can be discussed, utilizing the same theory. The following discussion is based on the well mixed reactors.

Starting with the well known equation (e.g. [5]),which describes the rate of heat generation:

$$\dot{Q}_R = \nu_i \; r \; \Delta H \; V_R \tag{1}$$

It is known that the expression of the reaction rate ($\nu_i \; r$) can be divided into the product of two functions, one of these depends on temperature, the other one is only the function of the concentration:

$$(\nu_i \; r) = k(T) \; f(c)$$

In the following, the thermal stability will be examined only, so the substitution of $f(c) \equiv c$ is introduced, i.e. the derived equations refer to the reactions of first order, but the thermal considerations are also valid for reactions of any kind of order.

The ARRHENIUS' equation is commonly accepted and valid for the description of the k(T) function:

$$k(T) = A \; e^{-\frac{E}{RT}} \tag{2}$$

In the case of tank reactors it is known [6] that the actual concentration c or the degree of conversion x , is the function of the initial concentration (c_o) and the mean residence time ($\bar{t}$); substituting Eq. (2) into this relation:

$$c = c_o(1 - x) = c_o \frac{1}{1 + k\bar{t}} = c_o \frac{1}{1 + Ae^{-\frac{E}{RT}}\bar{t}} \qquad (3)$$

i.e. the generated heat given by Eq. (1) is as follows:

$$\Delta Q_R = \nu_i \Delta H \, V_R \, c_o \frac{A e^{-\frac{E}{RT}}}{1 + Ae^{-\frac{E}{RT}}\bar{t}} \bar{t} .$$

Using simple transformations, the following equation of suitable form can be written:

$$\Delta \dot{Q}_R = \nu_i \Delta H \, V_R \, c_o \frac{1}{\bar{t}} \frac{A \bar{t} e^{-\frac{E}{RT}}}{1 + A \bar{t} e^{-\frac{E}{RT}}} \qquad (5)$$

If in Equation (5) all the quantities - with the exception of the temperature - are constants, then the heat generated in an adiabatic reactor will be proportional with the following function:

$$Y = \frac{e^{-\frac{1}{T}}}{1 + e^{-\frac{1}{T}}} \qquad (6)$$

For isotherm reactors, this seems to be less of a problem because the substitution T = constant theoretically holds. However, this is valid only in principle, chemical engineers are aware that isotherm reactors work in a similar manner to heat exchangers, and there exists a certain inner temperature (T) which differs from the temperature of the wall (T_1); this forms the boundaries of their working conditions and determines their dimensions. Therefore, in the practice either the amounts of heat generated at the mentioned temperatures or the quotient of these heat quantities have to be taken into account. Regarding Equation (4) at temperatures (T) and (T_1), and taking their quotient:

$$\Delta\dot{Q}_R^* = \frac{\Delta\dot{Q}_R}{\Delta\dot{Q}_{Rf}} = \frac{1 + \frac{1}{A\,\bar{t}}\, e^{\frac{E}{RT_1}}}{1 + \frac{1}{A\,\bar{t}}\, e^{\frac{E}{RT}}} \tag{7}$$

If in this case A, $\bar{t}$, E and R are constants, then a relation can be obtained which is similar to Equation (6):

$$Y^* = \frac{1 + e^{\frac{1}{T_1}}}{1 + e^{\frac{1}{T}}} \tag{8}$$

Plotting $\Delta\dot{Q}_R$ or $\Delta\dot{Q}_R^*$ vs. T, the result is a sigmoid heat generation curve, known from literature. As an example, HODOSSY's work [7] can be mentioned. Here the author examined the hydrogenation of furfural to furfuryl alcohol and plotted the measured values. The results were the mentioned sigmoid curves.

In addition, for setting up a relation with Equation (6) valid for adiabatic reactors, the numerator and denominator of Equation (8) is multiplied by [exp(- 1/T)] and transforming the result we obtain:

$$Y^* = \frac{e^{-\frac{1}{T}}}{1 + e^{-\frac{1}{T}}} + \frac{e^{\frac{1}{T_1} - \frac{1}{T}}}{1 + e^{-\frac{1}{T}}} \tag{9}$$

It is now evident that although the conditions are equal, why the degree of conversion in isotherm reactors is higher compared to the same one of adiabatic reactors. The first term of Equation (9) is identical with Equation (6) valid for adiabatic reactors, and to this a second term is added. If the latter is marked with Y_1, thus:

$$Y^* = Y + Y_1 \tag{10}$$

The above relation is shown in Fig. 1. Introducing the designation

$$e^{\frac{1}{T_1}} \equiv D$$

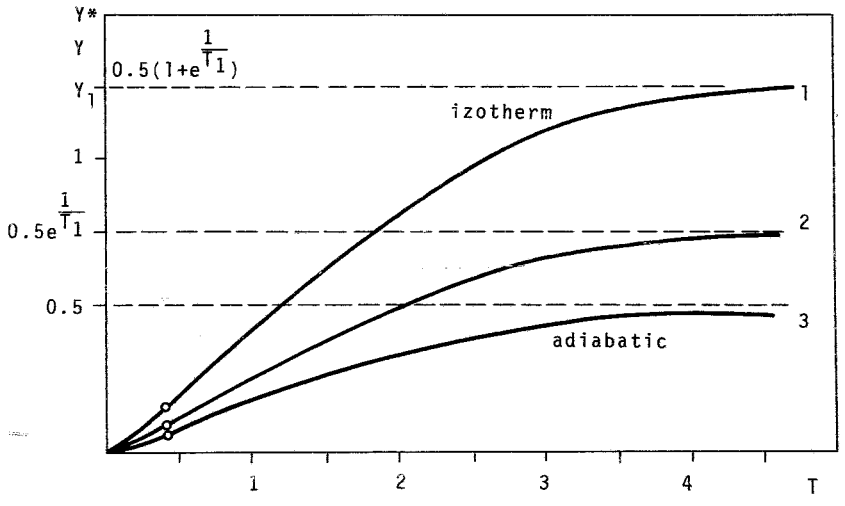

Fig. 1. 1 - $Y^* = Y + Y_1 = (1 + e^{1/T_1}) \frac{e^{-1/T}}{1 + e^{-1/T}}$

2 - $Y_1 = e^{1/T} \frac{e^{-1/T}}{1 + e^{-1/T}}$ $(T = 2.5)$; 3 - $Y = \frac{e^{-1/T}}{1 + e^{-1/T}}$

so the result is basically the same, but it is expressed differently as it is shown below:

$$Y^* = Y + \frac{D\, e^{-1/T}}{1 + e^{-1/T}} \tag{11}$$

or

$$Y^* = (1 + D) \frac{e^{-1/T}}{1 + e^{-1/T}} = (1 + D)\, Y \tag{12}$$

Although there are significant differences between the working conditions and characteristics of adiabatic and isotherm reactors, the conclusion can be drawn that they can be treated theoretically on the basis of the same principle.

This result provided encouragement to proceed further, transgressing the theory and methods usually applied in chemical engineering science, and to introduce the methods used in process control for the examination of the thermal stability of chemical reactors.

At first it was assumed that a chemical reactor as a whole is a dynamic system which can exist in different steady states. The response of the system was examined: if it is disturbed whether it returns to the previous steady state or does not. LJAPUNOV's first method was used in the examination of small disturbances, but if the disturbances were major, the non-linear model was solved and the plotted phase-plane provided the answer to the question.

The steady states of the system can be determined by the help of the

1. main isoclinics,
2. heat generation and removal curves,
3. bifurcating diagrams.

The last two methods can be applied well in practice and with their assistance the optimum working parameters of a reactor can be determined. The methods used and the experiments will be discussed in the following paper.

Acknowledgement

The authors are indebted to Mrs. M. Varga for her assistance in the mathematical analysis.

SYMBOLS

A pre-exponential factor (1/sec)

B feed rate (cu. metre/second)

c concentration (kg moles/cu. metre)

c_o concentration of the feed (kg moles/cu. metre)

E activation energy (kilocalories/kg mol)

ΔH heat of reaction (kilocalories/kg mol)

k reaction rate constant (1/second)

$\Delta\dot{Q}_R$ heat generation rate (kilocalories/second)

$\Delta\dot{Q}_{Rf}$ heat generation rate at the temperature of the wall (kilocalories/second)

$\Delta\dot{Q}_R^* = \Delta\dot{Q}_R/\Delta\dot{Q}_{Rf}$ (dimensionless)

r reaction rate (kg moles/cu. metre)

R gas constant (kilocalories/kg mol ^oK)

$\bar{t}$ mean residence time (second)

T temperature (^oK)

T_o feed temperature (^oK)

T_1 wall temperature (^oK)

V_R reactor volume (cu. metre)

x degree of conversion (dimensionless)

ν_i stoichiometric coefficient of the i-th component (dimensionless)

REFERENCES

1. WAGNER, C., Chem. Technik 18, 28 (1945)

2. VAN HEERDEN, C., Ind. Engng. Chem. 45, 1242 (1953)

3. BILOUS, O., AMUNDSON, N.R., A.I.Ch.E.J., 1, 513 (1955)

4. VOLTER, B.V., SZALNYIKOV, J.E., Ustoichivost rezhimov raboti khimicheskyh reaktorov. Izd. "Khimia" Moscow. 1972.

5. BRÖTZ, W., Grundriss der chemischen Reaktionstechnik, Verlag Chemie, Weinheim. 1970. II. Nachdruck. S. 283.

6. BENEDEK, P., LÁSZLÓ, A., A vegyészmérnöki tudomány alapjai. (The Foundations of Chemical Engineering Science.) Müszaki Könyvkiadó. Budapest, 1964.

7. HODOSSY, L., Brit. Chem. Engng. 9, 1277 (1968)

РЕЗЮМЕ

Неустойчивое поведение непостоянного типа больших химических реакторов является хорошо известным явлением. Как показывает практика, неустойчивость может быть довольно значительной и даже опасной, особенно в случае пуска или останова реактора. Часто замечали что у реакторов, работающих в режимах с высокой температурой и высокой степенью превращения, изменение скорости подачи вещества (B) концентрации (c_0) или температуры (T_0) приводило к неожиданному снижению температуры и конверсии. Кажется противоречивым тот факт, что незначительное изменение указанных параметров приводит к скачкообразному увеличению температуры и степени превращения. В практике об этом последнем явлении говорят, что реактор "загорелся", независимо от того действительно ли происходит горение или только неожиданный разогрев катализатора. В отличие от вышеописанного, авторы наблюдали и неоднократно воспроизвели при определенных критических параметрах такую неустойчивость, когда поведение реактора в определенных границах неожиданно изменялось, реактор осциллировал.

Обобщив результаты можно сказать, что существуют такие узкие неустойчивые условия работы реактора, которые нельзя описать уравнением теплового баланса системы.

Hungarian Journal
of Industrial Chemistry
Veszprém
Vol.1. pp. 563-576 (1973)

DETERMINATION OF THE ASH AND MOISTURE CONTENT OF MINERAL COALS BY NEUTRON SLOW-DOWN

G. FALUDI, E. HÁZI and Z. CSAPÓ

(Department of Radiochemistry, Veszprém University of Chemical Engineering)

Received: July 13, 1973.

The intensity of thermal neutrons in the vicinity of a neutron source emitting fast neutrons, depends on the concentration of the elements capable of slowing down the neutrons in the medium surrounding the source.

The possibilities for the determination of the ash and moisture content of mineral coals, were studied on the basis of this fact by the application of two sorts of geometrical arrangements. Factors interfering with the determinations were also studied. According to these investigations, the technique can be applied with coal of low ash content (up to 20 %) mainly for the purpose of ash content determination, with an error of ± 0.3 % ash content, whereas in the case of coal of high ash content (higher than 50 %) it can be used for humidity content determination, with an error of ± 0.2 % humidity.

INTRODUCTION

In the case of elements of low atomic number, from among the interactions between fast neutrons and matter - i.e. elastic scattering, inelastic scattering and nuclear reactions - it is first of all elastic scattering that occurs with a very high probability. The loss in energy brought about by the elastic scattering - to a very good approximation - is equal to the value

calculated on the basis of the equations of classical physics on elastic impact. Accordingly, the difference between the energy of the neutron before and after collision can be expressed by the following formula:

$$E_2 = E_1 \frac{A^2 + 2A\cos\vartheta + 1}{(A+1)^2} \tag{1}$$

where E_1 is the energy of the neutron before the collision,
E_2 is the energy of the neutron after the collision,
A is the mass number of the atom taking part in the collision,
ϑ is the angle of scattering

By introduction of the symbol

$$\left(\frac{A-1}{A+1}\right)^2 = \alpha$$

Equation (1) may be written in the following form:

$$\frac{E_2}{E_1} = \frac{1}{2}[(1+\alpha) + (1-\alpha)\cos\vartheta] \tag{2}$$

In the case of frontal collision, when $\vartheta = \pi$, the maximum decrease in energy brought about by one collision, i.e. the maximum relative decrease in energy can be deduced from Equation (2):

$$E_1 - E_{2_{min}} = (1-\alpha)E_1 \quad \text{and} \quad \frac{E_1 - E_{2_{min}}}{E_1} = 1 - \alpha \tag{3}$$

The higher the relative change in energy brought about by one collision, on the one hand, the number of collisions necessary for slowing down to a given final energy level is lower, and on the other hand, the path necessary for slowing down is shorter.

It is apparent from Equations (1), (2) and (3) that the loss in energy brought about by elastic collision is inversely proportional to the atomic number of the nucleus taking part in the collision. Nuclei of lower atomic number possess a stronger slowing down capability.

The aforesaid present a possibility for the determination of components which are of outstanding neutron moderating capability. If the mixture or solution to be studied is exposed to a fast neutron radiation of constant flux, the number (or intensity) of low-energy (thermal) neutrons will change in accordance with the concentration of the component of high neutron slowing down capability.

On the basis of the neutron slowing down capability of the hydrogen and carbon atoms, it is possible to determine the ash and moisture content of mineral coal; this problem is of a very high practical importance.

According to the papers published in literature, the principle of measurement based on the slowing down of neutrons has primarily been utilized in the development of techniques and apparatus serving the determination of the moisture content. For example,the moisture content of soil, concrete, wood, paper, sugar and ore mixtures, etc., has been measured in this way [1, 2, 3, 7, 9, 10, 12].

A number of authors have dealt with the application of this technique for the determination of the moisture content of mineral coal [1, 13], whereas its application for the purpose of ash content determination was so far rather limited [4].

DESCRIPTION OF THE MEASURING TECHNIQUE

It follows from the considerations on the slowing down path length - described in the preceding section - that the establishment of an optimal geometry is a very important condition of the applicability of the technique [6, 8]. Two - according to a number of point of view, basically different - geometric arrangements can be realized; these are schematically shown in Fig. 1. In the case of geometry realizing a "scattering of large space angle", the radio-isotipic neutron source, emitting fast neutrons, and the

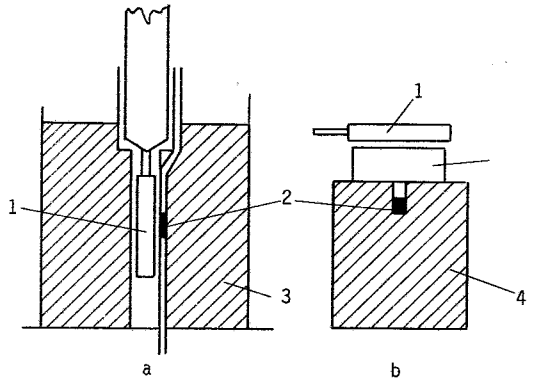

Fig. 1. The different arrangements of neutron source and detector a - "scattering of large space angle" geometry; b - "absorption-type" geometry; 1 - detector; 2 - neutron source; 3 - coal; 4 - paraffin

detector sensitive to slow neutrons, are placed in the immediate vicinity of each other. The measuring head containing the neutron source and the detector are immersed into the relatively large sample.

Taking the conclusion of KÜHN [1] - referring to the absolute value of the slowing down path lengths in hydrogen and carbon - into consideration and using a BF_3 counted tube as a detector (300 mm length and 38 mm diameter), a coal column of 600 mm height and 600 mm in diameter can be considered as an "infinite volume". The detector should be located in the middle of the coal column, in its longitudinal axis, whereas the optimum position for the neutron source is in the immediate vicinity of the detector, at a height of the middle part of the latter.

The change in the relative intensity of the slow neutrons, plotted against the diameter of the coal column for the case of a coal sample of 10 % ash and 3 % humidity content, of a maximum grain size of 6 mm and with application of a 9 mg Ra/Be neutron source is shown in Fig. 2 (the height of the coal column is 600 mm).

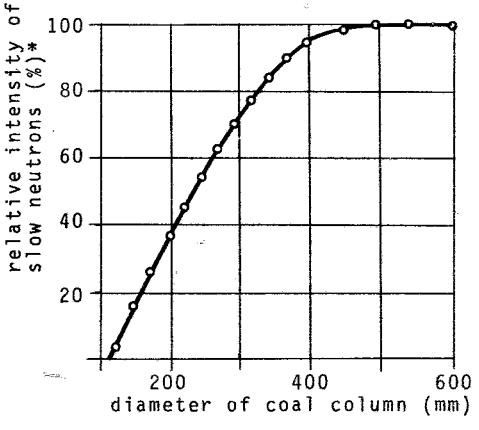

Fig. 2. The relation between the relative intensity of neutrons and geometry of coal column

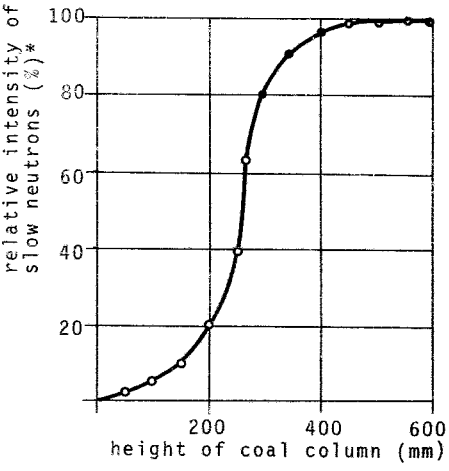

Fig. 3. How the relative neutron intensity depends on the geometry of the coal column

*Basis of reference: the intensity pertaining to "infinitely large volume".

The relative change in the intensity of the slow neutrons as plotted against the height of the coal column, in the case of the same coal sample, is shown in Fig. 3. (The diameter of the coal column was 600 mm and the distance between the bottom of the coal column and that of the detector was in all cases 100 mm.)

On the basis of Figs. 2 and 3, the minimum dimensions - "optimum dimensions" - pertaining to the maximum slow neutron intensity are the following: height 480 mm and diameter 400 mm of the coal column.

The calibration curve shown in Fig.4 is obtained if the optimal geometry is ensured and the measurement is carried out with identical space filling and the sample is of constant grain size and moisture content; the curve shows the relative change in the

intensity of slow neutrons, plotted against the ash content. On the basis of this calibration curve, and considering the scattering (σ) value calculated from the results of a large number of determinations (50), the error of the ash content determination changes in the case of different ash content ranges as illustrated by Table 1.

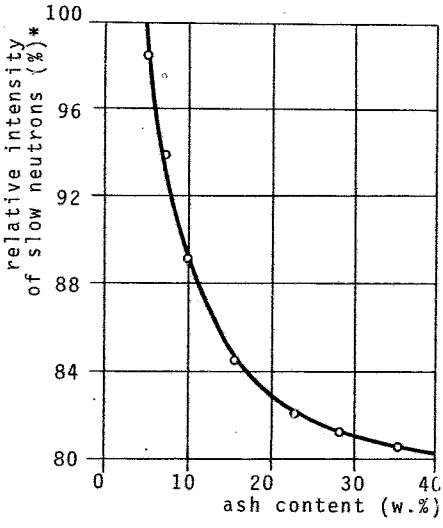

Fig. 4. Calibration curve ("scattering of large space angle" geometry

*Basis of reference: the intensity pertaining to the sample of 5 % ash content (particle size: 0 to 6 mm, moisture content: 10.6 %)

In practical application, in certain cases, the unchanged particle size distribution and constant level of moisture content is ab ovo assured on account of the coal processing technology applied, e.g. in the case of coal refuse utilization, where after desintegration, the ore and the refuse rock are separated in a hydrocyclone, or for example, in the utilization of ahidrated lignites in power stations.

Table 1

Ash content range	Absolute error	Relative error
6 - 15 %	± 0.29 % ash	± 2.9 %
15 - 30 %	± 0.45 % ash	± 1.5 %
above 30 %	± 0.6 % ash	± 1.2 %

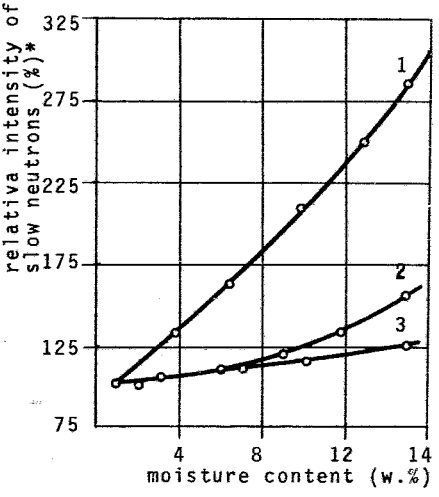

Fig. 5. The effect of moisture content of coal on the relative intensity of slow neutrons. Ash content (w.%): 1 - 78; 2 - 28; 3 - 10

*Basis of reference: the intensity measured on samples of the various coals containing 1 % moisture

If the measurement described in the foregoing is carried out with coal samples of constant ash, but variable moisture content, a calibration curve enabling moisture content determination is obtained; such a curve, established for three different sorts of coal containing different amounts of ash content, is shown in Fig. 5.

It is apparent from the curves shown in Fig. 5 that the sensitivity of the moisture content determination depends on the ash content of the coal: the technique is less sensitive in the case of coals of lower ash content. This effect can be explained by the high carbon content pertaining to a low ash content and the high neutron slow-down capability of carbon. Considering the statistical nature of radiometric measurements, the absolute error of the moisture determination can - for the coal samples of different ash content illustrated in Fig.5 - be compared on the basis of the data summarized in Table 2.

Table 2

Ash content	Absolute error of moisture content determination
10 %	± 0.54 % moisture content
28 %	± 0.36 % moisture content
78 %	± 0.22 % moisture content

If the constancy of moisture content and particle size distribution cannot be ensured in the ash content determination, random fluctuations in the moisture content may cause considerable errors in the ash determination. (A 1 % change in the moisture content corresponds, in the case of 10 % ash content, to a deviation of 2.1 % in ash content.)

In certain cases - especially when considering the unique requirements of industrial application - it may be justified to use "absorption-type" geometry, for example in the case of a continuous measurement carried out on material moved on a conveyor belt. In such an arrangement, a layer of well-defined thickness of the sample is placed between the fast neutron source and the slow neutron detector. The optimum layer thickness of the sample, dependent on a number of parameters, varies generally between 80 and 150 mm. This same geometry can also be applied for experimental laboratory measurements, because it is easy to handle on account of the relatively small amount of sample. For example, the application of various types of neutron detectors and factors interfering with the measurement can advantageously be studied with this geometry. The small amount of the needed sample also enables artificial coal "samples" to be synthetized in a wide ash content range. A calibration curve, plotted for the 5 to 100 % ash content range is ahown in Fig. 6. The layer thickness of the sample in this experiment was 100 mm, the particle size and moisture content of the sample was the same as of that used in the studies carried out with "high space angle" scattering. By comparing Figs. 4 and 6 (calibration curves), the drawback of the "absorption" geometry, i.e. its low sensitivity, becomes apparent.

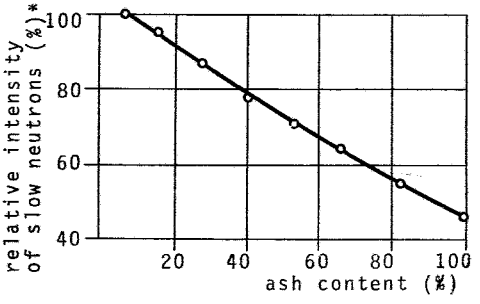

Fig. 6. Calibration curve ("absorption-type" geometry)

*Basis of reference: the intensity pertaining to a sample of 5 % ash content

INTERFERING FACTORS

If the volume weight or particle size of the samples or the chemical composition of the ash components in the samples used for ash - or moisture - content determination are different, it is to expected that interferences will occur.

As opposed to other radiometric ash or moisture determination techniques, changes in the chemical composition of the components of the ash do not interfere with the determination in the measuring technique based on the slowing-down of neutrons. This is explained by the fact that the elements which substitute each other are likewise of poor neutron slowing-down capability, as compared to the carbon or hydrogen atom.

Changes in the particle size distribution of the sample act through changes in the volume weight.

Changes in the volume weight act as an interfering factor since the number (concentration, [atom/cm^3]) of the atoms capable of slowing down neutrons (carbon and hydrogen) change even in the case of an identical ash and moisture content.

Figs. 7, 8 and 9 show the changes in the intensity of slow neutrons, plotted against the volume weight, for coal samples of a given ash content at different moisture content values. The limits of the volume weight intervals shown in the Figures correspond to the loosest and most compact space fillings possible, i.e. they are extreme values. With adequate particle size distribution ensured, it can be assumed that any spontaneous changes in space in filling do not surpass $\pm$ 0.01 g/cm^3 even in the case of industrial processes. Changes of this magnitude in volume weight - as can be judged from the calibration curves presented in Figs. 4 and 6 - cause an error of the magnitude shown in Table III. The data refer to coals of various ash contents and to both of the geometries.

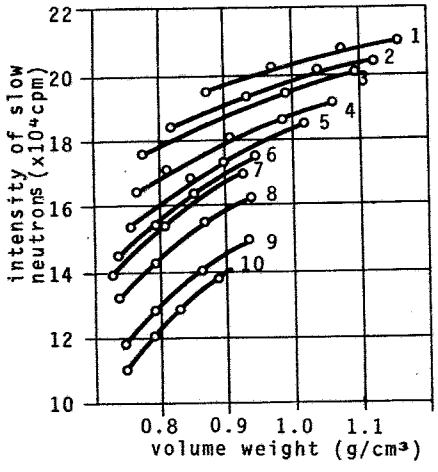

Fig. 7. The effect of volume weight of moist coal having 10 w.% ash content on the intensity of slow neutrons. Moisture content (w.%): 1 - 24.66; 2 - 21.68; 3 - 19.70; 4 - 16.76; 5 - 14.32; 6 - 11.80; 7 - 10.00; 8 - 6.39; 9 - 3.00; 10 - 0.50

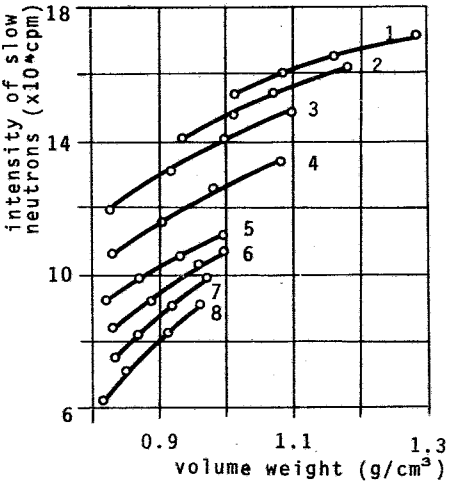

Fig. 8. The effect of volume weight of moist coal having 28 w.% ash content on the intensity of slow neutrons. Moisture content (w.%): 1 - 23.70; 2 - 20.74; 3 - 17.79; 4 - 14.86; 5 - 11.90; 6 - 8.98; 7 - 5.10; 8 - 2.00

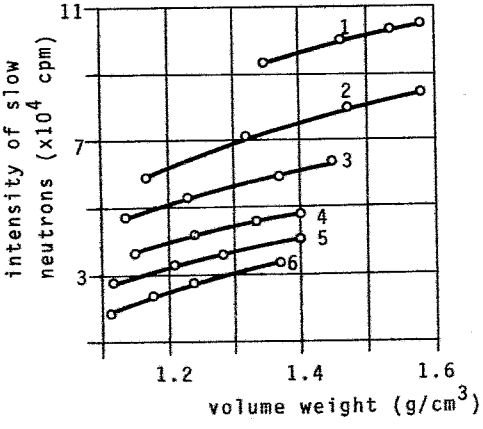

Fig. 9. The effect of volume weight of moist coal having 78 w.% ash content on the intensity of slow neutrons. Moisture content (w.%): 1 - 15.36; 2 - 12.48; 3 - 9.56; 4 - 6.60; 5 - 3.66; 6 - 0.66

Table 3

Ash content (%)	Absolute error in the ash content determination (%)
10	± 0.3
28	± 0.5
78	± 1.1

The interfering action of changes in the volume weight can be eliminated by a combination of the ash - or moisture - content determination, based on neutron slowing-down, with volume weight determination by gamma ray absorption. This is an already solved problem in the case of the determination of the humidity content of soils [5, 11].

DISCUSSION OF THE RESULTS

The method proposed in the foregoing enables the determination of two parameters that are of importance in connection with the production and processing of mineral coals, these parameters being ash content and moisture content. With coal samples of low ash content, the technique is mainly applicable for ash content determination, whereas in the case of coal samples of high ash content it is preferably used for the determination of the moisture content. In the case of coal of a high ash content (such as e.g. refuse) the determination of the moisture content - or its adjustment to a predetermined value - is important with a view to further processing (e.g. sintering in order to produce an additive to concrete, concrete production, and filling, etc.).

It is an advantage of the technique that the size of the material involved in the determination, i.e. the "sample size" is

very large, especially if the "large space angle scattering" geometry is applied. For example, practically all the material is measured, in case of a measuring sonde placed into a coal storage bunker, while it passes the sensor. Thus the information obtained can be regarded a very good average value. Further advantages are continuous operation and immediate availability of the results; the latter enables application for process control purposes as well.

Considering the advantages enumerated in the foregoing, the technique duly deserves intensive ineterst, when compared with the usual procedure involving sampling, drying for moisture determination and incineration for ash content determination, despite the fact that care must be exercised to overcome some interfering factors.

It is justified to combine the technique with other radiometric methods (e.g. gamma absorption, or reflexion) for the determination of the ash content in order to eliminate the interferences.

For practical application, considering industrial conditions, in the case of geometry producing "large space angle scattering" it is preferable to apply a Ra-226/Be or Am-241/Be neutron source, together with a BF_3-type counter tube.

REFERENCES

1. KÜHN, W., Atompraxis 5, 133 (1959)

2. KÜHN, W., Atompraxis 5, 335 (1959)

3. NEUHAUS, H., HOMBECK, F., KÜHN, W., Stahl und Eisen 82, 1017 (1962)

4. NAGY M., VARGA K., Energia és atomtechnika 15, 417 (1962)

5. NOVAKOVA, O., SLEZAK, V., Tesla Electronics 4, 16 (1971)

6. BESKIN, L.I., BOGDANOV, I.Ya., EMEL'YANOV, V.A., KIYANA, S., SINITSYN, V.I., Atomnaya energiya 31, 527 (1971)

7. STONE, I.F., Soil. Sci. Soc. Amer., Proc. 36, 261 (1972)

8. McCAULEY, G.N., STONE, I.F., Soil. Sci. Soc. Amer., Proc. 36, 246 (1972)

9. COUCHAT, P., RAMODIHARILAFY, I., Int. I. Appl. Radiat. Isotop. 23, 229 (1972)

10. POLLY, P., Arch. Techn. Messen. 435, 69 (1972)

11. NOVAKOVA, O., SLEZAK, V., Radioisotopy 13, 381 (1972)

12. VOTAVA, P., Radioisotopy 13, 423 (1972)

13. HAMPEL, M., Glückauf 109, 524 (1973)

РЕЗЮМЕ

Плотность термических нейтронов вблизи испускающего быстрые нейтроны источника зависит от концентрации элементов, тормозящих нейтроны.

Изучалось определение содержания пепла и влажности в каменных углях на основании вышеуказанного явления для случая двух экспериментальных установок. Авторы изучали влияющие на проведение эксперимента факторы. Данные экспериментов показали, что упомянутый метод применим для определения влажности с точностью до ±0,3% в случае углей с малым (до 20 весовых %) содержанием пепла, и с точностью до ±0,2% в случае углей с высоким содержанием пепла (более 50 весовых %).

СОДЕРЖАНИЕ

HUNGARIAN

Journal of

INDUSTRIAL CHEMISTRY

Edited by

the Hungarian Oil & Gas Research Institute (MÁFKI),
the Research Institute for Heavy Chemical Industries (NEVIKI),
the Research Institute for Technical Chemistry of the
Hungarian Academy of Sciences (MÜKKI),
the Veszprém University of Chemical Engineering (VVE).
Veszprém (Hungary)

Volume 1. **1973.** **Number 1.–4.**

CODEN: HJICAI

The "Hungarian Journal of Industrial Chemistry (Veszprém)" is a joint publication of the Veszprém scientific institutions of the chemical industry that deals with the results of applied and fundamental research in the field of chemical processes, unit operations and chemical engineering. The papers are published in three or four numbers at irregular intervals in one annual volume, in the English, Russian, French and German languages.

Editorial Office:
Veszprémi Vegyipari Egyetem,
"Hungarian Journal of Industrial Chemistry" Editorial Board:
H—8201 Veszprém, Schönherz Z. u. 10. Hungary.

CONTENTS

СОДЕРЖАНИЕ

A kiadásért felelős: Dr. Nemecz Ernő
Felelős szerkesztő: Dr. Bodor Endre
Példányszám: 950
Készült a Veszprémi Vegyipari Egyetem Sokszorositójában
Engedélyszámok: 92.907; 95.152; 88.382; 93.927
Áfész Sokszorosító üzem Vác. 925.74